CHAPTER ONE

INTRODUCTION

1.1 Background to the Study

Modern industrialized society has for some decades relied basically on single natural resource: petroleum. The total dependence on petroleum for liquid fuel transportation, heating fuels, plastics and petrochemicals, asphalt for road construction, packaging materials and modern medical devices has made it hard for the modern man to live without petroleum. Amongs all the applications of petroleum, energy generation is the most important. Energy has become a crucial factor for humanity to continue the economic growth and maintain high standard of living, especially after the inauguration of the industrial revolution in the late 18^{th} and 19^{th} century (IEA, 2007). According to the International Energy Agency (IEA) report (IEA, 2007, Shaid and Jama, 2011), the world will need 50% more energy in 2030 than today of which 45% will be accounted by China and India. The impact of energy isssues is more on the transportation than other areas of application. Globally, the transportation sector is the second largest energy consuming sector after industrial sector and accounts for 30% of the world's total delivered energy of which 80% is road transport. It is believed that the sector is currently responsible for nearly 60% of world's oil demand and will be the strongest growing energy demand sector in future (Atabani *et al.*, 2012). Meanwhile, petrodiesel fuel demand is growing at 35% which is greater than gasoline, kerosene and jet fuel (IEA, 2011).

However, for every positive benefit that petroleum has provided there seems to be a negative environmental ramification (Stewart and Joyce, 2012). Combustion engine emissions have resulted in growing concern over air quality and green house effects. It is believed that climate change is currently the most pressing global environmental problem. If the average global temperature increases by more than 20 $^{\circ}$C, up to one million living species could become

extinct and hundreds of millions of people could lose their lives (Ahmad *et al.*, 2012). It is expected that 4.1billion metric tons of carbon dioxide will be released to the atmosphere from 2020 to 2035. This is estimated to be about 43% increase for the aforementioned projected period (USEIAI 2010a, USEIAI 2010b).

Globally, the awareness of energy issues and environmental problems associated with burning fossil fuel has encouraged investigation on the possibility of using alternative sources of energy. Therefore, replacing petroleum with an inexpensive, renewable resource that can be produced in any country in the world would lead to a second green revolution for human needs (Mooney, 2009). Biofuel research has taken aim at replacing petroleum liquid fuels with chemicals derived from crop and forest residues, algae and birdlimed waste materials. Among them biodiesel seems very interesting for several reasons. It is highly biodegradable and has minimal toxicity. It can replace petrodiesel fuel in many different applications such as in boilers and internal combustion engines without major modifications. Also, biodiesel combustion has demostrated almost zero emissions of sulphates, aromatic compounds and other chemical substances that are destructive to the environment (Ahmad *et al.*, 2011, Cetinkaya *et al.*, 2005, Carraretto *et al.*, 2004).

Biodiesel is produced through a chemical process known as transesterification. Transesterification of vegetable oils with low molecular weight simple alcohols has been established as the best option to reduce the high viscosity, low volatility, heavy engine deposits and toxic substance formation associated with the direct use of vegetable oils (Tesser *et al.*, 2005). The relevance of biodiesel as an alternative fuel has received great attention which has grown in the last thirty years. Transesterification has remained the best method for biodiesel production. It involves the displacement of alcohol from ester by another alcohol in a process similar to hydrolysis except that alcohol is employed instead of water. The transesterification

process consists of a sequence of three consecutive reversible reactions which include conversion of triglycerides to monoglycerides. A two-step process involving esterification (acid-catalyzed) and subsequent transesterification (alkaline-catalyzed) has been suggested as the best approach in handling biodiesel feedstocks with high free fatty acid to prevent loss of the glycerides to soap formation (Mbaraka and Shanks, 2006). The glycerides are converted to glycerol and yield one ester molecule in each step. Since this reaction is reversible, excess amount of alcohol is often used to help drive the equilibrium towards the right. In the presence of excess alcohol, the forward reaction is pseudo-first order reaction and the reverse is a second order reaction. The choice of the catalyst and the nature of alcohol determine the type of initial species and the nature of fatty acid alkyl ester (FAAE) to be formed. Currently, the homogeneous base-catalyzed transesterification using methanol resulting in the corresponding fatty acid methyl esters (FAMEs) is the predominant technique applied for large scale production of biodiesel (Rayero *et al*., 2015). Application of methanol is necessitated by its wide availability and low-cost. The application of homogeneous base catalysts like NaOH and KOH at commercial level is highly encouraged because of their high catalytic activity compared to acid catalyst which are more corrosive (Wan and Hameed, 2011). The introduction of catalyst neutralization and washing has been among the most important stages of conventional purification steps employed to arrest the challenges of soap formation (Rayero et al., 2015). Also, the challenges of catalyst re-usability and the leaching of support or active sites which causes catalyst loss and decrease of the FAME yield have been serious challenges to heterogeneous catalyst application (Ilgen, 2012). A considerable amount of research has been conducted on feedstocks for biodiesel production, mainly using non-edible oil seeds including *jatropha curcas*, mahua, pongamia, camelina, cotton, karanja, neem, jojoba, moringa, rubber, passion seed, tobacco, salmon oil, tall, coffee ground, etc (Atabani *et al.*, 2012). However, in

all these investigations, little or no comprehensive work has been reported on so many underutilized tropical plant seed oils in Nigeria. Therefore, extensive research is required in the areas of fuel characterization, process optimization, engine performances and combustion emissions and kinetics of biodiesel production from sweet almond (*Prunus amygdalus*), African star apple (*Chrysophyllum albidium*), and African pear (*Dyacrodes edulis*) seed oils.

World production of almond was 2.9 million tons in 2013 with United States as the largest producer of 1.8 million tons (FAOSTAT 2014). The sweet almond variety is more widely distributed in Africa where it is mainly grown for the shade it provides in front of houses. In Nigeria the major use of this tree is for shade which it provides in front of houses, offices and markets. The fruits, when fully ripened fall to the ground and litter the environment. The oil yield of sweet almond seed oil (SASO) reported was 51.45 ± 3.92 % as an indication of its viability as a useful feedstock for various industrial purposes (Israel, 2008). African star apple is one of the indigenous wild fruit trees with enormous potentials for establishment (Ureigho and Ekeke, 2010). It has actually become a crop of commercial value in recent times. Within the pulp are three to five seeds which are not eaten. The seeds are dark brown shiny, obliquely ollipsoid to ovoid up to 2.8 cm long and 1.2 cm wide; its coat is hard, bony-shiny and dark brown when broken reveals white colored cotyledons. These are discarded after the pulp is consumed. It has been reported that African star apple seed oil (ASASO) of 21.51 % oil was extracted from the fruit seed using solvent extraction method (Audu, et al., 2013). The African pear otherwise called African plum or Safou, locally called ube among the Igbo's in southern eastern part of Nigeria belongs to the family of Burseraceae and botanically known as *Dacyrodes edulis*. It is an annual fruit of about 3cm in diameter and contains a leathery shelled stone surrounded by a pulpy pericarp of about 5mm thick. It is this portion that is eaten either raw or cooked and the seeds discarded (Bull and George, 2015; Ogunsuyi, 2015). Besides the

pulp contains 48% oil and a plantation can produce 7-8 tonnes of oil per hectare (Shikha and Rita, 2012; Awuno *et al.*, 2002).

1.2 Statement of the Problem

Globally, the Renewable Energy Network for 21st century (REN21) and other national strategies like the Nigerian Renewable Energy Master Plan (REMP), National Renewable Energy and Energy Efficiency Policy (NREEEP), Renewable Electricity Policy Guidelines (REPG) etc are geared towards arresting energy issues and environmental problems associated with burning fossil fuel before the year 2025. This has necessisated investigation on the possibility of using alternative sources of energy. The inability of various studied tropical feedstocks to meet the EU biofuel sustainability directive is threatening their viability as sources of alternative energy to petrodiesel. Few studies on the biofuel applications of *Prunus amygdalus, Chrysophyllum albidium* and *Dyacrodes edulis* were only focused on their potential application for biodiesel production (Giwa and Ogunbona, 2014, Ogunsuyi et al., 2015). Most studies on these feedstocks never established viable optimized routes for the biodiesel synthesis, engine performance-emission characteristics and kinetics of the oil transesterification process. This challenges their process scale-up, reactor design, simulation and control in both batch and continuous systems.

1.3. Research Aim and Objective

The aim of this research is to evaluate the optimization, engine performance and kinetics studies of base methanolysis of the selected seed oils for biodiesel production.

The specific objectives shall be:

1. To convert oil product extracted from the seed of from *Prunus amygdalus*, *Chrysophyllum albidium* and *Dyacrodes edulis* into biodiesel and to compare the final quality with international standard.
2. To characterize the oil and biodiesel samples.
3. To investigate process kinetics, optimization and effect of process variables on fuel properties.
4. To evaluate the engine performance, emission and combustion characteristics of the methyl esters and their blends in compression ignition diesel engine.
5. To investigate the application of response surface methodology (RSM) through central composite design (CCD), artificial neural network (ANN) as well as integrated modeling techniques in biodiesel production and engine combustion process.

1.4 Justification of Research

Currently, petro-diesel fuel demand is growing at 35% which is greater than gasoline, kerosene or jet fuel (IEA, 2011). Biodiesel has been established as better alternative renewable, non-toxic, biodegradable, sustainable and eco-friendly biofuel than petro-diesel (Atabani *et al.*, 2012). Biodiesel production helps rural development to restore degraded lands over a period and would therefore encourage rural employment generation in Nigeria. Also, its production can be raised easily and is less time consuming. Hence, biodiesel production would promote the small-medium enterprises in Nigeria and other African countries. Also, since it is safer to handle, transport, distribute and store than petroleum diesel, biodiesel application would not record fire hazards reported often on the usage of petroleum based fuels. Nigeria will not have

the need for payment of tariffs or similar taxes to other countries from which oil and petroleum diesel is imported. Therefore, researches and energy investments on biodiesel which is a better alternative to diesel would be highly rewarding.

The application of seed oils from sweet almond, African pear and African star apple sources for biodiesel production satisfy the EU sustainable biofuel directive as perennial plants, with their oil obtained from crop residues treated as waste in Nigeria. Harnessing the inexpensive and neglected seed oils as raw material for biodiesel production in Nigeria is an effective way to reduce the food-fuel strain on the use of traditional oils (palm oil, groundnut oil and palm kernel oil) (Giwa *et al.*,2014). It will offer a viable use to the waste-seed components of selected plant fruits especially now that the Nigerian government through its Sustainable Development Goals (SDGs) is advocating for a total return to green and nature.

1.5 Scope and Limitations of the Study

This work will be limited to the following:

- Oil extraction will be limited to solvent extraction method.
- Engine study of seeds with economically viable (high) oil yields.
- Evaluated properties of seed oil and biodiesel will be limited to vital physico-chemical properties.
- Engine performance and emission characteristic evaluation will be limited to the variation of BTE, BSFC, air/fuel ratio, volumetric efficiency, GFC, BSEC, exhaust gas temperature, and emissions of CO, CO_2, NOx and HC with brake power.
- Chemical kinetics study will be limited to esterification and transesterification processes.
- Process variables, modeling, optimization and statistical analysis will be limited to relevant tools like RSM, RSM-GA, ANN, NM simplex algorithm, and ANOVA.

CHAPTER TWO

LITERATURE REVIEW

2.1 Vegetable Oil Extraction

Globally, there are more than 350 oil bearing crops identified as potential sources of oil for industrial and domestic applications. The wide range of available feedstocks for industrial application represents one of the most significant factors of consideration (Demirbas, 2009). As much as possible, a viable oil feedstock should fulfill two main requirements: low production costs and large scale production. The availability of vegetable oil for various applications depends on the original climate, geographical location, local soil conditions and agricultural practices of any country. World annual vegetable oil production is about 0.107 billion tonnes which increased from 56 million tonnes in 1990 to 88 million tonnes in 2000. Leading the gains in vegetable oil production was a recovery in world palm oil output from 18.5 million tonnes in 1998 to 27.8 million tonnes in 2003 (Demirbas, 2009). Vegetable oils are basically water–insoluble and hydrophobic substances in plant kingdom that are made up of one mole of glycerol and three moles of fatty acids and are commonly referred to as triglycerides. The fatty acids vary both in carbon chain length and in number of unsaturated bonds (Fangrui and Hanna, 1999). Vegetable oil could be obtained from various parts of plants but more in abundance in either the fruit mesocarp or fruit seed. However, vegetable oil could be either edible (rape seed, soybean, peanut, sunflower, palm and coconut oil) or non-edible (jatropha, karanja, sea mango, algae and halophytes) (Aiwize and Achebo, 2012; Atabani *et al.*, 2012). Vegetable oil has found several industrial applications such as in production of biodiesel, biolubricants, resins, cosmetics, candle, etc. The use of edible oil sources for the above production process is not feasible as it raises serious concerns such as food versus fuel crises, major environmental

problems such as destruction of vital soil resources, deforestation and usage of much of the available arable land as well as the rapid growing gap between demand and supply of such oils in various countries. Figure 2.1 shows the classification oil extraction methods.

There are three main methods that have been identified for extraction of vegetable oil:

(i) Mechanical extraction

(ii) Enzymatic extraction

(iii) Solvent extraction.

Before the oil extraction takes place, seeds have to be either dried in the oven at 105°C for an hour or sun dried for about three weeks.

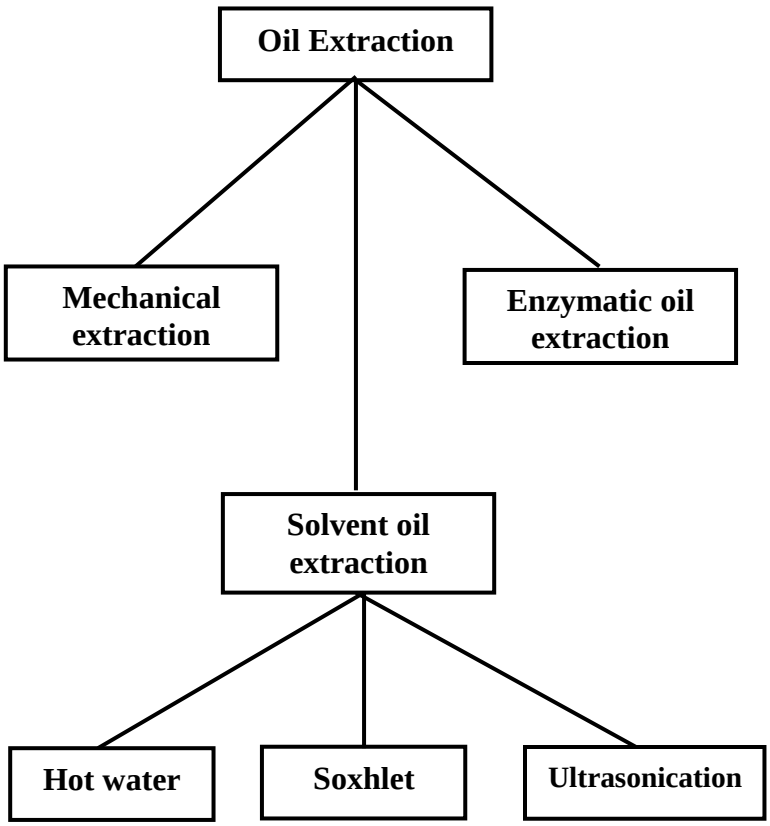

Figure 2.1: Classification of oil extraction processes (Atabani et al., 2012).

2.1.1 Mechanical extraction

The technique of oil extraction by mechanical presses is the most conventional one among other methods. In this type, either a manual ram press or an engine driven screw press can extract 68-80% of the available oil while the ram-press only achieves 60-65%. The oil extracted by mechanical presses needs further treatment of filtration and degumming. It has been found that pretreatment of the seeds such as cooking, can increase the oil yield of 89% after single pass and 91% after dual pass. (Mahanta and Shrivastava, 2011; Achten *et al.*, 2008).

2.1.2 Enzymatic oil extraction

Enzymatic oil extraction technique has emerged as a promising technique for extraction of oil. In this method suitable enzymes are used to extract oil from crushed seeds. Its main advantages are that it is environment friendly and does not produce volatile organic compounds. However the long process time is the main disadvantage associated with this technique (Mahanta and Shrivastava, 2011).

2.1.3 Solvent extraction (chemical extraction)

Solvent extraction is the technique of removing one constituent from a solid by means of a liquid solvent. It is also called leaching. There are many factors influencing the rate of extraction such as particle size, the type of liquid chosen, temperature and agitation. The small particle size is preferred. There are three methods that are used in this type and they are as follows: hot water extraction, sohxlet extraction and ultrasonic technique. Solvent extraction provides the best means of removing oil from the plant seeds, leaving a residue of less than 1% oil (Ochigbo and Paiko, 2011). Musa *et al* (2015) studied the effect of process variables (particle size, temperature and time) using ethanol as solvent but did not vary the solvent used

in oil extraction from the seeds of *Chrysophyllium albidium*. Tsakins *et al.* (1999) used normal hexane and mixture of chloroform/methanol in *Moringa olifera* seed oil extraction and obtained 35.7% and 31.2% oil yields respectively. Also Igbum *et al.* (2012) extracted PKO using thermal and solvent extraction methods. In the research, solvent extraction gave yield of 42.0 % while thermal extraction gave 41.26%. The application of n-hexane has been applied by several researchers because of its ability to extract high content of oil from plant seeds (Giwa and Ogunbona, 2014; Betiku and Adepoju, 2013; Adebayo *et al.*, 2012; Bello *et al.*, 2011).

2.2 Vegetable Oil Characterization

The Physico-chemical properties of vegetable oil are characterized based on AOAC (1990). The various quality parameters and their methods of analysis are presented briefly in Table 2.1.

Table 2.1: Methods for physico-chemical analysis for vegetable oil.

S/n	Property	Unit	Methods
1	Acid Value	mgKOH/g	AOAC Ca5a-40
2	Free fatty acid	mgKOH/g	AOAC Ca5a-40
3	Iodine value	mgKOH/g	AOAC 920:158
4	Saponification value	mgKOH/g	AOAC920:160/AOCS Cd3-2
5	Peroxide value	mgKOH/g	AOAC 965:133
6	Viscosity	mm^2/s	ASTMD-246
7	Density	kg/m^3	-
8	Calorific value	MJ/kg	-
9	Moisture content	mg/kg	Oven method

2.3 Biodiesel Production from Vegetable Oil

Direct use of vegetable oil as fuel for diesel engine can cause particle agglomeration, injector fouling due to its high viscosity and low volatility, which is about 10 to 20 times greater than petroleum diesel. The four techniques applied to reduce the high viscosity of vegetable oils are briefly discussed below.

2.3.1 Dilution with diesel fuel

Mainly vegetable oils are diluted with diesel to reduce the viscosity and improve the performance of the engine (Karaosmonoglu, 1999). This method does not require any chemical process. Singh and Singh (2010) reported that substitution of 100% vegetable oil for biodiesel fuel is not practicable. However, a blend of 20% vegetable oil and 80% diesel fuel was successful. The use of blends of rice brain oil, PP (Pistachia Palestine), waste cooking oil, palm oil, Soybean oil, cotton seed oil, rubber seed oil, rapeseed oil, *J. curcas oil, P. pinnata* oil with petro-diesel has been described in the literature (Pariwa 2010; Paramanik, 2003; Ma and Hanna, 1999).

2.3.2 Micro emulsion with immiscible liquids

A micro-emulsion is defined as a colloidal equilibrium dispersion of optical isotropic fluid microstructure with dimensions generally into 1-150nm range formed spontaneously from two normally immiscible liquids and one or more ionic or more ionic amphiphiles. Micro-emulsion process using solvents such as methanol, ethanol, hexanol, butanol and 1-butanol have been investigated by many researchers. Micro-emulsion with all these solvents has met the maximum viscosity requirement for diesel fuel. It has been demonstrated that short term performance of both ionic and non-ionic micro-emulsions of aqueous ethanol in soybean oil performed nearly as well as that of No. 2 diesel fuel (Singh and Singh 2010, Jain and Sharma 2010, Ma and Hanna, 1999).

2.3.3 Pyrolysis or thermal degradation of vegetable oils

Pyrolysis is the thermal decomposition of organic matters in the absence of oxygen and in the presence of a catalyst. The pyrolyzed material can be vegetable oil, animal fats, natural fatty acids or methyl esters of fatty acids. Many investigators have studied the pyrolysis of triglycerides to obtain suitable fuels for disesl engine. Thermal decomposition of triglycerides produces alkanes, alkenes, alkadines, aromatics and carboxylic acids (Mahanta and Shrivastava, 2011).The Pyrolysis of the vegetable oil can produce a product that has high cetane number, low viscosity, limited amounts of sulphur, water and sediments contents, acceptable copper corrosion values. However, ash contents, carbon residues and pour points might be unacceptable (Atabani *et al*., 2012). Also, it has been previously reported that Pyrolysis of vegetable oils produces more biogasoline than biodiesel fuel (Demirbas, 2003).

2.3.4 Transesterification (alcoholysis)

Among all these methods, transesterification seems to be the best option since the process can significantly reduce the high viscosity of vegetable oils (Fan, 2008). Furthermore, the physical properties of biodiesel produced by this simple process are very close to the petroleum diesel fuel. The different classifications of the transesterification process are presented in Figure 2.2 while simplified process flow chart of alkali-catalyzed biodiesel production is shown in Figure 2.3.

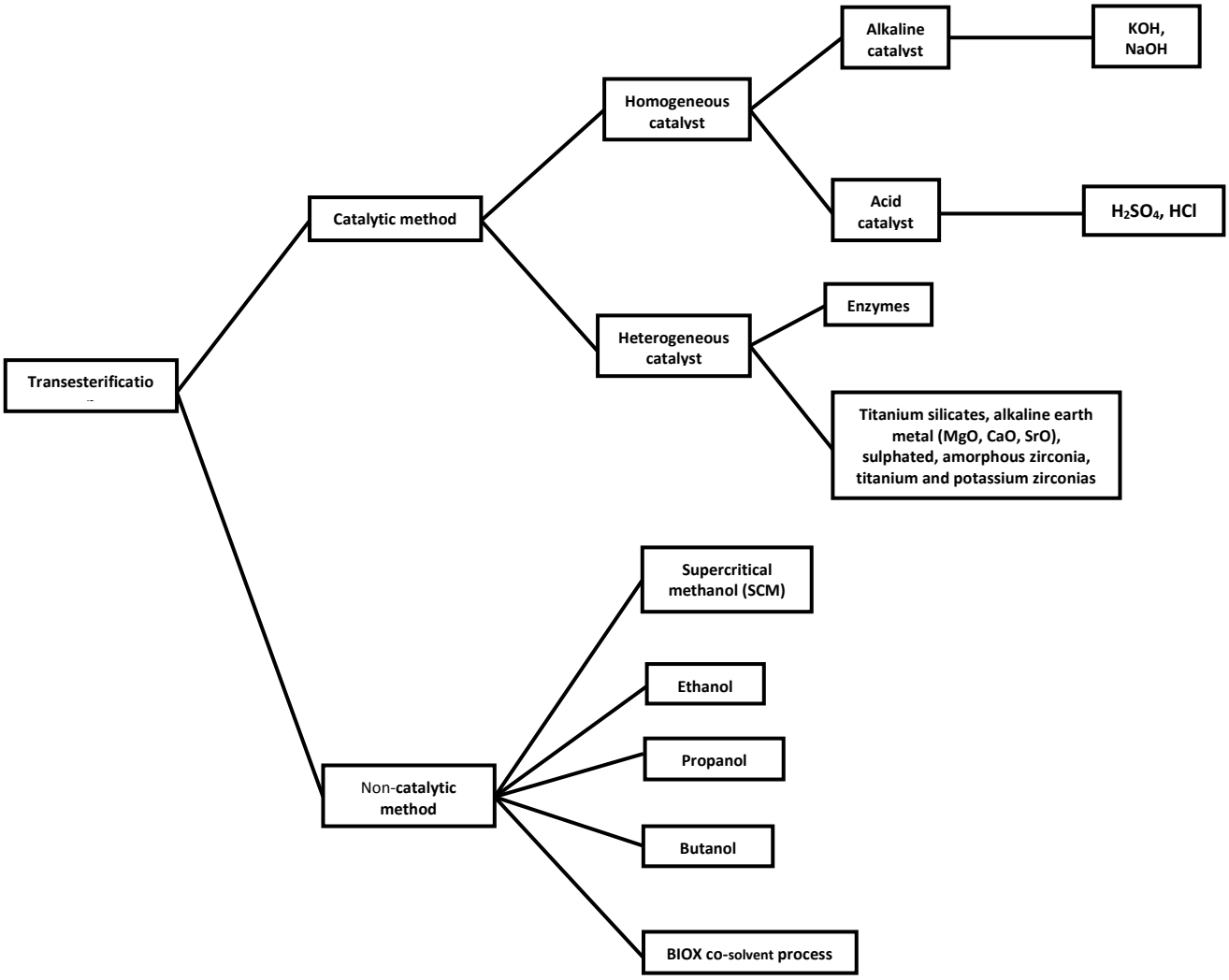

Figure 2.2: Classification of transesterification processes (Atabani *et al.*, 2012).

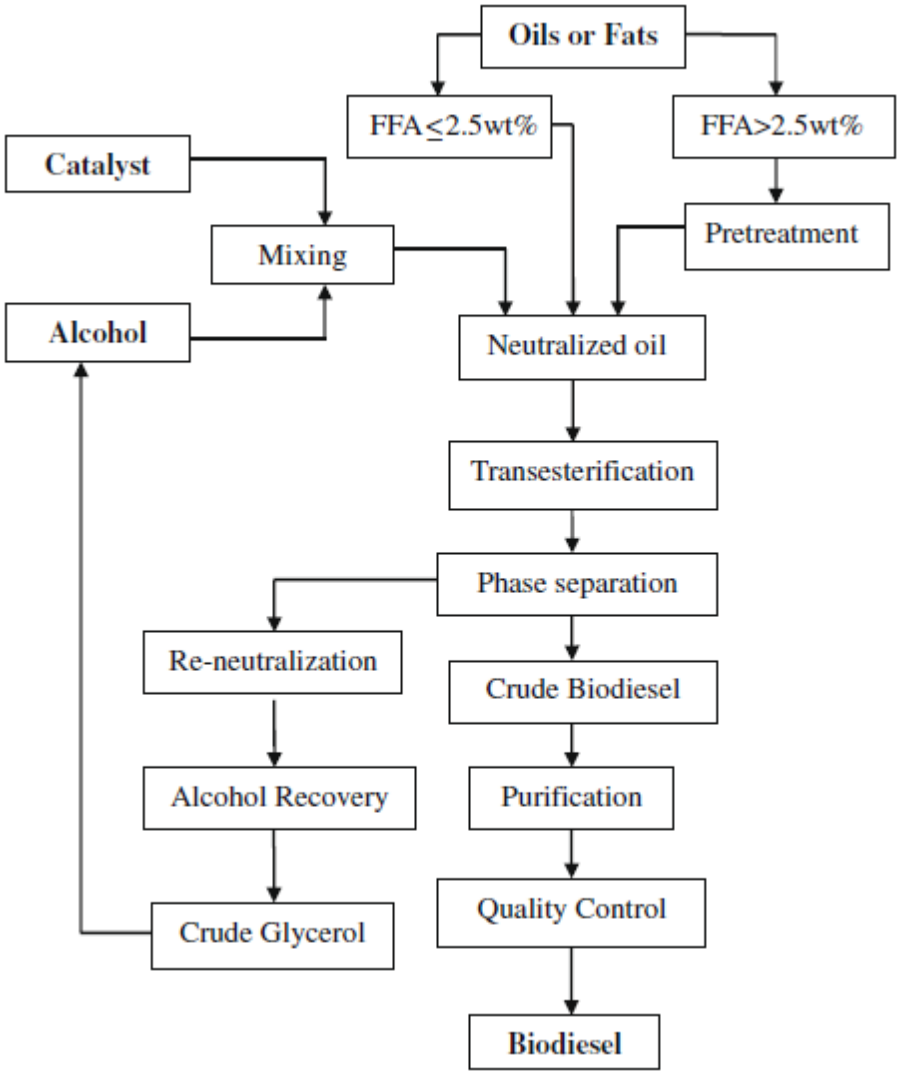

Figure 2.3: Simplified process flow chart of alkali-catalyzed biodiesel production (Leung *et al.*, 2010).

Transesterification is the displacement of alcohol from ester by another alcohol in process similar to hydrolysis except that alcohol is employed instead of water. The transesterification process consists of a sequence of three consecutive reversible reactions which include conversion of triglycerides to monoglycerides (Equation 2.1-2.3). The glycerides are converted to glycerol and yield one ester molecule in each step. Since this reaction is reversible, excess amount of alcohol is often used to help drive the equilibrium towards the

right. In the presence of excess alcohol, the forward reaction is pseudo-first order reaction and the reverse reaction a second order reaction (Nouriddini and Zhu, 1997).

$$\text{Triglyceride (Tg)} + \text{R'OH} \underset{K_2}{\overset{K_1}{\rightleftharpoons}} \text{Diglyceride (Dg)} + \text{R'COOR}_1 \quad (2.1)$$

$$\text{Diglycerides(Dg)} + \text{R'OH} \underset{K_4}{\overset{K_3}{\rightleftharpoons}} \text{Monoglyceride (Mg)} + \text{R''COOR}_2 \quad (2.2)$$

$$\text{Monoglycerides(Mg)} + \text{R'OH} \underset{K_6}{\overset{K_5}{\rightleftharpoons}} \text{Glycerol (Gl)} + \text{R'''COOR}_2 \quad (2.3)$$

$$\underset{\text{triglyceride}}{\begin{matrix}CH_2OCO\,R'\\CHOCO\,R''\\CH_2OCO\,R'''\end{matrix}} + \underset{\text{alcohol}}{3ROH} \leftrightarrow \underset{\text{glycerol}}{\begin{matrix}CH_2OH\\CHOH\\CH_2OH\end{matrix}} + \underset{\text{fatty acid alkyl ester (FAAE)}}{\begin{matrix}R'COOR\\R''COOR\\R'''COOR\end{matrix}} \quad (2.4)$$

The choice of the catalyst and the nature of alcohol determine the type of initial species and the nature of FAAE to be formed.

2.4 Mechanisms of the Transesterification Reaction

A two-step process of methanolysis involving esterification (acid-catalyzed) and subsequent transesterification (alkaline-catalyzed) has been suggested as the best approach in handling biodiesel feedstocks with high free fatty acid to prevent loss of the glycerides to soap formation (Mbaraka and Shanks, 2006). Fatty acids are a component of both oil and biodiesel. In chemical terms, they are carboxylic acids as shown in Figure 2.4a. Fatty acids which are not bound to some other molecules are known as free fatty acids. When free fatty acids react with a base, a fatty acid loses a hydrogen atom to form soap. Chemically, soap is the salt of fatty acid and could be represented in an idealized form as shown in Figure 2.4b. Glycerol is another important component of vegetable oil and by-product of biodiesel production. It can be represented as shown in Figure 2.4c. Also, alcohols such as methanol, ethanol, 1-butanol and1-propanol are used in biodiesel-making. They have the following molecular structures

(Figure 2.4d). Methanol is the most commonly used to make biodiesel and it is produced from natural gas. Ethanol is easily produced from plant sugars and this makes it more sustainable and renewable, but it more difficult to use because it easily forms emulsions which results in end product separation problems (especially while working with waste vegetable oils).

Transesterification is sometimes called alcoholysis, or if a specific alcohol, by corresponding names such as methanolysis or ethanolysis. Chemically biodiesel is a fatty acid alkyl ester shown in Figure 2.4e (methyl ester) and Figure 2.4f (ethyl ester). Its general form is shown in Figure 2.4g. The biodiesel ester contains a fatty acid chain on one side, and a hydrocarbon called an alkane on the other. Thus, biodiesel is a fatty acid alkyl ester. Compared to cetane which is an idealized petroleum molecule, alkyl esters are somewhat longer, and more importantly, contain two oxygen atoms (Figure 2.4h).

Vegetable oil is a mixture of many, compounds, primarily triglycerides and free fatty acids. A triglycride is a tri-ester of glycerol and three fatty acids. The molecular structure of triglyceride is shown in Figure 2.4.

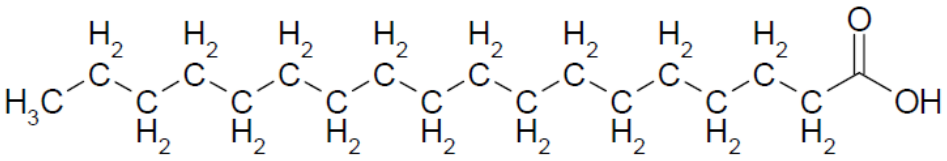

(a): Idealized fatty acid

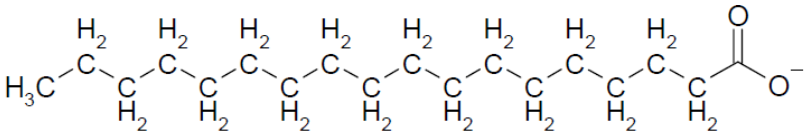

(b.) Idealized soap

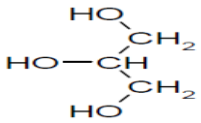

(c) Glycerol

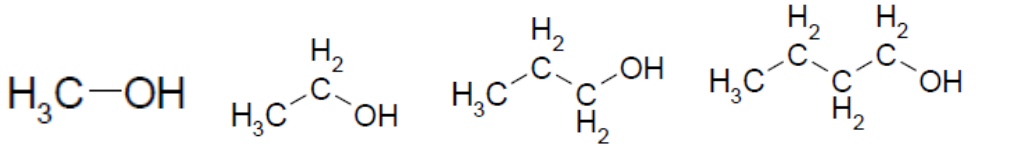

Methanol Ethanol 1-propanol 1-butanol

(d) Alcohols used in biodiesel production.

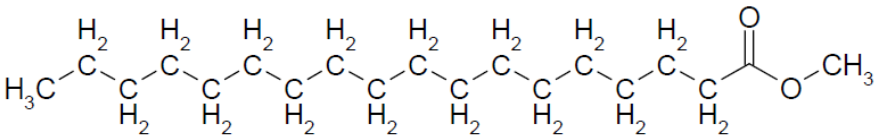

(e) Methyl ester.

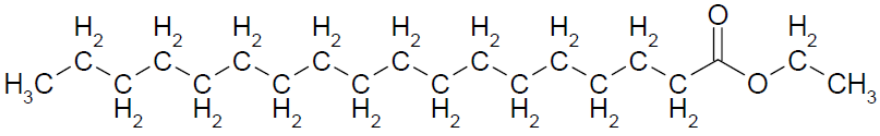

(f) Ethyl ester

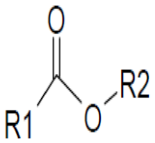

(g) Generalized ester structure

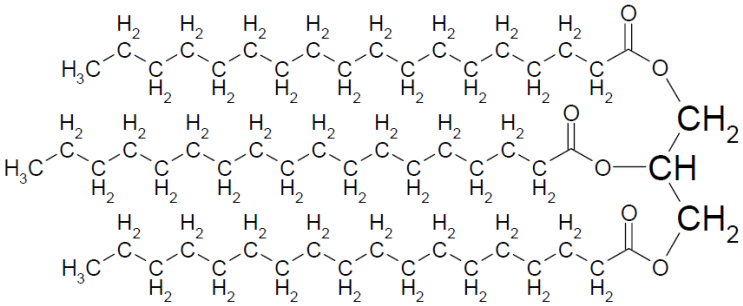

(h) Trigyceride

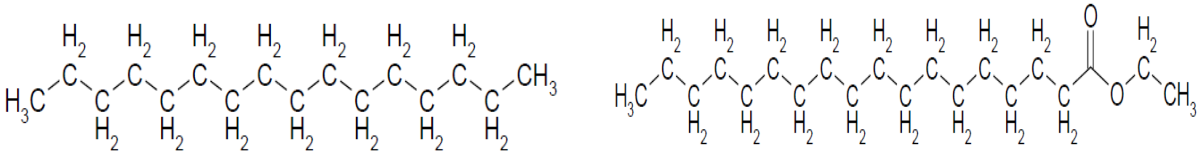

(i) Cetane versus Ethyl ester

Figure 2.4: Structures of chemical building blocks involved in transeterification process.

2.4.1 Mechanism of the transesterification reaction with an alkaline catalyst

The glycerides are converted to glycerol and yield one ester molecule in each step. Since this reaction is reversible, excess amount of alcohol is often used to help drive the equilibrium towards the right. In the presence of excess alcohol, the forward reaction is pseudo-first order reaction and the reverse is a second order reaction. The choice of the catalyst and the nature of alcohol determine the type of initial species and the nature of fatty acid alkyl ester (FAAE) to be formed. The mechanism of the transesterification reaction involving an alkaline homogeneous catalyst has been reported to follow series of sequential steps (Equations. 2.5-2.9) (Ma and Hanna, 1999).

Pre-Step:

$$OH + R'OH \leftrightarrow R'O^- + H_2O \tag{2.5}$$

or

$$NaOR' \quad \leftrightarrow \quad R'O^- \quad + \quad Na^+ \tag{2.6}$$

Step 1.

$$ROOCR_1 + O^-R' \leftrightarrow R_1 - \underset{\displaystyle OR'}{\overset{\displaystyle OR}{\overset{|}{\underset{|}{C}}}} - O^- \tag{2.7}$$

Step 2.

$$R_1 - \underset{\displaystyle OR'}{\overset{\displaystyle OR}{\overset{|}{\underset{|}{C}}}} - O^- + HOR' \quad \leftrightarrow \quad R_1 - \underset{\displaystyle OR'}{\overset{\displaystyle ROH^+}{\overset{|}{\underset{|}{C}}}} - O^- + O \tag{2.8}$$

Step 3.

$$R_1 - \underset{\displaystyle OR'}{\overset{\displaystyle ROH^+}{C}} - O^- \leftrightarrow R_1\,COOR + HOR \qquad (2.9)$$

Where R-OH – diglycerides, R_1 – long alkyl group and R' – short alkyl group.

For the mechanism of the transesterification reaction involving an alkaline homogeneous catalyst, the first step is the attack on the carbonyl carbon atom of the triglycerides molecule by the anion of the alcohol (methoxide ion) to form a tetrahedral intermediate. In the second step, the tetrahedral intermediate reacts with an alcohol (methanol) to generate the anion of the alcohol (methoxide ion). In the last step, rearrangement of the tetrahedral intermediate results in the formation of fatty acid ester and a diglyceride.

2.4.2 Mechanism of transesterification reaction with an acid catalyst

From the previous works reviewed, the kinetics study has concentrated on conventional feedstocks (palm oil, jatropha, soybean and sunflower) and only few attempts considered esterification processes. Water content and non-zero initial concentrations of free fatty acids is necessary to be addressed considering waste cooking oils and high free fatty acid content vegetable oils. The undesired saponification reaction requires more catalyst to achieve the same rate of reaction resulting in more soap and water formation. Scheme 1 presents a schematic reaction mechanism when an acid is used as catalyst, for a mono-, di- and triglycerides. The first stage (I) involves the protonation of the carbonyl group followed by the carbonation (II) which undergoes a nucleophilic attack. Alcohol is attached to the tetrahedral intermediate (III), and a new ester (IV) is obtained by the process glycerol elimination and catalyst regeneration.

The carbonation formed in step II is very reactive by which water must be avoided during reaction because this molecule can act as a nucleophile and generate carboxylic acids, which is a competitive reaction (Trejo-zarraga *et al.,* 2018). The prolongation of the oxygen in the carbonyl carbon of the fatty acid is the first step in the acid catalyzed reaction. The prolongation of the oxygen increases the positive charge of the carbonyl carbon which leads to a carbonation (Mbaraka and Shanks, 2006). A tetrahedral intermediate is produced after the nucleophile attack of the alcohol. The tetrahedral intermediate eliminates glycerol of the backbone forming a new ester and regenerating the catalyst (Meher *et al.,* 1999).

Jansri *et al.,* (2011) investigated the kinetics of methyl ester production from mixed crude palm oil using acid-alkaline catalyst. A two-stage process involving esterification and subsequent base-catalyzed transesterification of the palm oil was adopted. The optimum conditions for reducing high free fatty acid of 8-12 wt% of oil were 10:1 molar ratio of methanol to FFA and 10 wt% of sulphuric acid as catalyst. The transesterification reaction to convert triglyceride in the palm oil to methyl ester was found to be optimal using 6:1 molar ratio of methanol to oil, 0.6 wt% volume of NaOH as catalyst. The reactions were carried out over 20 minutes at 55 °C, 60 °C and 65 °C. The rate constants for the esterification forward and backward reaction were found to be 1.340 and 0.682 L/mol.min respectively. The transesterification stage rate constants for the forward reactions of Tg, Dg and Mg were 2.600, 1.186 and 2.303 L/mol.min respectively and 0.248, 0.227 and 0.022 L/mol.min for the reverse reactions respectively. However, their works considered only the impact of temperature on the rate of transesterification process. Kumar *et al.,* (2011), investigated the kinetics of base catalyzed transesterification reactions of mahua oil and jatropha oil used to prepare biodiesel. The effect of co-solvent and temperature were of main interest. In the presence of co-solvent, tetrahydrofuran (THF) methanolysis of mahua oil resulted in the increase of rate constants from

0.08 to 1.17 L^2 mol^{-2} min^{-1} at 28 °C and from 0.43 to 3.18 L^2mol^{-2} min^{-1} at 45 °C. The results obtained for jatropha oil were 0.50 and 2.76 $L^2mol^{-2}min^{-1}$ at 25 °C and1.26 and 4.56 L^2mol^{-2} min^{-1} at 45°C. Also, Rayero *et al.,* (2015), studied the kinetics of NaOH-catalyzed transesterification of sunflower oil with ethanol to produce biodiesel. They concluded that increase in the reaction temperature favoured the ethanolysis but the effects of catalyst concentration and ethanol-to-oil ratio were more than that of temperature. But the ethanolysis suffered heavily the effect of high soap and intermediate formation which were detrimental to the quality of the produced fatty acid ethyl ester.

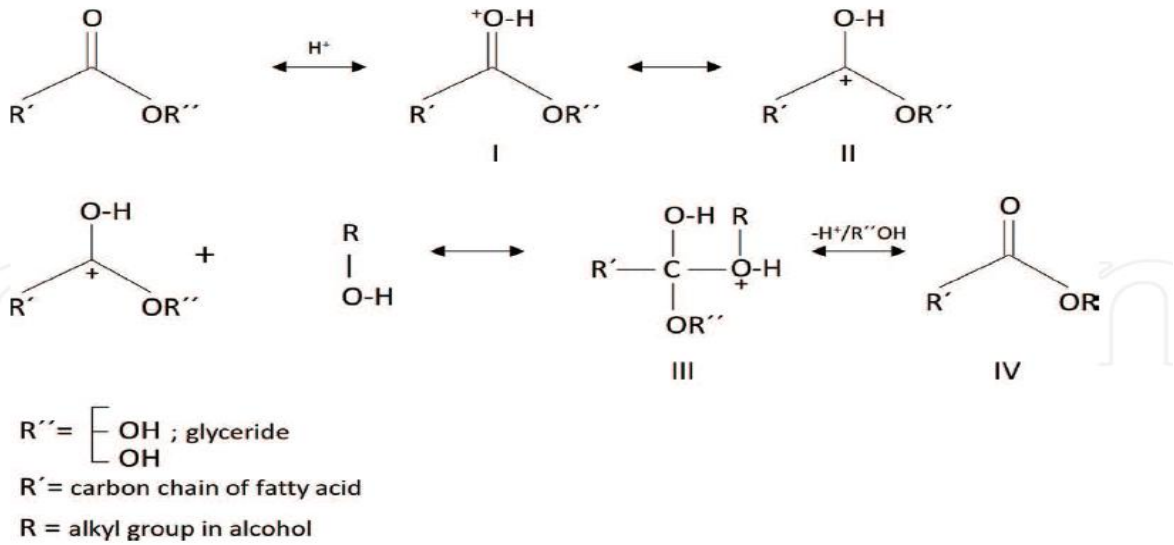

Scheme 1: Acid transesterification pathway (Trejo-zarraga *et al.,* 2018).

2.5 Kinetics of Transesterification Reaction

The earlier work performed by Freedman, *et al.,* (1986), set the step for most of the kinetics works. He studied transesterification of soybean oil using methanol and butanol at temperatures ranging from 20°C to 60°C, with molar ratios of alcohol to oil of 30:1 and 6:1. He

discovered that the forward reactions to be second order at 6:1 and pseudo-first order at 30:1(Turner, 2005). All the reverse reactions were found to be second order, rate constants were found to be function of temperature and Arrhenius equations was applied to derive the activation energies. Also, Noureddini and Zhu, (1997) again studied the kinetics of transesterification of soybean oil using the same reaction model proposed by Freedman *et al*, (1986) but took measurements at different mixing rates based on the stirrer's Reynolds number. They modified the Arrhenius equation and discovered that activation energy varied with Reynolds number. Also, their rate constants for the reverse direction of the first two reactions were larger than the rate constants in the forward direction. Darnoko and Cheryan, (2000) investigated the kinetics of palm oil transesterification. They found out that the best fit to data was a pseudo-second-order model for the initial stages of reaction, followed by first-order or zero-order kinetics. The reverse reactions were neglected for the reason that the equilibrium in the system is strongly shifted to ester formation because of excess methanol used.

Recently, more researches have been conducted and reported in the literature to improve on the earlier works. Jansri *et al.,* (2011) investigated the kinetics of methyl ester production from mixed crude palm oil using acid-alkaline catalyst. A two-stage process involving esterification and subsequent base-catalyzed transesterification of the palm oil was adopted. The optimum conditions for reducing high free fatty acid of 8-12wt% of oil were 10:1 molar ratio of methanol to FFA and 10wt% of sulphuric acid as catalyst. The transesterification reaction to convert triglyceride in the palm oil to methyl ester was found to be optimal using 6:1 molar ratio of methanol to oil, 0.6wt% volume of NaOH as catalyst. The reactions were carried out over 20 minutes at 55°C, 60°C and 65°C. The rate constants for the esterification forward and backward reaction were found to be 1.340 and 0.682 L/mol.min respectively. The transesterification stage rate constants for the forward reactions of Tg, Dg and Mg were 2.600,

1.186 and 2.303L/mol.min respectively and 0.248, 0.227 and 0.022L/mol.min for the reverse reactions respectively. However, their works considered only the impact of temperature on the rate of transesterification process. Kumar *et al*., (2011) investigated the kinetics of base catalyzed transesterification reactions of mahua oil and Jatropha oil used to prepare biodiesel. The effect of co-solvent and temperature were of main interest. In the presence of co-solvent, tetrahydrofuran (THF) methanolysis of mahua oil resulted in the increase of rate constants from 0.08 to 1.17$L^2mol^{-2}min^{-1}$ at 28°C and from 0.43 to 3.18$L^2mol^{-2}min^{-1}$ at 45°C. The results obtained for jatropha oil were 0.50 and 2.76$L^2mol^{-2}min^{-1}$ at 25°C and1.26 and 4.56$L^2mol^{-2}min^{-1}$ at 45°C. Also, Rayero et al., (2015) studied the kinetics of NaOH-catalyzed transesterification of sunflower oil with ethanol to produce biodiesel. They concluded that increase in the reaction temperature favoured the ethanolysis but the effects of catalyst concentration and ethanol-to-oil ratio were more than that of temperature. But the ethanolysis suffered heavily the effect of high soap and intermediate formation which were detrimental to the quality of the produced fatty acid ethyl ester.

2.6 Factors Affecting Transesterification Reaction Process

The process of transesterification brings about drastic change in viscosity of the vegetable oil the high viscosity component glycerol is removed and hence the product has low viscosity like the fossil fuels. The biodiesel production is totally miscible with mineral diesel in any proportion, flash point of the diesel is lowered after transesterification and the cetane number is improved. The yield of biodiesel in the process of transesterifiction is affected by several process parameters which include presence of moisture and free fatty acids (FFA), reaction time, reaction temperature, catalyst concentration and molar ratio of alcohol to oil (Parawira, 2004).

2. 6. 1 Temperature

Reaction temperature is one of the important factors that affect the yield of biodiesel. For example, higher reaction temperature increases the reaction rate and shortens the reaction time due to reduction in viscosity of oils. However, the increase in reaction temperature beyond the optimal level leads to decrease of biodiesel yield, because higher reaction temperature accelerates the saponification of triglycerides (Mathiyazhagan and Ganapathi, 2011) and causes methanol to vaporize resulting in decrease yield (Anitha and Dawn, 2010). Usually the transesterification reaction temperature should be below the boiling point of alcohol in order to prevent the alcohol evaporation. The range of optimal reaction temperature may vary from 50°C to 60°C depending on the oils and fats used (Mathiyazhagan and Ganapathi, 2011). Therefore, the reaction temperature near the boiling point of the alcohol is recommended for faster conversion by various literatures. At room temperature there is up to 78% conversion after 60mins and thus indicates that the methyl esterification of the FFAs could be carried out appreciably at room temperature but might require a longer reaction time. Temperature increases the energy of the reacting molecules and also improves the miscibility of the alcoholic polar media into a non- polar oily phase resulting in much faster reaction.

2. 6. 2 Reaction time

An increase in fatty acid esters conversion is observed when there is an increase in reaction time. The reaction is slow at the beginning due to mixing and depression of alcohol and oil. After that the reaction proceeds very fast. However the maximum ester conversion could be achieved within 90minutes. Further increase in reaction time does not increase the yield product i.e. biodiesel (mono alkyl ester). Besides longer reaction time leads to the reduction of end

product (biodiesel) due to the reversible reaction of transesterification resulting in loss of ester as well as soap formation (Jagadale and Juguikar, 2012).

2. 6. 3 Methanol to oil molar ratio

One of the most important parameters affecting the yield of biodiesel is the molar ratio of alcohol to triglycerides. Stoichiometrically, 3 moles of alcohol and 1 mole of triglycerides are required for transesterification to yield 3 moles of fatty acid methyl/ethyl esters and 1 mole of glycerol. In order to shift the reaction to the right it is necessary to either use excess alcohol or remove one of the products from the reaction mixture, the second option is usually preferred for the reaction to proceed to completion. The reaction rate is found to be highest when 100% excess methanol is used (Anitha and Dawn, 2010). Methanol, ethanol, propanol, butanol and amyl alcohol can be used in the transesterification reaction. Amongst these alcohols methanol is applied more frequently as its costs is low and it is physically and chemically advantageous (polar and shortest chain alcohol) over the other alcohols. In contrast, ethanol is also preferred compared to methanol since it is derived from agricultural products and is renewable and biologically less offensive in the environment. The effect of volumetric ratio of methanol and ethanol to oil was studied, results exhibited that highest biodiesel yield is nearly 99.5% at 1:6 oil/methanol. In comparison, biodiesel yield using methanol continuously increases with the raise of methanol molar ratio (Hossan and Boyle, 2009). The stoichiometric ratio for transesterification requires three mole of alcohol and one mole of triglycerides to yield three moles of fatty acid alkyl esters and one mole of glycerol. However more alcohol is preferred to shift the equilibrium for esters. Zhou *et al.,* (2003) studied the effect of alcohol / oil molar ratio on the single – phase base- catalyzed ethanolysis of sunflower oil. In that study, four molar ratio of ethanol to sunflower oil (6:1, 20:1, 25:1 and 30:1) were examined and found out that at ethanol / oil molar ratios of 20, 25 and 30:1, equilibrium was reached in 6 to 10 minutes at 23˚C

when 1.4wt% of potassium hydroxide was used while at the molar ratio of 6:1, equilibrium could not be reached even after 30 minutes. Increasing the molar ratio did favour the formation of esters, but the difference for the range of molar ratios from 25:1 to 20:1 was small. Meher *et al* (2006) concluded that the reaction was faster with higher molar ratio of methanol to oil while longer time was required for lower molar ratio (6:1) to get the same conversion. Canakii and Gerpen, (1999) investigated the effect of different alcohol types on transesterification. Methanol, ethanol 2-propanol and 1-butanol were tested for a 48h test period using sulphuric acid as catalyst at 3% concentration and molar ratio of alcohol to oil at 6:1. The conversion was 87.8%, 95.8%, 92.9% and 92.1% for methyl esters, ethyl ester, 2-propyl ester and 1-butyl ester respectively. Higher conversion was observed for the longer chain alcohols compared with methanol. The authors attributed this to the fact that higher reaction temperatures were chosen due to the higher boiling point of the long chain alcohols. Also the long chain alcohols can increase the solubility between the oil and alcohol since they are more non-polar than shorter chain alcohols.

2. 6. 4. Type and amount of catalyst

Biodiesel formation is also affected by the concentration of catalyst. Most commonly used catalyst for biodiesel production is sodium hydroxide (NaOH) or potassium hydroxide (KOH) (Mathiyazhagan and Ganapathi, 2011). The type and amount of catalyst required in the transesterification process usually depend on the quality of the feedstock and method applied for the transesterification process. For a purified feedstock, any type of catalyst could be used for the transesterification process. However, for feedstock with high moisture and free fatty acids contents, hetrogeneuous transesterification process is suitable due to high possibility of saponification process. The yield of fatty acid alkyl esters generally increase with increase in amount of catalyst. This is due to availability of more active sites by additions of larger amount

of catalyst in the transesterification process. However on economic perspective, larger amount of catalyst may not be profitable due to cost of the catalyst itself. Therefore, similar to the ratio of oil to alcohol, optimization process is necessary to determine the optimum amount of catalyst required in the transesterifiction process (Jagadale and Jugulkar, 2012; Kansedo, 2009). Triglycerides in vegetable oils and animal fats are immiscible with methanol. Consequently, catalyst is added to enhance the transesterification process and both homogeneous and heterogeneous catalysts can be used in this process (Fan, 2000).

Biodiesel production using homogenous alkaline catalyst has been comprehensively studied since it has several advantages over acid catalyst such as:

1. The transesterification reaction is faster and the reaction conditions are mild.

2. The consumption of methanol is significantly less.

3. The catalyst is less corrosive.

4. The acid catalyzed process requires a high methanol to oil molar and high acid catalyst concentration.

Commonly used alkaline catalysts include sodium hydroxide (NaOH), potassium hydroxide (KOH), sodium methoxide ($NaOCH_3$) and potassium methoxide ($KOCH_3$). Acid numbers for ultimate product using $NaOCH_3$ were significantly lower than those using NaOH. Sodium hydroxide is widely used in industrial biodiesel due to its cheapness and effectiveness. Meka *et al*., (2007) studied the effect of catalyst (sodium hydroxide) concentration on reaction time at two temperatures 50 and 60°C for safflower oil when the methanol / oil molar ratio was kept at 6:1. The authors found that in both cases, reaction time decreased proportional with increase in catalyst concentration from 1% to 2 % but soap was formed when catalyst

concentration was above 2%. Ataya *et al.,* (2006) performed canola oil transesterification experiment and found triglyceride conversion increased when the catalyst (NaOH) concentration increased from 1% to 3%. Rashid *et al.,* (2011) evaluated the effect of catalyst type and concentration on the rapeseed oil ester yields and observed that the hydroxide gave rise to higher yield than the counterpart methoxides.The results showed that 1% KOH was the optimal value when the concentration varied between 0.25% and 1.5%. This was in accordance with the result obtained by Meher *et al.,* (2006). The same trends were observed for varying the concentration of NaOH from 0% to 1.5%, which was also recommended by Freedman *et al.,* (1994). In contrast, Vicente *et al.,* (2004) drew a conclusion that biodiesel yields after separation and purification steps were higher for methoxide catalysts than for hydroxide catalysts when methanolysis of sunflower was conducted. The phenomenon of yield loss was ascribed to the fact that hydroxide catalysts could cause more triglyceride saponification and methyl ester dissolution in glycerol. Moreover, the reactions using NaOH catalyst were fastest of all. Though alkaline catalysts have many advantages as mentioned earlier, they are more sensitive to free fatty acid and water. Their application in vegetable oil transesterification can cause soap formation by neutralizing the free fatty acid in the oils which can partially consume the catalyst, thus reducing the biodiesel yield. Usually in basic conditions, the acceptable total FFA and water content are 0.5% and 0.1-0.3%, respectively (Williams *et al.,* 2007). Acid catalysts were preferred for biodiesel production when the FFA is high. The acids could be H_2SO_4, phosphoric acid, hydrochloric acid, organic sulphonic acid. Sulphuric acid and hydrochloric acid are commonly preferred (Goff *et al.,* 2004)

2. 6. 5. Mixing intensity

Oils and alcohols are not totally mixable, thus reaction can only occur in the interfacial region between the liquids and transesterification reaction is moderately slow process. So,

mixing between these two types of feedstock is necessary to promote contact between them, thereby, enhancing the transesterification reaction to occur (Kansedo, 2009; Jagadale and Jugulkar, 2012). Most literature indicate that during the transesterification reaction the reaction initially form a two phase liquid system. In general, the mixing intensity must be increased to ensure good and uniform mixing of the feedstock. When vegetable oils with high kinematic viscosity are used as the feedstock, intensive mechanical mixing is required to overcome the negative effect of viscosity to the mass transfer between oil, alcohol and catalyst (Kansedo, 2009; Jagadale and Jugulkar, 2012).

2. 6. 6 Free fatty acid and water content.

The FFA and moisture contents have significant effects on the transesterification of glycerides with alcohol using catalyst. The high FFA content (>1%w/w) will encourage soap formation and the separation of products will be exceedingly difficult and as a result it would have low yield of biodiesel product. In addition, formation of gels and foams hinders the separation of glycerol from biodiesel (Mathiyazlagan and Ganapathy, 2011). For instance, water content of waste cooking oil will accelerate the hydrolysis reaction and simultaneously reduce the amount of ester formation. To overcome this problem, supercritical methanol method was proposed. It may be noted that water has less influence in supercritical methanol method (Mathiyazhgan and Ganapathi, 2011). Therefore water content should not always exceed 0.5% to obtain 90% yield of biodiesel and it is more critical for an acid – catalyzed reaction than base catalyzed reaction. Jagadale and Jugulkar, (2012) stated the moisture levels of collected waste chicken fats being as high as 18%. Therefore, it is not possible to convert these oils to biodiesel by using a single process. One drawbacks of biodiesel is that there is an inverse relationship between biodiesel oxidative stability and its cold flow properties. Saturated compounds are less prone to oxidation than unsaturated compounds but they raise the cloud points of the fuel. The

reaction of FFA with alcohol produces ester, but also water that inhibits the transesterification of the triglycerides. This is due to the effect of the water produced when the FFAs react with the alcohol to form esters. This indicates that water formation is the primary mechanism limiting the completion of the acid catalyzed esterification reaction with FFA's. Igbum *et al.,* (2012) investigated the effects of transesterification variables above on *Telfari occidentals Hook f, Hura crepiltians L, Cucumerospsis manii and Canarium scheweinfunthi eng. I* and they discovered that alcohol (methanol to oil ratio of 6:1, generally showed a better property while the NaOH catalyst also showed better result than KOH. Temperature of 55˚C gave better yield than 38^{o}C while 30 minutes contact time gave better results than 5 minutes. Also Bello *et al.,* (2011) applied 6:1 methanol molar ratio with 4g/L sodium hydroxide catalyst concentration at 40°C to obtain 59% biodiesel yield.

2. 7 Properties and Characteristics of Biodiesel

Since biodiesel is produced from quite different scaled plants of varying origins and qualities, it is necessary to install a standardization of fuel quality to guarantee an engine performance without any difficulty (Balat and Balat, 2010). Austria was the first country in the world to define and approve the standards for rapeseed oil methyl esters as diesel fuel (Atabani *et al.,* 2012). Subsequently, other countries like Germany, Italy, France, the Czech Republic and United States followed (Meher *et al.,* 2006). Currently, the properties and qualities of biodiesel must adhere with the following international biodiesel standards specifications. The American Standard for Testing Materials (ASTM 6751-3), The European Union(EN14214) standards, Germany (DIN51606), Austria(ON) and Czech Republic(CSN) (Lin *et al.,* 2011). The physico-chemical fuel properties of biodiesel basically depend on the type of feedstock and their fatty acids composition.(Atadash *et al.,* 2010; Lin *et al.,* 2011). Additionally, the cetane number is

determined using ISO 5165 established by International Organization for Standardization (ISO) (Igbum *et al*., 2012)

2. 7. 1 Kinematic viscosity

This is the most important property of any fuel as it indicates the ability of a material to flow and therefore affects the fuel injection equipment and spray atomization particularly at low temperatures. The viscosity of biodiesel is 10-15 times greater than that of petro-diesel because of its large molecular mass and large chemical structure. In some cases at low temperature, it can become higher and solidifies, hence some literature has thought that higher viscosity of biodiesel can affect the volume flow and injection spray characteristics of the engine since at low temperature it may even compromise the mechanical integrity of the injection pump drive system (Rabe, 2010).

2. 7.2 Density and relative density

Density is the weight per unit volume and the denser an oil is the more energy it contains. According to ENISO3675/12185 and ASTMD1298, density should be tested at the temperature reference of 15 or 20°C (Torres- Jimenez *et al*., 2011). The relative density is needed to make mass to volume conversion, calculate flow and viscosity properties and equally use to judge the homogeneity of the biodiesel tanks (Sanford *et al.,* 2009).

2.7.3. Flash point (FP)

This is the temperature at which it will ignite when exposed to a flame or spark. The flash point varies inversely with the fuel volatility and it is higher than the prescribed limit of diesel fossil fuel, which is safe for transport handling and storage purpose (Atadash *et al.,*

2010). Usually biodiesel has a flash point of 150°C compared to 55-66°C for conventional diesel fuel (Sanford *et al*, 2009).

2.7.4. Cloud point (CP), pour point and cold filter plugging point (CFPP)

The partial or full solidification of the fuel may cause blockage of the fuel lines and filters, leading to fuel starvation, problems of starting, driving and engine damage due to inadequate lubrication. The cloud point is the temperature at which wax crystals first become visible when the fuel is cooled. Pour point is the temperature at which the amount of wax out of solution is sufficient to gel the fuel (the lowest temperature at which the fuel can flow). Generally, biodiesel has higher CP and PP compared to conventional diesel (Friday and Okano, 2011; Fernando *et al.,* 2007). Cold filter plugging point (CFPP) refers to the temperature at which the test filter starts to plugg due to fuel components that have started to gel or crystallize. It is an indicator of low temperature operability of fuels and reflects their cold weather performance as well as fuels limit of filterability (Masjuki, 2010).

2. 7. 5. Titre

This is the temperature at which oil changes from solid to liquid. Titre is very important because the transesterification process is fundamentally a liquid process and oils with the energy requirements and production cost are used for the biodiesel plant (Karmakar *et al*., 2010).

2.7.6. Cetane number (CN)

The cetane number (CN) is the indication of ignition characteristics or ability of fuel to auto-ignite quickly after being injected. Better ignition quality of the fuel is always associated with higher CN value. It is highly considered during the selection procedure of methyl esters for

use as biodiesel (Balat and Balat, 2010). Cetane number increases with increase in chain length of fatty acids and increase in saturation. A higher CN indicates shorter time between the ignition and the initiation of fuel injection into the combustion chamber (Karmakar *et al.*, 2010).

2.7.7. Oxidation stability

Oxidation stability is an indication of the degree of oxidation, potential reactivity with air and can determine the need for antioxidants. Oxidation occurs due to the presence of unsaturated fatty acid chains and the double bond in the parent molecule, which immediately react with the oxygen as soon as it is being exposed to air (Demirbas, 2009). The chemical composition of biodiesel fuel makes it more susceptible to oxidative degradation than fossil diesel fuel (Atadashi *et al*., 2010; Sanford *et al.,* 2009). A minimum of IP(110°C) of 3h is required for ASTM D 6751 where as a more stringent limit of 6h or greater is specified in EN14214 (Masjuki, 2010).

2. 7. 8 Lubrication properties

The lubrication properties of the biodiesel are better than diesel and this can help to increase the engine life (Atadashi *et al*., 2010). Also, the fatty acid alkyl esters (biodiesel) have improved lubrication characteristics (Lupuerta *et al.,* 2008), but they can contribute to the formation of deposits, plugging of filters, depending mainly on degradability, glycerol (and other impurities) content and cold flow properties etc. Also, Demirbas, (2008) stated that biodiesel provides significant lubricity improvement over diesel fuel. Xue *et al*., (2011) showed that higher lubricity of biodiesel might result in the reduced friction loss and thus improve the brakes effective power.

2. 7. 9 Acid value

Acid number or neutralization number is a measure of free fatty acids contained in fresh samples. Free fatty acids (FFAs) are the saturated or unsaturated monocarboxylic acid that occurs naturally in fats, oils and greases but are not attached to glycerol backbones. Higher amount of free fatty acids leads to higher acid value. Acid value is expressed as mgKOH required for neutralizing 1g of FAME. Higher acid content can cause severe corrosion in fuel supply system of an engine (Sharma and Singh, 2009).

2. 7. 10 Heating value / Heat of combustion

Heating value or heat of combustion is the amount of heating energy released by combustion of a unit value of fuels. One of the most important determinants of heating value is the moisture content of feedstock. It is not specified in the biodiesel standard ASTM D 6751 and EN 14214 but is prescribed in EN 14213 with a minimum of 35MJ/Kg (Rashid *et al.*, 2009).

2. 7.11 Free glycerine

Free glycerol refers to the amount of glycerol that is left in the finished biodiesel and its content depends on the production process. The higher yield of glycerol in biodiesel may be resulted from insufficient separation during washing of the ester product. It is insoluble in biodiesel so almost all glycerol are easily removed by settling or centrifugation. Free glycerol may remain either as suspended droplets or as the very small amount that is dissolved in the biodiesel. Higher glycerol can cause injector coking and damage to the fuel injection (Li *et al.*, 2010).

2.7.12 Total glycerol.

This is a measurement of how much triglyceride remains unconverted into methyl esters. It is calculated from the amount of free glycerin, monoglycerides, diglycerides and triglycerides. Each reaction step produces a molecule of methyl aster of a fatty acid. If the reaction is incomplete, then there will be triglyceride, diglycerides and monoglycerides left in the reaction mixture. Each of these compounds still contains a glycerol molecule that has not been released. The glycerol portion of these compoundsis referred to as bound glycerol, the sum is known as the total glycerol. Fuels that do not meet the specifications are prone to coking, thus may cause the formation of deposits on the injector nozzles, pistons and valves (Masjuki 2010).

2. 7.13 Water content and sediment.

These are housekeeping issues for biodiesel. Water can be present either as dissolved water or as suspended water droplets. Biodiesel can contain as much as 1500ppm of dissolved water while diesel fuel usually takes up about 50ppm. Sediment may consist of suspended rust and drit particles or it may originate from fuel as insoluble compounds formed during fuel oxidation (Masjuki, 2010). Water in the fuel generally cause two problems,; it can cause corrosion of engine fuel system components (rust) and with time result in acidic corrosion and attack fuel storage tanks. Water contamination can result to microbial growth. The species of yeast, fungi and bacterial can grow at the interface between the fuel and water at the bottom of a storage tank. The organism produces sludges and slimes that can cause filter plugging. Some of the organisms can convert the sulphur in the fuel to sulphuric acid which can corrode metal fuel tanks. Moreover, higher water contents can contribute to hydrolysis reaction that is responsible for converting biodiesel to free fatty acid which is also linked to fuel filter blockage (Fernando *et al.,* 2007).

2. 7.14. Sulfated ash

The ash content describes the amount of inorganic contaminants such as abrasive solid, catalyst residues and the concentration of soluble metal soaps contained in a fuel sample. The biodiesel is ignited and burned and then treated with sulphuric acid to determine the percentage of sulfated ash present in the biodiesel (Sanford *et al.,* 2009; Fernando *et al*, 2007).

2. 7.15. Carbon residue;

Carbon residue of the fuel is an indication of carbon depositing tendencies of the fuel after combustion. Carbon residue for biodiesel is more important than that in diesel fuel because it shows a high correlation with presence of free fatty acids, glycerides, soaps, polymers, higher unsaturated fatty acids and inorganic impurities. Although this residue is not solely composed of carbon, the term carbon residue is found in all standards because it has long been commonly used. (Meher *et al*., 2006).

2. 7. 16. Copper strip corrosion

The copper corrosion test measures the corrosion tendency of fuel when used with copper, brass or bronze parts. Corrosion resulting from biodiesel might be induced by some sulphur compounds by acids; hence the parameter is correlated with acid number (Atabani et al., 2012; Masjuki, 2010).

2. 7. 17. Cold soak filtration

This is the newest biodiesel requirement set in ASTMD6751. The cold soak filtration test is done to determine if catalyst form at low temperatures and do not redissolved when the biodiesel returns to a higher temperature.(Sanford *et al.*, 2009).

2. 7. 18. Visual inspection

The visual inspection test is used to determine the presence of water and particulates in biodiesel. It is measured as a haze value (Sanford *et al.,* 2009).

2. 7. 19. Phosphorus, calcium and magnesium

The specification from ASTMD 6751 state that phosphorus content in biodiesel must be less than 10ppm, calcium and magnesium combined must be less than 5ppm. Phosphorus is determined using ASTMD 6751 while calcium and magnesium are determined using EN14538 (Sanford *et al*., 2009).

2. 7. 20 Moisture contents

Moisture is the amount of water which cannot be converted to biodiesel. Moisture can react with the catalyst during transesterification which can lead to soap formation and emulsion. It is measured with ASTME203 standard test method for water (up to 1500ppm). In European standard, EN14214 has a Karl Fischer moisture specification of 0.050 wt % maximum (Karmakar *et al.,* 2010).

Table 2.2 contains the general parameters for the quality of biodiesel in accordance with ASTM 6751-3 and EN14214 specification as well as their test methods. The properties and characteristics of biodiesel after transesterification are important consideration as far as using vegetable oils as feedstocks for biodiesel production is concern (Igbum *et al.,* 2012). The ASTM system is the basis for defining product specification and measurement methods for most segments of fuels and industrial products in the US.

Table 2.2: Properties and qualities of biodiesel in comparison with petro-diesel (Atabani *et al.*, 2012).

Fuel properties	**Diesel**	**Biodiesel**		**Test methods**	
	ASTM D 9751	ASTM D 6751	EN 14214	ASTM	EN
Density (kg/m^3)	850	880	860-900	1298	3675
Viscosity @ 40˚C (cSt)	2.6	1.9-6.0	3.5-5.0	445	3104
Cetane number	40-55	47min.	51min.	613	5165ENISO
Iodine number	38.30	-	120max.	-	14111
Calorific value(MJ/kg)	42-46	-	35	-	14214
Acid value (mgKOH/g)	0.062	0.50max.	0.5max.	664	14104
Pour point	-35	-15 to10	-	97	-
Flash point (°C)	60-80	100-170	>120	93	3679ISODIS
Cloud point (°C)	-20	-3 to -12	-	2500	-
Cold filter plugging point (˚C)	-25	19	+5max.	6371	14214EN
Copper strip corrosion (3h @ 50˚C)	1	3max	1min.	130	2160
Carbon (wt%)	84-87	77	-	-	-
Hydrogen (wt%)	12-16	12	-	-	-
Oxygen (wt%)	0-0.31	11	-	-	-
Methanol content (%w/w)	-	-	0.20max.	-	14110EN
Water and sediment content	0.05	0.05max.	500[b]max.	2709	12937ENISO
Ash content(%w/w)	0.01	0.02	0.02	-	14214EN
Sulphur (%w/w)	0.05	0.05max.	10[b]	5453	20846ENISO
Sulphated ash (%w/w)	-	0.02	0.02	874	3987ENISO
Phosphorus content	-	0.001	10[b]	4951	14107EN
Free glycerine (%w/w)	-	0.02	0.02	6584	1410506EN
Monoglycerine (%w/w)	-	0.24	0.25	-	14105EN
Diglycerine (%w/w)	-	0.52	0.8	-	14105EN
Triglyceride(%w/w)	-	-	0.2	-	14105EN
Distillation temperature (˚C)	-	-	0.2	1160	-
Oxidation stability (h, 110˚C)	-	3min.	6min.	675	14112EN
Lubricity (HFRR:µm)	685	314	-	-	-
CCR 100% (mass %)	0.170(0.1)[d]	0.05max.	0.03max.	4530	10370ENISO

a – ppm, b- mg/kg, c- Determined at 25˚C, d- wt%, e- KJ /kg, f- Determined at 20 ˚C

2.8 Analytical Characterization of Biodiesel

2.8.1 Fourier transforms infrared spectrophotometeric analysis:

The FTIR spectroscopy has an excellent potential in providing qualitative and quantitative data for fuels including biodiesel without much vigor in sample preparation. It is used extensively as a quantitative analytical procedure for assessing edible oil quality parameter (Ma *et al.,* 1997). Similarly, it was developed for determining the acidity and moisture content in lubricants (Van de Voort *et al.,* 2006), as well as providing information about the functional groups in molecules and the structure of molecular vibration(Ndana *et al.,* 2013). There are two types of vibration: Stretching vibration and bending vibration. Stretching vibration motion is the type in which inter-nuclear distance between bonded atom increase and decrease along the bond axis while in bending vibration, the position of the bonded molecule change with respect to the bonded atom (the inter-atomic distance remain unchanged (Younis *et al.,* 2009).The intensity of an adsorption bands depends on the change in the dipole moment of the bond and the number of specific bonds present. The bond dipole results from the bond length and the charge difference between the two atoms. When the molecule absorbs a photon, it stretches and the bond length changes and leaves the charge difference which can be derived from the electronegativity values of the atom involved. FT-IR spectroscopy has seen extensive development and application in relation to qualitative and quantitative analysis and monitoring conditions of fatty acid methyl esters synthesis according to ASTM standards as reported in the literature (Knothe *et al*., 2005). Several researchers have worked in various capacities on FTIR spectroscopy analysis of different vegetable oils. Alexasandr, (2014) applied FTIR spectroscopy analysis to verify the FAME contents of biodiesel blends from commercially available biodiesel. Ndana *et al.,* 2013, used FTIR spectroscopy to evaluate the possible functional groups in each biodiesel produced from oils from the seeds of *Ricinus communis, Heavea brasilensis and Jatropha*

curcas. Mushtaq *et al.,* (2014) applied FTIR to analyze the functional groups in FAME produced from distaff thistle oil to confirm its production and characterization. Nwadike *et al.,* (2014) applied FTIR to determine the quality of biodiesel produced from groundnut seed oil, cow tallow oil and castor seed oil and their blends. The use of FTIR can overcome the challenges of longer time of sample preparation, costly technologies, advanced high technologies requiring experts' further interpretation, limitation of few amount of functional groups detection. Additionally, each type of vibration occurs at unique frequency called wave number making infrared spectroscopy a type of vibrational spectroscopy which collect more information about sample analyses when compared to other spectroscopy methods (Oyerinde and Bello, 2016)

There is always the need for measuring all infrared frequency simultaneously rather than individual as in dispersive method for sample analysis. The use of FTIR can overcome this limitation through the use of optical device called inter-ferometer that provides a unique type of signal which have an incorporated computer system and which can be used for analyzing the biodiesel and biodiesel blends. The infrared spectrum produced represents the finger prints of the sample with absorption peaks which corresponds to the frequency of vibration between the bonds of the atoms making up the biodiesel. Since each different material is a unique combination of atoms, no two compounds produce the exact same infrared spectrum. The size of the peaks in the spectrum is a direct indication of material present leading to qualitative analysis (Silverster *et al.,* 2013). FTIR spectroscopy analyses require the plot of intensities at each individual frequency in order to obtain quick sample identification. The measured signal is further processed by decoding the individual frequency which is accomplished through a mathematical technique called Fourier transformation. This is performed by the incorporated computer system of the FTIR spectrometer unit and presents the user the spectral result.

2.8.2. Gas chromatography-mass spectroscopy

Gas chromatography-mass spectroscopy (GC-MS) analysis mainly identifies the quality and quantity of the methyl esters present in the product sample (Elkady *et al.,* 2015). It is applied to ascertain specific methyl esters predominant in the produced FAME. The use of ordinary gas chromatography (GC) takes more time in sample preparation which involves derivatization of samples before the GC scan (Oyerinde and Bello, 2016) Hence the fitting of GC with MS gives better result and saves time as an advanced technique. This analytical technique also gives the distribution area for each component in the produced sample (Elkady *et al.,* 2015). Litty and Nithy (2012) analyzed the fatty acid composition of *Datura stramoinium* biodiesel using GC assisted with mass spectrometry while studying the influence of fatty acids on the fuel related characteristics. GC-MS is a hyphenated analytical technique that combines the separation properties of gas –liquid chromatography with the detection feature of mass spectroscopy to identify different substances within a test sample (Chuahan *et al.,* 2014). GC is used to separate the volatile and thermally stable constituents in a sample where as GC-MS fragments the analyte to be identified on the basis of its mass. Also the addition of mass spectrometer in it leads to GC-MS/MS. Superior performance is achieved by single and triple quadrupole moles (Sahih *et al.,* 2011; Rowley, 2001). Gas chromatography (GC) analysis is used to determine the distribution of methyl ester. For each sample standards, derivatizations are required to resolve the various saturated and unsaturated methyl esters in a biodiesel mixture. But MS provides detailed molecular weight information and requires only a very small amount of sample. GC-MS uses electron impact (EI) and chemical ionization (CI) techniques to achieve enhanced molecular ion, improved confidence in sample identification, significantly increased range of thermally labile and low volatility samples amenable for analysis, much faster analysis, improved sensitivity particularly for compounds that are hard to analyzed and

the many other features and options provide compelling reasons to use the GC-MS in broad range of areas (ISO 2002, ISO/IEC, 2005). GC-MS has been applied in varies areas of study such as environmental monitoring (Amirav *et al*., 2008), food, beverage, flavour and fragrance analysis (Robert and Adams, 2007), forensic and criminal cases (Hanidley and Adlard, 2001), biological and pesticides detection (Thermo fisher, 2011), security and chemical warfare agent detection (Eiceman, 2000; Kitson *et al.*, 1996), astro chemistry and geochemical research (Niessen, 2001), medicine and pharmaceutical applications (CDER 2000), petrochemical and hydrocarbon analysis (Grob and Barry, 2004), clinical toxicology (Gianneli and Imwinketried, 1999), industial applications (Cole, 2013) and academic research (Kalachova, 2012), as well as energy and fuel applications (Choi and Chung, 2015).

2.8.3 Thermo-gravimetric analysis (TGA)

Thermo-gravimetric analysis is one useful way for quantitative analysis of the produced biodiesel due to the large temperature difference due to the weight loss of oil and biodiesel. This allows one to determine the conversion (Elkady *et al.*, 2015). It is well known that biodiesel starts to thermally decompose at about 150°C and continues its thermal decomposition until complete vaporization. But parent vegetable oil begins its thermal degradation at a temperature approximately twice that of the biodiesel. Accordingly, the percentage of biodiesel conversion may be calculated using TGA (Chand *et al*., 2009). TGA is a method of thermal analysis in which changes in physical and chemical properties of materials are measured as a function of increasing temperature (with constant heating rate) or as a function of time with constant temperature and or constant mass loss. Changes in the mass of a sample are studied while the sample is subjected to a program. Hence, it is used to analyze the decomposition; thermal stability and kinetics of materials under a variety of conditions taking place in the sample.

There are three types of TG:

1. Dynamic TGA: In this type of analysis - the sample is subjected to conditions of continuous increase in temperature usually linear with time
2. Isothermal or static TGA: Here, sample is maintained at constant temperature for a period of time during which change in weight is measured.
3. Quasitatic TGA: In this technique, sample is heated to a constant weight at each of series of increasing temperature.

Siddharth and Sharma (2012) investigated the application of thermo gravimetric analysis for thermal degradation of *Jatropha curcas* and showed that the thermal degradation of all *Jatropha curcas* biodiesel (JCB) samples can be treated as a first order reaction.

2.8.4 Nuclear magnetic resonance (NMR)

Nuclear magnetic resonance is considered to be one of the reliable and rapid analysis used in quality control for biodiesel synthesis and can provide total methyl esters distributions (Oyerinde and Bello 2016; Mushtaq 2014). Proton NMR provides a good probe for biodiesel since ^{1}H is the most naturally abundant and most sensitive NMR active isotope. It is used to quantify the conversion of triglycerides into methyl esters because in proton NMR, distinct peaks are observed for the confirmation of methyl esters present in biodiesel (Mello et al, 2008). Also the ^{13}C NMR spectra of produced biodiesel are equally observed to support the confirmation from ^{1}HNMR. Mushtaq *et al.,* 2014 applied ^{1}HNMR and ^{13}C NMR on analysis of FAME produced from distaff thistle oil (DTO) and observed unsaturation in methyl esters as indicated by peaks σ130.16 and 127.88 ppm. Nuclear magnetic resonance (NMR) is an adaptable tool that is used as one of the best powerful methods for the interpretation of the structure of any compound (Sher, 2015). Knothe (2001), applied nuclear magnetic resonance

(NMR) spectroscope to determine the blend level of biodiesel and conventional diesel fuel and proved the method to be rapid and easy to use without requiring any hardware changes. Also, Morgenstan *et al.,* (2006), studied the kinetics of biodiesel production using proton nuclear magnetic resonance spectroscopy (^{1}HNMR) and was able to calculate their average degree of fatty acid unsaturation (Du = 1.32) in oil and methyl ester. Nuclear magnetic response (NMR) is a phenomenon in which particular atomic nuclei respond to the application of certain magnetic fields by absorbing or emitting electromagnetic radiation (Moudgil *et al.,* 1985). NMR has long been used by organic chemists, biochemists and physists as an analytical tool for the study of structures, confirmations, interactions and dynamics of molecules of homogeneous liquids or solids (Moudgil *et al.,* 1985). Quantifying biodiesel with alternative analytical tools such as proton nuclear magnetic resonance (^{1}HNMR) can provide total methyl distribution without significant sample pretreatment (Horst *et al.,* 2009). Biodiesel is composed of a mixture of monoalkyl esters of long- chain fatty acids of either vegetable oils or animal fats. Additional techniques such as mass spectrometry (MS) and proton nuclear magnetic resonance (^{1}HNMR) provide complementary information with different demands on sample preparation and allowance for sample variability. NMR data is sensitive to unique molecular environments which yield unique spectra for different molecules. Although MS is a more sensitive technique, NMR can provide detailed molecular information once a spectrum is acquired with sufficient high signal to noise ratio. For most samples generated in the biodiesel industry sample quantity is not an issue and NMR can be applied to biodiesel and biodiesel mixtures. NMR has been applied to monitor the transesterification reaction used in the production of biodiesel (Morgenstern *et al.,* 2016) and to monitor the oxidation of methyl esters in biodiesel (Knothe 2006). Previous work by Diehl and Randel has shown the ability of NMR to quantify blends of biodiesel and petroleum diesel (Diehl and Randel, 2007). Careful analysis with NMR can also

determine relative amounts of identified components within a mixture such as biodiesel. Knothe and Kenar have shown integral of resonance in ^{1}H spectral can be used to determine the relative amounts of fatty acids in vegetable oils and methyl esters mixtures when the source of the oil feedstock is known (Knothe and Kenar, 2004).

2.9 Modeling /OptimizationTechniques in the Production of Biodiesel

The desire for optimality is the inherent nature of humans such as a manufacturer wants to produce its products with the lowest cost, or a delivery company wants to deliver its products to all distributers with the shortest distance to save gasoline, time, etc. These are the typical examples which optimization theories can be applied to give optimal solutions. From the appearance of computers, mathematical theories of optimization have been developed and applied widely. The computer with its computing power has the ability to implement optimization theories very efficiently in the manner of time and cost. The goal of the optimization theories is the creation of a reliable method to optimize models by an intelligent process. Applications of these theories play more important roles for modern engineering and planning.

In real life scientists, engineers, and managers often collect a lot of data and usually fall into difficult situations how to select different factors to obtain desired results. Optimization is a process of how to trade off these factors to find the best solution by evaluating their combinations. Many engineering problems can be defined as optimization problems such as process design, logistics, process synthesis and analysis, telecommunication network, finding of an optimal trajectory for a robot arm, the optimal thickness of steel in pressure vessels, etc (Nam, 2012). Inpractice, optimization algorithms are able to solve these problems but to find the best solution for these problems is often not very easy and straightforward because they

include in large search spaces. It will be more challenging particularly in real life systems, which require optimal solutions in an acceptable amount of time. Optimization is a useful and important tool in the decision science and the analysis of physical systems. In order to use this tool, an objective function has to be defined. This objective function can be the cost, profit, time, etc. Normally, an objective function is modeled by unknown variables to describe its characteristics. And optimization algorithms define values of these variables to meet the requirements of this objective function. If the model is so simplistic, the solution will not reflect useful insights into practical systems. If the model is so complex, optimization algorithms may not give solutions. Therefore, models and optimization algorithms usually have to be complex enough to be handled by the computer. There are numerous optimization algorithms. Each is developed to solve a particular set of problems, and each has its own strength and weakness. Users usually have to evaluate a model and decide which algorithm is suited for (Nam, 2012).

Discrete and continuous optimization: Discrete optimization problems are known as integer programming problems. In discrete optimization problems, solutions make sense if and only if variables are integers. To meet this constraint, a good strategy is to solve problems with real variables and then round them up to the closest integers. This type of work is by no means guaranteed to give optimal solutions. In contrast with discrete optimization problems, continuous optimization problems are easier to solve because of the smoothness of continuous functions. Moreover, these problems have an infinite set of solutions with real values; therefore, we can use other information at any point to speculate the function's behavior. However, the same method cannot be applied to solve discrete optimization problems with a finite set of solutions, where points are close, may have different function values. Constrained and unconstrained optimization: constrained optimization problems arise from models which have constraints on variables. These can be the constraints of input variables or the constraints to

reflect relationships among variables, etc. Unconstrained optimization problems can be considered as particular cases of constrained optimization problems in which constraints of variables can be ignored without effect on the solution. Or these constraints can be counted as penalization terms in the objective functions of unconstrained problems.

Global and local optimization: local optimization algorithms converge much faster than global optimization algorithms. However, its solution is just a local one which is the minimum in the vicinity and it is not guaranteed to be the global solution which is the best of all minima. Stochastic and deterministic optimization: in some optimization problems, the model cannot be fully defined because it depends on quantities that are unknown at the time of formulation. Normally, a modeler can predict unknown quantities with some degree of confidence. Stochastic optimization algorithms will use these quantifications of the uncertainty to produce solutions that optimize the expected performance of the model. Vice versus with stochastic optimization algorithms, deterministic optimization algorithms assume that the model is fully specified. Each optimization algorithm has different techniques to converge iteratively to optimal solutions. Some use first derivatives, second derivatives, or function values, etc. to converge. Some accumulate information from previous iterations to predict its sequential convergence to target values. The optimization technique is a key to differentiate one algorithm from another. A good optimization algorithm should possess some following properties:

- Robustness: the algorithm has the ability to converge a wide range of problems in its category
- Efficiency: the algorithm can converge without too expensive computing cost. This cost can be understood as computing time and storage cost

- Accuracy: the algorithm can give solutions with precision. It is not very sensitive with errors when being implemented on computers.

Modeling in biodiesel is generally carried out with two different approaches; first, modeling biodiesel production process, simulation of transesterification reaction under variable amount of raw materials and catalyst and also reaction conditions. Second approach includes modeling the biodiesel combustion reaction and simulation of the different compositions of fuels in order to predict the engine performances and emissions.

The traditional one factor at a time method of analysis is time consuming and does not take into consideration the interation effects between the factors. Therefore, optimization method with respect to design of experiment is applied. To study the effects of process variables or independent variables on the objective function or response variable, experimental techniques such as central composite design (CCD), Placket-Burman experimental design and central composite rotatable design (CCRD)(Ghorbani *et al.,* 2011). Placket- Burman design is an orthogonal array that allows testing the largest number of factors with least number of observations (Montgomery, 1997).

2.9.1 Response surface methodology (RSM)

Response surface methodology (RSM) is a useful statistical technique which has been applied in research into complex variable processes. It employs mulitiple regression and correlation analysis as tools to assesss the effect of two or more independent factors on the dependent varaiables (Awolu and Layokun, 2013). Kalil *et al.,*(2000) have earlier described RSM as a good optimizer involving a collection of statistical techniques for designing experiments, building models, evaluating the effects of factors and searching for the optimum conditions. Based on the RSM the observed responses to design of experiments (DOE) are

fitted to a second-order or first-order function (Santiago-Urbina *et al.,* 2011). Such models belong to modeling techniques dealing with the development of non-parametric simulative models. Fractional factorial design is normally used to screen the variables such as reaction time, stirring speed, and ethanol oil molar ratio, type of catalyst and its concentrations and temperature. This results in a number of coded (low and high level) experimental runs. After identifying the most significant variables a central composite design (CCD) is applied to determine the critical values for these variables (optimizing the experiment) using standard computer system version. The main advantage of RSM is the capability to minimize the number of experimental runs needed to give adequate evidence for statistically acceptable result (Adepoju *et al.,* 2013) as well as makes it possible to predict the conditions required to obtain higher yield and determine the robustness (Delima *et al*., 2013). Using RSM in several fields such as chemical engineering process control and chemical analysis among many other applications is extensively studied.

To achieve maximum production of biodiesel yield, process variables including reaction temperature, methanol to oil ratio, weight of catalyst and reaction time have been used simultaneously in RSM method by performing central composite design (CCD) (Imadi *et al.,* 2007; Abdulla *et al.,* 2009). Kok *et al*., (2010) have used RSM to optimize the supercritical dimethyl carbonate (SCDMC) technology for biodiesel production by applying rotatable central composite design (RCCD). It has been applied in methanolysis optimization of some vegetable oil to biodiesel: *Sesame* oil (Betiku and Adepoju, 2013), *Neem* oil (Awolu and Layokun 2013), *Moringa oleifera* oil (Rashid *et al*., 2011), *Jatropha curcas* oil with high FFA (Tiwani *et al.,* 2007), animal fat (Jeong *et al.,* 2009), waste ripe seed oil (Yisan *et al.,* 2008), *Zanthoxylum bungeanum* seed oil using CaO as catalyst (Fan *et al.,* 2011) and cotton seed oil (Zhang *et al.,* 2010). Also, the application of factorial design and RSM for optimizing and expanding

production of biodiesel from combination of bioethanol and *Brassica carinata* oil is reported (Bouaid *et al*., 2009). According to the result of the work, a non-linear model developing would be an alternative to overcome the available problems in the long term storage of biodiesel.

Recently, Ganji *et al.*,(2017), focused on optimization of biodiesel combustion phenomena through parametric approach using response surface methodology (RSM) and computational fluid dynamics (CFD). The simulation responses such as indicated specific fuel consumption (ISFC), NOx and soot were analyzed using design of experiments (DOE). They concluded that NOx emissions evidently decreased and soot emissions increased with increasing rate of exhaust gas recirculation (EGR), increase in start of injection (SOI) increases NOx and reduces soot and ISFC while decrease in compression ratio (CR) increased soot emissions and ISFC and NOx is reduced.

2.9.2 Artificial neural network

Artificial neural network (ANN) approach has been one of the well known types of evolutionary computation method in the last decades. Artificial neural networks have shown great ability in solving complex nonlinear systems identification and control problems and can be described either as mathematical and computational models for non-linear function approximation, data classification, clustering and non parametric regression or as simulations of the behaviour of collections of model biological neurons (Ahmadi *et al.,* 2008). These networks are applied in many fields to model and predict the behaviour of unknown systems, very complex systems or both based on investigation of given input-output data (Ahmadian-Morghadam, 2012). ANNs are in fact non-linear computer algorithms which are extensively and successfully applied in different domains (Sulaiman *et al.,* 2010). ANN is a biologically inspired computational technique that imitates the behaviour and learning process of the human

brain. ANNs are universal approximators and their predictions are based on prior available data. It is therefore preferred in many data driven research applications over other theoretical and empirical models where predictive accuracy is of prime concern. The ANN technique has been extensively used in several applications in the fields of pattern recocgnitions; signal processing, function approximation, weather prediction and process simulations (Guo et al., 1997). The recent developments and potential application of ANN in diverse disciplines has motivated the present study. ANNs are essentially supervised learning methods, i.e. given an input and an output dataset; they have enough flexibility to model the nonlinear input output mapping. The methodology is generic and does not have any limitation to the type of dataset or the number of input-output variables. These generic ANN models provide flexibility to include other process parameters like tars, unconverted carbon, steam-to-biomass ratio (in the case of steam gasification) etc. or any other process parameter which are deemed necessary (Puig-Arnavat et al., 2013). There have been exhaustive studies on using different training algorithms for ANNs, e.g. Levenberg-Marquardt (LM), scaled conjugate gradient (SCG), Broyden-Fletcher-Goldfarb Shanno quasi-Newton (BFGS), gradient descent with momentum and adaptive learning rate (GDX), amongst many others (Plumb *et al.,* 2005). The LM gives accurate training results for moderate size neural networks. The other algorithms have disadvantage of slower convergence speed particularly for large networks. Based on the above reason, the LM backpropagation training algorithm is used here for minimising the mean squared error (MSE) between the network output and target output.

Various studies have proved that ANN is a powerful technique for process modeling of biofuels (Rajendra *et al*., 2009). Antonio *et al.,* (2006) accurately carried out simulation of transesterifiction for the production of Biodiesel from waste olive oil by applying ANN model and the results proved that ANN is a powerful alternative to experimental-testing needed to find

optimal parameters as well as a capable tool to process modeling. Ramadhas *et al.,* (2006) implemented four types of ANN models to predict the cetane number of biodiesel by applying multi layer feed forward (MLFEEN), radial base function (RBFN), generalized regression (GRNN) and recurrent network (RNN). Kumar *et al*., 2007, selected the best ANN for estimating properties of diesel biodiesel blends using seven neural network architectures with tree training algorithms within ten different types of weights and biases. Several researches have been conducted to prove the application of ANN in predicting engine performance and emission using fuel blends (Ghobadian *et al.,* 2009). Artificial neural network (ANN) model for predicting the brake power, torque and emissions of CO, CO_2, HC and NOx in relation to engine speed, load and fuel blends has been developed and the result showed high correlation coefficients (Kiani Deh kiani *et al.,* 2010) and backpropagation training algorithm is observed as appropriate to predict performance and exhaust emissions of engine for different speeds and different fuel blends (Ghorbani, *et al.,* 2009). It has been reported that the multi-input multi-output (MIMO) models show an improved performance over the multi-input single-output (MISO) models especially in handling multi-objective functions (Morad, *et al.,* 2010). A typical architecture topology for MIMO and MISO ANN are presented in Scheme 2.

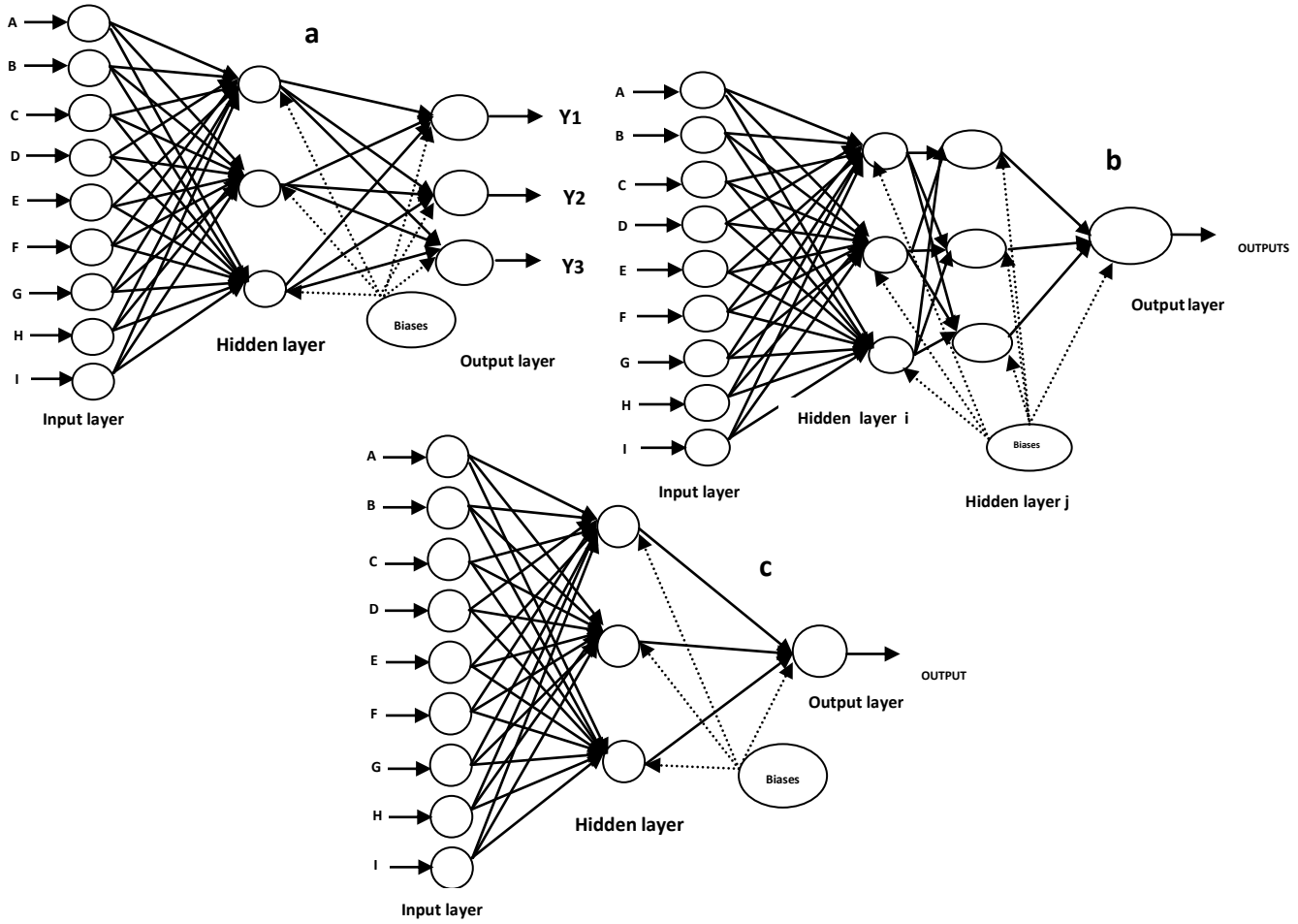

Scheme 2: Schematic diagram of MIMO (a-single layer, b- double hidden layer) and c- MISO back-propagation feed forward topology neural networks

2.9.3 Genetic algorithm.

The genetic algorithm (GA) is invented to mimic the natural behavior of evolution according to the Darwin principle of survival and reproduction (Zanchetta *et al.*, 2008). Unlike calculus-based methods, GA does not require derivatives, and it also has the ability to do a parallel search in the solution space simultaneously. Therefore, it is less likely to get trapped in local minima. Like the particle swarm algorithm and the differential evolution algorithm, GA starts by its initial population, and each individual is called a chromosome to represent a solution. During each generation, chromosomes will be evaluated according to their fitness

values and evolved to create new chromosomes for the next generation. New childish chromosomes can be produced in two different ways either by emerging from two parental chromosomes in current generation with the crossover operator or by modifying chromosomes with the mutation operator. In order to maintain the population size, all chromosomes have to go through the natural selecting process. The chromosomes with better genes or better fitness will have higher probability to go to the next generation and other ones with worse genes is more likely to be rejected. This procedure is repeated until the best chromosome close to the optimum solution can be obtained. Another big advantage of GA is that it can be applied in different domains, not just only in optimization problems. However, it still has the limitation of premature convergence and low local convergence speed. Therefore, GA is usually improved by research scholars (Hangyu *et al.,* 2006; Cheng and Ping, 2006).

2.9.4. Integrated model

Due to drawbacks of conventional models, there has been a massive tendency toward using combined methodologies to eliminate the disadvantages of single ones. One of the developed models include: export systems, statistical method, fuzzy logic, wavelet transform and genetic algorithm (GA). Among these, GA is cost effective and less time consuming technique (Rajendra *et al.,* 2009) than unplanned approaches and allows seeing interactions among experimental variables within the range studied, leading to better knowledge of the process and therefore reducing research time and cost (Bouaid *et al.,* 2009). ANN combined with genetic algorithm (GA) for predicting the optimum process parameters needed to reduce high FFA of any vegetable oil for complete transesterification is reported while conclusively it has been reported that a GA-ANN model is effective tool for predicting optimized pre-treatment process parameters for biodiesel production and using GA with RSM method based on CCRD

or other similar experimental techniques reduces time and cost of production (Jena *et al.*, 2010). In general using integrated models including GA, RSM and ANN offers a promising outlook in the estimation of the optimum variables for biodiesel production resulting in saving energy, cost and time (Ghorbani *et al* ., 2011).

2.9.5 Nelder-Mead's simplex algorithm

The simplex method is a direct downhill search method (Nelder and Mead, 1965). It is a simple algorithm to search for local minima and applicable for multidimensional optimization applications. Unlike classical gradient methods, this algorithm does not have to calculate derivatives. Instead it just creates a geometric simplex and uses this simplex's movement to guide its convergence. A simplex is defined as a geometrical figure which is formed by (n+1) vertices. Where n is the number of variables of an optimization function, and vertices are points selected to form a simplex. In each of the iteration, the simplex method will calculate a reflected vertex of the worst vertex through a centroid vertex. According to the function value at this new vertex, the algorithm will do all kinds of operations as reflection or extension, contraction, or shrink to form a new simplex. In other words, the function values at each vertex will be evaluated iteratively, and the worst vertex with the highest function value will be replaced by a new vertex which has just been found. Otherwise, a simplex will be shrunk around the best vertex, and this process will be continued until a desired minimum is met. Moreover, the convergence speed of this algorithm can also be influenced by three parameters α, β, γ (α is the reflection coefficient to define how far a reflected point should be from a centroid point; β is the contraction coefficient to define how far a contracted point should be when it is contracted from the worst point (Nam, 2012).

2.10 Performance and Combustion Evaluation of Biodiesel in Direct Injection Diesel Engine

Diesel fuel is largely consumed by the transportation sector and tests based on engine performance evaluation have established the feasibility of using vegetable oils, biodiesel derived from them and their blends with petrol-diesel in compression ignition engines (Haiter et al., 2012). Intensive research is on-going on the performance characteristics, combustion efficiency and emission qualities of these blends when applied in different proportions in stationary diesel engines (Elango and Senthilkumar, 2011).

2.10.1 Engine performance evaluation

Biodiesel application reduces the injector coking to a level significantly lower than the observed with No.2 diesel fuel. Engine performance parameters such as brake thermal efficiency, brake specific fuel consumption (BSFC) and brake specific energy consumption (BSEC) are calculated from the experimental data while the torque, brake power and fuel consumption values associated with CIE fuels are determined under certain operating conditions (Canakcii *et al.*, 2006). Other engine performance characteristics which vary with brake power include brake mean effective pressure, volumetric efficiency and gross fuel consumption while cylinder pressure and heat release vary with crank angle.

2.10.2 Exhaust emissions from biodiesel

Production of biodiesel is a complex task in considering to long term environmental effect. In cities across the world, the personal automobile is the only greatest polluter. The biodiesel impacts on exhaust emissions vary being a function of the type of biodiesel and the type of conventional diesel. Several studies on the performance and emission of compressed ignition engines, fuelled with pure biodiesel and its blends with diesel fuel have been conducted

and reported in the literature (Cardone *et al.,* 1998). The sulphur content of petrodiesel is 20-50 times that of biodiesels. Biodisel contain higher oxygen compared to petroleum diesel and the use of biodiesl in diesel engines have shown majestic reductions in emanation of CO, sulphur, PAH, smoke, PM and noise. However it emits more NOx emission than diesel. Petro-diesel fuel is largely consumed by the transportation sector and internal combustion engine have fallen victim of fossil fuel depletion and environmental degradation. In cities across the world, the personal automobile is the greatest combustion emission polluter. Carbon monooxide (CO) reacts with haemoglobin in the blood forming carboxyheamoglobin (H_6CO) rather than oxyhaemoglobin (H_6O_2), prevents oxygen transfer, causes headaches, nausea, fatigue to possible death, cardiovascular and neuro-behaviour, Sulphur dioxide causes bronchi-constriction, ear-nose-throat (ENT) irritation, respiratory illness, and aggravates existing heart diseases, nitrogen dioxide results in pulmonary fibrosis, lung tissue damage and pneumonia while particulate matter causes reduction in life expectancy, increase in chronic obstructive pulmonary disease and adverse effects on cardiovascular system (Agarwal, 2006). In Nigeria, the regulatory agency for environmental protection has stipulated maximum values of 20 mg/Nm^3 of particulate matter from pharmaceutical manufacturing as well as petroleum based and chemical industries, 300 mg/Nm^3 of NO_X, 500 mg/Nm^3 SO_X, and 500 mg/Nm^3 of CO from petroleum based and chemical industries (NASREA, 2009). The global warming potential of green house gases (GHGs) has been reported to be 296ppb for N_2O against 10 for CO_2 overtime horizon of 100years against 275 ppb and 315 ppb for N_2O and 27ppm and 360 ppm for CO_2 as pre-industrial and year 1997 concentrations respectively (Agarwal, 2006). Combustion engine emissions have resulted in growing concern over air quality and green house effects (Esonye, *et al.,* 2018)

Biodiesel has demonstrated a lot of promising characteristics such as reduction in exhaust emissions (Agarwal *et al.,* 2006). Regulated air pollutants include: CO, unburned HC, NO_X, particulate matter (PM) and polycyclic aromatic hydrocarbons and ozone-forming hydrocarbons. The net reduction in CO_2 emissions are estimated at 77-1048MJ of diesel and they increase as the amount of biodiesel blended with the diesel fuel increases (Demirbas, 2009). Helwani *et al.,* reported that combustion of neat biodiesel decreases CO_2 emissions by 46.7%, PM emission by 66.7% and unburned hydrocarbon by 45.32%. These results were obtained through green catalytic techniques.

2.10.3 Combustion efficiency

The combustion of fuels may be defined as a chemical combination of oxygen in the atmospheric air and hydrocarbons. The oxygen contents of biodiesel improve and facilitate the combustion process and decrease its oxidation potential. Demirbas, (2009) has reported that visual inspection of the injector types indicate no difference between biodiesel fuels and petro-diesel in testing. Diesel fuel is represented by $C_{16}H_{34}$ and releases 3.11kg of CO_2 per kilogram of fuel used in combustion (Atadashi *et al.,* 2010). Syed *et al.,* (2009) had reviewed different combustion characteristics such as ignition delay, ignition temperature and spray penetration of different biodiesel fuels. The air-fuel ratio (A/F) gives the minimum air requirement for complete combustion of a fuel. Adequate supply of air is essential for complete combustion and for obtaining maximum amount of heat. Depending on the amount of excess air supplied and the degree of mixing, the exhaust gas includes the products of complete combustion, CO_2, hydroxyl and aldehydes; and nitrogen compounds such as nitric oxide (NO) and nitrogen dioxide (NO_2). All these products except water and nitrogen are considered to be atmospheric pollutants. The primary aim of fuel production and use in industries is the provision of heat,

light and power. The combustion of these fuel release heat which is used to generate steam, heat other furnaces or heat space and to produce mechanical power directly in an internal combustion engine. The exhaust gases of the gas cycles leave the system at high temperature, and this is one of the reasons why the practical internal combustion engine have relatively lower thermal efficiency. For the vapour cycle, although the heat intake temperature is not very high, the condenser temperature is usually low.

Wilson, (2012), optimized diesel engine control parameters such as clearance volume, fuel injection pressure (FIP), nozzle-hole diameter, start of injection (SOI) and load using Taguchi design of experiments (DOE) in order to get the best performance in terms of NOx and BSFC. He also derived relations between operating parameters and responses and identified that the results of experimental data had a good agreement with the predicted results. It was also ascertained that among all the parameters FIP has a great influence on NOx emission. The study concluded that the design of experience (DOE) is an effective and efficient way to develop a robust design in order to get optimum performance and emissions. Also, it has been reported that the complexity of the in-cylinder combustion phenomena can be modelled using CONVERGETM computational fluid dynamics (CFD) software, in which turbulence modeling, combustion modeling and spray modeling can be used simultaneously to predict the performance and emission characteristics precisely (Ganji et al., 2016). Recently, Ganji *et al* (2016) focused on optimization of biodiesel combustion phenomena through parametric approach using response surface methodology (RSM) and computational fluid dynamics (CFD). The simulation responses such as indicated specific fuel consumption (ISFC), NOx and soot were analyzed using design of experiments (DOE). They concluded that NOx emissions evidently decreased and soot emissions increased with increase in rate of exhaust gas recirculation (EGR), increase in start of injection (SOI) increased NOx emission and reduced

soot release and ISFC while decrease in compression ratio (CR) increased soot emissions and ISFC with reduction in NOx emission.

Furthermore, Kaliamoorthy and Paramaswan, (2013) investigated the effects of engine parameters on the performance and emissions characteristics of a single cylinder 5.2kW diesel engine. Power, static injection pressure, injection timing, fuel fraction and compression ratio were considered as independent variables while brake power, fuel economy and emissions from blends of karanja oil biodiesel with petrodiesel using Taguchi based design of experiment. Qiang et al., (2016) reported that the efficient optimization algorithms are critical to the development of new engine technology. In their study, experimental investigations were carried out on optimizing the performance of a four-cylinder, turbocharged, direct-injection diesel engine running with soy biodiesel. An effective hybrid particle swarm optimization (PSO) and genetic algorithm (GA) method using a small population was developed and tested to optimize five operating parameters: EGR rate, pilot timing, pilot ratio, injection timing and injection pressure. Based on the measured engine performance and emissions, results show that the new hybrid algorithm can significantly speed up the optimization process and achieve a superior optimum as compared to the basic GA method. Also, Lotfan et al., (2016) investigated the combination of artificial neural network (ANN) and non-dominated sorting genetic algorithm 11 (NSGA-11) for modeling CO and NOx emission from direct injection dual-fuel (DDF) engine. The optimum values of intake temperature, mass flow rate of diesel and gaseous fuels were obtained for desired output power and engine speed via NSGA-11. Niu *et al.,* (2018) recently reported a novel online optimization approach based on engine physical model using NSGA-11 coupled with a support vector machine method (SVM). They proposed an enhancing training method to guarantee the accuracy of svm model. The study proposed a novel multi-objective online optimization approach for diesel engine fuel injection parameters and NOx and

soot emission. The process was tested on CRDI- assisted marine diesel engine (BSFC and maximum in-cylinder pressure). Some literature reports on the engine performance and combustion are presented in Table 2.3 (with engine models and specification) and 2.4.

Table 2.3: Some literature reports on engine performance, combustion and emission condition with engine models.

Engine specification	Halter *et al.*, 2012	Mishra *et al.*, 2014	Elango *et al.*, 2014	Karithikumar *et al.*, 2014
S	4	4	4	4
C	1	1	1	-
CR	17.5:1	17.5:1	17.5:1	-
WC	Yes	Yes	-	Yes
AC	No	No	yes	No
D1	Yes	Yes	Yes	-
SB	87.5/110min	87.5/110min	87.5/110min	87.5/110min
IT	23˚ BTDC	23˚ BTDC	23˚ BTDC	-
IP	220kg/cm^2	210 bar	200 bar	-
P	5.2KW	3.5KW	4.4KW	5Hp
LD	Eddy current Dynamometer	Eddy current Dynamometer	Eddy current Dynamometer	Spring load Dynamometer
Model	Kirloskar, Tv.1	Kirloskar, Tv.1	Kirloskar, Tv.1	Hindustan
Test Conditions				
(i)	1500rpm Constant speed varying load	1500rpm Constant speed varying load (5,25,75and 100)	1500rpm Constant speed varying load(19,20,30,40 and 50)	1500rpm varying load
(ii)	Mahua oil (25,50,75 and 100 blended)	Rice bran oil (0,5,10,15 and 20% blend)	Jatropha curcas oil	Cooking/esterified cooking oil (8:2, 9:1, 9.5:0.5)
(iii)	NDIR-AVL 444 Degas Analyzer AVL 437C smoke meter	Manatec Dsm-200 Smoke meter	AVL smoke meter, five gas analyzer	
Results	BTE↑, SFC↓, CO,CO_2,HC,O_2 NOx↓	SFC↑, BSEC↑, SO↑, bp↑,	SFC↑,BTE↓, EXGT,SO andNOx↑ HC and CO_2↓	S.g; SFC↓, M.E;BTE; ITE(9.5:0.5) ↑

C – Cylinder, AC – Air Cooled IT – Injection Time LD – Load Devices CR – Compression ratio, DI – Direct Injection , IP – Injection Pressure, WC – Water Cooled, SB – Stroke Bore, P – Rated Power ME –Mechanical efficiency, ↓ - decreas, ↑ - increase ,S_O – Smoke opacity

Table 2.4: Some literature reports on engine performance, combustion and emission condition.

Biodiesel feedstock		Engine	Operating Condition	Emission Results	References
Mustard oil methyl ester	BD MY	Horizontal, 1-cylinder, 4-stroke, AC, DI 1-Cylinder, 4-stroke, WC, RP: 5HP, RS: 1500 rpm	2200 rpm and 1kg load is used. At different engine load and fuel blend	Lower all HC, PM, NO_X emissions with fuel blend Decreases HC, CO_2, emission with an increase in fuel blend and increase in NO_x	(Hasib et al., .2011, Bannikov,2012)
Cotton seed oil methyl ester	BD MY	1-Cylinder, WC, NA, 4 stroke,DI 1-cylider, 4S,DI, NA, D:553cm^3, RP:4.476kW,RS:1800rpm	1100-1800 rpm Different speeds and different blends9B10,B20,B30) 1000-1600rpm and full load	CO, PM, Smoke emission reduced, NO_x increased 10% increase in NO_x and lower CO, 24%PM, 14% smoke compare with diesel fuel.	(Nabi et al., 2009, Hazar 2010)
Jatropha oil methyl ester	BD MY	1-Cylinder, WC, NA, 4 stroke, DI 1-Cylinder, 4S, WC, DI, RP: 8,82 kw, CR: 17:1, RS: 2000 rpm	Different speeds (1500 and 2000 rpm) and different load	Lower smoke, CO, HC and NO_x Decrease CO, HC and NOx with increase in engine speed	(Nabi et al., 2007, Huang et al., 2010)
Karanja oil methyl ester	BD MY	1-Cylinder, WC, NA, 4 stroke, DI 3 Cylinder, AVL make CI engine, CR: 18.1, WC, RS: 2200 rpm, P:44.1 kw	1200 rpm Full throttle at 1200 rpm, 1400 rpm and 2200 rpm and 20%, 50% and 100% blends	Lower smoke, CO. Engine noise emission and higher oxygen, combustion efficiency, NO_x Slightly increased CO, NO_x and reduce HC, PM and smoke with an increase in blending ratio	(Nabi et al., 2009,Sahoo et al., 2009)
Coconut oil methyl ester	BD MY	1-Cylinder, 4 stroke, AC, DI 1-Cylinder , 4 stroke , WC, NA, DI D: 638 cm^3, RP: 8.8 kw, RS: 2400 rpm.	2600 rpm Afull load varying speed condition	PM, Soot, CO, decrease and NO_x increase Reduces CO, HC emissions and higher NO_x emission	(Hossain et al., 2012, Habibullah et al., 2014)
Soy based biodiesel	BD MY	1-Cylinder, 4 stroke, WC, DI 1-Cylinder, 4 stroke, DI, CR: 16.5:1, RP: 11.03 kw, RS: 2000 rpm	1800 rpm under various load At full load and different engine speed	CO, PM decrease and NO_x BSFC increase Decrease CO, HC, NO_x and smoke by 27, 27, 5, 52% respectively	(Uddin Qj et al 2009)
Linseed oil methyl ester	BD MY	1-Cylinder, WC, NA, 4 stroke, DI 1-Cylinder, 4S, DI, RP: 4.4 kw, CR: 17.5:1, RS: 1500 rpm	1000 rpm At different loads, constant speed and different injection pressure	PM, CO, smoke lower and NO_x higher Decrease CO, HC and smoke emission but increase in NO_x	(NabiMd & Najmul 2008,Puhan et al 2009)
Neem oil methyl ester	BD MY	1-Cylinder, WC, NA, 4 stroke, DI 1-Cylinder, AC, DI, CR: 17.5:1, RP:4.4 kw, RS: 1500 r;pm	Various load At different blends, constant speed and different break power	NO_x, CO. HC and smoke reduced Lower CO, HC but increase NO_x and smoke emission with increase in fuel blend and engine load	(Mhia and Zagdul 2007,Elango and Senthilkumar 2010)

AC-air cooled, WC-water cooled, NA-natural aspirates, DI-direct injection, TC-turbocharged, PM-particulate matter

2.11 Characteristics of Selected Energy Crops

Three tropical energy crops selected for this study are African star apple, sweet almond and African pear. They are widely grown in Nigeria but their seeds are treated as waste. This makes their potentials to be neglected and underutilized.

2.11.1 African star apple (*Chysophyllum albidum*)

The physico-chemical properties of the African star apple fruit gave an indication of the usefulness of the fruit in brewing industry (Olufumilola and Oladapo, 2011). The juice of the fruit pulp has potentials as an ingredient of soft drink and can be fermented for wine and other alcohol production with unsaturated fatty acids being the main components of the oil (Ureigbo and Ehebe, 2010). The fruit contribute to improve health, nutrition, food security and income of the local communities (Houessou *et al.*, 2012). African star apples are among the under-utilized fruits in Nigeria (Olumifola and Oladapo, 2011) and seed of this plant have been rarely exploited for production of oil for commercial purposes despite the fact that it contains about 13% of edible oil (Musa et al 2015) while most often the seed are thrown away after the consumption of its juicy pulp (Ochigbo and Paiko, 2011, Audu *et al.,* 2013). Only few attempts on the extraction of oil from *C. albidium* in Nigeria are documented. Ochigbo and Paiko, (2011), worked on effect of solvent blending on the characteristics of oil extracted, Sam *et al.*, (2008) reported the extraction and classification of lipid from the seeds of *Chrysophyllum albidium.* The study was limited to phytochemical screening and fatty acid profile composition. Adebayo *et al.*, (2012), reported the oil extraction and characterization at 65˚C for 3-4 hours without explaining the reason for the choice of process condition. The following oil yield from the seed of *C. Albidium* has been reported 16.85%, 7.7%, 10.82%, 13.43%21.51%, 25.00% and 6.85% by Musa *et al.,* (2015), Sam *et al.,* (2008), Adebayo *et al.*, (2012), Ochigbo and Paiko,

(2011), Jayeoba *et al.,* (2007), Audu *et al.,* (2013); Ajiwe *et al*.,(1997) and Agbade *et al.,* (2012) respectively. Also, a sugar brix of 5.4 in the pulp and 0.9 in the peel as well as 13.4% reducing sugar from the juice have been reported (Olufumilola, 2011; Jayeoba *et al.,* 2007). These results are indications that star apple fruit can serve for multibiofuels production for biodiesel and bioethanol using the oil from the seed and sugar from the pulp.

2.11.2 Sweet almond (*prunus amygdalus)* fruit

World production of almond was 2.9 million tonnes in 2013 with United States as the largest producer of 1.8 million tonnes (FAOSTAT, 2014). Sweet almond tree is found in the south eastern and south southern parts of Nigeria where they are basically grown to provide shades to homes, offices and the environment. Their fruits litter the environment and are picked either by children or disposed off as wastes and as such their use as feedstock for biodiesel production would also serve as a waste disposal option in these areas. Although, Almond seed oil is from an edible feedstock, its application as a viable feedstock for biodiesel production may not likely compete with its use as food since it is not a staple food in so many parts of the world and not widely consumed in Africa. Giwa and Ogunbona, 2014, studied the extraction and characterization of the seed oil biodiesel from sweet almond obtained from Nigeria. Their study revealed that the seed oil has an oil yield of 51.45%, acid value of 1.07mg KOH/g and fatty acid composition of oleic acid (69.7%), linoleic acid (18.2%) and palmitic acid (9.3%). Their result equally showed that the cold flow properties were -3°C and -9°C for the cloud point and pour point respectively with the specific fuel properties found to satisfy both EN 14214 and ASTM D6751 biodiesel standards. Mehdic and Kariminia, (2011) also studied the optimization of biodiesel production from Iranian bitter almond oil using statistical approach. Their investigation revealed that at the following optimal conditions: temperature of 35°C, catalyst concentration of 1.4wt% and methanol to oil molar ratio of 9.7mol/mol, the actual values of the

product yield, biodiesel yield and biodiesel purity were 96.7, 94.7 and 97.9wt% respectively while the predicted values were 98.1, 96.3 and 98.2wt% respectively. Due to its high oil yield and abundance, oil from almond seed may be considered as Nigerian potential asset for biofuel and oleo chemical production (Israel, 2008).

2.11.3 African pear (*Dyacrodes edulis)*

The African pear belongs to the family of *Burseracea* and botanically known as *Dyacrodes edulis*. It is an indigenous fruit tree grown in low lands and plateau regions of West Central Africa and Gulf of Guinea (Ogunsyi, 2015). The major work carried out on the industrial application of African pear seed oil was reported by Ogunsyi, (2015), where he investigated on the application of the seed oil in biodiesel production. He discovered that the seed is a viable feedstock considering the fact that the seed contained about 59% oil and yielded an optimum value of 64.24% biodiesel at 60ºC, 7:1 methanol /oil molar ratio, at 850rpm for 120 minutes reaction time with KOH catalyst. Bull and George, 2015 equally assessed the fuel properties of biodiesel from African seed oil and obtained 80% biodiesel yield at 60 ºC , for 50 minutes reaction time using 1:6 oil/methanol molar ratio using 0.25g of NaOH as catalyst. Besides, the pulp contains 48% oil and a plantation can produce 7-8 tonnes of oil per hectare (Awono *et al.*, 2002; Shikha and Rita, 2012). However, much work is yet to be done in the use of African pear seed oil as a feedstock for biodiesel production.

2.12 Review of Some Related Works

Bhattacharyulu *et al* ., (2013), developed ANN model using MATLAB R 2008 b to correlate the effect of the operating parameters on the viscosity of biodiesel produced in an oscillatory baffled reactors. They showed that the comparison of viscosity of biodiesel and percentage error of the data points were under acceptable limits. This demonstrated that ANN has great potential in addressing the estimation problems related to yields incorporating the operating parameters of biodiesel production in saving time and energy and increase the accuracy of estimations.

Ahmadian -morghadam *et al.*, (2013), also applied artificial neural networks to develop a straight forward, accurate and time saving prognosticative model for alcohol production. Their results recommended artificial neural networks as a good means of effective recognizing patterns in data and accurately predicting ethanol concentration based on investigating inputs (sugar concentration, live yeast cells and dead yeast cells). The ethanol concentration evaluated in the experiments developed a simple accurate, nondestructive and time saving artificial neural networks model for estimation of ethanol concentration in batch ethanol fermentation from molasses based on live and dead yeast cell, sugar concentration.

Awolu and Layokun, (2013) investigated the optimization of biodiesel production from Neem (*Azadirachta ndica*) oil using a two step transesterification process and determination of qualities of neem oil biodiesel. The first step was carried out using 0.6w/w methanol – to- oil ratio in the presence of 1% w/w H_2SO_4 as an acid catalyst in 1h at 50°C while the second step was base (NaOH) transesterification of the product from the first step. The CCD optimization conditions for the second step were temperature (45°C to 65°C), catalyst concentration (0.45% to 1.45w/w), reaction time (45 to 65 minutes) and methanol /oil molar ratio (1.5 to 7.5).

Optimized biodiesel yield of 89.69% was produced at reaction time of 65 minutes, catalyst amount of 0.95g, temperature of 55°C and methanol / oil molar ratio of 4.5:1. The values of the physico-chemical properties were found to conform to international standards (ASTM). Their result concluded that neem biodiesel showed a general compliance with known standards coupled with its high yield which attested to the production viability and efficiency of neem biodiesel using tow-step transesterification process. The study demonstrates the usefulness of RSM for optimum conversion of *A. ndica* seed oil to methyl ester.

Also, De Lima *et al*., (2013) applied fractional factorial and central composite design and the variables of the reaction of transesterification of corn oil using ethyl alcohol. Reaction time, agitation speed, molar ratio ethanol: oil, type of catalyst, concentration of catalyst and temperature with the aim of optimizing the process conditions in order to achieve maximum efficiency of transesterification reaction and evaluated the effect of each variable and their interactions on yield. The factorial design was efficient in screening of insignificant variables applies in the optimization by the response surface method. The CCD resulted in optimized conditions being determined. A maximum performance was obtained when KOH is 156%mass/mass and ethanol /oil molar ratio of 10.9:1. The data obtained from the CCD were subjected to analysis of variance (ANOVA) with a 95% confidence level and correlation coefficient (R^2) of 0.9683 and the regression was found to be statically significant.

Srinivasarao *et al.,* (2013) applied statistical experimental designs for enhancing the ethanol production from cashew apple juice. The Plackett-Burman design was used initially to screen seven nutritional parameters which are critical and important in enhancing ethanol production. They found out that three parameters out of seven parameters were significan which were further optimized using CCD by RSM. The optimal values of the three variables obtained for maximum production of ethanol was g/l: ammonium chloride, 0.45, magnesium sulphate

0.08 and dipotassium phosphate 0.21 with 61.34g/l as predicted ethanol concentration against the laboratory yield of 59.80 g/l.

Kopia and Nithya, (2012) studied the influence of fatty acid composition in fuel related characteristics of *Datura stramonium linn* biodiesel by gas chromatography–mass spectrometry (GC-MS) and revealed that biodiesel samples with high monounsaturated can exhibit better fuel properties in terms of ignition quality, cloud point and heating value. They discovered the presence of 18 fatty acid methyl esters in *Datura stramonium* FAME with 16.69% saturated fatty acid, 65.59% monounsaturated and 17.72% polyunsaturated fatty acid. They showed that better understanding of fatty acid composition and correlating the fuel properties is of utmost importance in improving the optimal performance.

Mushtaq *et al.,* (2014) examined the production of biodiesel from distaff thistle (*Carthamus lanatus L.)* using alkali catalyzed transesterification. The optimum operating reaction condition of methanol to molar ratio (5:1), catalyst concentration (0.64%) and temperature (60°C) were applied to yield a 97% biodiesel. The values of fuel properties were found to be comparable with mineral diesel and in agreement with ASTM biodiesel standards. Also the synthesized fatty acid methyl ester (FAME) were confirmed and characterized by GC-MS, FTIR, ^{1}HNMR and ^{13}CNMR analyses and the results concluded that DTO appears to be an acceptable new none-edible oil feedstock for biodiesel industry.

Elkady *et al.,* (2015) investigated the production of biodiesel from waste vegetable oils through pretreatment followed by transesterification process in the presence of methanol using KM micro mixer reactor. The properties of the produced biodiesel were compared with its parent waste oil through different characterization techniques. The presence of methyl ester groups was confirmed using both GC-MS and FT-IR. Moreover, the thermal analysis of the

produced biodiesel and comparable waste oil indicated that the product after transesterification process began to vapourize at 120°C which makes it lighter than its parent oil which started to vapourize at around 300°C. A maximum biodiesel production yield of 97% was recorded.

Oyerinde and Bello, (2016) studied how Fourier transformation infrared (FT-IR) spectroscopy can be used to monitor homogeneous alkali catalyzed alcoholysis of peanut oil to produce biodiesel. The spectrum generated was used to identify the functional groups in the fuel sample for qualitative analysis and associated type of vibrations. Analyses on biodiesel blends with fossil diesel were also carried out with FT-IR spectroscopy. The result revealed that the biodiesel contained fatty acid methyl esters (FAME) which revealed the following functional groups with characteristics bands: C=O, -(CH_2)n-, C-O and C-H in the spectrum. They concluded that modern instrumentation such as FTIR spectroscopy is a veritable tool as an emerging technique for analysis of biodiesel even at low concentrations .It can be used for detecting the functional groups and indicate the amount of fatty acid methyl esters in biodiesel blends as a very good tool for both quantitative and qualitative analysis, indicating the biodiesel reactivity and stability. Hassan *et al.,* (2011) studied the application of modelling techniques for predicting and optimization of biodiesel production processes. They concluded that developed ANN-GA model is an effective tool for predicting optimized pre-treatment process parameters for biodiesel production. Also, RSM based on CCD was found to be a suitable approach for simultaneously studying of the effects of process variables on the biodiesel production. There was a good correlation between predicted engine performance and fuel related properties under varying conditions. In general, using integrated models including GA, RSM and ANN offers a promising outlook in the estimation of the optimum variables for biodiesel production resulting in saving of energy, cost and time.

Atapour and Kariminia, (2013) applied response surface methodology (RSM) to optimize the process of biodiesel production from Iranian bitter almond oil. Design of experiment was performed by application of a 5-level-3-factor central composite design in order to study the effect of different factors on the product yield, biodiesel yield and biodiesel purity. These factors were reaction temperature (30-70˚C), catalyst concentration (0.3-1.7w/w) and methanol to oil molar ratio (4.4-13.6mol/mol). A quadratic model was suggested for the prediction of biodiesel yield. Analysis of variance revealed that the factors were significant on the production process of biodiesel. For each factor, optimum value was determined as reaction temperature of 35˚C, catalyst (NaOH) concentration of 1.4wt% and methanol to oil molar ratio of 9.7mol/mol. At these optimal conditions, the actual values of the product yield, biodiesel yield and biodiesel purity were 96.7, 94.7 and 97.9 wt% respectively. At these conditions, the predicted values of the product yield, biodiesel yield and biodiesel purity were 98.1, 96.3 and 98.2 wt% respectively. The fuel properties of the biodiesel were measured and compared with those of Petroleum diesel, ASTM 6751 and EN 14214 biodiesel standards and reasonable compatibility was observed.

Dileep, (2016) in his experimental note presented the analysis and identification of fatty acid methyl esters composition in different vegetable oil (biodiesel) source using Perkin Elmer Clarus^{TM} 600 GC-MS. He identified 17 fatty acid methyl esters in polash biodiesel, 13 fatty acid methyl esters in kusum biodiesel, 11 fatty acids methyl esters in thumba biodiesel and 13 fatty acid methyl esters in mahua biodiesel.

Roy et al., (2013), studied the effects of fuel blends (2-20%) of pure canola oil, used canola oil biodiesel and blends of pure canola oil biodiesel with petrodiesel on DI injection engine on high idling operations with considerations on some engine performance (BSFC and fuel conversion efficiency) and combustion emission characteristics. They observed that only

CO and HC increased among all the tested emissions. Also, Pullen and Saeed (2014), researched on the effects of varying the different oil feedstocks (rape seed, sunflower, palm, soybean, corn, olive, used cooking oil, lard and beef tallow) and alcohol type on engine power, fuel economy and some exhaust emissions (O_2, CO, CO_2 and NO). The result showed that the fuel consumption increased to about 10% when running on pure biodiesel while maximum engine power was slightly reduced compared to petrodiesel. Additionally, methyl esters were found to perform indifferently to ethyl esters while ethyl esters showed quite improved cold flow characteristics. Furthermore, Ozener et al.,(2014), investigated the effects of soybean oil biodiesel-petrodiesel blends (B10, B20, B50) on steady state, single-cylinder direct injection engine running at 1200-3000rpm and observed that brake specific fuel consumption (BSFC), NOx and CO_2 increased while CO, HC emissions, ignition delay and premix peak decreased with addition of biodiesel. More so, Morshin et al., (2014), evaluated the integration of compressed natural gas (CNG) in diesel dual fuel (DDF) engine (HINO HO7C DDF) using diesel, biodiesel, diesel-CNG and biodiesel-CNG. They discovered that the horsepower of biodiesel was 10-20% higher than other fuel blends while biodiesel recorded increase in CO (15-32%) and NOx (6.67-7.03%) but reduction in HC (5.76-6.25%) emissions. Tuccar and Aydun (2013), had earlier reported the effects of microalgae biodiesel-petrodiesel blend (5, 10, 20, and 50 %) in diesel engine operation. The study revealed that microalgae biodiesel caused slight reduction in torque and brake values but exhibited improved emission conditions. Hossain et al., (2013), in their earlier study investigated on the blend of pyrolysis oil derived from de-inking sludge through an intermediate pyrolysis with biodiesel from waste cooking oil (WCO). The experiment which was tested on multi-cylinder indirect injection type CI engine showed that while considering brake thermal efficiency (BTE), peak cylinder pressure, peak

burn rate of combustion, CO_2 and NOx emissions, up to 20% blend can be used without applying ignition additives or surfactants for modification.

Wilson, (2012), optimized diesel engine control parameters such as clearance volume, fuel injection pressure (FIP), nozzle-hole diameter, start of injection (SOI) and load using Taguchi design of experiments (DOE) in order to get the best performance in terms of NOx and BSFC. He also derived relations between operating parameters and responses and identified that the results of experimental data had a good agreement with the predicted results. It was also ascertained that among all the parameters FIP has a great influence on NOx emission. The study concluded that the design of experience (DOE) is an effective and efficient way to develop a robust design in order to get optimum performance and emissions. Also, it has been reported that the complexity of the in-cylinder combustion phenomena can be modelled using CONVERGETM computational fluid dynamics (CFD) software, in which turbulence modeling, combustion modeling and spray modeling can be used simultaneously to predict the performance and emission characteristics precisely

Ayodele et al., (2017), recently optimized biodiesel production from waste groundnut oil (WGO), waste soybean oil (WSO) and waste palm kernel oil (WPKO) with high FFA contents using RSM. Esterification process was applied to reduce the high FFA contents of these waste vegetable oils. In their optimization study, the authors concentrated on the base catalyzed stage of the biodiesel production. Also, Odude et al., (2017) investigated the modeling and optimization of the production of fatty acid methyl esters from esterified palm kernel oil using calcined banana peel ash and pod husk ash as catalysts. The process employed central composite design of RSM to investigate the effects of the individual input variables and the RSM predicted the optimal conditions and the quadratic models for the two different

transesterification processes. More recently, Adepoju et al., 2018, studied the modeling and optimization of lucky nut biodiesel production from lucky nut seed oil with high FFA by pearl spar catalysed transesterification. The processes biodiesel involved oil extraction, oil esterification and transesterification. The authors considered paramount the optimization and modeling of only oil extraction and transesterification processes. These studies have significant inputs on the optimization of the two-step transesterification process. However, information on chemical kinetics is always complimentary to the optimization results of every chemical process. Chemical kinetics provides deep information on the factors that influence the rate of reaction, measures the rate and proposes clear explanation for the values obtained. It therefore provides clues that could help to design equipment to effect the necessary reactions on an industrial scale.

Freedman et al., (1986) studied transesterification of soybean oil using methanol and butanol at temperatures ranging from 20°C to 60°C, with molar ratios of alcohol to oil of 30:1 and 6:1. They discovered that the forward reactions to be second order at 6:1 and pseudo-first order at 30:1 while with methanol he found out that the forward reactions to be fourth order at 6:1 and pseudo-first order at 30:1. All the reverse reactions were found to be second order, rate constants were found to be function of temperature and Arrhenius equations was applied to derive the activation energies. Also, Noureddine and Zhu (1997) again studied the kinetics of transesterification of soybean oil using the same reaction model proposed by Freedman and colleagues but took measurements at different mixing rates based on the stirrer's Reynolds number. They modified the Arrhenius equation and discovered that activation energy varied with Reynolds number. Also, their rate constants for the reverse direction of the first two reactions were larger than the rate constants in the forward direction. Darnoko and Cheryan (2000) investigated the kinetics of palm oil transesterification. They found out that the best fit

to data was a pseudo-second-order model for the initial stages of reaction, followed by first-order or zero-order kinetics. The reverse reactions were neglected for the reason that equilibrium in the system is strongly shifted to ester formation because of excess methanol used. Jansri et al. (2011), investigated the kinetics of methyl ester production from mixed crude palm oil using acid-alkaline catalyst. A two-stage process involving esterification and subsequent base-catalyzed transesterification of the palm oil was adopted. The optimum conditions for reducing high free fatty acid of 8-12 wt% of oil were 10:1 molar ratio of methanol to FFA and 10 wt% of sulphuric acid as catalyst. The transesterification reaction to convert triglyceride in the palm oil to methyl ester was found to be optimal using 6:1 molar ratio of methanol to oil, 0.6 wt% volume of NaOH as catalyst. The reactions were carried out over 20 minutes at 55 °C, 60 °C and 65 °C. The rate constants for the esterification forward and backward reaction were found to be 1.340 and 0.682 L/mol.min respectively. The transesterification stage rate constants for the forward reactions of Tg, Dg and Mg were 2.600, 1.186 and 2.303 L/mol.min respectively and 0.248, 0.227 and 0.022 L/mol.min for the reverse reactions respectively. However, their works considered only the impact of temperature on the rate of transesterification process. Kumar et al., (2011) investigated the kinetics of base catalyzed transesterification reactions of mahua oil and jatropha oil used to prepare biodiesel. The effect of co-solvent and temperature were of main interest. In the presence of co-solvent, tetrahydrofuran (THF) methanolysis of mahua oil resulted in the increase of rate constants from 0.08 to 1.17 L^2 mol^{-2} min^{-1} at 28 °C and from 0.43-3.18 L^2mol^{-2} min^{-1} at 45 °C. The results obtained for jatropha oil were 0.50 and 2.76 $L^2mol^{-2}min^{-1}$ at 25 °C and1.26 and 4.5600$L^2mol^{-2}min^{-1}$ at 45°C.

Also, Rayero et al., (2015) studied the kinetics of NaOH-catalyzed transesterification of sunflower oil with ethanol to produce biodiesel. They concluded that increase in the reaction

temperature favoured the ethanolysis but the effects of catalyst concentration and ethanol-to-oil ratio were more than that of temperature. But the ethanolysis suffered heavily the effect of high soap and intermediate formation which were detrimental to the quality of the produced fatty acid ethyl ester.

2.13 Knowledge Gap

Until now, a full spectroscopic and chromatographic characterization and comparative analysis of the oil quality from the seeds of the above tropical trees have not been reported. This has prompted this research to conduct a detailed physico-chemical and spectroscopic studies of these seed oils to ascertain their useful industrial potentials and predict their shelf-life through the analysis of their resistance to oxidation. From the reviewed works, modeling and optimization of esterification step of the two-step transesterification has not received due attention even though the step is widely applied as a key pre-treatment process in handling biodiesel production from high free fatty acid content oils. Also there have not been any such reports on the African pear seed oil transesterification process. Therefore, this study presents for the first time the optimization and modeling of both stages of the two-step transesterification of African pear seed oil using response surface methodology and artificial neural network while comparing the predictive capabilities of both techniques. Also, from the previous works reviewed, the kinetics studies have concentrated on conventional feedstocks (palm oil, jatropha, soybean and sunflower) and only few attempts considered esterification processes. This research shall apply integrated use of Gauss-Jordan elimination method which has not been reported previously with simplified techniques of 4.0 3 GNU Octave software version 2016 to solve simultaneously the differential equations

It is obvious that currently the application of response surface methodology integrated with genetic algorithm (RSM-GA) in the optimization of diesel engine performance is scarcely reported in the literature. Notwithstanding, only few of these researches are on tropical seed oils while none is presented on *Dyacrodes edulis* and *sweet almond.* Also, considering the detailed literature reports reviewed, the application of Nelder-Mead (NM) simplex algorithm as a simpler, faster and energy saving approach that would enhance effective industrial scale up of laboratory results in biofuel production and usage is not found.

CHAPTER THREE

MATERIALS AND METHODS

3.1 Materials

3.1.1 Reagents and chemicals

The reagents and chemicals used in this work include the following: sodium hydroxide (99%, Sigma-aldrich), potassium hydroxide (loba chemie, gmbH) 85%),methanol ((Merck, Germany 99.5 % purity), carbon tetrachloride (chloroform), Wij's solution (iodine monochloride), potassium iodide solution, phenolphthalein (Merck Germany), powdered iodide (Fishon, England), hexane (99% purity, Merck Germany), sulphuric acid (98% min., Sg: 18300 BDH), hydrochloric acid, iodine, glacial acetic acid, iodine tetrachloride, starch indicator, potassium chloride, ethanol, etc.

3.1.2 Apparatus and analytical equipment

The apparatuses and analytical equipment used in this research include: petri dishes, thermo regulator heater with stirrer (Heizung chauffage, MGW-LAUDA, D6970, Lauda Konigshoffen, Germany). Electric digital precision weighing balance (Ohaus, Adventurer, model –AR 3130), pH meter (Hanna pH meter, model : 02895, India), rotary evaporator oven (model BTOV 1423), veisfar muffle furnance (PEW, Path Electrical Mimbai, India), fenantic portable viscometer (model VL Brookfield Eng. Labline, USA), abbe refractometer (model: WAY-25, Search tech. Instruments), semi-automatic cleveland flash point tester, oxygen bomb calorimeter (model XRY-1A), top load balance (Binatone; model KS-7020), water still (2Lit/hr, model No: 7652, Medica Inst. Mgt Coy, India), concentric rings, thermostatic water bath (model no; 6801TI, 6 holes, medica Inst. Mgt Coy, India), pH meter, digital (Exstick, India),

heating mantle (0-100^{o}C, Labline sunbine, India), sohxlet extractor (BEHR, Labor- Technik Ez100) and Magnetic stirrer (Model-124, Hp-1/8, max. speed -4000rpm, India).

3.2 Materials Collection and Preparation

3.2.1 Sourcing of seeds

The fresh fruits were harvested from Onitsha City in Anambra State of Nigeria. Anambra State is located in the South Eastern part of Nigeria. Geographically, Anambra state is located between latitude 5° 37' 60N and longitude 7° 10' 0E with equatorial type of climate.

3.2.2 Seed preparation/size reduction

The fruits were washed properly with water and separated into seeds and pulp. The clean seeds were sun-dried in the open for 7 days (for African pear) while for sweet almond and African star apple, the hulls containing the seeds were sun dried for 5 days to ensure free movement of the seeds as an indication of readiness for smooth seed separation. The seeds were manually separated from hulls by cracking and the seeds collected were sun-dried in the open for 7 days. Electric powered milling machine was used to crush the seeds into meals. The ground meal was sieved using ASTEM 11-70, EML 200- Haver- Boecker mechanical siever to obtain a size of 1.18mm sieve size. The ground meal was further placed on solar dryer for a period of 3 days to remove residual moisture. The pictoral representation of the fruit biomass components are shown in Plates A1.1-A1.3.

3.3 Oil Extraction and Degumming

A known weight (3.5kg) of the dried meal of seed was packed in a big fractionating column up to three quarter level and n-hexane was poured well above the level of the meal in

the column. It was closed with aluminum foil and sealed with masking tape and then left for a period of 24h. The mixture of oil and solvent was collected from the bottom of the column with beaker. This was repeated to extract more oil from the meal. The oil was thereafter recovered using rotary evaporator to distill off the solvent. After distillation, the oil was left in the open to totally dry up the remaining solvent completely. The oils were degummed by mixing the crude oil with about 3% by weight of warm water and the mixture was agitated mechanically using magnetic stirrer for 30 minutes at 70°C. This hydrates the phospholipids and gums thus making them insoluble in the oil. These were thereafter separated by settling using separating funnel to remove the gums, phosphosphides and lysophasidic acids, which are strong emulsifiers that lower the yields of neutral (flavourless) oil. The percentage yield of oil was determined using Equation (3.1).

$$Oil\ yield\ (\%) = \frac{weig\,ht\ of\ oil\ after\ degumming}{weig\,ht\ of\ seed\ meal\ taken} x100 \qquad (3.1)$$

3.4. Physico-chemical Characterization of the Oil

The physico-chemical properties of the seed oils were determined in accordance with Association of Official Analytical Chemist (AOAC, 2000) method (the acid value by AOAC Ca5a-40, saponification value by AOAC 920:160; iodine value by AOAC 920:158 and peroxide value by AOAC 965.33). The viscosity and specific gravity measurements were made using the Ostwald viscometer thermostatted at 40°C and thermal-hydrometer apparatus following the ASTM standards D445 and D1298, respectively, the density by using density bottle, moisture content by oven method. The ash content was determined by heating to dryness in Veisfar muffle furnace and the refractive index was measured with Abbe refractometer (Model: WAY-25, Search tech. Instruments). The colour was measured with a Lovibond 2000 Comparator tintometer ($5^1/_4$ "glass cell Model E, the tintometer Ltd, Salisbury, U.K) in

accordance with AOAC, (2000). All the analyses carried out on the physico-chemical parameters the oil were done in triplicates and the mean values and standard deviations were calculated and provided.

3.5 Oil Oxidation Stability Model Development and Statistical Analysis

The choice of time and temperature for the oxidation stability test was based on preliminary reports obtained (Borchain *et al.,* 2012). Oven test was used to evaluate the oxidative stability for composite oil fractions. Oil sample (50 g) were kept in equal portions in open flasks (30 ml), 30 mm diameter and 70 mm (height) in the dark (away from sunlight) in an oven (rotary evaporator oven, model BTOV 1423, India) at 65 °C and at room temperature (25 °C) for 60 days. A repeat of the above set-up was carried out with an addition of tertiary butyl hydroquinone (TBHQ) in the ratio of 1000:1 of oil to TBHQ. The resistance against oxidation was evaluated by the peroxide value (PV) in accordance with AOCS, (2000) cd-25 method. Oxidative stability (OS) of the seed oils in percentage was evaluated using Equation (3.2) as applied by Oladimeji *et al.,* (2013).

$$OS = \frac{(PV_i - PV_j)}{PV_j} X100 \quad (3.2)$$

Where PV_i –the peroxide value of the seed oil with antioxidant, PV_j – the peroxide value of the seed oil without antioxidant.

The experimental data obtained was used to develop the model using Levernberg Marquadt (LM) algorithm (with 0.0001 tolerance) on MATLAB 8.5 software version 2015. The accuracy of the model was tested by determining the coefficient of determination (R^2), adjusted

R^2 (Adj. R^2), root mean squared error (RMSE) and residual sum of squares (RSS). These were carried out using Equation (3.3)-(3.6).

$$R^2 = 1 - \frac{\sum_{i=1}^{n}(Y_{ip} - Y_{ie})^2}{\sum_{i=1}^{n}(Y_{ip} - Y_{e})^2} \quad (3.3)$$

$$Adj.R^2 = 1 - [(1 - R^2) \times \frac{n-1}{n-K-1}] \quad (3.4)$$

$$RMSE = \sqrt{\frac{\sum_{i=1}^{n}(Y_{ie} - Y_{ip})^2}{n}} \quad (3.5)$$

$$RSS = \sum_{i=1}^{n}(Y_{ie} - Y_{ip})^2 \quad (3.6)$$

where K, is the number of input variables, n is the number of data sets, Yie and Yip are actual and predicted output values of ith set, respectively, and Ye is average of actual output values.

3.6 Biodiesel Production

3.6.1 Preheating the oil

The oil was heated at 80°C for 30 minutes using Gallenkamp magnetic stirrer thermostat hot plate (Weiss Technik, England) to reduce the viscosity of the oil.

3.6.2 Preparation of sodium methoxide

This was prepared by adding NaOH (2% weight of the oil) to 175ml of methanol and stirred at 200 rpm until it dissolved completely for about two minutes in the reaction vessel.

3.6.3 Transesterification reaction

The sweet almond seed oil and African star apple seed oil were subjected to direct base transesterification reaction while African pear seed oil was subjected to two-step transesterification because of its high FFA. The two-step transesterification involves esterification followed by base transesterification.

3.6.3.1 Esterification

The APSO acid transesterification (esterification) was necessary because of its high FFA. The esterification was carried out using 50ml of methanol and 0.2ml of concentrated H_2SO_4 mixed together inside a 250 ml conical flask. The conical flask was inserted into a water bath at 50˚C. The mixture was later added to 200ml warmed (preheated) African pear seed oil (APSO) inside a 500ml conical flask and placed on magnetic stirrer with heater, continuously stirred for 1 hour 30 minutes for the esterification to take place. The reversible esterification is represented in Equation (3.7) (Freedman *et al.*, 1986).

$$FFA + ROH \underset{k_{12}}{\overset{k_{11}}{\rightleftharpoons}} RCOOR + H_2O \quad (3.7)$$

3.6.3.2 Base transesterification

The SASO, ASASO and esterified APSO were subjected to base transesterification separately. The calculated amount of NaOH-catalyst (NaOH:oil of 2%w/w) and methanol (at 6:1 molar ratio of methanol to oil) was added to the reaction mixture set at 65°C temperature and allowed to stand for 65 minutes reaction time. The base transesterification was carried out using a 500 ml volume reflux condenser fitted with thermo-regulator heater and stirrer. One hundred milliliter of oil was measured into the flask and was heated to the specified temperature. All reactions were carried out at atmospheric pressure with 0.20 wt% sodium hydroxide as catalyst at a speed of 140 rpm.

3.6.4 Biodiesel separation

After the base transesterification process the reaction mixture was allowed to settle for 24hours inside a separating funnel to allow clear separation of biodiesel from glycerin by gravity. The layer on the top was the biodiesel while the bottom layer was the glycerol. Thereafter the two layers were separated by settling using separating funnel. The biodiesel separation was carried out by decanting as the glycerol was drained off while the biodiesel remained.

3.6.5 Biodiesel washing

Warm distilled water at 50°C was added to the separated biodiesel and the mixture was shaken vigorously. The water was allowed to drain through the bottom of the separating funnel. This was carried out five times until a clear biodiesel was obtained.

3.6.6 Biodiesel drying

Anhydrous $CaCl_2$ (1:5 $CaCl_2$ to biodiesel weight ratio) was added to the biodiesel and held (kept) in an oven at 50˚C for 30minutes. The anhydrous $CaCl_2$ was later separated from the biodiesel by filteration to obtain a clear dry biodiesel. The weight of the biodiesel obtained from each sample was determined while the percentage yield of biodiesel was calculated using Equation (3.8).

$$Biodiesel\ yield\ (\%) = \frac{M_{biodieslel}}{M_{seed\ \ oil}} x100 \qquad (3.8)$$

Where $M_{biodiesel\ \ = weig\,ht\ of\ \ biodiesel\ \ obtained\ \ after\ \ separation}$

$M_{seed\ \ oil = weig\,ht\ of\ \ seed\ \ oil\ used\ \ for\ \ the\ transesterification}$

3.6.7 Physico-chemical characterization of the biodiesel

The physico-chemical analyses of the seeds oil biodiesel were determined by ASTM and AOAC, (2000) standard methods. The kinematic viscosity was determined by ASTM D-445 method, the density was determined by ASTM D-1298 method and the pour point determination was made using ASTM D-97 method. The flash point of the fuel was determined by ASTM D-93, the value of cloud point was estimated according to ASTMD-2500 and Acid value was measured following the ASTM D-664 method. The refractive index was determined using AOAC 921.08. The specific gravity was ascertained using AOAC 920.212 and iodine value using AOAC 920:159. The sulfur content and calorific value were determined according to ASTM D-4294 and ASTM D-246 rspectively. The moisture content was obtained using air-oven method using the Rotary Evaporator Oven (BTOV 1423). The cetane index (CI) was determined using correlation given by Krisnamgkura (1986) (Equation 3.9) while the cetane number (CN) was calculated by the equation developed by Patel (1999) (Equation 3.10). The

higher heating values (HHV) were determined using correlation applied by Sivaramakrishnan and Ravikumar, (2012) (Equations 3.11 to 3.14).

$$CI = 46.3 + \left({}^{54.58}/_{SV}\right) - 0.25IV \quad (3.9)$$

$$\mathrm{CN} = \mathrm{CI} - 2.6 \quad (3.10)$$

$$\mathrm{HHV} = 0.0317\mathrm{V} + 38.053 \quad (3.11)$$

$$\mathrm{HHV} = 0.4625\mathrm{V} + 39.450 \quad (3.12)$$

$$\mathrm{HHV} = -0.0259\rho + 63.776 \quad (3.13)$$

$$\mathrm{HHV} = 0.021\mathrm{FP} + 32.12 \quad (3.14)$$

Where SV - saponification value, IV- iodine value, V-viscosity, ρ - density and FP – flash point

3.6.8 FT-IR analysis of the oil and biodiesel

FT-IR analysis was performed to monitor the functional groups in biodiesel samples produced from the seed oil. The mid infrared spectra of oil and biodiesel samples were obtained in Fourier transform spectrometer by IR Affinity-1 Shimadzu, model No: 3116465. The FT-IR has SN ratio of its class of 30,000:1, 1 minute accumulator in the neighborhood of 2,100cm^{-1} peak to peak with a maximum resolution of 0.5cm^{-1} in the region of 400cm^{-1}-4000cm^{-1}. It has microlab software as supporting software. The method of sample introduction was through sample cell. Cleaning of the cell was done with trisolvent mixture of acetone-toluene-methanol before background collection. About 0.5ml of the sample (oil or biodiesel) was taken using the sample cell and introduced into the cell unit of the system. The scan results were obtained on the incorporated computer system as spectra. The peaks of the spectra obtained were identified

and interpreted to identify the functional groups in the molecules of the oil and biodiesel with the aid of structure correlation chart (Furnish *et al.,* 1989).

3.6.9 GC-MS analysis of the biodiesel

The fatty acid composition of the biodiesel samples was analyzed by gas-chromatography coupled with mass spectrometer according to AOCS official method Ce 2-66. The gas chromatographic analysis was made using GC-MS-QP2010 plus, Shimadzu. The GC column used was calibrated by injecting methyl ester standards and good separations were achieved by diluting the sample in a small amount of ethyl acetate. The carrier gas used was hydrogen and its flow rate was regulated at 41.27ml/mins while the column flows at 1.82ml/mins. The oven temperature was set at 80ºC before rising up at 6ºC/min until 340ºC. The identification of peaks was done by comparison of their retention time and mass spectra with mass spectra library (NIST05s LIB.) (Fu *et al.*, 2008).

3.7 Optimization and Modeling of Biodiesel Production

The influence of operating conditions such as temperature, reaction time, catalyst concentration and methanol/oil molar ratio on the biodiesel yield and viscosity were studied by varying one of them and keeping the others at constant values. Also, Response surface methodology (RSM) and artificial neural network (ANN) were used for optimization and modeling of the biodiesel production process respectively.

3.7.1 Effect of operating parameters on yield and viscosity

The the optimum conditions for reaction time (45, 50, 55, 60, 65, 70 minutes), catalyst concentration (0.5, 1.0, 1.5, 2.0, 2.5, 3.0 wt%), methanol/oil molar ratio (3:1, 4:1, 5:1, 6:1, 7:1, 8:1) and reaction temperature (45, 50, 55, 60, 65, 70°C) for biodiesel yield and viscosity. The choice of values were based on some preliminary investigations while optimization of the transesterification variables were done by considering each of them at a time while keeping others constant (catalyst concentration of 1.5wt%, methanol/oil molar ratio of 5:1, reaction time of 60minutes and reaction temperature of 60°C). The mixing rate and pressure were kept at 140rpm and atmospheric pressure respectively.

3.7.2 Optimization using RSM techniques

3.7.2.1 Experimental design and statistical analysis by RSM

The experimental design was developed using response surface methodology (RSM). RSM utilizes mathematical and statistical techniques to perform modeling and analysis of problems in which a respose of interest is influenced by several variables. The objective is to optimize the response from the tested variables. A standard RSM design called a central composite design (CCD) was applied to develop the experimental design for esterification process of African pear seed oil and transesterification reaction process of the seed oils.

There are four main operating conditions that affect both esterification and transesterification reactions which are reaction time, methanol to oil molar ratio (transesterification) or methanol to FFA molar ratio (esterification), reaction temperature and catalyst concentration. Table 3.1 and 3.2 contain the levels and range of the four independent variables studied for esterification of APSO and transesterication processes respectively. The variables range was selected based on results obtained from preliminary studies and literature

(Awolu and Layokun, 2013). The complete design matrixes of the experimental runs conducted are given in Table 3.3 and 3.4 for esterification of APSO and transesterification processes respectively.

In this study, the best fitted model based on the model fit summary and statistics analysis for linear, two-factor interactions, quadratic and cubic models of the RSM is quadratic for both the esterification and transesterification reactions. The quadratic model had the least standard deviations, closest (<0.2) difference between R-squared, adjusted R-squared, and predicted R-squared, highest lack of fit p-value and least sequential p-value. Hence, a second-order (Equation 3.15) was chosen for both esterifications of APSO and transesterification processes of all the seed oils.

$$Y = a_0 + \sum_{i=1}^{k} a_i x_i + \sum_{i=1}^{k} a_{ii} x_i^2 + \sum \sum_{i=1}^{k} a_{ij} x_{ij} + e \quad (3.15)$$

Where a_0 is a constant, a_i is the linear coefficient, a_{ij}-interactive coefficients, X_i and X_{ij} are the uncoded independent variables and Y is the predicted response (% free fatty acid or % biodiesel yield). K is the number of factors studied and response, a_0, a_i, a_{ii} and a_{ij} are the regression coefficient obtained for constant, linear, quadratic and interaction terms respectively; x_i and x_j are independent variables optimized in the experiment and e is random error. Regression analysis and analysis of variance (ANOVA) were performed using Design Expert 7.0.0 version software. The fitted polynomial equations obtained from regressional analysis was used to develop the response surface plots.

Table 3.1: Factors and their levels of CCD for the esterification process.

Variable	Symbols	Coded levels				
		-2	-1	0	1	2
Temperature (°C)	A	55	60	65	70	75
Catalyst conc. (w/w %)	B	5	10	15	20	25
Reaction time (minutes)	C	45	50	55	60	65
Molar ratio of methanol: FFA	D	6:1	9:1	12:1	15:1	18:1

Table 3.2: Factors and their levels of CCD for the transesterification process.

Variable	Symbols	Coded levels				
		-2	-1	0	1	2
Temperature (°C)	A	30	40	50	60	70
Catalyst conc. (w/w %)	B	0.5	1.0	1.5	2.0	2.5
Reaction time (minutes)	C	45	50	55	60	65
Oil/methanol molar ratio (mol/mol)	D	1:3	1:4	1:5	1:6	1:7

Table 3.3: The CCD for five-level-four-factor response surface analysis.

Run	Factor 1 A (˚C)	Factor 2 B (wt %)	Factor 3 C(min.)	Factor 4 D(mol/mol)	Responses	
					Actual %FFA	Predicted %FFA
1	-1	-1	-1	-1	-	-
2	1	-1	-1	-1	-	-
3	-1	1	-1	-1	-	-
4	1	1	-1	-1	-	-
5	-1	-1	1	-1	-	-
6	1	-1	1	-1	-	-
7	-1	1	1	-1	-	-
8	1	1	1	-1	-	-
9	-1	-1	-1	1	-	-
10	1	-1	-1	1	-	-
11	-1	1	-1	1	-	-
12	1	1	-1	1	-	-
13	-1	-1	1	1	-	-
14	1	-1	1	1	-	-
15	-1	1	1	1	-	-
16	1	1	1	1	-	-
17	-2	0	0	0	-	-
18	2	0	0	0	-	-
19	0	-2	0	0	-	-
20	0	2	0	0	-	-
21	0	0	-2	0	-	-
22	0	0	2	0	-	-
23	0	0	0	-2	-	-
24	0	0	0	2	-	-
25	0	0	0	0	-	-
26	0	0	0	0	-	-
27	0	0	0	0	-	-
28	0	0	0	0	-	-
29	0	0	0	0	-	-
30	0	0	0	0	-	-

Table 3.4: The CCD for five-level-four-factor response surface analysis.

Run	Factor 1 A (^{o}C)	Factor 2 B (wt %)	Factor 3 C (mins)	Factor 4 D (mol/mol)	Responses	
					Actual biodiesel yield (%)	Predicted biodiesel yield (%)
1	40	1.0000	50	1:4000	-	-
2	60	1.0000	50	1:4000	-	-
3	40	2.0000	50	1:4000	-	-
4	60	2.0000	50	1:4000	-	-
5	40	1.0000	60	1:4000	-	-
6	60	1.0000	60	1:4000	-	-
7	40	2.0000	60	1:4000	-	-
8	60	2.0000	60	1:4000	-	-
9	40	1.0000	50	1:6000	-	-
10	60	1.0000	50	1:6000	-	-
11	40	2.0000	50	1:6000	-	-
12	60	2.0000	50	1:6000	-	-
13	40	1.0000	60	1:6000	-	-
14	60	1.0000	60	1:6000	-	-
15	40	2.0000	60	1:6000	-	-
16	60	2.0000	60	1:6000	-	-
17	30	1.5000	55	1:5000	-	-
18	70	1.5000	55	1:5000	-	-
19	50	0.5000	55	1:5000	-	-
20	50	2.5000	55	1:5000	-	-
21	50	1.5000	45	1:5000	-	-
22	50	1.5000	65	1:5000	-	-
23	50	1.5000	55	1:3000	-	-
24	50	1.5000	55	1:7000	-	-
25	50	1.5000	55	1:5000	-	-
26	50	1.5000	55	1:5000	-	-
27	50	1.5000	55	1:5000	-	-
28	50	1.5000	55	1:5000	-	-
29	50	1.5000	55	1:5000	-	-
30	50	1.5000	55	1:5000	-	-

3.7.2.2 Development of artificial neural network (ANN)

ANN model is developed using MATLAB 8.5 software, 2015 version. A consolidated data set comprising of thirty (30) and twenty five (25) data sets for esterification and transesterification respectively were compiled and parameters like temperature at which the reaction is carried out, the time of reaction in minutes, the catalyst concentration as weight percent and the oil to methanol ratio were used as the independent input parameters. In this study, a three-layered feed-forward neural network with tangent sigmoid transfer function (tansig) at hidden layer and linear transfer function (purelin) at output layer was used. The sigmoid transfer function is given by Equation (3.16) and the linear activation function by Equation (3.17).

$$f(x) = 2[\frac{1}{1+e^{-2x}}] - 1 \tag{3.16}$$

$$f(x) = x \tag{3.17}$$

In the esterification process, the models developed are used for the production of the one dependent parameter: the free fatty acid reduction in each of the 30 independent runs. The backpropagation algorithm was used for network training, 66 percent of the data was taken for training set, 17 percent for validation and the rest of the data (17 percent) for the test set.

Considering the transesterification process, the models developed are used for the production of the one dependent parameter: the biodiesel yield in each of the 25 independent runs. The backpropagation algorithm was used for network training, 52 percent of the data was taken for training set, 13 percent for validation and the rest of the data (35 percent) for the test

set. The accuracy of the model was determined by using equations (3.18) to (3.20) as applied by Ahmadian -Morghadam *et al.,* (2013).

$$MAD = \sum_{i=1}^{n}(\left|\text{yi} - \text{y\^{}i}\right|)/\text{n} \quad (3.18)$$

$$MAPE = \sum_{i=1}^{n}\{(\left|\text{yi} - \text{y\^{}i}\right|)/\text{yi}\}/n \quad (3.19)$$

$$MSE = \sum_{i=1}^{n}\{(\left|\ \text{y\^{}i} - \text{yi}\ \right|)\text{\^{}}2\}/n \quad (3.20)$$

Where MSE – mean squared error

MAD - mean absolute deviation

MAPE - mean absolute percentage error

yi – actual biodiesel yield (%)

y^i - predicted biodiesel yield

3.8 Engine Performance, Pollutant Emission and Combustion Evaluation

A four-stroke, four-cylinder, water-cooled and direct-injection Perkins 4:108 diesel engine connected to an eddy current dynamometer which develops a power output of 112kW was used to study the performance, emission and combustion characteristics of the biodiesel, petrol-diesel and their blends. This is to ascertain the viability of using the biodisesel samples and their blends as alternative fuel to petrodiesel. The engine specifications are given in Table 3.5.

3.8.1 Precautions, preliminary checks and measurements

A rapid examination of the test bed was made. The positions of all controls were noted and such features such as the engine throttle and stop control were checked for correct functioning. The state of fuel supply, lubricant and cooling water were checked by starting the

pumps without the engine running. The ambient air temperature (Ta) and barometric pressure (Pa) were measured using thermometer and anaeroid barometer respectively.

Ambient temperature (Ta) = 28˚C = 301K

Barometric pressure, (Pa) = 0-95bar = 95kN/m^2

Gas constant for air (Ra) = 287J/kgK

Swept volume (given in the engine description manual) = 1.76 l/cycle

3.8.2 Dynamometer measurements

The diesel engine is clamped to a test bed and its shaft is connected to the hydraulic dynamometer. The torque exerted by the engine through the turning rotor is shown by the dynamometer dial indicator. When the engine torques exceeds 80Nm, weights graded in torque values are placed on the scale provided on the end of the spring scale as a support for the circular scale. The total torque (T) is calculated as shown in Equation (3.16). The brake power (bp) calculated by the dynamometer reading is given on the dynamometer circular scale. To increase the load on the engine, the wheel is rotated in the clockwise direction while rotating it in the anti-clockwise direction reduces the load on the engine.

3.8.3 Engine performance measurement

The water pumps to the engine and dynamometer were turned on after ambient temperature and pressure. Then, the biofuel blends density and calorific values were measured as stated in sections 3.4 and 3.6.7 respectively. The engine was connected to the battery terminal. The start button was pressed while the choke is in return position. The throttle was then placed at relative low speed (800rpm) and allowed to run idly for about 15minutes to attain

a uniform temperature. The value of the torque was recorded. The time for 50cm^3 of the fuel to be consumed at the speed of 1500rpm was measured by using the stopwatch.This is done by measuring the time for the fuel to move between appropriate spacers while the supply-tank fuel gauge is turned off. The manometer reading, exhaust temperature, oil temperature and oil pressure were measured. Also the readings on the two water systems for both engine and dynamometer namely: the water inlet temperature, water outlet temperature and water flow rate/head were measured. The process starting from recording the torque was repeated for higher torque values: 10, 20, 30, 40Nm. The parameters like, fuel volume flow rate, mass flow rate, air volume flow rate, brake power, brake mean effective pressure, swept volume, volumetric efficiency, brake thermal efficiency, specific fuel consumption, air/fuel ratio etc were calculated using Equations (3.21) to (3.37) as applied by Jindal *et al.*, (2013).

3.8.4 Engine combustion emission

The emissions characteristics from the exhaust were measured using Bacharach PCA_2-15068 model emission gas analyzer thong at the exhaust pipe end of the diesel engine. The digital gas analyzer records the amount of the each gas and temperature from the composite exhaust stream. The gas analyzer specifications are contained in Table 3.6.

Table 3.5: The CI engine specification.

S/n	Description	Specification
1	Make and Model	Perkins 4:108 (Plint and Paster)
2	Type	Four cylinder, vertical, direct injection, variable speed, water cooled stroke diesel engine
3	Bore	79.735mm
4	Stroke	88.90mm
5	Stroke length	0.089m
6	Compression ration	22.1
7	Orifice diameter	58.86cm
8	Maximum BHP	38
9	Power	112kW/150hp
10	Rated speed	1500-4000rpm
11	Loading device	Eddy current dynamometer
12	Injection pressure (barometer pressure)	0.95bar
13	Swept volume	1.76l/cycles
14	Engine number	108us7258
15	Dynamometer type	Heenam and Erdude, DP x 2 (Hydrauche)
16	Dynamometer capacity	112kw/150hp
17	Dynamometer maximum speed	7500rpm
18	Dynamometer centre height	2B x 337451
19	Dynamometer centre height	14.5″
20	Fuel gauge capacity	50,100,200cm^3
21	Drum size (water flow meter)	42″ x 27″
22	Exhaust pipe length	36″
23	Exhaust pipe diameter	3/2″
24	Indicator tapping	14mm in ND: 4 cylinder head
25	Coefficient discharge	0.6

Table 3.6: Operating conditions of the gas emission analyzer.

SN	Item	Condition
1	Model	Baracharach, PCA_2 No. 235, P/N 24-7305, S/N- QS1007, P.A 15068, New Kensington, USA
2	Weight	1.4 lb-analyzer, 0.5kg-probe
3	Dimensions	9H x 3W x 2.5D inch (22.9 x 7.6 x 6.3cm)
4	Operating conditions	
	Temperature	0-40°C (analyzer), 80°C max (probe tip)
	Humidity	15-90% relative humidity, non – condensing
	Air pressure	Atmospheric (analyzer), 10″ H_2O draft max (probe tip)
5	Power requirement	100-240VAC, 50/60Hz
6	Warm up time	60 seconds
7	Memory	500 complete combustion lest records
8	Interface	Printer – infrared (IrDA)/computer USB

$$T = T_R + T_W \tag{3.21}$$

$$\text{Brake mean effective pressure (Bmep)} = \frac{2b_p}{LANn} \tag{3.22}$$

$$= 675.82\frac{bp}{N} \tag{3.23}$$

$$\text{Volume flowrate (Va)} = \frac{\pi D^2}{4} \times K_D \times \frac{\sqrt{2\times 9.81\times hwRaTa}}{Pa} \tag{3.24}$$

$$= 0.00621\sqrt{hw} \tag{3.25}$$

$$\text{Mass flowrate (Ma)} \quad = \frac{P_a}{R_a T_a} \times \frac{\pi D^2}{4} \times K_D \sqrt{\frac{2\times 9.81\times hw R_a T_a}{P_a}} \tag{3.26}$$

$$= \quad 0.00683\sqrt{hw} \tag{3.27}$$

$$\text{Brake thermal efficiency } (\eta_{BT}) = \frac{bp}{mf Q_{net,v}} \tag{3.28}$$

$$\text{Swept volume } (V_s) = 1.76 \times 10^{-3} m^3/_{cycle} \tag{3.29}$$

$$\text{Swept volume } (V_s) = 0.00002933 Nm^3/s \tag{3.30}$$

$$\text{Fuel mass flowrate } (M_f) = \rho_f V_f \tag{3.31}$$

$$\text{Fuel volume flowrate } (V_f) = \frac{V}{t} \tag{3.32}$$

$$\text{Brake power } (b_p) = \frac{T\times N}{9549.305} \tag{3.33}$$

$$\text{Volumetric efficiency } (\eta_v) = \frac{V_a}{V_s} \tag{3.34}$$

$$\text{Brake specific energy consumption (BSEC)} = (\text{BSFC x } Q_{net,v})/100 \quad (3.35)$$

$$\text{Brake specific fuel consumption (BSFC)} = \frac{3600\,M_f}{b_p} \quad (3.36)$$

$$\text{Air} - \text{fuel ratio (A/F)} = \frac{M_a}{M_f} \quad (3.37)$$

Where: T_R- Torque reading from the spring dial, T_W -Torque indicated on the weight, b_p-brake power, D-cylinder bore, n-cylinder number, h_w-manometer depression, K_D-coefficient of discharge, Ta- ambient temperature, P_a-barometric pressure, R_a-gas constant for air, ρ_f-density of diesel fuel, T- engine torque, N-engine speed, L-piston stroke.

3.8.5 Performance, emission and combustion process optimization and modeling

In order to optimize the diesel engine performance and combustion emission characteristics, some modeling and optimization techniques were applied. The techniques used for the optimization were response surface methodology-genetic algorithm (RSM-GA) and Nelder-Mead (NM) simplex optimization technique. Also, multi-input multi-output artificial neural network (MIMO-ANN) was applied to model the processes. The response variables chosen were brake thermal efficiency (%), brake specific fuel consumption (Kg/kW-hr), carbon monoxide (%vol.), oxides of nitrogen (ppm) and hydrocarbon (ppm) emissions. The independent variables considered were engine load, fuel blend and engine speed.

3.8.5.1 Response surface methodology

A five –level three-factor central composite experimental design (CCD) was used in this study. Engine speed, load and fuel blend were the input variables. The factor levels were coded as -2 to +2 as shown in Table 3.7 with six axial points and six replications at the centre points leading to a total number of 20 experiments (Table 3.8).

Table 3.7: Independent variables in the experimental plan for CCD.

Variables		Coded levels				
		-2	-1	0	1	2
Load (Nm),	A	5	10	15	20	25
Fuel blend (% Vol.)	B	20	40	60	80	100
Speed (rpm)	C	1500	2000	2500	3000	3500

Table 3.8: CCD for five-level three-factor response surface analysis for engine combustion optimization.

Run	Factor A (Nm)	Factor B (%Vol.)	Factor C (rpm)	Responses				
				BTE (%)	BSFC (Kg/kW-hr)	CO (%Vol.)	NOx (ppm)	HC (ppm)
1	-1	-1	-1	-	-	-	-	-
2	-1	1	1	-	-	-	-	-
3	1	-1	1	-	-	-	-	-
4	1	1	-1	-	-	-	-	-
5	0	0	0	-	-	-	-	-
6	0	0	0	-	-	-	-	-
7	-1	-1	1	-	-	-	-	-
8	-1	1	-1	-	-	-	-	-
9	1	-1	-1	-	-	-	-	-
10	1	1	1	-	-	-	-	-
11	0	0	0	-	-	-	-	-
12	0	0	0	-	--	-	-	-
13	-2	0	0	-	-	-	-	-
14	2	0	0	-	-	-	-	-
15	0	-2	0	-	-	-	-	-
16	0	2	0	-	-	-	-	-
17	0	0	-2	-	-	-	-	-
18	0	0	2	-	-	-	-	-
19	0	0	0	-	-	-	-	-
20	0	0	0	-	-	-	-	-

Experimental data from CCD was analyzed using regression of Design Expert 7.0.0 version software. If a response is well modeled by a linear function of independent variables,

then the approximating function is the first-order model. If there is curvature in the system, then a polynomial of higher degree must be used, such as the second-order model (Silva et al., 2011). In this study, consideration was given to the summary of the model fit statistics result of the RSM linear, two-factor interactions, quadratic and cubic models. The quadratic model was suggested and selected by the Design Expert 7.0.0 software based on relevant criteria. Hence a second-order polynomial model (Equation (3.38)) was chosen.

$$Y = a_0 + \sum_{i=1}^{k} a_i x_i + \sum_{i=1}^{k} a_{ii} x_i^2 + \sum \sum_{i=1}^{k} a_{ij} x_{ij} + e \quad (3.38)$$

Where Y is the response variable, i and j are the linear and quadratic coefficient, respectively. K is the number of factors studied and response, a_0, a_i, a_{ii} and a_{ij} are the regression coefficient obtained for constant, linear, quadratic and interaction terms respectively; x_i and x_j are independent variables optimized in the experiment and e is random error.

3.8.5.2 RSM - genetic algorithm

The RSM models were tuned with genetic-algorithm for better optimized responses. Flowchart of the algorithm is shown in Figure 3.1 and the variables associated with the implementation of these procedures done in software are exposed in Table 3.9.

Table 3.9: Set genetic algorithm.

Functions mutations	Heuristic
Type of population	Bit string
Selection function	Stochastic uniform
Inheritance of	0.8
Population size	100^{th}

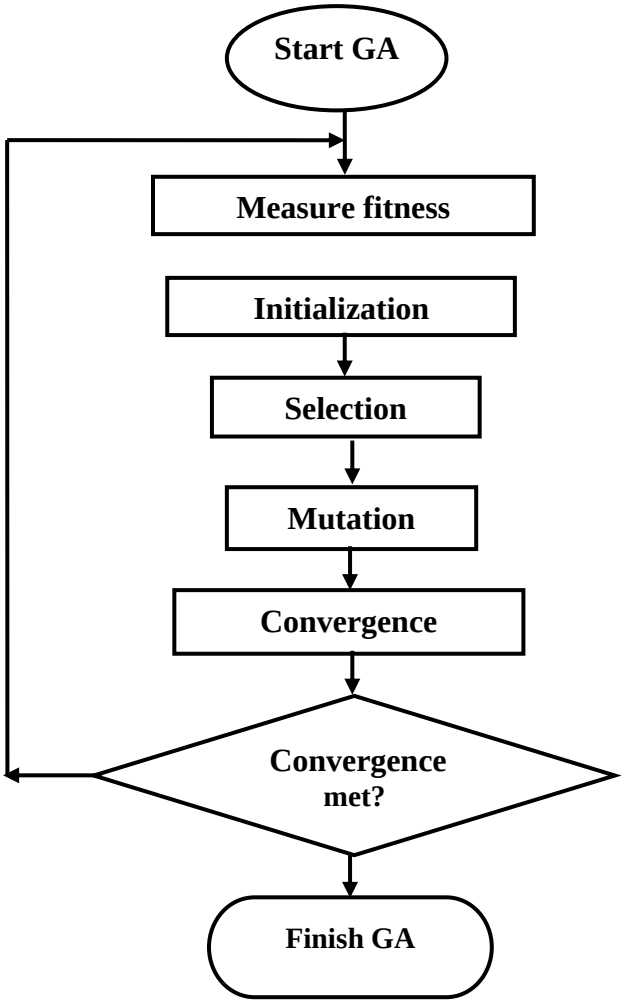

Figure 3.1: Flowchart of genetic algorithm.

3. 8. 5. 3 Development of artificial neural network (ANN)

A consolidated data set comprising of twenty(20) data set are compiled and parameters like fuel blend, load and speed were used as the independent input parameters. Neural network tool box V4 of MATLAB 8.5 version mathematical software was used for responses prediction by applying supervised learning paradigm. Levenberg Marquardt (LM) training algorithm on back propagation was used based on multi-input multi–output (MIMO) principle. In this study, multi-layer perception of three-layered feed-forward (MLPFFN) neural network with

hyperbolic tangent sigmoid transfer function (tansig) at hidden layer and logarithm sigmoid function (logsig) at output layer was used. The hyperbolic tangent and logarithmic sigmoid functions are presented in Equations (3.39) and (3.40) respectively.

$$f(x) = \frac{e^{x}-e^{-x}}{e^{x}+e^{-x}} \tag{3.39}$$

$$f(x) = \frac{1}{1+e^{-x}} \tag{3.40}$$

The output (y_i) of the ANN model is given as in Equation (3.41).

$$Y_j = f\left[\sum_{i=0}^{d(i-1)}(w_{ij}^{l} X_i^{l-1})\right] \tag{3.41}$$

Where *f* is a simple threshold function, *d* is the dimension of the network, *l* represents the number of layers and *l* w_{ij}^{l} is the weight which belongs to network with *l* layer, *i* input and *j* hidden layers. Equation (3.42) shows the mathematical representation of the ANN model weights.

$$W_{ij}^{l} \in \begin{cases} 1 \le l \le L\ layers \\ 0 \le i \le d^{l-1}\ input \\ 1 \le j \le d^{l}\ output \end{cases} \tag{3.42}$$

The models developed are used for the production of the five dependent parameters: brake thermal efficiency, brake specific fuel consumption and three emission characteristics (CO, NOx, and HC) in each of the 20 independent runs. ANN model is developed using MATLAB 8.5 version 2015 software. The propagation algorithm was used for network training, 70 percent of the data was taken for training set, 15 percent for validation and 15 percent of the data for the test set. Figure 3.2 represents the schematic flowchart of the proposed methodology.

Optimum neural network architecture is proposed by varying the number of hidden layers, transfer functions and number of neurons in each hidden layer. Deciding the optimum ANN architecture is often tricky as there is always a chance of picking up inconsistent patterns and also a risk of premature convergence during the optimisation of the weight and bias terms of the FFNN. Therefore multiple randomisation of the optimiser with different initial guess and multiple shuffles of the data segmentation in training, validation, testing sets have been adopted here to enable higher accuracy. The accuracy of the models was determined by using coefficient of correlation (R^2), root mean squared error (RMSE), standard error of prediction (SEP) and average absolute deviation (AAD) (Equations (3.43)-(3.47)) as applied by Sarve, *et al.*, (2015).

$$R^2 = 1 - \frac{\sum_{i=1}^{n}(Y_{ip} - Y_{ie})^2}{\sum_{i=1}^{n}(Y_{ip} - Y_e)^2} \tag{3.43}$$

$$RMSE = \sqrt{\frac{\sum_{i=1}^{n}(Y_{ie} - Y_{ip})^2}{n}} \tag{3.44}$$

$$SEP = \frac{RMSE}{Y_e} \times 100 \tag{3.45}$$

$$AAD = \frac{100}{n}\sum_{i=1}^{n}\frac{|Y_{ip} - Y_{ie}|}{|Y_{ie}|} \tag{3.46}$$

Where Y_{ie} is the experimental data, Yip is corresponding data predicted, Y_e is the mean value of experimental data and n is the number of experimental runs.

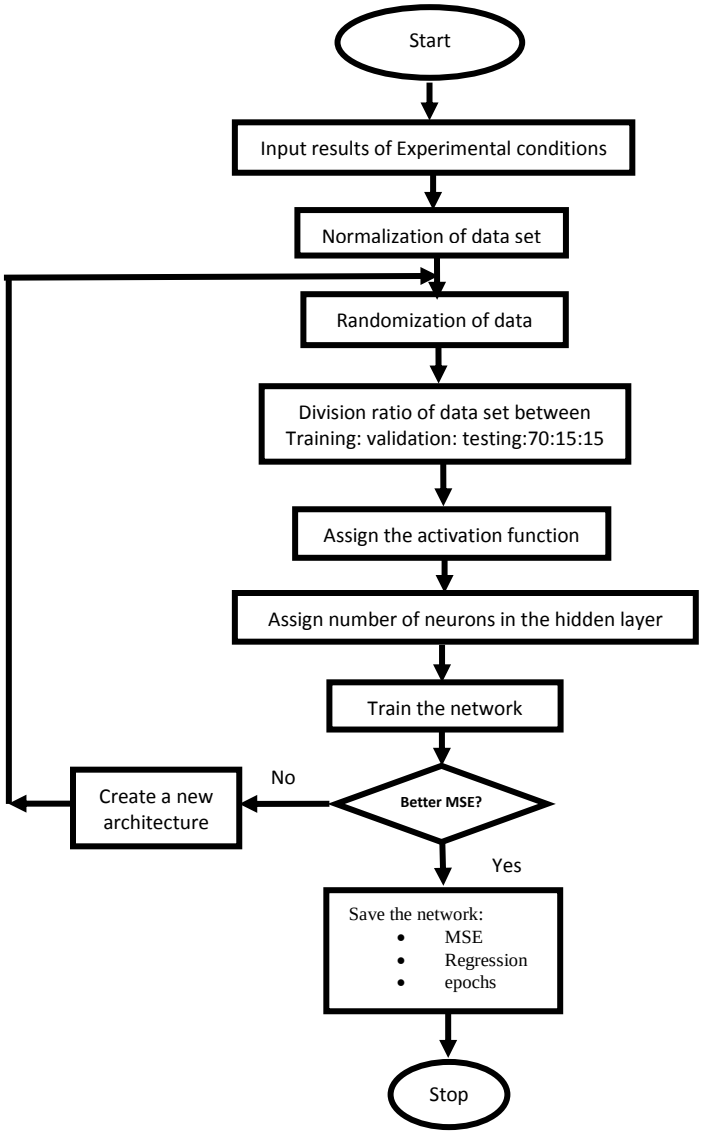

Figure 3.2: The flowchart of the ANN.

3.8.5.4 Nelder-Mead global optimization technique

The Nelder-Mead's simplex method is one of the most popular derivative free optimization algorithms in the fields of engineering, statistics, and sciences. This algorithm is favored and widely used because of its fast convergence and simplicity. The simplex method converges really well with small scale problems of some variables. It is the prime choice algorithm in Matlab optimization toolbox. The experimental data from the CCD was analyzed

using regression of Wolfran mathematica software, 2017 version and fitted to a second order polynomial model (Equation 3.31) and Nelder-Mead downhill optimization simplex technique was used to optimize the objective functions (BTE, BSFC, CO, NOx and HC). Moreover, the convergence speed of this algorithm depends on three parameters: the reflection coefficient that defines how far a reflected point should be from a centroid point; the contraction coefficient which defines how far a contracted point should be when it is contracted from the worst point and the reflected point in case the function value of the reflected point is smaller than the function value of the worst point and the expansion coefficient to define how far to expand from the reflected point in case a simplex moves on the right direction. The Nelder-Mead's simplex method algorithm can be summarized by the following steps (Nam, 2012) while more details are reported by Nelder and Mead, (1965).

Step 1: Get an initial simplex with random vertices and calculate their function values.

Step 2: Sort the vertices of the current simplex in the ascending order.

Step 3: Calculate the reflected points.

Step 4:

(a) Calculate the extended points.

(b) Replace the worst point by the extended points.

(c) Replace the worst point by the reflected points.

Step 5:

(a) Replace the worst point by the reflected points.

(b) Calculate the contracted points.

(c) Shrink the simplex.

(d) Then replace the worst points by the contracted points or replace the worst point by the reflected points.

Step 6: If the stopping conditions are not satisfied, the algorithm will return to step 2.

The experimental runs are shown with their co-ordinates on the simplex and in so doing in the boundary space of combinations required. The relative proportions of the components in each combination are properly described in the simplex (Figure 3.3) which represents the simplex of two dimensions which is an equilateral triangle.

The best match between the experimental results and the model predictions was determined on the basis of the residual norm (r) (Equation (3.47)), variance (S^2) (Equation (3.48)) and coefficient of determination (R^2).

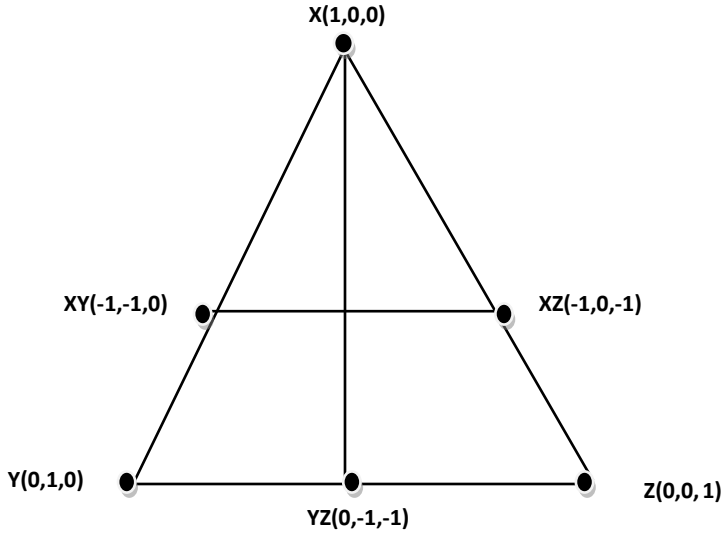

Figure 3.3: Factor notations on the simplex.

$$r = \sum_i (Y_{ip} - Y_{ie})^2 \quad (3.47)$$

$$S^2 = \frac{\sum (Y_{ip} - Y_e)^2}{n-1} \quad (3.48)$$

3.9 Chemical Kinetic Study

The rate of reaction and its mechanism as regards to the transesterification process of the three seed oils were investigated by considering both reversible and irreversible conditions.

3.9.1 Kinetics reaction conditions and sample analysis

The esterification process to convert the free fatty acid of African pear seed oil (APSO) into ester involved heating a known weight of African pear seed oil to the desired reaction temperature (55, 60 or 65 °C) and methanol was slowly added. The reactants were mixed for about 5 minutes before the required amount of concentrated sulphuric acid was added slowly and carefully as the catalyst. The molar ratio of methanol to FFA is 60:1 and with 5 wt% of sulphuric acid based on the FFA concentration (Berrios et al., 2007). The 4l-round bottomed flask was used. The remaining process conditions followed the approach applied in (Jansri et al., 2011) but the sampling time intervals in this study were 0, 0.3, 0.5, 2, 4, 6, 10, 20, 40, 60, 80 and 100 minutes while the speed of 140rpm was set for the stirrer. The amount of water in the esterification product was determined using Karl Fischer titration method (Jansri et al 2011).

The transesterification experiments were designed to determine the reaction rate constants and activation energies. A 6:1 molar ratio of methanol to SASO, esterified APSO and ASASO was used in all the experiments. To examine the temperature dependency of the

reaction rate constants, reactions at 55, 60 and 65 ˚C were studied. All reactions were carried out at atmospheric pressure with 0.20 wt% sodium hydroxide as catalyst and constant agitation of 140 rpm. During the course of experiment, 2 ml aliquot of the reaction mixture sample was withdrawn with a disposable pipette through an opening on the top of the reactor. The samples were collected in 10ml test tubes and kept in an ice bath at 5 ˚C prior to use in order to stop the reaction. Samples were withdrawn at the same specified time intervals as applied in the esterification process. The composition of sample was determined by GC on Perkin Elmer Claurus 600 model FID to ascertain the amount of triglycerides, diglycerides, monoglycerides, total methyl esters and glycerol in the biodiesel production batch reaction system. The GC specification is presented in Table 3.10.

Three different mixing intensities (200, 400 and 800 rpm) were used to investigate the effect of stirring rate on the rate of transesterification reaction. The rotational speed of the impeller was reset to 200 rpm, 400 rpm and 800 rpm, for reaction time of 100 minutes, temperature of 60 °C, methanol / oil molar ratio of 6:1 and 1.5 wt% catalyst concentrations. The reaction conditions followed those applied by Jansri et al., (2011) but the impeller speed was reset to 200 rpm, 400 rpm and 800 rpm.

Table 3.10: Operating conditions of gas chromatography analysis

SN	Item	Condition
1	Column	5"x1/4" internal diameter (i.d), glass column packed with 10 % silica 10 °C on 80-100mesh chromasorb HP at a temperature of 180 °C.
2	Detector	Flame Ionization Detector (FID),
3	Column temperature	185 °C (set point = 150 °C , increment = 35 °C)
4	Nitrogen flowrate	30 ml/min.
5	Hydrogen flowrate	20 ml/min
6	Air Pressure	12 lb/in^2
7	Sample size	0.3 µl
8	Attenuation	$2x10^4$
9	Backing off range	x100

3.9.2 Kinetic models and estimation of the rate constants

The mechanisms used to model the kinetics of transesterification are commonly (a) a three-step reaction mechanism and (b) a single-step reaction mechanism (Kumar *et al.*, 2011). The reversible esterification reaction is represented in Equation (3.49) (Freedman 1986). According to Noureddini and Zhu (1997) the mechanism of transesterification includes three consecutive reversible reactions yielding diglycerides and monoglycerides as intermediates. Equations (3.49) - (3.52) represent the stages of the reaction while Equation. (3.53) is the summary.

$$FFA + R'OH \underset{k_{12}}{\overset{k_{11}}{\rightleftharpoons}} RCOOR + H_2O \tag{3.49}$$

Where: FFA, R′OH, R′COOR and H_2O are free fatty acid, methanol, fatty acid methyl ester and water respectively.

$$Tg + R^{'}OH \underset{k_2}{\overset{k_1}{\rightleftharpoons}} Dg + FAME \tag{3.50}$$

$$Dg + R^{'}OH \underset{k_4}{\overset{k_3}{\rightleftharpoons}} Mg + FAME \tag{3.51}$$

$$Mg + R^{'}OH \underset{k_6}{\overset{k_5}{\rightleftharpoons}} Gl + FAME \tag{3.52}$$

$$\begin{matrix} CH_2OCOR \\ CHOCOR \\ CH_2OCOR \end{matrix} + 3ROH \leftrightarrow \begin{matrix} CH_2OH \\ CHOH \\ CH_2OH \end{matrix} + \begin{matrix} R'COOR \\ R''COOR \\ R'''COOR \end{matrix} \tag{3.53}$$

Triglycerides Alcohol Glycerol FAME

Where Mg, Dg, Tg, Gl, FAME and R′OH are monoglycerides, diglycerides, triglycerides, glycerol, fatty acid methyl ester and alcohol respectively.

3.9.3 Second-order reversible mechanism

Since both esterification and transesterification reaction stages are reversible and overall second-order (Jansri *et al.*, 2011), the rate equations that describe the disappearance of the species are presented in Eqs.(3.56-3.63).

$$\frac{\mathrm{d[FFA]}}{\mathrm{dt}} = -k_{11}[\mathrm{FFA}][\mathrm{Al}] + k_{12}\,[\mathrm{FAME}][\mathrm{Wt}] \tag{3.54}$$

$$\frac{\mathrm{d[Wt]}}{\mathrm{dt}} = k_{11}[\mathrm{FFA}][\mathrm{Al}] - k_{12}\,[\mathrm{FAME}][\mathrm{Wt}] \tag{3.55}$$

$$\frac{\mathrm{d[Tg]}}{\mathrm{dt}} = -k_{1}[\mathrm{Tg}][\mathrm{Al}] + k_{2}\,[\mathrm{Dg}][\mathrm{FAME}] \tag{3.56}$$

$$\frac{\mathrm{d[Dg]}}{\mathrm{dt}} = k_{1}[\mathrm{Tg}][\mathrm{Al}] - k_{2}\,[\mathrm{Dg}][\mathrm{FAME}] - k_{3}\,[\mathrm{Dg}][\mathrm{Al}] + k_{4}\,[\mathrm{Mg}][\mathrm{FAME}] \tag{3.57}$$

$$\frac{\mathrm{d[Mg]}}{\mathrm{dt}} = k_{3}[\mathrm{Dg}][\mathrm{Al}] - k_{4}\,[\mathrm{Mg}][\mathrm{FAME}] + k_{5}\,[\mathrm{Mg}][\mathrm{Al}] - k_{6}\,[\mathrm{Gl}][\mathrm{FAME} \tag{3.58}$$

$$\frac{\mathrm{d[Gl]}}{\mathrm{dt}} = k_{5}[\mathrm{Mg}][\mathrm{Al}] - k_{6}\,[\mathrm{Gl}][\mathrm{FAME}] \tag{3.59}$$

$$\frac{\mathrm{d[FAME]}}{\mathrm{dt}} = k_{1}[\mathrm{Tg}][\mathrm{Al}] - k_{2}\,[\mathrm{Dg}][\mathrm{FAME}] + k_{3}\,[\mathrm{Dg}][\mathrm{Al}] - k_{4}\,[\mathrm{Mg}][\mathrm{FAME}] + k_{5}\,[\mathrm{Mg}][\mathrm{Al}] - k_{6}\,[\mathrm{Gl}][\mathrm{FAME}] \tag{3.60}$$

$$\frac{\mathrm{d[Al]}}{\mathrm{dt}} = -\frac{\mathrm{d[FAME]}}{\mathrm{dt}} \tag{3.61}$$

Where [FFA], [Wt], [Tg], [Dg], [Mg], [Gl]. [Al] and [FAME] are concentrations of free fatty acids, water, triglycerides, diglycerides, monoglycerides, glycerol, alcohol and methyl esters respectively in the reaction mixture.

Differentiations of the concentrations with respect to time on the left hand side of Equations (3.54)-(3.61) were estimated from the slopes of experimental concentration-time curves at various reaction times using three-point method (Figures A7.1 – A7.3). The general

fitted regression model equations for esterification and transesterification are presented in Equations (3.62) and (3.63) respectively.

$$Y = At^{(x)} \tag{3.62}$$

$$Y = Y_0 + Aexp^{(\frac{t}{x})} \tag{3.63}$$

Where Y is the concentration of the species, $Y_{0,}$ A and x are model constants and the, t is time of reaction. The equation was further differentiated to get the slope of the fitted curve which corresponds to the differentiation of the concentrations with respect to time as they appeared on the right hand side of Equation (3.64) and (3.65). The second order differential systems of equation were transformed appropriately and resolved using least-squares regression technique with GNU Octave software version 4.03, 2016.

$$\begin{bmatrix} -a_{11} & a_{12} \\ a_{21} & -a_{22} \end{bmatrix} \begin{bmatrix} k_{11} \\ k_{12} \end{bmatrix} = \begin{bmatrix} \frac{dFFA}{dt} \\ \frac{dWt}{dt} \end{bmatrix} \tag{3.64}$$

$$\begin{bmatrix} -a_{11} & a_{12} & 0 & 0 & 0 & 0 \\ a_{21} & -a_{22} & -a_{23} & a_{24} & 0 & 0 \\ 0 & 0 & a_{33} & -a_{34} & a_{35} & -a_{36} \\ 0 & 0 & 0 & 0 & a_{45} & -a_{46} \\ a_{51} & -a_{52} & a_{53} & -a_{54} & a_{55} & -a_{56} \\ -a_{61} & a_{62} & -a_{63} & a_{64} & -a_{65} & a_{66} \end{bmatrix} \begin{bmatrix} k_1 \\ k_2 \\ k_3 \\ k_4 \\ k_5 \\ k_6 \end{bmatrix} = \begin{bmatrix} \frac{\mathrm{dTg}}{\mathrm{dt}} \\ \frac{\mathrm{dDg}}{\mathrm{dt}} \\ \frac{\mathrm{dMg}}{\mathrm{dt}} \\ \frac{\mathrm{dGl}}{\mathrm{dt}} \\ \frac{\mathrm{dFAME}}{\mathrm{dt}} \\ \frac{\mathrm{dOH}}{\mathrm{dt}} \end{bmatrix} \tag{3.65}$$

Where a_{11} –a_{66} are measured data points (concentrations); the dependent variables are the differentials of concentrations on the right hand side of Equation (3.64) and (3.65) and k_{11}, k_{12}, k_1, k_2, k_3, k_4, k_5 and k_6 are the rate constants. Rearranging Equation (3.64) (esterification) and Equation (3.65) (transesterification) according to Gauss-Jordan elimination method (Okullo and Temu, 2015, Kreyzig, 1999) and resolving gave the values of rate constants in dm^3/g.min.

3.9.4 Irreversible mechanism

Two models, pseudo second- and first-order models were considered under the irreversible transesterification mechanism.

3.9.4.1 Pseudo-second order irreversible model

According to kinetic studies of transesterification reaction in the literature, the mechanism includes three consecutive irreversible (Darnoko and Cheryan, 2000) reactions yielding fatty acid diglycerides and monoglycerides as intermediates. Equation (3.69) is the summary of Equation (3.66) to (3.68), which represents the stages of the reaction.

$$Tg + R'OH \xrightarrow{k_1} Dg + FAME \tag{3.66}$$

$$Dg + R'OH \xrightarrow{k_2} Mg + FAME \tag{3.67}$$

$$Mg + R'OH \xrightarrow{k_3} Gl + FAME \tag{3.68}$$

$$\underset{\text{Triglycerides}}{\begin{matrix}CH_2OCOR\\CHOCOR\\CH_2OCOR\end{matrix}} + \underset{\text{Alcohol}}{3ROH} \rightarrow \underset{\text{Glycerol}}{\begin{matrix}CH_2OH\\CHOH\\CH_2OH\end{matrix}} + \underset{\text{FAME}}{\begin{matrix}R'COOR\\R''COOR\\R'''COOR\end{matrix}} \tag{3.69}$$

Since simplified kinetic models suffice for practical purposes, experimental data were equally processed under the following assumptions (Ilgen, 2012; Darnoko and Cheryan, 2000).

1. A perfectly stirred batch reaction is considered.
2. The methanolysis reaction is constituted by three consecutive stages but assumed irreversible because of the excessive presence of methanol in the reaction (Ilgen, 2012).
3. The catalytically active species is sodium methoxide formed by reaction of NaOH with methanol which is a fast reversible reaction.

Assumming the best kinetic model for an irreversible mechanism to be pseudo-second order model, then the rate equation for the Tg hydrolysis would be as shown in Equation (3.70) (Darnoko and Cheryan, 2000; Levenspeil, 1999).

$$-r_{Tg} = \frac{-d[Tg]}{dt} = k[Tg]^2 \quad (3.70)$$

Integrating and rearranging of Equation (3.70) by integration yields Equation (3.71)

$$k_{Tg}\, t = \frac{1}{[Tg]} - \frac{1}{[Tg\,0]} \quad (3.71)$$

Where k is the overall rate constant, t is the reaction time; Tg_0 is the initial triglyceride concentration. A plot of reaction time (t) against $\frac{1}{[Tg]}$ will give a straight line if the model is valid. Similar approach was applied on the monoglycerides and diglycerides hydrolysis to get Equations (3.72) and (3.73).

$$k_{Dg}\, t = \frac{1}{[Dg]} - \frac{1}{[Dg_0]} \quad (3.72)$$

$$k_{Mg}\, t = \frac{1}{[Mg]} - \frac{1}{[Mg_0]} \quad (3.73)$$

3.9.4.2 First-order irreversible model

To determine the kinetics of the reaction based, the effect of reaction temperature and time were measured.

It was assumed that the catalyst was used in sufficient amount with respect to oil to shift the reaction equilibrium towards the formation of fatty acid methyl esters. Thus, the reverse

reaction could be ignored and change in concentration of the catalyst during the course of reaction can be assumed to be negligible (Zhang *et al.*, 2010). Also, since the concentrations of both Dg and Mg were found to be very low (Dg<2.9wt%, Mg<1.45wt %) compared to those of Tg (Tg> 94wt%) in the crude vegetabe oils used in this reaearch, the reaction could be assumed to be a single-step transesterification (Kumar et al., 2011). Therefore, the rate law of the transesterification reaction for forward reaction can be expressed by Equation (3.74) (Vujicic et al., 2010).

$$-r_{Tg} = \frac{-d[Tg]}{dt} = k'.[Tg].[ROH]^3 \quad (3.74)$$

Where [Tg] is the concentration of triglycerides and [ROH] that of methanol and k′ is the equilibrium rate constant. This overall reaction follows a second-order reaction rate law. However, due to the high molar ratio of methanol to oil, the change in methanol concentration can be considered as constant during reaction. This means that by taking methanol in excess, its concentration does not change the reaction order and it behaves as a first-order chemical reaction. Hence, the reaction would obey pseudo-first order kinetics (Zhang *et al.*, 2010) and finally, the rate expression can be written as in Equation (3.75).

$$-r_{Tg} = \frac{-d[Tg]}{dt} = k.[Tg] \quad (3.75)$$

Where k is modified rate constant and $k = k'[ROH]^3$. Assuming that the initial triglyceride concentration was $[Tg_0]$ at time t =0, and at time t it falls down $[Tg_t]$. The integration of above Equation (3.76) for t = 0, $[Tg]= [Tg_0]$ and at t = t, $[Tg] =[Tg_t]$ gives the following equation:

$$-\ln[Tg] + \ln[Tg_0] = kt \quad (3.76)$$

Based on the above considerations, the rate data from the seed oils of African pear, sweet almond and African star apple transesterification reaction in ground seeds would fit with Equation (3.76). To test this rate equation, -ln[Tg] was plotted against time. In this procedure, the weight percentage of Tg was used as concentration because $[Tg]_0/[TG]$ is a concentration ratio and its value is independent of units, provided that the same units are used for both $[Tg]_0$ and [Tg]. Least-square approximation was applied in fitting a straight line to the experimental data, and in each case the coefficient of determination (R^2) was determined.

3.9.5 Activation energy determination

Finally, activation energies of the reactions taking place were estimated using the calculated rate constants and temperatures at which they were observed in Arrhenius equation (Equation (3.77).

$$\log_{10} k = \frac{-Ea/2.303R}{T} + A \quad (3.77)$$

Where E_a = Activation energy,

R = Gas constant

A = Arrhenius constant or frequency factor.

CHAPTER FOUR

RESULTS AND DISCUSSION

4.1 Seed Oil and Biodiesel Characterization

The seed oils were characterized by ascertaining their physico-chemical properties and their functional groups through the FT-IR analysis. Also, the biodiesel from the seed oils were characterized for physico-chemical properties, functional groups and fatty acid compositions.

4.1.1 Physico-chemical properties of the seed oils and biodiesel

Table 4.1 contains the results of the physico-chemical properties of the seed oils. The physico-chemical properties of the biodiesel from the seed oils are presented in Table 4.2. The results are presented in comparison with the relevant international standards such as ASTM D 6751 and EN 14214.

The oil content is a key factor influencing the choice of plant seeds as potential feedstock for biodiesel and other industrial products. The percentage oil yields of sweet almond (60.15%) and African pear (55.70%) appear more commercially viable for biofuel purposes than African star apple seed oil yield (13.35%) which is quite low when compared with most oil feedstocks (peanut -50%, sesame seed -5%, olive seed-40%, castor seed-50%, sunflower seed-35%) as reported by Ofoefule *et al.,* (2013). It implies that the seeds of African star apple would contain more proximate compositions of ash, crude fibre, carbohydrate, protein and nitrogen than the seeds of sweet almond and African pear. This indicates that the African star apple seed may not be a good seed of abundant oil for biodiesel production but genetically modified breeds can be developed which could produce seeds with higher oil yields. The golden and pale yellow colours of SASO and APSO are of high aesthetic qualities, while

that of ASASO is dark red. The results are the same with the colours obtained by earlier researchers while ASASO has similar colour with *Luffa cylindrica* and *Cucumis melo* (Ibeto *et al.,* 2012).

The high moisture content of vegetable oil is an indication of poor processing practice; it promotes oil oxidation rancidity and equally affects the biodiesel yield negatively. The results obtained for SASO, APSO and ASASO (0.57, 0.55 and 0.79%) are all quite low compared with 5.32% obtained by Ofoefule *et al.,* (2013) for tiger nut seed oil and 5.006% by Isreal, (2008) for almond seed oil. Lotero *et al.,*(2005) has advised for moisture content of vegetable oils to be below 0.5% in order to obtain high yield of biodiesel (>90%). This is owing to the fact that high moisture content in oils promotes deterioration, oxidative rancidity and soap formation during transesterification. Therefore, the values obtained in this study are expected to promote biodiesel yield above 90%. African star apple has moisture content of about 0.22 and 0.24% higher than sweet almond and African pear seed oils respectively. This would translate to lower biodiesel yield from African star apple while the effect of oil moisture content of seed oils from sweet almond and African pear on biodiesel yield would be almost the same since they have very close moisture content.

The saponification value serves as important parameters in determining the suitability of the oil for soap making. It is equally used for checking impurities (Ofoefule *et al.,* 2013). Its value is inversely proportional to the molecular weight of the oil (Audu *et al.,* 2012). It means that the lower the saponification value the larger the molecular weight of fatty acids in the glycerides. The values obtained for SASO, APSO and ASASO are 165.50, 250.72 and 201.66 mgKOH/g respectively. These values are in close agreement with results obtained from other feedstocks prominantely used for biodiesel production such as jatropha seed

(193.55mgKOH/g), castor (202mgKOH/g), soybean (220.78mgKOH/g), linseed (188.71mg/KOH/g) etc (Demirbas, 2003). This implies that the saponification values of the seed oils in this study would have no negative effect on their application for biodiesel production. Similar results have been previously reported by other reasearchers on African star apple. Audu *et al.,* (2013) obtained 193.7mgKOH/g, Musal *et al.,* (2015) obtained 228mgKOH/g though Agbede *et al.,* (2012) obtained 327mgKOH/g while Ochigbo and Paiko, (2011) got 246.84mgKOH/g. The value obtained for SASO is the lowest among the three seed oils studied but it is more than twice the value of 65.92mgKOH/g reported for *Luffa Cylindrica* by Ibeto *et al.,* (2012) and higher than 161.1mgKOH/g reported by Ofoefule *et al.,* (2013) from tiger nut. The Saponification value obtained from APSO appeared highest among the three seed oil samples used. This implies that APSO would contain the highest percentage of fatty acids among the three seed oils (Oyerinde and Bello, 2016). The high saponification value obtained from APSO is in agreement with the values of 250mgKOH/g and 253mgKOH/g reported for edible oil like palm kernel oil and coconut oil respectively as (Musa *et al.,* 2015), but far higher than the value of 171.10mgKOH/g reported by Ogunsuyi, (2015) from African pear. The variations of the saponification values results obtained in this study from the ones reported by other researches on the same feedstocks could be due to variations in locality, climate and processing methods. The saponification value of the methyl esters decreased significantly when compared with the values obtained from their seed oils and follows the trends observed in tiger nut oil (Ofoefule *et al*., 2013) and corn oil (De lima *et al*., 2013).

Iodine value is the measure of the degree of unsaturation of oil (Nzikou *et al.,* 2009). Iodine value is classified thus; less than 115 as non-drying as, greater than 130 as drying and between 130 and150 as semi-drying. Therefore, all the three oil samples are all non-drying oil

samples. The iodine value should be less than 120g I_2/100g of oil sample for the seed oil to be suitable as feedstock for biodiesel production (EN 14214). Also, it has been reported that oils having high unsaturation of fatty acids, when heated are prone to polymerization of the glycerides, causing formation of deposits and thereby compromising oxidative stability (Mittelbach, 1996). Therefore, the values obtained for the three seed oils (SASO-35.77, APSO-50.96 and ASASO-37.57g/100g) do suggest high suitability for biodiesel production. Also Giwa and Ogunbona, (2014) obtained 92.3g/100g for SASO, Audu *et al.,* (2013) obtained 33.18g/100g and 83.56g/100g for ASASO and *Luffa cylindrical* respectively, while Musa *et al.,* (2015) obtained 30.0g/100g for ASASO. Literature value for APSO is rare. The iodine value is an index of the number of double bonds within a mixture of fatty acid contained in biodiesel. Therefore, it is a measure of the total unsaturation of a fatty material. The iodine value of 28.02, 45.06 and 32.86g/100g for SASOME, APSOME and ASASOME respectively showed slight decrease in the values obtained from the parent seed oils. This is owing to the transesterification process the seed oils have undergone. However, the results satisfy the specification of 120g/100g (maximum) recommended by EN 14214 standards. Iodine value of APSOME is highest and this indicates that it would possess the highest unsaturation characteristics among the three methyl esters produced. The values are all lower than 98.38g/100g obtained from tiger nut biodiesel (Ofoefule *et al.,* 2013).

Peroxide value is an index of rancidity and hence provides information on oil quality and stability. High peroxide value in vegetable oil suggests absence of low levels of antioxidant. Also, Codex Alimentarius Commission has recommended a maximum value of 10 meq oxy/kg for edible oils such as groundnut seed oils. Therefore, the peroxide values of the seed oils (SASO-1.48, APSO-1.88 and ASASO-1.60 meq.oxy/kg) in this research satisfy the

Codex Alimentarius Commission recommendation and clearly suggest that the seed oils are fairly stable and may not readily become rancid during storage (Audu *et al.,* 2013). The values obtained in this study are in consistence with the values obtained previously for ASASO by Audu *et al.,* (2013) (1.96meq oxy/g), Akubugwo and Ugbogu, (2007) (1.80meq oxy/g), Musa *et al.,* 2015 (1.45meq oxy/g), Adebayo *et al.,* 2012 (1.57meq oxy/g) and 45.20meq oxy/g obtained by Ogunsuyi, (2015) for APSO. The higher value obtained by Ogunsuyi, (2015) could be attributed to method of processing and handling of the raw seeds.

Acid values provide an indication of age and quality of the oil or fat. It has a direct correlation with free fatty acid (FFA) content of oils and fats. Percentage FFA is obtained by multiplying acid value by 0.503 (Ofoefule *et al.,* 2013). Many researchers have reported that free fatty acid (FFA) above 2% in oil require pretreatment for optimal conversion into biodiesel (Ramadhas *et al.,* 2005). This is owing to the fact that high FFA results in losing the oil to soap (Mushtaq *et al.,* 2014). The FFA content of APSO (3.28%) is higher than the values obtained from SASO (1.40%) and ASASO (1.44%). Hence, African pear seed oil requires two-step transesterification for optimal conversion to biodiesel. However, the FFA of APSO is lower than the value (12.33%) obtained by Ogunsuyi, (2015) for the same APSO and 4.49% obtained by Ofoefule *et al.,* (2013) for tiger nut. Also, Ibeto *et al.,* (2012), obtained 47.12% and 51.4% from paw-paw and orange seed oils respectively. The difference observed in some cases here with the same feedstocks could be attributed to the age of the seed, geographical location where the seeds where obtained and storage conditions. However, considering FFA of the seed oils from this study, they can be used for industrial purposes such as the production of biodiesel and biolubricant. The values obtained in this study are within the limit of ASTM D 6751 and EN 14214 as indication of high biodiesel potentials. However, the high acid value obtained

from APSO was reduced to 0.26% after the esterification process prior to transesterification. Also, the final values of the FFA content of the fatty acid methyl ester produced from the three seed oils were less than 0.26% and compares with the standards (ASTM D 6751, EN 14214). It implies that their application in diesel engines would not cause severe corrosion on the fuel supply systems.

The refractive index indicates the level of optimal clarity of crude oil sample relative to water. When the biodiesel temperature is near to the cloud point, a cloudy state appears and refractive index changes showing that the refractive index is a significant parameter to evaluate the state of a biodiesel. Although, the standard of refractive index is not stipulated in the ASTM D and EN standards, the values (SASO-1.4402, APSO-1.4269 AND ASASO-1.4438) obtained in this study are in the same range with 1.46 obtained from *Arachies hypogeal* (Ibeto *et al.,* 2012) and 1.467 obtained from corn oil (De Lima *et al*., 2013).

The values of specific gravity of oil required for biofuel is very important for effective functioning of the injection engines through maintaining the optimal air to fuel ratio, promote efficient combustion and reduce particulate matter emissions (Ibeto *et al.,* 2012). The specific gravity values of all the seed oils studied were in the range of 0.83 to 0.88. These values are within the standard of 0.87-0.90 for biodiesel (Ibeto *et al.,* 2012). Since the values obtained are within the standard limit of ASTM D 6751 and EN 14214 (Table 4.2), it is expected that the biodiesel produced in this work would function well in diesel fuel injection systems.

Viscosity is important in determining optimum handling, storage and operational conditions because biodiesel fuel need to have suitable flow characteristics to ensure that adequate supply reaches injectors at different operating temperatures. Also, oils with high viscosity can form droplets on injection which causes poor atomization but oils with very low

viscosity can produce biodiesel with low viscosity which may not provide sufficient lubrication for precision fill of the fuel injection pumps (Atabani et al., 2012). The viscosity of the seed oils (SASO-6.05, APSO-5.82 and ASASO-5.55cp) are consistent with 3.70 cp for APSO (Ogunsuyi, 2015), and 4.23 cp for SASO (Giwa and Ogunbona, 2014). However, the high value obtained from SASO shows that it could be used as lubricants in engine parts in the tropics with little pretreatment. Also, values obtained are all comfortably within the 1.9-6.0 mm^2/s standards of ASTM D. The values are slightly lower than 8.08 mm^2/s reported by Ofoefule *et al.*, (2013), on tiger nut, 4.23 mm^2/s reported by Giwa and Ogunbona, (2014) on SASOME and 5.6 mm^2/s reported by Bull and George, (2015) on APSOME, but compared very well with 2.60 mm^2/s obtained by Ogunsuyi, (2015) on African pear seed oil. Moreover, the viscosities of the fatty acid methyl esters are found to be lower than their corresponding seed oils due to transesterification. This is very important for the efficiency of their application in the engine since many diesel engines use high technological injection pumps which do not tolerate very viscous fluids as these may clog fuel filters.

Usually, biodiesel has flash point of 150° C compared to 55-66°C for conventional diesel fuel (Sanford et al., 2009). The seed oils methyl esters have safer values of flash point (SASOME-136, APSOME-125 and ASASOME-126°C). The flash points of the parent seed oils were higher but transesterification process reduced the flash points. These values of flash point makes the fatty acid methyl esters from all the seed oils safe for transport handling and storage purposes since flash point is the temperature at which fuel sample will ignite when exposed to flame or spark. The flash point values in this study are quite low compared to 182°C obtained by Ogunsuyi, (2015) from APSOME but in agreement with the result of 144 °C obtained by Bull and George, (2015). The variation could be due to method of processing.

The cold flow properties of the methyl esters were measured by determination of cloud point (CP) and pour point (PP). These are important low temperature fuel parameters. Specifications for CP and PP are not in the biodiesel standards of EN 14214 though ASTM D 6757 requires that CP be reported probably because each country has different climatic conditions. Also, the solidification of fuel may cause blockage of the fuel lines and filteres, leading to fuel starvation, engine starting problems and engine damage due to poor lubrication. As reported here, SASOME has high CP and PP values, while APSOME and ASASOME have values which are quite within the -15 to +10 and -3 to +12 ASTM D 6757 standards for CP and PP respectively. The different results are based on variation in percentage of long-chain unsaturated fatty acids which are probably more in APSOME and ASASOME than SASOME (Giwa and Ogunbona, 2014). However, the values obtained from SASOME is in agreement with results of Bull and George, (2015) (CP-2.7°C, and PP 15.2°C), as well as Awolu and Layokun, (2013) (CP-8°C and PP-4°C). Moreover, since the pour point is the lowest temperature at which frozen oil can flow and is used to specify the cold temperature instability of fuel oil, this implies that the produced biodiesel from these seed oils would perform well in very cold and temperate regions.

The ash contents of the biodiesel samples (0.1, 0.1 and 0.1%) were the same and above the maximum limit of ASTM D 6751 (0.02%) and EN 14214 (0.02%). This indicates that they may likely have very high mineral contents that would lead to presence of some air pollutants like SO_X and NO_X (Ofoefule et *al*., 2013). However, the air pollutants that might be emitted would be quite less than those proposed by other researchers on tiger nut methyl esters and its blends since the latter feedstock has up to 1.13% ash content (Ofoefule *et al*., 2013). The ash content of the methyl esters in this study are found to be lower than the values obtained from

the corresponding seed oils (SASO-1.02, APSO-1.50 and ASASO-1.22%) showing improved fuel quality because of the transesterification process.

The calorific values (SASOME-31.17, APSOME-34.42 and ASASOME-32.83MJ/kg) are below diesel fuel ASTM D 9751 (42-46MJ/kg) standard but within the minimum limit of EN 14214 standard of 35MJ/kg. These results support the values obtained on higher heating values based on flash point (34.MJ/kg). Since the deviation of the calorific values from the standard is not wide, the biodiesel samples in this study would burn with expected optimal release of energy. Based on the results, biodiesel obtained from African pear is expected to release highest amount of energy on combustion followed by African star apple.

Cetane number (CN) measures the tendency of the fuel to self-ignite at a particular temperature and pressure in the cylinder when the fuel is injected. The cetane numbers (SASOME-70.40, APSOME-55.20 and ASASOME-64.57) of the three seed oil biodiesel are above the minimum limits of ASTM and EN (47 and 57 respectively). This shows that they all have good ignition quality. It implies that SASOME would give lowest delay period for fuel ignition and injection initiation into combustion chamber, followed by ASASOME and APSOME (Sivaramakrishnan and Ravikumar, 2012). This could be due to higher chain length of fatty acids and increase in saturation in SASOME than in the other biodiesel samples. The values obtained are equally above the standard (40 – 55) set for petro-diesel. This could be explained to be due to higher oxygen content which is typical of biodiesel fuel. Also, Sivaramakrishnan and Ravikumar,(2012) obtained CN values of 63, 54, 45, 49, 54 and 62 from babassu, rapeseed, soyabean, sunflower, peanut and palm oil methyl esters respectively.

Table 4.1: Physico-chemical properties of SASO, APSO and ASASO.

S/n	Parameters	Results		
		Sweet almond	African pear	African star apple
1.	Oil yield (%)	60.15(2.51)	55.70(2.14)	13.36(2.80)
2.	Colour	Golden	Pale yellow	Dark red
	Red units	4.0(0.2)	2.10(0.1)	5.4(0.5)
	Yellow units	40.00(6.5)	31.0(5.0)	55(8.5)
3.	Specific gravity	0.8552(0.007)	0.8885(0.006)	0.8346(0.005)
4.	Moisture content (%)	0.57(0.05)	0.55(0.045)	0.79(0.038)
5.	Refractive Index	1.4472(0.009)	1.4269(0.008)	1.4515(0.009)
6.	Saponification value (mg KOH/g)	165.50(3.49)	250.72(3.50)	201.66(3.49)
7.	Iodine value (g/100g)	35.77(0.66)	50.96(0.58)	37.57(0.64)
8.	Peroxide value (milli eq. oxy/kg)	1.48(0.02)	1.88(0.03)	1.60(0.02)
9.	Acid value (mgKOH/g)	2.805(0.35)	6.57(0.25)	2.88(0.30)
10.	Free fatty acid as oleic (%)	1.402(0.27)	3.28(0.30)	1.44(0.29)
11.	Ash content (%)	1.02(0.02)	1.50(0.02)	1.22(0.02)
12.	Viscosity (cp)	6.05(0.34)	5.82(0.29)	5.55(0.25)
13.	Smoke point (˚C)	40(2.3)	30(1.7)	35(1.5)
14.	Titre point (˚C)	52(1.79)	36(1.72)	45(1.76)
15.	Flash point (˚C)	157(2.34)	149(2.22)	135(1.89)
16.	Cloud point (˚C)	10(0.24)	-2(0.11)	-3(0.15)

Values are means of triplicate determination and standard deviation (SD) are given in parenthesis

Table 4.2: Result of the seed oil FAME physico-chemical characterization compared with standard

Parameter	Results			Standards		
	SASO FAME	APSO FAME	ASASO FAME	ASTM D 9751	ASTM D 6751	EN 14214
Biodiesel yield (%)	94.36	93.025	86.49	-	-	-
Specific gravity	849.1	851.7	819.5	850	880	860-900
Moisture content (%)	0.02	0.031	0.026	-	-	-
Refractive index	1.4402	1.4269	1.4438	-	-	-
Acid value (mgKOH/g)	0.46	0.92	0.32	0.062	0.50	0.50
Free fatty acid (%)	0.23	0.10	0.16	0.31	0.25	0.25
Iodine value (mgKOH/g)	28.02	45.06	32.86	42-46	-	120max.
Saponification value (mgKOH/g)	161.05	242.51	189.03	-	-	-
Ash content (%)	0.10	0.10	0.10	0.01	0.02	0.02
Viscosity (cp)	2.84	2.31	2.19	2.6	1.9-6.0	3.5-5.0
Smoke point	34	24	25	-	-	-
Fire point	40	27	36	-	-	-
Flash point	136	125	126	60-80	100-170	120
Cloud point	10	-2	-3	-20	-3 to 12	-
Pour point	4	-6	-8	-35	-15 to 10	-
Calorific value (MJ/Kg)	31.17	34.42	32.83	42-46	-	35
Conductivity (Us/CM)	0.40	0.86	0.52	-	-	-
Cetane index	73.0	57.80	67.16	-	-	-
Cetane number	70.40	55.20	64.57	40-55	47min	51min
Higher heating value(HHV)[a] (MJ/kg)	34.72	34.50	34.52	-	-	-
Higher heating value(HHV)[b] (MJ/kg)	40.76	40.52	40.46	-	-	-
Higher Heating value(HHV)[c] (MJ/kg)	63.75	63.75	63.75	-	-	-

a- based on flash point, b- based on viscosity, c- based on density, min-minimum, max- maximum

4.2 Fourier Transform Infra-red Characterization of the Seed Oils and their Biodiesel

Figures A3.1-A3.6 show the absorption of spectra of the intensity maps for sweet almond, African pear and African star apple seed oils and their biodesels at frequency region of 450-4000cm^{-1}. The result was analyzed and compared with known signature of identified materials in the FTIR library (Furnish *et al.,* 1989). There is similarity in the infrared absorption spectrum intensities. The spectra of peak position and shapes which shows that the main components of the vegetable oils are closely the same. The specific peaks 891.42 cm^{-1}, 895.28 cm^{-1} and 764.04 cm^{-1} in SASO, APSO and ASASO respectively indicate the presence of =C-H functional groups and possess bending type of vibration appearing at low energy and frequency regions in the spectra. They are double bonded and attributed to unsaturation. They are part of fatty acids with unsaturated bond in the triglycerides. The 980.20cm^{-1} and 949.32cm^{-1} represents the value of conjugated fatty acid glycerides (Wang et al., 2012). This also applies to the band region between 1319.88 -1501.30 cm^{-1}, 1318.68 cm^{-1} and 1346.90 -1578.50 cm^{-1} for SASO, APSO and ASASO respectively and can be ascribed to the bending vibrations of methyl group in the triglyceride. The 1721.32 cm^{-1}, 1721.32 cm^{-1}and 1655.70 cm^{-1} for SASO, APSO and ASASO respectively can be ascribed to the stretching vibrations of C=O. These indicate the presence of carbonyl functional groups that appear as R-C(OR)-O in the vegetable oils. It has been proposed that peaks around these regions (3008 and1654 cm-1) correspond to unsaturated double bonds of =CH; cis and –C=C; cis respectively and can be used as an indication of the degree of unsaturation of a triglyceride (Rohman, 2017). The peaks at 3134.08 - 3265.3 cm^{-1} from APSO spectral are attributed to the stretching vibrations of =C-H group. The characteristics bands of 2419.98cm^{-1} appear with C=C for SASO while the regions between

3384.98-359.28 cm^{-1}, 3790.20 cm^{-1} and 3384.96-3539.38 cm^{-1} can be ascribed to O-H stretching vibrations which are single bonded and appeared at high energy levels of the spectra. They indicate the presence of water molecules. The presence of unsaturated characteristics in the seed oils shows their relevance as feedstocks for biodiesel production (Lei *et al.,* 2017, Knothe, 2010).

The transesterification process of seed oils to convert them to their corresponding FAMEs can be illustrated by monitoring shifting trends on the functional groups using FT-1R (Ahmad *et al.,* 2014).

4.2.1 FTIR result of SASO and SASOME in comparison

Table 4.3 contains peaks identified from the spectrum of SASO and SASOME as they appeared in Figures A3.1 and A3.2. The peak analyses of both spectra show significant differences effected by the ester groups. The specific peak 891.42cm^{-1} indicates the presence of =C–H functional groups and posseses bending type of vibrations appearing at low energy and frequency region in the spectra. The peak is double bonded and attributed to as unsaturated. It is part of fatty acid methyl ester with unsaturated bond in the triglyceride and ester (Oleate and linoleate) (Saifuddin and Refai, 2014). The characteristics peaks found in the region of 1076.70cm^{-1} and 1196.40cm^{-1} show split stretching of C–O and rocking vibration of C–O as carbonyl groups for SASO and SASOME respectively (Saifuddin and Refai 2014; Conceicao *et al.,* 2007). It could be observed that 1188.64cm^{-1} in the oil sample got split into two concrete signals at 1134.60cm^{-1} and 1196.36cm^{-1}. The band regions between 1319.88 – 1501.30cm^{-1} and 1319.88 – 1566.92cm^{-1} for SASO and SASOME spectral, respectively can be ascribed to the

bending and rocking vibrations of methyl group in the glyceride and ester (Gunstone, 2004). The band regions between 1721.32cm^{-1}-1840.98cm^{-1} and 1721.32cm^{-1}- 1813.96cm^{-1} for SASO and SASOME spectra respectively can be ascribed to the stretching vibrations of C=O group indicating the conversion of the triglyceride to methyl esters. The characteristic bands of 2419.98cm^{-1} and 2400.68cm^{-1} appear with C=C (alkenes group) for SASO and SASOME respectively. Also, the band regions between 3384.98 – 3597.28cm^{-1} and 3384.98 – 3608.86cm^{-1} for SASO and SASOME, respectively can be ascribed to O–H stretching vibrations, which are single bonded and appear at high energy levels. The single bond functional group O-H was observed to be prevalent in the biodiesel with stretch vibrations (Younis *et al*., 2009). The presence of water molecule was evidenced by the hydrogen bonding (Ndana *et al.,* 2013). The presence of C-H at 1319.88, 1474.28 and 1566.92 cm^{-1} regions of the SASOME spectrum can be attributed to the properties such as pour and cloud points that influences the performance of biodiesel during cold weather engine operation (Ndana *et al.,* 2013). However, the presence of carbon to carbon (C=C) unsaturated bonds can cause the biodiesel samples to remain in liquid state but may be liable to poor storage stability due to oxidation. This implies that the biodiesel would not need cold flow improver for better performance. All the absorptions corresponding to C-O and C=O stretches indicate that the biodiesel product contains ester functional groups typical to any biodiesel type, while the following groups: C–H, C=H, and O–H indicated biodegradability of the oil and produced biodiesel(Menkiti et al., 2016).

Table 4.3: FT-IR main characteristic band positions for SASO and SASOME.

SASO			SASOME		
Wave number (cm^{-1})	Type of vibration	Functional group	Wave number (cm^{-1})	Type of vibration	Functional group
891.42	Bending	=C-H	891.42	Bending	=C-H(alkenes)
1076.70	Bending	C-O-C	1041.96	Stretching	C-O
1188.64	Stretching	C-O	1134.60	Split rocking	C-O
1319.88	Bending/rocking	CH_2	1196.40	Split rocking	C-O
1424.10	Bending/rocking	CH_2	1319.88	Bending/Rocking	CH_2
1501.30	Bending/rocking	CH_2	1474.28	Bending/Rocking	CH_2
1721.32	Stretching	C=O	1566.92	Bending/Rocking	CH_2
1840.98	Stretching	C=O	1721.32	Stretching	C=O
2419.98	Symmetrical/ Stretching	C=C	1813.96	Stretching	C=O
3384.98	Stretching	O-H	2400.68	Symmetrical/ Stretching	C=C
3597.28	Stretching	O-H	3384.98	Stretching	O-H
			3608.86	Stretching	O-H

4.2.2 FTIR result of APSO and APSOME in comparison

Table 4.4 contains the main functional groups present at both the optimum produced APSOME and its parent APSO. The most characteristics absorption peaks are indicated in Figures A3.3 and A3.4 for APSO and APSOME respectively. The absorption peaks appearing at 760.18cm^{-1} and 756.32cm^{-1} for APSO and APSOME respectively represent the bending vibrations of alkenes and overlapping of rocking vibrations of methylene for both samples. The other ones at 895.28 and 930.02cm^{-1} represents the bending vibrations of C–H and =C–H functional groups for alkanes and alkenes unsaturated class. The 1165.48cm^{-1} and 1161.62cm^{-1} stretching vibrations of APSO and APSOME spectra respectively represent the single bond

carbonyl functional groups (C–O). The characteristics peaks found at 1223.38cm^{-1} for APSO and 1258.12$cm^{-1}$for APSOME indicate the bending vibrations of C–O–C. The band regions of 1346.90 – 1578.50cm^{-1} in the APSO spectrum can be asserted to the bending vibration of $–CH_2$ methyl groups in the fatty acid and 1319.88 – 1566.92cm^{-1} regions in the APSOME spectrum represent the stretching vibrations of $–CH_2$ methyl groups in the biodiesel (Gunstone, 2004). The 1721.32cm^{-1} and 1732.90cm^{-1} in the APSO and APSOME spectral respectively are attributed to C–O groups with the stretching mode of vibration. These indicate the presence of carbonyl functional groups that appear as R_1–C(OR)–O in the vegetable oil and R_1–C (OCH_3)=O in biodiesel. The peaks at the regions of 3134.08 – 3265.3cm^{-1} and 3149.52 – 3261.46cm^{-1} in the APSO and APSOME spectra respectively are attributed to the stretching vibrations of =C–H alkene groups. The peak 3790.20$cm^{-1}$for both APSO and APSOME with stretching mode of vibration is ascribed to the presence of O-H groups and are single bonded at high energy regions of the spectra (Shut *et al.*, 2010; Younis *et al*., 2009; Smith, 1999).

Table 4.4: FT-IR main characteristic band positions for APSO and APSOME

APSO			APSOME		
Wave number (cm^{-1})	Type of vibration	Functional group	Wave number (cm^{-1})	Type of vibration	Functional group
760.18	Bending	C-H	756.32	Bending	=C-H
895.28	Bending	C-H	930.02	Stretching	=C-H
1165.48	Stretching	C-O	1161.62	Stretching	C-O
1223.38	Bending	C-CO-O	1258.12	Bending	C-CO-O
1346.90	Bending	CH_2	1319.88	Bending	CH_2
1439.54	Bending	CH_2	1447.26	Bending	CH_2
1578.50	Bending	CH_2	1566.92	Stretching	CH_2
1659.56	Bending	C=C	1655.70	Bending	C=C
1721.32	Stretching	C=O	1732.90	Stretching	C=O
3134.08 - 3265.32	Stretching	=CH,C=C	3149.52-3261.46	Stretching	=CH,C=C
3790.28	Stretching	O-H	33790.28	Stretching	O-H

4.2.3 FTIR result of ASASO and ASASOME in comparison

Table 4.5 contains the functional groups of ASASO and ASASOME extracted from Figures A3.5 and A3.6. It is observed that the 640.52cm^{-1} for ASASO and 640.20cm^{-1} for ASASOME vibrations respectively are bending and out of plane and indicate the presence of–(CH_2) functional groups. The 764.04cm^{-1} for ASASO is ascribed to the rocking vibrations of alkenes and methylene groups (=C-H and–(CH_2)n) while 763.56cm^{-1} for ASASOME represents same functional groups but with bending of alkenes and overlapping of rocking vibrations of methylene. The peaks between 949.32–1134.60cm^{-1}represents the C-O stretching vibrations for

ASASO while 979.44 – 1133.64cm^{-1} represents bending vibrations of the same carbonyl groups for ASASOME. The stretching vibrations of the C-O-C groups could be ascribed to the wave numbers of 1261.98cm-^{1} (ASASO) and 1257.00 (ASASOME) while there is the appearance of bending vibrations of –CH_2 at 1362.34cm^{-1} for ASASO and 1318.68cm^{-1} for ASASOME. Peak 1474.28cm-^{1} for ASASO contains –CH_2 group with bending vibrations while 1442.04cm^{-1} contains –CH_2 bending and rocking vibrations. The methylene group (C=C) appeared at peaks of 1655.70cm^{-1} for ASASO and 1657.92cm^{-1} for ASASOME with stretching and bending vibrations respectively. The stretching vibrations of C–O ester group was observed at 1740.62–1875.72cm^{-1} for ASASO and 1835.25cm^{-1} for ASASOME while at high energy bands of 3384.96 – 3539.38cm^{-1} for ASASO and 3384.96 – 3539.16cm^{-1} for ASASOME appeared the hydrogen group (O-H).

Table 4.5: FT-IR main characteristic band positions for ASASO and its biodiesel.

ASASO			ASASOME		
Wave number (cm^{-1})	Type of vibration	Functional group	Wave number (cm^{-1})	Type of vibration	Functional group
640.52	Bending	– (CH_2)	640.20	Bending	– (CH_2).
764.04	Rocking	C-H	763.56	Bending	=C-H
949.32	Stretching	C-O	979.44	Bending	C-O
1134.60	Stretching	C- O	1133.64	Bending	C-O
1261.98	Stretching	C-O-C	1257.00	Stretching	C-O-C
1362.34	Bending	CH_2	1318.68	Bending	CH_2
1474.28	Bending	CH_2	1442.04	Bending	CH_2
1655.70	Bending	=CH,C=C	1657.92	Bending	=CH,C=C
1740.62	Stretching	C=O			
1875.72	Stretching	C=O	1835.25	Stretching	C=O
3384.96-3539.38	Stretching	O-H	3384.96-3539.16	Stretching	O-H

The FT–IR spectra have been used to identify the functional groups and the peaks corresponding to various stretching and bending vibrations in the vegetable oil and their biodiesel. It is observed that the esters have two characteristically strong absorption bands arising from C=O around 1721.32–1875.72$cm^{-1}$and that of C-O at 1138.64–1196.40cm^{-1}(Soares *et al.,* 2008). The C=O group indicates the presence of carbonyl functional groups that show the conversion of triglycerides in the seed oils to methyl esters (Oyerinde and Bello, 2016). The stretching and bending vibrations of CH_3, CH_2 and CH group in the biodiesel samples lie in the reported ranges: 1318.68 – 1566.92 similar to results observed by other researchers (Oyerinde and Bello, 2016; Elkady *et al.,* 2015; Ahmad *et al.,* 2014; Ndana *et al.,* 2013). The single bond functional group O-H was observed to be prevalent in all the samples with both stretch and hydrogen bonding. The change in wavenumber of the functional groups between the seed oils

and their methyl esters as they appeared on their spectra indicates that the fatty acids reacted to form ester. These results reflect the conversion of the triglycerides to methyl esters. The presence of C-H indicates prevalence of properties such as pour and cloud points that affect the performance of biodiesel during cold weather engine operation (Younis *et al.,* 2008). The presence of carbon to carbon (C=C) can cause the biodiesel samples to remain in liquid state but may be liable to possible oxidation during storage. However, all the observed absorptions corresponding to C=O stretches show that the biodiesel products from the three seed oils contain ester functional groups described in any biodiesel type.

4.3 GC-MS Characterization of the Methyl Esters

The fatty acid composition of sweet almond, African pear and African star apple seed oil methyl esters were analysed by gas chromatography coupled with mass spectrometer. The identification of peaks was done by comparison of their retention time and mass spectra with mass spectra library (NIST05s LIB.) (Fu *et al.*, 2008).

4.3.1 GC-MS characterization of SASOME

The fatty acid chromatogram showing the different components present in SASOME is shown in Figure A4.1. Twenty four (24) peaks were recorded which showed different fatty acid methyl esters and few non-fatty acid components present. The major fatty acid component present in SASOME is oleic acid followed by α-linolenic acid, palmitic acid and stearic acid. Other organic compounds detected by the GC-MS in SASOME include hexadecane, hexadimethylacetal, octanal and pentanal. These results are in line with the results obtained by Botinestean *et al.*, (2012), who identified decane, tetralin and hexadimethylacetal in tomato seed oil by GC-MS. Similarly, Sharmila and Jeyanthi, (2011), had identified over six non-fatty acid methyl esters through GC-MS of *Cladophora vagabund.* From Table 4.6, SASOME contains a total of 37.74% saturated fatty acid, 41.42% monounsaturated fatty acid and 13.90% polyunsaturated fatty acids.

Table 4.6: Fatty acid profile of SASO FAME.

Peak	Retention time	Fatty Acid	Amount (%)
1.	3.766	Capric acid methyl ester	1.06
2.	3.929	Caprylic acid methyl ester	1.36
3.	4.201	Stearic acid methyl ester	1.32
4.	4.695	Eicosenic acid methyl ester	7.14
5.	5.192	Erucic acid methyl ester	0.73
6.	5.572	Palmitic acid methyl ester	7.88
7.	6.407	Lignoceric acid methyl ester	4.75
8.	6.845	Oleic acid methyl ester	40.34
9.	8.179	α- Linolenic acid methyl ester	8.07
10.	10.076	Palmtoleic acid methyl ester	0.58
11.	12.171	Elaidic acid methyl ester	0.09
12.	13.953	Arachidic acid methyl ester	4.30
13.	15.953	Behenic acid methyl ester	3.71
14.	15.868	Myristic acid methyl ester	3.69
15.	18.111	Octanal	0.69
16.	18.185	Margaroleic acid methyl ester	1.45
17.	19.260	Hexadecane	1.56
18.	20.347	Hexanaldimethyl acetal	1.41
19.	21.214	Linoleic acid methyl ester	0.83
20.	21.582	Gadoliec acid methyl ester	0.14
21.	23.130	Lauric acid methyl ester	1.53
22.	23.410	γ-linolenic acid methyl ester	3.41
23.	23.875	Vaccenic acid methyl ester	1.78
24.	24.512	Pentanal	1.97

4.3.2 GC-MS characterization of APSOME

The fatty acid chromatogram showing the different components present in APSOME is shown in Figure A4.2. Twenty four (25) peaks were recorded which showed different fatty acid methyl esters and few non-fatty acid components present (Table 4.7). Similarly, Sharmila and Jeyanthi, (2012) had previously identified 31 peaks representing different organic compounds including fatty acids in *Cladophora vagabunda* methyl esters. Among the saturated fatty acids methyl esters in the APSOME sample are caprylic, capric, palmitic, stearic, arachnidic, behenic, lignoceric, eicosenic and gadolic while the monounsaturated fatty acids identified were Erucic, oleic, palmitoleic and vaccenic acid. The polyunsaturated fatty acids present are linolenic, α- linloei and γ- linoleic. A total saturated fatty acids of 14.78%, monounsaturated fatty acids of 75.50% polyunsaturated fatty acid of 6.41% contained in the methyl ester (Figure 4.1). The oleic acid content is high (62.12%). It

implies that the oleic acid content of APSOME is far higher than 15-20% reported for cotton seed oil (Ogunsuyi, 2015), compares with 64.10% reported for rapeseed oil and below 83.60% reported for hazelnut kernel (Demirbas, 2003). This result justifies African pear biodiesel as possessing good biofuel quality. Other organic compounds detected in the APSOME by the GC-MS include tetradecane, dodecane, eicosane, octadecane, nonadecane and hexadecane. Similar detection of non-fatty acid compounds on GC-MS analysis of some seed oils has been reported by other researchers (Botinestean *et al.*, 2012; Sharmila and Jeyanti, 2011).

Table 4.7: Fatty acid profile of APSO FAME.

Peak	Retention time	Fatty acid	Amount (%)
1.	3.773	Erucic acid methyl ester	0.06
2.	3.936	Caprylic acid methyl ester	0.50
3.	4.208	Capric acid methyl ester	1.01
4.	5.198	α -liniolenic acid methyl ester	2.90
5.	5.577	Palmitoleic acid methyl ester	1.61
6.	6.850	Eicosenic acid methyl ester	0.40
7.	8.187	Elaidic acid methyl ester	1.01
8.	10.089	Margaroleic acid methyl ester	0.77
9.	11.648	Behenic acid methyl ester	2.01
10.	12.182	Linoleic acid methyl ester	3.51
11.	13.574	γ –linolenic acid methyl ester	1.40
12.	13.964	Palmitic acid methyl ester	9.05
13.	14.949	Vaccenic acid methyl ester	0.38
14.	15.508	Oleic acid methyl ester	62.12
15.	16.879	Lignoceric acid methyl ester	1.05
16.	17.500	Stearic acid methyl ester	9.01
17.	18.123	Myristic acid methyl ester	0.15
18.	18.195	Gadoliec acid methyl ester	0.51
19.	19.270	Arachidic acid methyl ester	0.31
20.	20.359	Tetradecane	0.41
21.	21.598	Dodecane	0.61
22.	23.142	Eicosane	0.81
23.	24.525	Octadecane	0.22
24.	25.601	Nonadecane	0.51
25.	26.493	Hexadecane	0.75

4.3.3 GC-MS Characterization of ASASOME

The chromatogram of the ASASOME product from the base transesterification of ASASO for the fatty acid components characterization by using gas chromatography coupled with mass spectroscopy is shown in Figure A4.3. The profile is contained in Table 4.8. Twenty one (21) peaks were recorded which showed different fatty acid methyl esters present. Other researchers have identified such number of peaks while using GC-MS to analyze methyl esters; Koria and Nithia, (2012) identified 18 peaks from *Datura stramoniun Linn* biodiesl while Sharmila and Jeyanthi, (2012) identified 31 peaks representing different organic compounds including fatty acids in *Cladophora vagabunda* methyl esters. Among the saturated fatty acids methyl esters in the sample are caprylic, capric, palmitic, stearic, behenic, lauric, myristic, lignoceric, eicosenic and arachidic, while the monounsaturated fatty acids identified were erucic, oleic, and palmitoleic. The polyunsaturated fatty acids present are linoeic, α-linolenic and γ- linolenic. ASASOME contains 27.71% saturated fatty acids, 53.30% monounsaturated fatty, acids and 18.99% polyunsaturated fatty acids (Figure 4.1). Its oleic acid content (50.5%) is the highest fatty acid content, followed by palmitic acid (20.66%) and linoleic acid (13.97%). The oleic acid component of ASASOME (50.5%) compares with those of sesame seed oil (52.8%) and peanut kernel oil (48.3%) reported previously as good feedstocks for biodiesel production (Oyerinde and Bello, 2016; Ferdous *et al.,* 2012; Demirbas, 2003).

Table 4.8: Fatty acid profile of ASASO FAME using GC-MS.

Peak	Retention time	Fatty acid	Amount(%)
1.	3.774	Eicosenic acid methyl ester	2.14
2.	3.936	Erucic acid methyl ester	0.09
3.	4.208	Oleic acid methyl ester	50.50
4.	5.198	Palmitic acid methyl ester	20.66
5.	5.576	Linoleic acid methyl ester	13.97
6.	6.850	Stearic acid methyl ester	1.01
7.	8.186	α -linolenic acid methyl ester	0.21
8.	10.087	Caprylic acid methyl ester	0.95
9.	12.182	Behenic acid methyl ester	0.59
10.	13.966	Myristic acid methyl ester	1.23
11.	15.511	Lignoceric acid methyl ester	1.65
12.	16.578	Palmitoleic acid methyl ester	0.09
13.	18.125	Butrycic acid methyl ester	1.44
14.	18.195	Arachidic acid methyl ester	1.01
15.	19.273	Oxalic acid (pentadecyl ester)	0.22
16.	20.363	Phthalic acid methyl ester	2.00
17.	21.601	Lauric acid methyl ester	0.70
18.	23.149	Capric acid methyl ester	0.31
19.	24.526	Elaidic acid methyl ester	0.40
20.	25.602	γ- linolenic acid methyl ester	0.43
21.	26.493	Gadoleic acid methyl ester	0.40

4.3.4 Effects of fatty acid compositions of the methyl esters on their fuel characteristics

Figure 4.1 contains the distribution of the fatty acid compositions of the methyl esters. A total of 37.74% saturated fatty acid (SFA), 41.42% monounsaturated fatty acid (MUSFA) and 13.90% polyunsaturated fatty acids (PUSF) were found to be contained in SASOME. ASASOME contains 27.71% saturated fatty acids, 53.30% monounsaturated fatty, acids and 18.99% polyunsaturated fatty acids while APSOME contains 14.78% saturated fatty 75.50% monounsaturated fatty acids and 6.41% polyunsaturated fatty acids. It is observed that APSOME and ASASOME are composed of more unsaturated fatty acids than SASOME.

In biodiesel standards, the specifications that a biodiesel must meet are related with composition and structure of fatty acids inherent in the biodiesel (Mittlebach and

Remschnodt, 2004). These qualities include cetane number, kinematic viscosity, oxidative stability and cold flow properties in the form of cloud and pour points (Knothe, 2009). Other essential properties influenced by fatty acid components of biodiesel, but not contained in biodiesel standards are exhaust emission, lubricity and heat of combustion (Knothe, 2012). Knothe, (2009) has reported that methyl oleate can be the desirable fatty acid among the other common fatty acids that can enrich the fuel properties of biodiesel produced. The presence of low levels of saturated and polyunsaturated fatty acids and the prevalence of high levels of monounsaturated fatty acids in biodiesel sample equally enhance properties of high quality biodiesel (Knothe, 2009). In this study, the methyl esters are observed to contain high levels of monounsaturated fatty acids (SASOME-41.42%, APSOME-75.5% and ASASOME-53.3%). Therefore, they would possess good fuel properties.

The higher composition of unsaturated fatty acids in a feedstock enhances biodiesel cloud point and decreases its oxidation stability (Sharma et al., 2008). The presence of higher composition of unsaturated fatty acids in the methyl esters (APSOME-81.91%, ASASOME-72.29% and SASOME-53.32%) would therefore enhance their cold flow properties like cloud point and pour point. However, poor oxidative stability would be exhibited more by APSOME, followed by ASASOME and least from SASOME in the biodiesels. The high viscous nature of waste cooking oils or used frying oils is reported to be due to their high saturated and less unsaturated fatty acids (Knothe, 2006) and this could cause micro-crystal formations that are dangerous to fuel lines and engine filters (Srivasta and Prasad, 2001). This is in agreement with the result of this study as it is observed that SASOME possessing more saturated fatty acids is more viscous than APSOME and ASASOME. It means that the application of APSOME and ASASOME would have little or no tendency of inherent viscosity problem and engine blockage.

Again a high value of cetane number (CN) above 80 has been observed in saturated fatty acid methyl esters (FAME), a medium range (55-58) in monounsaturated FAME and low value (20-40) in feedstock predominant in unsaturated fatty acids (Koria and Nithya, 2012). In the present study, the cetane number is found to be in the medium range (average of 63.39) (Table 4.2), reflecting the dominance of monounsaturated fatty acids. Highly saturated compounds like tallow methyl ester has cloud point of 17°C while palm oil methyl ester possesses cloud point of 13°C. On the contrary, feedstock with relatively low concentrations of saturated long chain fatty acids such as linseed, olive, rape seed and safflower oils tend to yield biodiesel with cloud point less than 0°C (Koria and Nithya, 2012). In this study, African pear seed oil biodiesel cloud point was determined as -2 °C which supports the occurrence of more unsaturated fatty acid than saturated fatty acids.

Awolu and Layokun, (2013) have reported that biodiesel fuel with more unsaturated fatty acid composition has lower heating value and thermal efficiency and equally emits lower HC, CO and smoke. It implies that APSOME and ASASOME are expected to emit lower HC, CO and smoke compared to SASOME that is more saturated.

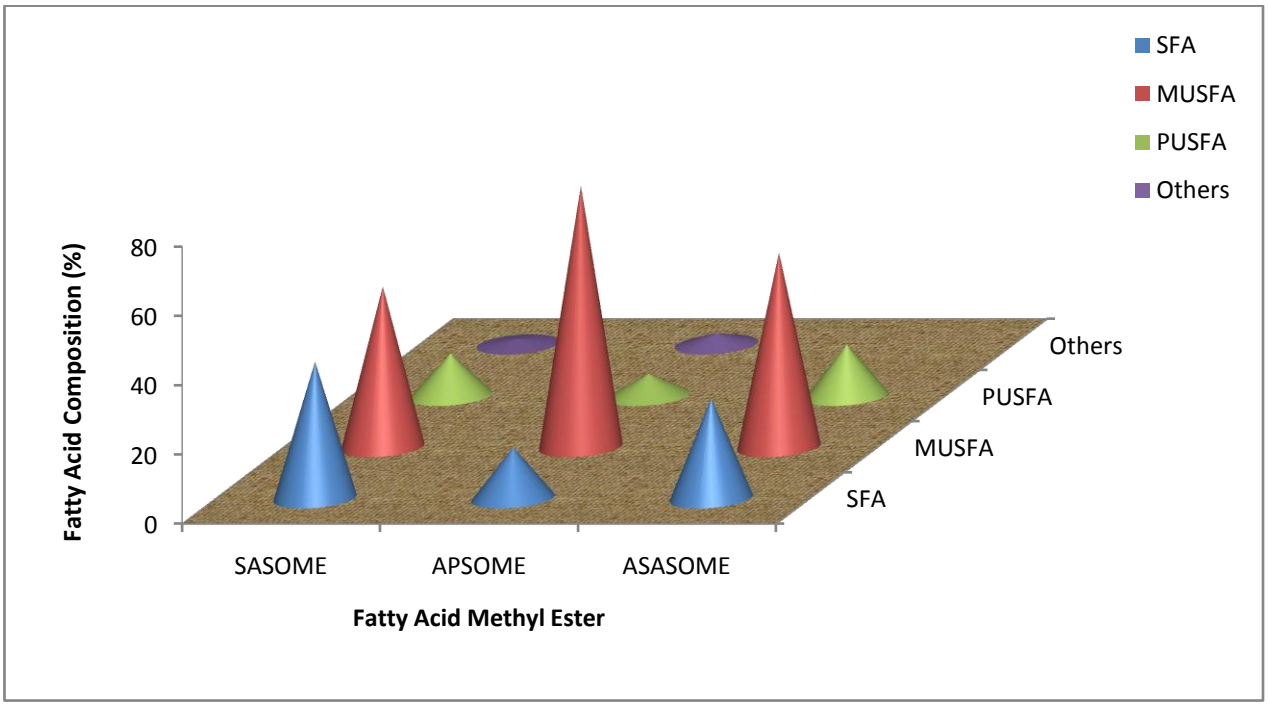

Figure 4.1: Fatty acid distribution in the methyl esters.

4.5 Seed Oils Oxidation Stability Analysis

Oxidation stability is an indication of the degree of oxidation and potential reactivity with air and can determine the need for antioxidants (Atabani et al., 2012). The oxidation of biodiesel fuel occurs due to the presence of unsaturated fatty acid chains and double bonds in the parent molecule which react with oxygen as soon as it is being exposed to air (Atadashi et al., 2010). Therefore, studies of the parent oil oxidation stability would give timely background knowledge of the biodiesel susceptibility to degradation. Figures 4.2 and 4.3 illustrate the change in peroxide values at room temperature and during heating at elevated temperatures (65^{o}C) for 60 days respectively. Oxidation process is influenced by such factor like temperature, air, peroxide, light and extraneous materials (Atadashi *et al.,* 2010). The peroxide values were followed up in order to study the effect of storage at room temperature and in accelerated conditions on the oxidation stability of the raw seed oils and in their combination with antioxidant (tertiary butyl hydroquinone) The peroxide values of the raw oils of SASO and ASASO were lower than those of APSO and the peroxide values of APSO was found to be above SASO and ASASO all through the 60 days period studied. This could be attributed to the higher unsaturated fatty acid and free fatty acid originally contained in APSO (Figure 4.1). The rate of increase in the peroxide values of the seed oils at both temperatures initially was very slow. The rate was observed to be significantly slow up to 10 days at elevated temperature and 20 days at room temperature. These periods of oxidation could be taken to represent the induction periods (Borchani *et al.,* 2010). It implies that high temperature promotes oxidation. Similar results have been reported for raw sesame oil (18 days) and olive oil (23 days) (Borchani *et al.,* 2010).

The same trend observed in Figures 4.2 and 4.3 was repeated in Figures 4.4 and 4.5 where the seed oils were in mixture with tertiary butyl hydroquinone (TBHQ). At the same corresponding storage times, the values of peroxide values of seed oils in mix with TBHQ

were observed to be lower than those of the seed oils with no antioxidant. This may be attributed to the reduction of the degree of unsaturation of the seed oils by the antioxidant which translated to lower oxidation rates. At room temperature and after storage period of 60 days, SASO, ASASO and APSO peroxide values were 22.67, 30.51 and 26.11 meqO_2/kg oil against 15.48, 18.47 and 17.10 meqO_2/kg oil for the mix of the seed oils with TBHQ respectively. Again, at elevated temperature the values of peroxide value for SASO, APSO and ASASO were 265.05, 280.12 and 272.91 meqO_2/kg oil for mix of the seed oils with TBHQ respectively. It shows that the rate of oxidation increases with temperature. Also, the primary oxidation products, lipid hydroperoxides are relatively stable at room temperature, while at high temperatures, they are readily decomposed to alkoxy radicals and then form aldehydes and short-chain hydrocarbons (Eunok and David, 2006). Therefore, storing the methyl esters at room temperature would provide best condition that would promote better oxidation stability.

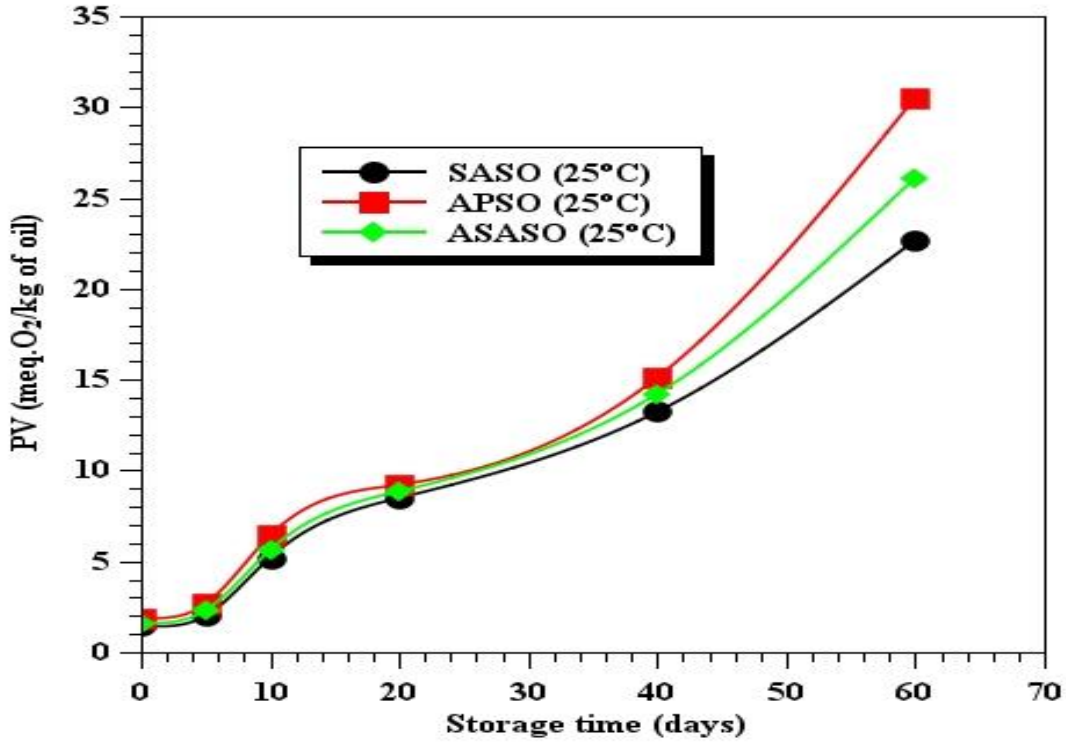

Figure 4.2: Change in peroxide value during storage period at room temperature (25 °C)

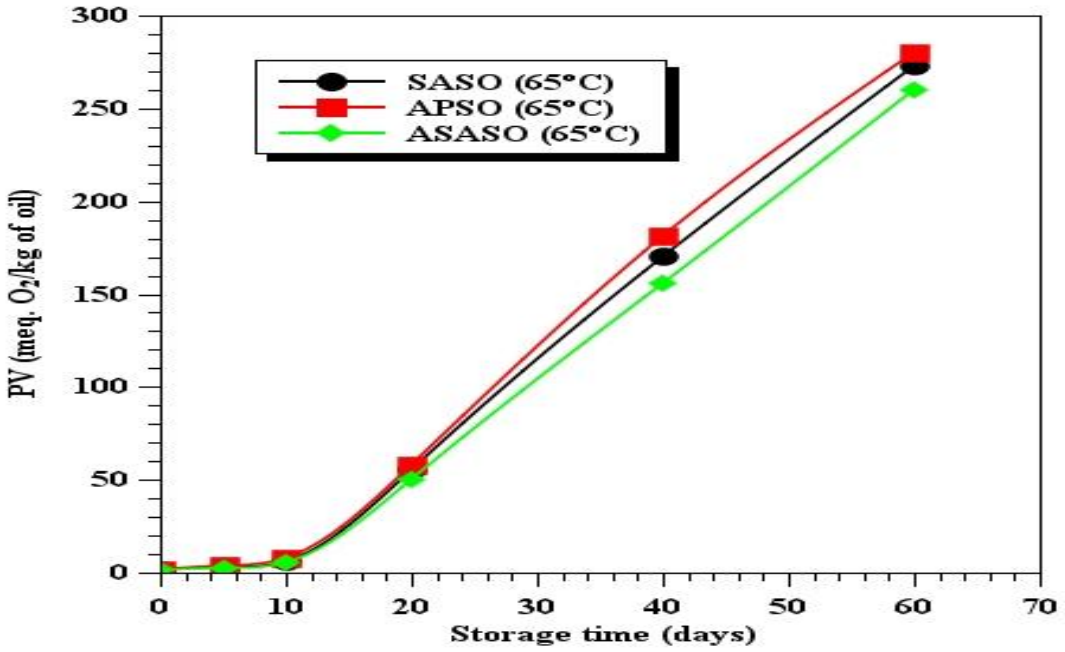

Figure 4.3: Change in peroxide value during storage period at elevated temperature (65°C).

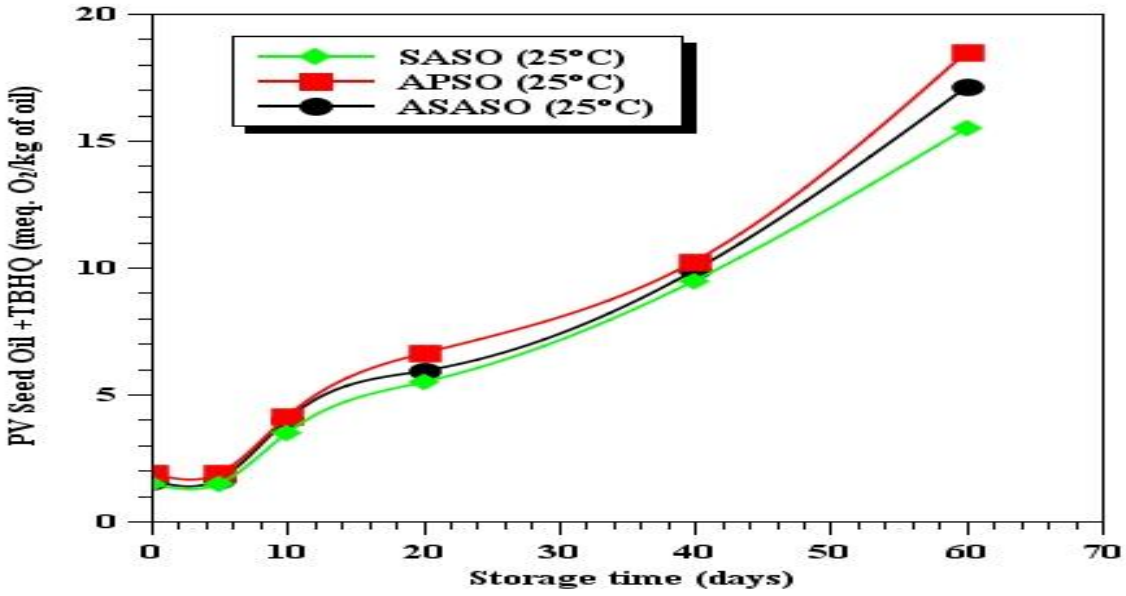

Figure 4.4: Change in peroxide value during storage in mix with TBHQ at room temperature (25 °C).

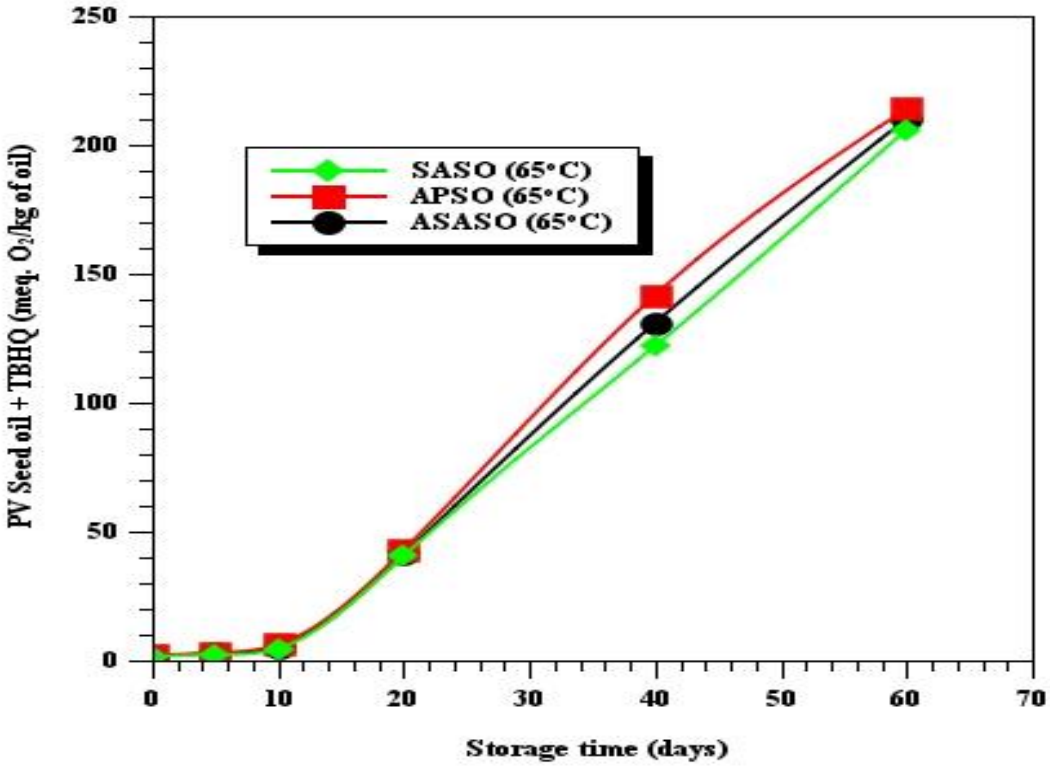

Figure 4.5: Change in peroxide value during storage in mix with TBHQ at elevated temperature (65 °C).

Figure 4.6 and 4.7 show the regression exponential model plots of the variation of oxidation stability of the seed oils of sweet almond, African pear and African star apple against storage time at room temperature and elated temperature respectively. The model equation is presented in Equation 4.1 with A as the amplitude, t as the e-folding time and Y_0 as the offset. Equation 4.1 was fitted with the experimental results obtained to yield the following final equations (Equation 4.2-4.7). Conversely, Oladimeji *et al.*, (2013), had reported the successful modeling of oxidative stability of palm olein, soybean oil and linseed oil using a linear regression model. The linear model could have been possible because their study was for a shorter period of 7 days but in this study, a long period of 60 days was studied. Also, their study modeled oxidation stability of refined oils with mixture of antioxidants while in this study some portions of the oils were not mixed with antioxidants. However, the oxidative stability models from both studies were characterized

by high values of regression correlation coefficients (above 0.92) which indicate good fitness of the data.

$$Y = Y_0 + Ae^{(-x/t)} \quad (4.1)$$

$$Y_{SASO\ 25°C} = 32.22 - 32.29e^{(-x/2.83)} \quad (4.2)$$

$$Y_{APSO\ 25°C} = 33.89 - 33.91e^{(-x/2.15)} \quad (4.3)$$

$$Y_{ASASO\ 25°C} = 32.22 - 32.29e^{(-x/2.50)} \quad (4.4)$$

$$Y_{SASO\ 65°C} = 32.22 - 32.29e^{(-x/7.02)} \quad (4.5)$$

$$Y_{APSO\ 65°C} = 32.22 - 32.29e^{(-x/3.19)} \quad (4.6)$$

$$Y_{ASASO\ 65°C} = 32.22 - 32.29e^{(-x/7.15)} \quad (4.7)$$

Table 4.9 contains the analysis of the model fitness that was carried out by determining the coefficient of dtermination (R^2), the root mean squared error (RMSE) and residual sum of squares (RSS) using Levenberg-Marquandt algorithm approach. The high values of R^2 (>0.92) indicated good agreement between the model values and the experimental data. However, SASO and ASASO oxidation stability model at 65 °C and 25 °C respectively showed the best fit with R^2 (>0.97). It shows that among all the models, less than 7.10% of the variability is not explained by the observed responses. It equally indicates the unexplained total variation which can be caused by other variables excluded from the model parameter (Adepoju *et al.,* 2018). The model provides accurate description of the

experimental data by indicating successful correlation. Exponential regression model developed described the variation of oxidation stability of the seed oils against storage time and the analysis of variance validated the model with low root mean squared error (RMSE): 0.5923<RMSE<3.1574, high coefficient of determination (R^2):0.950<R^2<0.999 and low residual sum of squares (RSS): 10<RSS<72 to validate the model. Also, based on the oxidation stability results, the above tropical seed oils are prone to oxidative degradation during storage period. The addition of antioxidants would be an effective way of ensuring oxidative stability and improved shelf life both at room temperature and elevated temperatures.

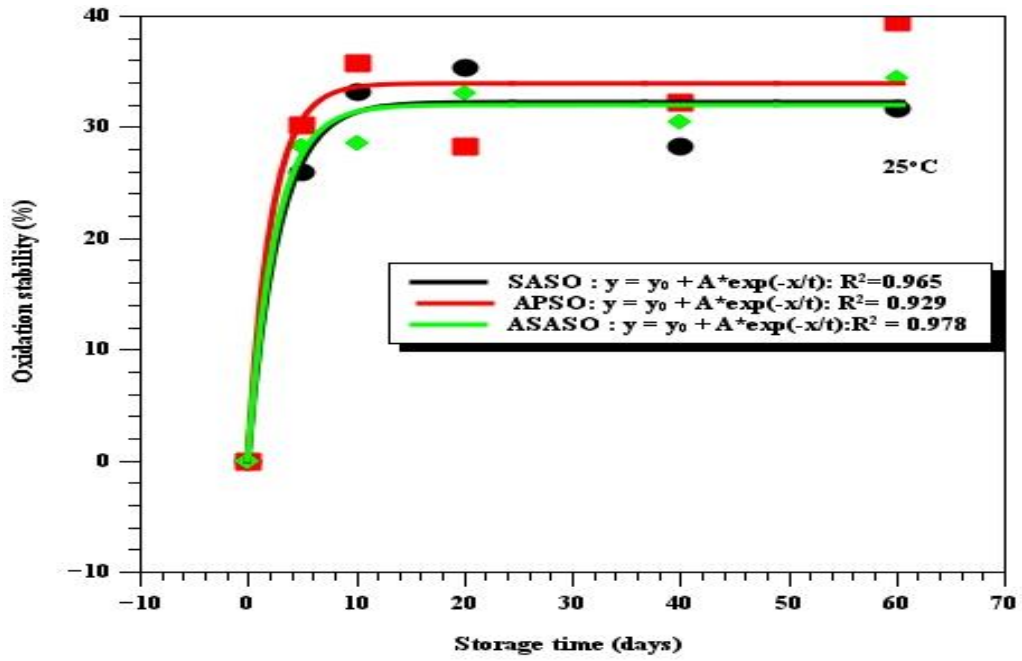

Figure 4.6: Oxidation stability of SASO, APSO and ASASO against storage time at room temperature (25°C).

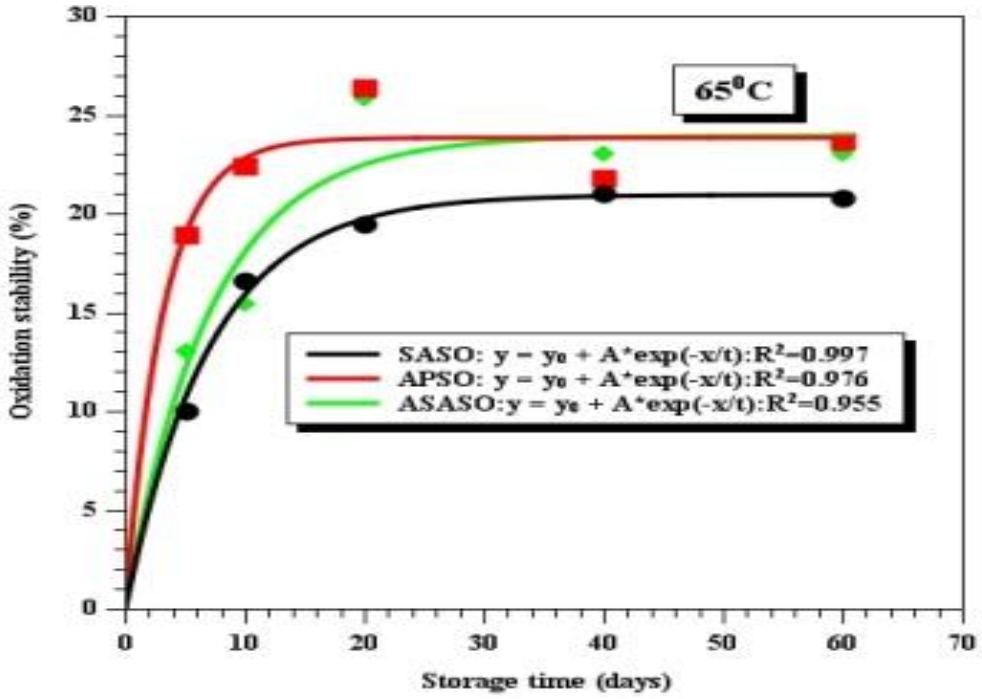

Figure 4.7: Oxidative stability of SASO, APSO and ASASO against time at elevated temperature (65 °C).

Table 4.9: Oxidation stability model analysis.

Sn	Oxidation stability	Best model equation	RMSE	Chi ^{2}/df	RSS	R^2	Adj.R^2
1	SASO at25°C	Y= 32.22-32.29e$^{(-x/2.83)}$	3.1574	9.96	29.9080	0.965	0.912
2	APSO at 25°C	Y= 33.89-33.91e$^{(-x/2.15)}$	4.8503	2.35	70.9080	0.929	0.823
3	ASASO at 25°C	Y= 32.22-32.29e$^{(-x/2.50)}$	2.4815	6.15	18.4744	0.977	0.944
4	SASO at 65°C	Y= 32.22-32.29e$^{(-x/7.02)}$	0.5923	3.51	1.0525	0.997	0.992
5	APSO at 65°C	Y= 32.22-32.29e$^{(-x/3.19)}$	1.8964	3.59	10.7896	0.9763	0.941
6	ASASO at 65°C	Y= 32.22-32.29e$^{(-x/7.15)}$	2.6269	6.90	20.7024	0.9548	0.887

4.6 Optimization of Biodiesel Production

4.6.1 Effect of operating conditions on biodiesel yield and viscosity

The results of the variation of the methyl ester yields and viscosity of sweet almond, African pear and African star apple seed oils with process conditions are presented in Table A5.1. Figures 4.8 to 4.15 show the plots of the biodiesel yield (wt %) and viscosity (mm^2/s) as functions of the operating conditions.

4.6.1.1 Effect of temperature on biodiesel yield

Figure 4.8 shows the effect of temperature on the biodiesel yield of the feedstocks. The influence of temperature on methyl ester yields during sweet almond, African pear and African star apple seed oils transesterification using NaOH catalyst was investigated over the temperature range of 40-75 °C. The yields of sweet almond methyl ester (SASOME), African pear seed oil methyl ester (APSOME) and African star apple seed oil methyl ester (ASASOME) were observed to increase with increase in temperature up to 65˚C. Increase in temperature increases the energy of the reacting molecules and also improves the miscibility of the alcoholic polar media into a non-polar oily phase (Dennis *et al.*, 2009). These could result in a much favoured reaction as observed here before 65°C. However, the lower yields observed at reaction temperature below 65°C could be due to the inability of the supplied heat to reduce the viscosities of the oils. After the maximum yields obtained at 65˚C, the yield decreased. This could be due the fact that at elevated temperatures, saponification reaction is favoured over transesterification (Nagaranja, *et al.*, 2014; Veranda *et al.*, 2011). Also, at elevated temperature beyond methanol boiling point (65°C), methanol could significantly get lost from the reaction mixture. These could justify the decrease in yield of the methyl esters with increase in temperature beyond 65˚C as obtained in this study. Ealier researchers have reported that transesterification should be processed between

60-70˚C (Moreira *et al.*, 2010, Leung and Guo, 2006). It could therefore be asserted that 65°C is the optimum temperature for maximum ester yields (95.5, 94.5 and 80.50% for SASOME, APSOME and ASASOME respectively).

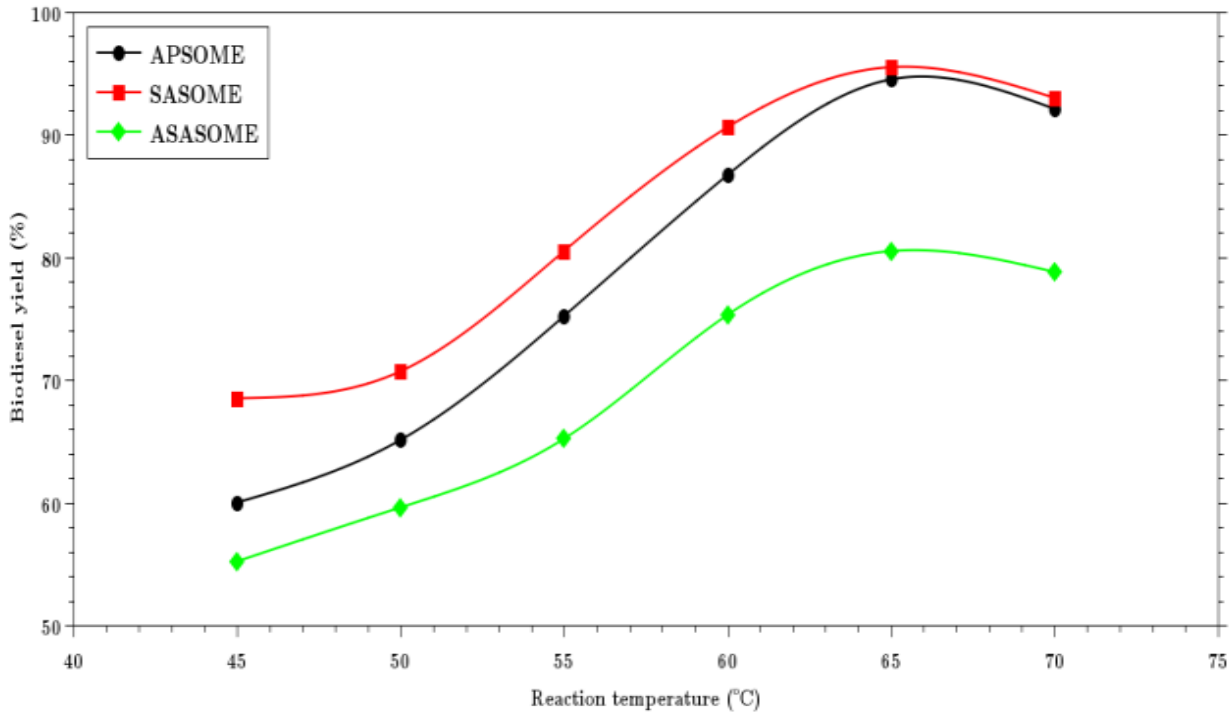

Figure 4.8: The effect of reaction temperature on yield.

4.6.1.2 Effect of temperature on biodiesel viscosity

The effect of reaction temperature on methyl esters viscosity studied between 45-70 °C is shown in Figure 4.9. The viscosity of the biodiesel samples increased slightly with increase in reaction temperature. Since the saponification reaction is more favoured at elevated temperature, more soap which is more viscous would be formed as the temperature increases. Furthermore, soaps allow emulsification which causes glycerol-ester phases separation to be less sharp (Mushtaq *et al.*, 2014). This could explain why the viscosity kept on increasing with increase in temperature. However, from 65˚C where there are highest yields of 80.50%, 95.50% and 94.50% for ASAOME, SASOME and APSOME respectively, the change in the viscosities of the methyl esters became less significant. Since the viscosities obtained at the optimum yield temperature are 3.42mm^2/s, 3.48mm^2/s and

3.55mm^2/s for ASAOME, SASOME and APSOME respectively, and they compare with ASTM and EN standards (Table 4.2), 65°C could be selected as the optimum temperature for efficient viscosity.

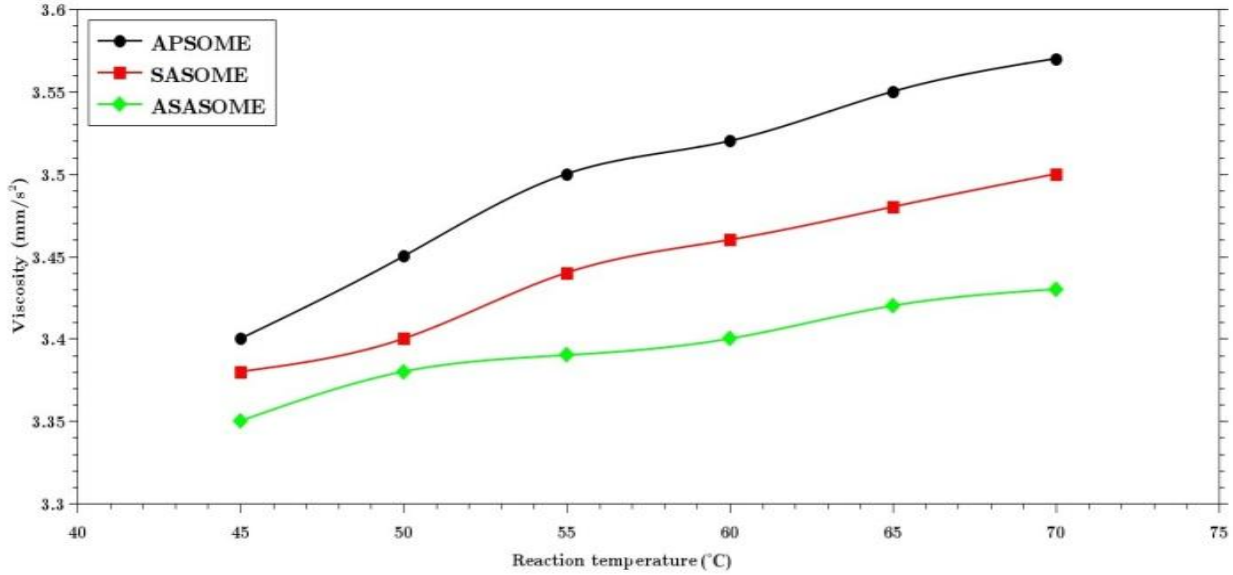

Figure 4.9: The effect of reaction temperature on viscosity.

4.6.1.3 Effect of reaction time on biodiesel yield

The effects of reaction time between 45-75 minutes on SASOME, APSOME and ASASOME yield is shown on Figure 4.10. It was observed that the yields increased significantly as the reaction time increased. This is due to the fact that longer reaction creates more contact time for the reacting species. Maximum yields of 94.40%, 92.50% and 84.50%, for SASOME, APSOME and ASASOME, respectively at 65 minutes. However, with additional five minutes reaction time, 2.10%, 2.70% and 4.60%, decrease in yields respectively was observed. Similar observations have been made, where the methyl yield reaches a maximum at reaction time below 90 minutes, and remains relatively constant with further increase in the reaction time (Alamu *et al*., 2007). Excessive reaction time during catalyzed transesterification favours backward reaction which causes reduction in yield (Dennis *et al.,* 2009). In this study, the observed decrease in yield of the methyl esters beyond 65 minutes reaction time could be because the backward reaction was favoured at

higher reaction time beyond 65 minutes and this could have resulted in a loss of methyl esters as well as cause more fatty acids to form soaps.

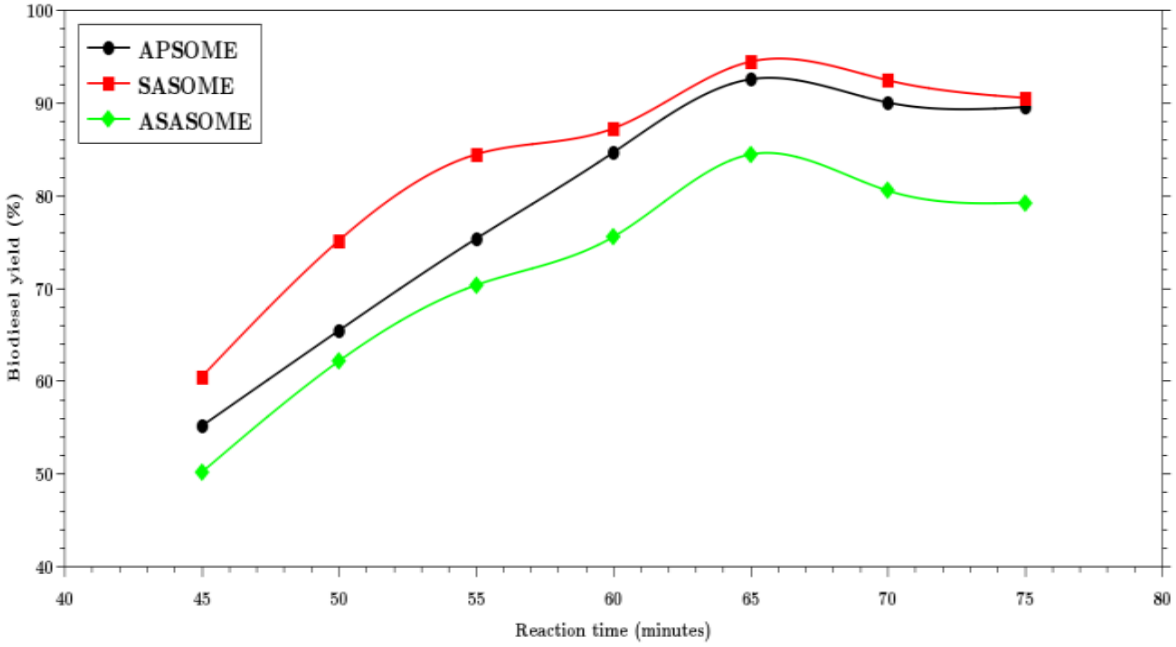

Figure 4.10: Effect of reaction time on yield.

4.6.1.4 Effect of reaction time on biodiesel viscosity

Figure 4.11 shows the effect of reaction time on the viscosity of the SASOME, ASASOME and APSOME produced within 45-75 minutes reaction time. The viscosites are observed to decrease with increase in reaction time but had a slight increase from 65minutes to 70 minutes reaction time in the case of ASASOME before it became steady (Figure 4.8). Lowering the viscosity of triglycerides is one of the key reasons of transesterification process. The lowest achievable kinematic viscosity were 2.0mm^2/s, 2.88mm^2/s and 2.91mm^2/s for ASASOME, SASOME and APSOME respectively which gave 65.30, 64.18 and 67.30% decrease in the kinematic viscosities of the respective parent seed oils. Hence, it could be asserted that as the reaction proceeds, the viscosities decrease while FAME yield increases till 65minutes, after which the reverse becomes the trend. The increase in viscosity

from 65 minutes time could be due to soap formation (more viscous) which is favoured at longer reaction time.

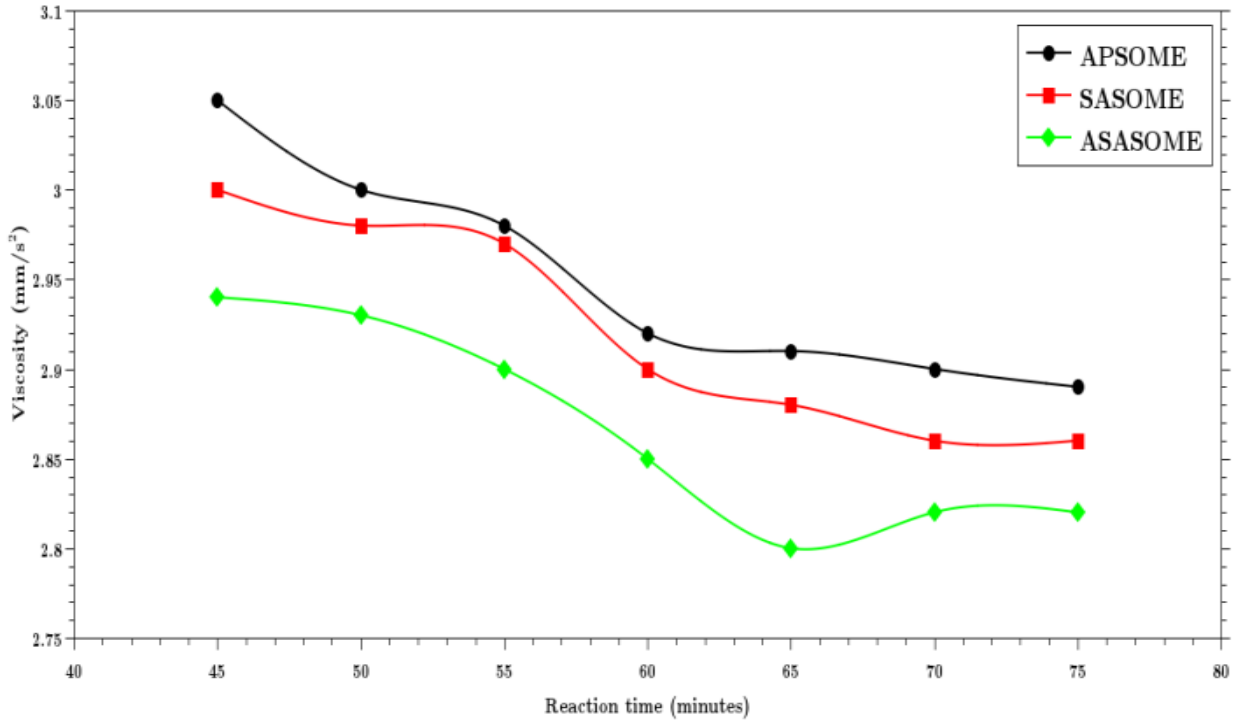

Figure 4.11: Effect of reaction time on viscosity.

4.6.1.5 Effect of catalyst concentration on biodiesel yield

Figure 4.12 shows the effect of NaOH catalyst concentration on the methyl esters yield. It was observed that the biodiesel yields increased when the catalyst concentration increased from 0.5wt% to 1.5wt%. The lower yields observed at lower catalyst concentrations was because an insufficient amount of catalysts result in an incomplete conversion of the triglycerides into fatty acid methyl esters (Leung and Guo, 2006). Optimum ester yield at 1.5wt.% of catalyst while using NaOH catalyst has been reported (Dennis et al., 2009). However, the methyl esters yields decreased when the catalyst concentration increased from 2.0wt% to 3.0wt%. This could be due to the fact that the higher concentration of NaOH catalyst favours saponification reaction. Also, the formation of water when the excess catalyst is added has been reported to inhibit transesterification

and favour hydrolysis (Mathiyazhagan and Ganapathi, 2011). The optimum catalyst amount in this study was found to be 1.5wt% for APSOME and 2.0wt% for both SASOME and ASASOME. The maximum yield obtained at these optimum catalyst concentrations were 86.5, 93.6 and 86.4% for APSOME, SASOME and ASASOME, respectively.

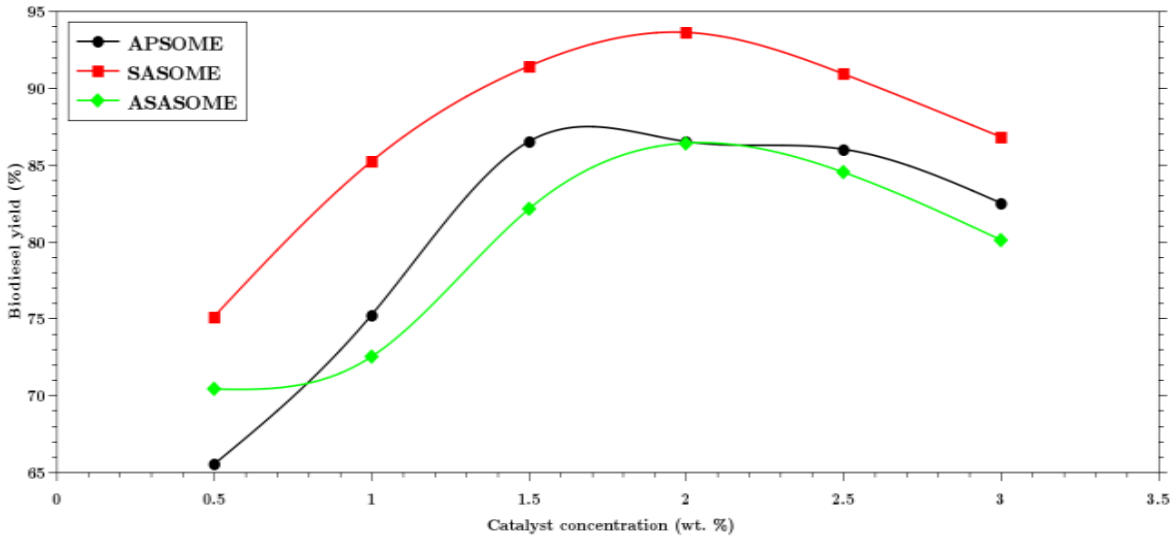

Figure 4.12: Effect of catalyst concentration on yield.

4.6.1.6 Effect of catalyst concentartion on biodiesel viscosity

The effects of catalyst concentration on the viscosity of biodiesel produced from the three feedstocks are shown in Figure 4.13. The viscosity of the produced FAME kept on decreasing with increase in catalyst concentration. However, after 2.5wt% catalyst concentration it became almost steady for APSOME and SASOME. However, for all the seed oils, the effect of catalyst concentration on viscosity became less noticeable after 2.0wt% catalyst concentration. Beyond 2.0wt% catalyst concentration, the yield decreased from maximum values of 86.40% and 93.60% for ASASOME and SASOME, respectively. Maximum APSOME yield of 86.50% with 1.5wt% catalyst concentration at higher viscosity of 3.45mm^2/s was observed against 2.71mm^2/s and 2.81mm^2/s obtained in the case of ASASOME and SASOME respectively. However, these values are found to be within the international standard of 1.9-6.0 mm^2/s (ASTM D 6751).

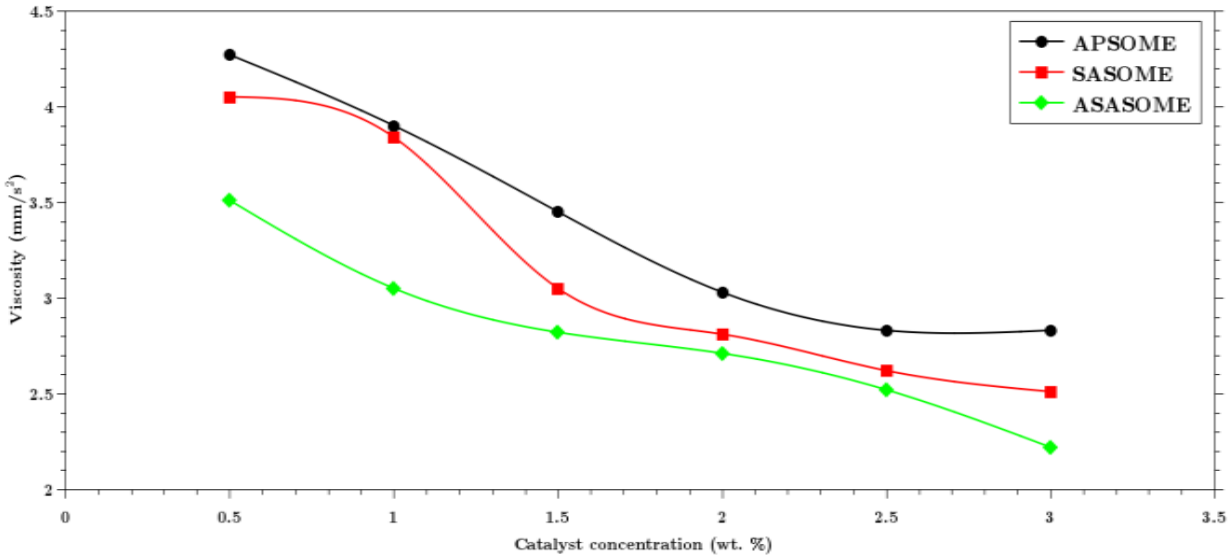

Figure 4.13: Effect of catalyst concentration on viscosity.

4.6.1.7 Effect of methanol to oil molar ratio on biodiesel yield

The effect of methanol to oil molar ratios on the biodiesel yiels from the three seed oils are shown in Figure 4.14. The effect of methanol to oil molar ratio was studied between 3:1 and 8:1 molar ratios. It was observed that increase in the molar ratio from 3:1 to 8:1 increases steadily the yields from 64.5, 76.5 and 60.1% to 85.7, 93.5 and 88.0% for ASASOME, SASOME and APSOME, respectively. Stoichiometrically, 3 moles of alcohol are required for 1 mole of triglyceride in transesterification to produce 3 moles of fatty acid ester and 1 mole of glycerol (Dennis *et al.*, 2009). However, in practice, higher molar ratio is needed to drive the reaction to completion at a faster rate (Dennis *et al.*, 2009). Therefore, it was observed that ester yield increased with increase in molar ratio beyond 3:1 methanol to oil molar ratio. It is equally observed that as the molar ratio rises above a certain level (7:1), it started having no significant effect on the biodiesel yield. Several studies have reported similar results about molar ratio (Anwar and Rashid, 2007). But among the molar ratio studied, molar ratio of 8:1 and 7:1 gave the best results of 93.5% and 87.68% biodiesel

yields for SASOME and APSOME respectively. Considering economic factors, the ASASOME optimum methanol to oil molar ratio could be selected to be at 6:1 that gave 82.5% methyl ester yield. At ratio higher than 8:1 methanol/oil molar ratio, the yield seemed to increase insignificantly for APSOME. This could be due to the diminution of the catalyst concentration by excess of alcohol according to Liu *et al.,* (2007). Similar explaination goes for the observed insignificant increase of biodiesel yield beyond 6:1 methanol to oil molar ratio. Beyond the optimal molar ratios, increasing the molar ratios does not have significant increase in biodiesel yield but rather increases the cost for alcohol recovery (Leung and Guo, 2006).

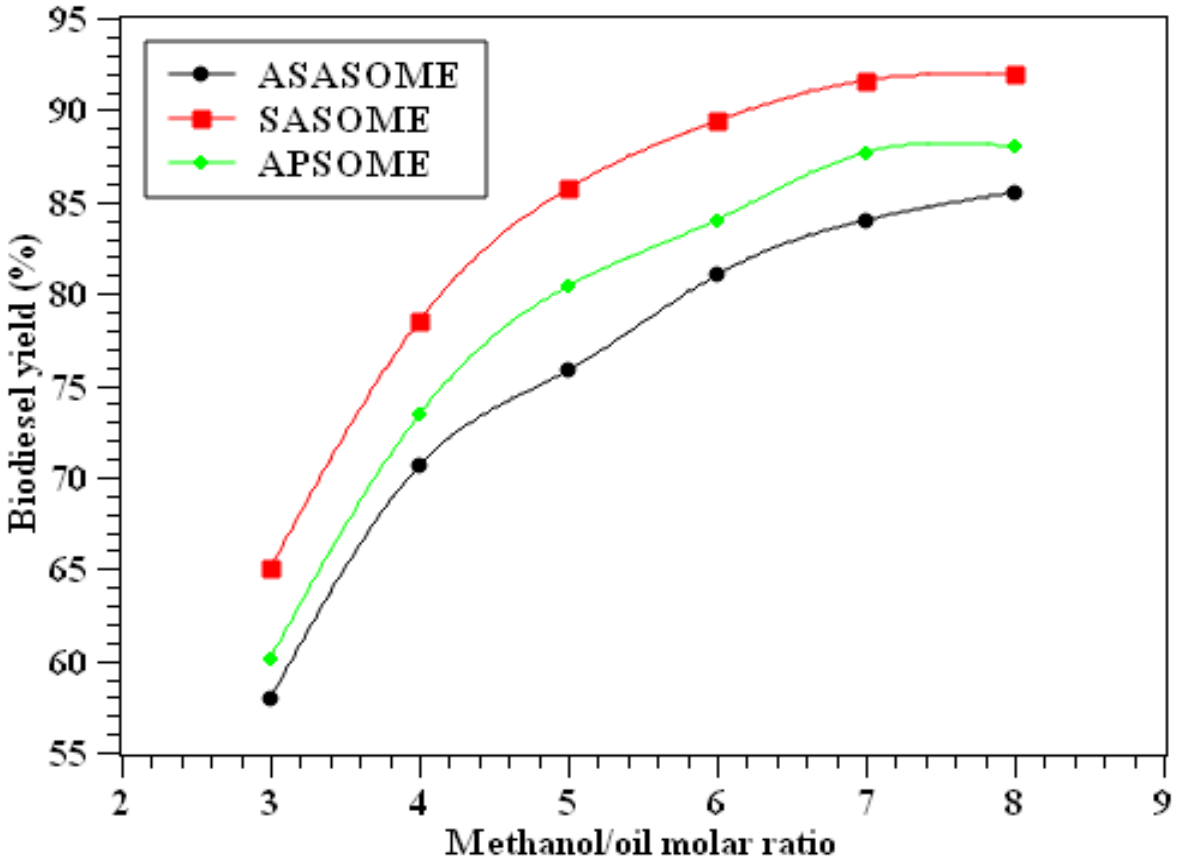

Figure 4.14: Effect of methanol/oil molar on yield.

4.6.1.8 Effect of methanol to oil molar ratio on biodiesel viscosity

The effect of methanol to oil molar ratios on the methyl esters viscosity is shownin Figure 4.15. The viscosities decreased significantly with increase in the methanol to oil molar ratios until 6:1 molar ratio. It was observed that from 6:1 metanol to oil molar ratio, the viscosity of the methyl esters showed no much significant decrease. Then from molar ratio of 7:1, the viscosity of APSOME and ASASOME started increasing while that of SASOME appeared almost steady. This could be because glycerol which is a by-product of the reaction would largely dissolve in the excessive methanol and subsequently inhibit the reaction of methanol to reactants and catalyst, thus interfering with the separation of glycerine (Ismaila *et al.*, 2016). The poor phase separation could have caused increase in the viscosity of the methyl esters produced. Since the optimum yields of the methyl esters were selected on economic basis to be at 6:1 methanol to oil molar ratio, and the viscosities increase beyond this ratio, the same ratio (6:1) could be selected for optimum viscosities of 2.55, 2.69 and 2.7 mm^2/s for ASAOME, SASOME and APSOME respectively.

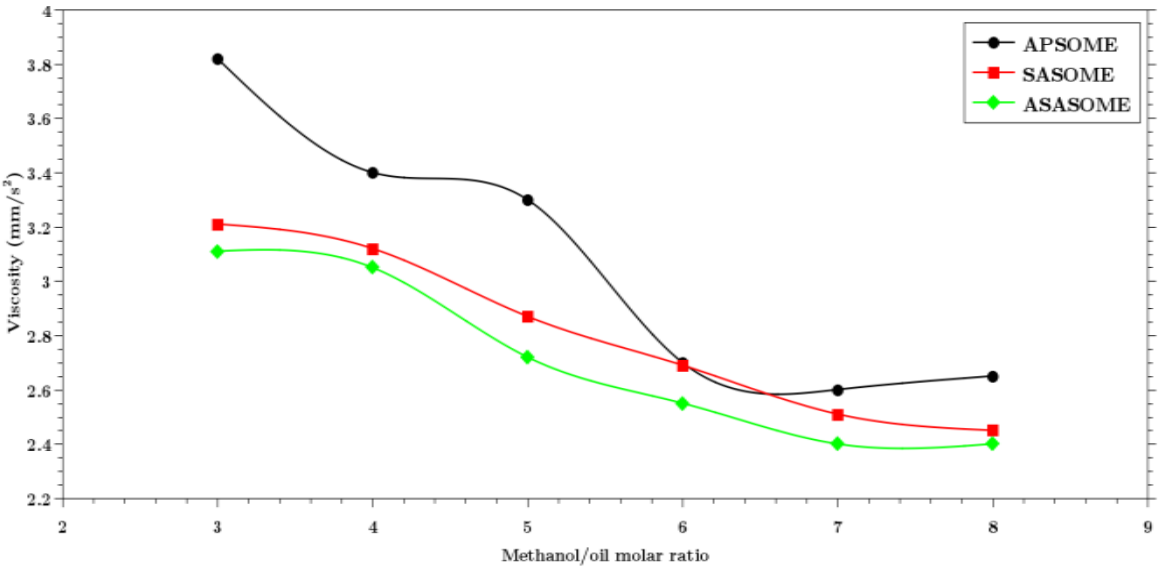

Figure 4.15: Effect of methanol/oil molar on viscosity.

Therefore, the study of the effects of production variables shows that the methylic transesterification of the APSO, SASO and ASASO is optimized at mixing rate of 140rpm, temperature of 65°C, reaction time of 65 minutes, methanol to oil molar ratio of 6:1 and catalyst concentration of 1.5wt%, 2.0wt% and 2.0wt% respectively to produce methyl ester yields of 94.50%, 95.50% and 85.70% and viscosity of 2.60mm^2/s, 2.45mm^2/s and 2.40mm^2/s respectively.

4.6.2 Optimization of biodiesel production using RSM

4.6.2.1 African pear seed oil esterification optimization using RSM

The responses obtained from different experimental runs carried out by combination of four variables are presented in Table 4.10. The four experimental variables interactions gave a total of 30 experimental runs which comprises of 24 individual runs and 6 similar runs.

Table 4.10: Central composite design of APSO esterification with actual, RSM and ANN predicted values.

Run	A (˚C)	B (wt %)	C (min.)	D(mol/mol)	Actual %FFA	predicted	
						RSM	ANN
1	-1	-1	-1	-1	0.95	0.9305	0.8847
2	1	-1	-1	-1	0.89	0.7310	0.9417
3	-1	1	-1	-1	0.90	0.7303	0.8748
4	1	1	-1	-1	1.00	0.7286	0.9836
5	-1	-1	1	-1	0.48	0.4723	0.5024
6	1	-1	1	-1	0.66	0.6652	0.6698
7	-1	1	1	-1	0.84	0.7540	0.5724
8	1	1	1	-1	1.00	0.9735	1.0433
9	-1	-1	-1	1	0.46	0.6780	0.5836
10	1	-1	-1	1	0.72	0.7329	0.7618
11	-1	1	-1	1	0.57	0.6357	0.5309
12	1	1	-1	1	0.85	0.7325	0.8393
13	-1	-1	1	1	0.92	1.0749	0.8652
14	1	-1	1	1	0.84	0.7950	0.8520
15	-1	1	1	1	0.66	0.7276	0.6686
16	1	1	1	1	1.05	1.2719	1.0476
17	-2	0	0	0	0.49	0.5745	0.5303
18	2	0	0	0	0.55	0.5807	0.6973
19	0	-2	0	0	0.74	0.7806	0.7281
20	0	2	0	0	0.68	0.6787	0.6873
21	0	0	-2	0	0.57	0.5292	0.6556
22	0	0	2	0	1.20	1.3240	1.1788
23	0	0	0	-2	1.11	0.9741	1.0900
24	0	0	0	2	1.00	0.9760	1.1047
25	0	0	0	0	0.99	0.9767	0.9102
26	0	0	0	0	1.00	0.9767	0.9102
27	0	0	0	0	1.00	0.9767	0.9102
28	0	0	0	0	1.00	0.9767	0.9102
29	0	0	0	0	0.99	0.9767	0.9102
30	0	0	0	0	1.00	0.9767	0.9102

4.6.2.1.1 Combined effects of operating parameters on the esterification response. The esterification process of the African pear seed oil was analyzed based on the various solutions obtained at possible reacting conditions from the model predictive equation. RSM flexibility in navigating the design space makes it to be considered appropriate. The equation was solved for the various interactive effects on esterification process to minimize the free fatty acid content of African pear seed oil for maximum biodiesel yield. The interaction between only two factors was considered at any instance while setting the other variables at their mean coded value of zero. The interactive effects of adjusting the process variables within the design space were monitored using 3D surface plots and every significant interaction effects. The analyses and optimization exercise were completed using the Design Expert 7.0.0 version and the graphical solutions are presented in Figures 4.16a to 4.16f

Figure 4.16a represents the combined effect of catalyst concentration and temperature on the APSO FFA reduction while maintaining the reaction time and molar ratio at 55 minutes and 12:1 respectively. It could be observed that increase of catalyst concentration at low temperature up to about 65^{o}C results in low FFA. But beyond this temperature, the FFA increases at all amounts of catalyst used. After 65 ^{o}C the cumulative curves of FFA reduction looked like a stretched "u" letter shape within the catalyst concentration of 5-25wt%, which shows that the lowest FFA appeared in the range of 5-15 wt%.

Fig 4.16b shows the effects of temperature and reaction time on the FFA reduction of APSO for improved biodiesel yield. This was done by keeping catalyst concentration and methanol to oil molar ratio at constant values of 15.0wt% and 12:1 respectively. Lowest value of FFA was obtained at reaction time and temperature between 45-60minutes and 55-

70 ^{o}C respectively. It implies that beyond these reaction time and temperature ranges, the backward reaction is more favoured as less concentration of the reactants could not promote effective forward reaction according to collision theory. Otherwise, the water formed during esterification can be constantly removed from the reaction mixture to enable the forward reaction to continue beyond the optimum temperature and reaction time conditions observed.

Figure 4.16c shows the observed interaction effect of temperature and molar ratio of methanol to FFA. The quadratic effect of temperature and molar ratio were identified with smooth curves. The process response (%FFA) is minimized in a similar fashion as the methanol to oil molar ratio is increased from low value of 6:1 to mean value between 12-14w/w%. The quadratic effect of methanol/ oil molar ratio is observed to be more significant than the temperature. Increasing the methanol amount beyond the optimum range showed no significant effect to acid value or FFA. This could be due to the effect of water produced during the esterification (Berchmans and Hirata, 2008). The %FFA has been found to increase due to the hydrolysis of triglycerides in the presence of moisture and oxidations (Berchmans and Hirata, 2008). The oxidation of the high unsaturated fatty acids of APSO might occur easily and result in more release of more free fatty acid. At low temperature the conversion efficiency is noted to be very low (about 10% only). With increase in temperature the conversion takes place at a faster rate. At higher reaction temperatures, beyond 65^{o}C there is a chance of loss of methanol. Since high reaction temperature increase the production cost of biodiesel through high energy supply, the optimum conditions of temperature observed in this study would make economic sense.

Figure 4.16d shows the plot of the combined effects reaction time and catalyst concentration. The temperature and methanol/oil molar ratio were kept at constant values of 65^{o}C and 12:1 respectively. The quadratic effect of reaction time is observed to be more than that of catalyst concentration, which is observed through the smoother curve of the

reaction time than catalyst concentration. It implies that reaction time has more effect than catalyst concentration. At all values of catalyst concentration, the FFA of APSO is minimized within the range of 45-60 minutes reaction time. It means that running the esterification at the observed optimum reaction time accommodates 5-25wt% range of catalyst concentration for minimum FFA result. However, at higher temperature beyond 60^{o}C, the %FFA increases which could be due to loss of collision theory controlled reaction. Also, at lower temperature below 50^{o}C clearly results in poor FFA reduction, which could be due to short of enough kinetic energy for the reactants.

Figure 4.16e represents the combined effects of methanol/oil molar ratio and the catalyst concentration on the FFA reduction while keeping the temperature and reaction time at constant values of 65^{o}C and 55 minutes respectively. At all the range of values studied from the two combining variables, the FFA values were all low (below 0.43%). It shows that the effect of the methanol/oil molar ratio and catalyst concentration is very significant. However, the quadratic effect of methanol/oil molar ratio appears more than that of catalyst concentration. The minimum value of the %FFA (less than 0.30 wt%) appeared between 12:1-15:1 methanol/oil molar ratio irrespective of the catalyst concentration. Therefore, considering this range of methanol/oil molar ratio, lowest catalyst concentration of 5wt% is advantageous as the FFA content of APSO can conveniently be reduced at low raw material costs.

Figure 4.16f represents the plot showing the results of the effects of reaction time and molar ratio of methanol to oil while maintaining catalyst concentration and temperature of the reaction contant at 15wt% and 65^{o}C respectively. As expected for a typical controlled minimization process, the free fatty acid content of African pear seed oil decreases readily with increase in reaction time at all methanol to oil molar ratios. This is explained to mean that the more the reaction stays, the more the free fatty acid of the seed oil is converted to methyl ester and water and the more the FFA reduces. Reaction time

could be observed to have significant effect on the African pear seed oil FFA reduction or conversion to methyl ester. This agrees with results of Jansri *et al,* (2011) who observed over 92% conversion of FFA content of mixed crude palm oil within 5 min of commencement of esterification reaction. However, increasing the reaction time beyond 60minutes results in the increase in %FFA. This means that beyond this reaction, the backward reaction which favours free fatty acid formation is favoured, irrespective of the molar ratios. The minimum FFA was obtained between 9:1- 15:1 methanol/oil molar ratio.

4.6.2.1.2 APSO esterification ANOVA analysis and model fitting. The F-value, lack of fit and R-squared value tests were performed using analysis of variance (ANOVA) to calculate the significance of each type of model. The only model that satisfied the criteria is found to be quadratic model and hence it was selected. The effect of each parameter was evaluated using the quadratic model as shown in Table 4.11. Many appraisal techniques such as coefficient of determination (R^2), adjusted coefficient of determination (adj. R^2) and coefficient of variation (C.V) were used to weigh the adequacy of the model as used by other researchers (Sarve *et al.,* 2015). The Model F-value of 3.61 implies the model is significant and that there is only a 0.95% chance that a model F-value this large could occur due to noise. Values of "Prob> F" less than 0.0500 indicate model terms are significant. In this case the linear coefficients A, B, C; the cross-products, AB, AC, AD, BD, CD, and the quadratic coefficients, A^2, C^2, D^2 are significant model terms. Values greater than 0.1000 indicate the model terms are not significant. It shows that the effect of most independent variables on the APSO FFA reduction was significantly high. It could be ascertained that the degree of significant effect of the process parameters is in the order of: temperature > reaction time > catalyst concentration > molar ratio. In addition, the squares of temperature, reaction time and methanol/oil molar ratio are significant in the African pear seed oil esterification process. This could mean that these factors whose square are significant have

better effect on the esterification process (Awolu and Layokun, 2013). The "Lack of Fit F-value" of 0.8355 implies the 'Lack of Fit' is not significant relative to the pure error. The non-significant lack of fit is good because it shows that the model will be well fitted (Ohale et al., 2017). "Adeq Precision" measures the signal to noise ratio. A ratio greater than 4 is desirable (Table 4.12). The ratio of 6.791 indicates an adequate signal and that this model can be used to navigate the design space. The coefficient of variation (C.V) is the ratio of the standard deviation of estimate to the mean value of the observed response and as well independent of the unit (Ohale, *et al.,* 2017). It is also a measure of reproducibility and repeatability of the models (Chen *et al.*, 2011). Therefore, the C.V value of 38.86 shows the model is reasonably reproducible. Apart from the F-value, lack of fit and C.V, the R-squared of 0.8077 also shows that more than 80% of the overall variability can be explained by the empirical models of the Equations. The adj. R-squared and the predicted R-squared values of 0.7769 and 0.7214 respectively for the quadratic model are in reasonable agreement since the difference is less than 0.2 (Uzoh *et al.,* 2019).

4.6.2.1.3 APSO esterification model equations. The selected models in terms of the coded, actual and actual significant terms are given in Equations (4.8), (4.9) and (4.10) respectively. The equation in terms of coded factors can be used to make predictions about the response for given levels of each factor. By, defaults, the high levels of the factors are coded +2 and the low levels of the factors are coded as -2. The coded equation is useful for identifying the relative impact of the factors by comparing the factors coefficients, while the equation in terms of actual factors can be used to make predictions about the response for actual levels of each factor (Ohale *et al.,* 2017). Analyzing the obtained model, it is observed that factors B and D present negative effects, showing that at lower factor values, lower FFA are obtained while the interactive effects of AB, AC, AD, BC and CD were

significantly negative, showing that increase in the levels of the variables results in a increase in FFA (Zanette *et al.*, 2011).

APSO FFA reduction (%) = +0.25 +0.13 A - 0.039 B + 0.11 C - 0.065D - 0.11 AB - 0.078 AC – 0.004688AD - 0.066 BC + 0.023BD - 0.14CD + 0.12A^2 + 0.026B^2 + 0.16 C^2 + 0.13 D^2 (4.8)

APSO FFA reduction (%) = +3.53644 -0.081207 * Temperature (+ 0.089730 * Catalyst Conc. - 0.078066 * Reaction Time + 0.033304 * methanol/oil molar ratio -1.07188E-003 * Temperature * Catalyst Conc. - 7.84375E-004 * Temperature * Reaction Time -7.81250E-005 * Temperature * methanol/oil molar ratio -6.59375E-004 * Catalyst Conc. * Reaction Time +3.80208E-004 * Catalyst Conc. * methanol/oil molar ratio -2.34896E-003 * Reaction Time * methanol/oil molar ratio +1.18469E-003 * Temperature^2 +2.59687E-004 * Catalyst Conc.^{2} +1.62219E-003 * Reaction Time^2+3.51997E-003 * methanol/oil molar ratio^2 (4.9)

APSO FFA reduction (%) = +3.53644 -0.081207 * Temperature + 0.089730 * Catalyst Conc. - 0.078066 * Reaction Time -1.07188E-003 * Temperature * Catalyst Conc. - 7.84375E-004 * Temperature * Reaction Time -7.81250E-005 * Temperature * methanol/oil molar ratio +3.80208E-004 * Catalyst Conc. * methanol/oil molar ratio -2.34896E-003 * Reaction Time * methanol/oil molar ratio +1.18469E-003 * Temperature (°C)^2 +1.62219E-003 * Reaction Time (min)^2+3.51997E-003*methanol/oil molar ratio^2 (4.10)

Table 4.11: ANOVA for response surface quadratic APSO esterification model.

Source	Sum of Squares	Df	Mean Square	F-Value	p-value Prob> F	
Model	2.73	14	0.2	3.61	0.0095	Significant
A- Temperature (°C)	0.38	1	0.38	7.1	0.0177	
B-Catalyst conc. (wt%)	0.36	1	0.36	6.6	0.04295	
C-Reaction time (min)	0.31	1	0.31	5.68	0.0308	
D-Methanol/oil molar ratio	0.1	1	0.1	1.86	0.1929	
AB	0.36	1	0.36	6.6	0.04295	
AC	0.43	1	0.43	8.2	0.01303	
AD	0.52	1	0.52	9.62	0.0029	
BC	0.07	1	0.07	1.29	0.2745	
BD	0.31	1	0.31	5.68	0.0308	
CD	0.32	1	0.32	5.88	0.0284	
A^2	0.38	1	0.38	7.12	0.0175	
B^2	0.018	1	0.018	0.34	0.5673	
C^2	0.72	1	0.72	13.35	0.0024	
D^2	0.44	1	0.44	8.15	0.0121	
Residual	0.81	15	0.054			
Lack of fit	0.29	10	0.02916	0.54	0.8355	Not significant
Pure error	8.33	5	1.66			
Cor. Total	3.54	29				

Table 4.12: Summary of APSO esterification regression values.

Std. Dev.	0.23	R^2	0.8077
Mean	0.6	AdjR^2	0.7769
C.V. %	38.86	Pred R^2	0.7214
PRESS	4.67	Adeq Precision	6.791

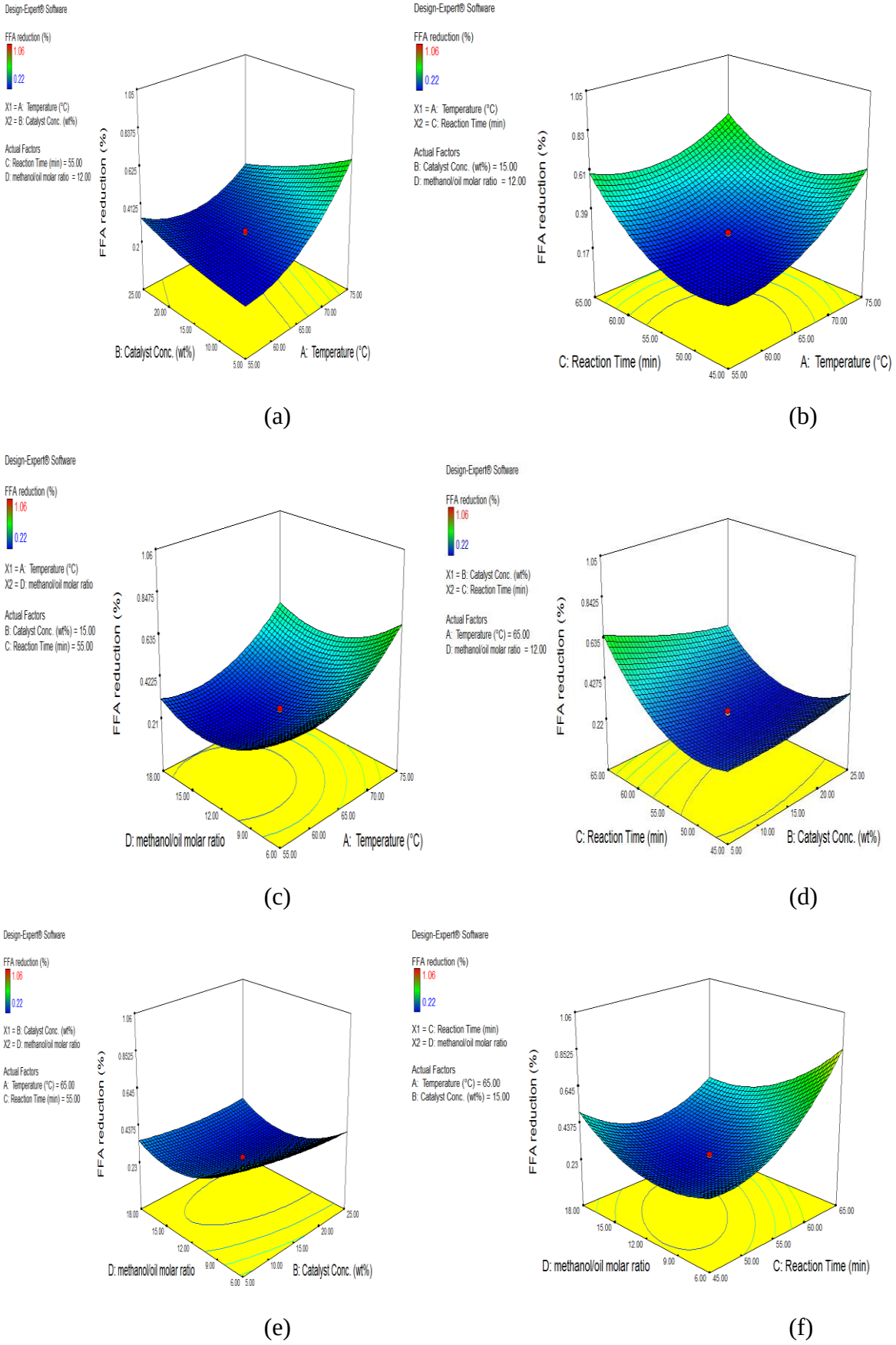

Figure 4.16: The 3D response surface plot of the effects of the variables on APSO FFA reduction

(a). Catalyst concentration and temperature (b). Reaction time and temperature
(c). Oil/methanol ratio and temperature (d). Reaction time and catalyst concentration
(e). Oil/methanol ratio and catalyst concentration (f). Oil/methanol ratio and reaction time

,

,

4.6.2.1.4 Esterification optimization process. The optimization exercise for the reduction of free fatty acid content of African pear seed oil through esterification process was conducted separately utilizing the flexibility of Design Expert 7.0.0 optimization tool function. Equation 4.9 was solved and the solution represents the optimized process conditions where minimum response of 0.29% FFA is obtained when the temperature is 55°C, concentration of H_2SO_4 is 5wt%, methanol to FFA molar ratio of 13:1 at reaction time of 60minutes (Table 4.13). Experiment was then performed using the optimal result and the results were in close agreement (0.29% predicted and 0.26% experimental). This value of FFA is observed to be within the limit of ASTM D 6751 and EN 14214 standard of 0.25%. The optimum value obtained in this research would promote the potential of biodiesel production from the esterified oil for high yield of methyl ester.

Table 4.13 : Optimum values of APSO free fatty acid reduction through esterification

Variables	Optimum values	%FFA		
		Experimental	Predicted	Desirability
Temperature (°C)	55			
Catalyst concentration (wt%)	5.0	0.26	0.29	1.00
Reaction time (min)	60			
Methanol /FFA molar ratio	13:1			

4.6.2.2 APSO esterification ANN modeling

4.6.2.2.1 Network training. The multilayer perception (MLP) technique used in this research was developed in MATLAB 8.5 version with four input neuron representing the process independent variables (temperature, reaction time, catalyst concentration and methanol to FFA molar ratio), a single hidden layer of 10 neurons and an output layer consisting of one neuron representing the percentage of FFA reduction . In order to reduce

the deviations of predictions from experimental values, a trial and error technique was employed to determine the adequate number of neurons required in the hidden layer. The multilayer perception architecture is shown in Figure 4.17. A total of 20(66%) of experimental result was used to train the network, 5(17%) of the experimental result was used to validate the training while the remaining 5(17%) was used for testing (Figure 4.18). After the selection of the hidden number of neurons a number of training runs were performed to look out for the best possible weights in error propagation framework and the final selected network architecture was trained for 15 iterations. The mean square error of the training, validation and testing network is 1.63705e-3, 2.41426e-2 and 1.0294e-2 with regression coefficients of 0.98149, 0.6906 and 0.9306 respectively (Figure 4.19). The linear fit model ($Y=0.89 * T + (0.12)$) generated by the validation outputs versus target plots shown in Figure 4.19 was used to predict the ANN model values: where Y = the ANN model value, T(target) = the experimental value used to generate the corresponding ANN value.

The graph of the correlation between the experimental value and the predictions by ANN and RSM is shown in Figure 4.20. It is clearly observed from the trends of ANN and RSM predictions against the experimental values for the respective runs that ANN and RSM had strong prediction capabilities but the ANN demonstrated stronger prediction and model developing capability.

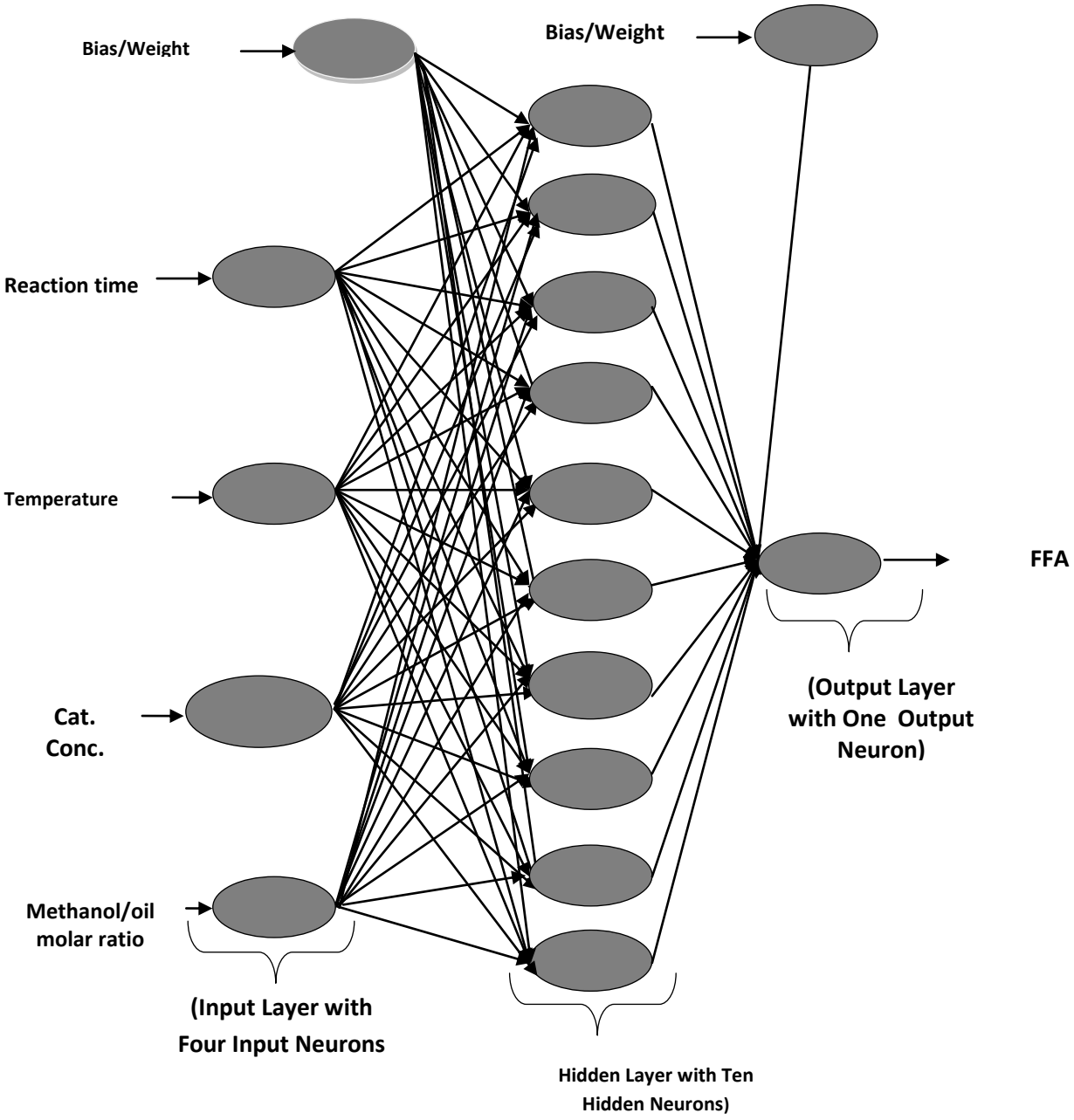

Figure 4.17: A typical ANN model architecture of the topology of the APSO FFA reduction

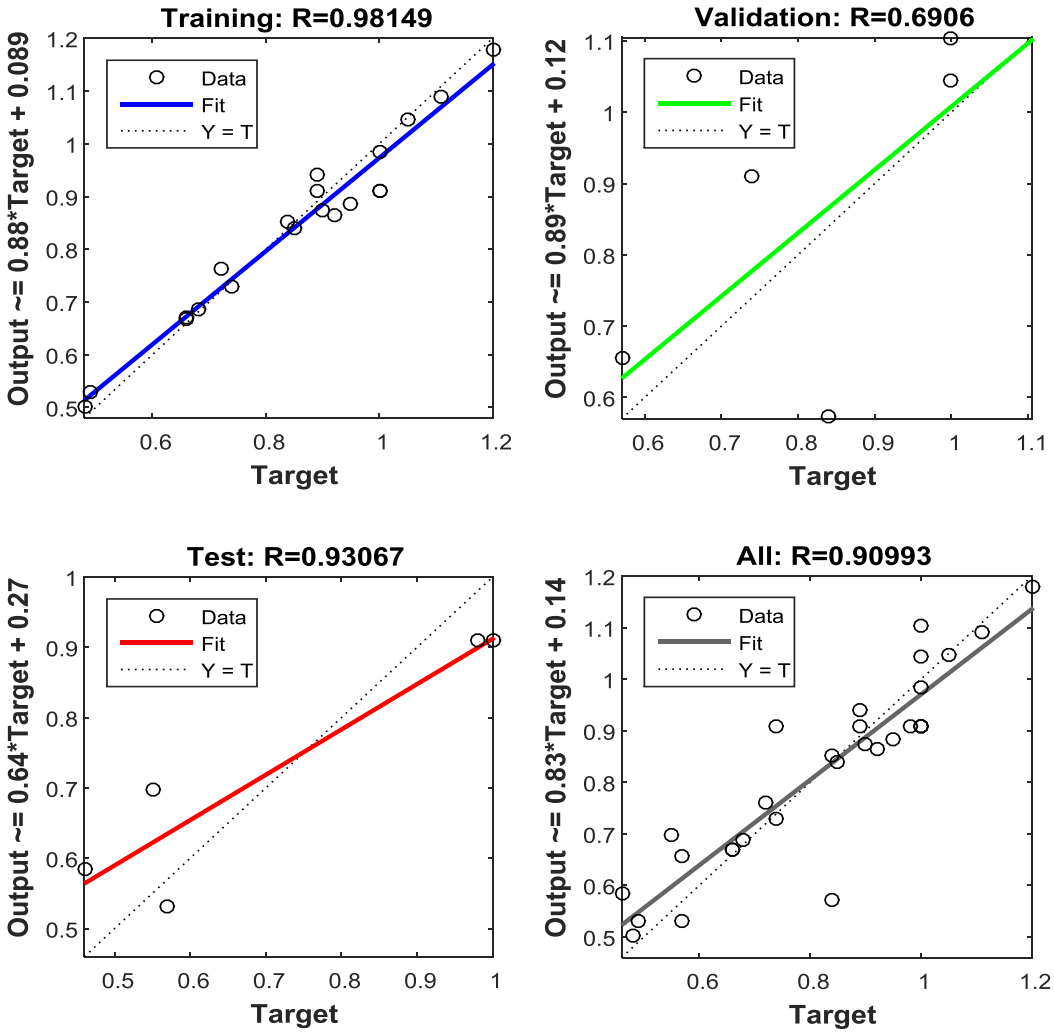

Figure 4.18: ANN regression values for training, test, validation and over all model for APSO esterification

Results

	Samples	MSE	R
Training:	20	1.63705e-3	9.81488e-1
Validation:	5	2.41426e-2	6.90595e-1
Testing:	5	1.02941e-2	9.30665e-1

Figure 4.19: MSE and R values for training, validation and testing of APSO esterification.

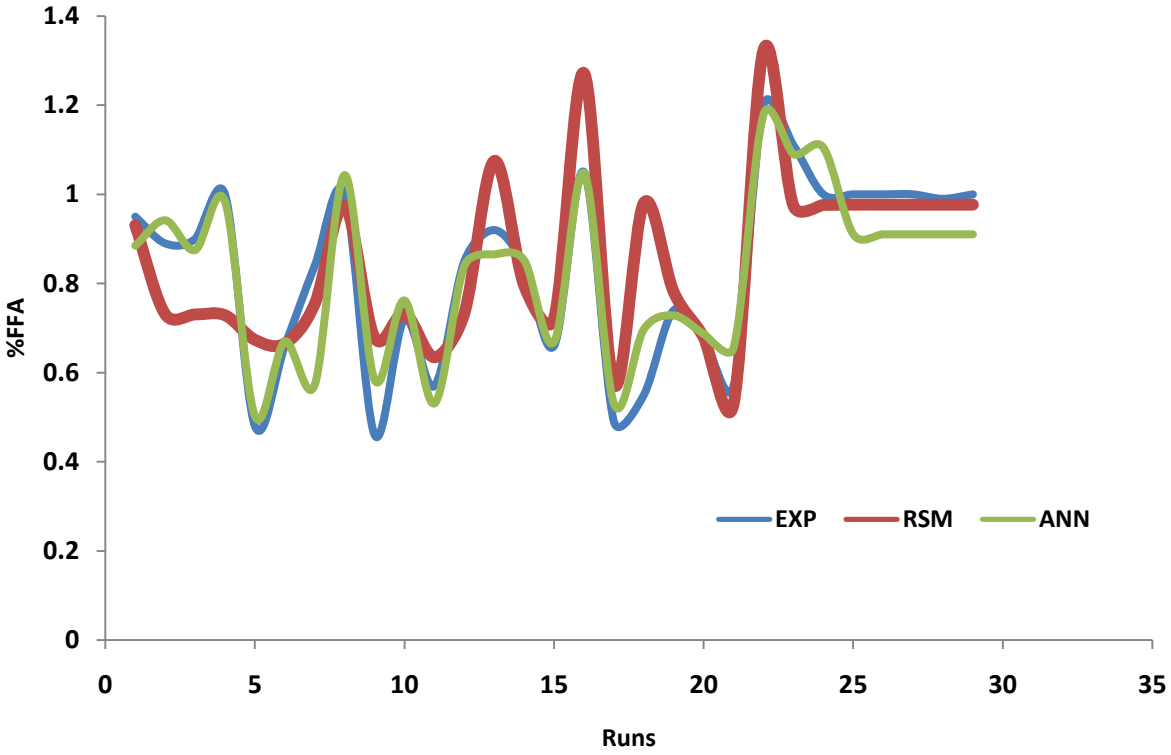

Figure 4.20: Comparison between experimental and predicted FFA using ANN and RSM.

4.6.2.3 RSM optimization of SASO transesterification process

A central composite design was applied to develop a correlation between the factors affecting transesterification reaction and the methyl ester yield. The complete design matrix, experimental and predicted responses is presented in Table 4.14. The experimental values of SASOME content obtained ranged from 66.84 wt% to 94.36 wt %.

Table 4.14: The CCD of five-level four-factor response surface study of SASOME production.

Run	Factor 1 A (^{o}C)	Factor 2 B (wt %)	Factor 3 C (mins)	Factor 4 D(mol/mol)	Actual value (%)	Predicted value (%)
1	40	1.0000	50	1:4000	80.7700	79.2754
2	60	1.0000	50	1:4000	70.5400	71.6404
3	40	2.0000	50	1:4000	66.8400	66.3137
4	60	2.0000	50	1:4000	69.6100	69.5587
5	40	1.0000	60	1:4000	84.8860	86.3597
6	60	1.0000	60	1:4000	87.6560	87.6047
7	40	2.0000	60	1:4000	83.9560	83.2380
8	60	2.0000	60	1:4000	86.7260	86.0330
9	40	1.0000	50	1:6000	67.7700	67.1823
10	60	1.0000	50	1:6000	71.5400	70.3273
11	40	2.0000	50	1:6000	65.8400	65.9606
12	60	2.0000	50	1:6000	69.7100	69.7556
13	40	1.0000	60	1:6000	85.8860	84.2066
14	60	1.0000	60	1:6000	86.6560	86.9016
15	40	2.0000	60	1:6000	85.9560	84.5349
16	60	2.0000	60	1:6000	86.7260	87.3499
17	30	1.5000	55	1:5000	74.4780	76.3376
18	70	1.5000	55	1:5000	80.0180	79.3776
19	50	0.5000	55	1:5000	78.1780	79.7043
20	50	2.5000	55	1:5000	86.3180	76.0110
21	50	1.5000	45	1:5000	60.1320	61.6583
22	50	1.5000	65	1:5000	94.3640	94.1967
23	50	1.5000	55	1:3000	77.2480	78.8357
24	50	1.5000	55	1:7000	76.9420	77.3425
25	50	1.5000	55	1:5000	76.8431	76.5521
26	50	1.5000	55	1:5000	76.8431	76.5527
27	50	1.5000	55	1:5000	76.8431	76.5521
28	50	1.5000	55	1:5000	76.8431	76.5521
29	50	1.5000	55	1:5000	76.8431	76.5521
30	50	1.5000	55	1:5000	76.8431	76.5521

4.6.2.3.1 SASOME production RSM quadratic model ANOVA analysis. The F-value, lack of fit and R-squared values tests were performed using analysis of variance (ANOVA) to calculate the significance of each type of model. The only model that satisfied the criteria is found to be quadratic model and hence it was selected. The effect of each parameter was evaluated using the quadratic model as shown in Table 4.15. Many appraisal techniques such as coefficient of determination (R^2), adjusted coefficient of determination (adj. R^2) and coefficient of variation (C.V) were used to weigh the adequacy of the model as used by other researchers (Sarve *et al.,* 2015). Values of "Prob> F" less than 0.0500 indicate model terms are significant. In this case A, B, C, AB, AC, BD, $A^{2,}$ and B^2 are significant model terms. Values greater than 0.1000 indicate the model terms are not significant. The Model F-value of 5.75 implies the model is significant. There is only a 0.09% chance that a "Model F-Value" this large could occur due to noise. The "Lack of Fit F-value" of 0.2429 implies the Lack of Fit is not significant relative to the pure error. There is a 24.29% chance that a "Lack of Fit F-value" this large could occur due to noise. Non-significant lack of fit is good. It shows that the effect of most independent variables on the SASO transesterification was significantly high. It could be ascertained that the degree of significant effect of the process parameters is in the order of: reaction time > temperature, catalyst concentration > molar ratio. Temperature and catalyst concentration have equal effect. In addition, the squares of temperature, reaction time and catalyst concentration are significant in the African pear seed oil transesterification process. This could mean that these factors whose square are significant have better effect on the esterification process (Awolu and Layokun, 2013). The non-significant lack of fit is good because it shows that the model will be well fitted (Ohale *et al.*, 2017). "Adeq Precision" measures the signal to noise ratio. A ratio greater than 4 is desirable (Table 4.16). The ratio of 8.148 indicates an adequate signal and that this model can be used to navigate the design space. The coefficient of variation (C.V) is the ratio of the standard deviation of estimate to the mean

value of the observed response and as well independent of the unit (Ohale *et al.*, 2017). It is also a measure of reproducibility and repeatability of the models (Chen *et al.*, 2011). Therefore, the C.V value of 6.75shows the model is reasonably reproducible. Apart from the F-value, lack of fit and C.V, the R-squared of 0.9429 shows that more than 94% of the overall variability can be explained by the empirical models of the Equations. The adj. R-squared and the predicted R-squared values of 0.8562 and 0.6947 respectively for the quadratic model are in reasonable agreement since the difference is less than 0.2 (Uzoh *et al.*, 2019).

4.6.2.3.2 SASOME production RSM model equations. The selected models in terms of the coded, actual and significant terms are given in Equations (4.11), (4.12) and (4.13) respectively. The equation in terms of coded factors can be used to make predictions about the response for given levels of each factor. By, defaults, the high levels of the factors are coded +2 and the low levels of the factors are coded as -2. The coded equation is useful for identifying the relative impact of the factors by comparing the factors coefficients, while the equation in terms of actual factors can be used to make predictions about the response for actual levels of each factor (Ohale *et al.*, 2017). Analyzing the obtained model, it is observed that none of factors present negative effects, while the interactive effects of AB, AC, AD, and BD were significantly negative, showing that increase in the levels of the variables results in a decrease in SASOME yield (Zanette *et al.*, 2011).

Table 4.15: ANOVA for SASOME yield response surface quadratic model.

Source	Sum of Squares	Df	Mean Square	F Value	p-value Prob> F	
Model	2157.2	14	154.09	5.75	0.0009	significant
A- Temperature	181.5	1	181.5	6.77	0.0200	
B-Catalyst Conc.	181.5	1	181.5	6.77	0.0200	
C-Reaction Time	190.2	1	190.2	7.09	0.0167	
D-methanol/oil molar ratio	28.17	1	28.17	1.05	0.3216	
AB	169	1	169	6.3	0.024	
AC	144	1	144	5.37	0.035	
AD	1	1	1	0.037	0.8495	
BC	36	1	36	1.34	0.2647	
BD	196	1	196	7.31	0.0163	
CD	9	1	9	0.34	0.5709	
A^2	1015.05	1	1015.05	37.86	< 0.0001	
B^2	304.76	1	304.76	11.37	0.0042	
C^2	92.19	1	92.19	3.44	0.0835	
D^2	48.76	1	48.76	1.82	0.1975	
Residual	402.17	15	26.81			
Lack of Fit	319.33	10	31.93	1.93	0.2429	not significant
Pure Error	82.83	5	16.57			
Cor Total	2559.37	29				

Table 4.16: Summary of SASOME yield regression model.

Std. Dev.	5.18	R^2	0.9429
Mean	76.77	Adj R^2	0.8562
C.V. %	6.75	PredR^2	0.6947
PRESS	1958.64	Adeq Precision	8.148

SASOME yield (%w/w) = +86.83+2.75 * A+2.75 * B+0.75 * C+1.08 * D-3.25 * A * B -3.00 * A * C-0.25 * A * D +1.50 * B * C -3.50 * B * D +0.75 * C * D -6.08 * A^2-3.33 * B^2 -1.83 * C^2- 1.33 * D^2 (4.11)

SASOME yield (%w/w) = -85.75000 +2.75833 * Temperature +21.37500 * Cat Conc +2.42917 * Reactionn Time +4.75000 * Molar ratio -0.16250 * Temperature * Cat Conc -0.015000 * Temperature * Rxn Time -6.25000E-003 * Temperature * Molar ratio +0.15000 * Cat Conc * Rxn Time -1.75000 * Cat Conc * Molar ratio +0.037500 * Rxn

Time * Molar ratio -0.015208 * Temperature^2 - 3.33333 * Cat Conc^2 -0.018333 * Rxn Time^2-0.33333 * Molar ratio^2 (4.12)

SASOME yield (%w/w) = -85.75000 +2.75833* Temperature +21.37500 * Cat Conc +2.42917 * Rxn Time -0.16250 * Temperature * Cat Conc -0.015000 * Temperature * Rxn Time +0.15000 * Cat Conc * Rxn Time -1.75000 * Cat Conc * Molar ratio +0.037500 * Rxn Time * Molar ratio -0.015208* Temperature^2 - 3.33333 * Cat Conc^2 (4.13)

4.6.2.3.3 SASOME production factors interative effects. Figure 4.21A shows the 3D surface plot of the effects of catalyst concentration and temperature on the biodiesel yield of sweet almond seed oil (SASO) while keeping the reaction time and methanol/ oil molar ratio constant at 55minutes and 5.0 respectively. The result shows that the combined effects of the two variables are significant while considering the smoothness of their curves. This is revealed by the circular nature of the contour plot between catalyst loading and temperature on sweet almond methyl ester yield. This result agrees with the result of the ANOVA analysis where the linear terms, interactive terms and quadratic terms of both variables are all significant. Similar trend has been recorded by other researchers (Awolu and Layokun, 2013). Simultaneous increase in temperature and catalyst concentration resulted in significant increase SASOME yield. This could be due to the joint positive effect both increase in kinetic energy and concentration of the reactants. Maximum yield was obtained at about 60^{o}C and 2.5 wt% of temperature and catalyst concentration. Beyond this temperature, the yield starts decreasing more especially at catalyst concentration beyond 2.0 wt% probably due to loss of methanol whose boiling point is (68^{o}C). Reports had revealed similar observations where a negative effect was shown at higher reaction temperature (>65 °C) and catalyst loading (>3.5 wt%) and this phenomenon was attributed to increase in viscosity of the reaction mixture at high catalyst loading (Tshizanga *et al.,* 2017).

Figure 4.21B shows the effects of oil/methanol molar ratio and temperature on SASO biodiesel yield. The catalyst concentration and reaction time was kept constant at 1.5wt% and 55minutes respectively. Temperature effect is found to be far more significant

than methanol/oil molar ratio. The SASOME yield increased with increase in temperature irrespective of the value of the methanol/oil molar ratio. This is supported by the ANOVA result where methanol/oil molar ratio was found to be insignificant as linear and quadratic terms. Other researchers have reported a different result showing high significant effect of alcohol/oil molar ratio (Siver *et al.,* 2011). The difference in result is clearly due to the variation of the alcohol type (ethanol) and range of molar ratio (3:1 -15:1) studied. Optimum temperature was observed to be between 50-65^{o}C which is comfortably reported as the most ideal temperature for biodiesel production (Odude *et al.,* 2017). Beyond this temperature, the SASOME yield begins to fall and this could be due to widely accepted reason of loss of methanol.

Figure 4.21C shows the 3D plot of interactive effects of reaction time and catalyst concentrations on SASOME yield. The temperature and methanol/oil molar ratio were kept constant at 50^{o}C and 5:1 respectively. The effect of catalyst concentration showed very high response compared to that of reaction time. The smoother curve of catalyst concentration shows that its quadratic is more significant than reaction time. This is supported by the ANOVA result. Maximum yield of SASOME was obtained at reaction time range of 55-60 minutes and 1.5-2.50wt% catalyst concentration. Beyond these ranges the yields starts going down and this could be due to the fact that longer reaction time favours backward reaction (saponification reaction) while high loading of the catalyst increases the viscosity of the biodiesel and difficulty in product separation. Similar range of results has been reported where highest yield of neem seed oil biodiesel was obtained at 60 all catalyst concentration (Awolu and Layokun, 2013).

Figure 4.21D contains the effect of oil/methanol ratio and catalyst concentration keeping other factors constant at 50^{o}C and 55 minutes for temperature and reaction time respectively. The effect of both factors is almost the same on the biodiesel yield. Simultaneous increase in both variables results in the significant increase in the SASOME

yield. Increase in the yield was observed at all methanol/ oil ratio within 0.5-2.00 wt% catalyst concentration. Similarly, high yields were obtained at all catalyst concentration while the molar ratio was within 3:1-6:1. Beyond these ranges, the yield goes down significantly even with increase in catalyst concentration. This could be that, excess catalyst produced emulsions and the produced sweet almond biodiesel had difficulty in the separation phase (Silver *et al.,* 2011). Additionally, excess catalyst NaOH reacts with methanol to form soap which inhibits biodiesel yield (Rashid and Anwar, 2008).

Figure 4.21E contains the effect of oil/methanol ratio and reaction time keeping other factors constant at 50^{o}C and 1.5 wt% for temperature and catalyst concentration respectively. Simultaneous increase in both variables resulted in yield increase until a certain point when it began to decrease. The smooth curves of both variables show that they had very significant effect on the yield of sweet almond seed oil biodiesel. The effect of both factors is almost the same on the biodiesel yield. Maximum yield of SASOME was obtained around 60 minutes and 6:1 methanol /oil molar ratio. Beyond these points, increase in reaction time could have favoured the backward reaction due to lower concentration of the SASO triglyceride while increase in molar ratio could have resulted in poor separation and recovery of glycerol (Silver *et al.,* 2011). This result is quite in agreement with most available reports in literature where a molar ratio of 6:1 is generally considered the most appropriate for methanol (Ma and Hanna, 1999). Also, methanol/oil molar ratio beyond 10:1 increases the polarity of the reaction mixture thereby resulting in the solubility of glycerol and this promotes the reversible reaction (Ayodele *et al.,* 2017).

Figure 4.21F contains the effect of reaction time and temperature while keeping other factors constant at 5.0 and 1.5 wt% for methanol/oil molar ratio and catalyst concentration respectively. Obviously, the smoother curve of temperature shows its higher significant effect on the yield of SASOME than reaction time. This is in agreement with the ANOVA result where both the linear and quadratic terms of temperature were all more

significant than those of reaction time. However, the ANOVA results still show that the interactive term of temperature and reaction time was very significant. Increase in temperature results in higher reaction rate by increasing the kinetic energy of the reacting molecules. It has been reported earlier that increase in biodiesel yield with increase in temperature is in agreement with Arrhenius equation (Ayodele *et al.*, 2017). Beyond 60^{o}C where maximum yield was obtained, the yield started decreasing irrespective of the reaction time. This decrease could be as a result of the closeness of the reaction temperature to the boiling point of methanol which could result in its escape from the reacting mixture. This optimum temperature would entail low cost of production as energy requirement for the SASO transesterification is comparatively low. Likewise, beyond 60 minutes reaction time, saponification might have been favoured more due to less concentration of the reactants to push the reaction in the forward direction.

The response values obtained by inserting the independent values are the predicted values of the model. These values are compared to the actual and experimental values. As it can be seen in Figure 4.22, the actual values were distributed relatively near to the predicted value line. This implies that there is a good correlation between the actual and predicted values. This shows that the CCD is well fitted into the model and thus can be used to perform the optimization operation for transesterification of SASO.

The optimization exercise for the maximum response of SASOME was conducted by utilizing the flexibility of the Design Expert 7.0.0 version numerical optimization tool function. A total of 11 solutions were generated with their desirability. The selected best solution represents the optimized process conditions where SASOME maximum response was obtained as 92.58wt% and validated at 91.09wt%. The optimum values of the process conditions are as contained in Table 4.17.

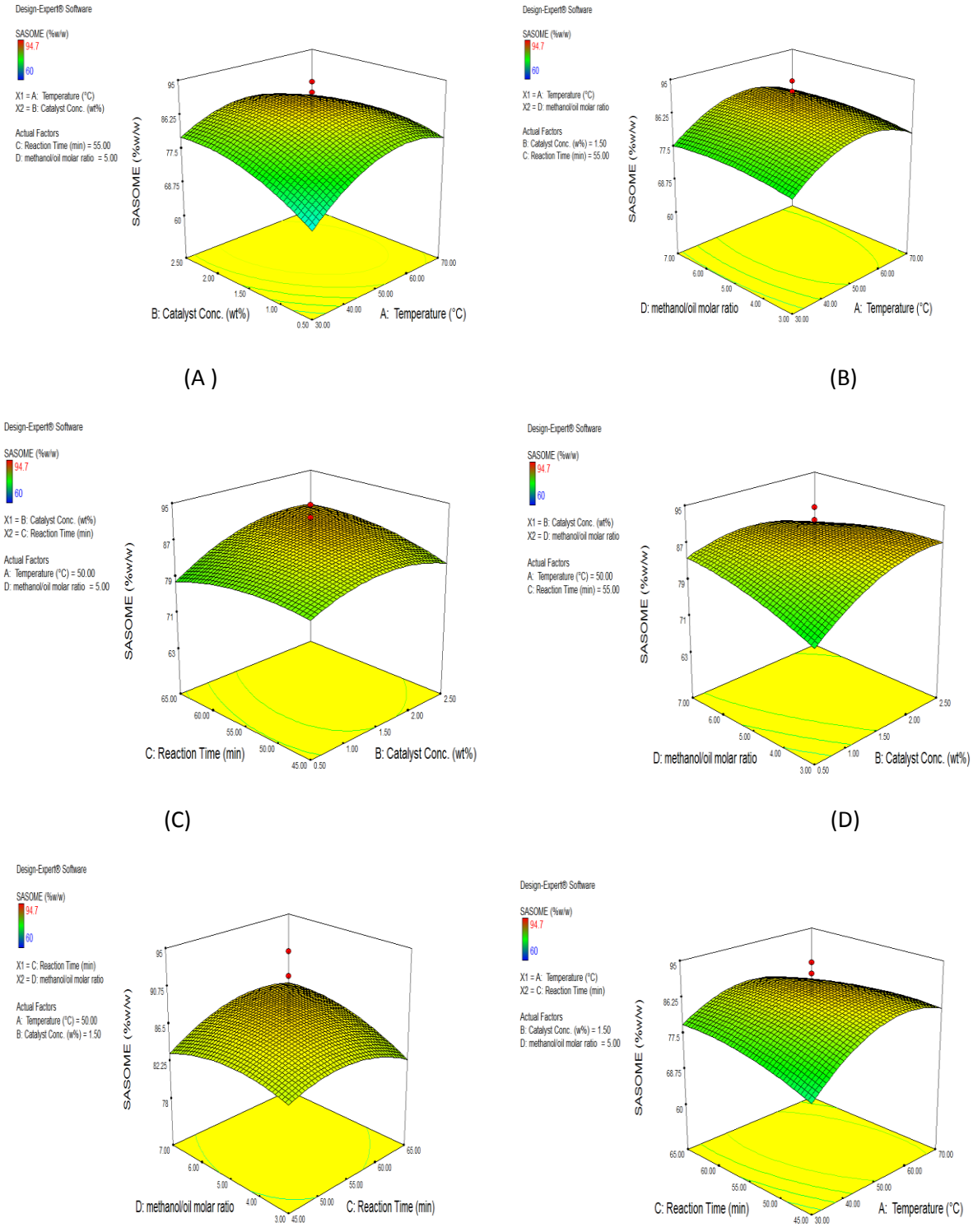

Figure 4.21: The 3D response surface plot of the effects of the variables on SASOME yield

(A). Catalyst concentration and temperature (B). Oil/methanol ratio and temperature
(C). Reaction time and catalyst concentration (D). Oil/methanol ratio and catalyst concentration
(E). Oil/methanol ratio and reaction time (F). Reaction time and temperature,

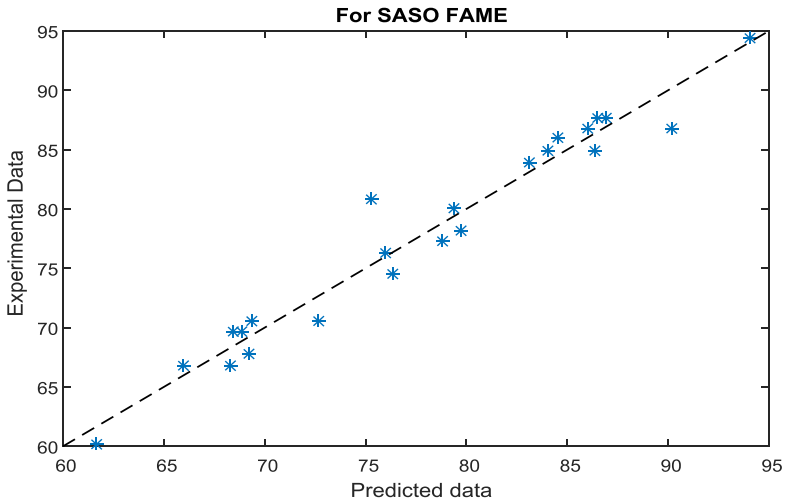

Figure 4.22: Linear correlation between predicted versus actual values for SASOME yield.

Table 4.17: CCD optimum predicted conditions for SASO transesterification and validation experiments.

Variables	Optimum values	%SASOME yield		
		Experimental	Predicted	Desirability
Temperature (°C)	50.03			
Catalyst concentration (wt%)	2.04	92.58	91.09	0.906
Reaction time (min)	58.52			
Methanol /oil molar ratio	4.66			

4.6.2.4 RSM optimization of APSO transesterification process

A CCD was applied to develop a correlation between the factors affecting transesterification reaction and the methyl ester yield. The complete design matix, experimental and predicted responses is presented in Table 4.18. The experimental values of APSOME content obtained ranged from 46.6 wt% to 92.92 wt %.

Table 4.18: CCD of five-level four-factor response surface study of APSOME production.

Run	Factor 1 A (^{o}C)	Factor 2 B (wt %)	Factor 3 C (mins)	Factor 4 D (mol/mol)	Actual value (wt%)	Predicted value (wt%)
1	40	1.0000	50	1:4000	80.2600	75.6469
2	60	1.0000	50	1:4000	87.8200	89.2357
3	40	2.0000	50	1:4000	69.5600	70.9757
4	60	2.0000	50	1:4000	78.2500	77.3469
5	40	1.0000	60	1:4000	86.6200	88.0357
6	60	1.0000	60	1:4000	85.3100	84.4069
7	40	2.0000	60	1:4000	87.0500	86.1469
8	60	2.0000	60	1:4000	85.7400	85.3007
9	40	1.0000	50	1:6000	69.1300	70.4480
10	60	1.0000	50	1:6000	66.8200	66.8193
11	40	2.0000	50	1:6000	69.6600	68.5593
12	60	2.0000	50	1:6000	67.2500	67.7130
13	40	1.0000	60	1:6000	86.8200	85.6193
14	60	1.0000	60	1:6000	85.3500	84.7730
15	40	2.0000	60	1:6000	87.6500	86.5130
16	60	2.0000	60	1:6000	85.8400	88.4493
17	30	1.5000	55	1:5000	78.7450	80.1118
18	70	1.5000	55	1:5000	76.1250	75.6368
19	50	0.5000	55	1:5000	77.0050	78.3718
20	50	2.5000	55	1:5000	77.8650	77.3768
21	50	1.5000	45	1:5000	46.6450	46.3118
22	50	1.5000	65	1:5000	92.9250	94.4368
23	50	1.5000	55	1:3000	77.4350	78.8995
24	50	1.5000	55	1:7000	78.5142	79.1054
25	50	1.5000	55	1:5000	80.2193	80.1340
26	50	1.5000	55	1:5000	80.2192	80.1340
27	50	1.5000	55	1:5000	80.2193	80.1340
28	50	1.5000	55	1:5000	80.2194	80.1340
29	50	1.5000	55	1:5000	80.2192	80.1340
30	50	1.5000	55	1:5000	80.2193	80.1340

4.6.2.4.1 APSOME production RSM model ANOVA analysis. The F-value, lack of fit and R-squared values tests were performed using analysis of variance (ANOVA) to calculate the significance of each type of model. The only model that satisfied the criteria is found to be quadratic model and hence it was selected. The effect of each parameter was evaluated using the quadratic model as shown in Table 4.19. Many appraisal techniques such as coefficient of determination (R^2), adjusted coefficient of determination (adj. R^2) and coefficient of variation (C.V) were used to weigh the adequacy of the model as used by other researchers (Sarve et al., 2015). There is only a 0.03% chance that a "Model F-Value" this large could occur due to noise. Values of "Prob> F" less than 0.0500 indicate model terms are significant. In this case A, B, C, AB, AC, BD, A2, B2 and C2 are significant

model terms. Values greater than 0.1000 indicate the model terms are not significant. The "Lack of Fit F-value" of 0.1431 implies the Lack of Fit is not significant relative to the pure error. There is a 14.31% chance that a "Lack of Fit F-value" this large could occur due to noise. Non-significant lack of fit is good. It shows that the effect of most independent variables on the APSO transesterification was significantly high. It could be ascertained that the degree of significant effect of the process parameters is in the order of: temperature > reaction time > catalyst concentration > molar ratio. In addition, the squares of temperature, reaction time and catalyst concentration are significant in the African pear seed oil transesterification process. This could mean that these factors whose square are significant have better effect on the esterification process (Awolu and Layokun, 2013). The non-significant lack of fit is good because it shows that the model will be well fitted (Ohale *et al.*, 2017). "Adeq Precision" measures the signal to noise ratio. A ratio greater than 4 is desirable (Table 4.20). The ratio of 9.282 indicates an adequate signal and that this model can be used to navigate the design space. The coefficient of variation (C.V) is the ratio of the standard deviation of estimate to the mean value of the observed response and as well independent of the unit (Ohale *et al.*, 2017). It is also a measure of reproducibility and repeatability of the models (Chen *et al.*, 2011). Therefore, C.V value of 7.85 shows that the model is reasonably reproducible. Apart from the F-value, lack of fit and C.V, the R-squared of 0.9271) shows that more than 92% of the overall variability can be explained by the empirical models of the Equations. The adj. R-squared and the predicted R-squared values of 0.9154 and 0.715 respectively for the quadratic model are in reasonable agreement since the difference is less than 0.2 (Uzoh *et al.*, 2019).

4.6.2.4.2 APSOME production RSM model equations. The selected model in terms of the coded, actual and significant terms is given in Equations (4.14), (4.15) and (4.16) respectively. The equation in terms of coded factors can be used to make predictions about

the response for given levels of each factor. By, defaults, the high levels of the factors are coded +2 and the low levels of the factors are coded as -2. The coded equation is useful for identifying the relative impact of the factors by comparing the factors coefficients, while the equation in terms of actual factors can be used to make predictions about the response for actual levels of each factor (Ohale *et al.*, 2017). Analyzing the obtained model, it is observed that none of factors present negative effects, while the interactive effects of AB, AC, AD, BD and CD were significantly negative, showing that increase in the levels of the variables results in a decrease in APSOME yield (Zanette *et al.*, 2011).

Table 4.19: ANOVA for APSOME response surface quadratic model

Source	Sum of Squares	Df	Mean Square	F Value	p-value Prob> F	
Model	3393.27	14	242.38	6.88	0.0003	Significant
A- Temperature	498.68	1	498.68	14.15	0.0019	
B-Catalyst Conc.	200.68	1	200.68	5.7	0.0306	
C-Reaction Time	205.42	1	205.42	5.83	0.0301	
D-methanol/molar ratio	36.01	1	36.01	1.02	0.328	
AB	191.82	1	191.82	5.44	0.034	
AC	318.62	1	318.62	9.04	0.0088	
AD	3.42	1	3.42	0.097	0.7596	
BC	26.52	1	26.52	0.75	0.3993	
BD	394.02	1	394.02	11.18	0.0044	
CD	4.62	1	4.62	0.13	0.7222	
A^2	1489.33	1	1489.33	42.27	< 0.0001	
B^2	311.27	1	311.27	8.83	0.0095	
C^2	195.79	1	195.79	5.55	0.0312	
D^2	51.39	1	51.39	1.46	0.2459	
Residual	528.48	15	35.23			
Lack of Fit	445.65	10	44.56	2.69	0.1431	not significant
Pure Error	82.83	5	16.57			
Cor Total	3921.75	29				

Table 4.20: Summary of APSOME yield regression values.

Std. Dev.	5.94	R^2	0.9271
Mean	75.65	AdjR²	0.9154
C.V. %	7.85	PredR²	0.7150
PRESS	2686	Adeq Precision	9.282

APSOME (%w/w) = +86.83 + 4.56 * A +2.89 * B +1.72 * C +1.22 * D - 3.46 * A * B - 4.46 * A * C -0.46 * A * D +1.29 * B * C - 4.96 * B * D +0.54 * C * D - 7.37 * A^2 -3.37 * B^2 -1.87 * C^2 -1.37 * D^2 (4.14)

APSOME (%w/w) = -138.0 + 3.61479 * Temperature +26.97917 * Catalyst Conc. + 3.01625 * Reaction Time (min) +6.85625 * methanol/molar ratio -0.17313 * Temperature * Catalyst Conc. - 0.022313 * Temperature * Reaction Time - 0.011562 * Temperature * methanol/molar ratio +0.12875 * Catalyst Conc. * Reaction Time - 2.48125 * Catalyst Conc. * methanol/molar ratio + 0.026875 * Reaction Time * methanol/molar ratio -0.018422 * $Temperature^2$ - 3.36875 * $Catalyst\ Conc.^2$ -0.018688 * $Reaction\ Time^2$ -0.34219 * $methanol/molar\ ratio^2$ (4.15)

APSOME (%w/w) = -138.00000+3.61479 * Temperature +26.97917 * Catalyst Conc. + 3.01625 * Reaction Time (min) -0.17313 * Temperature * Catalyst Conc. - 0.022313 * Temperature * Reaction Time - 2.48125 * Catalyst Conc. * methanol/molar ratio -0.018422 * $Temperature^2$ - 3.36875 * $Catalyst\ Conc.^2$ -0.018688 * $Reaction\ Time^2$ (4.16)

4.6.2.4.3 APSOME production factors interactive effects. Then, the effects of the transesterification parameters on the biodiesel yield were investigated and the obtained findings are given in Figures 4.23(A-F).

Figure 4.23A shows the plot of the effects of catalyst concentration and temperature on the biodiesel yield while keeping the reaction time and methanol/ oil molar ratio constant at 55minutes and 5.0 respectively. The result shows that the combined effects of the two variables are significant while temperature showed more significant effect than catalyst concentration. This is revealed by the circular nature of the contour plot between catalyst loading and temperature on methyl ester yield. This result agrees with the result of the ANOVA analysis. Similar trend has been recorded by other researchers (Awolu and Layokun, 2013). Simultaneous increase in temperature and catalyst concentration resulted in significant increase APSOME yield. This could be due to the joint positive effect both increase in kinetic energy and concentration of the reactants. Maximum yield was obtained at about 60^oC and 2.5 wt% of temperature and reaction time. Beyond this temperature, the yield starts decreasing probably due to loss of methanol whose boiling point is (68^oC). Reports had revealed similar observations where a negative effect was shown at higher reaction temperature (>65 °C) and catalyst loading (>3.5 wt %) and this phenomenon was

attributed to increase in viscosity of the reaction mixture at high catalyst loading (Tshizanga *et al.,* 2017).

Figure 4.23B shows the effects of oil/methanol molar ratio and temperature on biodiesel yield. The catalyst concentration and reaction time was kept constant at 1.5wt% and 55minutes respectively. It was observed that increment of methanol/oil molar ratio up to the level of 7:1, the APSOME content increases, beyond 7:1 methanol/oil molar ratio there is no significant effect of methanol/oil molar ratio on APSOME yield. Temperature effect is found to be far more significant than methanol/oil molar ratio. This is supported by the ANOVA result where methanol/oil molar ratio was found to be insignificant. Other researchers have reported a different result showing high significant effect of alcohol/oil molar ratio (Siver *et al.,* 2011). The difference in result is clearly due to the variation of the alcohol type (ethanol) and range of molar ratio (3:1 -15:1) studied. Optimum temperature was observed to be within 50-65^{o}C which is comfortably reported as the most ideal temperature for biodiesel production (Adepoju *et al*., 2018; Awolu and Layokun, 2013). Beyond this temperature, the APSOME yield begins to fall and this could be due to widely accepted reason of loss of methanol.

Figure 4.23C shows the interactive effects of reaction time and catalyst concentrations.. The effect of reaction time showed very high response compared to that of catalyst concentration. The temperature and methanol/oil molar ratio were kept constant at 50^{o}C and 5:1 respectively. The smoother curve of catalyst concentration shows that its quadratic is more significant than reaction time. This is supported by the ANOVA result. Maximum yield of APSOME was obtained at reaction time range of 55-60 minutes and 1.5-2.50wt%catalyst concentration. Beyond these ranges the yields starts going down and this could be due to the fact that longer reaction time favours backward reaction (saponification reaction) while high loading of the catalyst increases the viscosity of the biodiesel and difficulty in product separation. Similar range of results has been reported where highest

yield of neem seed oil biodiesel was obtained at 60 all catalyst concentration (Awolu and Layokun, 2013).

Figure 4.23D contains the effect of oil/methanol ratio and catalyst concentration keeping other factors constant at 50^{o}C and 55 minutes for temperature and reaction time respectively. The effect of both factors is almost the same on the biodiesel yield. Simultaneous increase in both variables results in the significant increase in the APSOME yield. Increase in the yield was observed at all methanol/ oil ratio within 0.5-2.00 wt% catalyst concentration. Similarly, high yields were obtained at all catalyst concentration while the molar ratio was within 3:1-6:1. Beyond these ranges, the yield goes down significantly. This could be that, excess catalyst produced emulsions and the biodiesel that is produced has difficulty in the separation phase (Silver *et al.,* 2011). Additionally, excess catalyst NaOH reacts with methanol to form soap which inhibits biodiesel yield (Rashid and Anwar, 2008).

Figure 4.23E contains the effect of oil/methanol ratio and reaction time keeping other factors constant at 50^{o}C and 1.5 wt% for temperature and catalyst concentration respectively. Simultaneous increase in both variables resulted in yield increase until a certain point when it began to decrease. The smooth curves of both variables shows that they are very significant effect on the yield of African pear seed oil biodiesel. The effect of both factors is almost the same on the biodiesel yield. Maximum yield of APSOME was obtained around 60 minutes and 6:1 methanol /oil molar ratio. Beyond these points, increase in reaction time could have resulted formation of soap due to lower concentration of the reactants while increase in molar ratio could have resulted in poor separation and recovery of glycerol (Silver *et al.,* 2011). This result is quite in agreement with most available reports in the literature where a molar ratio of 6:1 is generally considered the most appropriate for methanol (Ma and Hanna, 1999). Also, methanol/oil molar ratio beyond 10:1 increases the

polarity of the reaction mixture thereby resulting in the solubility of glycerol and this promotes the reversible reaction (Ayodele *et al.*, 2017).

Figure 4.23F contains the effect of reaction time and temperature while keeping other factors constant at 5.0 and 1.5 wt% for methanol/oil molar ratio and catalyst concentration respectively. Obviously, the smoother curve of temperature shows its higher significant effect on the yield of APSOME than reaction time. This is in agreement with the ANOVA result where both the linear and quadratic terms of temperature were all more significant than reaction time. However, the ANOVA results still show that the interactive term of temperature and reaction time was very significant. Increase in temperature results in higher reaction rate by increasing the kinetic energy of the reacting molecules. It has been reported earlier that increase in biodiesel yield with increase in temperature is in agreement with Arrhenius equation (Ayodele *et al.*, 2017). Beyond 60^{o}C where maximum yield was obtained, the yield started decreasing. This decrease could be as a result of the closeness of the reaction temperature to the boiling point of methanol which could result in its escape from the reacting mixture. This would entail low cost of production as energy consumption is very low. However, the effects of both factors are almost the same. Likewise, beyond 60 minutes reaction time, saponification might have been favoured more due to less concentration of the reactants to push the reaction in the forward direction.

The response values obtained by inserting the independent values are the predicted values of the model. These values are compared to the actual and experimental values. As it can be seen in Figure 4.24, the actual values were distributed relatively near to the predicted value line. This implies that there is a good correlation between the actual and predicted values. This shows that the CCD is well fitted into the model and thus can be used to perform the optimization operation for transesterification of APSO.

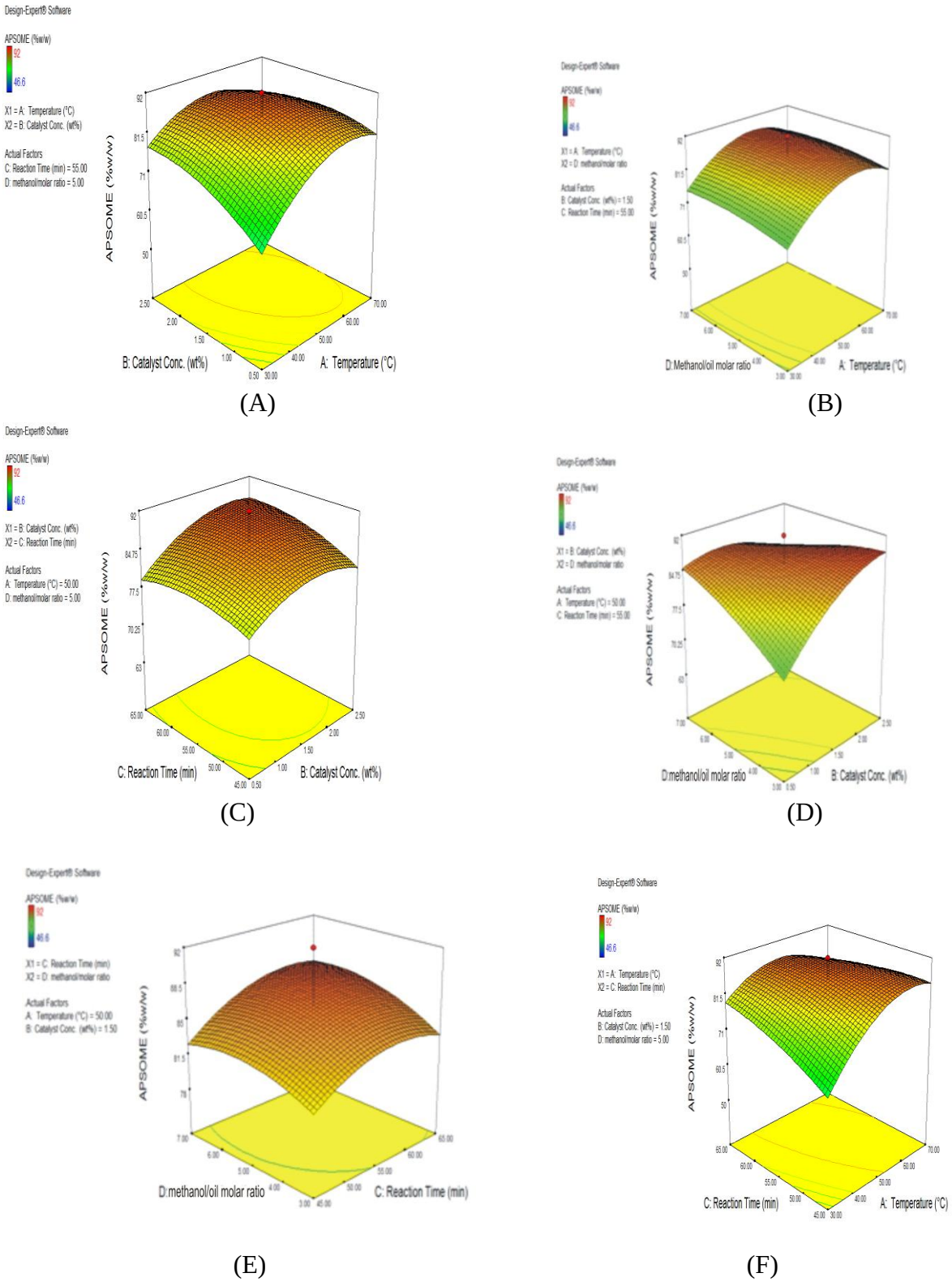

Figure 4.23: The 3D response surface plot of the effects of the variables on APSOME yield
(A) Catalyst concentration and temperature (B) Methanol/Oil ratio and catalyst concentration, (C) Reaction time and catalyst concentration, (D) Methanol/Oil ratio and temperature, (E) Methanol/Oil ratio and reaction time, (F). Reaction time and temperature,

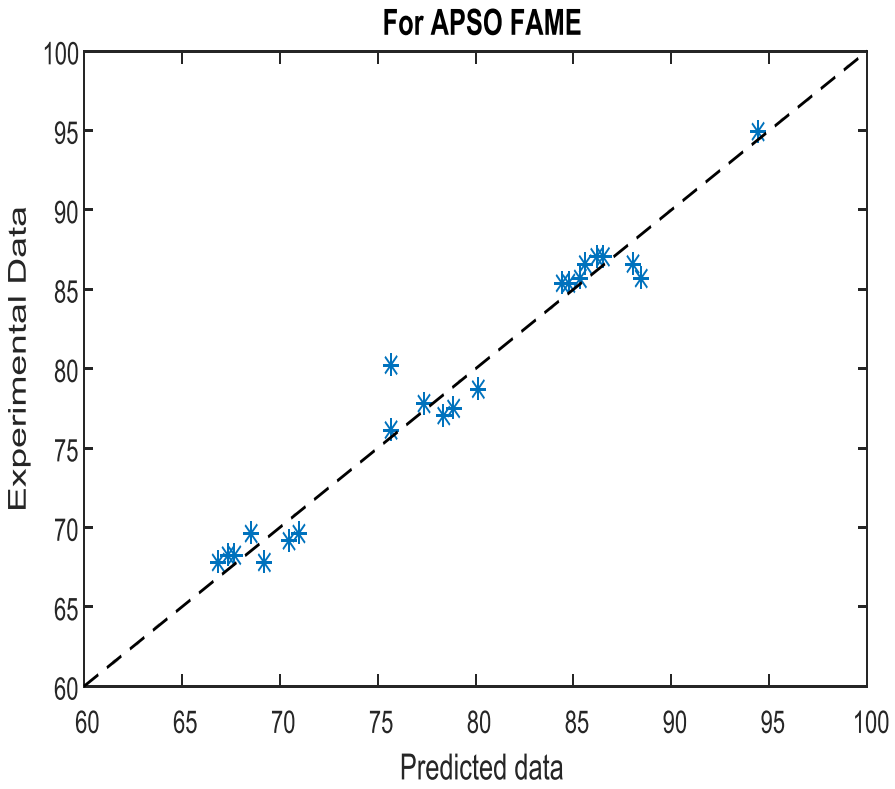

Figure 4.24: Linear correlation between Predicted versus actual yield for APSOME yield

The optimization exercise for the maximum response of APSOME was conducted by utilizing the flexibility of the Design Expert 7.0.0 version numerical optimization tool function. A total of 12 solutions were generated with their desirability. The selected best solution represents the optimized process conditions where APSOME maximum response was obtained as 94.55wt% and validated at 95.03wt%. The optimum values of the process conditions are as contained in Table 4.21.

Table 4.21: CCD optimum predicted conditions of APSO transesterification and validation experiments.

Variables	Optimum values	%APSOME yield		Desirability
		Experimental	Predicted	
Temperature (°C)	63.92			
Catalyst concentration (wt%)	1.88	94.55	95.027	1.00
Reaction time (min)	58			
Methanol /oil molar ratio	6.86			

4.6.2.5 RSM optimization of ASASO transesterification process

The complete CCD matix developed to correlate between the factors affecting transesterification reaction and the methyl ester yield, experimental and predicted responses is presented in Table 4.22. The experimental values of ASASOME content obtained ranged from 60.78 wt% to 86.5 wt %.

Table 4.22: Central composite design of five-level four-factor response surface study of ASASOME production.

Run	Factor 1 A (^{o}C)	Factor 2 B(wt %)	Factor 3 C (mins)	Factor 4 D(mol/mol)	Actual value (%)	Predicted value (%)
1	40	1.0000	50	1:4000	60.7800	61.1287
2	60	1.0000	50	1:4000	67.0200	66.1187
3	40	2.0000	50	1:4000	71.8000	70.8987
4	60	2.0000	50	1:4000	69.0400	72.8887
5	40	1.0000	60	1:4000	65.2360	66.8347
6	60	1.0000	60	1:4000	74.4760	74.8247
7	40	2.0000	60	1:4000	79.2560	79.6047
8	60	2.0000	60	1:4000	85.4960	84.5947
9	40	1.0000	50	1:6000	60.7800	61.4839
10	60	1.0000	50	1:6000	67.0200	67.9739
11	40	2.0000	50	1:6000	71.8000	72.7539
12	60	2.0000	50	1:6000	78.0400	76.2439
13	40	1.0000	60	1:6000	68.2360	65.6899
14	60	1.0000	60	1:6000	74.4760	75.1799
15	40	2.0000	60	1:6000	79.2560	79.9599
16	60	2.0000	60	1:6000	86.4960	86.4499
17	30	1.5000	55	1:5000	66.8980	66.9243
18	70	1.5000	55	1:5000	79.3780	78.4043
19	50	0.5000	55	1:5000	62.1180	62.1443
20	50	2.5000	55	1:5000	84.1580	83.1843
21	50	1.5000	45	1:5000	65.6820	64.7083
22	50	1.5000	65	1:5000	80.5940	80.6203
23	50	1.5000	55	1:3000	73.1380	71.5591
24	50	1.5000	55	1:7000	75.8410	76.4329
25	50	1.5000	55	1:5000	78.3258	79.0154
26	50	1.5000	55	1:5000	78.3358	79.0154
27	50	1.5000	55	1:5000	78.3358	79.0154
28	50	1.5000	55	1:5000	78.3258	79.0154
29	50	1.5000	55	1:5000	78.3258	79.0154
30	50	1.5000	55	1:5000	78.3258	79.0154

4.6.2.5.1 ASASOME production RSM model ANOVA analysis. The F-value, lack of fit and R-squared value tests were performed using analysis of variance (ANOVA) to

calculate the significance of each type of model. The only model that satisfied the criteria is found to be quadratic model and hence it was selected. The effect of each parameter was evaluated using the quadratic model as shown in Table 4.23. Many appraisal techniques such as coefficient of determination (R^2), adjusted coefficient of determination (adj. R^2) and coefficient of variation (C.V) were used to weigh the adequacy of the model as used by other researchers (Sarve et al., 2015). Values of "Prob> F" less than 0.0500 indicate model terms are significant. In this case A, B, C, AB, AC, BD, A^2, and B^2 are significant model terms. Values greater than 0.1000 indicate the model terms are not significant. The Model F-value of 4.44 implies the model is significant. There is only a 0.35% chance that a "Model F-Value" this large could occur due to noise. The "Lack of Fit F-value" of 0.3294 implies the Lack of Fit is not significant relative to the pure error. Non-significant lack of fit is good. It shows that the effect of most independent variables on the ASASO transesterification was significantly high. It could be ascertained that the degree of significant effect of the process parameters is in the order of: temperature > catalyst concentration > reaction time > molar ratio. In addition, the squares of temperature, catalyst concentration and molar ratio are significant in the African star apple seed oil transesterification process. This could mean that these factors whose square are significant have better effect on the esterification process (Awolu and Layokun, 2013). The non-significant lack of fit is good because it shows that the model will be well fitted (Ohale *et al.*, 2017). "Adeq Precision" measures the signal to noise ratio. A ratio greater than 4 is desirable (Table 4.24). The ratio of 8.134 indicates an adequate signal and that this model can be used to navigate the design space. The coefficient of variation (C.V) is the ratio of the standard deviation of estimate to the mean value of the observed response and as well independent of the unit (Ohale, *et al*., 2017). It is also a measure of reproducibility and repeatability of the models (Chen *et al.,* 2011). Therefore, the C.V value of 5.62 shows that the model is reasonably reproducible. Apart from the F-value, lack of fit and C.V, R-

squared value of 0.898 also shows that more than 89% of the overall variability can be explained by the empirical models of the equations. The adj. R-squared and the predicted R-squared values of 0.726 and 0.665 respectively for the quadratic model are in reasonable agreement since the difference is less than 0.2 (Uzoh *et al.*, 2019).

4.6.2.5.2 ASASOME production RSM quadratic model equations. The selected models in terms of the coded, actual and significant terms are given in Equations (4.17), (4.18) and (4.19) respectively. The equation in terms of coded factors can be used to make predictions about the response for given levels of each factor. By, defaults, the high levels of the factors are coded +2 and the low levels of the factors are coded as -2. The coded equation is useful for identifying the relative impact of the factors by comparing the factors coefficients, while the equation in terms of actual factors can be used to make predictions about the response for actual levels of each factor (Ohale *et al.*, 2017). Analyzing the obtained model, it is observed that none of factors present negative effects, while the interactive effects of AB and AC were significantly negative, showing that increase in the levels of the variables results in a decrease in ASASOME yield (Zanette *et al.*, 2011).

Table 4.23: ANOVA for ASASOME response surface quadratic model.

Source	Sum of Squares	df	Mean Square	F Value	p-value Prob> F	
Model	1170.28	14	83.59	4.44	0.0035	significant
A- Temperature	200.33	1	200.33	10.63	0.0053	
B-Catalyst Conc.	107.95	1	107.95	5.73	0.0302	
C-Reaction Time	116.6	1	116.6	6.19	0.0251	
D-methanol/oil molar ratio	50.75	1	50.75	2.69	0.1215	
AB	15.8	1	15.8	0.84	0.3743	
AC	15.8	1	15.8	0.84	0.3743	
AD	103.99	1	103.99	5.52	0.0322	
BC	2.33	1	2.33	0.12	0.7302	
BD	90.73	1	90.73	4.82	0.0444	
CD	6.38	1	6.38	0.34	0.5694	
A^2	364.79	1	364.79	19.36	0.0005	
B^2	91.18	1	91.18	4.84	0.0443	
C^2	15.2	1	15.2	0.81	0.3833	
D^2	153.98	1	153.98	8.17	0.0119	
Residual	282.59	15	18.84			
Lack of Fit	194.69	10	19.46	1.03	0.3294	Not significant
Pure Error	87.90	5	17.56			
Cor Total	1452.87	29				

Table 4.24: Summary of ASASOME yield regression values.

Std. Dev.	4.34	R-Squared	0.898
Mean	77.3	Adj R-Squared	0.726
C.V. %	5.62	Pred R-Squared	0.665
PRESS	1627.72	Adeq Precision	8.134

ASASOME (%w/w) = +84.00 +2.89 * A +2.12 * B +2.20 * C +1.45 * D -0.99 * A * B - 0.99 * A * C +2.26 * A * D +0.38 * B * C +2.38 * B * D + 0.63 * C * D - 3.65 * A^2 - 1.62 * B^2 - 0.74* C^2 - 2.37* D^2 (4.17)

ASASOME (%w/w) = +11.54062 +1.12196 * Temperature + 1.41333 * Catalyst Conc. +1.07267 * Reaction Time - 0.049688 * Temperature * Catalyst Conc. - 4.96875E-003 * Temperature * Reaction Time +0.056406 * Temperature * methanol/oil molar ratio +0.038125 * Catalyst Conc. * Reaction Time +1.19062 * Catalyst Conc. * methanol/oil molar ratio +0.031562 * Reaction Time * methanol/oil molar ratio -9.11719E-003 * Temperature ^{2} - 1.61938 * Catalyst Conc.^{2} - 7.44375E-003 * Reaction Time ^{2} - 0.59234 * methanol/oil molar ratio^2 (4.18)

ASASOME (%w/w) = +11.54062 +1.12196 * Temperature + 1.41333 * Catalyst Conc. +1.07267 * Reaction Time + 0.30833 * methanol/oil molar ratio + 0.056406 * Temperature * methanol/oil molar ratio +1.19062 * Catalyst Conc. * methanol/oil molar ratio - 9.11719E-003 * Temperature ^{2} - 1.61938 * Catalyst Conc.^{2} - 0.59234 * methanol/oil molar ratio^2 (4.19)

The optimization exercise for the maximum response of ASASOME was conducted by utilizing the flexibility of the Design Expert 7.0.0 version numerical optimization tool function. A total of 9 solutions were generated with their desirability. The selected best solution represents the optimized process conditions where ASASOME maximum response was obtained as 85.91wt% and validated at 86.85wt%. The optimum values of the process conditions are as contained in Table 4.25.

Table 4.25: CCD optimum predicted conditions of ASASO transesterification with validation experiments

Variables	Optimum values	% ASASOME yield		
		Experimental	Predicted	Desirability
Temperature (°C)	65.62			
Catalyst concentration (wt%)	2.14	85.91	86.85	1.00
Reaction time (min)	62.04			
Methanol /oil molar ratio	5.88			

Figure 4.25A shows the 3D surface plot of the effects of catalyst concentration and temperature on the biodiesel yield of African star apple seed oil (ASASO) while keeping the reaction time and methanol/ oil molar ratio constant at 55minutes and 5.0 respectively. The result shows that the combined effects of the two variables are significant while considering the smoothness of their curves. This is revealed by the circular nature of the contour plot between catalyst loading and temperature on African star apple methyl ester yield. This result agrees with the result of the ANOVA analysis where the linear terms, interactive terms and quadratic terms of both variables are all significant. Similar trend has been recorded by other researchers (Awolu and Layokun, 2013). Simultaneous increase in temperature and NaOH (catalyst) concentration resulted in significant increase ASASOME

yield. This could be due to the joint positive effect both increase in kinetic energy and concentration of the reactants (triglycerides and methanol). Maximum yield of ASASOME was obtained at about 60^{o}C and 2.5 wt% of temperature and catalyst concentration. Beyond this temperature, the yield of ASASOME starts decreasing more especially at NaOH concentration beyond 2.0 wt% probably due to loss of methanol whose boiling point is (68^{o}C). Reports had revealed similar observations where a negative effect was shown at higher reaction temperature (>65 °C) and catalyst loading (>3.5 wt%) and this phenomenon was attributed to increase in viscosity of the reaction mixture at high catalyst loading (Tshizanga *et al.,* 2017).

Figure 4.25B shows the effects of African star apple oil/methanol molar ratio and temperature on ASASO biodiesel yield. The catalyst (NaOH) concentration and reaction time was kept constant at 1.5wt% and 55minutes respectively. A quadratic term of temperature is found to be more significant than methanol/oil molar ratio. This is depicted on the more smoothness of temperature curve The ASASOME yield increased with increase in temperature irrespective of the value of the methanol/oil molar ratio. This is supported by the ANOVA result where methanol/oil molar ratio was found to be insignificant as linear and quadratic terms. Other researchers have reported a similar result showing high significant effect of alcohol/oil molar ratio (Siver *et al.,* 2011). Optimum temperature was observed to be between 50-65^{o}C which is comfortably reported as the most ideal temperature for biodiesel production (Awolu and Layokun, 2014). Beyond this temperature, the ASASOME yield begins to fall and this could be due to widely accepted reason of loss of methanol.

Figure 4.25C shows the 3D plot of interactive effects of reaction time and catalyst concentrations on ASASOME yield. The temperature of reaction and methanol/oil molar ratio were kept constant at 50^{o}C and 5:1 respectively. The effect of catalyst concentration showed very more significant effect than reaction time. The smoother curve of catalyst

concentration shows that its quadratic is more significant than reaction time. This is supported by the ANOVA result. Maximum yield of ASASOME was obtained between reaction time of 60-65 minutes and 2.0-2.50wt% NaOH (catalyst) concentration. Beyond this catalyst concentration, high loading of the catalyst could have increased the viscosity of the biodiesel and difficulty in product separation. Similar range of results has been reported in literature (Awolu and Layokun, 2013).

Figure 4.25D contains the effect of oil/methanol ratio and catalyst concentration on ASASOME yield while keeping temperature and reaction time constant at 50^{o}C and 55 minutes respectively. The effect of both factors is almost the same on the biodiesel yield. Simultaneous increase in both variables results in the significant increase in the ASASOME yield. Increase in the yield was observed at all methanol/ oil ratio until 2.00 wt% catalyst concentration. Similarly, high yields were obtained at all catalyst concentration while the molar ratio was within 3:1-6:1. Beyond these ranges, the yield goes down significantly with increase in both catalyst concentration and methanol/oil molar ratio. This could be that, excess catalyst produced emulsions and the produced biodiesel had difficulty in the separation phase (Silver *et al.,* 2011). Additionally, excess catalyst NaOH could have reacted with methanol to form soap which inhibits biodiesel yield (Rashid and Anwar, 2008).

Figure 4.25E contains the effect of oil/methanol ratio and reaction time on African star apple seed oil methyl ester (ASASOME) yield keeping temperature and catalyst concentration constant at 50^{o}C and 1.5 wt% respectively. The methanol/oil molar ratio is shown to have smooth curves while reaction time lacks smooth curve. This implies that the quadratic term of methanol/oil molar ratio is significant on the biodiesel produced while that of reaction time is not. This is in agreement with the ANOVA p-values. Conversely, the linear terms of reaction time is significant while that of molar ratio is not. Maximum yield of ASASOME was obtained at highest reaction time of 65 minutes and 6:1 methanol /oil

molar ratio. This result is quite in agreement with most available reports in literature where a molar ratio of 6:1 is generally considered the most appropriate for methanol (Ma and Hanna, 1999). Also, methanol/oil molar ratio beyond this value could increase the polarity of the reaction mixture thereby resulting in the solubility of glycerol and this promotes the reversible reaction (Ayodele et al., 2017).

Figure 4.25F contains the effect of reaction time and temperature while keeping other factors constant at 5.0 and 1.5 wt% for methanol/oil molar ratio and catalyst concentration respectively. Obviously, the smoother curve of temperature shows its higher significant effect on the yield of ASASOME than reaction time. This is in agreement with the ANOVA result where both the linear and quadratic terms of temperature were all more significant than those of reaction time. Increase in temperature results in higher reaction rate by increasing the kinetic energy of the reacting molecules. It has been reported earlier that increase in biodiesel yield with increase in temperature is in agreement with Arrhenius equation (Ayodele *et al.,* 2017). Beyond 60^{o}C where maximum yield was obtained, the yield started decreasing irrespective of the reaction time. This decrease could be as a result of the closeness of the reaction temperature to the boiling point of methanol which could result in its escape from the reacting mixture. This optimum temperature would entail low cost of production as energy requirement for the ASASO transesterification is comparatively low.

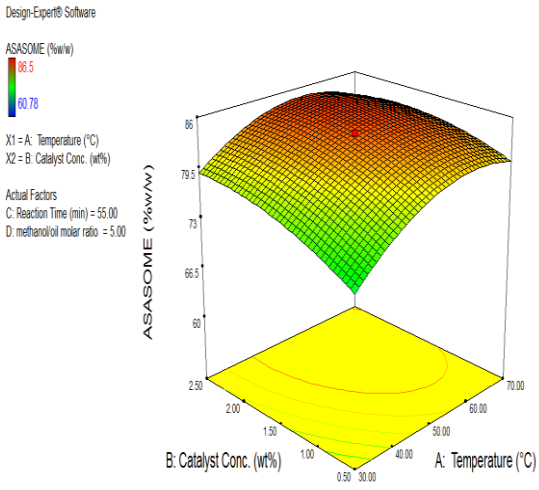

(A)

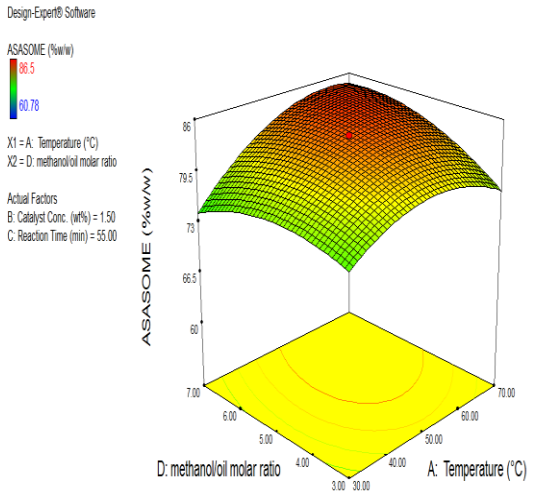

(B)

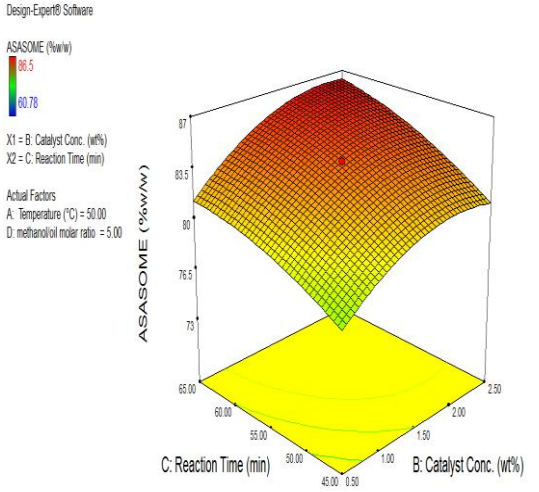

(C)

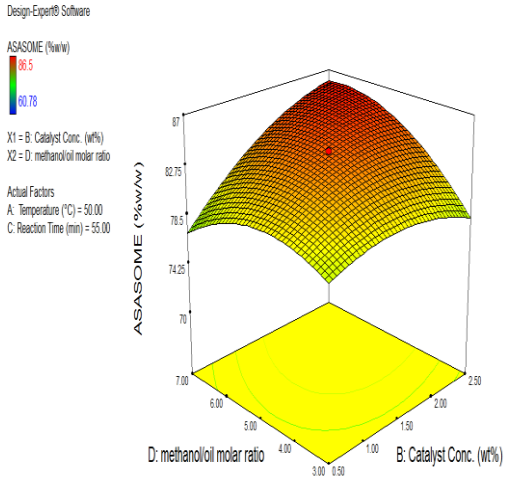

(D)

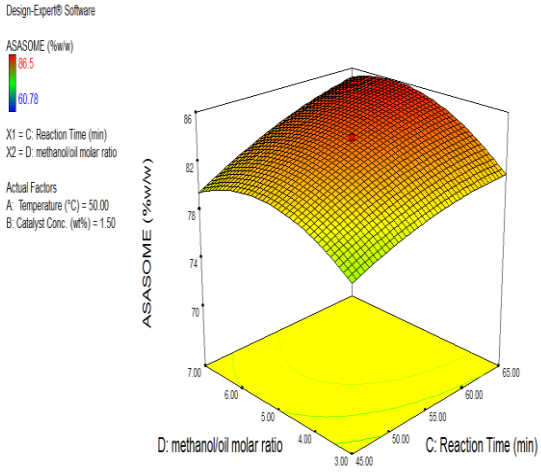

(E)

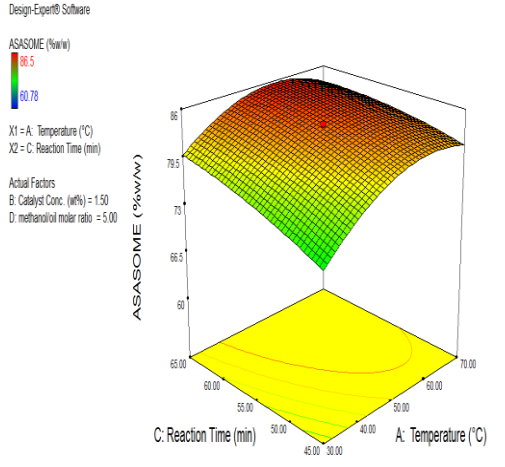

(F)

Figure 4.25: The 3D response surface plot of the effects of the variables on ASASOME yield.
(A). Catalyst concentration and temperature (B). Oil/methanol ratio and temperature
(C). Reaction time and catalyst concentration (D). Oil/methanol ratio and catalyst concentration
(E). Oil/methanol ratio and reaction time (F). Reaction time and temperature,

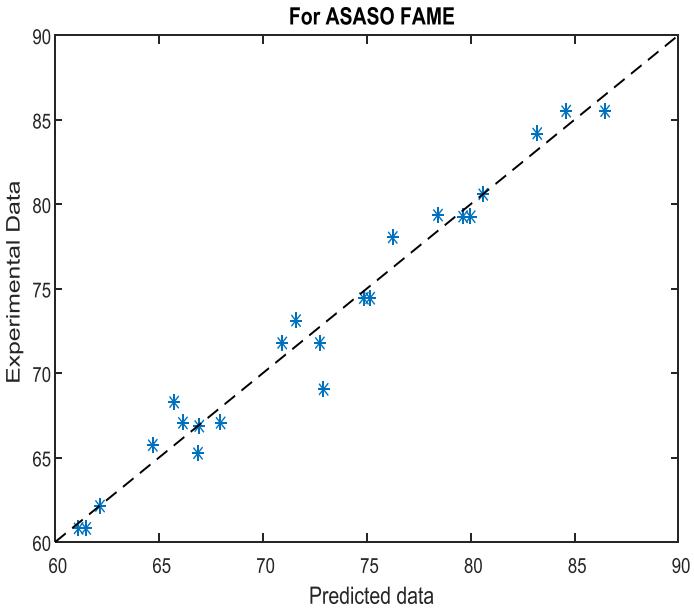

Figure 4.26: Linear correlation between predicted versus actual yield for ASASOME yield.

4.6.2.6 The summary of the seed oil RSM optimized conditions.

The summary of the optimized conditions for the SASO, APSO and ASASO methanolysis is presented in Table 4.26. A validation experiment was then performed using the optimal results of the numerical optimization executed by Design Expert 7.0.0 software. The results of the validation experiments were found to be in reasonable agreement with that of statistical model. Therefore, the optimal responses and their conditions provided in Table 4.26 were established as viable routes for maximum biodiesel yield, reduced energy consumption and low operating cost through RSM.

Table 4.26: Summary of optimized criteria for the seed oils transesterification using RSM.

Process parameters	Results		
	SASO	APSO	ASASO
Reaction time (min)	58.52	58.00	62.04
Oil/methanol ratio	1:4.66	1:6.86	1:5.88
Reaction temperature (°C)	50.03	63.92	65.62
Catalyst concentration (wt %)	2.04	1.88	2.14
Predicted methyl content (%)	91.09	95.03	86.85
Experimental methyl content (%)	92.58	94.55	85.91

4.6.3 Artificial neural networks (ANN) modeling

The optimum architecture topology of ANN (4:10: 1) model in this case is shown in Figure 4.27. It consists of three layers: input layer with four input variables, hidden layer with ten hidden neurons and an output layer with single output variable. All neurons from hidden layer have tan-sigmoid transfer function (tansig) and the output layer neuron has linear transfer function (purelin). As observed from Figure 4.16, the connections consist of weights and biases between inputs and neurons as well as between neurons from different layers.

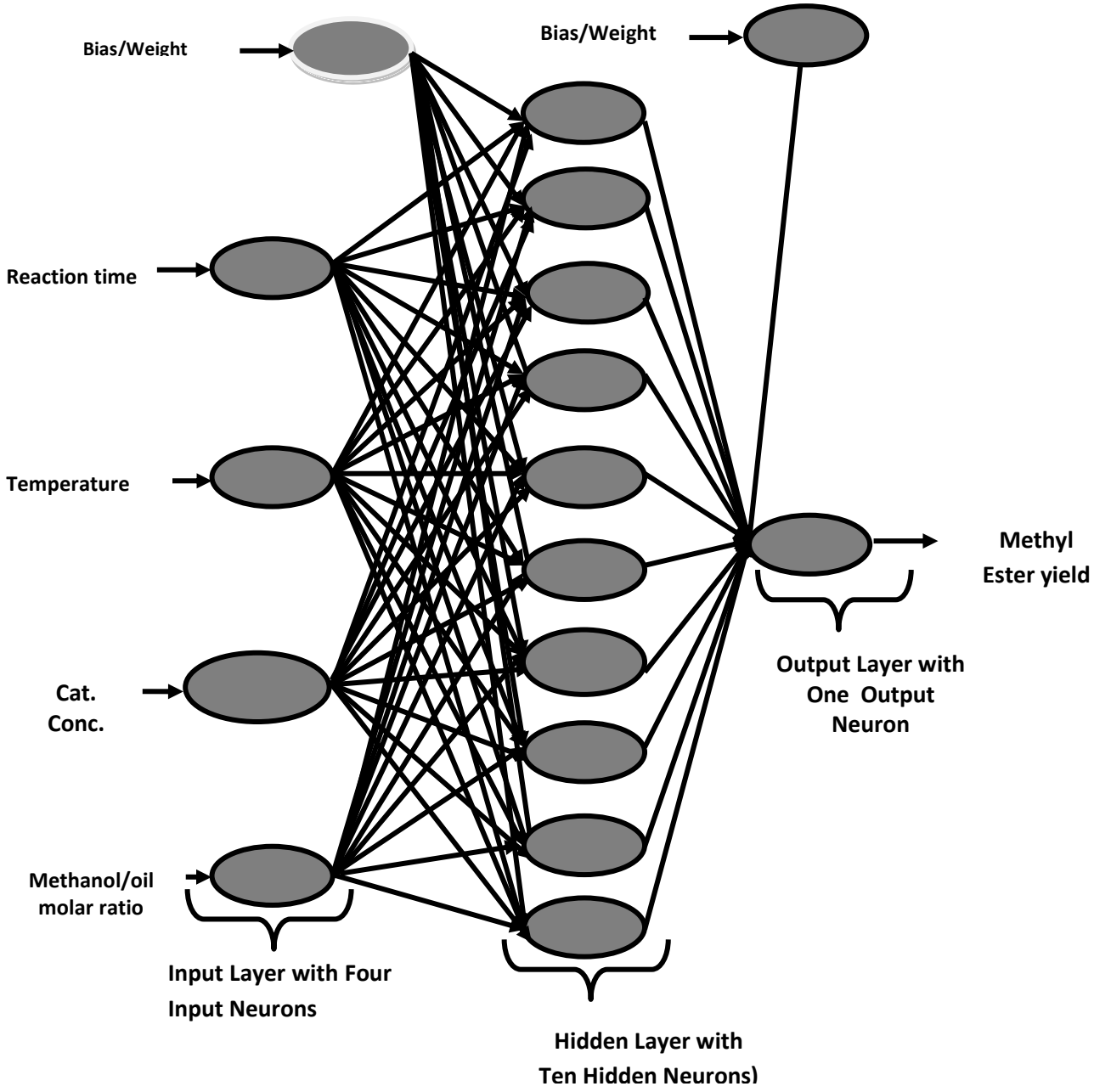

Figure 4.27: Typical ANN architecture of the topology of the seed oils'methanolysis.

4.6.3.1 Artificial neural network modeling of SASOME production

Total data set of 25 points as shown in Table 4.27 was used in developing ANN model by MATLAB 8.5. Figure 4.28 shows the relationship between output and target with high coefficient of determination (R=0.96637) and low standard error of estimation using ANN as contained in Table 4.27. It is observed that the regression coefficients of training, testing, validation and overall model developed using ANN is shown in Figure 4.29. The values on the X-axis are the target values, or the experimental values input to develop the model whereas the values on the Y-axis are the values predicted by the ANN model developed. As can be seen from these high regression values, the values predicted are very close to the actual yield values for all data set and an indication of successful development of the ANN model. Also Table 4.28 summarizes the statistical results for training and validation sets of artificial neural network models. These results indicate forecasting error measurements based on difference between the model and actual values. By this consideration, these training data, the lowest standard deviation, mean absolute deviation, mean absolute percentage error and the highest R^2 were calculated for SASOME yield. For validation data, however, the lowest standard deviation, mean absolute deviation mean absolute percentage error and the higher R^2 were observed for biodiesel yield. The maximum value of the response is 95.45% obtained at 60°C, catalyst concentration of 1.5g, reaction time of 65 minutes and methanol/oil ratio of 1:5. Calculated statistics as shown in Table 4.28 indicate that ANN provides a desirable means of efficiently recognizing the patterns in data and predicting biodiesel yield in agreement with Figure 4.30 (MSE Vs Epochs). It showed high coefficient of correlation (R = 0.9664).

Table 4.27: Sample of data of artificial neural network of SASOME.

Run	Factor 1 A (^{o}C)	Factor 2 B(wt%)	Factor 3 C (mins)	Factor 4 D (mol/mol)	Actual value (%)	Predicted value (%)
1	40	1.0000	50	1:4000	80.7700	83.0520
2	60	1.0000	50	1:4000	70.5400	70.8070
3	40	2.0000	50	1:4000	66.8400	61.9403
4	60	2.0000	50	1:4000	69.6100	73.3347
5	40	1.0000	60	1:4000	84.8860	87.9489
6	60	1.0000	60	1:4000	87.6560	85.8663
7	40	2.0000	60	1:4000	73.9560	74.4695
8	60	2.0000	60	1:4000	86.7260	87.1048
9	40	1.0000	50	1:6000	67.7700	63.6320
10	60	1.0000	50	1:6000	71.5400	75.6868
11	40	2.0000	50	1:6000	65.8400	68.1964
12	60	2.0000	50	1:6000	69.7100	74.0382
13	40	1.0000	60	1:6000	74.8860	74.2280
14	60	1.0000	60	1:6000	86.6560	87.9548
15	40	2.0000	60	1:6000	85.9560	90.1428
16	60	2.0000	60	1:6000	86.7260	82.6761
17	30	1.5000	55	1:5000	74.4780	73.1443
18	70	1.5000	55	1:5000	80.0180	80.1113
19	50	0.5000	55	1:5000	78.1780	78.2802
20	50	2.5000	55	1:5000	86.3180	81.3596
21	50	1.5000	45	1:5000	60.1320	57.3792
22	50	1.5000	65	1:5000	94.3640	95.4555
23	50	1.5000	55	1:3000	77.2480	76.4045
24	50	1.5000	55	1:7000	76.9420	75.3852
25	50	1.5000	55	1:5000	76.8431	77.8612

Table 4.28: Model statistics for the artificial neural network model of SASOME

Performance	Values
MSE	6.0035
MAE	2.7860
MAD	1.8930
Minimum Absolute Error	0.0933
Maximum Absolute Error	4.32820
R	0.96637

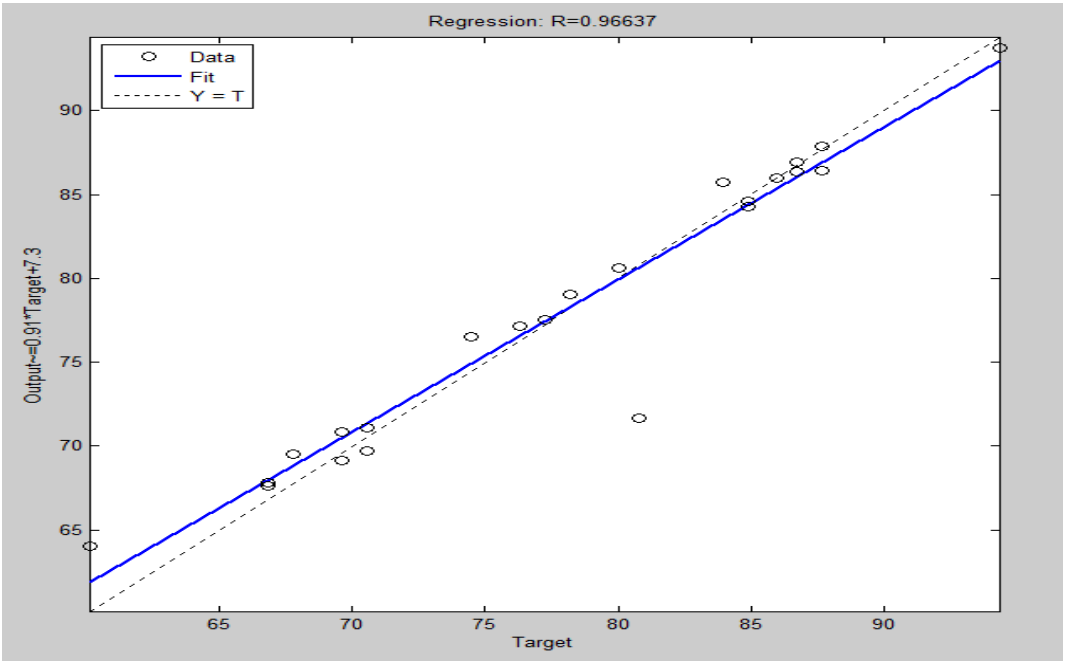

Figure 4.28: ANN plot showing the predicted output and the actual output for SASOME

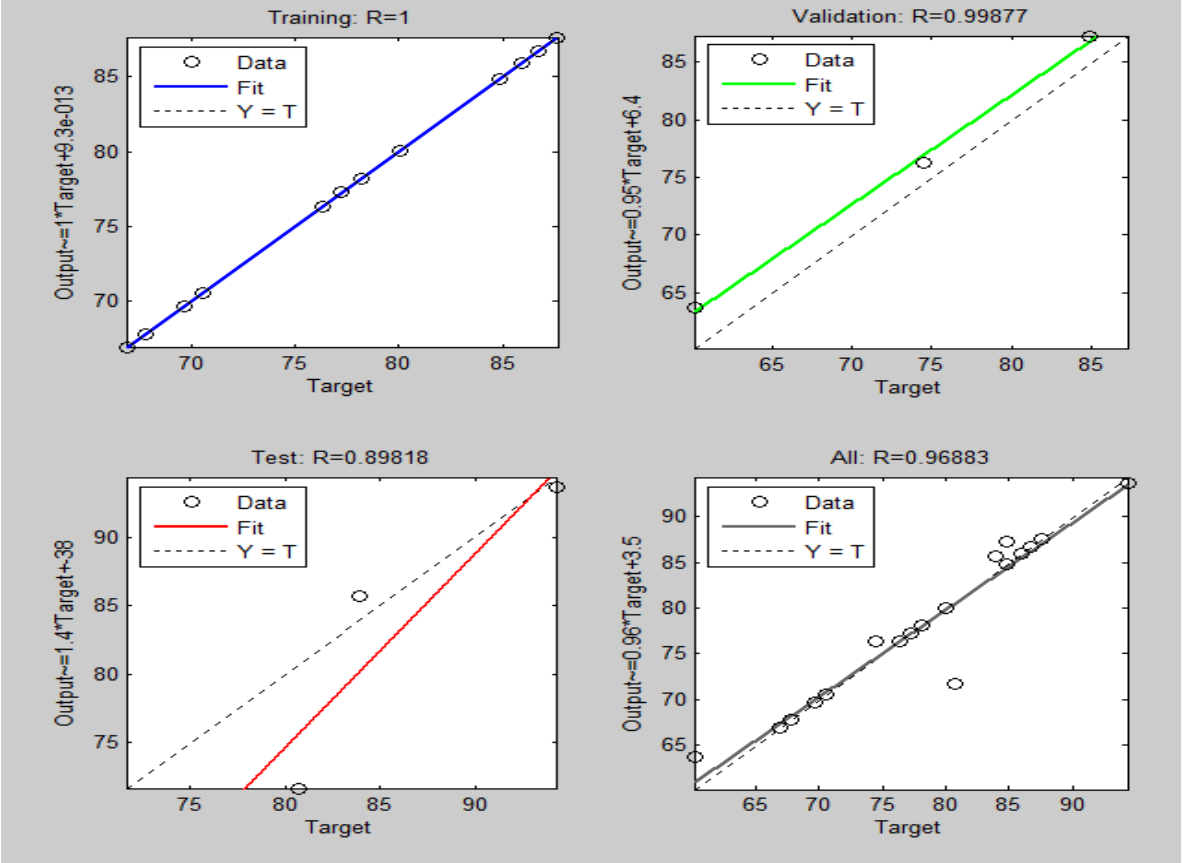

Figure 4.29: ANN regression values for training data; test data; validation data and overall model for SASOME

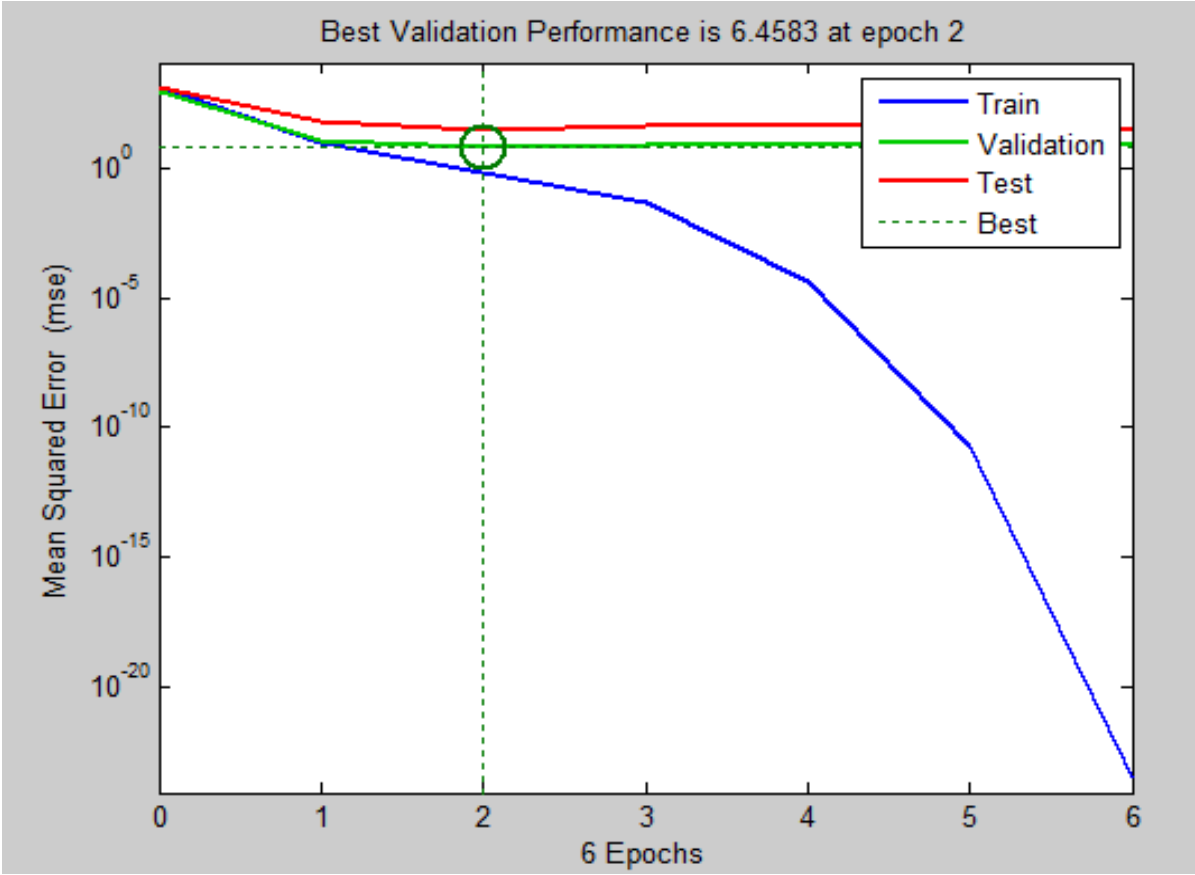

Figure 4.30: Plot indicating the best performance validation in terms of MSE with respect to the number of iterations for SASOME.

4.6.3.2 Artificial neural network (ANN) modeling of APSOME production

Total data set of 25 points as shown in Table 4.29 was used in developing ANN model by MATLAB 8.5. All models constructed from the data set were characterized by a great response for all input variables from the leaning set. Figure 4.31 shows the relationship between the output and the target with high coefficient of determination (R=0.97196) and low standard error of estimation using ANN as contained in Table 4.29. Almost all the data scattered around the 45° line and that shows excellent compatibility between the experimental results and ANN predicted data. The regression coefficients of training, testing, validation and overall model developed using ANN is shown in Figure 4.32 and all prediction set had very good values of R (1.000, 0.9951, 0.8456 and 0.97171 respectively) with low value of MSE (Figure 4.33). The values on the x-axis are the target

values or the experimental values used to develop the model while the values on the y-axis are the values predicted by the model. The models constructed from this data set were characterized by a huge response for all input variables from the learning set which exhibited good relation between inputs (reaction temperature, reaction time, oil to methanol molar ratio and catalyst concentration) and the output (biodiesel yield). As mentioned earlier, the validation of results was tested using 25 sets of data. The comparison showed the behavior of such neural network models in predicting biodiesel yield. In addition, Table 4.30 summarizes the statistical results. These results indicate forecasting error measurements based on differences between the model and actual values. For validation data, the low standard deviation, mean absolute deviation, mean absolute percentage error and high R^2 were observed for biodiesel yield. The calculated statistics indicate that ANN provides a desirable way of understanding the patterns in data and predicating methyl ester yield based on investigating parameters (inputs). The results of this study are in agreement with the works available in literature (Bhattacharyulu *et al.,* 2013; Ahmadian-Morghadam *et al.,* 2013).

Table 4.29: Sample of data used to develop artificial neural network for APSOME.

Run	Factor 1 A(^{o}C)	Factor 2 B(wt%)	Factor 3 C(mins)	Factor 4 D (mol/mol)	Actual value (%)	Predicted value (%)
1	40	1.0000	50	1:4000	80.2600	80.0910
2	60	1.0000	50	1:4000	67.8200	73.0778
3	40	2.0000	50	1:4000	69.5600	69.5676
4	60	2.0000	50	1:4000	68.2500	68.3166
5	40	1.0000	60	1:4000	86.6200	86.7414
6	60	1.0000	60	1:4000	85.3100	85.2270
7	40	2.0000	60	1:4000	87.0500	88.2719
8	60	2.0000	60	1:4000	85.7400	86.5910
9	40	1.0000	50	1:6000	69.1300	69.4590
10	60	1.0000	50	1:6000	66.8200	67.7630
11	40	2.0000	50	1:6000	69.6600	66.4099
12	60	2.0000	50	1:6000	67.2500	68.1794
13	40	1.0000	60	1:6000	86.8200	86.2429
14	60	1.0000	60	1:6000	85.3500	79.6197
15	40	2.0000	60	1:6000	87.6500	87.1192
16	60	2.0000	60	1:6000	85.8400	85.6321
17	30	1.5000	55	1:5000	78.7450	78.9258
18	70	1.5000	55	1:5000	76.1250	76.0502
19	50	0.5000	55	1:5000	77.0050	76.6884
20	50	2.5000	55	1:5000	77.8650	74.0572
21	50	1.5000	45	1:5000	59.9450	60.0572
22	50	1.5000	65	1:5000	94.9250	99.3069
23	50	1.5000	55	1:3000	77.4350	77.5250
24	50	1.5000	55	1:7000	78.5142	79.2240
25	50	1.5000	55	1:5000	80.2193	81.0040

Table 4.30: Model statistics for the artificial neural network model of APSOME.

Performance	Biodiesel
MSE	1.3112
MAE	1.6588
MAD	1.3112
Minimum Absolute Error	0.009
Maximum Absolute Error	5.7303
R	0.97196

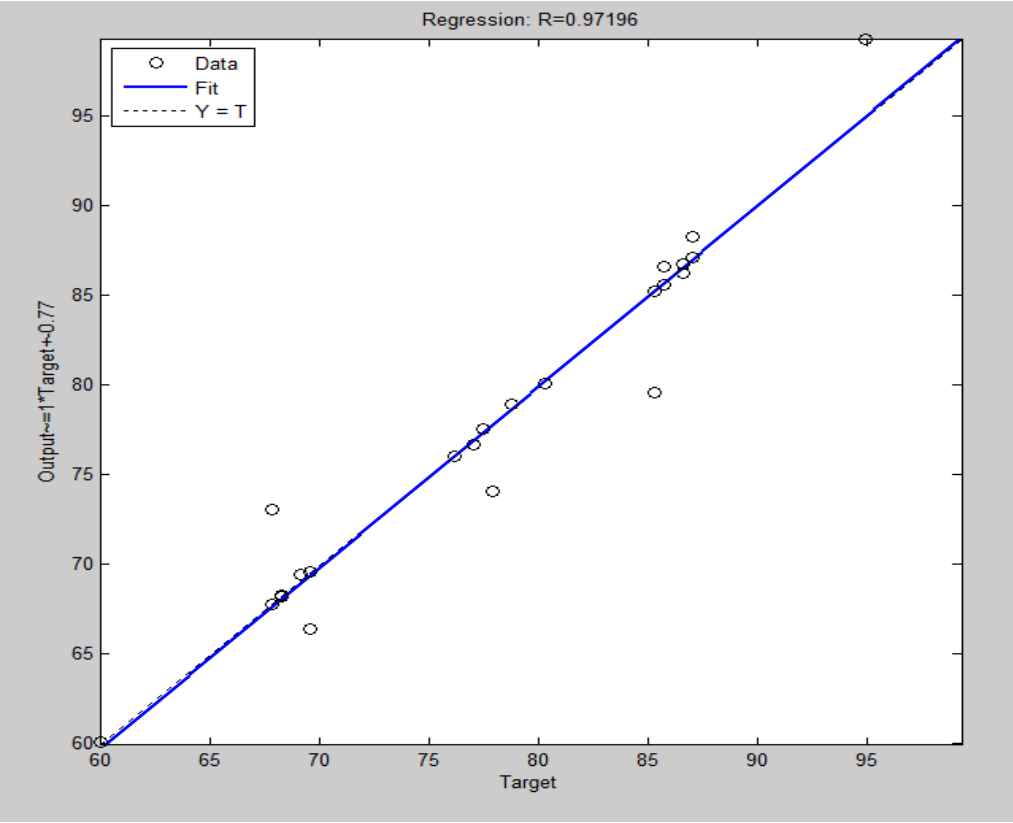

Figure 4.31: Desired output and actual network base on randomized data for APSOME

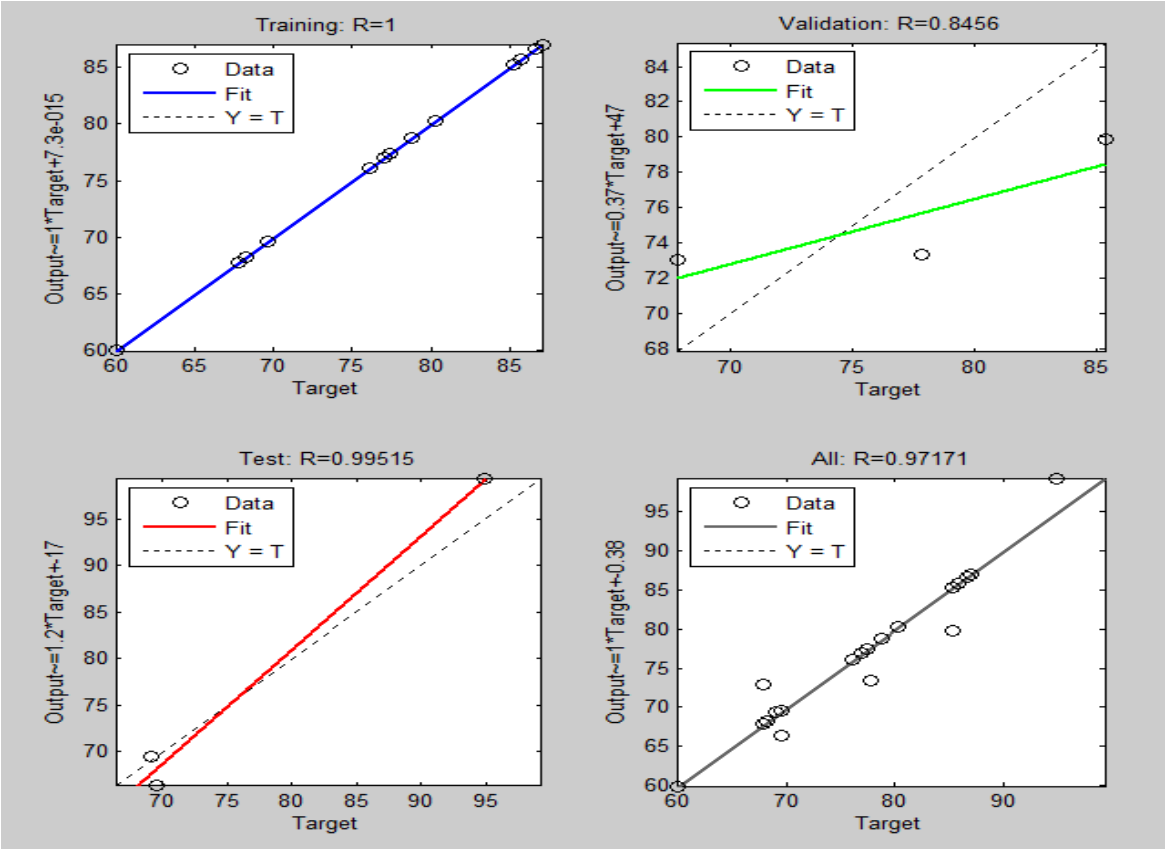

Figure 4.32: Regression values for training data, test data, validation data and overall model for APSOME

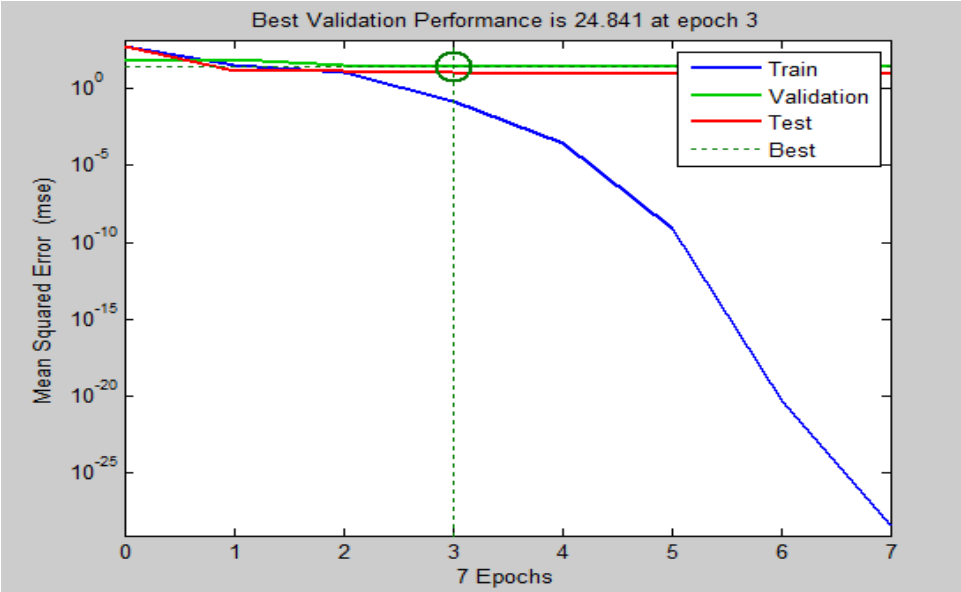

Figure 4.33: RMSE for training, testing and validation data for the ANN model developed.

4.6.3.3 Artificial neural network (ANN) modeling of ASASOME production

Figure 4.34 shows the relationship between output and target with high coefficient of determination (R=0.913) and low standard error of estimation using ANN as contained in Table 4.31. It is observed that the regression coefficients of training, testing, validation and overall model developed using ANN as shown in Figure 4.35 were all above 0.95. The values on the X-axis are the target values, or the experimental values input to develop the model whereas the values on the Y-axis are the values predicted by the ANN model developed. As can be seen from these high regression values, the values predicted are very close to the actual yield values for all data set and an indication of successful development of the ANN model. Also, Table 4.21 summarizes the statistical results for training and validation sets of artificial neural network models. These results indicate forecasting error measurements based on difference between the model and actual values. By this consideration, these training data, the lowest standard deviation, mean absolute deviation, mean absolute percentage error and the highest R^2 were calculated for ASASOME yield. For validation data, however, the lowest standard deviation, mean absolute deviation mean

absolute percentage error and the higher R^2 were observed for biodiesel yield. Calculated statistics as shown in Table 4.32 indicates that ANN provides a desirable means of efficiently recognizing the patterns in data and predicting biodiesel yield in agreement with Figure 4.36, (MSE Vs Epochs). The results obtained are in close agreement with the previous research results obtained Rajendra *et al.,* (2009).

Table 4.31: Sample of data used to develop artificial neural network for ASASOME.

Run	Factor 1 A (^oC)	Factor 2 B (wt%)	Factor 3 C (mins)	Factor 4 D(mol./mol.)	Actual value (%)	Predicted value (%)
1	40	1.0000	50	1:4000	60.7800	60.8638
2	60	1.0000	50	1:4000	67.0200	67.0210
3	40	2.0000	50	1:4000	71.8000	71.8008
4	60	2.0000	50	1:4000	69.0400	69.1294
5	40	1.0000	60	1:4000	65.2360	65.3154
6	60	1.0000	60	1:4000	74.4760	74.5044
7	40	2.0000	60	1:4000	79.2560	84.0478
8	60	2.0000	60	1:4000	85.4960	86.5986
9	40	1.0000	50	1:6000	60.7800	61.8232
10	60	1.0000	50	1:6000	67.0200	67.0475
11	40	2.0000	50	1:6000	71.8000	67.5013
12	60	2.0000	50	1:6000	78.0400	78.0598
13	40	1.0000	60	1:6000	68.2360	66.7983
14	60	1.0000	60	1:6000	74.4760	74.5004
15	40	2.0000	60	1:6000	79.2560	79.3307
16	60	2.0000	60	1:6000	86.4960	85.5202
17	30	1.5000	55	1:5000	66.8980	63.2870
18	70	1.5000	55	1:5000	79.3780	79.3931
19	50	0.5000	55	1:5000	62.1180	62.1202
20	50	2.5000	55	1:5000	84.1580	84.2487
21	50	1.5000	45	1:5000	65.6820	65.7245
22	50	1.5000	65	1:5000	80.5940	80.6667
23	50	1.5000	55	1:3000	73.1380	73.1728
24	50	1.5000	55	1:7000	75.8410	75.9921
25	50	1.5000	55	1:5000	78.3258	78.3425

Table 4.32: Model statistics for the artificial neural network model ASASOME.

Performance	Biodiesel
MSE	2.803446
MAE	1.211945
MAD	0.762586
Minimum Absolute Error	0.0008
Maximum Absolute Error	5.3426
R	0.98139

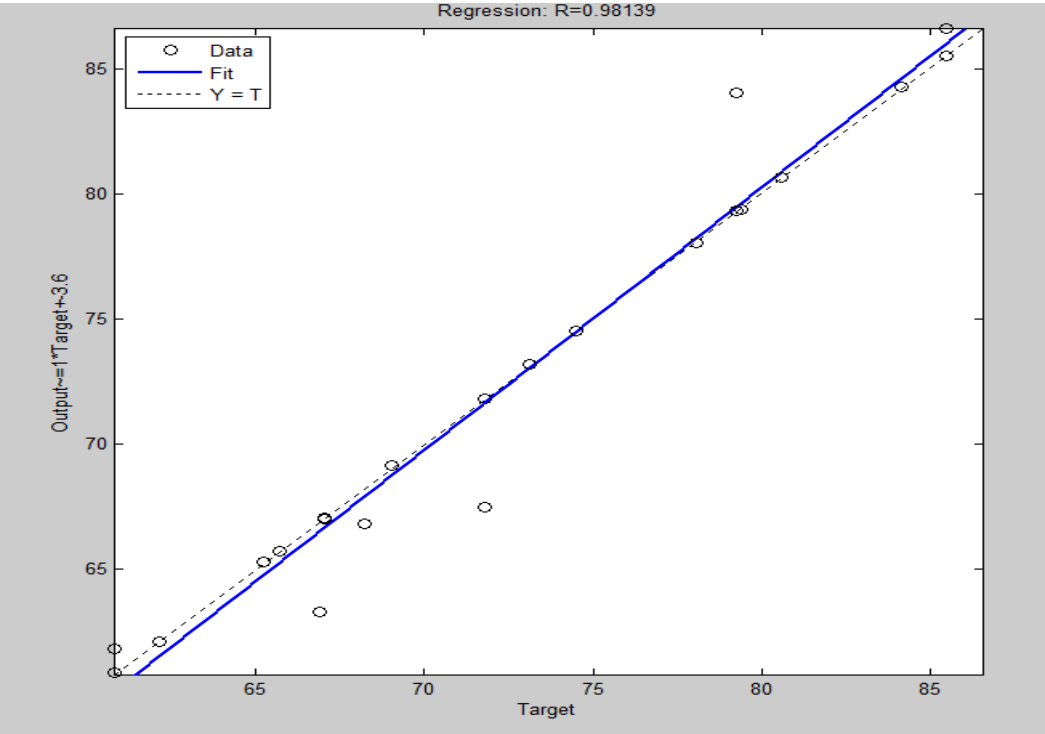

Figure 4.34: Plot showing the predicted output and the actual output.

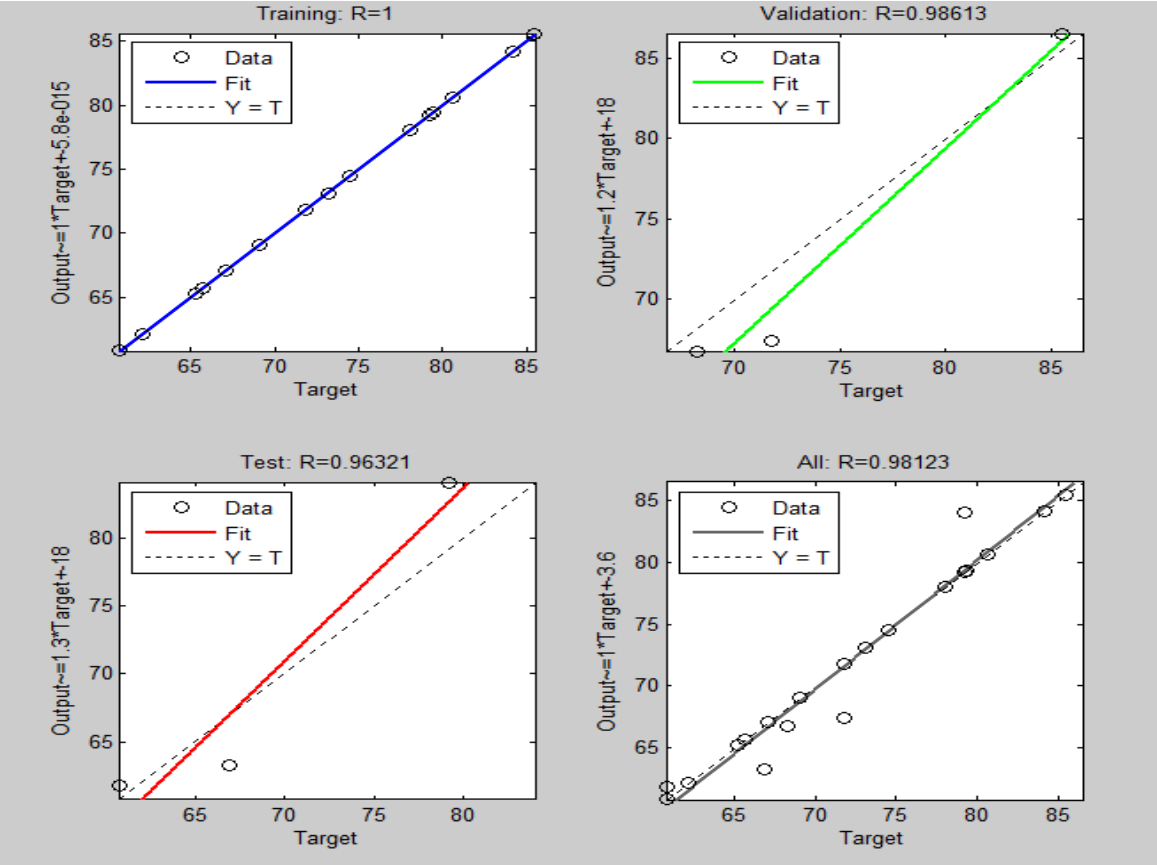

Figure 4.35: Plot showing the regression values actual and predicted yield.

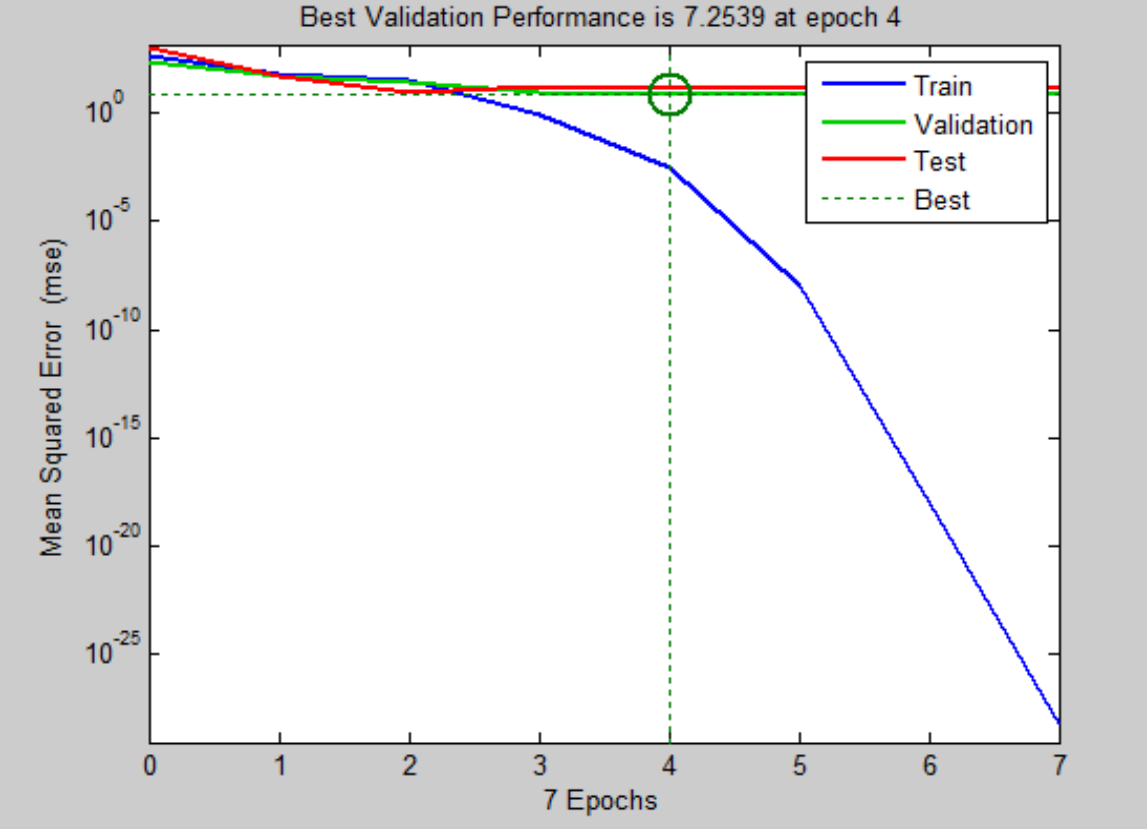

Figure 4.36: Plot indicating the best performance validation in terms of its MSE with respect to the number of iterations.

4.7 Engine Performance, Pollutant Emission and Combustion Characteristics Study

The African pear seed oil methyl ester (APSOME) and sweet almond seed oil methyl ester (SASOME), their blends with petrodiesel and the unblended petrodiesel were run in perkins 4:108 diesel engine to determine and compare their engine performance and combustion emissions characteristics. The engine speed was run at constant speed of 1500rpm while the engine load was varied from 5-40Nm. The blends of 25:75(B25), 50:50(B50) and 75:25(B75) perecentage volume ratios were choosen based on earlier reports (Haiter et al., 2012). The unblended biodiesels were coded B100. The results are presented in Tables A4.1 for petrodiesel and Tables A4.2-A4.9 for APSOME and SASOME blends.

4.7.1 Physico-chemical characterization of the B100, their blends and petro-diesel

Tables 4.34 and 4.35 contain the results the physico-chemical characterization of the fuel blends of SASOME and APSOME with petrodiesel. The results are compared with the ASTM D 6751 standards.

The kinematic viscosities of all the blends of SASOME with petro diesel were all within the range (1.9-6.0 mm^2/s) required for use in the engines. The values decreased with decrease in the amount of biodiesel in each blend. The values were found to decrease from 4.05mm^2/s for B100 to 3.50mm^2/s for B25. The viscosity of biodiesel is reported to be 10-15 times greater than that of petrodiesel because of biodiesel large molecular mass and chemical structure (Rabe, 2010). Therefore, more petrodiesel in the blends is expected to lower the viscosity of the blends.This is expected to improve the fuel flow and injection characteristics of the blends with more petrodiesel. Elango *et al.,* (2014) had reported similar results, where 4.2 mm^2/s at B20 and 4.6 mm^2/s at B50 using jatropha diesel oil.

However, all the blends had specific gravity values lower than the 0.880 tolerable limits allowable for effective air fuel injection systems as specified in the ASTM D 6751standards.

The ash content of the blends increases with increase in the amount of petrodiesel in the blend. This could be due to increase in the amount of mineral elements introduced from the petro-diesel. The increase in ash content with decrease in the amount of biodiesel in the blends shows that blends with more biodiesel would likely result in decrease in the emission of some air pollutants like SO_x and NO_x.

The saponification values of the blends showed little or no appreciable changes with the blends, though the saponification values were higher at B100 and lower at B25. B100 of SASOME had 161.05mgKOH/g while the lowest blends of B25 had 160.0mgKOH/g. However, the slight decrease in the values could be due to lack of saponifiable matter or fatty acids in the petro-diesel.

The flash point values were found to decrease from B100 to B25 blend (as the biodiesel content decreases) but all the values obtained were all above the 60˚C recorded for diesel. The B100 flash point was 136˚C while the values at lower blends decreased to 98.0˚C at B25 blends. The values of the flash points of all the blends fall within the 100-170°C allowable limit for ASTM D 6751 standard. This shows that none of the SASOME blends would have tendency of fire outbreaks nor be classified as hazardous material. However, the values obtained for all the blends were all within the -3 to12 °C (cloud point) and -15 to 10 °C (pour point) stipulated by ASTM D6751 standards.

The calorific values of all the SASOME blends were below the value (43.5MJ/kg) recorded for petrodiesel. The values increased with increase in petrodiesel blends. However, the lowest value was obtained from B100 (31.18MJ/kg) and the highest by B25 (35.28MJ/kg). These results indicate that all the blends would all burn with high release of energy.

The values of the sulphur content were found to increase with increase in petrodiesel in the blend. This is due to the fact that petrodiesel contains very high sulphur content which is very minimal in biodiesel. B100 had sulphur content of 2.11pm while B25 had 13.72ppm sulphur content against 30.50ppm recorded for the petrodiesel. This indicates that there is a clear correlation between the ash content and sulphur content in biodiesel. The result of the sulphur content of the blends is equally in line with 20-50% of diesel fuel values already reported by Demirbas, (2003). Although, high levels of sulphur in fuel when combined with water vapour forms sulphuric acid which has corrosive effect on the engine components, sufficient level of sulphur content in fuel is essential for the lubricating and functioning of fuel system machinery such as fuel pumps and injectors (He *et al.,* 2008). However, the sulphur content values obtained for B100 and the blends are in compliance with the Environmental Protection Agency (EPA) regulation standard (15ppm max) on high way diesel fuel, which took effect from June 1st, 2006.

The copper strip corrosion result showed class 1 value for all the blends as well as the petrodiesel. The corrosion tendencies of the fuels are induced by some sulphur compounds (Atabani *et al.,* 2010). Since the results obtained in this study for the SASOME and its blends are below the No. 3 maximum ASTMD 6751 standards, the fuel blends would not have corrosion tendency when used with copper, brass or bronze parts.

Table 4.33: The physico-chemical characteristics of the SASOME blends with diesel

S/n	Parameters	B100	B75	B50	B25	Diesel	ASTMD 6751
1	Viscosity(mm^2/s)	4.05	4.00	3.92	3.50	3.21	1.9-6.0
2	Specific gravity	0.849	0 .844	0.840	0.835	0.83	0.880
3	Ash content	0.1	0.19	1.00	1.15	-	0.02
4	Acid value(mgKOH/g)	0.46	0.40	0.40	0.38	-	0.50
5	Sap. value (mgKOH/g)	161.05	160.0	160.50	165.0	-	-
6	Free fatty acid (%)	0.23	0.20	0.20	0.19	-	0.25
7	Refractive index	1.4402	1.266	1.311	1.470	-	-
8	Calorific value(MJ/kg)	31.18	32.48	33.88	35.28	43.5	-
9	Flash point(°C)	136	116	107	98.0	60	100-170
10	Cloud point(°C)	10	8.0	7.5	6	8	-3 to 12
11	Pour point(°C)	4	3	4	8	9	-15 to 10
12	Sulphur content(ppm)	2.11	5.91	11.01	13.72	30.5	15ppm
13	Copper corrosion	Class 1	Class 1	Class 1	Class1	Class1	No. 3 max

Sap. - saponification

The kinematic viscosities of all the blends of African pear seed oil methyl ester (APSOME) with petrodiesel were all found to be higher than the petro-diesel and within the range (1.9-6.0 mm^2/s) required for use in the diesel engines. The values decreased with decrease in the amount of biodiesel in each blend. The kinematic viscosity results obtained in this study follow the trend of results obtained by Elango and Sentinkumar (2014) in jatropha diesel oil blends with diesel. They obtained viscosities of 4.2mm^2/s and 4.6mm^2/s at B20 and at B50 blends respectively. The results obtained in this study are all within the 1.9-6.0 mm2/s standard recommended by international standards (ASTM D6751). Therefore, there would be no tendency of the fuel blends to give any fuel injection flow challenges. However, all the blends had specific gravity values within the tolerable limits of

0.88 (ASTM D 6751) allowable for effective air fuel injection systems. The ash content of the blends increases with increase in the amount of petrodiesel in the blend. This could be due to increase in the amount of mineral elements introduced from the petro-diesel (Ofoefule et al., 2015). This could result in the increase in the emissions of some air pollutants. Both SASOME and APSOME blends had similar trends in ash content.

The saponification values of the blends showed no significant changes with the blends, though the saponification values were higher at B100 and lower at B25. B100 of APSOME had 242.51mgKOH/g while the lowest blends of B25 had 224.68mgKOH/g. However, the slight decrease in the values could be due to lack of saponifiable matter or fatty acids in the petro-diesel added to the biodiesel.

The flash point values decreased with increase in petrodiesel in the blends. It was observed that the flash point of B25 (88°C) was lower than the minimum 100°C stipulated by ASTM D 6751. This was because the B100 of APSOME had lower flash point (125°C) than 136°C recorded by SASOME B100. Therefore, blending the biodiesels with petrodiesel of lower flash point (60°C) definitely caused the B25 to have such very low flash point. This would make B25 to have tendencies of fire outbreaks and be classified as hazardous. Similarly, the flash point of jatropha biodiesel blend with petro-diesel has been reported low with higher amount of petrodiesel in the blends (98˚C for B50 and 79˚C for B20) (Elango and Senthilkumar, 2011). Also, the calorific values decreased with increase in biodiesel in the blends. Such trend has been observed by Elango and Senthilkumar, (2011) (40.877 MJ/kg at B50 and 43.093 MJ/kg at B20). However, the values obtained for all the blends were all within the -3 to12 °C (cloud point) and -15 to 10 °C (pour point) stipulated by ASTM D 6751 standards.

The values of the sulphur content were found to increase with increase in petrodiesel in the blend. B100 had sulphur content of 3.11pm while B25 had 13.72ppm sulphur content against 30.50ppm recorded for the petrodiesel. This indicates that there is a clear correlation

between the ash content and sulphur content in biodiesel blends with petrodiesel. However, the sulphur content values obtained for B100 and the blends is in compliance with the Environmental Protection Agency (EPA) Regulation Standard (15ppm max) on high way diesel fuel, which took effect from June 1st, 2006. High levels of sulphur in fuel, combines with water vapour to form sulphuric acid, which is the main component of acid rain that causes corrosive wearing on cylinder liners. However, sufficient level of sulphur content in fuel is essential for the lubricating and functioning of fuel system machinery such as fuel pumps and injectors (He, 2008). The result of the sulphur content is equally in line with 20-50% of diesel fuel values already recommended by Demirbas, (2003). The result of the copper corrosion belonged to class 1. This value is quite low compared to the maximum of No. 3 maximum limit stipulated by ASTM D 6751. It implies that the blends would not have corrosion tendencies on copper, brass and bronze materials.

Table 4.34: The physico-chemical characteristics of the APSOME blends with diesel.

Sn	Parameters	B100	B75	B50	B25	Diesel	ASTM D 6751
1	Viscosity(mm^2/s)	3.52	3.47	3.4	3.3	3.2	1.9-6.0
2	Specific gravity	0.852	0 .85	0.846	0.84	0.83	0.880
3	Ash content	0.1	0.19	1	1.15	-	0.02
4	AcidValue(mgKOH/g)	0.92	1.01	1.28	1.49	-	0.50
5	Sap. Value (mgKOH/g)	242.51	239.68	227.11	224.68	-	-
6	Free fatty acid (%)	0.46	0.52	0.79	0.81	-	0.25
7	Refractive index	1.4269	0.42	1.4111	1.4069	-	-
8	Calorific value(MJ/kg)	34.42	35.8	37.2	38.7	43.5	-
9	Flash point(°C)	125	109	100	88	60	100-170
10	Cloud point(°C)	-2	6	7	7.5	8	-3 to 12
11	Pour point(°C)	-6	-1	5	7	9	-15 to 10
12	Sulphur content(ppm)	3.11	5.91	11.01	13.72	30.5	15ppm
13	Copper corrosion	Class 1	Class 1	Class 1	Class 1	Class1	No. 3 max

Sap. – saponification

4.7.2 Engine performance results

The engine performance was evaluated based on the variations of the following engine chararcteristics: torque, brake thermal efficiency, brake specific fuel consumption, brake gross fuel consumption, volumetric efficiency, air/fuel ratio, brake specific energy consumption and brake mean effective pressure with brake power. It is worthy of note, that the influence of biodiesel on engine performance depends on the relationship between the fuel injection system and the fuel properties (oxygen content, density, viscosity, and higher heating value (HHV) of biodiesel) (Habibullah *et al.,* 2015). Hence, it is wise to relate the performance of the engine to the fuel characteristics or properties.

4.7.2.1 Variation of torque with brake power

Figure 4.37 (A) and (B) shows the relationship between brake power and torque for SASOME and APSOME respectively. The engine torque was varied between 5 to 40Nm while the brake power ranged between 0.785 to 6.283kW. It is observed from that there is a linear relationship between the brake power and corresponding load. The increase in the torque or load results in increase in brake power. The same trend is observed in the B100, its blends (B25, B50 and B75) and the petro-diesel. This is possible because, brake power is a product of the load or torque and speed of the engine. Therefore, running the engine at specific speed and varying load gave a linear relationship. Since the same conditions of operation were applied to both SASOME and APSOME, the same characteristics were observed for both of them on the relationship between engine torque and brake power.

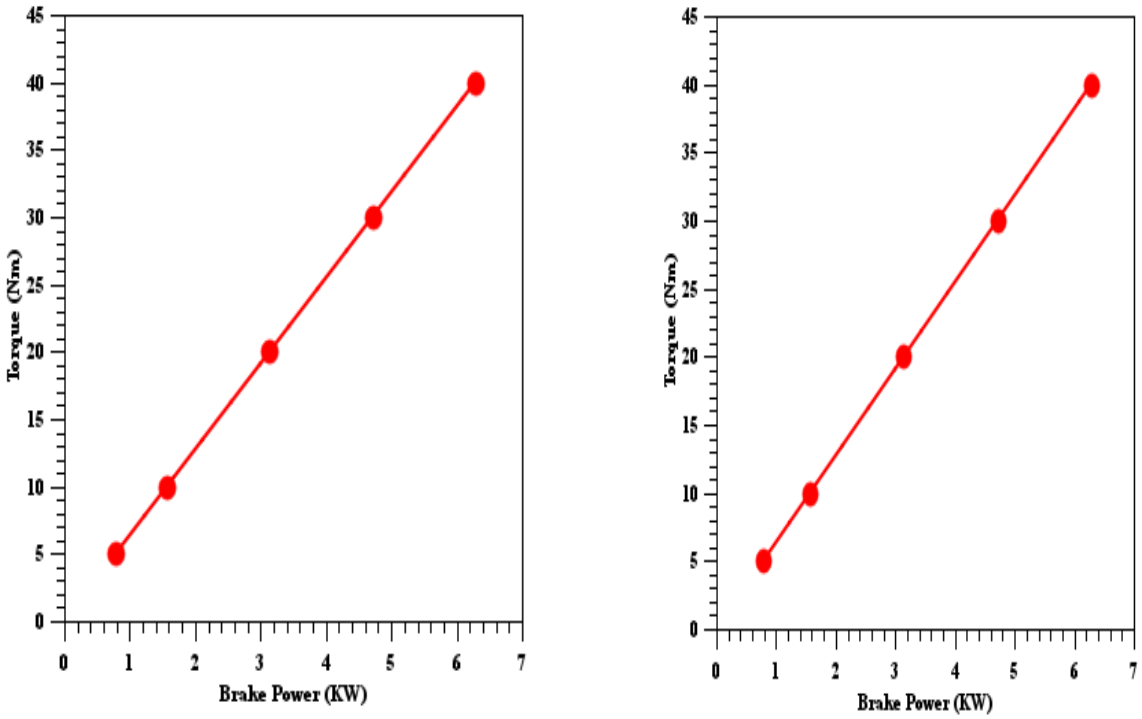

(A) (B)

Figure 4.37: Variation of torque against brake power, (A)-APSOME, (B)-SASOME.

4.7.2.2 Variation of brake thermal efficiency with brake power

Tables A6.10 and A6.11 contains the values of brake thermal efficiencies of APSOME and SASOME respectively, for B100, petrodiesel and various blending ratios (B100, B75, B50 and B25) obtained at different brake powers. The variation of brake thermal efficiency (BTE) of the engine with various blends is shown in Figure 4.38 and compared with the brake thermal efficiency obtained using petrodiesel. The BTE increases with increase in brake power and decreases with increase in fuel mass flowrate (m_f). This is because BTE is a ratio of brake power (bp) to the product of fuel mass flowrate and calorific value. It is observed that BTE of all the blends are low at all load levels. Among the blends, B25 is found to have the lowest thermal efficiency of 30.00% and 32.09% for SASOME and APSOME respectively while for diesel it is 26.5. But for B50 and B75 it increased to 40.22% for SASOME and 36.22% for APSOME respectively. It is observed that as the portion of biodiesel fuel in the blends increases, the thermal efficiency increases. Considering SASOME at lower loads, B25 and diesel showed maximum BTE of 9.17% and 7.0% respectively, compared to other blends which had high BTE above 10%. This has

been suggested by Mishva *et al.*, (2014) to be due to additional lubricity provided by the biodiesel and presence of oxygen in biodiesel that resulted in improved combustion as compared to diesel. It was observed that between brake powers of 4.712kW (30Nm torque) and 6.283kW (40Nm toque), the difference in the thermal efficiency is insignificant compared to the change observed between the lower brake powers. It implies that 30Nm load at 1500rpm engine speed would give the best brake thermal efficiency among the range of factors studied. Similar results have been reported in the literature (Venkanna *et al.*, 2009). Hence, engines fueled by African pear and sweet almond seed oil biodiesels would run smoothly with longer maintenance intervals than those fueled by petro-diesel.

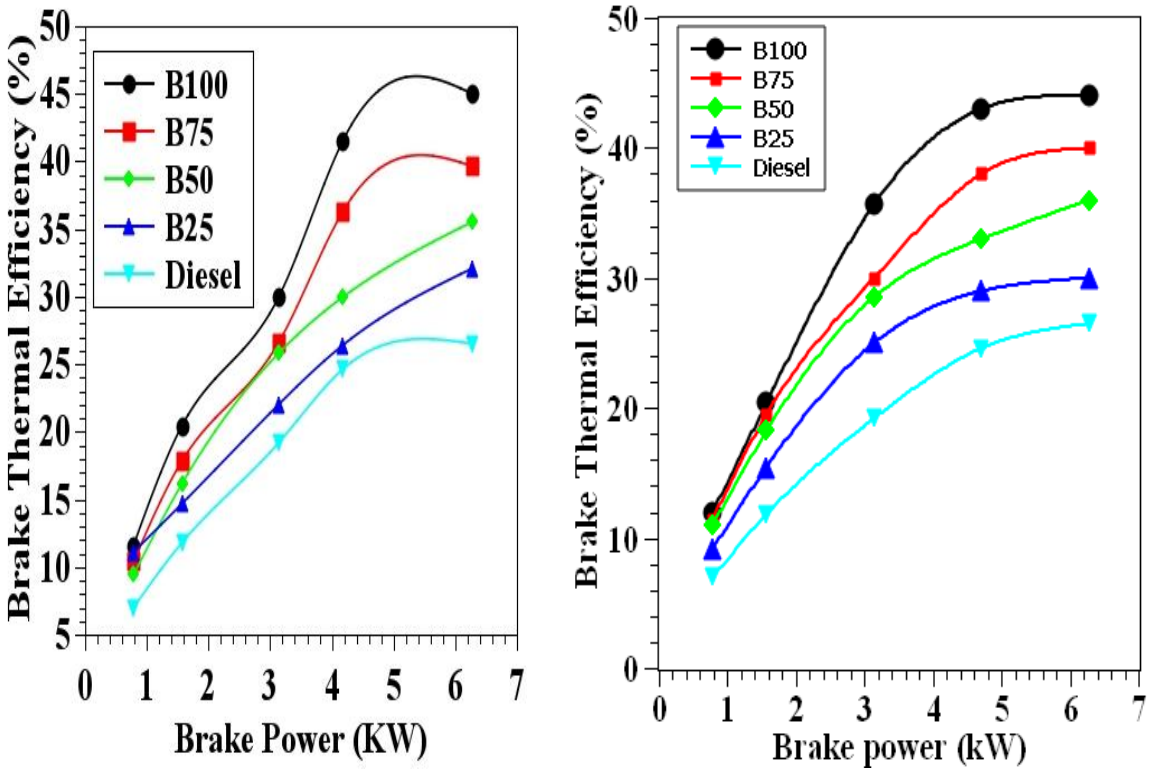

(A) (B)

Figure 4.38: Variation of brake thermal efficiency with brake power, (A)-APSOME, (B)- SASOME.

4.7.2.3 Variation of brake specific fuel consumption with brake power

Tables A6.12 and A6.13 contains the values of brake specific fuel consumption of APSOME and SASOME respectively for the various fuel blends at different brake powers. Figure 4.39 shows the variation of specific fuel consumption with brake power. From the

graph, it is observed that as engine brake power increases, specific fuel consumption decreases for all the fuel blends. Brake specific fuel consumption (BSFC) of biodiesel was higher than diesel at higher load. This could be due to less heating value and higher density of biodiesel (Mishva *et al*; 2014) that resulted in higher fuel flow-rate (on weight basis). Also, higher proportions of the biodiesel in the blends increase the viscosity which resulted in the increase in the specific fuel consumption (Elango *et al.,* 2011). Moreso, as the concentration of biodiesel increases, the fuel consumption tends to decrease for both SASOME and APSOME blends because mass flowrate of the fuel decreases. The minimum specific fuel consumption for B25 fuel is 1.11kg/kW-hr for SASOME and 1.19kg/kW-hr for petro-diesel. The specific fuel consumption for B50, B75 and B100 were 0.968kg/kW-hr, 0.96kg/kW-hr and 0.96kg/kW-hr at lowest load (5Nm) against 1.19 kg/kW-hr for diesel. It was equally observed that the B25 blends is close to diesel in the BSFC value while the values of APSOME blends were found to be higher than those of SASOME for the different blends. Of interest is the fact that, the negative changes observed on the BSFC with increase in brake powers were not uniform. It decreased with increase in power, while there was no significant difference in the BSFC between 30Nm and 40Nm. Therefore, the minimum specific fuel consumptions for SASOME and APSOME blends could be obtained at brake power of 4.712kW (30Nm).

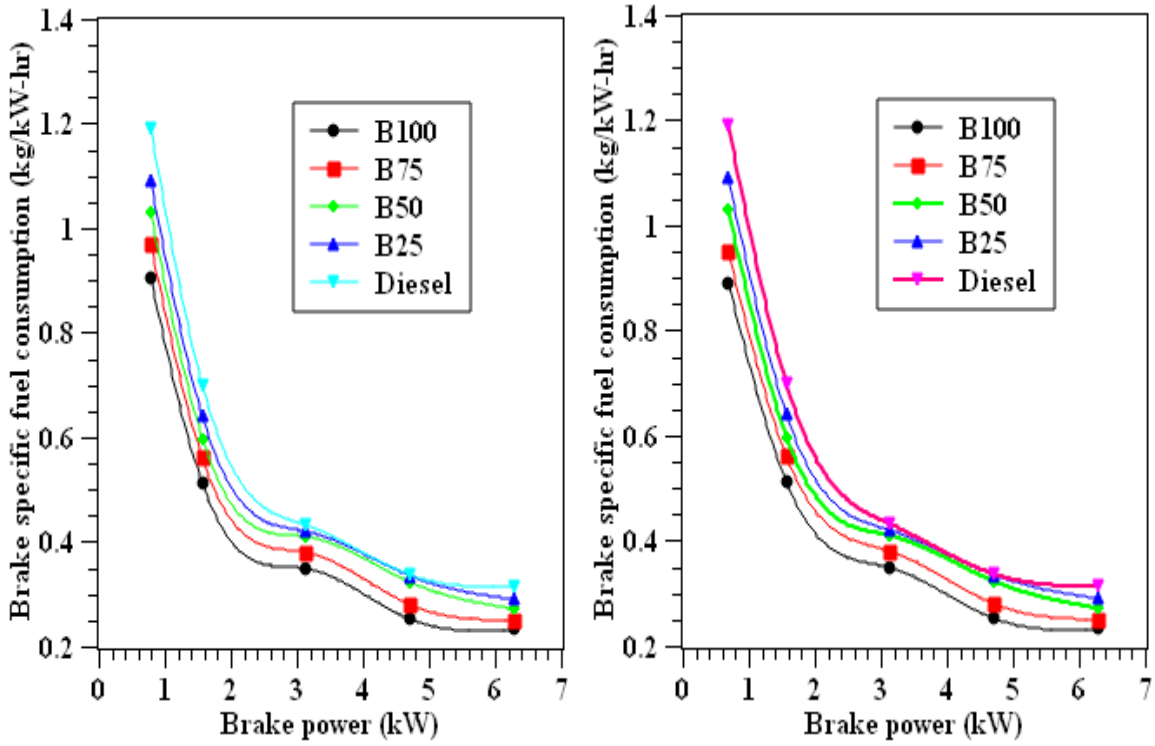

Figure 4.39: Variation of brake specific fuel consumption with brake power, (A)-APSOME, (B)-SASOME.

4.7.2.4 Variation of specific energy consumption with brake power

Tables A6. 14 and A6.15 contains the values of brake specific energy consumption of APSOME and SASOME respectively for various blending ratios and at different brake powers. Figure 4.40 (A) and (B) represents the trend lines for break specific energy consumption for both APSOME and SASOME respectively.

Since biodiesel blends have different calorific values, viscosity and density, therefore BSFC may not be a better reliable tool to compare the fuel consumption per unit power developed. Wahome *et al., (*2013) has therefore, advocated for brake specific energy consumption (BSEC) to be used to compare the biodiesel blends on the basis of energy required to develop unit power output.Brake specific energy consumption (BSEC) is the energy required to develop unit power output (Wahome *et al.*, 2013). It is a product of the brake specific fuel consumption and the calorific values (Q_{net}) of the fuel. Therefore, it would increase with increase in the fuel consumption and fuel mass flowrate but would

decrease with increase in brake power or load. In this study, brake specific energy consumption was found to be higher at lower loads and eventually decreased at full loads. The brake specific energy consumption of the blends with biodiesel was found to be lower than that of diesel. It indicates that energy released by biodiesel to develop unit power is more than that of petrodiesel fuel (Mishva *et al.*, 2014). Similar to the non-uniform negative changes observed on the BSFC with increase in brake powers, BSEC decreased with increase in power, while there was not significant difference in the BSEC between 30Nm and 40Nm. It therefore implies that the minimum specific energy consumptions for SASOME and APSOME blends could be obtained at brake power of 4.712kW (30Nm).

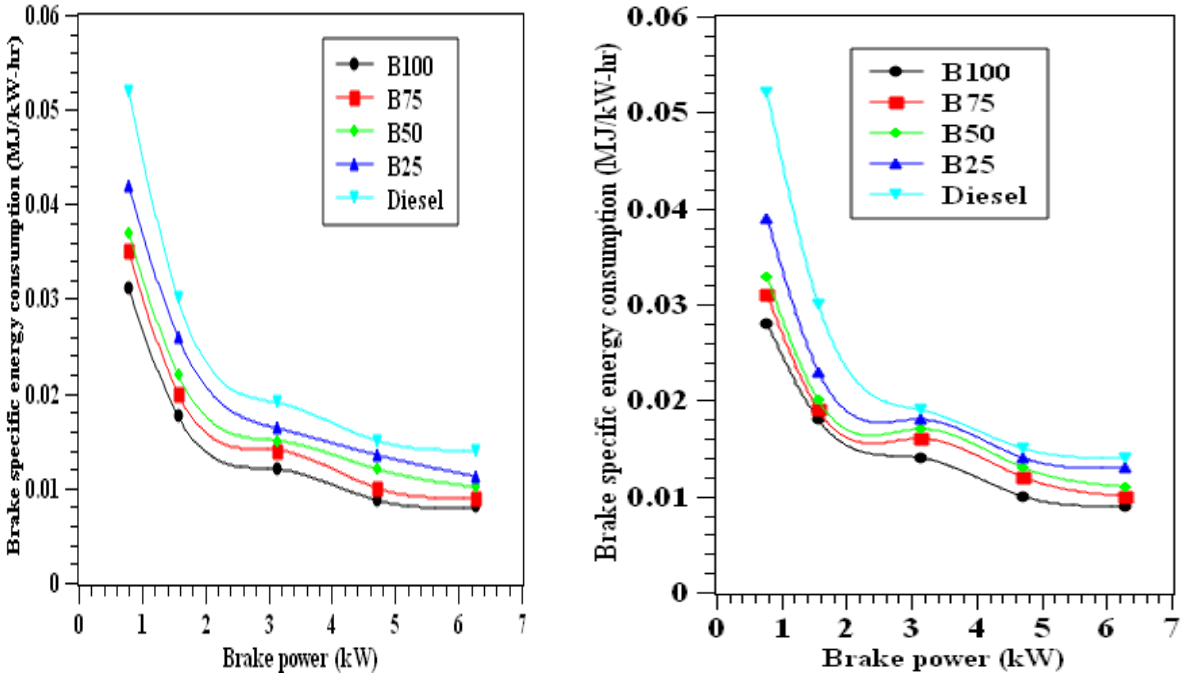

(A) (B)

Figure 4.40: Variation of blends' brake specific energy consumption with brake power, (A)-APSOME, (B)-SASOME.

4.7.2.5 Variation of gross fuel consumption with brake power

Tables A6.16 and A6.17 contains the values of gross fuel consumption of APSOME and SASOME respectively for various blending ratios and at different brake powers. Figure 4.41 (A) and (B) represents the variation of gross fuel consumption with brake power for both APSOME and SASOME respectively.

The gross fuel consumption is found to increase with increase in brake power. The highest gross fuel consumption was observed for diesel at 40Nm load (5.46 $\times 10^{-4}$kg/s) followed by B75 (5.34 $\times 10^{-4}$kg/s) and B25. (5.22$\times 10^{-4}$kg/s) for SASOME, but APSOME had its highest gross fuel consumption at B25 (5.06$\times 10^{-4}$kg/s) followed by B50 (4.752$\times 10^{-4}$kg/s) and B75 (4.43$\times 10^{-4}$kg/s). The B25 blend of both methyl esters has closer values with the petrodiesel than other blends as shown in Figures 4.30. The values of gross fuel consumption obtained for APSOME were less than their corresponding values for SASOME. This could be explained to be due to higher viscosity and density of SASOME than obtained for APSOME.

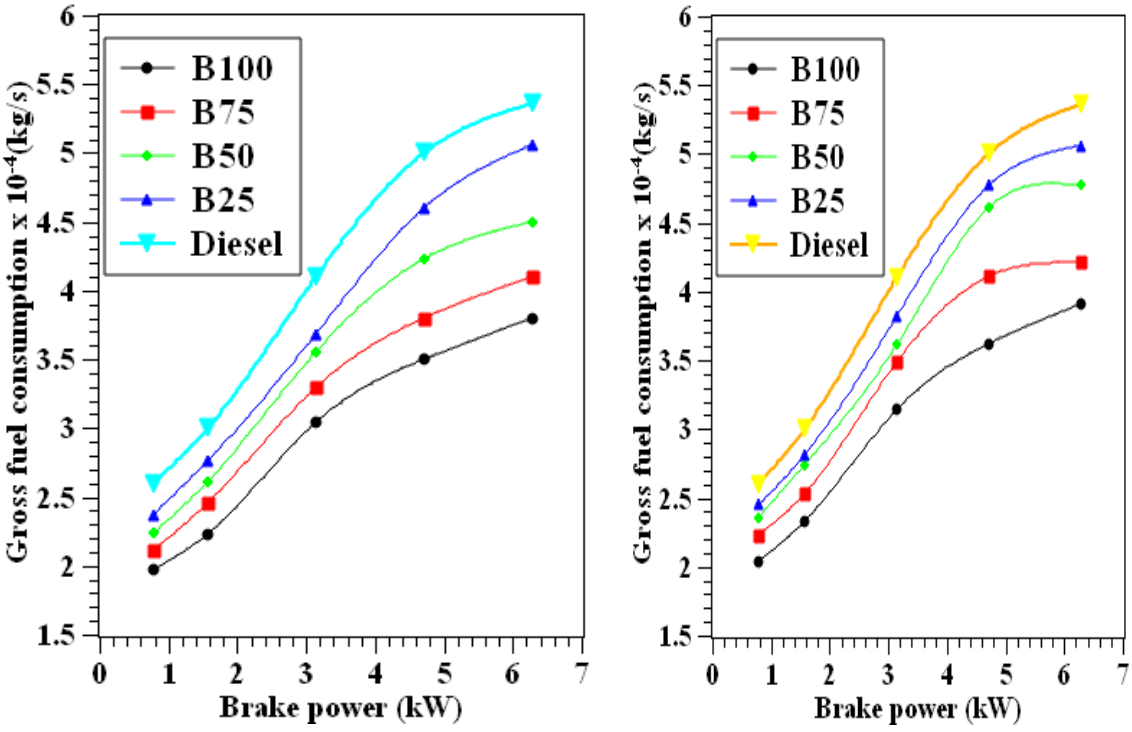

Figure 4.41: Variation of blends' gross fuel consumption against brake power, (A)-APSOME, (B)-SASOME.

4.7.2.6 Variation of air/fuel ratio with brake power

The variation of air/fuel ratio of SASOME and APSOME blends with load is presented in Tables A6.18 and A6.19 respectively. These were measured at different values of brake powers. Figures 4.42 A and B shows the variation of air/fuel ratio with brake power for APSOME and SASOME blends with petro-diesel respectively. The air/fuel ratio (A/F) gives the minimum air requirement for complete combustion of a fuel. Adequate supply of air is essential for complete combustion and for obtaining maximum amount of heat. It is observed that for each of the blends, the higher the load and brake power values, the less the amount of air/fuel ratio. It means that less amount of air is required for the combustion of the fuel blends at higher brake powers than at lower brake powers. This is due to the observed less specific fuel consumptions of the blends at higher brake powers. Also, the petro-diesel had the least air/fuel ratio while the blends with more biodiesel had higher values of air/fuel ratio. This could be due to the higher presence of hydrocarbon in the structure of biodiesel ($C_{22}H_{43}O_2$) than that of petrodiesel ($C_{16}H_{34}$) (Atadashi *et al.*, 2010).

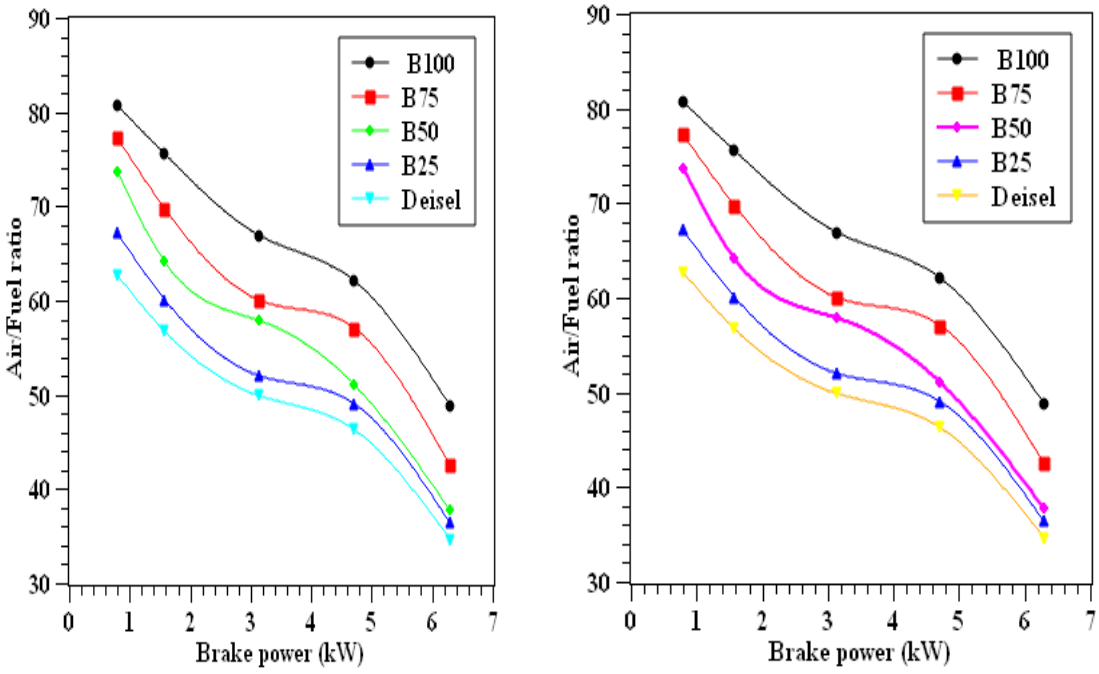

(A) (B)

Figure 4.42: Variation of fuel blends air/ fuel ratio with brake power (A)-APSOME, (B)-SASOME.

4.7.2.7 Variation of brake mean effective pressure with brake power

Tables A6.20 and A6.21 contains the values of brake mean effective pressure (B_{mep}) of APSOME and SASOME respectively and their variours blends ratios and at different brake powers. The variations of Bmep with brake power are shown in Figure 4.43. The B_{mep} depends on the brake power engine speed. It conventionally increases with increase in brake power, and decreases with increase in engine speed. Therefore, the brake mean effective pressure (B_{mep}) values of all the blends were the same at different specific loads, because the same value of speed was used. There was a sharp increase from 10Nm torque, while from there was equal gradient for all the brake powers from 10-40Nm. The deviation observed between the first and second brake power points and the rest of the points was because the lowest brake power was generated with 5Nm torque, while the rest had equal difference of 10Nm. Both SASOME and APSOME had same values at specific load points. However, the highest value of 2.31 bar was obtained at highest torque of 40Nm (full load) and 0.354 bar was obtained at 5Nm torque.

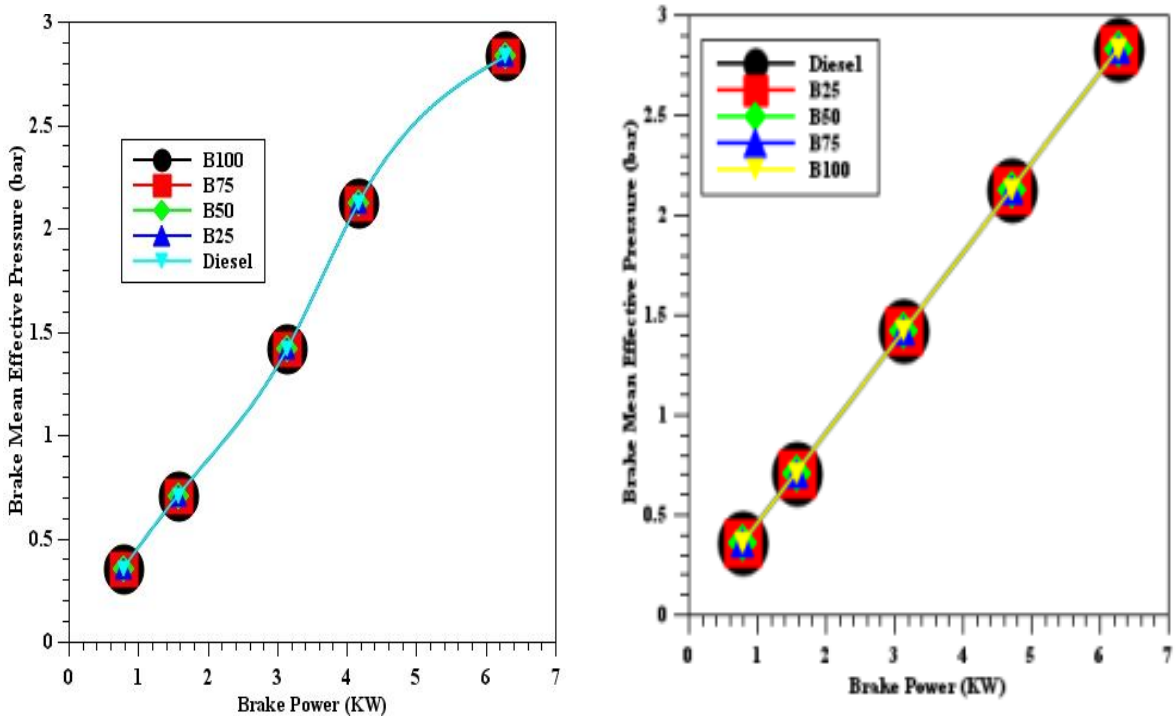

(A) (B)

Figure 4.43: Variation of blends' brake mean effective pressure with brake power, (A)-APSOME, (B)-SASOME.

4.7.2.8 Variation of volumetric efficiency with brake power

Tables A6.22 and A6.23 contain the values of volumetric efficiency of APSOME and SASOME respectively for various blending ratios and at different brake powers. The variation of the volumetric efficiency (η_v) with brake power is shown in Figure 4.44. It is observed that it followed similar trend with the brake mean effective pressure (B_{mep}). The volumetric efficiency (η_v) is the ratio of the air volumetric flowrate (V_a) to the swept volume (V_s). Therefore, it increases with increase in air volumetric flowrate. The highest value of 88.82 % was obtained for all the blends at brake power of 6.23 kW and torque of 40Nm while the lowest value of 67.26 % was obtained at brake power of 0.785 kW and torque of 5.0 Nm. Lower values below 80% obtained at lower brake powers could have been caused by increase in residual gas, poor back flow from inlet manifold to combustion chamber and higher gas temperature in the cylinder than in the inlet manifold. The same values were recorded for both SASOME and APSOME because the same amount or volume of fuel was measured for all the blends.

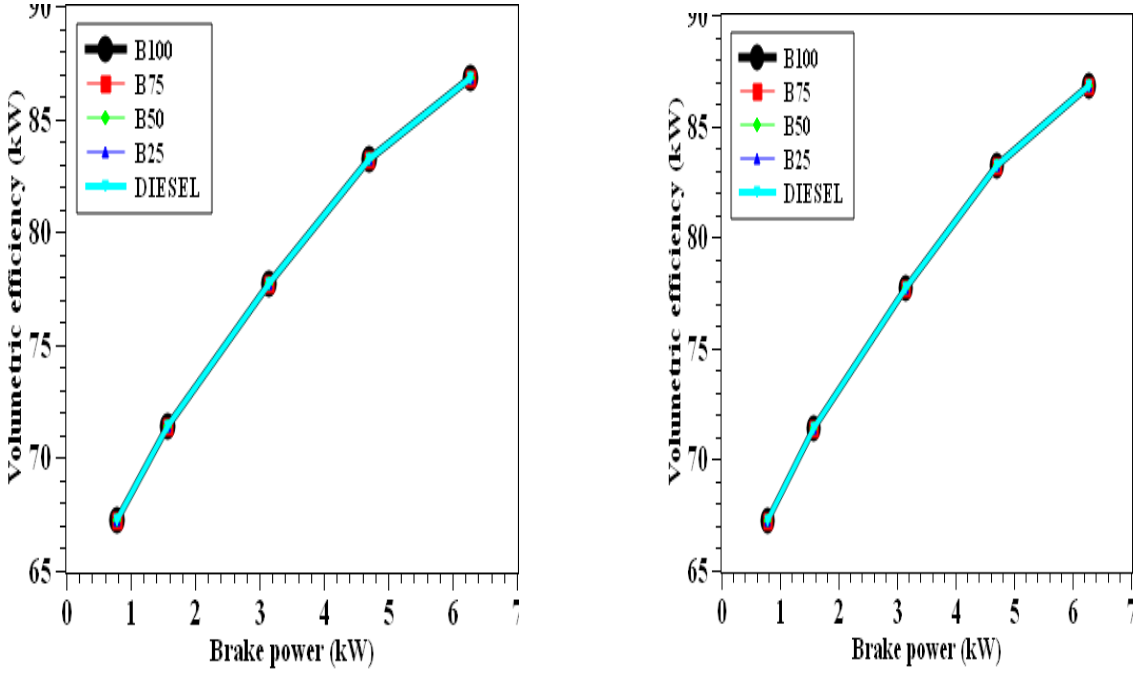

(A) (B)

Figure 4.44: Variation blends volumetric efficiency with brake power, (A)-APSOME, (B)-SASOME.

4.7.3 Combustion and emission characteristics

The combustion and exhaust emission chararcteristics of the various blends of APSOME and SASOME in comparison with petrodiesel are studied by measuring the exhaust gas temperature, carbon monoxide, carbon dioxide, oxides of nitrogen and hydrocarbon emissions obtained at various values of brake powers.

4.7.3.1 Variation of exhaust gas temperature with brake power

Tables A6.24 and A6.25 contain the values of exhaust gas temperature of APSOME and SASOME respectively for various blending ratios and at different brake powers. Figure 4.45 (A) and (B) represents the variation of exhaust gas temperature with brake power for APSOME and SASOME respectively.

Exhaust gas temperature is an indication of the extent of conversion of heat into work, which happens inside the cylinder. The exhaust gas temperature for various blends showed an upward trend with increase in the brake power in all the blends. This trend is similar to what was observed previously using *jatropha curcas* on Kirloskar Tv.1 diesel engine and Five-gas analyzer (Elango, 2014). The increase in the exhaust gas temperature may be due to the high viscosity of the biodiesel which results in changes in the injection characteristics (Haiter *et al.,* 2012). The highest exhaust gas temperatures recorded for B100 in this study are 241˚C and 232˚C for SASOME and APSOME B100 respectively, at full load (40Nm). At all loads, petro-diesel is found to have the highest exhaust gas temperature (250°C) while B25 recorded the highest exhaust temperature (248 and 238°C for APSOME and SASOME respectively) among the blends at full load. The highest exhaust gas temperature obtained was below 260°C against about 349°C recorded by Haiter *et al.,* (2012) using mahua oil methyl ester. The difference in the results could be due to the difference in the feedstock and the diesel engine used the studies.

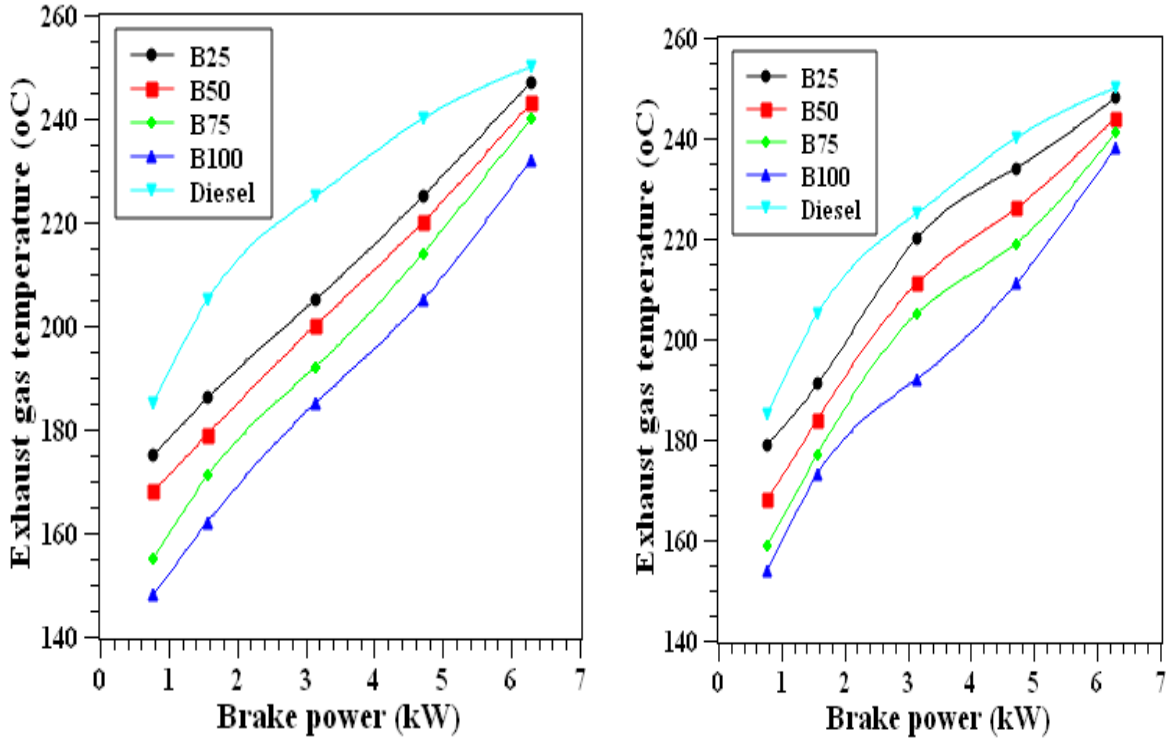

(A) (B)

Figure 4.45: Variation of blends' exhaust gas temperature with brake power (A)-APSOME, (B)-SASOME.

4.7.3.2 Variation of CO emission with brake power

Tables A6.26 and A6.27 contain the values of CO emissions of APSOME and SASOME respectively for various blending ratios and at different brake powers. The variation of carbon monoxide (CO) with brake power is shown in Figure 4.46 (A) and (B) for APSOME and SASOME blends with diesel respectively in comparison with diesel fuel. In general, CO is produced from partial combustion because of insufficient oxygen to produce CO_2. It is a product of the imperfect combustion of hydrocarbon fuels and is affected by engine speed, air-fuel ratio, fuel pressure, fuel type, and injection timing (Habibullah *et al.,* 2015). The carbon monoxide emissions are found to have slight increase with increase in load. This is not surprising as at higher brake powers, incomplete combustion tendency would be higher due to high rate of fuel injection which would result in small amounts of other compounds (CO and aldehydes) which could eventually degrade into carbon (ii) oxide (Atadashi *et al.,* 2010). Although, the CO emission for B25, B50, B75

and B100 fuels were not much different from those of diesel at low and medium loads, it is observed that the engine emits more CO for diesel at lowest brake power conditions than in the other blends. Similar results have been reported by Elango and Senthilkumar, (2011). Meanwhile, at full load the CO emission for B100 of SASOME and APSOME became about 3.86% and 10.71% respectively higher than that of diesel.

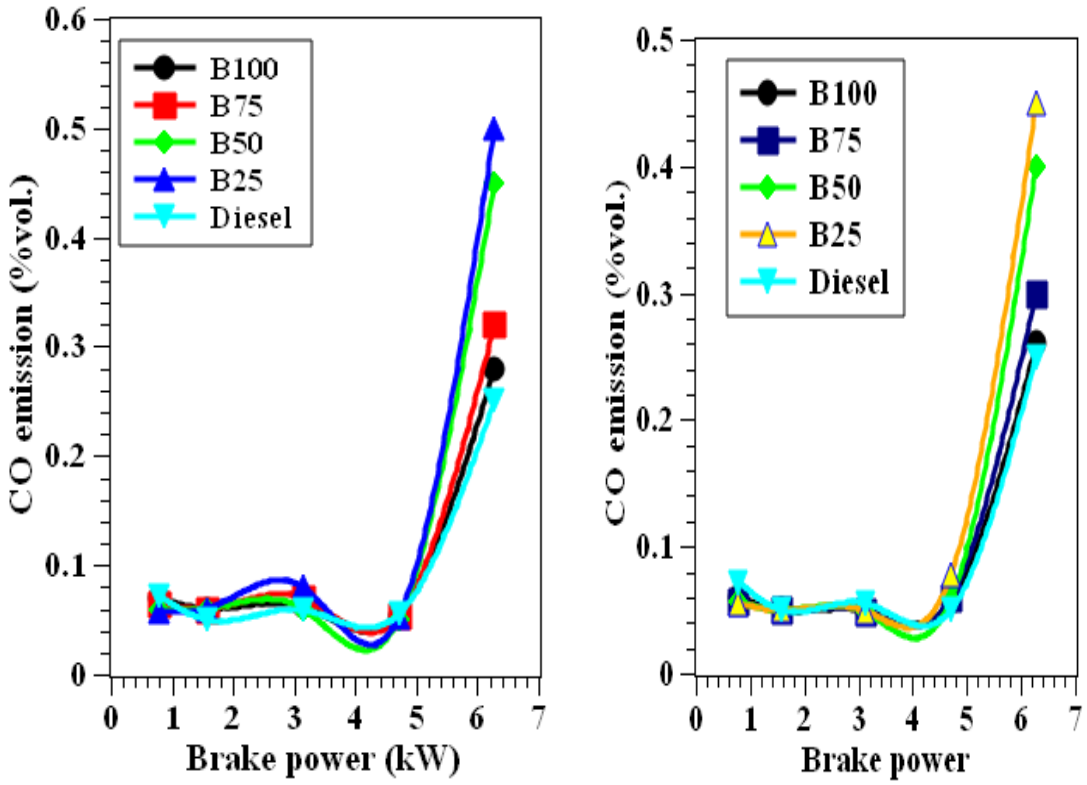

(A) (B)

Figure 4.46: Variation of blends' CO emission with brake power (A)-APSOME, (B)-SASOME.

4.7.3.3 Variation of CO_2 emission with brake power

Tables A6.28 and A6.29 contains the values of CO_2 emissions of APSOME and SASOME respectively for various blending ratios and at different brake powers. Figure 4.47 shows the variation of carbon dioxide (CO_2) with brake power. Complete combustion inside the combustion chamber increase carbon dioxide (CO_2) emissions. The CO_2 emission increases with load and concentration of biodiesel blends while B100 emits the highest CO_2 which indicates the complete combustion of the fuel. Higher density of the blends increases

the fuel flow rate as the load increases which in turn increases the CO_2 emission with load. Huzayyin *et al.*, (2004) have reported increase in CO_2 emissions for jojoba biodiesel blends for all engine loads. Fortunately, the CO_2 emission from biodiesel engines can be absorbed by the plants for photosynthesis. Therefore, the CO_2 level in the atmosphere may be kept in balanced condition due to the increased greenery and plants cultivated to yield bio-fuels.

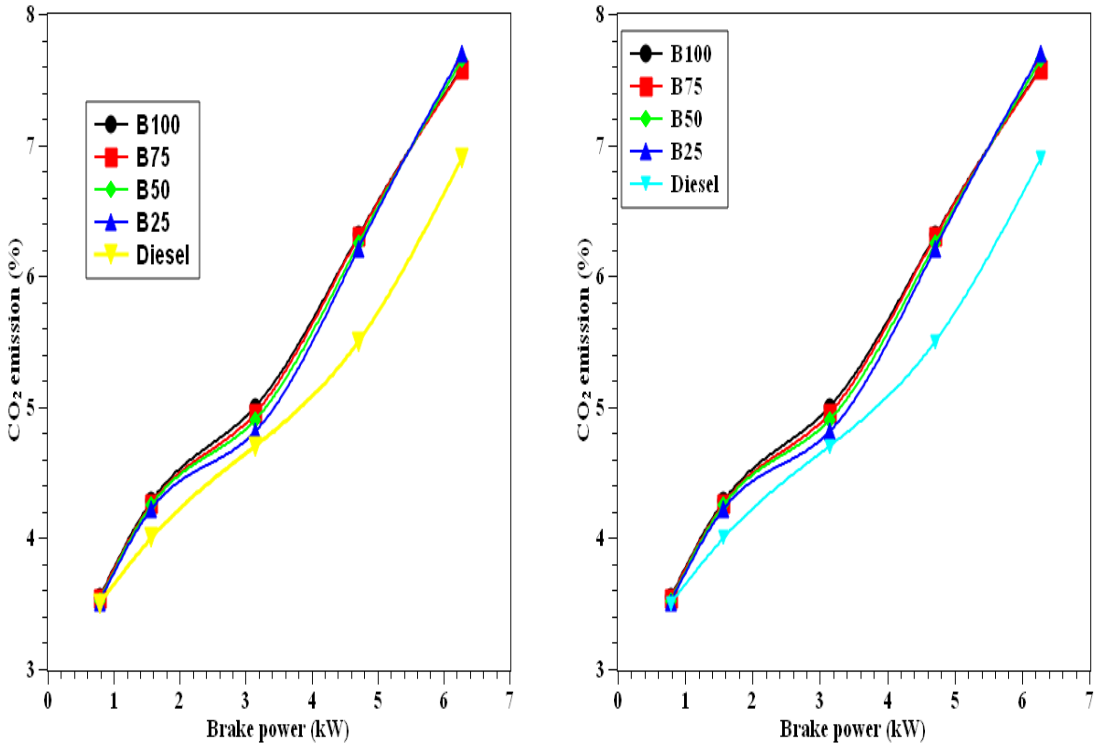

Figure 4.47: Variation of blends' CO_2 emission with brake power (A)-APSOME, (B)-SASOME.

4.7.3.4 Variation of NOx emission with brake power

Tables A6.30 and A6.31 contain the values of oxides of nitrogen emissions of APSOME and SASOME respectively for various blending ratios and at different brake powers. The variation of oxides of nitrogen (NOx) with brake power is shown in Figure 4.48A and Figure 4.48B for SASOME and APSOME respectively. NO_x emission is observed to increase significantly with load. Haiter *et al.*, (2012), have reported that oxygenated fuels results in higher combustion temperature which promotes higher NOx formation (oxidation of nitrogen molecules at high temperature inside the cylinder is the

cause of NOx formation as by-product). Therefore, the presence of oxygenated biodiesel in the blended fuels could have resulted in their higher NO_x formation than found in diesel fuel. Also, at high engine torque, combustion temperature is increased because of the slow cooling rate and poor atomization in the premixed region (Habibullah *et al.*, 2015). Conversely, lower NOx emission has been observed by several researchers while applying ethanol-gasoline blends and this was attributed to higher heat of vapourization of ethanol which reduces the combustion temperature. The results obtained in this study agree with the reports of Elango and Senthilkumar, (2011). However, based on this study, to obtain a minimal NOx emission requires running the engine at low brake power and with B25 fuel blend while the adjustment of the injection timing and introduction of exhaust gas recirculation have been suggested as ways of reducing the NOx emissions of biodiesel (Nabi *et al.*, 2008).

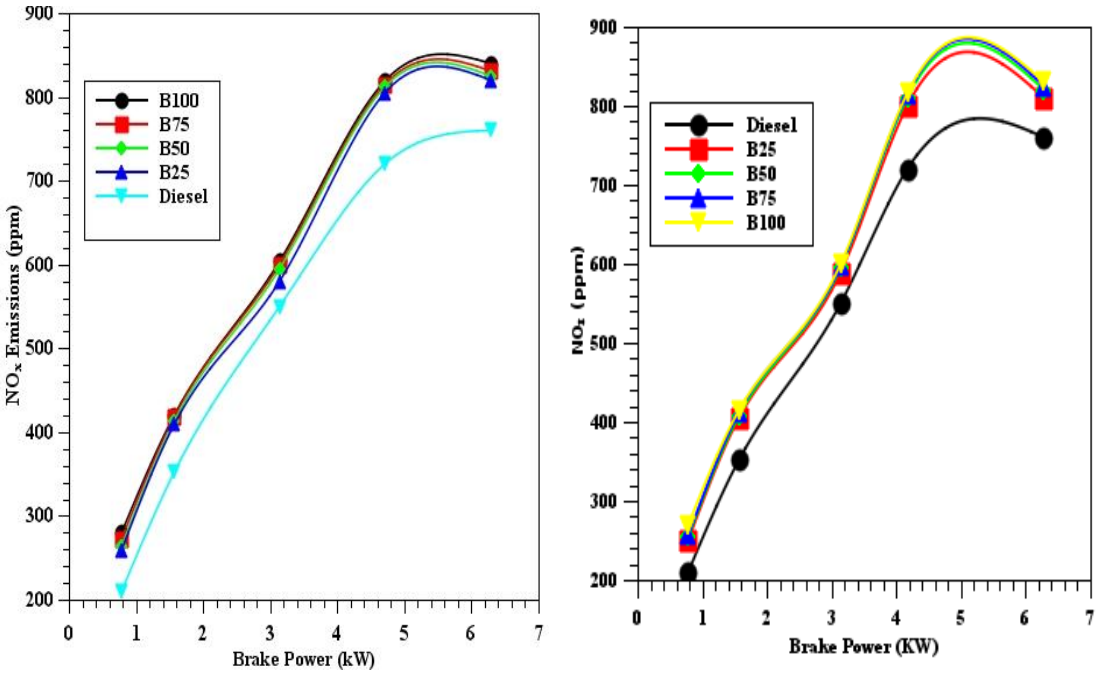

(B) (B)

Figure 4.48: Variation of blends' NOx emission with brake power (A)-APSOME, (B)-SASOME.

4.7.3.5 Variation of HC emission with brake power

Tables A6.32 and A6.33 contain the values of HC emissions of APSOME and SASOME respectively for various blending ratios and at different brake powers. The variation of hydrocarbon (HC) emissions with brake power is shown in Figure 4.49. The emission of various fuels is lower in low and medium loads but increased at higher loads. This could be because at higher loads, when more fuel is injected into the engine cylinder, the availability of free oxygen is relatively less for the reaction (Haiter *et al.*, 2012). Also, at higher loads the increase in viscosity increases the emission levels (Elango and Senthilkumar, 2011). Equally, it was observed that the higher the biodiesel in the blends, the lower the HC emission. This is because higher oxygen contents of the biodiesel promotes complete combustion and reduce HC emissions (Habibullah, *et al.*, 2015).

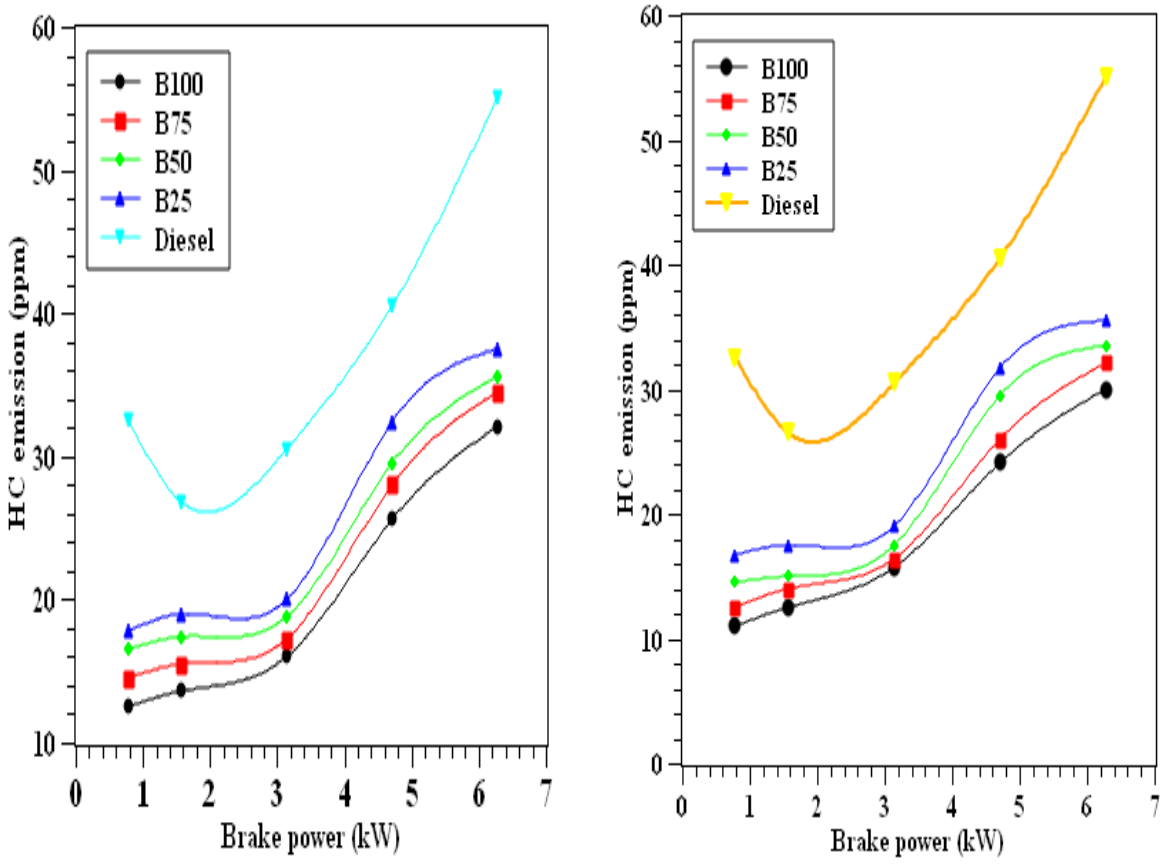

Figure 4.49: Variation of blends' HC emission with brake power (A)-APSOME, (B)-SASOME.

4.7.3.6 Variation of percentage emissions with fuel blend

Tables A6.34 and A6.35 contain the values of the percentage change in emissions of APSOME and SASOME respectively for various blending ratios and at different brake powers against petro-diesel. Figure 4.50 A and B show the percentage change in the exhaust emissions against blends of SASOME and APSOME respectively, with diesel. The exhaust emissions include CO, CO_2, HC and NO_x, from the oil blends of B100, B75, B50 and B25 at 5, 10, 20, 30 and 40Nm. At high torque of 40Nm the percentage change of CO, and HC showed decrease in values as the biodiesel content in the blends increases, while CO_2 and NO_X showed increase in values with increase in biodiesel in the blends. The percentage change in the CO emissions at 5 and 20 Nm for all the blends were negative for both SASOME and APSOME though the values of SASOME were higher than their corresponding values of APSOME (Table A6.48 and Table A6.49). The percentage change of CO at 10N were the same for all the blends for both SASOME and APSOME but was zero for SASOME and 20% for APSOME. The value of the percentage change of CO emission at 30Nm was highest for B25 followed by B75 and least for B100 for SASOME (-3.38%) (Table A6.34) and B50 for APSOME (1.69) (Table A6.35). The percentage emission change of CO was more pronounced than other emission at low biodiesel blends but same with CO_2 and NO_X at B100. The percentage change of NO_X emission showed least values at 40Nm and B25 blend (6.58% for SASOME and -7.89% for APSOME). However, all the values of percentage change for NO_X showed decrease in values as the amount of petrodiesel increases in the blends. Highest values were recorded with B100 and least values with B25. All the values were positive, while the values of APSOME were all higher than their corresponding SASOME values. The percentage change of the CO_2 emissions of the blends with diesel showed decrease in values as the amount of biodiesel in the blends increases at 40Nm. The trends at 40Nm for SASOME repeated for APSOME while the trend did not repeat at other torque units. The percentage change of the HC emissions of the

blends with diesel showed irregular trends at 5, 10 and 30Nm torques but had similar trends of decrease in values at 20Nm and 40Nm for SASOME as the biodiesel content of the blends increases. Also, the percentage change of the emissions for APSOME and SASOME at 40Nm showed similar trends. However, the emissions of all the pollutants except NO_X decreased with biodiesel used. This agrees with the EPA, 2002 recommendations (EPA, 2002).

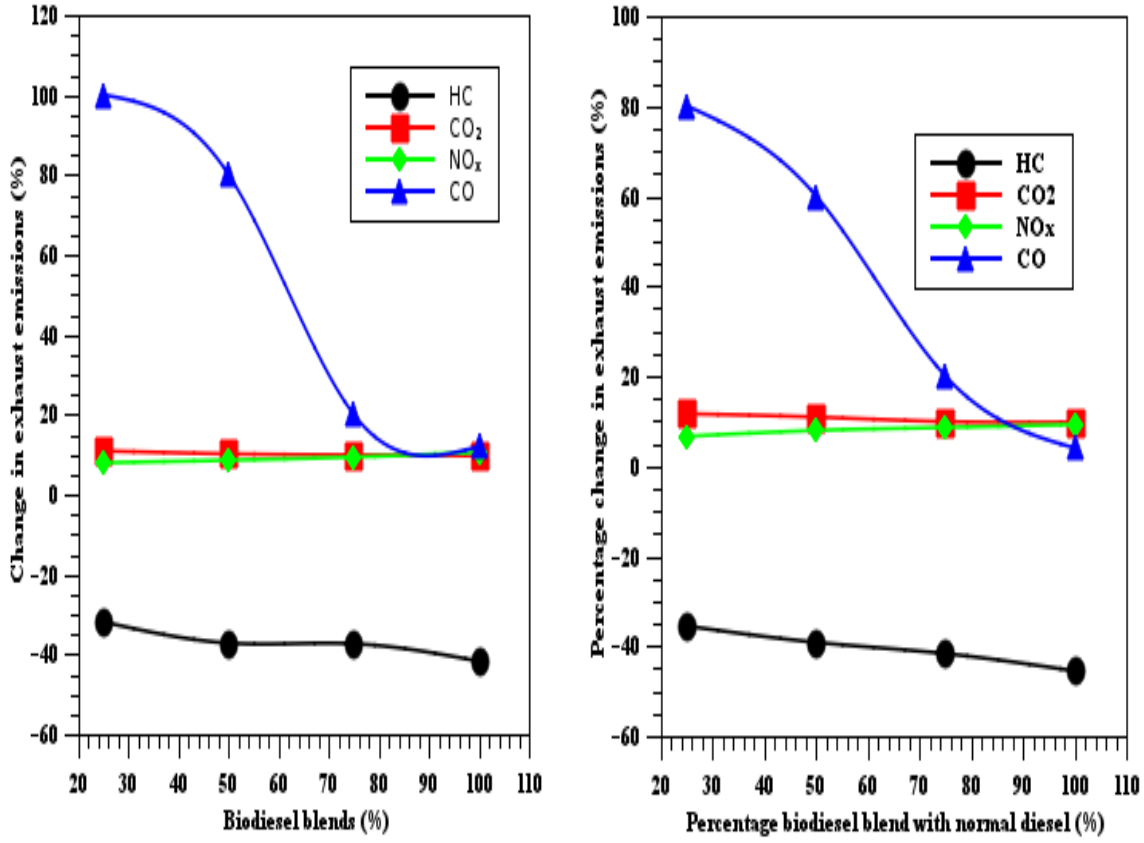

(A) (B)

Figure 4.50: Variation of blends' change in exhaust emissions with biodiesel blends (A)-APSOME, (B)-SASOME.

4.8. Optimization of the engine performance and combustion emission characteristics

4.8.1 Response surface methodology

A central composite design (CCD) was applied to develop a relationship between the factors affecting the engine performance (brake thermal efficiency and brake specific fuel consumption) and combustion emissions (CO, NOx and HC). The experimental design matrix and the RSM predicted results for SASOME process optimization a are exposed in Table 4.35.

Table 4.35: The CCD of experiment of the three variables with the experimental and observed RSM responses for SASOME.

Run	Factors			Responses									
				BTE		BSFC		CO		NOx		HC	
	A(Nm)	B(%vol.)	C(rpm)	Exp. Value	Pred. Value	Exp. Value	Pred. Value	Exp. Value	Pred. Value	Exp. Value	Pred. Value	Exp. Value	Pred. Value
1	10	40	2000	16.4000	16.913	0.6300	0.546	0.040	0.172	220	320.6932	20.8700	29.9236
2	10	80	3000	14.5500	15.1782	0.6700	0.4815	0.4500	0.353	356	385.9432	23.6100	30.7111
3	20	40	3000	20.1500	20.8982	0.4700	0.4540	0.1790	0.2263	300	516.6932	31.3900	37.0111
4	20	80	2000	31.5500	32.8707	0.3200	0.3290	0.1790	0.2463	800	858.9432	19.2500	23.7111
5	15	60	2500	27.6100	27.9420	0.3700	0.3941	0.4700	0.4527	600	599.9773	39.6200	37.3457
6	15	60	2500	27.6100	27.9420	0.3700	0.3941	0.4700	0.4527	600	599.9773	39.6200	37.3457
7	10	40	3000	14.4400	13.4270	0.4000	0.2465	0.2560	0.2927	850	791.1932	27.9600	27.3848
8	10	80	2000	19.2100	19.4695	0.7300	0.5015	0.2860	0.3427	740	523.4432	35.9400	34.2048
9	20	40	2000	25.7700	25.1495	0.5900	0.2940	0.0480	0.2490	375	345.1932	28.5300	25.3148
10	20	80	3000	19.6200	20.1145	0.7300	0.7690	0.1430	0.1142	523	422.4432	39.6200	34.4523
11	15	60	2500	27.6100	27.9420	0.3700	0.3941	0.4700	0.4527	600	599.9773	39.6200	37.3457
12	15	60	2500	27.6100	27.9420	0.3700	0.3941	0.4700	0.4527	600	599.9773	39.6200	37.3457
13	5	60	2500	14.4500	13.9099	0.2700	0.5048	0.1790	0.1664	459	531.4318	31.9800	27.0008
14	25	60	2500	31.5500	29.0824	0.4700	0.5398	0.0950	0.0036	665	592.4318	25.0400	26.1333
15	15	20	2500	17.1500	17.4899	0.3500	0.3523	0.3310	0.1741	320	205.6818	26.1100	22.6108
16	15	100	2500	25.6100	24.942	0.4800	0.6223	0.1790	0.2319	200	314.1818	24.7200	24.3333
17	15	60	1500	28.5500	28.3174	0.2600	0.3373	0.4410	0.2641	620	643.4318	32.2100	29.8708
18	15	60	3500	31.5500	31.7749	0.4100	0.4773	0.1790	0.2519	721	677.4318	39.6200	39.3457
19	15	60	2500	27.6100	27.9420	0.3700	0.3941	0.4700	0.4527	600	599.9773	39.6200	37.3457
20	15	60	2500	27.6100	27.9420	0.3700	0.3941	0.4700	0.4527	600	599.9773	39.6200	37.3457

4.8.1.1. RSM optimization of SASOME BTE

4.8.1.1.1 ANOVA analysis and model fitting of SASOME BTE. Considering Table 4.36, the SASOME BTE model F-value of 15.98 implies that the model is significant and there is only a 0.01% chance that a "Model F-Value" this large could occur due to noise. Values of "Prob> F" less than 0.0500 indicate model terms are significant. In this case A, B, AB, A^2 and C^2 are significant model terms. Values greater than 0.1000 indicate the model terms are not significant. The non-significant lack of fit (F-value of 1.02) shows that the model will be well fitted (Ohale *et al.*, 2017). Table 4.37 contains the summary of the response regression analysis. Also, the "Pred R-Squared" of 0.6804 is as close to the "Adj R-Squared" of 0.8765 as one might normally expect since the difference between them is below 0.2. This indicates lack of block effect or a possible problem with the model and/or data. "Adeq Precision" measures the signal to noise ratio. A ratio greater than 4 is desirable. The ratio of 13.121 obtained here indicates an adequate signal. This model can therefore be used to navigate the design space. The coefficient of variation (C.V) is the ratio of the standard deviation of estimate to the mean value of the observed response and as well independent of the unit (Ohale, *et al.*, 2017). It is also a measure of reproducibility and repeatability of the models (Chen *et al.*, 2011). It implies that, the C.V value of 9.58 recorded here shows that the model is reasonably reproducible. Apart from the F-value, lack of fit and C.V, the R-squared value of 0.9652 equally shows that more than 96% of the overall variability can be explained by the empirical models of the Equations.

4.8.1.1.2 Fitted RSM model equations. The selected models in terms of the coded, actual and significant terms are given in Equations (4.20), (4.21) and (4.22) respectively. The equation in terms of coded factors can be used to make predictions about the response for given levels of each factor. By, defaults, the high levels of the factors are coded +2 and the low levels of the factors are coded as -2. The coded equation is useful for identifying the

relative impact of the factors by comparing the factors coefficients, while the equation in terms of actual factors can be used to make predictions about the response for actual levels of each factor (Ohale *et al.*, 2017).

Table 4.36: ANOVA for the SASOME BTE response quadratic model.

Source	Sum of Squares	df	Mean Square	F-Value	p-value Prob> F	
Model	724.77	9	80.53	15.98	< 0.0001	Significant
A-Load	44.23	1	44.23	8.77	0.0142	
B-Fuel Blend	85.56	1	85.56	16.97	0.0021	
C-Speed	15.1	1	15.1	3	0.1141	
AB	103.82	1	103.82	20.6	0.0011	
AC	3.64	1	3.64	0.72	0.415	
BC	0.11	1	0.11	0.022	0.8853	
A^2	57.67	1	57.67	11.44	0.007	
B^2	3.33	1	3.33	0.66	0.4352	
C^2	343.76	1	343.76	68.2	< 0.0001	
Residual	50.41	10	5.04			
Lack of Fit	25.70	5	5.14	1.02	0.328	Not significant
Pure Error	24.71	5	4.94			
Cor Total	775.18	19				

Table 4.37: Summary of SASOME BTE regression values

Std. Dev.	2.25	R-Squared	0.935
Mean	23.43	Adj R-Squared	0.8765
C.V. %	9.58	Pred R-Squared	0.6804
PRESS	534.59	Adeq Precision	13.121

BTE (%) = +27.28 + 2.10 * A +2.93 * B +1.23 * C +3.60 * A * B + 0.67 * A * C - 0.12 * B * C + 4.58 * A^2 -1.10 * B^2 -11.18 * C^2 (4.20)

BTE (%) = -35.18395 -1.87269 * Load +0.027909 * Fuel Blend +0.056295 * Speed + 9.00625E-003* Load * Fuel Blend + 6.75000E-005 * Load * Speed -2.93750E-006 * Fuel Blend * Speed + 0.045795 * Load ^{2} - 6.87784E-004 * Fuel Blend^2 -1.11805E-005 * Speed^2 (4.21)

BTE (%) = -35.18395 -1.87269 * Load + 0.027909 * Fuel Blend +9.00625E-003* Load * Fuel Blend + 0.045795 * Load ^{2} - 1.11805E-005 * Speed^2 (4.22)

4.8.1.1.3 Main and interactive effects of process conditions. The advantage of RSM is that the main and interactive effects of the variables could be observed. Figure 4.51a shows the 3D plot of the interactive effect of fuel blend and engine load on the brake thermal efficiency of sweet almond seed oil methyl ester (SASOME) while keeping the speed of the diesel engine at a constant rate of 2500 rpm. Studying the fuel blend and engine load is critical on the determination of brake thermal efficiency of diesel engine. Normally, the brake thermal efficiency of a diesel engine increases with increase in biodiesel in the fuel blend. It was observed that the higher the biodiesel content in the fuel blend, the higher the brake thermal efficiency, more especially at engine load above 15 Nm. This phenomenon which is due to the lubricating effect of the biodiesel due to its oxygen content that promotes efficient combustion. The engine load showed smoother curve than fuel blend which implies that its quadratic term is more significant than that of fuel blend. Also, the ANOVA result supports the significant effect of both factors on BTE of SASOME as it was observed that both terms have their linear terms significant. However, highest brake thermal efficiency of the 4:108 Perkins diesel engine was observed at full engine load with 100% SASOME, while the lowest BTE was observed to occur at about 15Nm engine load and blend of 20% volume of SASOME and 80% volume of petrodiesel.

Figure 4.51b shows the interactive effect of engine speed and engine load on the engine brake thermal efficiency while keeping the fuel blend at a constant concentration of 60% volume. Highest brake thermal efficiency was observed at engine load above 20 Nm and at optimum engine speed of 2500rpm. The thermal efficiency was observed to increase with speed until about 2500rpm when it started reducing. Conversely, the BTE started decreasing with increase in engine load until about 15 Nm when it eventually started increasing steadily until the highest load of 25Nm. Figure 4.51c shows the combined effect of engine speed and SASOME fuel blend on the brake thermal efficiency of the diesel

engine while keeping the engine at a constant load 15Nm. The effect of speed showed similar trend with that observed on the study of effect of engine speed and engine load on the engine brake thermal efficiency but the trend of fuel blend followed a converse direction.

It was observed that the interactive effect of load and fuel blend (Figure 4.51a) has the greatest effect (BTE >38%), followed by load and speed (BTE < 35%), ((Figure 4.51b) and least by speed and fuel blend (BTE < 31%), (Figure 4.51c). This observation is supported by the ANOVA result where the interactive terms of load and fuel blend is most significant based on the p-value.

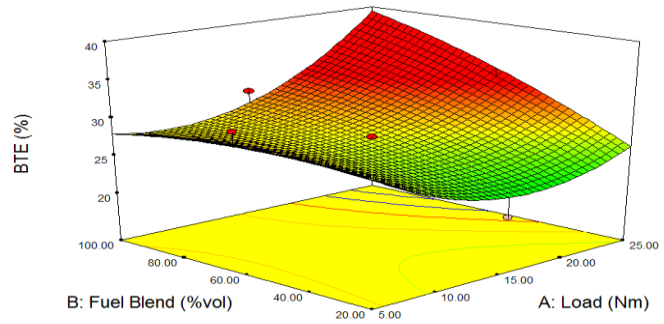

(a)

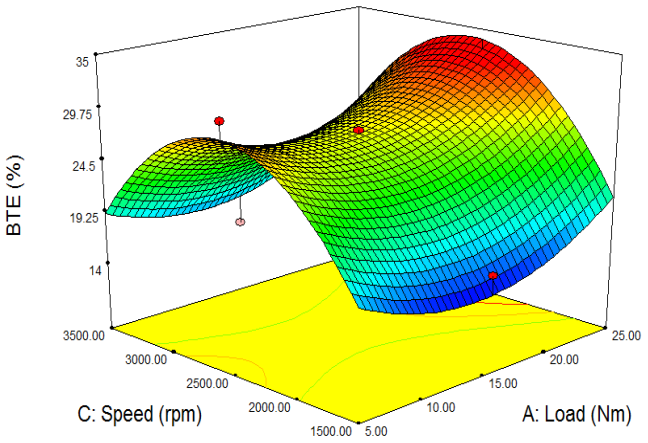

(b)

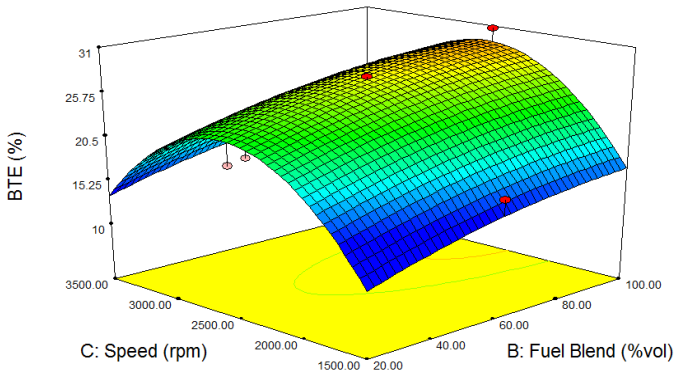

(c)

Figure 4.51: The 3D response surface plots of the interaction effects of the variables on BTE:
(a) -fuel blend versus load, (b) - speed versus load, (c)-speed versus fuel blend

4.8.1.1.4 SASOME BTE optimization process. The optimization exercise for the maximum BTE performance of Perkins 4:108 diesel engine run with blends of SASOME was conducted by utilizing the flexibility of the Design Expert 7.0.0 version numerical optimization tool function. A total of 11 solutions were generated with their desirability. The selected best solution represents the optimized process conditions where maximum BTE response was obtained as 32.05%. The optimum values of the process conditions are as contained in Table 4.38.

Table 4.38: RSM optimum values of process parameters for maximum SASOME BTE response

Variables	Optimum values	Predicted BTE (%)	Desirability
Engine load (Nm)	24.12		
Fuel blend (%vol.)	55.68	30.0538	1.00
Engine speed (rpm)	2407.08		

4.8.1.2 RSM optimization of SASOME BSFC

4.8.1.2.1 ANOVA analysis and model fitting of SASOME BSFC. Table 4.39 contains the ANOVA analysis of the SASOME BSFC model. The Model F-value of 13.82 implies the model is significant. It also means that there is only a 0.02% chance that a "Model F-Value" this large could occur due to noise. In this case A, B, AB, A^2 are significant model terms. The "Lack of Fit F-value" of 1.80 implies the “Lack of Fit” is not significant relative to the pure error and there is a 26.77% chance that a "Lack of Fit F-value" this large could occur due to noise. Non-significant lack of fit is good. The "Pred R-Squared" of 0.6973 is as close to the "Adj R-Squared" of 0.8586 as one might normally expect (Table 4.40). This may indicate a large block effect or a possible problem with your model and/or data. "Adeq Precision" measures the signal to noise ratio and a ratio greater than 4 is desirable. Therefore, a ratio of 13.045 obtained in this study indicates an adequate signal and that the

model can be used to navigate the design space. Therefore, the C.V value of 6.28 shows that the model is reasonably reproducible. Apart from the F-value, lack of fit and C.V, the R- squared value of 0.928 shows that more than 92% of the overall variability can be explained by the empirical models of the Equations.

Table4.39: ANOVA for the SASOME BSFC response quadratic model.

Source	Sum of Squares	df	Mean Square	F Value	p-value Prob> F	
Model	0.14	9	0.016	13.82	0.0002	Significant
A-Load	0.044	1	0.044	38.13	0.0001	
B-Fuel Blend	0.022	1	0.022	19.34	0.0013	
C-Speed	3.24E-03	1	3.24E-03	2.84	0.1231	
AB	0.024	1	0.024	21.18	0.001	
AC	2.45E-03	1	2.45E-03	2.14	0.1738	
BC	8.00E-04	1	8.00E-04	0.7	0.4222	
A^2	6.51E-03	1	6.51E-03	5.69	0.0382	
B^2	1.54E-03	1	1.54E-03	1.34	0.2731	
C^2	4.11E-03	1	4.11E-03	3.59	0.0872	
Residual	0.011	10	1.14E-03			
Lack of Fit	7.34E-03	5	1.47E-03	1.8	0.2677	not significant
Pure Error	4.08E-03	5	8.17E-04			
Cor Total	0.15	19				

Table 4.40: Summary of SASOME BSFC regression values.

Std. Dev.	0.024	R-Squared	0.9283
Mean	0.39	Adj R-Squared	0.8586
C.V. %	6.28	Pred R-Squared	0.6973
PRESS	0.031	Adeq Precision	13.045

4.8.1.2.2 The SASOME BSFC RSM model equations. The selected models in terms of the coded, actual and significant terms are given in Equations (4.23), (4.24) and (4.25) respectively.

BSFC (kg/kW-h) = +0.42 +0.066 * A +0.047 * B +0.018* C +0.055 * A * B - 0.018 * A * C -0.010 * B * C +0.049 * A^2 +0.024 * B^2 +0.039 * C^2 (4.23)

BSFC (kg/kW-h) = +0.62976 -0.011866 * Load -2.03523E-003 * Fuel Blend -1.33932E-004 * Speed +1.37500E-004 * Load * Fuel Blend -1.75000E-006* Load * Speed -

2.50000E-007 * Fuel Blend* Speed +4.86364E-004 * $Load^2$+1.47727E-005 * Fuel $Blend^2$+3.86364E-008 * $Speed^2$ (4.24)

BSFC (kg/kW-h) = +0.62976 -0.011866 * Load -2.03523E-003 * Fuel Blend +1.37500E-004 * Load * Fuel Blend +4.86364E-004 * $Load^2$ (4.25)

4.8.1.2.3 Main and interactive effects of factors on SASOME BSFC. The combined effect of the SASOME fuel blend and engine load on the BSFC performance of Perkins 4:108 diesel engine is shown on Figure 4.52a The speed of the engine was kept constant at 2500rpm. It was observed that simultaneous increase on the both factors studied resulted in increase in the engine BSFC. The increase in BSFC is found to be more significant at extreme units of the factors. The increase in BSFC with increase in fuel blend could be due to the reduced calorific value and greater density of the fuel blend as the concentration of biodiesel increases (Xue *et al.,* 2011). It implies that the loss of calorific value of biodiesel was compensated with higher fuel consumption (Pullen and Saeed, 2014). The SASOME BSFC was observed to be minimal (below 0.5kg/kW-h) at all fuel blends below 20Nm and at all loads while the concentration of biodiesel in the blend is below 60%volume.

Figure 4.52b represents the 3D plots of the interactive effect of engine speed and load on the brake specific fuel consumption of the SASOME blend while keeping fuel blend constant at 60%vol. It was clearly shown that the lowest brake specific fuel consumption is obtained at lowest load and speed. Typically, higher speed encourages low fuel consumption, this fact is observed from 20Nm and as the speed increases from 1500rpm up to about 3000rpm. Beyond this speed range the trend reversed. Similar results have reported on the decrease in the BSFC with increase in speed up to 2000rpm where beyond this speed the authors observed increase in the BSFC of rapeseed oil methyl esters blends (Pullen and Saeed, 2014). Also, as the load increases from 5Nm up to 15Nm, the BSFC is observed to decrease while beyond this load unit, there was significant increase in the BSFC with increase in the load.

Figure 4.52c represents the 3D plots of the combined effect of engine speed and fuel blend on the brake specific fuel consumption of the SASOME blend while keeping load constant at 15Nm. The trend observed in the interactive effect of speed and load is repeated in the case of speed and fuel blend. It is clearly shown that there was a steady increase in BSFC with increase in the fuel blend more especially speeds below 2500rpm. This could be due to increase in the fuel viscosity and density as the concentration of biodiesel in the blend increases.

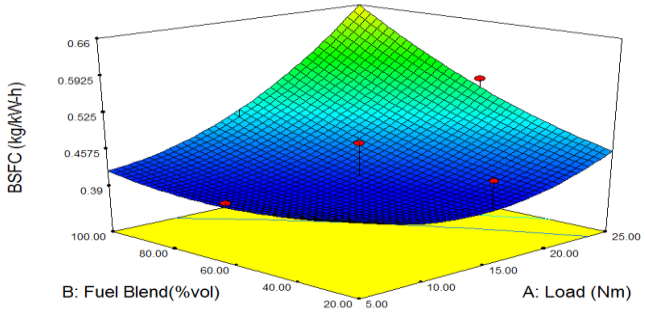

(a)

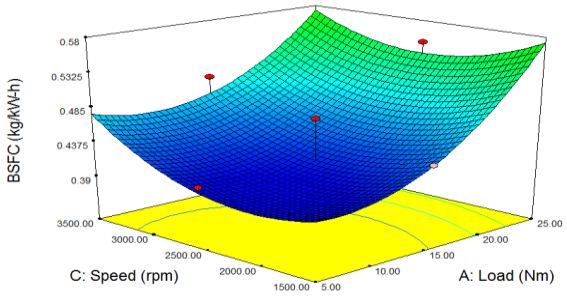

(b)

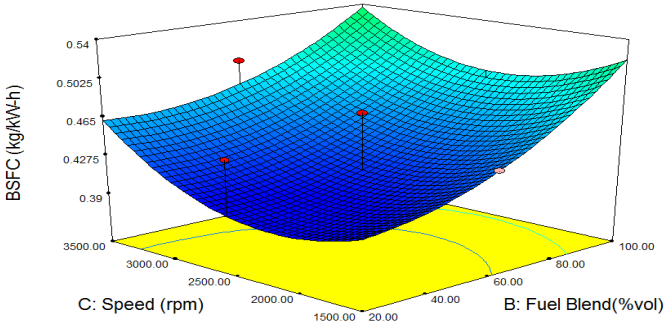

(c)

Figure 4.52: The 3D response surface plots of the interaction effects of the variables on SASOME BSFC: (a) -fuel blend versus load, (b)- speed versus load, (c)-speed versus fuel blend

4.8.1.2.4 SASOME BSFC optimization process. The optimization exercise for the minimum BSFC of Perkins 4:108 diesel engine run with blends of SASOME was conducted by utilizing the flexibility of the Design Expert 7.0.0 version numerical optimization tool function. A total of 15 solutions were generated with their desirability. The selected best solution represents the optimized process conditions where minimum BSFC response was obtained as 0.3906kg/kW-h. The optimum values of the process conditions are as contained in Table 4.41.

Table 4.41: RSM optimum values of process parameters for minimum SASOME BSFC response

Variables	Optimum values	Predicted BSFC (kg/kW-h)	Desirability
Engine load (Nm)	7.09		
Fuel blend (%vol.)	53.13	0.390657	1.00
Engine speed (rpm)	2019.89		

4.8.1.3 RSM optimization of SASOME CO emission

4.8.1.3.1 SASOME CO emission ANOVA analysis and model fitting. The ANOVA analysis of the CO emission model is shown in Table 4.42. The Model F-value of 12.49 implies that the model is significant and there is only a 0.02% chance that a "Model F-Value" this large could occur due to noise. In this study C, AB, B^2 and C^2 are significant model terms. Values greater than 0.1000 indicate the model terms are not significant. The "Lack of Fit F-value" of 1.83 implies the “Lack of Fit” is not significant relative to the pure error and there is a 26.13% chance that a "Lack of Fit F-value" this large could occur due to noise. Also, the "Pred R-Squared" of 0.6703 is very close to the "Adj R-Squared" of 0.8448 (Table 4.43). This indicates no possible problem with the model and/or data. "Adeq Precision" of 9.436 indicates an adequate signal. This model can therefore be used to navigate the design space. The coefficient of variation (C.V) of 6.28 shows the model is

highly reproducible. The R- squared value of 0.9183 shows that more than 91% of the overall variability can be explained by the empirical models of the Equations.

Table 4.42: ANOVA for the SASOME CO emission response quadratic model.

Source	Sum of Squares	df	Mean Square	F Value	p-value Prob> F	
Model	0.066	9	7.37E-03	12.49	0.0002	Significant
A-Load	5.78E-04	1	5.78E-04	0.98	0.3458	
B-Fuel Blend	1.19E-03	1	1.19E-03	2.01	0.1863	
C-Speed	4.82E-03	1	4.82E-03	8.16	0.0109	
AB	4.38E-03	1	4.38E-03	7.42	0.0195	
AC	7.80E-04	1	7.80E-04	1.32	0.2769	
BC	9.46E-04	1	9.46E-04	1.6	0.2341	
A^2	1.64E-04	1	1.64E-04	0.28	0.6093	
B^2	0.02	1	0.02	34.29	0.0002	
C^2	4.35E-03	1	4.35E-03	7.37	0.0217	
Residual	5.90E-03	10	5.90E-04			
Lack of Fit	3.82E-03	5	7.63E-04	1.83	0.2613	not significant
Pure Error	2.08E-03	5	4.17E-04			
Cor Total	0.072	19				

Table 4.43 : Summary of SASOME CO emission regression values

Std. Dev.	0.024	R-Squared	0.9183
Mean	0.39	Adj R-Squared	0.8448
C.V. %	6.28	Pred R-Squared	0.6703
PRESS	0.031	Adeq Precision	9.436

4.8.1.3.2 SASOME CO emission RSM quadratic model equations. The selected models in terms of the coded, actual and significant terms are given in Equations (4.26), (4.27) and (4.28) respectively. The equation in terms of coded factors can be used to make predictions about the response for given levels of each factor.

CO emission (%vol) = +0.33 +7.600E-003 * A -0.011 * B +0.014 * C +0.013 * A * B -9.875E-003 * A * C +0.011 * B * C -7.727E-003 * A^2 +0.086 * B^2 +0.040 * C^2 (4.26)

CO emission (%vol) = +0.75635 +3.57818E-003 * Load -7.87733E-003 * Fuel Blend -1.86864E-004 * Speed +3.28125E-005 * Load * Fuel Blend -9.87500E-007 * Load * Speed +2.71875E-007 * Fuel Blend * Speed -7.72727E-005 * Load ^{2} +5.36080E-005 * Fuel Blend ^{2} +3.97727E-008 * Speed^2 (4.27)

CO emission (%vol) = +0.75635 -1.86864E-004 * Speed -7.87733E- 003 * Fuel Blend -1.86864E-004 * Speed +3.28125E-005 * Load * Fuel Blend +5.36080E-005 * Fuel Blend ^{2} +3.97727E-008 * Speed^2 (4.28)

4.8.1.3.3 Main and interactive effect of factors on SASOME CO emission. The interactive effect of SASOME fuel blend and load on the carbon monoxide emission while keeping the speed at a constant value 2500rpm is shown on Figure 4.53a. The fuel blend is observed to have more significant effect than engine load on the CO emission. The CO emission was observed to decrease with increase in fuel blend up to 80% vol. at all loads. This could be due to the higher oxygen content (10-11%) of biodiesel that promotes the efficient engine combustion and reduced CO emission. Beyond 80%vol. fuel blend the CO was found to increase in the same rate till 100 % vol. concentration. It appeared that the minimum CO emission (below 0.3%vol) could be obtained within the range of 60-80 %vol. at almost all the studied load range (5-25Nm). Reports of many studies have presented that increase biodiesel content of blends results in decrease in CO emission, although levels range widely and with operating condition (Pullen and Saeed, 2014).

The interactive effects of engine speed and load on the SASOME CO emission is shown in Figure 4.53b. A constant fuel blend of 60% vol. was used. Increase in engine speed resulted in decreased CO emission. This could be due to turbulence intensity increase in the engine cylinder that improves combustion (Celikten et al., 2012).

Figure 4.53c represents the 3D plot of the combined effect of engine speed and SASOME fuel blend on the CO emission when the engine load is kept at 15Nm. Increase in both speed and fuel blend decreased the CO emission significantly. This could be attributed to the joint effects of increase in engine turbulence and oxygen content of the fuel blend. The minimum CO emission was observed to occur while the fuel blend is within 60-80%vol. and speed range of 1500-2500rpm.

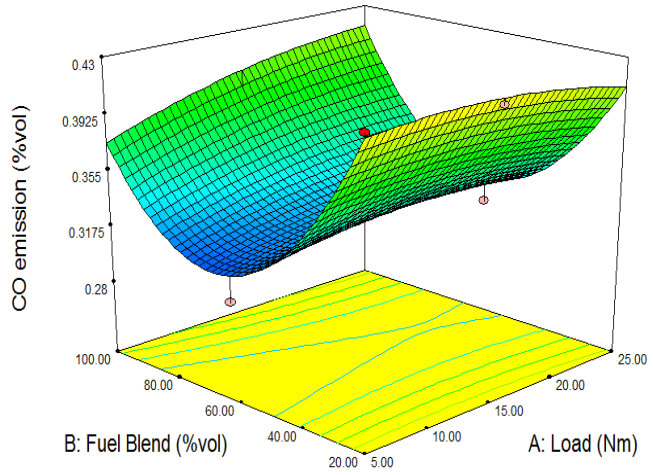

(a)

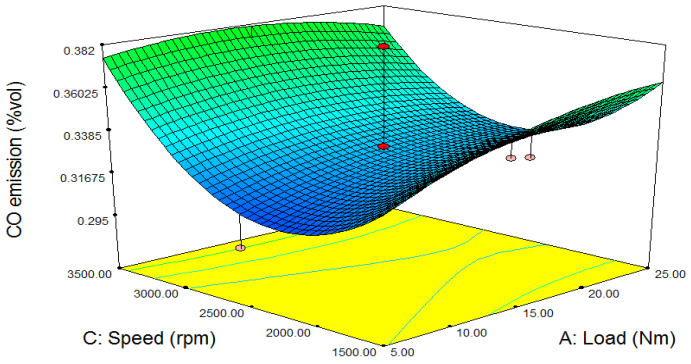

(b)

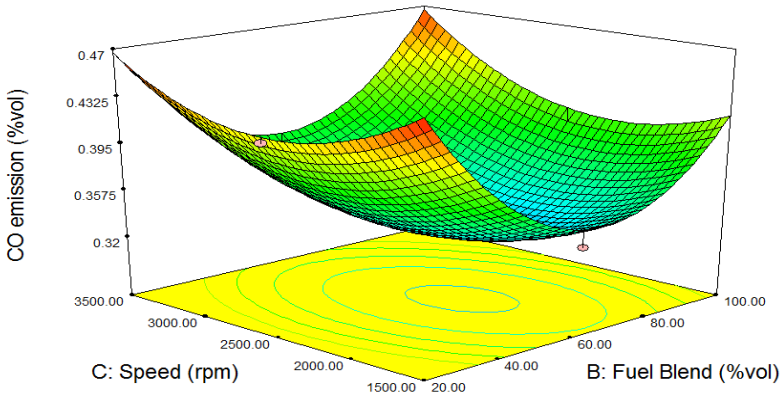

(c)

Figure 4.53: The 3D response surface plots of the interaction effects of the variables on CO emission: (a) -fuel blend versus load, (b) - speed versus load, (c)-speed versus fuel blend

4.8.1.3.4 SASOME CO emission optimization process. The optimization exercise for the minimum CO of Perkins 4:108 diesel engine run with blends of SASOME was conducted by utilizing the flexibility of the Design Expert 7.0.0 version numerical optimization tool function. A total of 6 solutions were generated with high desirability. The selected best solution represents the optimized process conditions where minimum CO response was obtained as 0.306%vol. The optimum values of the process conditions are as contained in Table 4.44.

Table 4.44: RSM optimum values of process parameters for minimum SASOME CO response

Variables	Optimum values	Predicted CO (%vol.)	Desirability
Engine load (Nm)	5.00		
Fuel blend (%vol.)	66.43	0.306751	0.933
Engine speed (rpm)	2183.74		

4.8.1.4. RSM optimization of SASOME NOx emission

4.8.1.4.1 ANOVA analysis and model fitting. The SASOME NOx emission model F-value of 31.23 implies that the model is significant (Table 4.45). There is only a 0.01% chance that a "Model F-Value" this large could occur due to noise. In this case B, AC, A^2, B^2 and C^2 are significant model terms. The "Pred R-Squared" of 0.8772 is as close to the "Adj R-Squared" of 0.9347 as one might normally expect with the difference between them being less than 0.2 (Table 4.46). "Adeq Precision" measures the signal to noise ratio. A ratio greater than 4 is desirable. A ratio of 14.504 obtained in this study indicates an adequate signal and that the model can be used to navigate the design space. Also, the C.V value of 1.91 shows the model is very reproducible. More so, the R- squared value of 0.9652 shows that more than 96% of the overall variability can be explained by the empirical models of the Equations.

Table 4.45: ANOVA for the SASOME NOx emission response quadratic model.

Source	Sum of Squares	df	Mean Square	F Value	p-value Prob> F	
Model	53094	9	5899.33	31.23	<0.0001	Significant
A-Load	152.1	1	152.1	0.81	0.3906	
B-Fuel Blend	1081.6	1	1081.6	5.73	0.0378	
C-Speed	6.4	1	6.4	0.034	0.8576	
AB	3.12	1	3.12	0.017	0.9002	
AC	910.12	1	910.12	4.80	0.0051	
BC	105.13	1	105.13	0.56	0.4728	
A^2	4490.46	1	4490.46	23.77	0.0006	
B^2	2298.27	1	2298.27	12.17	0.0058	
C^2	6578.27	1	6578.27	34.82	0.0002	
Residual	1888.95	10	188.9			
Lack of Fit	224.67	5	44.89	0.237	0.4215	Not significant
Pure Error	1664.24	5	332.85			
Cor Total	54982.95	19				

Table 4.46 : Summary of SASOME CO emission regression values

Std. Dev.	13.74	R-Squared	0.9656
Mean	718.55	Adj. R-Squared	0.9347
C.V. %	1.91	Pred. R-Squared	0.8772
PRESS	28742.97	Adeq. Precision	14.504

4.8.1.4.2 SASOME NOx RSM quadratic model equations. The selected models in terms of the coded, actual and significant terms are given in Equations (4.29), (4.30) and (4.31) respectively while equation in terms of coded factors can be used to make predictions about the response for given levels of each factor.

NOx (ppm) = +659.44 -3.90 * A +10.40 * B +0.80 * C -0.62 * A * B -3.37 * A * C +3.63 * B * C + 40.41 * A^2 +28.91 * B^2+48.91* C^2 (4.29)

NOx (ppm) = +1108.86534 -11.57523 * Load -2.11131 * Fuel Blend -0.24412 * Speed -1.56250E-003 * Load * Fuel Blend -3.37500E-004 * Load * Speed
+9.06250E-005 * Fuel Blend * Speed +0.40409 * $Load^2$ + 0.018068 * Fuel Blend ^{2} + 4.89091E-005 * Speed ^{2} (4.30)

NOx (ppm) = +1108.86534 -2.11131 * Fuel Blend -3.37500E-004 * Load * Speed + 0.40409 * $Load^2$ + 0.018068 * $Fuel\ Blend^2$
+ 4.89091E-005 * $Speed^2$ (4.31)

4.8.1.4. 3 Main and interactive effects of factors on the SASOME NOx emission. The interactive effect of fuel blend and engine load on the NOx emission of SASOME blends is shown in Figure 4.54b. The simultaneous increase of both fuel blend and engine load resulted in shorter ignition delay which resulted in low amount of fuel involved in the premixed combustion. This could have resulted in lower initial rate of heat release that reduced the NOx emission until about 60% vol. fuel blend and 15Nm engine load. Increase in engine load from 15Nm was found to increase NOx emission probably due to higher combustion temperature. The interactive effect of fuel blend and engine speed (Figure 4.54b) as well as that of the engine load and speed (Figure4.54c) is observed to follow the same trend observed in Figure 4.54a.

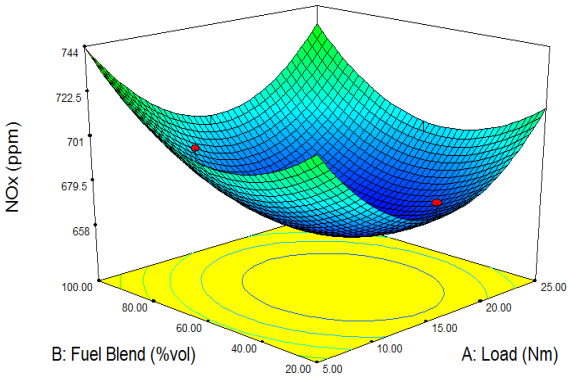

(a)

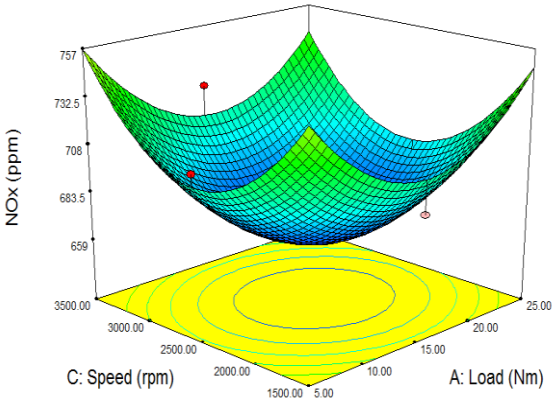

(b)

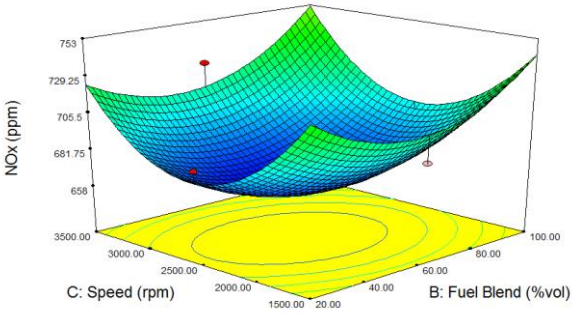

(c)

Figure 4.54: The 3D response surface plots of the interaction effects of the variables on NOx emission: (a) -fuel blend versus load, (b) - speed versus load, (c) - speed versus fuel blend

4.8.1.4.4 SASOME NOx optimization process. A total of 15 solutions were generated with their desirability by the numerical optimization tool function of Design Expert 7.0.0 version. The selected best solution represents the optimized process conditions where minimum NOx response was obtained as 659.71ppm. The optimum values of the process conditions are as contained in Table 4.47.

Table 4.47: RSM optimum values of process parameters for minimum SASOME NOx response

Variables	Optimum values	Predicted NOx (ppm)	Desirability
Engine load (Nm)	17.11		
Fuel blend (%vol.)	54.98	369.71	0.933
Engine speed (rpm)	2452.08		

4.8.1.5 RSM optimization of SASOME HC emission

4.8.1.5.1 ANOVA analysis and model fitting. The summary of SASOME HC emission model ANOVA and its regression are resented in Tables 4.48 and 4.49 respectively. Model F-value of 91.00 implies the SASOME HC model is significant. The "Lack of Fit F-value" of 1.09 implies that the Lack of Fit is not significant relative to the pure error. There is a 22.13% chance that a "Lack of Fit F-value" this large could occur due to noise. The "Pred R-Squared" of 0.9356 is in reasonable agreement with the "Adj R-Squared" of 0.9771 while "Adeq Precision" ratio of 23.247 indicates an adequate signal.

The coefficient of variation (C.V) value of 2.03 shows the model is reasonably reproducible. Apart from the F-value, lack of fit and C.V, the R- squared value of 0.9879 shows that more than 98% of the overall variability can be explained by the empirical models of the Equations.

Table 4.48: ANOVA for the SASOME HC emission response quadratic model.

Source	Sum of Squares	df	Mean Square	F Value	p-value Prob> F	
Model	376.68	9	41.85	91	<0.0001	significant
A-Load	0.05	1	0.05	0.11	0.7474	
B-Fuel Blend	4.52	1	4.52	9.82	0.0106	
C-Speed	0.49	1	0.49	1.06	0.3271	
AB	6.18	1	6.18	13.43	0.0044	
AC	2.61	1	2.61	5.68	0.0385	
BC	2.7	1	2.7	5.88	0.0358	
A^2	2.22	1	2.21	4.82	0.0491	
B^2	243.27	1	243.27	528.93	<0.0001	
C^2	2.62	1	2.62	5.70	0.0378	
Residual	4.6	10	0.46			
Lack of Fit	2.50	5	0.501	1.09	0.3158	Not significant
Pure Error	2.09	5	0.419			
Cor Total	381.28	19				

Table 4.49: Summary of SASOME HC emission regression values

Std. Dev.	0.68	R-Squared	0.9879
Mean	33.41	Adj R-Squared	0.9771
C.V. %	2.03	Pred R-Squared	0.9356
PRESS	24.55	Adeq Precision	23.247

4.8.1.5.2 SASOME HC emission RSM model equations. The selected models in terms of the coded, actual and significant terms are given in Equations (4.32), (4.33) and (4.34) respectively. The equation in terms of coded factors can be used to make predictions about the response for given levels of each factor.

HC (ppm) = +29.53 -0.071 * A +0.67 * B -0.22 * C -0.88 * A * B -0.57 * A * C -0.58 * B * C -0.80 * A^2 +9.41 * B^2 - 0.85 * C^2 (4.32)

HC (ppm) = +36.93339+ 0.50739 * Load-0.61933 * Fuel Blend +5.75548E-003 * Speed-2.19688E-003 * Load * Fuel Blend -5.71250E-005 * Load * Speed -1.45313E-005 * Fuel Blend * Speed -7.99545E-003 * Load ^{2} +5.87841E-003 * Fuel Blend^2 -8.49545E-007 * Speed ^{2} (4.33)

HC (ppm) = +36.93339 - 0.61933 * Fuel Blend -2.19688E-003 * Load * Fuel Blend - 5.71250E-005 * Load * Speed -1.45313E-005 * Fuel Blend * Speed -7.99545E-003 * Load ^{2} +5.87841E-003 * Fuel Blend^{2} -8.49545E-007 * Speed ^{2} (4.34)

4.8.1.5.3 Main and interactive effects of factors on HC emission. Figure 4.55a shows the interactive effect of both fuel blend and load on HC emission while speed of the engine was set constantly at 2500rpm. It was observed that irrespective of the engine load, the HC emission decreased significantly with increase in fuel blend up to about 70% vol. biodiesel concentration in the blend. The increase in oxygen content and higher cetane number (CN) of biodiesel must have led to more complete combustion and shortened combustion delay respectively. Also, it was observed that the simultaneous increase in both speed and load resulted in the HC emission (Figure 4.55b). However, the lowest HC emission was achieved at lowest factor conditions. The combined effect of speed and engine load had most significant reduction on the HC emission. Figure 4.55c shows that the combined effect of fuel blend and engine speed on HC emission follows the same trend with that of the effect of fuel blend and engine load.

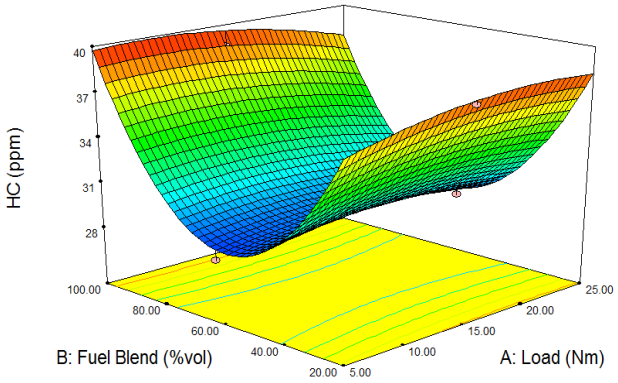

(a)

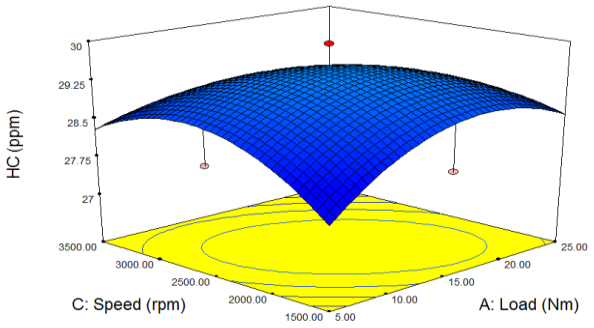

(b)

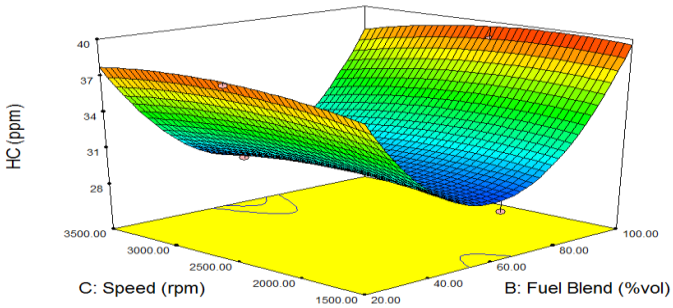

(c)

Figure 4.55: The 3D response surface plots of the interaction effects of the variables on HC emission: (a) -fuel blend versus load, (b) - speed versus load, (c)-speed versus fuel blend

4.8.1.5.4 SASOME HC emission optimization process. The optimization exercise for the minimum HC of Perkins 4:108 diesel engine run with blends of SASOME was conducted by utilizing the flexibility of the Design Expert 7.0.0 version numerical optimization tool function. A total of 13 solutions were generated with their desirability. The selected best solution represents the optimized process conditions where minimum HC

response was obtained as 27.89ppm. The optimum values of the process conditions are as contained in Table 4.50.

Table 4.50: RSM optimum values of process parameters for minimum SASOME HC emission response

Variables	Optimum values	Predicted HC (ppm)	Desirability
Engine load (Nm)	6.32		
Fuel blend (%vol.)	58.49	27.8938	1.00
Engine speed (rpm)	1548.14		

4.8.2 RSM-GA optimization results for SASOME engine performance and emission

The RSM was integrated with genetic algorithm (GA) for simultanous optimization of the emission variables and engine performance parameters. The global optimized conditions for the responses are contained in Table 4.51 and these show improved conditions and responses. The results of the experimental values obtained were very close to the ones calculated from the model. Results suggested that the optimal conditions attained had the least error and can be practically applied in the viability and feasibility analysis of the application of seed oil derived from sweet almond in biodiesel production.

Table 4.51: Optimal conditions for engine performance and combustion of SASOME in CI engine using RSM-GA.

Responses	Optimized values	Experimental values	Optimum conditions		
			Load(Nm)	Fuel blend (%Vol.)	Speed(rpm)
BTE (%)	31.0182	32.50	20	80	1980
BSFC(Kg/kW-hr)	0.1898	0.1553	10	15	2700
CO (% Vol.)	0.0421	0.0455	25	60	2550
NOx(ppm)	174.8259	175.89	15	20	2450
HC(ppm)	22.0714	21.5788	15	60	2400

4.8.3 Optimization of APSOME engine performance and combustion emission using RSM

A central composite design (CCD) was applied to develop a relationship between the factors affecting the engine performance (brake thermal efficiency and brake specific fuel consumption) and combustion emissions (CO, NOx and HC). The experimental design matrix and the response surface results for process optimization a are exposed in Table 4.52.

Table 4.52: CCD of experimental and observed RSM responses for APSOME.

Run	Factors			Responses									
				BTE(%)		BSFC(kg/kW-hr)		CO(%vol.)		NOx(ppm)		HC(ppm)	
	A(Nm)	B(%vol.)	C(rpm)	Exp. value	Pred. value	Exp. value	Pred. value	Exp. value	Pred. value	Exp. value	Pred. value	Exp. value	Pred. value
1	10	40	2000	14.5600	14.8314	0.5710	0.4654	0.0500	0.0418	300	309.5625	22.4000	22.3720
2	10	80	3000	20.0400	25.7264	0.6430	0.6031	0.4000	0.4316	800	803.8125	24.6700	26.8170
3	20	40	3000	30.0500	27.2689	0.1430	0.1361	0.1880	0.1588	400	425.3125	30.4000	31.7495
4	20	80	2000	35.0000	36.9689	0.4290	0.4206	0.3870	0.3658	800	638.8125	20.1500	20.3195
5	15	60	2500	32.0000	32.4520	0.3500	0.3600	0.4800	0.4591	670	664.7500	35.9400	35.3468
6	15	60	2500	32.0000	32.4520	0.3500	0.3600	0.4800	0.4591	670	664.7500	35.9400	35.3468
7	10	40	3000	33.4600	28.7789	0.1430	0.1520	0.2750	0.2825	400	392.6875	29.6600	28.0495
8	10	80	2000	21.6700	21.7389	0.4430	0.3997	0.0480	0.2025	525	531.1875	35.9400	35.1495
9	20	40	2000	34.9900	36.5914	0.2140	0.2037	0.3580	0.4517	344	341.6875	29.6600	30.0720
10	20	80	3000	31.6700	31.6864	0.3570	0.3405	0.1880	0.2215	770	771.9375	24.4000	24.9870
11	15	60	2500	32.0000	32.4520	0.3500	0.3600	0.4800	0.4591	670	664.7500	35.9400	35.3468
12	15	60	2500	32.0000	32.4520	0.3500	0.3600	0.4800	0.4591	670	664.7500	35.9400	35.3468
13	5	60	2500	19.6600	17.1311	0.1090	0.1022	0.2750	0.2650	650	649.6250	22.4000	22.3205
14	25	60	2500	25.6100	25.8511	0.1430	0.1399	0.4000	0.4247	321	329.8750	24.6700	24.1905
15	15	20	2500	13.5600	14.4986	0.6430	0.5932	0.1200	0.1307	334	362.1250	29.6600	27.3780
16	15	100	2500	30.0500	29.8236	0.2140	0.2139	0.3900	0.4040	830	830.3750	24.6700	23.3930
17	15	60	1500	21.6700	22.8586	0.1430	0.1587	0.4000	0.2037	634	648.6250	38.7000	38.5980
18	15	60	3500	26.0000	27.5236	0.2500	0.2444	0.0690	0.0700	691	674.8750	30.4000	30.9430
19	15	60	2500	32.0000	32.4520	0.3500	0.3600	0.4800	0.4591	670	664.7500	35.9400	35.3468
20	15	60	2500	32.0000	32.4520	0.3500	0.3600	0.4800	0.4591	670	664.7500	35.9400	35.3468

4.8.3.1 RSM optimization of APSOME BTE

4.8.3.1.1 ANOVA analysis and model fitting of APSOME BTE. The APSOME BTE model ANOVA analysis and its summary are presented in Tables 4.53 and 4.54 respectively. The Model F-value of 10.64 implies that the model is significant. There is only a 0.01% chance that a "Model F-Value" this large could occur due to noise. Values of "Prob> F" less than 0.0500 indicate model terms are significant. In this study, B, AB, A^2 and C^2 are significant model terms. Values greater than 0.1000 indicate the model terms are not significant. The non-significant lack of fit shows that the model will be well fitted (Ohale *et al.,* 2017). The "Pred R-Squared" of 0.6452 is as close to the "Adj R-Squared" of 0.8203 as one might normally expect since the difference between them is below 0.2. This indicates lack of block effect or a possible problem with the model and/or data. "Adeq Precision" measures the signal to noise ratio. A ratio greater than 4 is desirable. The ratio of 10.60 indicates an adequate signal. This model can therefore be used to navigate the design space. The coefficient of variation (C.V) is the ratio of the standard deviation of estimate to the mean value of the observed response and as well independent of the unit (Ohale, *et al.,* 2017). It shows the degree of reproducibility and repeatability of the models (Chen *et al.,* 2011). Therefore, the C.V value of 13.19 shows the model is reasonably reproducible. In addition to the F-value, lack of fit and C.V, the R- squared value of 0.9054 shows that more than 90% of the overall variability can be explained by the empirical models of the equations.

4.8.3.1.2 APSOME BTE RSM quadratic model equations. The selected models in terms of the coded, actual and significant terms are given in Equations (4.35), (4.36) and (4.37) respectively. The equation in terms of coded factors can be used to make predictions about the response for given levels of each factor. By, defaults, the high levels of the factors are coded +2 and the low levels of the factors are coded as -2. The coded equation is useful for identifying the relative impact of the factors by comparing the factors coefficients, while

the equation in terms of actual factors can be used to make predictions about the response for actual levels of each factor (Ohale *et al.,* 2017).

Table 4.53: ANOVA for the APSOME BTE response quadratic model.

Source	Sum of Squares	df	Mean Square	F Value	p-value Prob> F	
Model	1037.39	9	115.27	10.64	0.0005	Significant
A-Load	29	1	29	2.68	0.1329	
B-Fuel Blend	85.56	1	85.56	7.9	0.0185	
C-Speed	15.1	1	15.1	1.39	0.265	
AB	103.82	1	103.82	9.58	0.0113	
AC	3.64	1	3.64	0.34	0.5747	
BC	0.11	1	0.11	0.01	0.9216	
A^2	59.59	1	59.59	5.5	0.041	
B^2	25.16	1	25.16	2.32	0.1585	
C^2	472.29	1	472.29	43.59	< 0.0001	
Residual	108.34	10	10.83			
Lack of Fit	57.47	5	11.49	1.06	0.4170	Not significant
Pure Error	50.87	5	10.17			
Cor Total	1145.73	19				

Table 4.54: Summary of APSOME BTE regression values

Std. Dev.	3.29	R-Squared	0.9054
Mean	24.95	Adj. R-Squared	0.8203
C.V. %	13.19	Pred. R-Squared	0.6452
PRESS	864.81	Adeq. Precision	10.603

BTE (%) = +30.69 +1.70 * A +2.92 * B +1.23 * C +3.60 * A * B +0.68 * A * C -0.12 * B * C + 4.65 * A^2-3.02 * B^2-13.10 * C^2 (4.35)

BTE (%) = -47.36900 -1.93533 * Load +0.17225 * Fuel Blend + 0.065918 * Speed +9.00625E-003 * Load * Fuel Blend + 6.75000E-005 * Load * Speed -2.93750E-006 * Fuel Blend * Speed + 0.046550 * Load ^{2} -1.89062E-003 * Fuel Blend ^{2} -1.31050E-005 * Speed ^{2} (4.36)

BTE (%) = -47.36900 +0.17225 * Fuel Blend +9.00625E-003 * Load * Fuel Blend -2.93750E-006 * Fuel Blend * Speed +0.046550 * Load^2

-1.31050E-005 * Speed ^{2} (4.37)

4.8.3.1.3 APSOME BTE factors interactive effects. Figure 4.56a shows the 3D plot of the interactive effect of fuel blend and engine load on the brake thermal efficiency of African pear seed oil methyl ester (APSOME) while keeping the speed of the diesel engine at a constant rate of 2500 rpm. The brake thermal efficiency of a diesel engine typically increases with increase in biodiesel concentration in the fuel blend. It was observed that higher biodiesel content in the fuel blend results in the increase in the brake thermal efficiency, more especially at engine load above 15 Nm. This phenomenon which is due to the lubricating effect of the biodiesel and its oxygen content promotes efficient combustion. The engine load showed smoother curve than fuel blend which implies that its quadratic term is more significant than that of fuel blend. Also, the ANOVA result supports the significant of the interactive effect both factors on BTE of APSOME. However, highest brake thermal efficiency of the 4:108 Perkins diesel engine was observed at full engine load with 100% APSOME, while the lowest BTE was observed to occur at about 15Nm engine load and blend of 20% volume of APSOME and 80% volume of petrodiesel.

Figure 4.56b shows the interactive effect of engine speed and engine load on the engine brake thermal efficiency while keeping the fuel blend at a constant concentration of 60% volume. Highest brake thermal efficiency (above 35%) was observed at engine load above 20 Nm and at optimum engine speed of 2500rpm. The thermal efficiency was observed to increase with speed until about 2500rpm when it started reducing. Conversely, the BTE started decreasing with increase in engine load until about 15 Nm when it eventually started increasing steadily. Figure 4.56c shows the combined effect of engine speed and APSOME fuel blend on the brake thermal efficiency of the diesel engine while keeping the engine at a constant load of 15Nm. The effect of speed showed similar trend with that of effect of engine speed and engine load on the engine brake thermal efficiency, but the trend of fuel blend followed an opposite direction. It was observed that the

interactive effect of load and fuel blend (Figure 4.56a) has the greatest effect (BTE >38%), followed by load and speed (BTE < 35%), ((Figure 4.56b) and least by speed and fuel blend (BTE < 32%), (Figure 4.56c). This observation is supported by the ANOVA result where the interactive terms of load and fuel blend is most significant based on the lowest value of p-value and highest value of F-value.

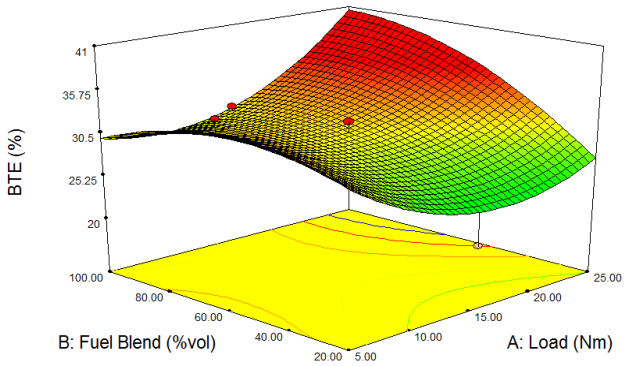

(a)

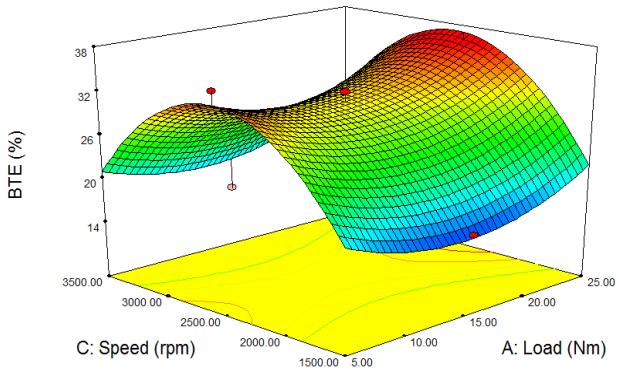

(b)

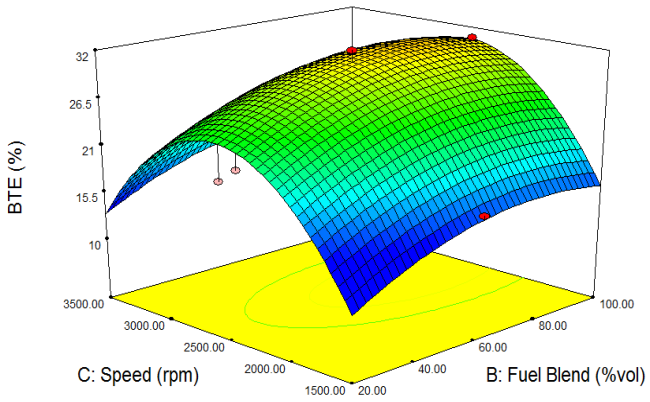

(c)

Figure 4.56: The 3D response surface plots of the interaction effects of the variables on APSOME BTE:
(a) -fuel blend versus load, (b) - speed versus load, (c)-speed versus fuel blend

4.8.3.1.4 APSOME BTE optimization process. The optimization exercise for the maximum BTE performance of Perkins 4:108 diesel engine run with blends of APSOME was conducted by utilizing the flexibility of the Design Expert 7.0.0 version numerical optimization tool function. A total of 10 solutions were generated with their desirability. The selected best solution represents the optimized process conditions where maximum BTE response was obtained as 36.07%. The optimum values of the process conditions are as contained in Table4.55.

Table 4.55: RSM optimum values of process parameters for maximum APSOME BTE response

Variables	Optimum values	Predicted BTE (%)	Desirability
Engine load (Nm)	23.0		
Fuel blend (%vol.)	77.02	36.07	1.00
Engine speed (rpm)	2298.11		

4.8.3.2 RSM optimization of APSOME BSFC

4.8.3.2.1 APSOME BSFC RSM model ANOVA analysis. The APSOME BSFC model ANOVA analysis and its summary are presented in Tables 4.56 and 4.57. The Model F-value of 15.87 implies the model is significant. There is only a 0.01% chance that a "Model F-Value" this large could occur due to noise. Values of "Prob> F" less than 0.0500 indicate model terms are significant. In this investigation, A, B, C, AB, and C^2 are significant model terms. The "Lack of Fit F-value" of 1.06 implies the Lack of Fit is not significant relative to the pure error and there is a 47.35% chance that a "Lack of Fit F-value" this large could occur due to noise. Non-significant lack of fit is good. The "Pred R-Squared" of 0.6936 is as close to the "Adj R-Squared" of 0.8757 as one might normally expect. This may indicate a large block effect or a possible problem with your model and/or data. Things to consider are model reduction, response transformation, outliers, etc. "Adeq Precision" measures the signal to noise ratio. A ratio greater than 4 is desirable. The ratio of 14.426 indicates an adequate signal. This model can be used to navigate the design space.

The coefficient of variation (C.V) is the ratio of the standard deviation of estimate to the mean value of the observed response and as well independent of the unit (Ohale et al 2017). It is also a measure of reproducibility and repeatability of the models (Chen et al., 2011). Therefore, C.V value of 6.16 shows the model is reasonably reproducible. Apart from the F-value, lack of fit and C.V, the R- squared value of 0.9346 shows that more than 93% of the overall variability can be explained by the empirical models of the Equations.

4.8.3.2.2 APSOME BSFC RSM model equations. The selected models in terms of the coded, actual and significant terms are given in Equations (4.38), (4.39) and (4.40) respectively. The equation in terms of coded factors can be used to make predictions about the response for given levels of each factor.

Table 4.56: ANOVA for the APSOME BSFC response quadratic model.

Source	Sum of Squares	df	Mean Square	F Value	p-value Prob> F	
Model	0.12	9	0.013	15.87	<0.0001	significant
A-Load	0.03	1	0.03	35.98	0.0001	
B-Fuel Blend	0.017	1	0.017	20.23	0.0011	
C-Speed	5.62E-03	1	5.62E-03	6.66	0.0274	
AB	0.018	1	0.018	21.75	0.0009	
AC	8.61E-04	1	8.61E-04	1.02	0.336	
BC	6.61E-05	1	6.61E-05	0.078	0.7851	
A^2	2.38E-03	1	2.38E-03	2.82	0.1239	
B^2	4.18E-03	1	4.18E-03	4.96	0.0501	
C^2	8.30E-03	1	8.30E-03	9.84	0.0106	
Residual	8.43E-03	10	8.43E-04			
Lack of Fit	4.35E-03	5	8.69E-04	1.06	0.4735	not significant
Pure Error	4.08E-03	5	8.17E-04			
Cor Total	0.13	19				

Table 4.57: Summary of APSOME BSFC regression values

Std. Dev.	0.029	R-Squared	0.9346
Mean	0.47	Adj R-Squared	0.8757
C.V. %	6.16	Pred R-Squared	0.6936
PRESS	0.039	Adeq Precision	14.426

BSFC (kg/kW-h) = +0.42 +0.054 * A +0.041 * B +0.024 * C +0.048 * A * B -0.010 * A * C -2.875E-003*B*C+0.017*A^2 +0.037 * B^2 + 0.052 * C^2 (4.38)

BSFC (kg/kW-h) = +0.71594 -4.40042E-003 * Load - 3.33603E-003 * Fuel Blend - 2.14952E-004 * Speed +1.19687E-004 * Load * Fuel Blend -1.03750E-006 * Load (Nm) * Speed -7.18750E-008 * Fuel Blend* Speed +1.73971E-004 * Load ^{2}+2.29408E-005* Fuel Blend^2

+5.17054E-008 * Speed^2 (4.39)

BSFC (kg/kW-h) = +0.71594 -4.40042E-003 * Load - 3.33603E-003 * Fuel Blend - 2.14952E-004 *Speed+1.19687E-004*Load*FuelBlend+5.17054E-008*Speed^2 (4.40)

4.8.3.2.3 APSOME BSFC factors interactive effects. The combined effect of the APSOME fuel blend and engine load on the BSFC performance of Perkins 4:108 diesel engine is shown on Figure 4.57a The speed of the engine was kept constant at 2500rpm. It was observed that simultaneous increase on the both factors studied resulted in increase in the engine BSFC at fuel blend and engine load beyond 80% and 20Nm respectively. The increase in BSFC is found to be more significant at extreme units of the factors. The increase in BSFC with increase in fuel blend could be due to the reduced calorific value and greater density of the fuel blend as the concentration of biodiesel increases (Xue *et al.*, 2001). The loss of calorific value of biodiesel was compensated with higher fuel consumption (Pullen and Saeed, 2014). The BSFC was observed to be minimal (below 0.42kg/kW-h) at fuel blend between 60 -80%vol. and 15-20Nm engine loads.

Figure 4.57b represents the 3D plots of the interactive effect of engine speed and load on the brake specific fuel consumption of the APSOME blend while keeping fuel blend constant at 60%volume. It was clearly shown that lowest brake specific fuel consumption is obtained at lowest load and speed. Typically higher speed encourages low fuel consumption, this fact is shown at higher loads from 20Nm and as the speed increases from 1500rpm up to about 3000rpm. Similar results have reported on the decrease in the BSFC with increase in speed up to 2000rpm, beyond this speed the authors observed increase in the BSFC of rapeseed oil methyl esters blends (Celikten *et al.*, 2012). Also, as the load increases from 5Nm up to 15Nm, the BSFC is observed to increase steadily. The minimum BSFC was obataine at lowest load (5Nm) and speed between 1500-2500rpm.

Figure 4.57c represents the 3D plots of the combined effect of engine speed and fuel blend on the brake specific fuel consumption of the APSOME blend while keeping load constant at 15Nm. The trend observed in the interactive effect of speed and load is repeated in the case of speed and fuel blend. It is clearly shown that there was a steady increase in

BSFC with increase in the fuel blend more especially speeds below 2500rpm. This could be due to increase in the fuel viscosity and density as the concentration of biodiesel in the blend increases. But the BSFC was observed to be minimized at about 60%vol. fuel blend and engine speed between 200-2500rpm.

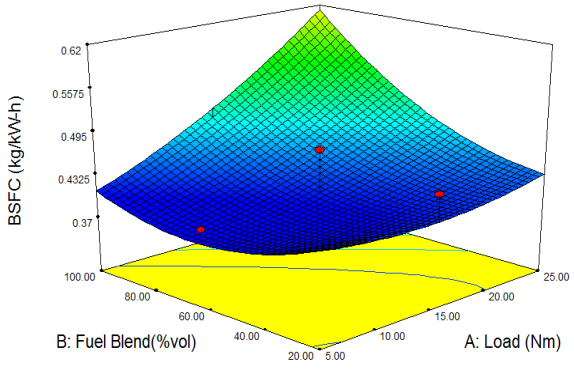

(a)

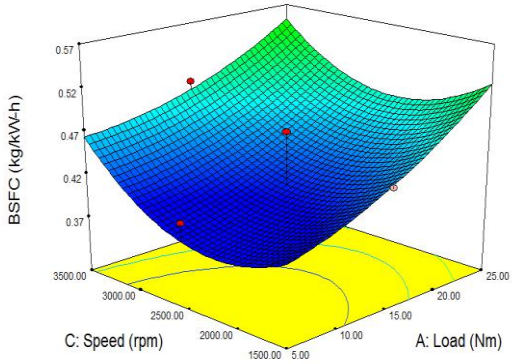

(b)

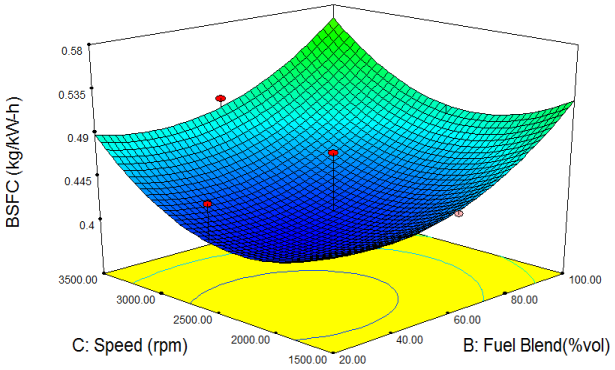

(c)

Figure 4.57: The 3D response surface plots of the interaction effects of the variables on APSOME BSFC:
(a) -fuel blend versus load, (b) - speed versus load, (c)-speed versus fuel blend.

4.8.3.2.4 APSOME BSFC optimization process. The optimization exercise for the minimum BSFC of Perkins 4:108 diesel engine run with blends of APSOME was conducted by utilizing the flexibility of the Design Expert 7.0.0 version numerical optimization tool function. A total of 14 solutions were generated with their desirability. The selected best solution represents the optimized process conditions where minimum BSFC response was obtained as 0.3989kg/kW-h. The optimum values of the process conditions are as contained in Table 4.58.

Table 4.58: RSM optimum values of process parameters for minimum APSOME BSFC response

Variables	Optimum values	Predicted BSFC (kg/kW-h)	Desirability
Engine load (Nm)	12.93		
Fuel blend (%vol.)	35.16	0.3989	1.00
Engine speed (rpm)	1985.19		

4.8.3.3 RSM optimization of APSOME CO emission

4.8.3.3.1 APSOME CO emission RSM model ANOVA analysis. The APSOME CO emission model ANOVA analysis and its summary are presented in Tables 4.59 and 4.60 The Model F-value of 11.15 implies the model is significant. There is only a 0.04% chance that a "Model F-Value" this large could occur due to noise. Values of "Prob> F" less than 0.0500 indicate model terms are significant. In this case C, B^2 and C^2 are significant model terms. Values greater than 0.1000 indicate the model terms are not significant. If there are many insignificant model terms (not counting those required to support hierarchy), model reduction may improve your model. The "Lack of Fit F-value" of 2.47 implies the Lack of Fit is not significant relative to the pure error. There is a 17.14% chance that a "Lack of Fit F-value" this large could occur due to noise. Non-significant lack of fit is good. The "Pred R-Squared" of 0.5779 is close to the "Adj R-Squared" of 0.8279 as one might normally

expect. Adeq Precision" measures the signal to noise ratio. A ratio greater than 4 is desirable. A ratio of 9.975 indicates an adequate signal and it means that this model can be used to navigate the design space.

The coefficient of variation (C.V) is the ratio of the standard deviation of estimate to the mean value of the observed response and a measure of reproducibility and repeatability of the models (Chen *et al.,* 2011). Therefore, the C.V value of 6.88 shows the model is reasonably reproducible. The R- squared value of 0.9094 shows that more than 90% of the overall variability can be explained by the empirical models of the Equations.

4.8.3.3.2 APSOME CO emission quadratic model equation. The selected models in terms of the coded, actual and significant terms are given in Equations (4.41), (4.42) and (4.43) respectively. The equation in terms of coded factors can be used to make predictions about the response for given levels of each factor.

Table 4.59: ANOVA for the APSOME CO emission response quadratic model.

Source	Sum of Squares	df	Mean Square	F Value	p-value Prob> F	
Model	0.073	9	8.07E-03	11.15	0.0004	Significant
A-Load	1.10E-03	1	1.10E-03	1.52	0.2453	
B-Fuel Blend	3.60E-04	1	3.60E-04	0.5	0.4967	
C-Speed	5.11E-03	1	5.11E-03	7.06	0.024	
AB	1.68E-03	1	1.68E-03	2.32	0.1583	
AC	9.68E-04	1	9.68E-04	1.34	0.2743	
BC	1.15E-03	1	1.15E-03	1.59	0.2357	
A^2	8.60E-04	1	8.60E-04	1.19	0.3013	
B^2	8.88E-03	1	8.88E-03	12.27	0.0057	
C^2	0.018	1	0.018	24.21	0.0006	
Residual	7.24E-03	10	7.24E-04			
Lack of Fit	5.15E-03	5	1.03E-03	2.47	0.1714	not significant
Pure Error	2.08E-03	5	4.17E-04			
Cor Total	0.08	19				

Table 4.60: Summary of APSOME CO emission regression values

Std. Dev.	0.027	0.024	R-Squared	0.9094
Mean	0.39	0.39	Adj R-Squared	0.8279
C.V. %	6.88	6.28	Pred R-Squared	0.5779
PRESS	0.045	0.031	Adeq Precision	9.975

CO emission (%vol) = +0.33 +0.011 * A -6.000E-003 * B +0.023 * C +0.014 * A * B -0.011 * A * C +0.012 * B * C -0.018 * A^2
+0.057 * B^2+0.080 * C^2 (4.41)

CO emission (%vol) = +0.89172 +6.92955E-003 * Load - 5.70511E-003 * Fuel Blend - 3.77991E-004 * Speed +3.62500E-005* Load * Fuel Blend -1.10000E-006 * Load * Speed +3.00000E-007 * Fuel Blend (%vol) * Speed -1.76818E-004 * Load ^{2}+3.55114E-005 * Fuel Blend ^{2}+7.98182E-008 * Speed ^{2} (4.42)

CO emission (%vol) = +0.89172 - 3.77991E-004 * Speed +3.55114E-005 * Fuel Blend ^{2}+7.98182E-008 * Speed ^{2} (4.43)

4.8.3.3.3 APSOME CO emission factors interactive effect of factors. The interactive effect of APSOME fuel blend and load on the carbon monoxide emission while keeping the speed at a constant value 2500rpm is shown on Figure 4.58a. The fuel blend is observed to have more significant effect than engine load on the CO emission. The CO emission was observed to decrease with increase in fuel blend up to 80% vol. at all loads. This could be due to the 10-11% oxygen content of biodiesel that promotes the efficient engine combustion and reduced CO emission. Beyond 80%vol. fuel blend the CO emission was found to increase in the same rate till 100 % vol. concentration. It appeared that the minimum CO emission (below 0.3%vol) could be obtained within the range of 60-80 %vol. at almost all the load range (5-25Nm) studied. Reports of many studies have presented that increase in biodiesel content of blends results in decrease in CO emission, although levels range widely and with operating condition (Pullen and Saeed 2014). In this study, this was confirmed below 60%vol. biodiesel concentration and at all the loads studied.

The interactive effect of engine speed and load on the APSOME CO emission while keepin fuel blend constantly at 60% vol concentration is shown in Figure 4.58b. Increase in engine speed resulted in decreased CO emission. This could be due to turbulence intensity increase in the engine cylinder that improves combustion (Celikten *et al.*, 2012). But beyond 2500rpm, the trend reversed, probably due to decrease in air/fuel ratio at high engine speed.

Figure 4.58c represents the 3D plot of the combined effect of engine speed and APSOME fuel blend on the CO emission when the engine load is kept at 15Nm. Increase in both speed and fuel blend decreased the CO emission significantly. This could be attributed to the joint effects of increase in engine turbulence and oxygen content of the fuel blend. The minimum CO emission was observed to occur while the fuel blend is within 60-80%vol. and engine speed range of 1500- 2500rpm.

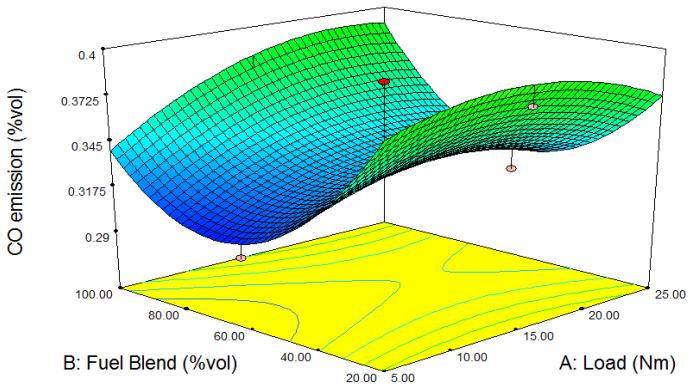

(a)

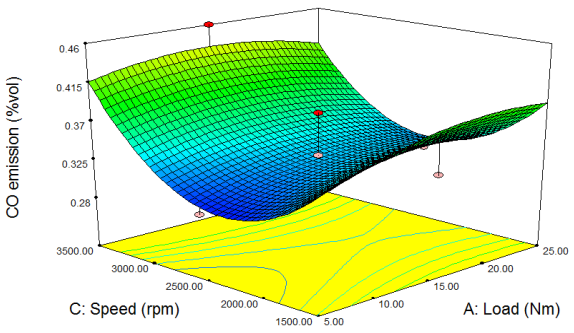

(b)

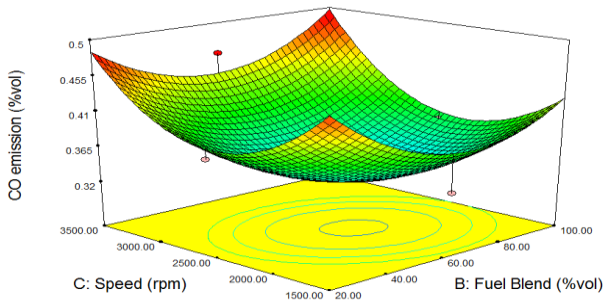

(c)

Figure 4.58: The 3D response surface plots of the interaction effects of the variables on APSOME CO emission: (a) -fuel blend versus load, (b) - speed versus load, (c)-speed versus fuel blend

4.8.3.3.4 APSOME CO emission optimization process. The optimization exercise for the minimum CO of Perkins 4:108 diesel engine run with blends of APSOME was conducted by utilizing the flexibility of the Design Expert 7.0.0 version numerical optimization tool function. A total of 7 solutions were generated with their desirability. The selected best solution represents the optimized process conditions where minimum CO response was obtained as 0.2976%vol. The optimum values of the process conditions are as contained in Table 4.61.

Table 4.61: RSM optimum values of process parameters for minimum APSOME CO response

Variables	Optimum values		
		Predicted CO (%vol.)	Desirability
Engine load (Nm)	5.00		
Fuel blend (%vol.)	68.19	0.2976	0.986
Engine speed (rpm)	2274.01		

4.8.3.4 RSM optimization of APSOME NOx emission

4.8.3.4.1 APSOME NOx emission RSM quadratic model ANOVA analysis. The APSOME NOx emission quadratic model ANOVA analysis and its summary are presented in Tables 4.62 and 4.63 respectively. The Model F-value of 77.73 implies the model is significant. There is only a 0.01% chance that a "Model F-Value" this large could occur due to noise. Values of "Prob> F" less than 0.0500 indicate model terms are significant. In this case B, AB, A^2, B^2 and C^2 are significant model terms. Values greater than 0.1000 indicate the model terms are not significant. The "Pred R-Squared" of 0.9221 is as close to the "Adj R-Squared" of 0.9732 as one might normally expect with the difference between them being less than 0.2. "Adeq Precision" measures the signal to noise ratio. A ratio greater than 4 is desirable. Your ratio of 22.131 indicates an adequate signal. This model can be used to navigate the design space.

The coefficient of variation (C.V) is also a measure of reproducibility and repeatability of the models (Chen et al., 2011). Therefore, the C.V value of 1.2 shows the model is reasonably reproducible. Also, the R-squared value of 0.9859 shows that more than 98% of the overall variability can be explained by the empirical models of the Equations.

4.8.3.4.1 APSOME NOx RSM quadratic model equations. The selected models in terms of the coded, actual and significant terms are given in Equations (4.44), (4.45) and (4.46) respectively. The equation in terms of coded factors can be used to make predictions about the response for given levels of each factor.

Table 4.62: ANOVA for the APSOME NOx emission response quadratic model.

Source	Sum of Squares	df	Mean Square	F Value	p-value Prob> F	
Model	51926.97	9	5769.66	77.73	< 0.0001	Significant
A-Load	78.4	1	78.4	1.06	0.4783	
B-Fuel Blend	396.9	1	396.9	5.35	0.0433	
C-Speed	16.9	1	16.9	0.23	0.6435	
AB	512	1	512	6.9	0.0253	
AC	264.5	1	264.5	3.56	0.0884	
BC	128	1	128	1.72	0.2184	
A^2	4420.02	1	4420.02	59.55	< 0.0001	
B^2	3102.96	1	3102.96	41.81	< 0.0001	
C^2	5225.46	1	5225.46	70.4	< 0.0001	
Residual	742.23	10	74.22			
Lack of Fit	542.13	5	108.43	1.46	0.3486	Not significant
Pure Error	200.10	5	40.o2			
Cor Total	52669.2	19				

Table 4.63: Summary of APSOME NOx emission regression values.

Std. Dev.	8.62	R-Squared	0.9859
Mean	719.8	Adj R-Squared	0.9732
C.V. %	1.2	Pred R-Squared	0.9221
PRESS	4101	Adeq Precision	22.131

NOx (ppm) = +661.16 -2.80 * A + 6.30 * B - 1.30 * C - 8.00 * A * B -5.75 * A * C - 4.00 * B*C+40.09*A^2+33.59*B^2+43.59*C^2 (4.44)

NOx (ppm) = +1042.82841 - 9.66977 * Load -1.81182 * Fuel Blend - 0.20463 * Speed - 0.020000 * Load * Fuel Blend - 5.75000E-004 * Load * Speed - 1.00000E-004* Fuel Blend * Speed + 0.40091 * Load ^{2}
+0.020994 * Fuel Blend ^{2} +4.35909E-005* Speed ^{2} (4.45)

NOx (ppm) = +1042.82841 -1.81182 * Fuel Blend -0.020000 * Load * Fuel Blend +0.40091 * Load ^{2} +0.020994 * Fuel Blend ^{2} +4.35909E-005* Speed ^{2} (4.46)

4.8.3.4.3 Main and interactive effects of factors on APSOME NOx emission. The 3D plots of the combined effects of both fuel and engine load on the NOx emission is presented in Figre 4.59a. Initial increase in both factors resulted in significant decrease in the NOx

emission. The simultaneous increase of both fuel blend and engine load might have resulted in shorter ignition delay which resulted in low amount of fuel involved in the premixed combustion (Figure4.59a). This could have resulted in lower initial rate of heat release that reduced the NOx emission until about 60% vol. fuel blend and 15Nm engine load. Increase in engine load from 15Nm was found to increase NOx emission probably due to higher combustion temperature. The interactive effect of fuel blend and engine speed (Figure 4.59b) as well as the engine load and speed (Figure 4.59c) is observed to follow the same trend observed above.

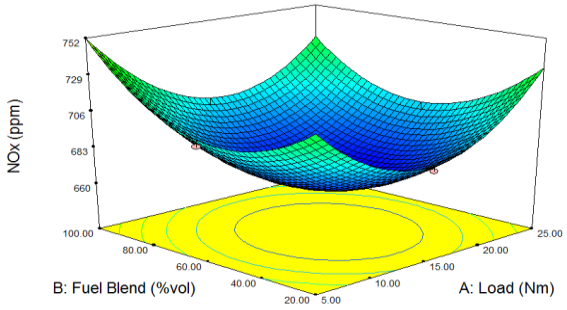

(a)

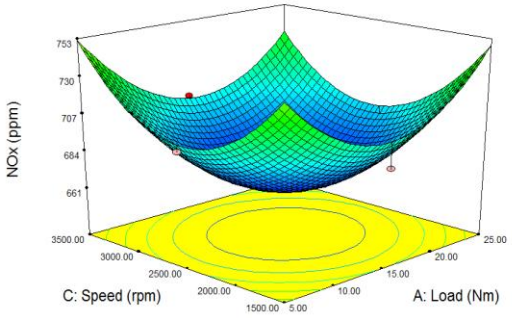

(b)

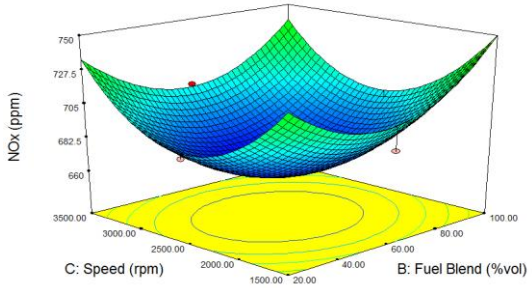

(c)

Figure 4.59: The 3D response surface plots of the interaction effects of the variables on APSOME NOx emission: (a) -fuel blend versus load, (b) - speed versus load, (c) - speed versus fuel blend.2

4.8.3.4.4 APSOME NOx optimization process. The optimization exercise for the minimum NOx of Perkins 4:108 diesel engine run with blends of APSOME was conducted by utilizing the flexibility of the Design Expert 7.0.0 version numerical optimization tool function. A total of 15 solutions were generated with their desirability. The selected best solution represents the optimized process conditions where minimum NOx response was obtained as 664.63ppm. The optimum values of the process conditions are as contained in Table4.64.

Table 4.64: RSM optimum values of process parameters for minimum APSOME NOx response

Variables	Optimum values	Predicted NOx (ppm)	Desirability
Engine load (Nm)	13.41		
Fuel blend (%vol.)	45.11	464.63	1.0
Engine speed (rpm)	2554.41		

4.8.3.5 RSM optimization of APSOME HC emission

4.8.3.5.1 APSOME HC emission quadratic model ANOVA analysis and fitting. The APSOME HC emission model ANOVA analysis and its summary are presented in Tables 4.65 and 4.66 respectively. The Model F-value of 91.0 implies the model is significant. There is only a 0.01% chance that a "Model F-Value" this large could occur due to noise. Values of "Prob> F" less than 0.0500 indicate model terms are significant. In this case B, AB, AC, BC, A^2, B^2 and C^2 are significant model terms. The "Lack of Fit F-value" of 1.09 implies the Lack of Fit is not significant relative to the pure error. There is a 22.13% chance that a "Lack of Fit F-value" this large could occur due to noise. The "Pred R-Squared" of 0.9356 is in reasonable agreement with the "Adj R-Squared" of 0.9771. "Adeq Precision"

measures the signal to noise ratio. A ratio greater than 4 is desirable. The ratio of 23.247 indicates an adequate signal. This model can be used to navigate the design space.

The coefficient of variation (C.V) value of 2.03 shows the model is reasonably reproducible. Apart from the F-value, lack of fit and C.V, the R- squared value of 0.9879 shows that more than 98% of the overall variability can be explained by the empirical models of the Equations.

4.8.3.5.2 APSOME HC emission RSM quadratic model equations. The selected models in terms of the coded, actual and significant terms are given in Equations (4.47), (4.48) and (4.49) respectively. The equation in terms of coded factors can be used to make predictions about the response for given levels of each factor.

Table 4.65: ANOVA for the APSOME HC emission response quadratic model

Source	Sum of Squares	df	Mean Square	F Value	p-value Prob> F	
Model	376.68	9	41.85	91	<0.0001	significant
A-Load	0.05	1	0.05	0.11	0.7474	
B-Fuel Blend	4.52	1	4.52	9.82	0.0106	
C-Speed	0.49	1	0.49	1.06	0.3271	
AB	6.18	1	6.18	13.43	0.0044	
AC	2.61	1	2.61	5.68	0.0385	
BC	2.7	1	2.7	5.88	0.0358	
A^2	2.3	1	2.3	5.0	0.0491	
B^2	243.27	1	243.27	528.93	<0.0001	
C^2	2.42	1	2.42	5.26	0.0445	
Residual	4.6	10	0.46			
Lack of Fit	2.53	5	0.506	1.09	0.3158	Not significant
Pure Error	2.07	5	0.414			
Cor Total	381.28	19				

Table 4.66: Summary of APSOME HC emission regression values

Std. dev.	0.68	R-squared	0.9879
Mean	33.41	Adj. R-squared	0.9771
C.V. %	2.03	Pred. R-squared	0.9356
PRESS	24.55	Adeq. Precision	23.247

$$HC\ (ppm) = +29.53 - 0.071 * A + 0.67 * B - 0.22 * C - 0.88 * A * B - 0.57 * A * C - 0.58 * B * C - 0.80 * A^2 + 9.41 * B^2 - 0.85 * C^2 \quad (4.47)$$

$$HC\ (ppm) = +36.93339 + 0.50739 * Load - 0.61933 * Fuel\ Blend + 5.75548E-003 * Speed - 2.19688E-003 * Load * Fuel\ Blend - 5.71250E-005 * Load * Speed - 1.45313E-005 * Fuel\ Blend * Speed - 7.99545E-003 * Load^2 + 5.87841E-003 * Fuel\ Blend^2 - 8.49545E-007 * Speed^2 \quad (4.48)$$

$$HC\ (ppm) = +36.93339 - 0.61933 * Fuel\ Blend - 2.19688E-003 * Load * Fuel\ Blend - 5.71250E-005 * Load * Speed - 1.45313E-005 * Fuel\ Blend * Speed - 7.99545E-003 * Load^2 + 5.87841E-003 * Fuel\ Blend^2 - 8.49545E-007 * Speed^2 \quad (4.49)$$

4.8.3.5.3 APSOME HC emission interactive effects of factors. Figure 4.60a shows the interactive effect of both fuel blend and load on HC emission while speed of the engine was set constantly at 2500rpm. It was observed that irrespective of the engine load, the HC emission decreased significantly with increase in fuel blend up to about 70% vol. biodiesel concentration in the blend. The increase in oxygen content and higher cetane number (CN) of biodiesel must have led to more complete combustion and shortened combustion delay respectively. From Figure 4.60b, simultaneous increase in both speed and load resulted in the increase of HC emission. However, the lowest HC emission was achieved at lowest factor conditions. The combined effect of speed and engine load had most significant reduction effect on the HC emission.

The combined effect of engine speed and fuel blend on HC emission of APSOME – petrodiesel blend run on CI diesel engine is shown on Figure 4.60c. The engine load was

kept constant at 15Nm. It was observed that at almost all speed (1500-3500rpm), increase in the fuel blend significantly reduced the hydrocarbon emission. This continued until about 70% vol. concentration of biodiesel in the blend before the reveres trend took over. The decrease in the HC emission could have been caused by improved combustion due to high oxygen content in the biodiesel but the reverse trend could have been due to low air-fuel ratio at higher blends.

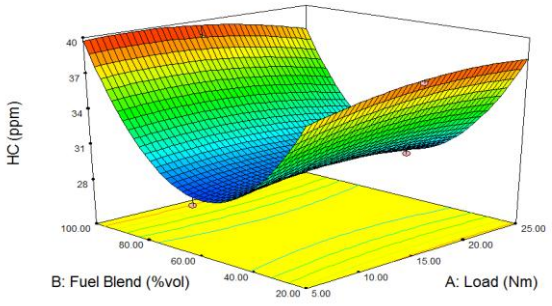

(a)

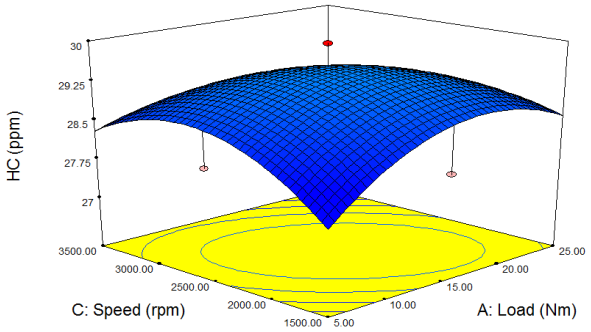

(b)

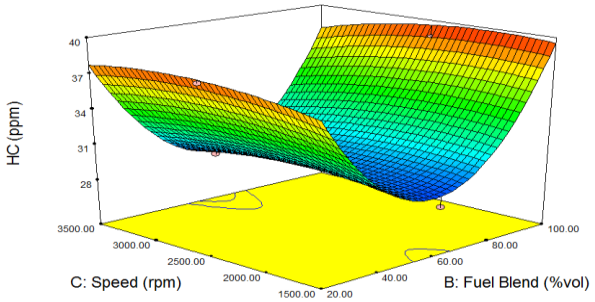

(c)

Figure 4.60: The 3D response surface plots of the interaction effects of the variables on APSOME HC emission: (a) -fuel blend versus load, (b) - speed versus load, (c)-speed versus fuel blend.

4.8.3.5.4 APSOME HC emission optimization process. The optimization exercise for the minimum HC of Perkins 4:108 diesel engine run with blends of APSOME was conducted by utilizing the flexibility of the Design Expert 7.0.0 version numerical optimization tool function. A total of 13 solutions were generated with their desirability. The selected best solution represents the optimized process conditions where minimum HC response was obtained as 27.75ppm. The optimum values of the process conditions are as contained in Table 4.67.

Table 4.67: RSM optimum values of process parameters for minimum APSOME HC response

Variables	Optimum values	Predicted HC (ppm)	Desirability
Engine load (Nm)	5.43		
Fuel blend (%vol.)	57.32	27.75	1.00
Engine speed (rpm)	1581.11		

4.8.4. RSM-GA optimization results for APSOME engine performance and emission

The RSM was therefore integrated and tunned with genetic algorithm (GA) for simultanous optimization of the emission variables and engine performance parameters. The optimized conditions for the responses are contained in Table 4.68 and these show improved conditions and responses in comparison with RSM . Using the RSM-GA optimized solution, the experimental run for *Dyacrodes edulis* seed oil biodiesel in CI engine was carried out. The results of the experimental values obtained were very close to the ones calculated from the model. Results suggested that the optimal conditions attained had the least error and can be practically applied in the viability and feasibility analysis of the application of seed oil derived from African pear in biodiesel production.

Table 4.68: Optimal conditions for engine performance and combustion of APSOME in CI engine using RSM-GA.

Responses	Optimized values	Experimental values	Optimum conditions		
			Load (Nm)	Fuel blend (%Vol.)	Engine speed (rpm)
BTE (%)	38.0303	41.010	22	80	1990
BSFC(Kg/kW-hr)	0.0679	0.0511	10	85	2000
CO (% Vol.)	0.0507	0.0500	15	20	2800
NOx(ppm)	232.3047	234.05	15	65	3500
HC(ppm)	20.8474	21.3321	24	60	2400

4.8.5 Modeling of the engine combustion using ANN

Total data set of 20 points was used in developing the ANN model using MATLAB 8.5 version 2015 software The optimum architecture of ANN (3:7:5) model is shown in Figure 4.61 consisting of three layers as input layer with three input variables, hidden layer with seven neurons, and output layer with five output variables. All models constructed from the data set were characterized by a great response for all input variables from the leaning set.

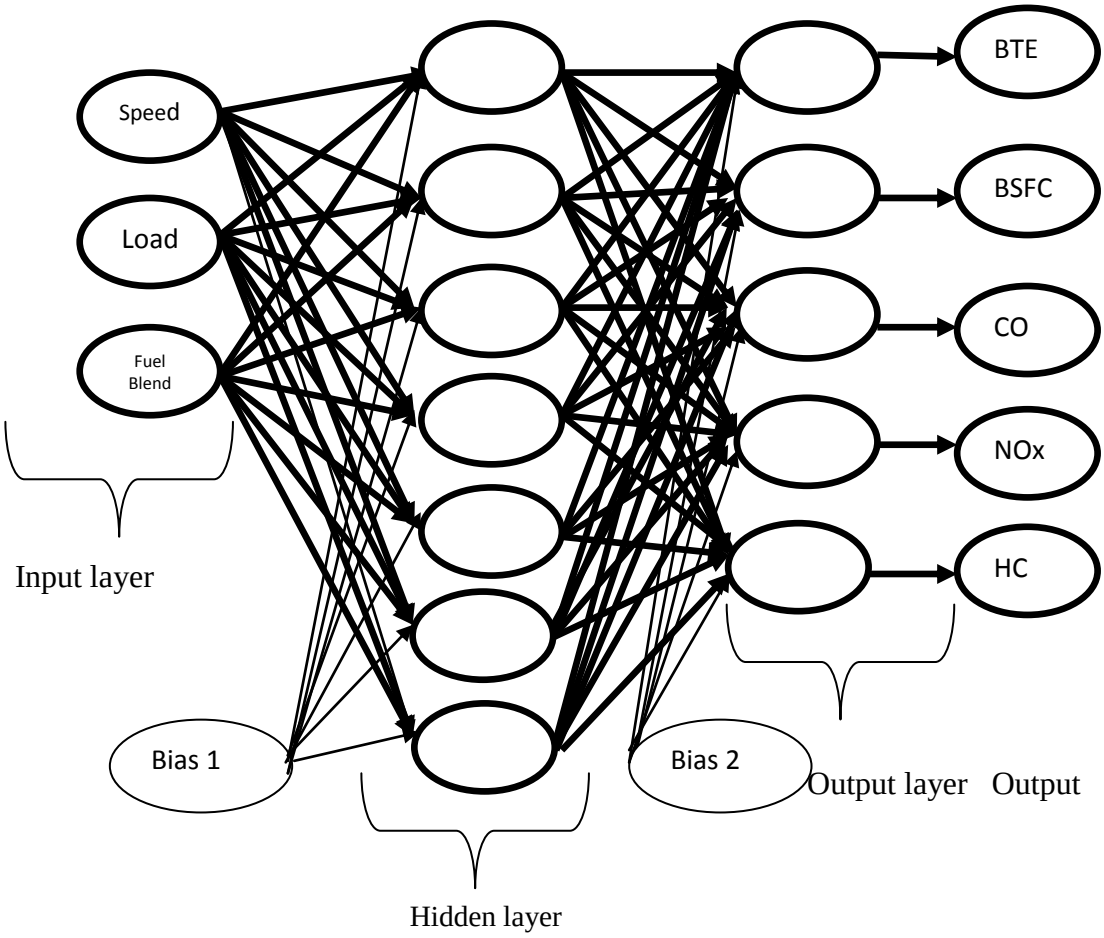

Figure 4.61: ANN Architecture topology of the MIMO ANN model with single hidden layer.

4.8.5.1 ANN modeling of SASOME engine combustion

The optimum architecture of the ANN model was determined based on three steps: (1) optimum number of neurons, (2) selection of of the best backpropagation training algorithm and (3) testing and validation of the model. A number of neural network architectures and topologies were selected and investigated for the estimation and prediction of the responses (BTE, BSFC, CO, NOx and HC). This is due to the fact that the choice of an optimal neural network and architecture and topology is critical for successful application of ANN. Multi-input multi output algorithm was selected. The scatter diagram for all inputs and all output that compare the experimental data versus the computed neural network data in training, testing, validation and all predictions networks are shown in Figure 4.62 with very good values of R (0.95705, 0.82799, 0.94531 and 0.94419 respectively). Almost all the data scatter around the 45° line that is the indication of excellent compatibility between the experimental results and ANN predicted data. The values of R between experimental responses and ANN predicted responses in all the cases suggest that the developed ANN model, which was trained using experimental data was precise predicting the engine combustion performance and combustion emission pollutants. The results are in close agreement with the values of 0.9487,0.999, 0.929 and 0.999 obtained for engine torque, SFC,CO and HC emissions respectively by Ghobadian et al, (2009).Table 4.69 contains the experimental and corresponding predicted values by MIMO-ANN model.

Table: 4.69: CCD experimental and ANN predicted values of SASOME combustion responses.

Run	Factors			Responses									
				BTE(%)		BSFC(kg/kW-hr)		CO(%vol.)		NOx(ppm)		HC(ppm)	
	X_1(Nm)	X_2(%vol.)	X_3(rpm)	Exp. Value	Pred. Value	Exp. Value	Pred. Value	Exp. Value	Pred. Value	Exp. Value	Pred. Value	Exp. Value	Pred. Value
1	10	40	2000	16.4000	16.0205	0.6300	0.2917	0.0400	0.4078	220	169.9340	20.8700	38.5850
2	10	80	3000	14.5500	15.5874	0.6300	0.7340	0.4500	0.2238	356	568.5032	23.6100	33.9617
3	20	40	3000	20.1500	28.7505	0.3700	0.2097	0.1790	0.2332	300	686.6027	31.3900	32.4973
4	20	80	2000	31.5500	32.5049	0.3200	0.3577	0.1790	0.0931	800	878.6045	19.2500	15.0818
5	15	60	2500	27.6100	33.0900	0.3700	0.4351	0.4700	0.2993	600	789.8506	39.6200	31.3923
6	15	60	2500	27.6100	33.0900	0.3700	0.4351	0.4700	0.2993	600	789.8506	39.6200	31.3923
7	10	40	3000	14.4400	19.2044	0.4000	0.4114	0.2560	0.2452	850	567.1557	27.9600	25.0069
8	10	80	2000	19.2100	19.7060	0.7300	0.6418	0.2860	0.2503	740	553.8622	35.9400	29.0880
9	20	40	2000	15.7700	16.4166	0.2900	0.2249	0.0480	0.3597	375	383.5505	28.5300	32.0095
10	20	80	3000	19.6200	33.1303	0.8300	0.3652	0.1430	0.0444	523	936.6085	39.6200	5.1594
11	15	60	2500	27.6100	33.0900	0.3700	0.4351	0.4700	0.2993	600	789.8506	39.6200	31.3923
12	15	60	2500	27.6100	33.0900	0.3700	0.4351	0.4700	0.2993	600	789.8506	29.8600	31.3923
13	5	60	2500	30.4500	14.7208	0.2700	0.7713	0.1790	0.4231	459	434.4348	31.9800	40.2257
14	25	60	2500	31.5500	35.9799	0.6300	0.3350	0.0950	0.2821	665	920.9339	25.0400	28.6118
15	15	20	2500	17.1500	15.7765	0.3500	0.1918	0.3310	0.3677	320	252.0775	26.1100	26.3670
16	15	100	2500	27.6100	18.5194	0.4800	0.5946	0.1790	0.0557	200	651.1502	24.7200	24.5390
17	15	60	1500	31.5500	24.2868	0.2600	0.3401	0.4410	0.4117	600	570.1177	32.2100	44.5222
18	15	60	3500	31.5500	31.6404	0.4100	0.5019	0.1790	0.3136	721	863.3832	39.6200	28.1274
19	15	60	2500	27.6100	33.0900	0.3700	0.4351	0.4700	0.2993	600	789.8506	39.6200	31.3923
20	15	60	2500	27.6100	33.0900	0.3700	0.4351	0.4700	0.2993	600	789.8506	39.6200	31.3923

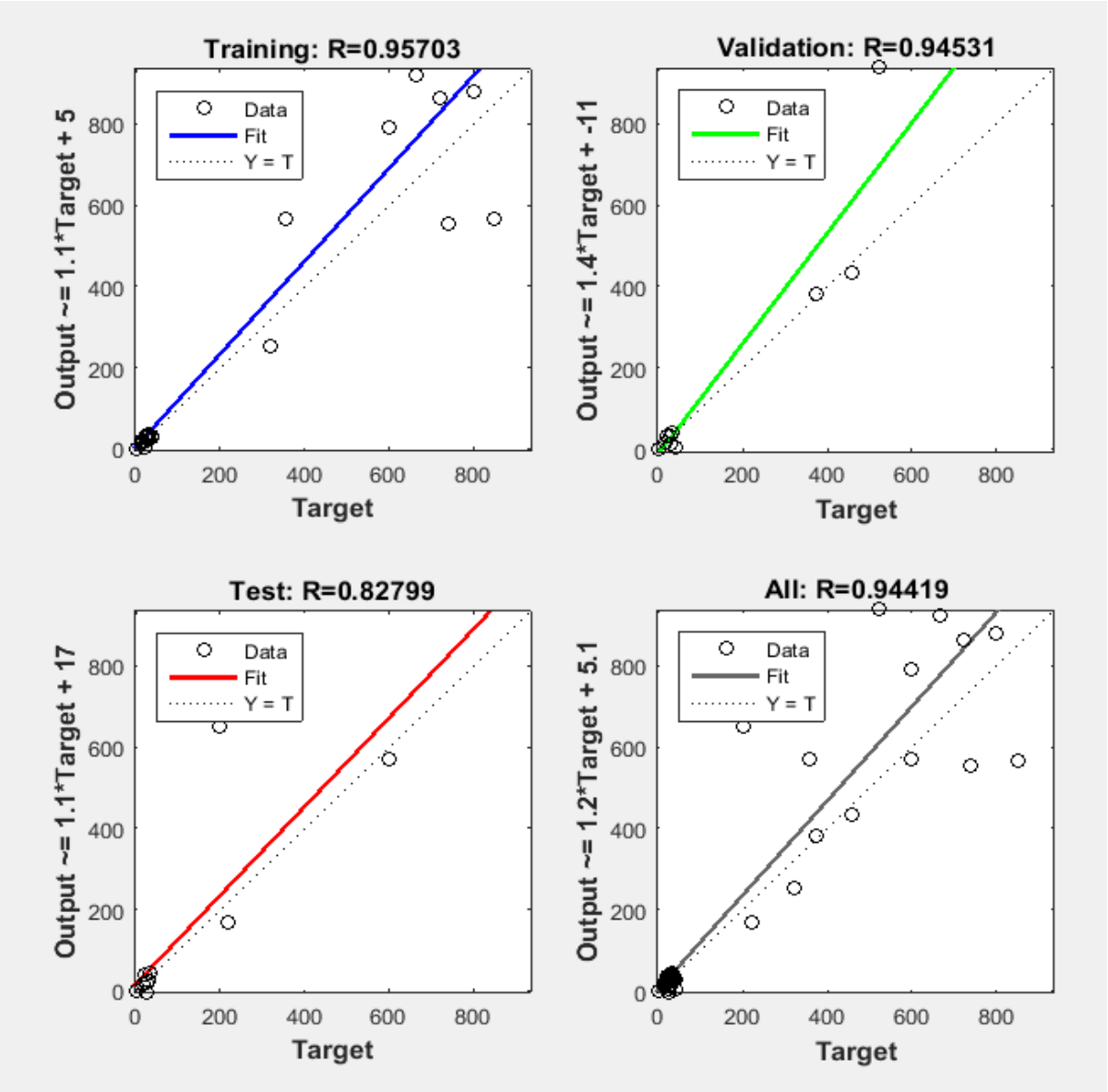

Figure 4.62: SASOME MIMO neural network model with training, validation, test and all prediction set.

4.8.5.2 ANN modeling of APSOME engine combustion

The mean and standard deviation values provide the statistic summary of the dataset to facilitate the reproducibility. The statistical analysis of the input and output variables are represented by the mean and standard variations. The mean vectors for the input and the output are 15, 60, 2500 and 27.45, 0.312, 0.311, 492.45, 30,12 respectively while the standard deviations for the input and out variables are 4.5883, 18.353, 458.83 and 6.80,

0.165, 0.1595, 197.419, 5.866 respectively. Total data set of 20 points as shown in Table 4.70 was used in developing the ANN model using MATLAB 8.5 version 2015 software. All models constructed from the data set were characterized by a great response for all input variables from the leaning set. The scatter diagram for all inputs and all output that compare the experimental data versus the computed neural network data in training, testing, validation and all predictions networks are shown in Figure 4.63 with very good values of R (0.97385, 0.89468, 0.9929 and 0.94237 respectively). It is observed from these figures that the ANN represents an excellent accuracy in modeling the responses. The results are in close agreement with the values of 0.9487, 0.999, 0.929 and 0.999 obtained for engine torque, SFC, CO and HC emissions respectively by Ghobadian et al, (2009). The predictive capability of the ANN model is shown through the statistical analysis presented in Table 4.71.

The ANN result of APSOME follows the same trend with SASOME as discussed in section 4.5.4.5 but with better correlation than SASOME optimization model.

Table: 4.70: CCD experimental and ANN predicted values of APSOME combustion responses.

Run	Factors			Responses									
				BTE(%)		BSFC(kg/kW-hr)		CO(%vol.)		NOx(ppm)		HC(ppm)	
	X_1(Nm)	X_2(%vol.)	X_3 (rpm)	Exp. Value	Pred. Value	Exp. Value	Pred. Value	Exp. Value	Pred. Value	Exp. Value	Pred. Value	Exp. Value	Pred. Value
1	10	40	2000	13.5600	11.8578	0.5710	0.6717	0.0500	0.0038	300	383.0	22.4000	28.2545
2	10	80	3000	20.0400	32.5081	0.6430	0.4345	0.4000	0.4250	400	353.0	24.6700	45.3663
3	20	40	3000	30.0500	27.5804	0.1430	0.0980	0.1880	0.1104	400	325.5	30.4000	30.1466
4	20	80	2000	35.0000	28.3235	0.4290	0.3014	0.1880	0.4677	800	809.8	20.1500	26.3376
5	15	60	2500	32.0000	34.6426	0.3500	0.3838	0.4800	0.4097	670	808.2	35.9400	38.9669
6	15	60	2500	32.0000	34.6426	0.3500	0.3838	0.4800	0.4097	670	808.2	35.9400	38.9669
7	10	40	3000	33.4600	30.0084	0.1430	0.2751	0.2750	0.1043	400	392.8	29.6600	31.3052
8	10	80	2000	21.6700	17.9762	0.1430	0.1584	0.0480	0.2505	525	444.7	35.9400	35.4270
9	20	40	2000	34.9900	30.6330	0.2140	0.2429	0.3580	0.3256	344	264.8	28.6600	24.0054
10	20	80	3000	31.6700	27.7684	0.3570	0.2556	0.1880	0.4759	300	643.1	24.4000	24.1361
11	15	60	2500	32.0000	34.6426	0.3500	0.3838	0.4800	0.4097	670	808.2	35.9400	38.9669
12	15	60	2500	32.0000	34.6426	0.3500	0.3838	0.4800	0.4097	670	808.2	35.9400	38.9669
13	5	60	2500	19.6600	27.5849	0.1090	0.5050	0.2750	0.0951	850	829.7	22.4000	43.3401
14	25	60	2500	25.6100	31.2259	0.1430	0.2002	0.4000	0.2983	221	268.3	24.6700	16.0220
15	15	20	2500	13.5600	17.7495	0.6430	0.4808	0.1200	0.1393	334	314.9	29.6600	35.1653
16	15	100	2500	30.0500	20.7541	0.2140	0.1096	0.3900	0.6083	400	602.7	24.6700	22.4035
17	15	60	1500	21.6700	19.9857	0.1430	0.2544	0.4000	0.2424	334	463.6	38.7000	33.5086
18	15	60	3500	26.0000	34.1399	0.2500	0.2780	0.0690	0.3187	221	702.1	30.4000	41.0963
19	15	60	2500	32.0000	34.6426	0.3500	0.3838	0.4800	0.4097	670	808.2	35.9400	38.9669
20	15	60	2500	32.0000	34.6426	0.3500	0.3838	0.4800	0.4097	670	808.2	35.9400	38.9669

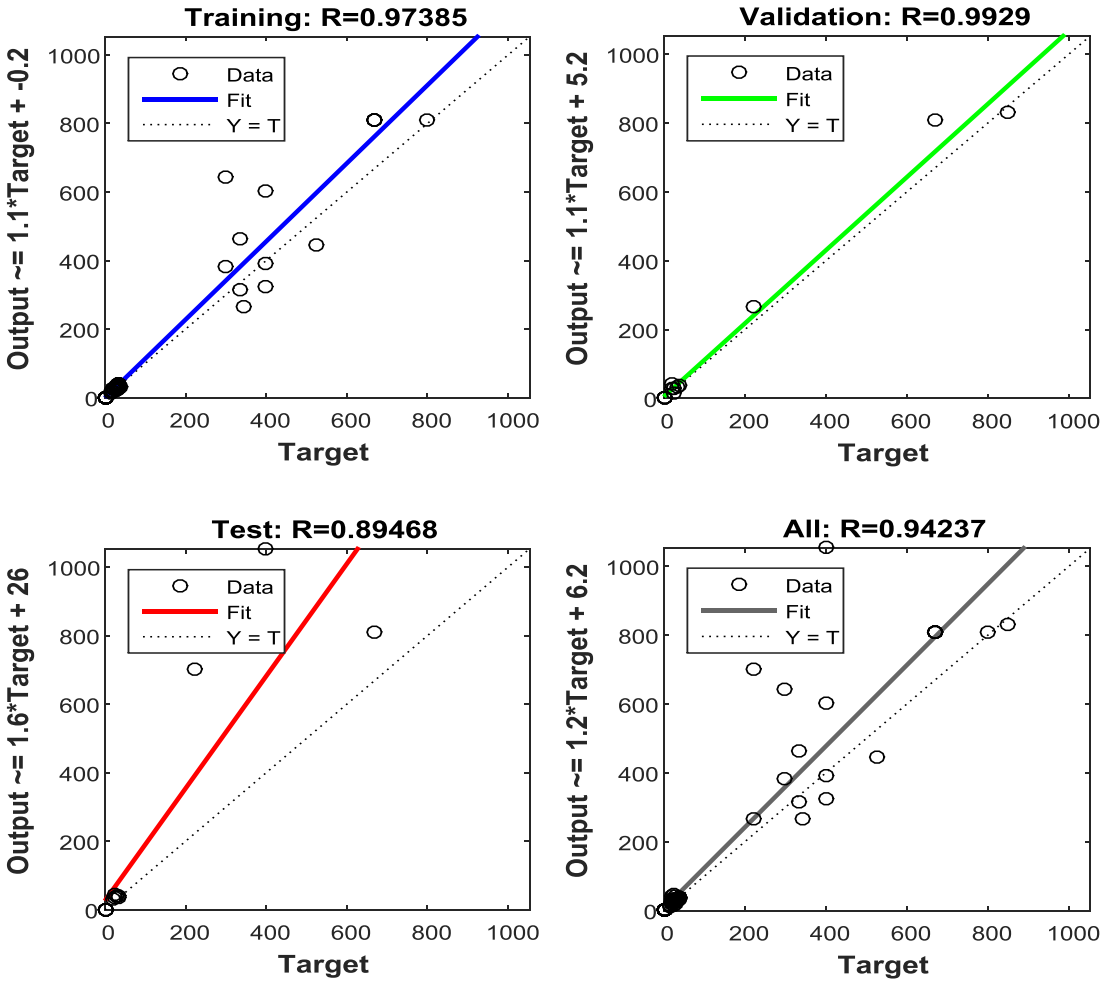

Figure 4.63: APSOME MIMO neural network model with training, validation, test and all prediction set.

Table 4.71: Predictive capabilities of ANN model on APSOME combustion.

Responses	AAD	RMSE	SEP	R^2
BTE (%)	5.510	2.03	7.44	0.998
BSFC (kg/kW-hr)	0.110	$4.5x10^{-4}$	0.14	0.811
CO (%vol.)	0.128	$4.9x10^{-4}$	0.157	0.730
NOx (ppm)	209.59	1,471.90	238.42	0.601
HC (ppm)	6.552	1.749	7.88	0.842

4.8.6. Nelder -Mead techniques optimization results

The independent variables load(X), fuel blend (Y) and enfgine speed (Z) were considered as process conditions for the maximization of the brake thermal efficiency and minimization of the brake specific fuel consumption as well as the exhaust emissions (CO, NOx and HC) using Nelder-Mead simplex optimization techniques. Both the combustion characteristics of SASOME and the APSOME were optimized.

4.8.6.1 Nelder -Mead techniques for SASOME combustion optimization

The model equations obtained for the SASOME responses based on Nelder-Mead simplex techniques are presented in Equations (4.51-4.54). Where X, Y and Z represent the independent variable: engine load, fuel blend and engine speed respectively. Table 4.72 contains the experimental and predicted responses. Figures 4.64- 4.68 show the response surface plots based on the model developed. It is the ratio of the standard error of estimate to the mean value of the observed response as a measure of reproducibility of the model. From the result, the R^2 of all the responses are all above 0.99 showing excellent correlation between the experimental values and the predicted values from the model. The optimized conditions are presented in Table 4.73.

$$BTE(X,Y,Z) = 0.83629 - \ 0.00023548Z)Z + X(-49.7773 + \ Y(-0.614959 - 0.00411549Y + 0.000034025Z) + X(3.36372 + 0.0163374X - 0.0006875Y + 0.0016095Z) + (-0.017295 + 0.000013515Z)Z \quad (4.50)$$

$$BSFC(X,Y,Z) = 11.9029 + Y(-0.0251429 + 0.000549107Y - 0.0000046425Z) + (-0.01241 + \ 3.24x10^{-6}Z)Z + X(0.314619 + \ Y(-0.00170714 - 0.0000347321Y - 7.5x10^{-7}Z) + X(-0.0433143 + 0.000361905X + 0.00014Y + 0.0000208Z) + (0.000292 - 1.83x10^{-7}Z)Z) \quad (4.51)$$

$$CO(X,Y,Z) = -1.03735 + Y(0.58106 - 0.00444446Y + 1.575x10^{-6}Z) + \ (-0.015132 - 2.864x10^{-6}\ Z)Z + X(0.21897 + \ Y(-0.0404682 + 0.000287318Y + 2.875x10^{-7}Z) + X(-0.0423913 + 0.000880696X - 0.00020925Y + 5.25x10^{-6}Z) + (-0.0012955 - 2.27x10^{-7}Z)Z) \quad (4.52)$$

$$NOx(X,Y,Z) = -11777.1 + Y(294.232 - 1.18214Y - 0.04565Z) + (1.261 + 0.0024Z)Z + X(947.219 + X(-27.7543 + 0.498095X + 0.2285Y - 0.0035Z) + Y(-18.9096 + 0.0646429Y - 0.00203Z) + (0.0133 - 0.000012Z)Z \quad (4.53)$$

$$HC(X,Y,Z) = -845.877 + Y(17.1236 - 0.105817Y - 0.00140875Z) + (0.33831 - 0.00007826Z)Z + X(44.8903 + X(-0.563078 + 0.0394106X + 0.0031125Y - 0.0006033Z) + Y(-1.11441 + 0.00646262Y + 0.000092325Z) + (-0.005577 + 3.912x10^{-6}Z)Z) \quad (4.54)$$

Table: 4.72: Experimental and Nelder-Mead predicted values of SASOME combustion responses.

Run	Factors			BTE (%)		BSFC (kg/kW-hr)		CO(%vol.)		NOx(ppm)		HC(ppm)	
	X(Nm)	Y(%vol.)	Z(rpm)	Exp. Value	Predicted Value	Exp. Value	Predicted Value	Exp. Value	Predicted Value	Exp. value	Predicted Value	Exp. value	Predicted Value
1	10	40	2000	16.4000	16.400	0.6300	0.6300	0.1790	0.1789	220	220.057	20.8700	20.8735
2	10	80	3000	14.5500	14.440	0.6300	0.6300	0.1869	0.1879	356	491.587	23.6100	23.6177
3	20	40	3000	20.1500	20.151	0.3700	0.3700	0.0399	0.03992	300	300,069	31.3900	31.9841
4	20	80	2000	31.5500	31.5514	0.3200	0.3200	0.2559	0.2519	800	800.115	19.2500	19.2612
5	15	60	2500	27.6100	27.6112	0.3700	0.3700	0.4700	0.4799	600	600.081	39.6200	39.6268
6	15	60	2500	27.6100	27.6112	0.3700	0.3700	0.4700	0.4799	600	600.081	39.6200	39.6268
7	10	40	3000	14.4400	14.5507	0.4000	0.4000	0.5799	0.2749	850	850.057	27.9600	27.9635
8	10	80	2000	19.2100	19.2107	0.7300	0.7300	0.1789	0.1879	740	721.081	35.9400	35.9477
9	20	40	2000	15.7700	15.771	0.2900	0.2900	0.1429	0.1879	375	375.069	28.5300	28.5352
10	20	80	3000	19.6200	19.6214	0.8300	0.8300	0.0949	0.1879	523	523.115	39.6200	39.6268
11	15	60	2500	27.6100	27.6112	0.3700	0.3700	0.4700	0.4799	600	600.081	39.6200	39.6268
12	15	60	2500	27.6100	27.6112	0.3700	0.3700	0.4700	0.4799	600	600.081	29.8600	29.8708
13	5	60	2500	30.4500	30.4505	0.2700	0.2700	0.1789	0.1879	459	459.058	31.9800	31.3952
14	25	60	2500	31.5500	31.5517	0.6300	0.6300	0.2859	0.2641	665	665.099	25.0400	25.0492
15	15	20	2500	17.1500	17.1507	0.3500	0.3500	0.1789	0.1879	320	356.085	26.1100	26.8275
16	15	100	2500	27.6100	31.5508	0.4800	0.4800	0.1789	0.1879	200	200.123	24.7200	24.7325
17	15	60	1500	31.5500	31.5517	0.2600	0.2600	0.4410	0.4422	600	599.977	32.2100	26.1124
18	15	60	3500	31.5500	23.621	0.4100	0.4100	0.1790	0.1789	721	721.081	39.700	38.0733
19	15	60	2500	27.6100	27.6112	0.3700	0.3700	0.4700	0.4799	600	600.081	39.6200	39.6268
20	15	60	2500	27.6100	27.6112	0.3700	0.3700	0.4700	0.4799	600	600.081	39.6200	39.6268

Table 4.73: SASOME Nelder-Mead statistical analysis.

S/n	Response	Variance	R^2
1	BTE	1.17524×10^{-6}	0.99347
2	BSFC	1.7828×10^{-9}	0.99569
3	CO	1.86692×10^{-9}	0.99432
4	NOx	8.67484×10^{-3}	0.99176
5	HC	17.01647×10^{-5}	0.99765

Table: 4.74: Nelder-Mead optimized conditions for SASOME combustion.

Responses	Optimized values	Experimental values	Optimum conditions		
			Load(Nm)	Fuel blend(vol.%)	Speed(rpm)
BTE (%)	33.5075	36.50	5	78.95	1465.5
BSFC(kg/kW-hr)	0.1573	0.1453	10	26	2500
CO (%vol.)	0.0399	0.0303	10	40	2000
NOx(ppm)	170.259	168.58	10	39.43	2000
HC(ppm)	19.7062	20. 94	10	39.43	2000

Further more, combustion of the sweet almond seed oil biodiesel blends in Perkins 4:108 diesel engine was analyzed based on the various solutions obtained at possible engine conditions from the model predictive equations of Nelder-Mead algorithm. These equations were solved for the various interaction effects on the brake thermal efficiency of the engine, brake specific fuel consumption, and the exhaust emissions in form of carbon (ii) oxide, oxides of nitrogen and hydrocarbons at any point of the interaction between two factors: engine load and fuel blend only. The relationship between the variable and the responses can be presented on the graphical drawing, placing the experimental levels of each variable on the one side and the type of interactions between the test variables on the other hand which allows the deducing of the optimum conditions.

Figure 4.64 to 4.68 show the 3-dimensional surface plots for the responses under viable optimum conditions. The line graph helps to determine the relationships between two sets of values, with one data set always being dependent on the other set. The other variables were set at their mean value of zero (0). Every significant effect on the responses and the combined effects were monitored using 3D surface plots. Studying the fuel blend and engine load is critical on the determination of brake thermal efficiency of diesel engine. Normally, the brake thermal efficiency of a diesel engine increases with increase in biodiesel in the fuel blend. This phenomenon which is due to the lubricating effect of the biodiesel and its oxygen content which promotes efficient combustion are observed at fuel blends beyond 60% content of biodiesel in the blend. Irrespective of the amount of African pear seed oil biodiesel in the blend, the higher loads content promoted high brake thermal efficiency of the Perkins 4:108 CI diesel engine. It became obvious that the fuel blend has more significant effect on the brake thermal efficiency than the load within the range studied. Figure 4.64 shows the effect of load (x) and fuel blend (y) on the brake thermal efficiency while keeping the speed constant at 3000rpm. The quadratic effect of engine fuel blend is observed with clear smooth curves on reference surface plots. The response is maximized at lowest engine loads when the amount of sweet almond oil biodiesel in the blend is high and engine torque is low. It shows that high amount of biodiesel promotes efficient combustion due to its high oxygen content. Figure 4.65 shows the observed interaction of the effect of load (x) and fuel blend (y) on the brake specific fuel consumption while keeping the speed constant at 3000rpm. The quadratic effect of engine fuel blend is observed with smooth curves on reference surface plots. The response is maximized at lowest engine loads when the amount of sweet almond oil biodiesel in the blend is high. It is observed that increasing the fuel blend from 60% vol. resulted in high brake specific fuel consumption at lower engine loads. The minimum value BSFC obtainable at about 25 Nm load and minimum fuel blend (20%vol.). It implies that decrease in the amount of sweet

almond biodiesel in the blend and at maximum engine torque would minimize the brake specific fuel consumption of the diesel engine. The effect of fuel blend is found to be stronger than load on BSFC. Fig. 4.66 displays the interactive effect of load (x) and fuel blend (y) on the response of percentage CO emission while keeping the speed constant at 3000rpm. The lowest CO emission was obtained around 5Nm load and exteme fuel blends (highest and lowest values). This is due to the strong effects of fuel blend quadratic terms. It could be observed that the optimum CO emission is obtainable at about 70%vol. blend of sweet almond seed oil with petro-diesel. The highest emission was obtained at 25Nm load and 80% biodiesel-petrodiesel blend. But at very high fuel blends towards 100% biodiesel blend and highest load considered (25Nm), the emission increased. Figure 4.67 shows the effect of load (x) and fuel blend (y) on the NOx emission while keeping the speed constant at centre point. The result shares similarity with the one obtained in the case of CO emission, but the combined effects the two factors are more significant on CO emission than on NOx emission. Also, it is observed that increase in the torque units and fuel blend increases the NOx emission. This result is expected since these combined conditions icreases the oxygen content and temperature of engine combustion which translates to high NOx formation. Figure 4.68 shows the effect of load (x) and fuel blend (y) on the HC emission while keeping the speed constant at 3000rpm. The result follows the same trend with the one obtained in the case of CO emission. The quadratic effect of both engine load and fuel blend are observed with clear smooth curves on reference surface plots, showing their strong effects on the HC emissions from the diesel engine. The presence of oxygen in the sweet almond seed oil biodiesel supports combustion and consequently, HC emission reduced gradually as the amount of biodiesel increases in the blends. But as the engine loads increase, more especially at high biodiesel concentrations beyond 70% vol. the impacts of viscosity increase the emission levels of the blends.

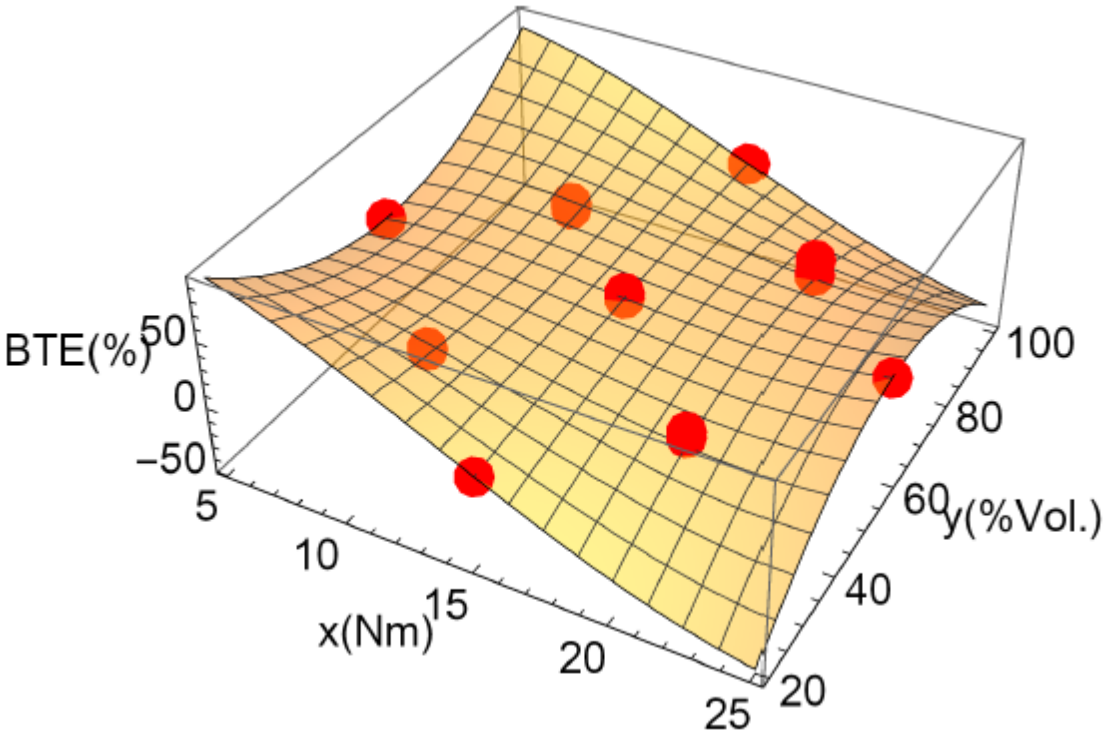

Figure 4.64: Response surface plots for fuel blend and load interaction on SASOME brake thermal efficency based on Nelder-Mead.

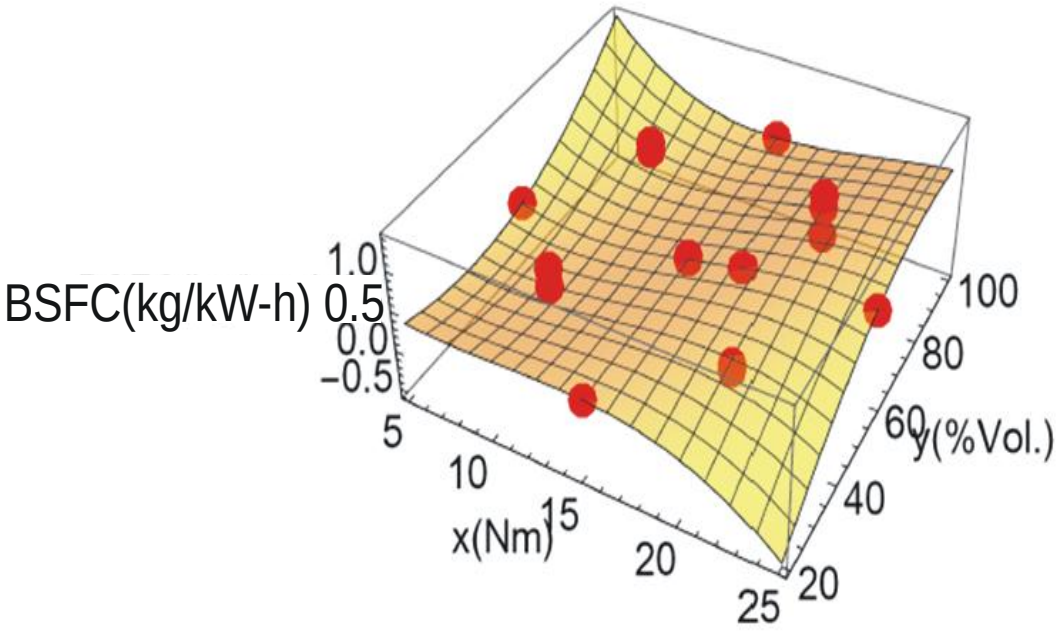

Figure 4.65: Response surface plots for fuel blend and load interaction on APSOME brake specific fuel consumption based on Nelder-Mead.

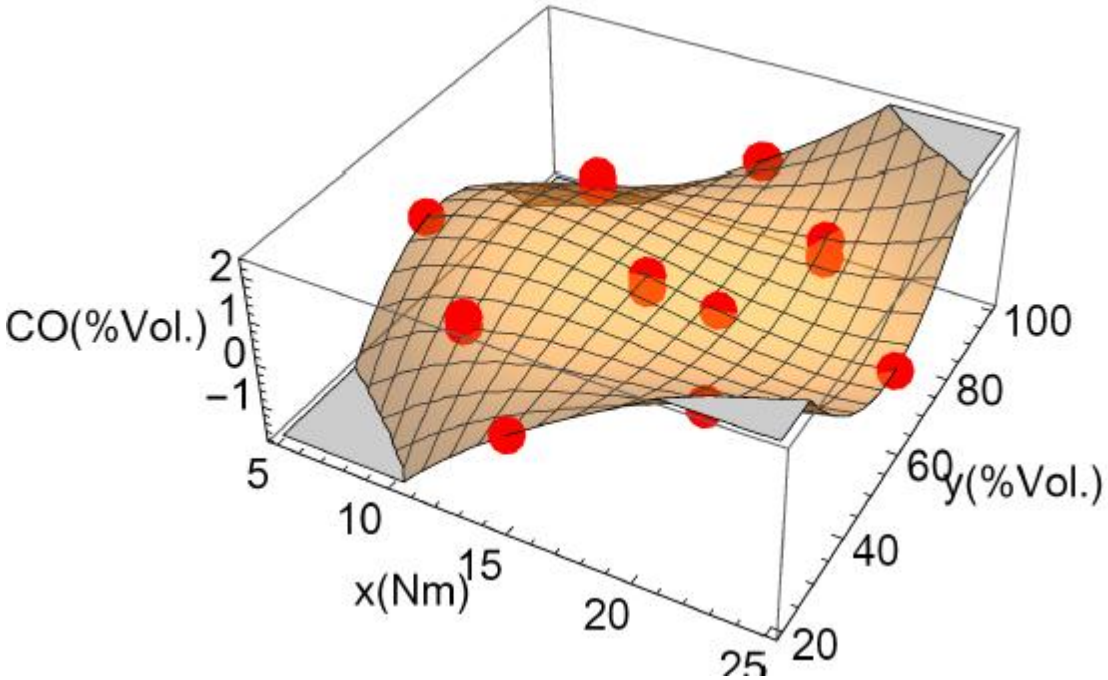

Figure 4.66: Response surface plots for fuel blend and load interaction on SASOME CO emission based on Nelder-Mead

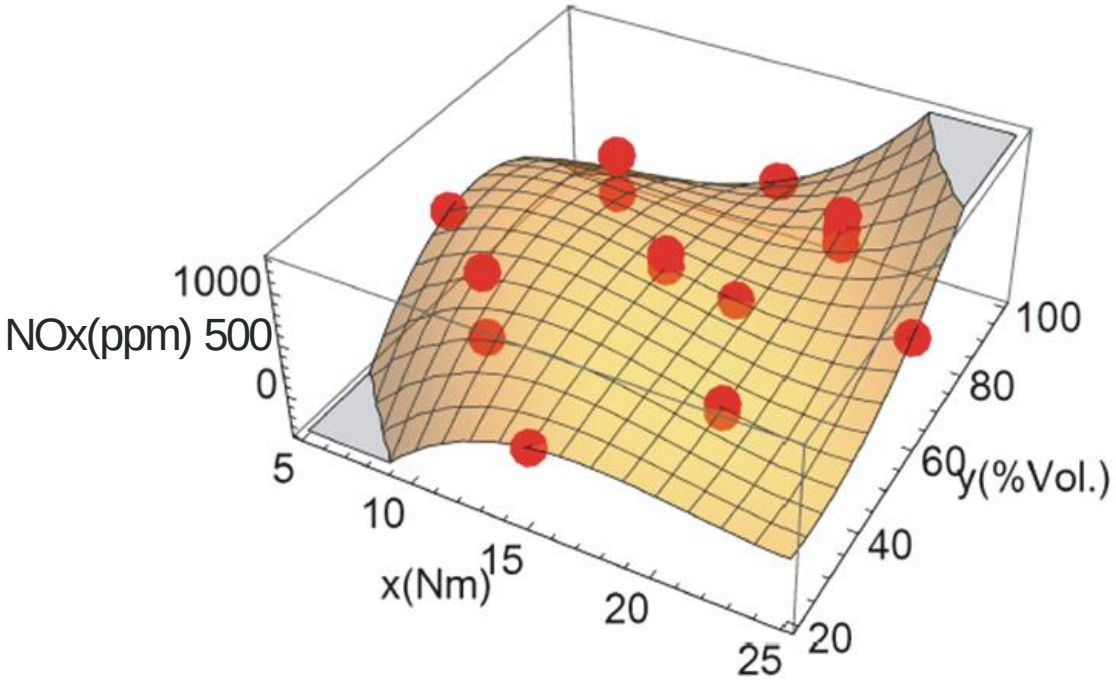

Figure 4.67: Response surface plots for fuel blend and load interaction on SASOME NOx emission based on Nelder-Mead

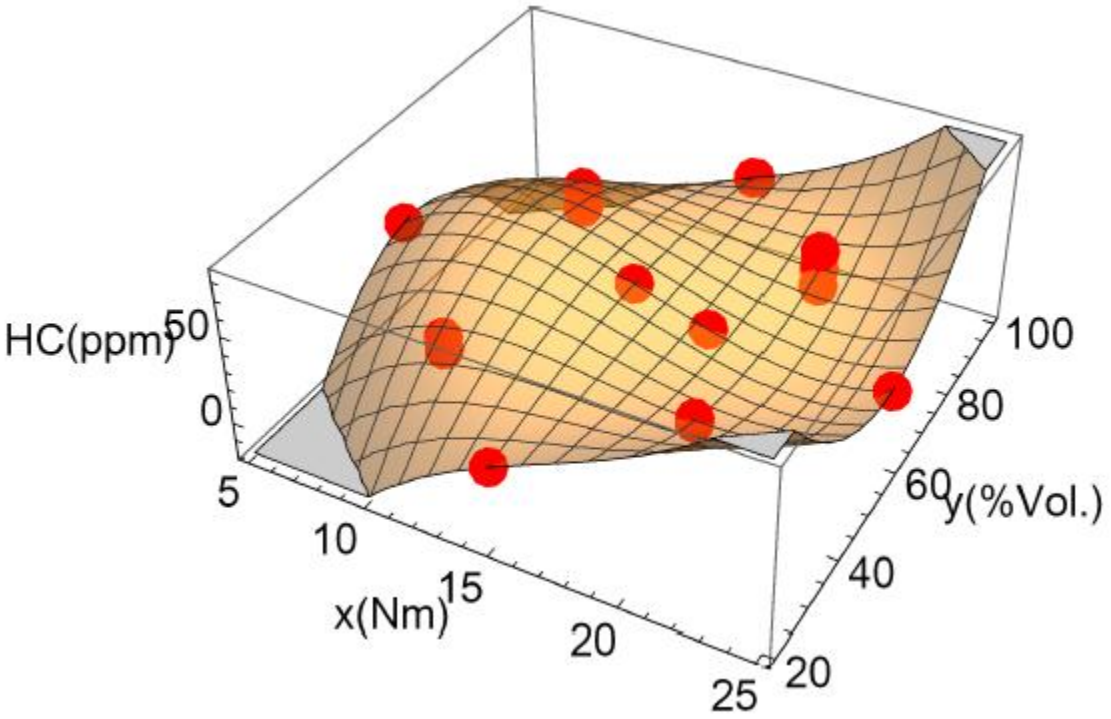

Figure 4.68: Response surface plots for fuel blend and load interaction on SASOME HC emission based on Nelder-Mead.

4.8.6.2 APSOME optimization using Nelder-Mead technique

Fitted model equations for the APSOME responses based on Nelder-Mead simplex approach are given by Equations (4.55-4.59). The experimental values and the corresponding predicted values are presented in Table 4.75. It is the ratio of the standard error of estimate to the mean value of the observed response as a measure of reproducibility of the model. From the result, the R^2 of all the responses are all above 0.99 as an indication of excellent correlation between the experimental and the predicted values from the model (Table 4.76). Also, the proper balancing of the points on the 3D surface plots (Figures 4.69-4.73) supports better correlation of the predicted values with the experimental than obtained from other methods applied in this study. The optimized criteria are presented in Table 4.77.

$$BTE\ (X,Y,Z) = -680.343 + Y(13.3959 - 0.104918Y - 0.00111675Z) + (0.13575 + 7.18\,x10^{-6}Z)Z + X(63.8257 + Y(-0.649368 + 0.00656973Y + 0.00005785Z) + X(-1.62829 + 0.0234786X - 0.009165Y + 0.0004112Z) + (-0.015334 - 3.6x10^{-7}\mathrm{Z})\mathrm{Z}) \quad (4.55)$$

$$BSFC(X,Y,Z) = 1.24441 + Y(-0.0574896 + 0.0000484547Y + 0.000046425Z) + (-0.002788 + 2.68\,x10^{-7}Z)Z + X(0.75222 + Y(-0.00394486 + 4.0522x10^{-8}Y - 2.3225x10^{-6}Z) + X(-0.0419247 + 0.0000972161X - 0.00033975Y + 5.97x10^{-6}Z) + (0.0000165 - 1.34x10^{-8}Z)Z) \quad (4.56)$$

$$CO(X,Y,Z) = -18.5164 + Y(0.0847986 + 0.000951655Y + 2.1x10^{-7}Z) + (-0.013098 - 2.82x10^{-6}\,Z)Z + X(0.870891 + Y(-0.00272074 + 0.0000540687Y + 1.075x10^{-7}Z) + X(0.870891 + X(-0.00903648 + 0.000792033X - 0.00014675Y + 7.69x10^{-6}Z) + (-0.0005181 + 1.41x10^{-7}Z)Z) \quad (4.57)$$

$$NOx(X,Y,Z) = -20872.9 + Y(336.782 - 2.66694Y + 0.0029Z) + (8.848 - 0.002052Z)Z + X(1249.74 + X(-23.381 + 0.73391X + 0.11475Y - 0.00715Z) + Y(-20.9555 + 0.165171Y - 0.0008525Z) + (-0.2678 + 0.0001026Z)Z) \quad (4.58)$$

$$HC(X,Y,Z) = -611.046 + Y(9.68615 - 0.0551429Y - 0.000989Z) + (0.27367 - 0.00005772Z)Z + X(37.0296 + X(-0.775187 + 0.0318097X + 0.0010075Y - 0.0003363Z) + Y(-0.587743 + 0.00331057Y + 0.00005257Z) + (-0.00699 + 2.885x10^{-6}Z)Z) \quad (4.59)$$

Table 4.75: Experimental and Nelder-Mead predicted values of APSOME combustion responses.

Run	Factors			Responses									
				BTE(%)		BSFC(kg/kW-hr)		CO(%vol.)		NOx(ppm)		HC(ppm)	
	X(Nm)	Y(%vol.)	Z(rpm)	Exp. Value	Pred. Value	Exp. Value	Pred. Value	Exp. Value	Pred. Value	Exp. Value	Pred. Value	Exp. Value	Pred. Value
1	10	40	2000	13.5600	13.47	0.5710	0.575	0.0500	0.055	300	305	22.4000	22.55
2	10	80	3000	20.0400	19.98	0.6430	0.639	0.4000	0.421	400	403	24.6700	24.70
3	20	40	3000	30.0500	30.67	0.1430	0.144	0.1880	0.192	400	403	30.4000	30.55
4	20	80	2000	35.0000	34.96	0.4290	0.430	0.1880	0.192	800	799	20.1500	19.99
5	15	60	2500	32.0000	32.10	0.3500	0.360	0.4800	0.475	670	677	35.9400	36.05
6	15	60	2500	32.0000	32.10	0.3500	0.360	0.4800	0.475	670	677	35.9400	36.05
7	10	40	3000	33.4600	33.55	0.1430	0.144	0.2750	0.280	400	406	29.6600	30.04
8	10	80	2000	21.6700	20.89	0.1430	0.145	0.0480	0.050	525	531	35.9400	35.45
9	20	40	2000	34.9900	34.49	0.2140	0.215	0.3580	0.360	344	350	28.6600	29.00
10	20	80	3000	31.6700	30.87	0.3570	0.359	0.1880	0.192	300	305	24.4000	24.50
11	15	60	2500	32.0000	32.10	0.3500	0.360	0.4800	0.475	670	677	35.9400	36.05
12	15	60	2500	32.0000	32.10	0.3500	0.360	0.4800	0.475	670	677	35.9400	36.05
13	5	60	2500	19.6600	20.05	0.1090	0.110	0.2750	0.281	850	855	22.4000	25.05
14	25	60	2500	25.6100	25.72	0.1430	0.144	0.4000	0.430	221	230	24.6700	23.97
15	15	20	2500	13.5600	13.45	0.6430	0.648	0.1200	0.121	334	335	29.6600	30.04
16	15	100	2500	30.0500	29.91	0.2140	0.215	0.3900	0.400	400	409	24.6700	25.00
17	15	60	1500	21.6700	21.55	0.1430	0.145	0.4000	0.425	334	345	38.7000	37.98
18	15	60	3500	26.0000	26.18	0.2500	0.270	0.0690	0.070	221	237	30.4000	30.58
19	15	60	2500	32.0000	32.10	0.3500	0.360	0.4800	0.475	670	677	35.9400	36.05
20	15	60	2500	32.0000	32.10	0.3500	0.360	0.4800	0.475	670	677	35.9400	36.05

Table 4.76: APSOME Nelder-Mead statistical analysis.

S/n	Response	Variance	R^2
1	BTE	4.4656×10^{-6}	0.99347
2	BSFC	9.18061×10^{-11}	0.99651
3	CO	2.37532×10^{-11}	0.99342
4	NOx	3.97798×10^{-4}	0.99651
5	HC	1.47744×10^{-7}	0.99432

Table: 4.77: Nelder-Mead optimized conditions for APSOME combustion.

Responses	Optimized values	Experimental values	Optimum conditions		
			Load (Nm)	Fuel blend (vol.%)	Speed (rpm)
BTE (%)	34.963	42.010	10	69.587	980
BSFC(Kg/kW-hr)	0.1096	0.0502	20	5	2650
CO (% vol.)	0.0500	0.0450	10	40	2000
NOx(ppm)	220.973	232.05	10	38.35	2000
HC(ppm)	20.1524	20.534	10	38.215	2000

The combustion of the African pear seed oil biodiesel blends in Perkins 4:108 diesel engine was analyzed based on the various solutions obtained at possible engine conditions from the model predictive equations of Nelder-Mead. These equations were solved for the various interaction effects on the brake thermal efficiency of the engine, brake specific fuel consumption, and the exhaust emissions in form of carbon (ii) oxide, oxides of nitrogen and hydrocarbons at any point of the interaction between two factors: engine load and fuel blend only. The relationship between the variable and the responses can be presented on the graphical drawing, placing the experimental levels of each variable on the one side and the type of interactions between the test variables on the other hand which allows the deducing of the optimum conditions. Figs 6a-6e show the 3-dimensional surface plots for the responses under viable optimum conditions. The line graph helps to determine the relationships between two sets of values, with one data set always being dependent on the other set. The other variables were set at their mean value of zero (0). Every significant effect on the responses and the combined effects were monitored using 3D surface plots (Figures 4.69-4.73). Studying the fuel blend and engine load is critical on the determination of brake thermal efficiency of diesel engine. Normally, the brake thermal efficiency of a diesel engine increases with increase in biodiesel in the fuel blend. This phenomenon which is due to the lubricating effect of the biodiesel and its oxygen content which promotes efficient combustion are observed at fuel blends beyond 60% content of biodiesel in the blend. Irrespective of the amount of African pear seed oil biodiesel in the blend, the higher loads content promoted high brake thermal efficiency of the Perkins 4:108 CI diesel engine. It became obvious that the fuel blend has more significant effect on the brake thermal efficiency than the load within the range studied. Figure 4.69 shows the effect of load (x) and fuel blend (y) on the brake thermal efficiency while keeping the speed constant at 3000rpm. The lowest thermal efficiency was obtained around 10Nm load and 70% biodiesel-petrodiesel blend. Figure 4.70 shows the observed interaction of the effect of load

(x) and fuel blend (y) on the brake specific fuel consumption while keeping the speed constant at 3000rpm. The quadratic effect of engine load is observed with clear smooth curves on reference surface contours. The response is minimized at lowest and extreme high engine loads when the amount of African pear oil biodiesel in the blend is low. At these extreme conditions of loads, increasing the fuel blend from 40% vol. up to 100% vol. resulted in high brake specific fuel consumption. However, at the average loads units considered (between 10-15Nm), the brake specific fuel consumption was highest at minimal amount of biodiesel in the fuel blend (below 40% vol.). The lowest BSFC was obtained at about 15 Nm load irrespective of the fuel blend. The effect of load is stronger than that of fuel blend. Figure 4.71 displays the interactive effect of load (x) and fuel blend (y) on the response of percentage CO emission while keeping the speed constant at 3000rpm. The lowest CO emission was obtained around 5Nm load and irrespective of the biodiesel-petrodiesel blend. The highest emission was obtained at 25Nm load and 80% biodiesel-petrodiesel blend. A very interesting result is recorded in which a minimal amount of carbon monoxide is emitted at low factors and average fuel blends with high engine load. But at very high fuel blends towards 100% biodiesel blend and highest load considered (25Nm), the emission increased. Figure 4.72 shows the effect of load (x) and fuel blend (y) on the NOx emission while keeping the speed constant at centre point. The result shares similarity with the one obtained in the case of CO emission. Figure 4.73 shows the effect of load (x) and fuel blend (y) on the HC emission while keeping the speed constant at 3000rpm. The result follows the same trend with the one obtained in the case of CO emission.

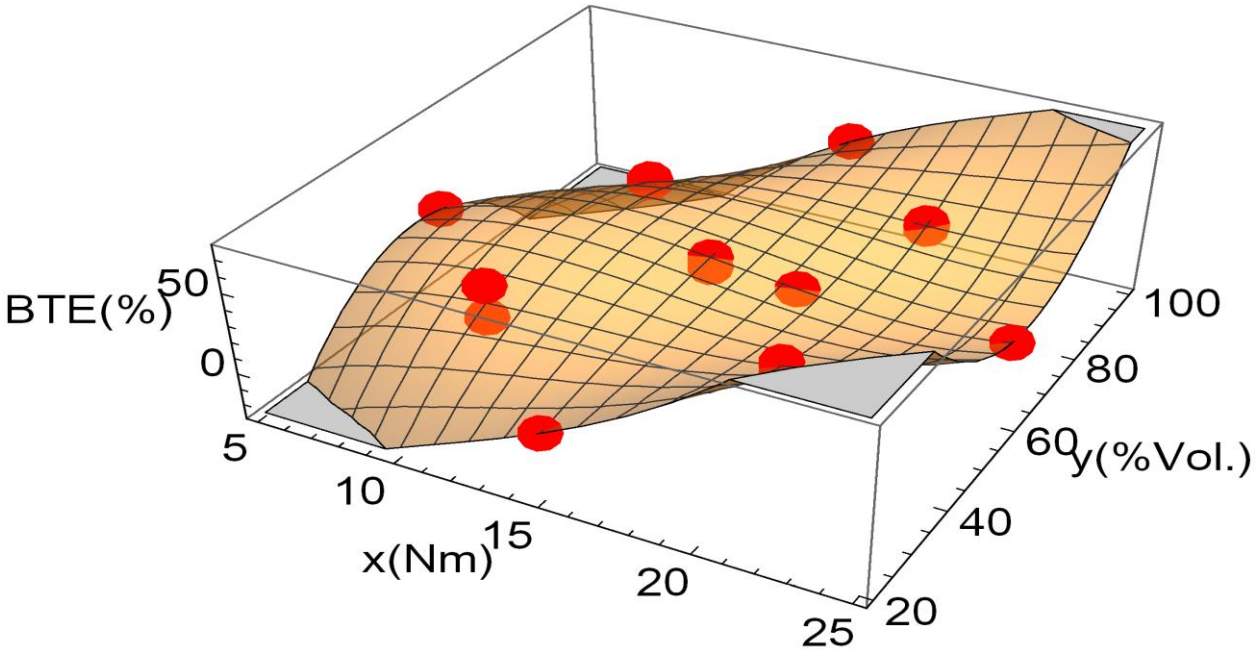

Figure 4.69: Response surface plots for fuel blend and load interaction on APSOME brake thermal efficiency based on Nelder- Mead.

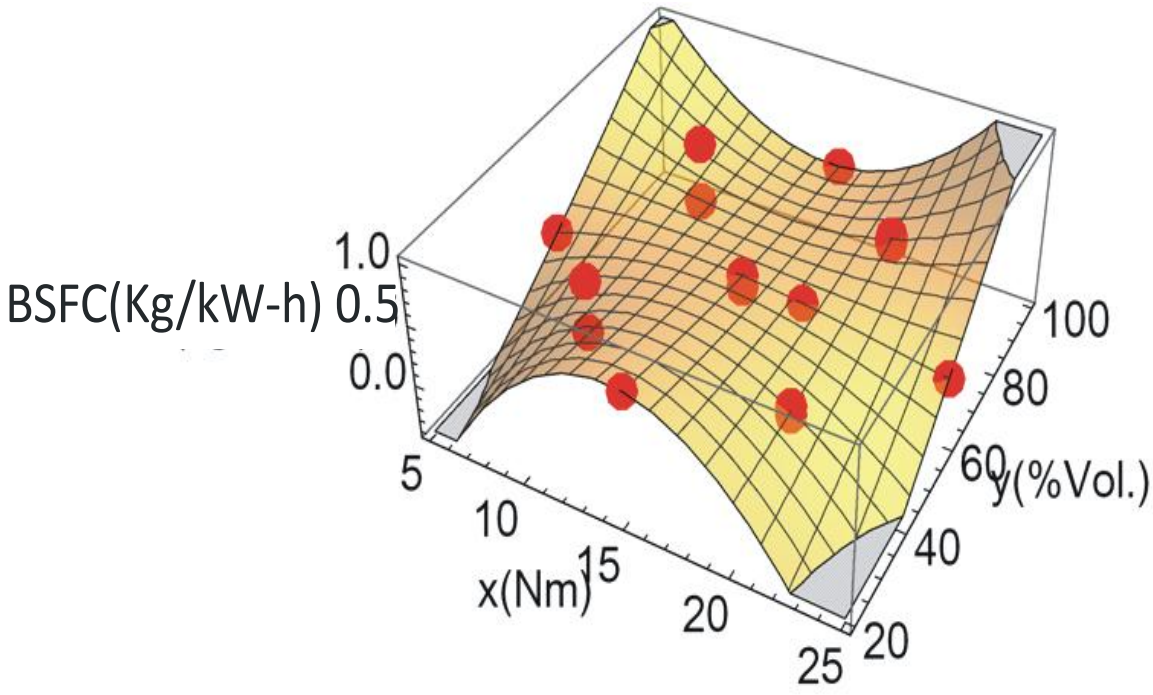

Figure 4.70: Response surface plots for fuel blend and load interaction on APSOME brake specific fuel consumption based on Nelder-Mead.

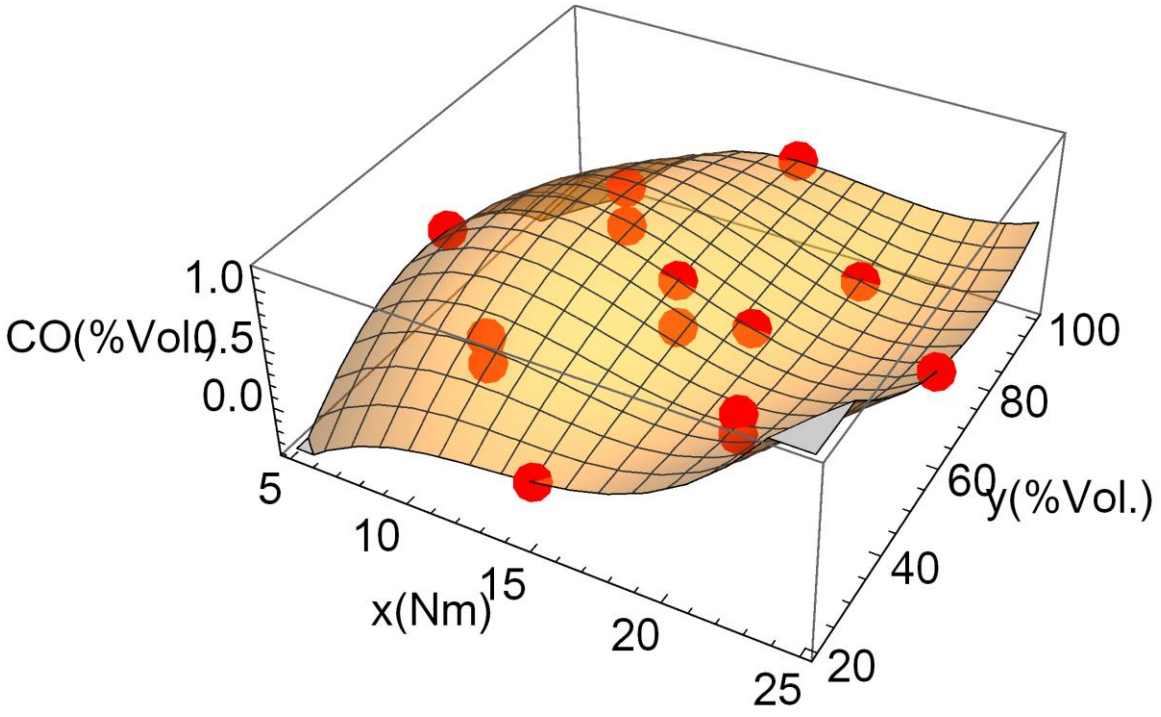

Figure 4.71: Response surface plot for fuel blend and load interaction on APSOME CO emission based on Nelder-Mead.

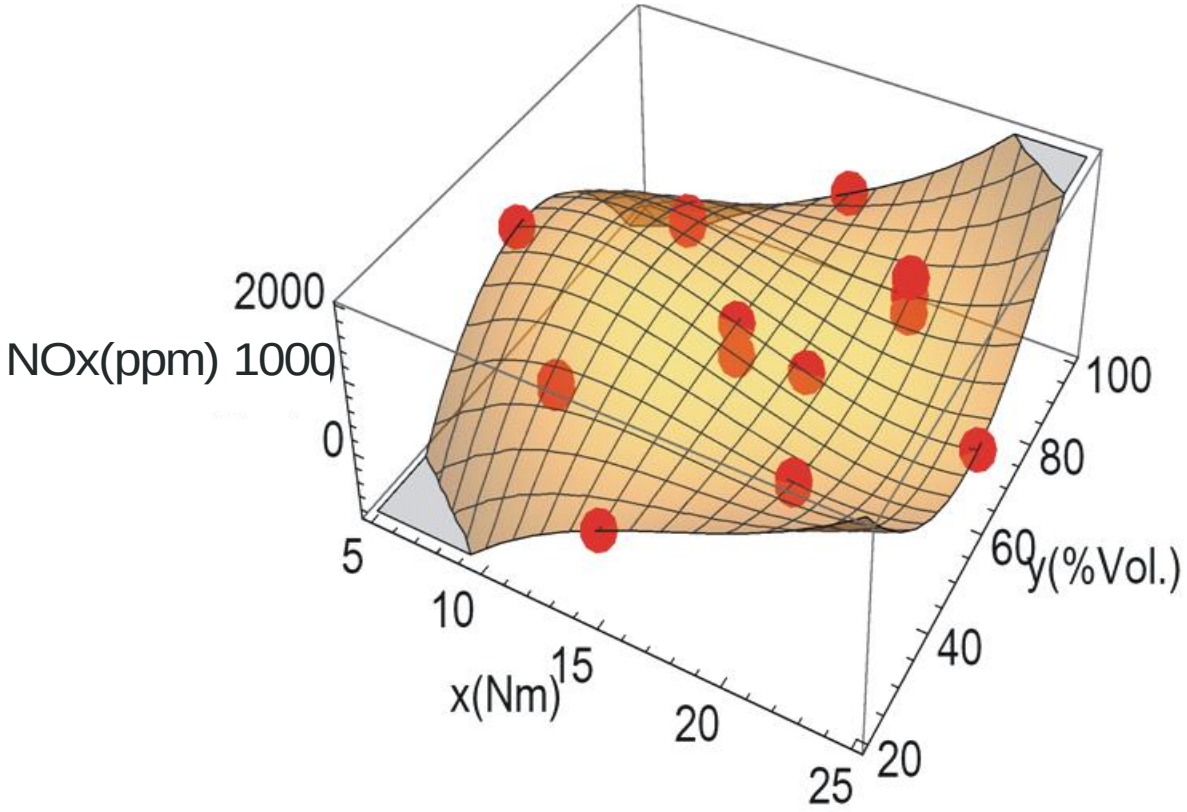

Figure 4.72: Response surface plots for fuel blends and load interaction on APSOME oxides of nitrogen emission based on Nelder-Mead.

.

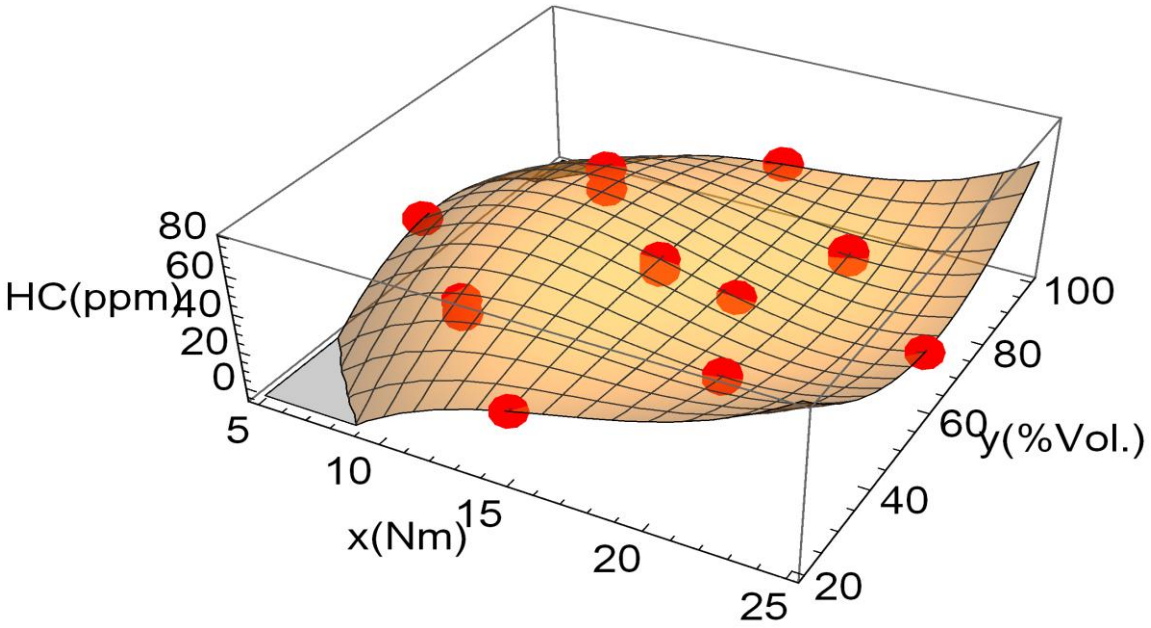

Figure 4.73: Response surface plots for fuel blend and load interaction on APSOME hydrocarbon emission based on Nelder-Mead.

4.9 Chemical Kinetics Result

The chemical kinetic study involves the esterification of the African pear seed oil (APSO), transesterification of the esterified APSO, sweet almond seed oil (SASO) and African star apple seed oil (ASASO). The effect of temperature on the rate of esterification (FFA reduction) and transesterification were determined at 55, 60 and 65^{o}C.

4.9.1 Esterification chemical kinetics modeling

The graphical representation of the esterification reaction compositions are shown in Figures 4.74-4.76. It was observed that the rate of change of the concentration followed a power regression model with high correlation coefficients ($0.80<R^2$). From Figure 4.77, there is no clear difference on the rate of FFA reduction between 60 and 65 °C. But considering 55 °C and other temperatures, moving from 55 °C up to 60 °C and 65 °C showed a significant effect of temperature on the rate of FFA reduction in contrast to some literature reports (Jansri et al., 2011) for the same temperature ranges. With an initial 7.9 wt% FFA, after 2 min, up to 94.94 wt% reduction in FFA was achieved at all temperature while at 90 min., the FFA was reduced to about 0.2 wt%, 0.15 wt% and 0.13 wt% for 55, 60 and 65 °C respectively. This result appears improved compared to the result previously reported (Prateepchaukul *et al.,* 2007) where less than 2 wt% after 90 mins at 60 °C was reported and but this result is in closer agreement with other previous results (Freedman, *et al.,* 1986) where better than 92 % conversion of FFA within 5 min was obtained.

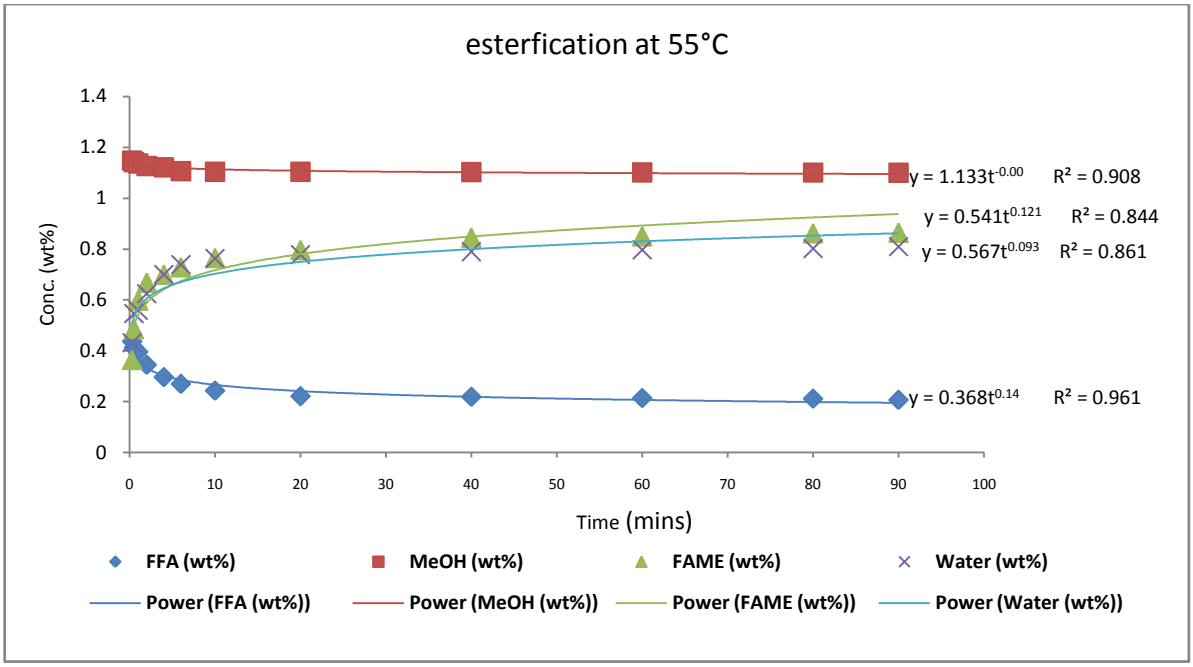

Figure 4.74: Composition of esterification reaction products at 55˚C.

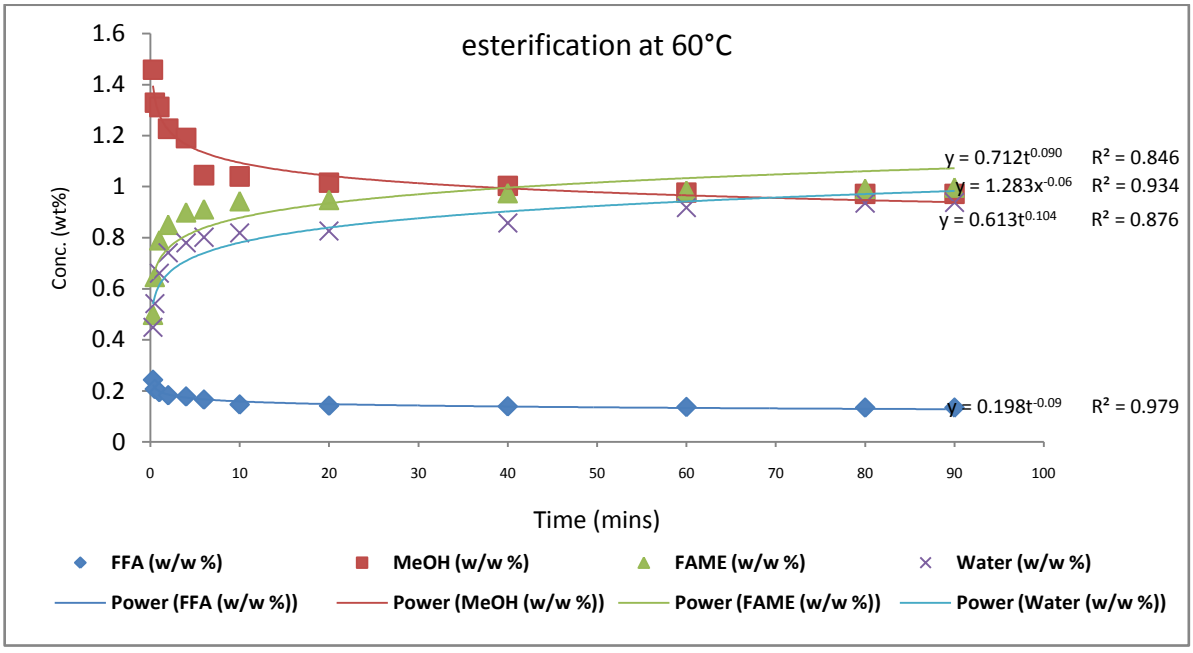

Figure 4.75: Composition of esterification reaction products at 60˚C.

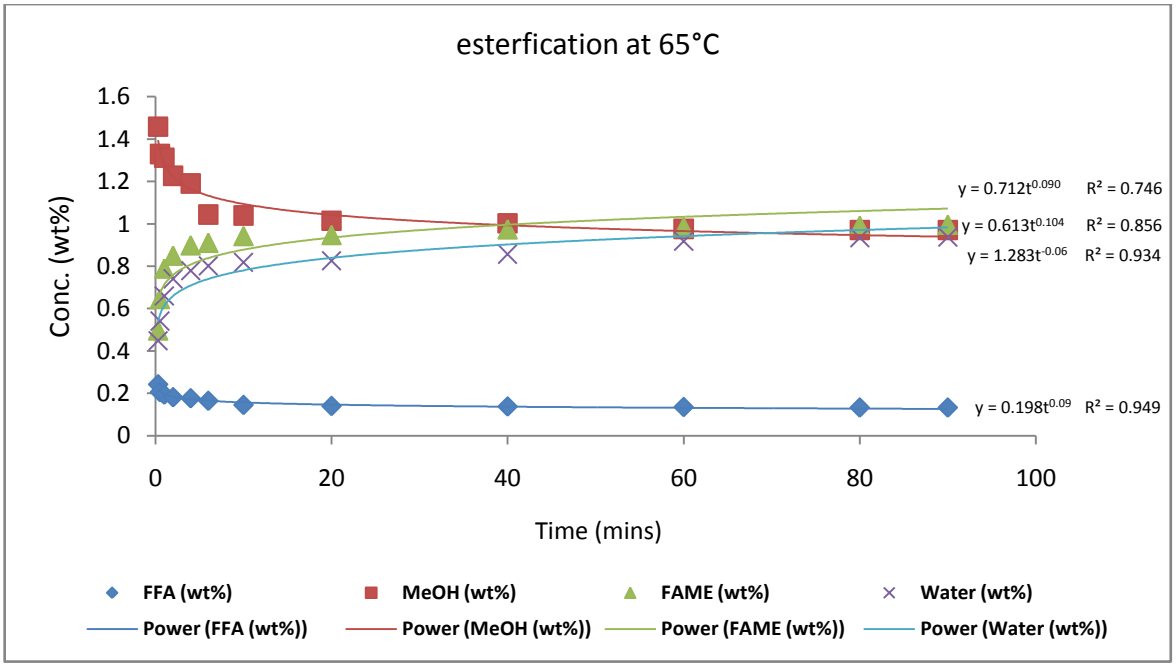

Figure 4.76: Composition of esterification reaction products at 65˚C.

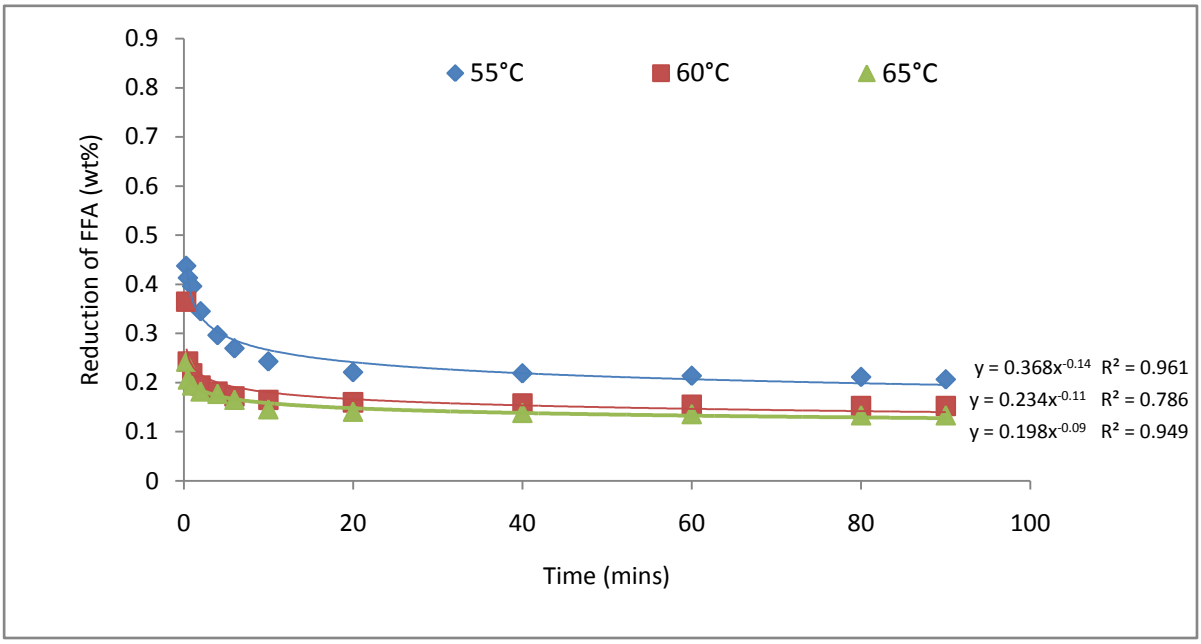

Figure 4.77: The effect of reaction temperature on FFA reduction.

The best-fit values of the rate constants were used for obtaining approximate activation energy for the reversible reaction process of the esterification by looking for a linear regression relationship between the logarithm of the rate constants and the inverse of the absolute temperature with high values of R^2 for both forward and backward reactions (Figure.4.78). The slopes were used for estimating activation energies using Arrhenius equation and the results are contained in Table 4.78. The results are similar to those previously reported (Gomez-Castro, et al., 2011). The activation energy of the forward esterification reaction was higher than the reverse reaction which indicates that the formation of FFA through the backward reaction requires lesser energy. This means that the APSO esterification would be favoured by higher temperature within the range studied. Also, for more effective conversion of the FFA in the APSO into FAME and water, water could be removed from the product stream instantly so as to favour the forward reaction.

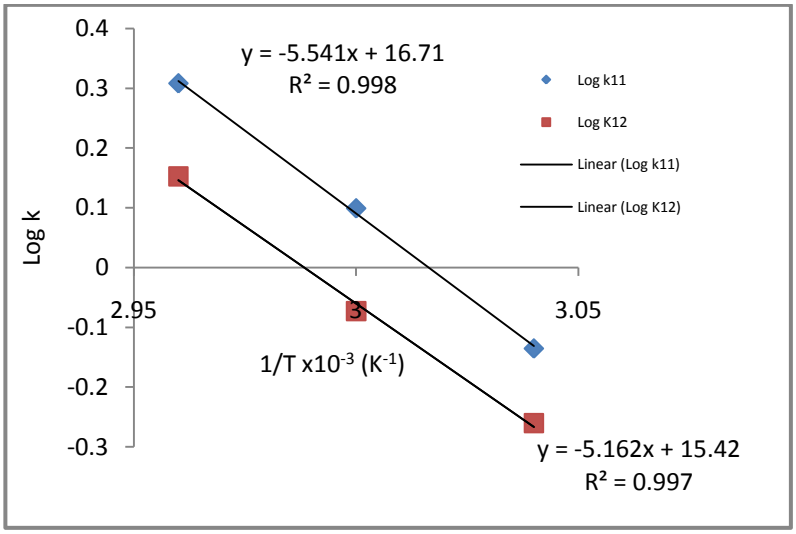

Figure 4.78: Plot of log k vs 1/T APSO esterification reversible models.

Table 4.78: Summary of esterification rate constants (L/g.min) and activation energy values for reversible model.

Temperature (°C)	k_{11}	k_{12}
55	0.732	0.5490
60	1.255	0.8450
65	2.031	1.4210
E_a(kJ/mol.)		
FFA-Wt	106.09	-
Wt – FFA	-	98.79
R^2	0.998	0.997

4.9.2 Transesterification kinetics results

The reaction rate constants and activation energies for triglycerides (Tg), diglycerides (Dg) and monoglycerides (Mg) hydrolysis were ascertained on the basis of both reversible and irreversible second-order consecutive reaction mechanisms.

Figures 4.79, 4.80 and 4.81 show the progress of the transesterification reaction of sweet almond seed oil, African pear seed oil and African star apple seed oils for reaction temperatures of 55°C, 60°Cand 65°C. The values of the Tg, Dg, Mg, methyl esters and alcohol obtained are presented in Tables A7.1-A7.9. The catalyst concentration was 0.1wt % of NaOH and methanol/ oil ratio of 6:1 at mixing speed of 140rpm. The choice of the reaction conditions was based on the previous conditions studied for both reversible and irreversible mechanisms in the literature (Jansri et al., 2011, Darnoko and Cheryan, 2000). The initial stage of the reaction produced fatty acid methyl esters (FAMEs) rapidly. The rate then reduced and finally reached almost equilibrium in about 80 minutes for all the temperatures for the three seed oils. The Dg and Mg contents were minimal (< 2.89wt %), while the amounts of Tg were above 94 %. This

result is similar to that reported on mahua oil (92-93wt% of Tg) and in contrast to that reported on pongamia oil, in which Tg, Dg, and Mg were found to be the weight ratio of 42:26:11 respectively, (Kumar *et al.,* 2011).

It is observed that the glycerol concentration increased with increase in FAME but was not in relative proportion to that of FAME. This has been suspected to be due to the effects of the intermediate products (Dg and Mg) (Darnoko and Cheryan, 2000). Also, the triglycerides concentration reduced as the reaction progresses due to its conversion to ester. The Tg concentration after 60 minutes was less than 15% for all the seed oil methyl esters at all the temperatures. The highest concentration of Dg and Mg were observed in the first 2 minutes for SASO, APSO and ASASO, after which they started decreasing until after 80 minutes when they appeared at equilibrium. Similar results have been reported on palm oil transesterifican, in which the highest concentrations of Dg and Mg were observed in the first minute and reached equilibrium after 60 minutes (Darnoko and Cheryan, 2000). The higher duration observed in this study could be due to the variation in the seed oil compositions (since palm oil has different fatty acid composition from the seed oils reported in this study) or the different catalysts used.

The values of Tg were greater than Dg and Dg was greater than Mg values for all the temperature and for all the seed oils. It was observed that the higher the temperature, the lower the values of Tg, Dg and Mg for respective reaction times, but the higher the temperature, the higher the values of FAME. This could be probably because as the temperature moves from 55°C towards the 65°C, the closer it gets to the boiling point of methanol (68°C) (Darnoko and Cheryan, 2000). This condition gives better reaction condition for higher conversion of glycerides (Figure 4.82). It was clear that the difference in the concentrations of FAMEs within the studied temperature ranges was not significant at respective reaction times. This could be

due to the closer range of 10^{o} C reaction temperature. Therefore, it could be that other factors other than temperature, such as mixing intensity, concentration of reactants (catalyst and alcohol) had more effects on the seed oils' Tg conversion to methyl esters. However, closer look at the effect of the range of temperature studied on the rate of transesterification shows no initial lag period previously reported on soybean transesterification (Noureddini and Zhu, 1997). The possible reason for the absence of lag period is formation of methyl esters, which acted as a solvent for the reactants, and consequently, making the the reaction mixture a homogeneous single phase. This is obvious in the higher concentration of FAME achieved within the first few minutes of the reaction time. Also, mass transfer effects are known to dominate at lower temperatures (Kumar *et al.,* 2011).

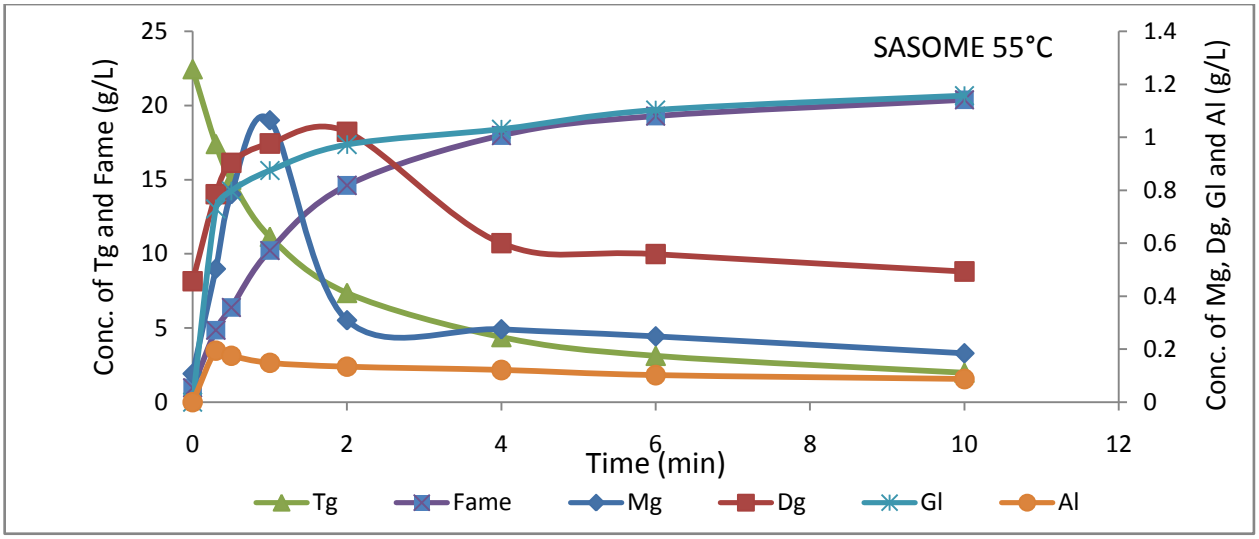

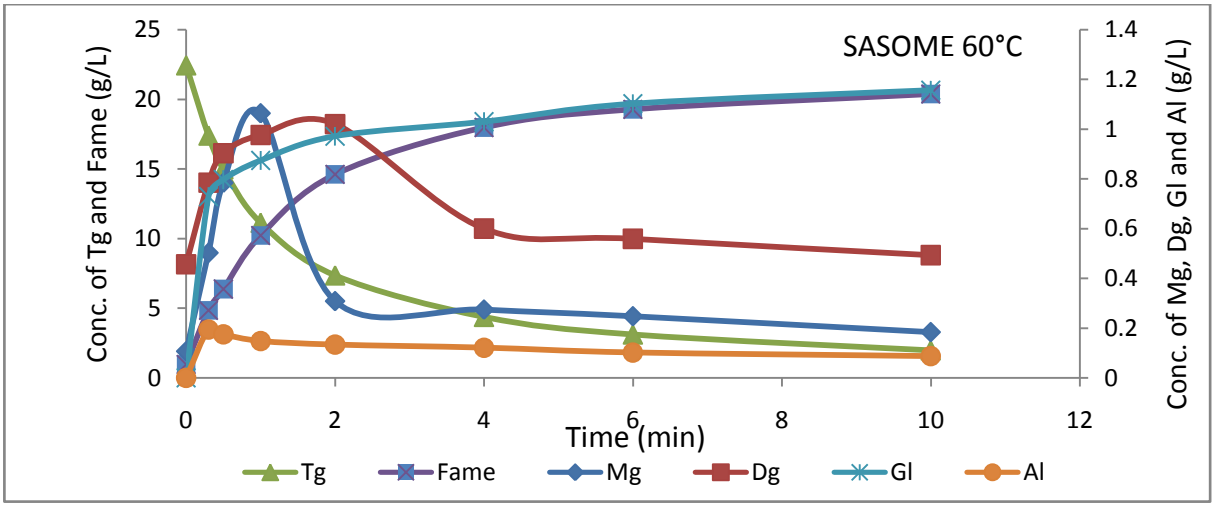

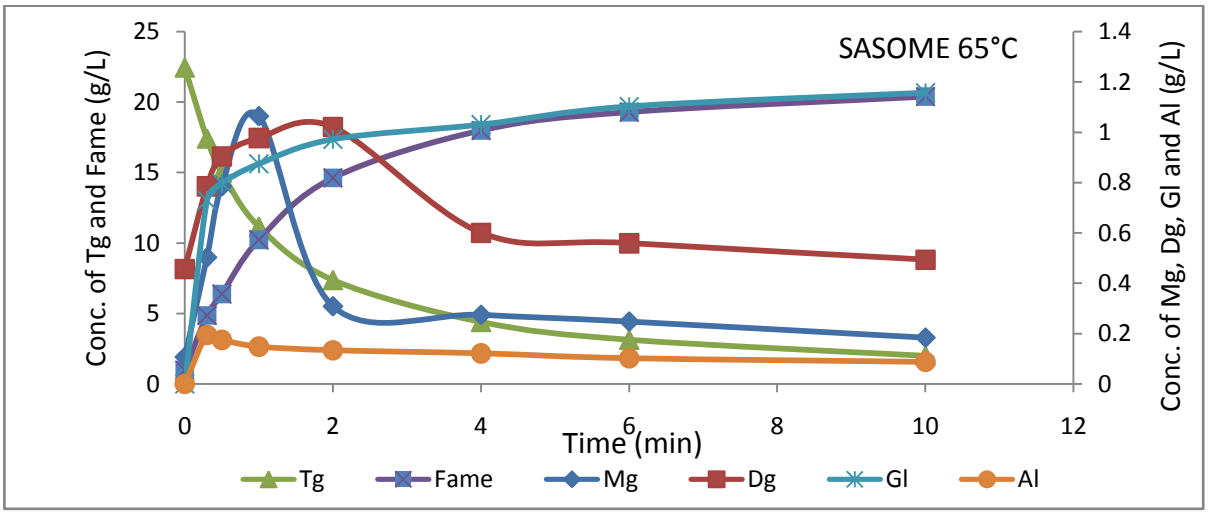

Figure 4.79: Composition of reaction products for SASOME at 55˚C, 60˚C and 65˚C.

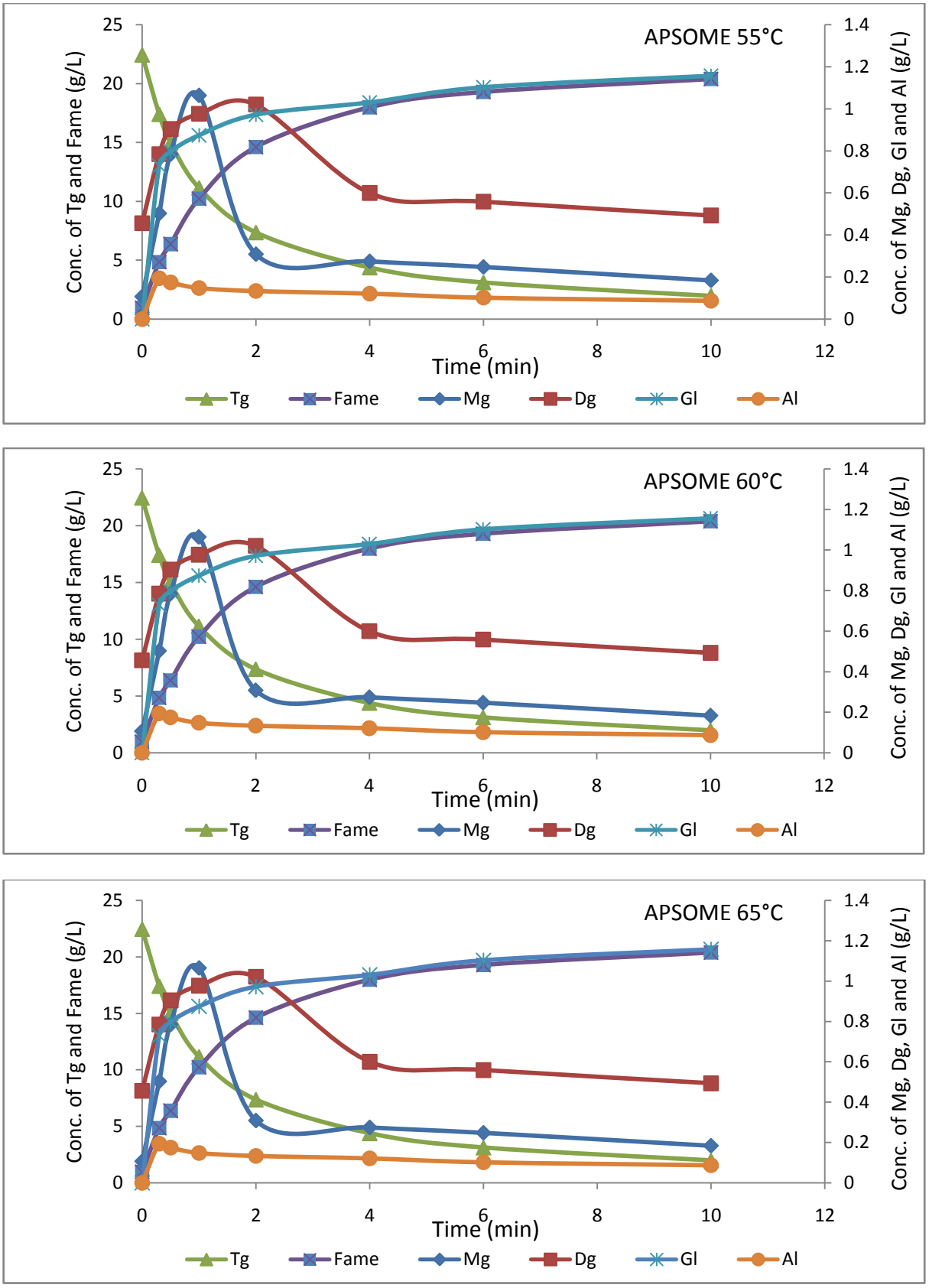

Figure 4.80: Composition of reaction products for APSOME at 55˚C, 60˚C and 65˚C.

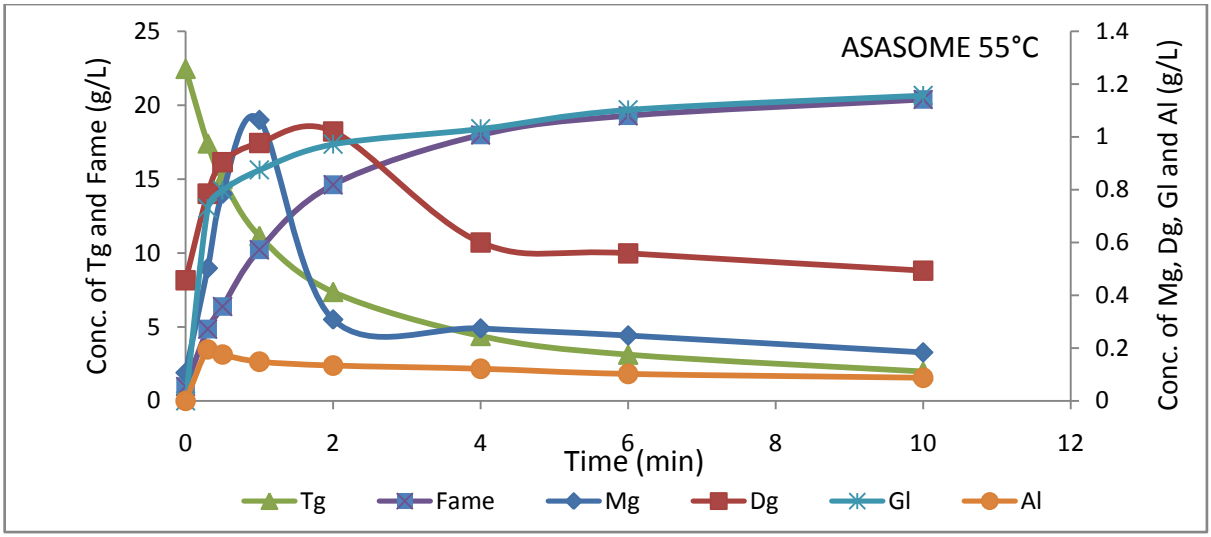

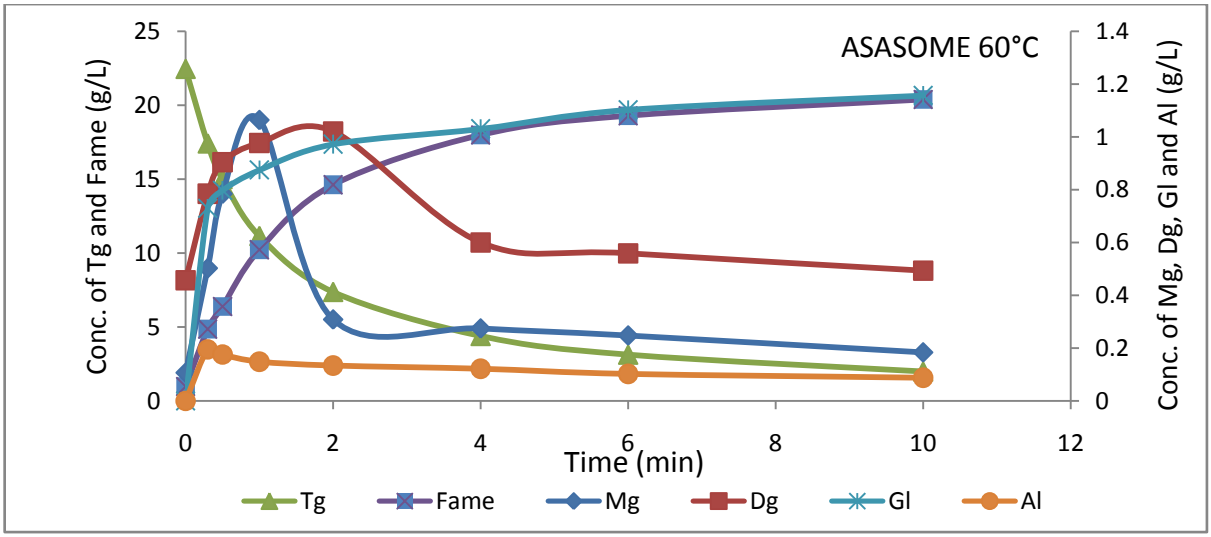

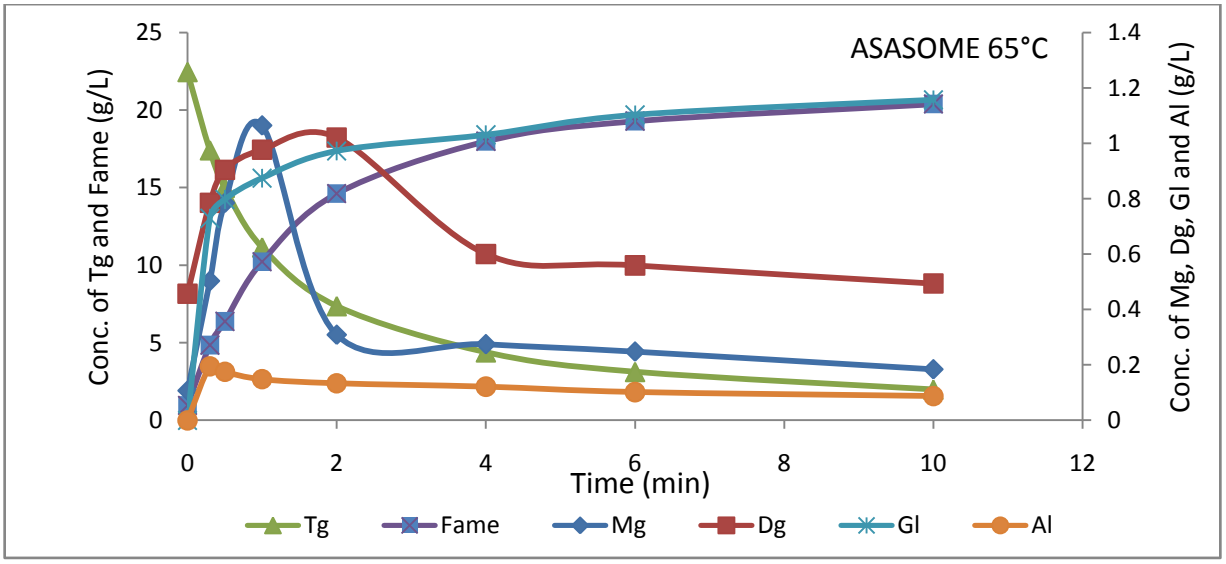

Figure 4.81: Composition of reaction products for ASASOME at 55˚C, 60˚C and 65˚C.

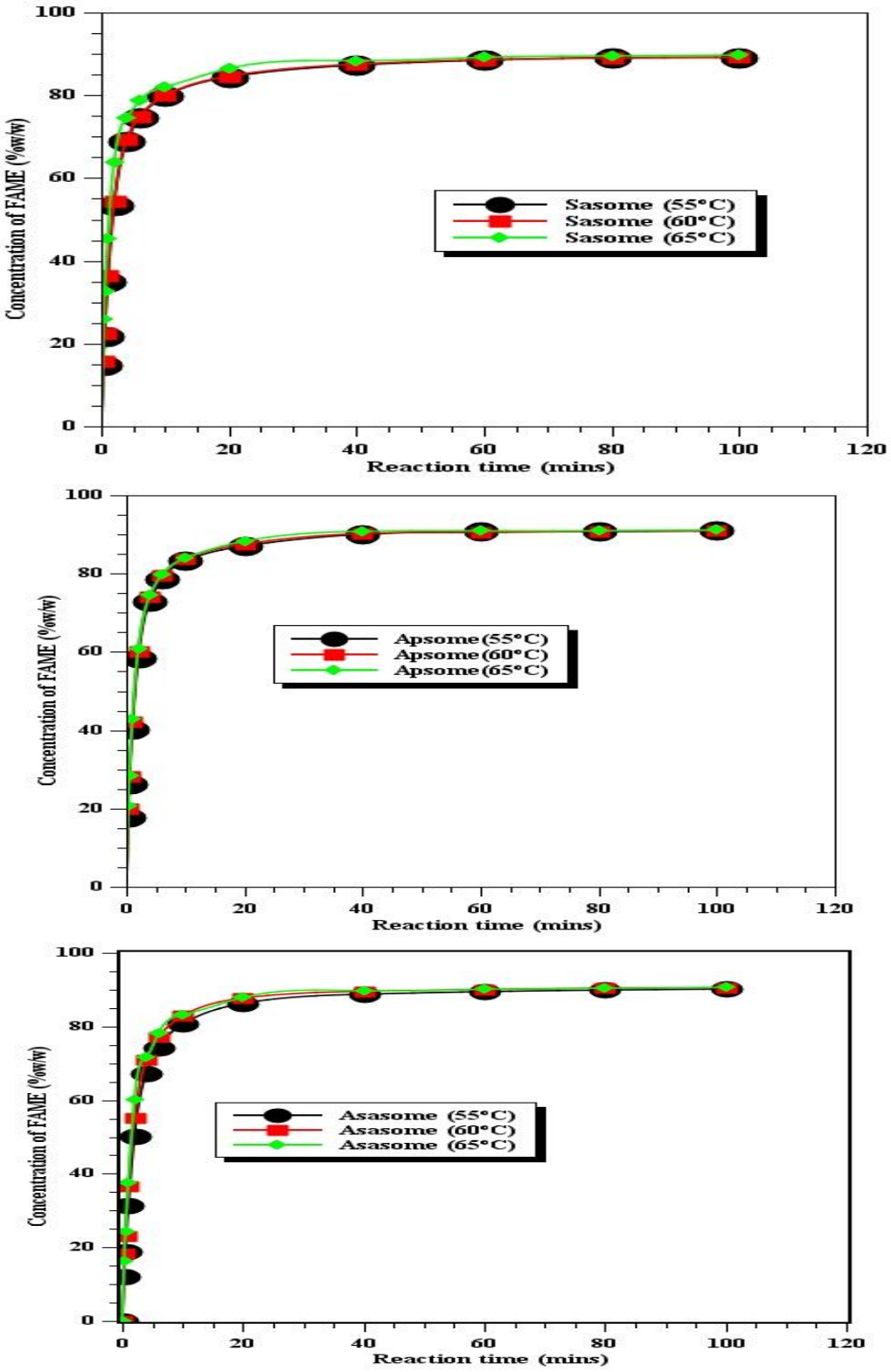

Figure 4.82: Effect of reaction temperature on the transesterification reaction for SASOME, APSOME and ASASOME

4.9.3 Effect of mixing on rate of reaction

Effect of mixing intensities or stirring rate on the hydrolysis of the seed oil is depicted in Figures 4.83, 4.84, 4.85 and Table A7.10. The choice of mixing rate was based on preliminary reports from the literature (Okullo and Temu, 2015). A constant high temperature of 60°C was considered. Transesterification without mixing occurs only at the interface of the two layers causing increase in the duration of reaction (Jansri *et al*., 2011). But increase in mixing intensity, helps to breake down the intermolecular forces, making the oil/methanol solution homogeneous without phase formation. In this study, increase in mixing rates (200, 400 and 800rpm) had significant effects the triglycerides conversion to methyl esters. The effect of mixing was more noticeable in APSO and ASASO conversion than that of SASO. Initially when the reaction rate was set at 140rpm and at 60°C, after 6 minutes reaction time, only about 74.91, 79.38 and 77.11wt% yield of methyl esters were obtained from SASO, APSO and ASASO conversions respectively but at 800rpm, 80.92, 90.21 and 90.31wt% were obtained for SASO, APSO, and ASASO respectively. The results obtained are similar to those of Noureddine and Zhu, (1997) and Okullo and Temu, (2015) with soybean and Jatropha feedstocks respectively, while the slight variations could be as a result of the difference in mixing intensities worked on. Nouriddine and Zhu, (1997) worked on 150, 300 and 600rpm while Okullo and Temu, (2015) worked on 600, 700 and 800rpm.

This shows that increase in mixing rate increased the rate of reaction by reducing the time required to achieve higher conversion of the Tg. However, it was observed that after 40 minutes reaction time, the difference in yield of methyl ester became less than 2wt% after 20 minutes. It means that the effect mixing intensity becomes quite unnecessary beyond 40 minutes. The reason could be that the methyl ester produced is soluble in oil and methanol, and could have acted as a co-solvent. This could have made the system homogenous and resulted in

only chemical-reaction-controlled kinetics beyond 40 minutes. No large differences were observed in Tg conversion to FAME between 400rpm and 800rpm in case of SASOME and between 200rpm and 400rpm for APSOME. Conversely, there was significant difference between the three mixing intensities for ASASOME up to 20 minutes reaction time. Also, 800rpm showed highest conversion among the three oil conversion all through the reaction time. No optimal mixing rate was detected as the highest mixing rate of 800rpm was the most favorable in the mixing range under investigation.

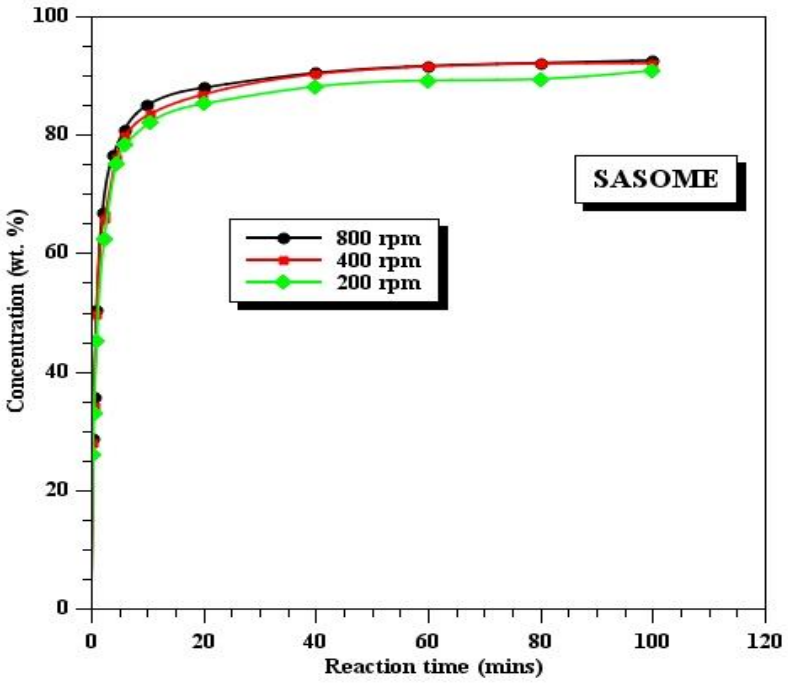

Figure 4.83: Effect of mixing on SASO triglyceride conversion.

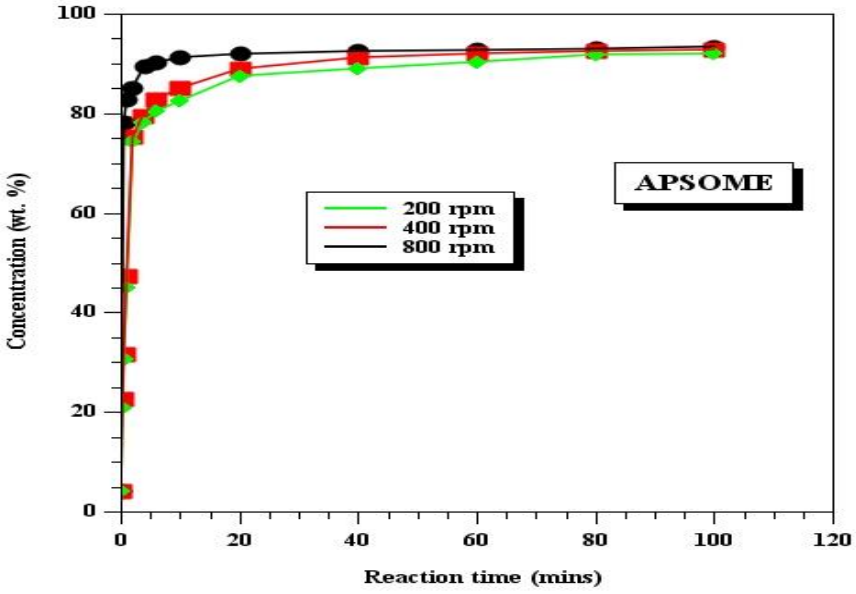

Figure 4.84: Effect of mixing on APSO triglyceride conversion.

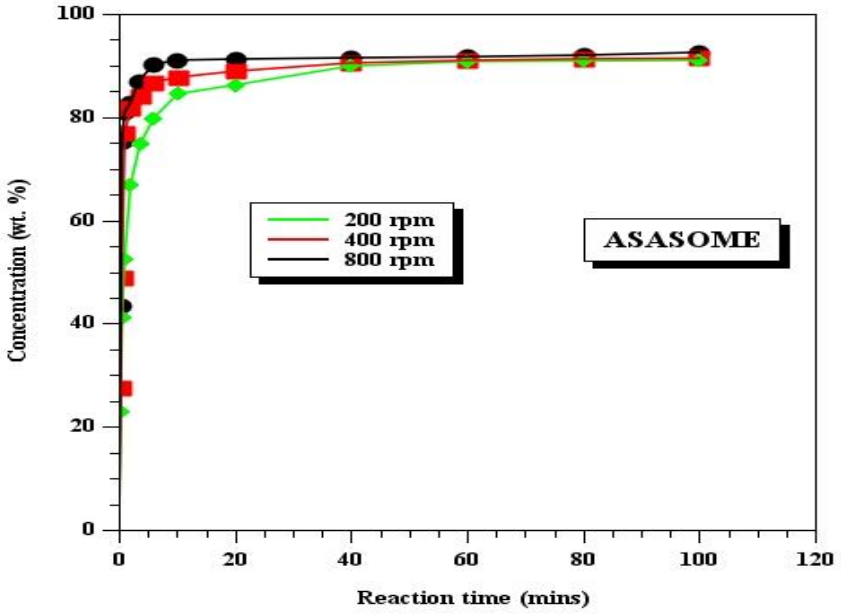

Figure 4.85: Effect of mixing on ASASO triglyceride conversion.

4.9.4 Second order irreversible base transeasterification model

Least-square approximation was applied, in fitting a straight line to the experimental data according to a model developed based on Tg hydrolysis and the second-order reaction rate as shown in Equation 4.60 (Darnoko and Cheryan, 2000; Leveinspel, 1999). In each case the coefficient of determination (R^2) was determined.

$$\frac{-d[Tg]}{dt} = k[Tg]^2 \qquad (4.60)$$

Integration of Equation (4.60) gives Equation (4.61).

$$k_{Tg}\, t = \frac{1}{[Tg]} - \frac{1}{[Tg0]} \qquad (4.61)$$

Where k is the overall pseudo-rate constant, t is the reaction time, Tg_0 is the initial triglyceride concentration.

A plot of reaction time (t) against $\frac{1}{[Tg]}$ gave a straight line as shown in Figure A7.4 with high values of coefficient (R^2) (Tables 4.23 to 4.25) to show that the model is valid. The plots for the three temperatures (55, 60 and 65^{o}C) is shown in Figure A7.4, the slope is k_{Tg} (wt%$^{-1}$min). It is observed that k increased with temperature. Finally, activation energies of the reaction taking place were estimated using the calculated rate constants and temperatures at which they were observed in Arrhenius equation (Equation (3.79)).

The Dg and Mg relationship with time followed the same trend (Figure A7.5 and A7.6) with that of Tg. The values of rate constants of APSO transesterification were found to be about 4% higher than that of SASO and ASASO for Tg hydrolysis and Mg hydrolysis while the value

of rate constants for Dg hydrolysis of ASASO was higher thanthose of SASO and APSO Dg hydrolysis (Table 4.79, 4.80 and 4.81). These variations in rate constants could be attributed to composition of glycerides and FFA in the seed oils which may result in differing mixing rates in methanol (Kumar *et al.,* 2011).

Although, the kinetics of base-catalyzed transesterification of sweet almond seed oil, African pear seed oil and African star seed oil are not yet documented in the literature, the values of the activation energy obtained for SASOME is similar to 14.7 and 14.2 kcal/min obtained for Tg and Dg hydrolysis of palm oil reported by Darnoko and Cheryan (2000), at same temperature. The values for the three seed oils studied in this research compared favourably (22.43 for 28.50 and 23.23 kcal/min for SASO, APSO and ASASO respectively). The values of rate constants for the Tg hydrolysis obtained in this research is about factor of 4 higher than that determined by Darnoko and Cheryan, (2000) for palm oil at same conditions and about factor 2 lower than the values reported by Rayero *et al.,* (2015) on the kinetics of NaOH catalyzed transesterification of sun flower oil with ethanol. The difference in fatty acid compositions of the feedstocks could be the reason for the slight variations in the results.

Also, the percentage conversion of Tg recorded for the seed oils ranged between 89-91% and their values compared with 91% obtained by Kumar *et al.,* (2011), 98% obtained by Darnoko and Cheryan (2000) after 1hour. The model predicts that maximum monoglycerides yield decreases as the reaction temperature increases. This could be due to the fact that the conversion of monoglyceride into glycerol has the highest activation energy among the three transesterification steps. The results show that kinetic constants of the first step (hydrolysis of Tg into Dg and biodiesel) has the smallest values. It is therefore, the slowest and the rate determining step.

Then the higher activation obtained for monoglycerides hydrolysis clearly shows that higher temperature favours the reaction step more than the other steps with lower activation (for multiple reaction). The positive value of the activation energy supports the exothermic nature of transesterification process (Reyero *et al.*, 2015). The increase in k at higher temperature and the order of magnitude of k is $k_{Mg}>k_{Dg}>k_{Tg}$ was similarly recorded by Darnoko and Cheryan, (2000).

Table 4.79: Summary of the kinetics result for second-order irreversible reactions of SASOME.

Glyceride	Temperature(T) (°C)	(K)	1/T x10^3(K^{-1})	k (wt%/min)	E_a (Kcal/mol.)
Tg ⟶ Dg	55	328	3.05	0.00960 (R^2 = 0.98)	12.76
	60	333	3.00	0.01010 (R^2 = 0.99)	
	65	338	2.96	0.01610 (R^2 = 0.98)	
Dg ⟶ Mg	55	328	3.05	0.00838 (R^2 = 0.98)	
	60	333	3.00	0.00845 (R^2 = 0.97)	15.83
	65	338	2.96	0.01592 (R^2 = 0.97)	
Mg ⟶ Gl	55	328	3.05	0.01650 (R^2 = 0.98)	
	60	333	3.00	0.02930 (R^2 = 0.99)	22.43
	65	338	2.96	0.04090 (R^2 = 0.98)	

Table 4.80: Summary of the kinetics result for second-order irreversible reactions of APSOME.

Glyceride	Temperature(T) (°C)	(K)	1/T x10^3(K^{-1})	k (wt%/min)	E_a (Kcal/mol.)
Tg ⟶ Dg	55	328	3.05	0.00960 (R^2 = 0.97)	12.76
	60	333	3.00	0.01010 (R^2 = 0.99)	
	65	338	2.96	0.01610 (R^2 = 0.98)	
Dg ⟶ Mg	55	328	3.05	0.00838 (R^2 = 0.98)	
	60	333	3.00	0.00845 (R^2 = 0.97)	15.83
	65	338	2.96	0.01592 (R^2 = 0.98)	
	55	328	3.05	0.01650 (R^2 = 0.99)	
Mg ⟶ Gl	60	333	3.00	0.02930 (R^2 = 0.98)	22.43
	65	338	2.96	0.04090 (R^2 = 0.98)	

Table 4.81: Summary of the kinetics result for second-order irreversible reactions for ASASOME.

Glyceride	Temperature(T) (°C)	(K)	1/T x10^3(K^{-1})	k (wt%/min)	E_a (Kcal/mol.)
Tg ⟶ Dg	55	328	3.05	0.00710 (R^2 = 0.98)	2.707
	60	333	3.00	0.00870 (R^2 = 0.97)	
	65	338	2.96	0.00910 (R^2 = 0.97)	
Dg ⟶ Mg	55	328	3.05	0.02390 (R^2 = 0.99)	7.30
	60	333	3.00	0.03040 (R^2 = 0.99)	
	65	338	2.96	0.03210 (R^2 = 0.98)	
Mg ⟶ Gl	55	328	3.05	0.01600 (R^2 = 0.97)	23.33
	60	333	3.00	0.03710 (R^2 = 0.97)	
	65	338	2.96	0.04090 (R^2 = 0.99)	

4.9.5 First-order irreversible model

By ignoring the intermediate reactions of diglyceride and monoglyceride, the three steps have been combined in a single step (Birla *et al.,* 2012). However, due to the high molar ratio of methanol to oil, the change in methanol concentration can be considered as constant during reaction. This means that by taking methanol in excess, its concentration does not change the reaction order and it behaves as a first order chemical reaction (Zhang *et al.,* 2010). Least-square approximation was applied, in fitting a straight line to the experimental data, and in each case the coefficient of determination (R^2) was determined. The overall pseudo rate constants determined from the slopes of the straight line plots of ln [Tg] against t shown in Figures A7.9 are presented in Tables 4.82, 4.83 and 4.84 for SASOME, APSOME and ASASOME respectively. As can be seen from Figure A7.9, in the reactions conducted at 55, 60 and 65°C, there was a decrease in the coefficient of determination for the pseudo first-order kinetic model. The coefficient of determination is especially important because the value of R^2 x100 represents

the percentage of original uncertainty as explained by the linear model. Figure A7.9 shows that the reaction at these temperatures does not fit the pseudo first-order reaction kinetic model better. This is supported by the lower values of coefficient of determination obtained from the first-order fitted plots ($R^2 < 0.80$) against high coefficient of determination obtained on the second-order irreversible kinetic model ($R^2 > 0.97$). Similar results have been reported on the kinetics of hydrolysis of nigella sativa (*black cumin*) seed oil catalyzed by native lipase in ground seed where pseudo first-order rate equation at 20, 30 and 40°C; and the pseudo second-order equation at 50, 60 and 70°C (Dandik and Aksoy, 1992). Therefore, it could be that hydrolysis of some oils to methyl esters follows first-order irreversible kinetic models at low temperature ranges (20-40°C). The low temperature ranges is reported to favour the activity of native lipase better than at higher temperatures and this resulted in different mechanisms. But such low temperatures would not favour maximum ester yield in this study because they are far below the reported optimum temperature (Darnako and Cheryan, 2000). Darnako and Cheryan, 2000, has observed that at latter reaction stages (beyond 30 mins) of palm oil hydrolysis to methyl ester, the first-order or zero-order reaction model is the best fitted. Similar observation was made on this study where as from 20 minutes reaction, the reaction follows first-order model with high coefficient of determination ($R^2 > 0.94$). This is shown in Figure A7.10 These stages showed low reaction rate due to reduction in the reactants concentration. It implies that at low temperatures and latter stages of methanolysis of the vegeatble oils progesses very slowly and follow first-order kinetic model.

Table 4.82: First-order model reaction rate constant for SASOME

Glyceride	Temperature (°C)	Reaction rate constant (min^{-1})	R^2
Triglyceride	55	0.0429	0.81
	60	0.0476	0.80
	65	0.0458	0.77

Table 4.83: First-order model reaction rate constant for APSOME

Glyceride	Temperature (°C)	Reaction rate constant (min^{-1})	R^2
Triglyceride	55	0.0431	0.80
	60	0.0437	0.80
	65	0.0439	0.80

Table4.84: First-order model reaction rate constant for ASASOME

Glyceride	Temperature (°C)	Reaction rate constant (min^{-1})	R^2
Triglyceride	55	0.0408	0.82
	60	0.0420	0.81
	65	0.0428	0.81

4.9.6 Second-order reversible model

The rate constants values for the first forward reactions were higher, implying that there was no resistance by mass transfer at the initial stage. This supports the lack of lag period in the first stage of the reaction. However, as the temperatures increased the rate constants values increased slightly. The rate determining step for the reversible reaction was determined to be the hyrolysis of Dg to Tg (the slowest step). Considering forward reactions alone, the reaction Dg to Mg (k_3) is slower than those of Tg to Dg (k_1) and Mg to Gl (k_5). High concentrations of Tg and Dg did offset the reversible reaction effects even at high temperatures.

Figures A7.11-A7.13 shows the plot of log vs 1/T. The slopes gave the activation energies (Ea) and the intercepts gave the pre-exponential factors. As seen from Tables 4.85, 4.86 and

4.87 forward reactions for the first reaction steps (Tg to Dg and Dg to Mg) have lower activation energies than their reverse counterparts which theoretically would mean more favourable reverse reactions. However, high concentrations of Tg and Dg and chemically controlled kinetics resulted in more favoured forward reactions, especially at high temperatures.

Higher temperature favoured hydrolysis of APSO monoglycerides to glycerol, SASO diglycerides to triglycerieds, and ASASO diglycerides to monoglycerides in the reversible mechanism. But monoglyceride hydrolysis to glycerols was favoured by higher temperature under irreversible mechanism. The rate constants proved that at all temperatures, the hydrolysis of Dg to Mg of SASO, and Tg to Dg of both APSO and ASASO were the rate determining steps for irreversible reaction condition. Considering the reversible reaction mechanism, the hydrolysis of SASO Mg to Dg, and ASASO Dg to Tg were the rate determining steps while the hydrolysis of Mg to Dg, Dg to Tg and Tg to Dg at 55°C, 60°C and 65°C respectively, were the rate determining step for APSO.

Table 4.85: Summary of rate constants (L/g.min) and activation energy for SASOME for reversible model.

Temperature (°C)	Tg ⇌ Dg		Dg ⇌ Mg		Mg ⇌ Gl	
	k_1	k_2	k_3	k_4	k_5	k_6
55	0.0408	0.0201	0.0356	0.0102	0.0701	0.0370
60	0.0529	0.0622	0.0459	0.0252	0.1245	0.0631
65	0.0984	0.0896	0.0676	0.0721	0.1738	0.0892
E_a(J/mol.)	79.02	139.43	58.17	96.05	83.60	80.94
C	$1.86x10^{11}$	$4.78x10^{20}$	$7.24x10^{4}$	$6.76x10^{13}$	$2.74x10^{11}$	$3.71x10^{11}$
R^2	0.928	0.951	0.966	0.987	0.992	0.996
RMSE	0.07346	0.10576	0.03639	0.06663	0.0244	0.0166
RSS	0.00539	0.011185	0.001324	0.004440	0.000599	0.000276

Table 4.86: Summary of rate constants (L/g.min) and activation energy for APSOME for reversible model.

Temperature (°C)	Tg ⇌ Dg		Dg ⇌ Mg		Mg ⇌ Gl	
	k_1	k_2	k_3	k_4	k_5	k_6
55	0.0442	0.0241	0.0476	0.0113	0.1049	0.0517
60	0.0476	0.0430	0.0851	0.2172	0.2010	0.1011
65	0.0493	0.0597	0.1347	0.2540	0.3319	0.1570
E_a(kJ/mol.)	41.019	84.28	71.36	74.25	104.55	102.16
C	$1.17x10^5$	$1.62x10^{11}$	$1.51x10^{10}$	$1.56x10^{11}$	$2.05x10^{16}$	$2.46x10^{16}$
R^2	0.986	0.992	0.727	0.998	0.999	0.997
RMSE	0.01640	0.02480	0.1468	0.01017	0.00363	0.01892
SSE	0.000269	0.000615	0.021564	0.0001035	0.000013	0.0003580

Table 4.87: Summary of rate constants(L/g.min) and activation energy for ASASOME for reversible model.

Temperature (°C)	Tg ⇌ Dg		Dg ⇌ Mg		Mg ⇌ Gl	
	k_1	k_2	k_3	k_4	k_5	k_6
55	0.1002	0.0112	0.0270	0.0613	0.0680	0.0220
60	0.1740	0.0300	0.0591	0.1512	0.0950	0.0570
65	0.3289	0.047	0.1691	0.2693	0.2013	0.0925
E_a(J/mol.)	109.04	133.07	166.45	136.04	97.717	132.62
C	$2.27x10^{16}$	$1.99x10^{19}$	$1.33x10^{25}$	$4.57x10^{20}$	$3.02x10^{14}$	$4.56x10^{19}$
R^2	0.989	0.975	0.977	0.996	0.922	0.985
RMSE	0.03802	0.06971	0.08419	0.02855	0.09488	0.05468
RSS	0.0014459	0.004859	0.00708	0.0008153	0.0090025	0.0029902

CHAPTER FIVE

CONCLUSION AND RECOMMENDATION

5.1 Conclusion

The seed oils of sweet almond, African pear and African star apple belong to the oleic group, possess high monounsaturated fatty acids and oil yields but African star apple has comparatively low yield. The seed oils are prone to oxidative degradation during storage and the variation of their rate of oxidation stability at room and elavated temperatures follows exponential regression model. The addition of antioxidant (TBHQ) improved the oils shelf life. Transesterification process improved the fuel qualities of the vegetable oils. The biodiesels would possess enhanced cold flow properties, low thermal efficiency and poor storage stability. Physico-chemical properties of the biodiesels and blends of sweet almond seed oil methyl ester (SASOME) and African pear seed oil methyl ester (APSOME) with petro-diesel satisfied relevant international standards. The esterification of APSO and transesterification of the seed oils followed second-order regression models based on RSM. The bodiesel yields were highly optimized at mild reaction conditions, short reaction times and low reaction material requirements while ANN showed better predictions. Higher oxygen content and viscosity of SASOME and APSOME were responsible for their better engine performance and emission characteristics than petrodiesel. Excellent correlation of results of engine performance and emission characteristics of the experimental and predicted values was in the following order: Nelder-Mead>RSM-GA>MIMO-ANN. The irreversible second-order model of the power rate law best described the conversion of triglycerides with time. The present study revealed that the seed oils' methanolysis is highly viable.

5.2 Contribution to Knowledge

Though many researchers have contributed efforts to address the issues of biodiesel, the technology is yet to be fully exploited. This research through the results obtained has:

- Established the optimized viable routes which the following processes could be operated: African pear seed oil esterification, transesterification of seed oils derived from sweet almond, African pear and African star apple and engine performance and emissions of *Prunus amygdalus* and *Dyacrodes edulis* in Perkins 4:108 model CI diesel engine.
- Established the rate determining steps, reaction order and thermodynamics requirements of both reversible and irreversible consecutive methanolysis reaction of the selected seed oils.
- Established the influence of fatty acid composition and the functional groups on the fuel related properties of methyl esters derived from *Prunus amygdalus, Chrysophyllum albidium* and *Dyacrodes edulis* seed oils.
- Established the induction time and oxidation regression model for the seed oils.

5.3 Recommendations

1. The seed oils of African pear and sweet almond can be harnessed for biodiesel productions since they are highly underutilized in Nigeria.
2. The application of antioxidants would help to promote the oxidative stability and improve the shelf-life of the selected seed oils and similar highly unsaturated feedstocks to enhance their biodiesel potentials.

3. The adjustment of the injection timing and introduction of exhaust gas recirculation is suggested as ways of reducing the high NOx emissions of the biodiesel from African pear and sweet almond seed oils.
4. Application of Gauss-Jordan elimination method is recommended as a simpler and faster approach for solving simultaneously the differential equations of reversible three-step consecutive rate equations of homogeneous transtesterfication reaction.
5. Application of Nelder-Mead should be exploited the more in solving chemical process control problems.

REFERENCES

Abdoli, M. A., Mohamadi, F., Ghobadian, B. & Fayyazu, E. (2014). Effective parameters on biodiesel production from feather fat oil as a cost-effective feedstock. *International Journal of Environmental Research, 8*(1), 139-148.

Abdullah, A. Z., Razali, N., & Lee, K. T. V.(2009). Optimization of mesoporous K/SBA – 15 catalyzed transesterification of palm oil using response surface methodology. *Fuel Processing Technology, 90,* 958 – 964.

Achten, W. M. J., Verchit, L., Mathisjs Franken, Y. J., Singh, E., Arts, V. P. & Muijs, R. B. (2008). Jatropha biodiesel production and use. *Biomass Bionergy, 32*(12), 1063-84.

Adebayo, S. E., Orheuba, B. A., Adeoye, P. A., Musa, J. J. & Fase, O. J. (2012). Solvent extraction and characterization of oil from African star apple (*Chrysophyllum albidium)* seeds, *AcademicResearch International. Nat. & Appl.,3*(2), 178-183.

Adepoju, T. F. & Olawale, O. (2014). Acid-catalyzed esterification of waste cooking oil with high FFA for biodiesel production.*Chemical and Process Engineering Research, 21*, 80-84.

Adepoju, T. F., Ojdiran, J. O. & Okumola, A. A. (2013). An Optimization Approach to Oil extraction from *Chrysophyllum albidium* oil seeds and its quality characterization. *International Journal of Innovative Research and Studies*, *2* (10), 56-71.

Adepoju, T. F., Rasheed, B., Olatunji, O. M., Ibeh, M. A. Ademiluyi, F. T. & Olatunbosun, B. E. (2018). Modeling and optimization of lucky nut biodiesel production from lucky nut seed by pearl spar catalysed transesterification. *Heliyon* 4, e00798. doi: 10.1016/j.heliyon.2018. e00798.

Adewusi, H. G. & Bada, S. O. (1997). Preliminary information on the Ecology of *Chrysophyllum albidium* in West and Central Africa. In Proceedings of a National Workshop on the Potentials of Star Apple in Nigeria 16.25.

Adeyanju, A. A. (2008). Effect of seeding of wood ash on biogas production using pig waste and cassava peels. *J. Eng. Appl. Sci*., *3,* 242-245.

Agbede, O. O., Alade, A.O., Adebayo, C. A., Salain, K.K, & Bakere T. (2012). Evaluation of chosen fruit seeds oil as potential biofuels. *Int. Agro Phys., 26,* 199-202.

Agunbiade, S.O. & Olanlokun, J. O. (2006). Evaluation of some nutritional characteristics of Indian almond (*Prunus amygdalus) Pakistan J. Nutr*., *5*, 316-318.

Ahmad, A. L., Mat Yasin, N .H., Derek, C. J. C. & Lim, J. K. (2011). Microalgae as a sustainable energy source for biodiesel production: a review. *Renew Sustain. Energy Rev. 15*(1), 584-93.

Ahmad, A., Barat, G., Gholamhassan, N. & Ali, M. (2013). Design, fabrication and evaluation of a novel biodiesel processor system. *International Journal of Renewable Energy Tech. Research, 2*(12), 249-225.

Ahmad, M., Sadia, H., Zafar, M., Sultana, S. M.A. & Khan, Z. (2012). The production and quality assessment of mustard oil biodiesel. A cultivated potential oil seed crop. *Energy Sources Part A*: *34,* 1480-1490.

Ahmadian-Morghadam, H., Elegado, F. B. & Nayve, R. (2013). Prediction of ethanol concentration in biofuel production using artificial neural networks. *American Journal of Modelling and Optimization, 1* (3), 31-35.

Ahring, B. & Westermann, P. (2007). Co-production of bioethanol with other biofuels. In Olsson, edition, Biofuels, Springer Berlin/herdelberg 289-302.

Ajiwe, V. I. E., Okeke, C. A., Nnabuike, B., Ogunleye, G. A. & Elebo, E.(1997). Application of oils from African star apple (*Chrysophyllum africanum),* horseeye bean (*Mucuna sloanu)* and African pear (*Dacyodes edulis)* seeds. *Bioresource Technology, 59*, 259-261.

Akpan, U. G., Jimoh, A. & Mohammed, A. D. (2006). Extraction, characterization and modification of castor seed oil. *Leonardo Journal of Science, 8*, 43-52.

Alamu, O. J., Waheed, M. A., Jekayinfa, S. O., Akintola, T. A. (2007). Optimal transesterification duration for biodiesel production from Nigerian palm kernel oil. Agric Eng Int: CIGR Ejournal 2007; IX.

Alemayehu, G. (2014) . Anaerobic co-digestion of biodegradable municipal solid waste with human excreta for biogas production. A review. *American Journal of Applied Chemistry, 2* (4), 55-62.

Alfa, A. (2010). Extraction of oil and proximate analysis of Nigerian mango seed kernel. B.Eng. Degree Thesis, Dept of Chem. Engr. Featuring Nigerian State,14-29.

Ali, J. E., Rashid, J. & Rana, J. E. (2010). The importance of almond (*Prunus amygdalus L.),* and its bye-products. *Food Chemistry, 120* (2), 349-360.

Ali, J., Hadi, A., Shashin, R., Moshen, N. & Fatemeh, A. (2014). Investigation and energy balances for biogas production from cow and poultry manure. *International Journal of Renewed Energy Research, 4*(2), 312-320.

Ali, M. N. & Mohammed, M. K. (2014). Comparative studies on bioethanol production with immobilized cells of *S. cerevisiae* local stain and *S. cerevisiae* MTCC170 by stationary and shaking fermentation methods. *Intl. J. of Current Microbial and Applied Sci., 3*(1), 380-390.

Alom, T. & Amirav, A. (2006). Isotope abundance analysis method and software for improved sample identification with supersonic gas chromatography / mass spectrometry. *Rapid Common Mass spectron, 20*, 2579-2588.

Amirav, A., Gorin, A., Polak, M. & Fialkov, A.B. (2008). Gas chromatography –mass spectrometry with supersornic molecular beams. *J. Mass spectrum, 43*, 141-163.

Amon, T., Amon, B., Kryvoruchko, V., Zollitsch, W., Mayer, K. & Gruter, L. (2007). Biogas production from maize and dairy cattle manure ---Influence of biomass composition on methane yield. *Agriculture, Ecosystem and Environment, 118,* 173-182.

Animasaun, D. A., Krirhnamurthy, R., Ingalhalli, R. S. & Ramani, N. D. (2014). A preliminary attempt of ethanol production from Fig (*Ficus Carca*) and Date (*Phoenix dactylifera*) fruits using *Saccharomyces cerevisiae. Int. J. Pure Appl. Biosci., 2*(2), 174-180.

Anitha, A. & Dawn, S. S. (2010). Performance characteristic of biodiesel produced from waste groundnut oil using supported heteropolyacids. *International Journal of Chemical Engineering and Applications, 1*(3), 261-265.

Antunes, F. A.F., Chandel, A.K., Milessi, T.S.S., Santos, J.C., Rosa, C. A. & Da Silva, S. S. (2014). Bioethanol production from sugar bagasse by a novel Brassilian pentose fermenting

yeast *Scheffersomyces Shehatae* UFma-Hm 52.2: Evaluation of fermentation medium. *Int. J. of Chem. Engr*., *2014*, 8pp.

AOAC, (2000). Official methods of analysis, (13th Edition). Association of Official Analytical Chemists, Washington, DC.

Atabani, A. E., Silitonga, A. S., Irfan, A. B., Mahlia, T. M. I., Masjuki, H. H. & Mekhilef, S. (2012). A comprehensive review on biodiesel as an alternative energy resource and its characteristics. *Renewable and Sustainable energy review, 16*, 2070- 2093.

Audu, T. O. K., Aluyor, E.O. Egualeoma, S. & Momoh, S.S. (2013). Extraction and characterization of *Chrysophyllum albidium* and *Luffa cylindrical* seed oils. *Petroleum Technology Development Journa*l, *3*(1), 1-7.

Awolu, O. O. & Layokun, S. K. (2013). Optimization of two-step transesterification production of biodiesel from neem (*Azadirachta indica*) oil. *Int. J. of Energy and Environmental Engineering, 4*, 39.

Balusu, R., Paduru, R. M., Seenaya, G. & Reddy, G. (2004). Production of ethanol from cellulose biomass by *Clostridium thermocellum* SSI9 in submerged fermentation screening of nutrients using Plackett Durman design. *Applied Biochem. Biotechnol., 117*, 133-144.

Bannikov, M. & Vasilev, I.(2012) Combustion characteristics of the mustard methyl esters. *Key Eng Mater* 510:406-12.

Barbara S (2004) Analytical techniques in science. Infrared spectroscopy; fundamentals and application. Wiley, London, New York.

Bello, E. I., Fade-Aluko, A.O., Anjorin, S. A. & Mogaji, T.S. (2011). Nut (dika nut) *Irvingia gabonensis*) oil biodiesel as alternative fuel for diesel engines. *J. Petro. Technology and Alternative Fuels, 2*(9),176-180.

Beng, G.O. & Kelvin, R.L. (2009). Strategy for adapting wine yeast for Bioethanol production. *Int. J. Mol. Sci., 10*, 385-394.

Berchamans, H. J. & Hirata, S. (2008) Biodiesel production from crude *Jatropha curcas L*. seed oil with high content of FFA. *Bioresource Tech.* 99, 1716-1721.

Berrios, M. J., Siles, M. A. & Martin, A. (2007). Kinetic study of esterification of free fatty acids (FFA) in sunflower oil. *Fuel, 86*, 2383-2388.

Betiku, E. & Adepoju, T. F. (2013). Methanolysis optimization of sesame (*Sesamum indicum)* oil to biodiesel and fuel quality characterization. *International Journal of Energy and Environmental Engineering, 4*(9), 1-8.

Bhattacharyulu, Y. C., Ganvir, V. N., Aditaya, A. & Ramming, A. (2013). Modeling of neem oil methyl esters production using ANN. *International Journal of Computer Application 70(27)*. 0925-8887.

Blesner, D. M. (2006). Validating chromatographic methods: A practical guide. John Willey and Sons.

Botinestean, C., Hadaruga, N. G., Hadaruga, D. J. & Jiami, I. (2012). Fatty acids composition by gas Chromatography-mass spectrometry (GC-MS) and most important physical –chemical parameteters of tomato seed oil (TSO). *J. of Agroalimentary Process & Techn*., ***18***(1), 89-94.

Camilli, R., Reddy, C. M., Coercer, D. R., Van Mooy, B. A. S., Jakuba, M. V. & Kinsey, J. C. (2010). Tracking hydrocarbon plume transport and biodegradation at deepwater horizon. *Science; 330,* 201-4.

Carraretto, C., Macor, A., Mirandola, A., Stoppato, A. & Tonon, S. (2004). Biodiesel as alternative fuel: Experimental analysis and energetic evaluations. *Energy Convers. Manage., 29* (12-15), 2095-11.

CDER, (1994). Reviewer Guidance: Validtion of Chromatographic methods. FDA.

CDER, (2000). Guidance for industry analytical Procedures and Methods Validation.FDA

Centikaya, M., Ulusoy, Y., Tekin, Y. & Kaaraosmanoghua, F. (2005). Engine and winter road test performances of used cooking oil originated biodiesel. *Energy Convers. Manage., 46*(7-8), 1279-20.

Cheng, L. H & Ping, W. Y. (2006). Genetic algorithm with a hybrid crossover operator and its convergence. *Computer Engineering and Application, 16*, 22-24.

Choi, M. H. & Chung, B. C. (2015). Bringing GC-MS profiling of steroids into clinical applications. *Mass Spectron Rev., 34*(2), 219-36.

Christian, D. P. & Lederle, P. E. (1984). Seed properties and water balance in desert granivores, southwest. *Nat., 29*, 181-8.

Cole, J. (2013). Introducing Auto SRM, MRM Simplicity for High Performance Results. Application Brief No. ABS 2298.

Conceicao, M. M., Fermardes, V. J., Araiyo, A.S., Farais, M. F., Santos, I. M. & Souza, A. G.(2007).Thermal and oxidative degradation of castor oil biodiesel. *Journal of Energy Fuel, 21* (1), 1522 – 1527.

Dahunsi, S. O. & Oranusi, U. S. (2013). Co-digestion of food waste and human excreta for biogas production. *British Biotechnology Journal, 3*(4), 485-499.

Dandik, L. & Aksoy, H. A. (1992). The kinetics of hydrolysis of *Nigella sativa* (Black Cumin) seed oil catalyzed by native lipase in ground seed. *JAOCS*, 69, (12), 1239-1240.

Darnoko, D. & Cheryan, M. (2000). Kinetics of Palm oil transesterifiction in a batch reactor. *JAOCS. 77*, 1263- 1267.

De Lima, A. P., De lima, A. L., Santos, D. Q. & Neto, W. B. (2013). Application of factorial design and response surface mechanism to optimize ethyl biodiesel production from corn oil. *Rev. Virtual Quim, 5*(5), 817-827.

Demirbas, A. (2003). Biodiesel fuels from vegetable oils via catalytic and noncatalytic supercritical alcohol transesterification and other methods, A survey. *Energy Conversion Management, 44*, 2093-2104.

Dennis Y.C. Leung, D.Y. Xuan, C., Wu, M. K. & Leung, H (2009) A review on biodiesel production using catalyzed transesterification, *Applied Energy* 87 1083–1095.

Ediri, B. A. & Nosa, A. O. (2012). A comprehensive review of biomass resources and biofuels production potential in Nigeria. *Research Journal in Engineering and Applied Science, 1*(3), 149-155.

Ehiagbonare, J. E., Onyibe, H. I. & Okoegwale, E. E. (2008). Studies on the isolation of normal and abnormal seedlings of *Chrysophyllum albidium*: A step toward sustainable management of the taxon in the 21st century. *Sci. Res. Essay, 3*(12), 567-570.

Eiceman, P (2000). Gas Chromatography. In Meyers R. A. (ed). Encyclopedia of Analytical Chemistry Applications, Theory and Instrumentation, Chichester Wiley.

Elango, T., & Senthilkumar, T. (2010) Effect of methyl esters of neem and diesel oil blends on the combustion and emission characteristics of a CI engine. *ARPN J Eng Appl Sci.* 5:80–5.

Elkady, M. F., Ahmed, Z. & Ola, B. (2015). Production of biodiesel from waste vegetable oil via KM micromixer. *Journal of Chemistry, Volume 2015,* Article ID 630168, 9pp.

Emmanuel, I. M. & Francis, O.A. (2010). Comparative evaluation of different organic fertilizers on the soil fertility Improvement, leaf mineral compositions and growth performance of African cherry nut (*Chrysophyllum albidium L.)* seedlings. *Journal of American Science, 6*(8), 217-9.

Evan, D. D., Sunny, I. & Karl, R. (2012). The bioethanol industry in sub-saharan Africa: History, challenges and prospects. *Journals of Biomedicine and Biotechnology, 2012*, 1-11.

Ezeoha, S. L. & Idike, F. I. (2007). Biogas production potential of cattle paunch manure. *Journal of Agricultural Engineering and Technology (JAET), 15*, 25-31.

Falodun, A & Ikhatua,M. I. (2012). The essential oil components of *Irvingia gambonensis* and *Irvingia wombolu* from southern Nigeria. *Canadian Journal of Pure & Applied Sci*. *6*(2), 1955-1957

Fan, X. (2008). Optimization of biodiesel production from crude cotton seed oil and waste vegetable oil; conventional and ultrasonic irradiation methods. Ph.D thesis, Department of Food Technology, Clemson University.

Fan, X., Wang, X. & Chem. F. (2011). Biodiesel production from crude cotton seed oil: An optimization process using response surface methodology. *The open fuels energy Sci., 4,* 1-8.

Fangrui, M. & Hanna, M. A. (1999). Biodiesel production: A review. *Bioresource Technology, 70,* 1-15.

FAOSTAT (2014). Production /Crops for almond with shell" food and agriculture Organization of United Nations, Statistics division, 65-120.

Ferdous, K., Uddin, M.R., Khan, M. R. and Islam, M.A.(2012). Biodiesel from sesame oil: base catalyzed transesterification. International journal of Engineering and technology, 1(4), 420-431.

Fernando, S., Karra, P., Hernandez, R. & Tha, S. K. (2007). Effect of incompletely converted soybean oil on biodiesel quality. *Energy, 32* (5), 844-51.

Forsan, F. K., Oduro, E.K. & Hammond – Donkoh, E. (2004). Performance of Jatropha oil blends in a diesel engine. *Renewable Energy, 29*, 1135-45.

Freedman, B., Butterfield, R. O. & Pryde, E. H. (1986). Transesterification kinetics of soybean oil. *JAOCS, 63*, 1375-1380.

Friday, J. B. & Okano, D. (2011). *Calophyllum inophyllum* (Kamani): Available from: http://www.agroforestry.net/tti/*calophyllum-kamani.pdf* (cited 05.03.16)

Fu, C., Mielenz, J. R., Xiao, X., Hamilton, C. Y. & Rodrigwiz, M. (2011). Genetic manipulation of lignin reduces recalcitrance and improves ethanol production from switch grass. *Proas, 108*, 3803-8.

Fu, Y. J., Zu. Y. G., Wang. L. L., Zhang, N. J., Liu. W., Li, S. M. & Zhang, S. (2008). Determination of fatty acid methyl esters in biodiesel produced from yellow horn oil by RP-LC-RID. *Chromatographia, 67*, 9-14.

Furnish, B. S., Hannaford, A. J., Smith, P. W. G. &Tatchell, A. R. (1989), Vogel's textbook of practical organic chemistry, 5th ed., Longman group, UK, 1412-1422.

Galadima, A. & Garba, Z, N. (2009). Catalytic synthesis of ethyl ester from Some common oils. *Science World Journal,* 4, 1-5.

Ghorbani, H., Nikbakht, A. M., Tahatabaei, M., Hosseini, M. & Mohammadi, P. (2011). Application of modeling techniques for prediction and optimization of biodiesel production process. Int. Conf. on Biotechnology and Environment Mgt (IPCBEE) *18,* 7-12.

Gianneli, P. C. & Imwinkelried, E. J. (1999). Drug Identification: Gas Chromatography In scientific Evidence. Vol. 2, Lexis law publishing, Charlottesuille.

Giovanilton, F., Silva Fernando, L., Camargo Andrea, L. O. & Ferreira, F. (2011). Application of response surface methodology for optimization of biodiesel production by transesterification of soybean oil with ethanol, *Fuel Processing Technology* 92, 407–413.

Giwa, S. & Ogunbona, C. (2014). Sweet almond (*Prunus amygdalus dulcis*) seeds as a potential feedstock for Nigerian biodiesel automotive project. *Rev. Ambient Aqua*, 9 (1), 35-48.

Grrob, R. L & Barry, E. F. (2004). Modern Practice of gas Chromatography: Wiley-interscience, New York.

Gryglewiezs, P. (1999). Rapeseed oil methyl ester preparation using heterogeneous catalyst. *Biores. Tech., 70,* 249- 253.

Gunstone, E. D. (2004). Rapeseed and canola oil: Production process, properties and uses. *JAOCS 33,* 132 – 139,

Gupta, P., Singh, R.S., Sacham A., Vidyarth A.S. & Gupta, A. (2012). Study on biogas production by anaerobic digestion of garden waste. *Fuel, 95*, 495-498.

Habibullah, M. Rizwanul Fattah, I. M. Masjuki, H. H. and Kalam, M. A. (2015) Eff ects of palm-coconut biodiesel blends on the performance and emission of a single-cylinder diesel engine Energy Fuels 29, 734−74.

Habibullah, M., Masjuki, H. H., Kalam, M. A., Rizwanul Fattah, I. M, Ashraful, A. M., Mobarak, H. M. (2014) Biodiesel production and performance evaluation of coconut, palm and their combined blend with diesel in a single-cylinder diesel engine. *Energy Convers. Manage* 87:250-7.

Haiter, L. A., Ran, R., Arumugham, S. & Thyargarjan, K. (2012). Performance, emission and combustion evaluation of diesel engine using methyl esters of mahua oil. *International Journal of Environmental Science, 3* (1), 639-649.

Handley, A. J. & Adlard, E. R. (2001). Gas Chromatographic Techniques and Applications Sheffield Academic, London

Hangyu, K., Jing, L. & Yong, S. (2006). Improving crossover and mutation for adaptive genetic algorithm. *Computer Engineering and Application, 12,* 93-96.

Hanumanth, M., Hebbal, O. D., & Narindgi, M. C. (2012). Extraction of biodiesel from vegetable oils and their comparisons. *International Journal of Advanced Scientific Research & Technology, 2*(9), 242-2450.

Hasib, Z. M, Hossain, J, Biswas, S, & Islam, A. (2011) Bio-diesel from mustard oil: a renewable alternative fuel for small diesel engines. *Mod. Mech. Eng.* 1:77 -83.

Hazar, H. (2010) Cotton methyl ester usage in a diesel engine equipped with insulated combustion chamber. *Appl. Energy* 87:134-40.

He, B. B., Van Garpen, J. H. & Thompson, J. C. (2008). Suphur content in selected oils and fats and their corresponding methyl esters. *Applied Engineering & Agric., 2008,* 223-226.

Hingu, S., Golgate, P. R. & Rathod, V. K. (2010). Synthesis of biodiesel from waste cooking oil using sonochemical-reactors" *Ultrasonicsonochemistry, 17,* 827-832.

Hossain, M. A, Chowdhury, S. M., Rekhu, Y., Faraz, K. S.,& Islam, M. U. (2012) Biodiesel from coconut oil: a renewable alternative fuel for diesel engine. In: International conference on aerospace, mechanical, automotive and materials engineering (ICAMAME 2012), Kualalumpur, Malaysia..

Houesson, L. G., Lougbegnon, T. O., Gbesso, F. G. H., Anagorau, L. E. S. & Sinsin, B. (2012). Ethno-botanical study of the African star apple (*Chrysophyllum albidium G. Don)* in the Southern Benin. *West Africa Journal of Ethnobiology and Ethnomedicine, 8,* 40 1-10.

Huang. J, Wang, Y., Qin, J. B. & Roskilly, A. P. (2010)Comparative study of performance and emissions of a diesel engine using Chinese pistache and jatropha biodiesel. *Fuel Process Technol*. 91:1761–7.

Huzayyin A.S., Bawady A.H., Rady M.A., Dawood A., (2004), Experimental evaluation of diesel engine performance and emission using blends of jojoba oil and diesel fuel. Energy Convers Manag 45, 2093–112.

Ibeto, C. N., Okoye, C. O. B & Ofoefule, A. U. (2012). Comparative study of the physico-chemical characterization of some oils as potential feedstock for biodiesel production. *ISRN Renewable Energy* 2012, 5p

Igbum, O. G., Leke, L., Ande, S., Okoronkwo, M.U. & Nwadinigwe, C.A. (2012). Effects of transesterification variables on the characteristics of the methyl esters obtained from four virgin tropical seed oils in Nigeria. *International Research Journal of Pure & Applied Chemistry, 2*(4), 230-478.

Ikhatua, M. J., Eghareoba, R. K. A. & Asa, L. N. (2010). Microbial spoilage of *Irvingia* kernels in Benin city Nigeria. *Archives of Applied Science Research, 2*(5), 168-176.

Ilgen. O. (2012). Reaction kinetics of doyomite catalyzed transesterification of canola oil and methanol. *Fuel Processing Technology 95*, 62-66.

Imadi, S. B., Bandaru, V. R, Somalanka, S. R, & Garapati, H. R.(2007). Optimization of medium constituents for the production of citric acid from byproducts using Doehlert experimental design. *Enzyme Microb. Technol., 40,* 1367-1372.

Internatioanl Organization for Standardization (2002). Quality Management System, Fundamentals and Vocabulary ISO 9000: 2000(E).

International Energy Agency, (2011). Oil marketer reports, Total OECD12 month moving average demand Vs year. 1year growth. Pans, France: Organisation for economic Co-operation and development.

Irini, A., Prawit, K., Anne, B.T., Maria, S., & Prasad, K. (2009). Bioethanol, biohydrogen and biogas production from wheat straw in a biorefinery concept. *Bioresources Technology, 100*, 2562-2568.

Ismail, S., Ahmed, A.S., Reddy, A. and Hamdan, S. (2016). Biodiesel Production from Castor Oil by Using Calcium Oxide Derived from Mud Clam Shell, *Journal of Renewable Energy* 2016, 8 pp http://dx.doi.org/10.1155/2016/5274917

ISO/IEC: 17025(2005). General Requirement for Competence of testing and caliberation laboratories Paragraphs *5*, 5-5.6

Israel, S. A. (2008). Chemical qualities of oil from some fresh and market vegetable crops within Kwara State of Nigeria. *Biokemistri, 20*(2),71-75.

Jagadale, S .S. & Jugulkar, L. M. (2012). Review of various reactions on production of chicken fat based biodiesel. *J. of Modern Eng. Research, 2*(2), 407-411.

Javidialesaadi, A. & Raeissi, V. (2013). Biodiesel Production from high free fatty acid content oils. Experimental investigation of the pretreatment step. 4th International Conference on Environmental Science and Development – ICESD 2013(5), 474-475.

Jayeoba, O. J., Ige, M. M., Omolaiye, J. A., Gbadamosic, S. O., Ogunbanjo, R. O. & Abiola, I. O. (2007). Chemical composition and physical properties of African star apple (*Chrysophyllum albidium). ASSET 7*(1), 37-42.

Jenke, D. (1996). Chromatographic method validation: A review of current practices and procedures: General concepts and guides. *Liq. Chrom & Rel. Technol., 19*, 737-757.

Jeong, G. T., Yang, H. S. & Park, D. H. (2009). Optimization of transesterification of animal fat ester using response surface methology. *Bioresource Tech., 100*, 25-30.

Jindal, S. (2009). The effects of engine parameters on the combustion characteristics, performance and emission of CI engines running on biodiesel and SVO. Ph.D. thesis, CTAE Udaipair.

Jones, J. M., Saddawi, A., Dooley, B. Mitchell, E. J. S., Werner, J., Waldron, D. J. Weatherstone, S. & Williams, A. (2015) Low temperature ignition of biomass. *Fuel Processing Technology* 134, 372-377.

Joseph, J. K. (1995). Physico-chemical attributes of wild mango *(Irvingia gabonensis)* seeds. *Bioresource Tech., 53*, 179-181.

Joshua, M., Garba, M.A., Chidi, N., Audu, A.A & Abduljalat, D. (2011). Comparative Study of biodiesel from kernel oils of *Jatropha curcas* and *Azadirachta indica* in Zaria, Nigeria. *International Journal of Pharmaceutical Research and Innovation 4*, 10-15.

Jubiano, M., Rocha Jnr., J. G. & Bauerfelo, G. E. (2014). Biodiesel synthesis with alkaline catalyst a new refractometric monitoring and kinetic study. *Fuel*. *125*, 164-172.

Kafuku, G. S. & Mbarawa, M. (2010). Biodiesel production from croton megalocarpus oil and its process optimization. *Fuel*, *89*, 2556-60.

Kalachova, P. (2012). Analysis of emerging persistent organicpollutants using GC-M/MS SeTAC, Berlin.

Karaosmonoglu, F. (1999). Vegetable oils fuels: A review. *Energy Sources Part A, 21*, 221-227.

Karithikur, S., Ragavanandham, V., Kanagaray, S., Manikumar, R., Asha, A. & Achary, A. (2011). Preparation, characterization and engine performance characteristics of used cooking sunflower oil-based bio-fuels for diesel engine. *Advanced Material Research, 984-985*, 913-923

Karmakar, A., Karmakar, S. & Mukherjee, S. (2010). Properties of various plants and animals feedstock for biodiesel production. *Bioresource Technol., 101*(91), 7201-10.

Kasendo, J. B. (2009). Synthesis of biodiesel from palm oil and sea mango oil using sulfated zirconia catalyst. M.Sc. Thesis, University of Sains, Malaysia.

Kitson, F. G., Larsen, B.S. & Ewen, C. N. (1996). Gas chromatography and mass spectrometry; A practical guide. Academic Press, Boston.

Knothe, G. Biodiesel and renewable diesel: a comparison (2010). *Prog. Energy Combust. Sci*. 36(3): 364-73

Knothe, G. (2001). Determing the blend levels of mixtures of biodiesel with conventional diesel fuel by fibre-optic near infra red spectroscopy and H magnetic resonance spectroscopy. *J. America Oil Chem. Sci*., *78*, 1025.

Knothe, G. (2009). Improving biodiesel fuel properties by modifying fatty ester composition. *Energy and Environmental Science, 2*, 759-766.

Knothe, G. (2012). Synthesis and Characterization of long chain 1, 2-dioxo compounds. *Chemistry and Physiscs of lipids*, *50*, 14-34.

Knothe, G., Knahl, J. & Van Gerpen, J. (2005). The biodiesel handbook, AOCS press Champaign, IL; p.42.

Koria, L. & Nithya, G. (2012). Analysis of *Datura stramonium linn*, biodiesel by GC –MS and influence of fatty acid composition on fuel related characteristics". *J. of phytology*, *4*(1), 06-09.

Kreyzig, E. (1999). Advanced engineering mathematics, John Wiley and Sons Inc. Singapore.

Krinamgkura, K. A. (1986) A simple method for estimation of cetane index of vegetable oil methyl esters. *J. Am Oil Chem Soc*. *63*(4), 552-553.

Kumar, G. R., Ravi, R. & Chadh, A. (2011). Kinetic studies of base-catalyzed transesterification reaction of non-edible oils to prepare biodiesel. The effect of co-solvent and temperature. *Energy and Fuels*, *25*, 2826-2832.

Leakey, R. R. B., Greenwell, P., Hall, M.N., Atangana, A.R., Usoro, C., Anegbeh, P. O., Fondoun, T.M. & Tchoundjeu, Z. (2005). Domestication of *Irvingia gabonensis* tree-to-tree variation in food-thickening properties and in fat and protein contents of *dika* nut. *Food Chem,*. *90*, 365-378.

Lei, S., Zhilong, L., Jinhong, L., & Zhenxing, Q., (2017). Analysis of Edible Vegetable oils by infrared absorption spectrometry, *Advances in Engineering research*, 86: 286-289.

Leke, L., Ogbanje, A. A., Terje, D.H. & Ikyaagba, T. (2013). Production of biogas from maize cobs. *International Journal of Energy and Environment (IJEE) 4*(1), 153-160.

Leung, D. Y. C. & Guo, Y. (2006). Transesterification of neat and used frying oil: optimization for biodiesel production. *Fuel Process Technol*. 87:883-90.

Levenspiel, O. (1999). Chemical Reaction Engineering, John Wiley and Sons Inc. New York.

Li, Z., Deng, L., Lu, J., Guo, X., Yang, Z. & Tan, T. (2010). Enzymatic synthesis of fatty acid methyl esters from crude rice bran oil with immobilized *Candidachin. J. Chem. Eng., 18*(5), 870-5.

Lin, B. F., Huang, J. H. & Huang, D. Y. (2009). Experimental study of the effects of vegetable oil methyl ester on DI diesel engine performance characteristics and pollutant emission. *Fuel, 88*(9), 1779-85.

Linde, M. Jakobsson, E., Galbe, M., Zacchi, G. (2007). Team pretreatment of dilute H_2SO_4 – impregnated wheat straw and SSF with low yeast & enzymes loading for bioethanol production. *Biomass and Bioenergy, 32*(4), 326-332.

Liu, Y., Lolero, E., Goodwin, J.G. (Jr) and Mo, X. (2007) .Transesterification of poultry fat with methanol using Mg-Al hydrotalcite derived catalysts. *Applied Catalysis, 331,* 138 – 148.

Ma, F. & Hanna, M. A. (1999). Biodiesel production: A review. *Bioresource Technology, 70*, 1-15.

Martin, M. A. (2010). First generation biofuels complete. *N. Biotechnol, 27*, 596-608

Masjuski, H. H. (2010). Biofuel engine: a new challenge. Inaugural lecture. University of Malaysia.

Mathiayzhagan, M. & Ganapathi, A. (2011). Factors affecting biodiesel production. *Research in Plant Biology, 1*(2)1-5.

Maurer, H. H., Pfeger, K. & Webner, A.A. (2007). Mass spectral and GC data of drugs, poisons, pesticides, pollutants and their metabolites. Wheiheim wiley VCH.

Mbaraka, I. & Shanks, B. (2006). Conversion of oils and facts using advanced mesoporous heterogeneous catalyst, *J. Am. Oil Chem. Soc*., *83*, 79-91.

Mehdic, A. & Kariminia, H.(2011). Optimization of biodiesel production from Iranian bitter almond oil using statistical approach. *Applied Energy, 88* (7), 2377-2381.

Meher, L., Sagar, D. & Nack, S. (2006). Technical aspects of biodiesel production by transesterifiction - A review. *Renewable and Sustainable Energy Reviews, 10,* 248-268.

Mehmet, M. O., Ahmet, U., Esin, E. & Derya, A. (2011). Characteristics of some almond kernels and oils. *Scientia Horticultural, 127*(3), 330-333.

Menkiti, M. C., Agu, C. M., & Udeigwe, T. K. (2016). Kinetic and parametric studies for the extractive synthesis of oil from *Terminalia catappa L.* kernel. Reac. Kinet. Mecha. Cat. doi 10.1007/s11144-016-1101-y

Mhia Md, Z. & Shahadat, M. H. H. (2007) Making biodiesel and performance test of a diesel engine using diesel-biodiesel blends as a fuel with inlet air preheating attachment. Int Conference, *Mech Eng* 1–6.

Mishva, A., Tiwari, G. S., Jindal, S. & Mihta, A. K. (2014). Performance Evaluation of Rice bran biodiesel in small size agricultural diesel engines. *Agric. Eng. Int. CIGR Journal, 16*(1), 84-89.

Mittelbach, M. (1996). Diesel fuel derived from vegetable oils: Specification and quality control of biodiesel. *Bioresource Technol*., *56*, 7-11.

Mittelback, M. & Gangl, S. (2001). Long storage stability of biodiesel made from rape seed and used frying oil. *JOACS 78*, 573-7.

Mittlebach, M. & Remschnodt, C. (2004). Biodiesel the comprehensive handbook. Boersedruck Ges MBH, Vienna.

Montgomery, D. C. (2001). Design and analysis of experiments, fifth ed. John Wiley & Sons, New York.

Mooney, B. P. (2009). The second green revolution? Production of plant biodegradable plastics. *Biochem. J., 418,* 219-32.

Morad, N. A., Zin, R., M., Yusof, K. M. and Abdul Aziz., M. K. (2010) Process Modelling of Combined Degumming and Bleaching in Palm Oil Refining Using Artificial Neural Network *J. Am. Oil Chem. Soc.* 87,1381-1388 , DOI 10.1007/s11746-010-1619-5

Moreira, A. l., Dias, J. M., Almeida, M. F. & Alvim-ferraz, C. M. (2010). Biodiesel production through transesterification of poultry fat at 30˚C. *Energy & Fuels, 24*(10), 5717-5721.

Morgenstern, M., Cline, J. & Catald, S. (2006). Determination of the kinetics of biodiesel production using proton nuclear magnetic resonance spectroscopy (^{1}H NMR). *Energy & Fuel, 20*(4), 1350-1353.

Mshandete, A. M. & Parawira, W. (2009). Biogas technology research in selected sub saharan African countries: A review. *African Journal of Biotechnology 8*(2), 116-125.

Musa, U., Isa, A.G., Mohammed, J. A., Mohammed, U. G., Usman, Z. & Alharsan, B. (2015). Extraction of *Chrysophyllum albidium* seed oil, optimization and characterization. *Chemical and Process Engineering Research, 30*, 1-8.

Mushtaq, A., Shazia, S., Lee, K.T., Ahmed, Z.A., Haleema, S., Muhammed, Z., Taibi Ben, H., Muhammed, A. A.& Rasool, B. T. (2014). Distaff Thistle Oil: A possible new non-edible feedstock for biogas energy. *International Journal of Green Energy, 10*, 1-27.

Nabi, M. N, Hoque, S. M. N. & Akhter, M. S. (2009). Karanja (Pongamia Pinnata) biodiesel production in Bangladesh, characterization of karanja biodiesel and its effect on diesel emissions. *Fuel Process Technol* 90:1080–6.

Nabi, M. N., Akhter, M. S. & Islam, K. F. (2007). Prospect of biodiesel production from Jatropha curcas, a promising non edible oil seed in Bangladesh. In: International conference on mechanical engineering (ICME, Dhaka, Bangladesh) proceedings;.

Nabi, M. N., Rahman, M. M. & Akhter, M. S. (2009). Biodiesel from cotton seed oil and its effect on engine performance and exhaust emissions. *Appl. Therm. Eng*. 29:2265–70.

Nabi, M. N. & Najmul Hoque, S. M. (2008). Biodiesel production from linseed oil and performance study of a diesel engine with diesel bio-diesel fuels. *Mech Eng* 39 (1):40–4.

Nam, D. P. (2012). Improved Nelder Mead's method and applications. Ph.D. thesis, Department of Electrical and Computer Engineering, Auburn University, Aubarn, Alabama

Ndana, M., Grace, J. J., Baba, F. H. & Mohammed, U. M. (2013). Fourier transform infrared spectrometyric analysis of functional groups in biodiesel produced from oil of *recinum communis, hevea brasiliences* and *jatropha curcas* seeds. *Int . J. of Sc. Envi. & Tech., 2*(6), 1116-1121.

Nelder, J. A., & Mead, R. (1965), A simplex method for function minimization, Computer

Nieseen, W. M. A. (2001). Current practice of gas chromatography-mass spectrometry. Marcel Dekkor, New York, NY.

Nnabuchi, M. .N, Akubuko, F.O, Augustine, C. & Ugwu, G. Z. (2012). Assessment of the effect of co-digestion of chicken dropping and cow dung on biogas generation. *Global Journal of Science Frontier Research (A),12* (7), 20-26.

Noureddini, H. & Zhu, D. (1997). Kinetics of transesterification of soybean oil. *JAOCS 74* (11), 1457-1461.

Nzikou, J. M., Kimbongiula, A., Matos, L., Loumouamou, B., Pambou-Tobi, N.P.G., Ndangui, C.B., Abena, A. A., Siluo, T., Scher, J. & Desobry, .S. (2009). Extraction and characterization of seed kernel oil from mango (Magnifera Indica). *Research Journal of Environments and Earth Science, 2*(1), 31-35.

Oboh, I. O., Aluyor, E. O. & Audu, T. O. K. (2009). Use of *Chrysophyllum albidium* for the removal of metal irons from aqueous solution, *Scientific Research and Essay, 4*(6), 632-635.

Ochigbo, S. S. & Paiko, Y. B. (2011). Effects of solvent blending on the characteristics of oils extracted from the seeds of *Chrysophyllum albidium .I.J.S.N, 2*(2), 352-358.

Octave, S. & Thomas, D. (2009). The locks and keys to industrial metabolism. *Biochem. 91*, 659-64.

Odude, V. O., Adesina, A. J., Oyetunde, O.O., Adeyemi, O. O., Ishola, N. B., Anietie Okon Etim, A. O., & Betiku, E. (2017). Application of Agricultural Waste-Based Catalysts to Transesterification of Esterified Palm Kernel Oil into Biodiesel: A Case of Banana Fruit Peel Versus Cocoa Pod Husk, *Waste and Biomass Valorization*, https://doi.org/10.1007/s12649-017-0152-2.

Ofoefule, A. U., Ibeto, C.N., Okoro, U.C. & Onukwuli, O. D.(2013). Biodiesel production from tigernut (*Cyprus esculentus*) oil and characterization of its blend with petrodiesel. *Physical Review and Research International,* 3(2), 145 - 153

Ogunsina, B. S., Bhatnagan, A.S., Indira, T. N. & Radha, C. (2012). The proximate composition of African bush mango kernels (*Irvingia gabonensis)* and characteristics of its oil. *Ife Journal of Science*, 14 (1), 177-183.

Ohale, P. E., Uzoh, C. F., & Onukwuli, O. D.(2017). Optimal factor evaluation for the dissolution of alumina from azaraegbelu clay in acidic solution using RSM and ANN comparative analysis. *South African Journal of Chemical engineering*, 43-54

Okafor, J. C. (1985). Commercial production of ogbono and ugiri. In information series ob Agriculture in Anambra State. How to grow selected fruit Trees. Booklet No. 4, 25-30.

Okoye, C. O. B. & Ibeto, C. N. (2010). Analysis of different grounds of fruits juice with emphasis on the sugar and race metal content, *Bioresource, 7*, 493-495.

Okullo, A.A. & Temu, A. K. (2015), Modelling the kinetics of jatropha oil transesterification. *Energy and Power Engineering, 7,* 135-143.

Olowoyeye, J. (2013). Comparative studies on biogas production using six different animal dungs. *Journal of Biology, Agric and Health care, 3*(15), 9-11.

Olufumilola, A. A. & Oladapo, A. S. (2011). Physico-chemical properties of African star apple (*Chrysophylum albidum)* components. *Nutrition and Food Science, 41*(1), 8-11.

Orheoba, B. A., Ideh, P.A., Adebayo, S.E. & Nwankwo, C.C. (2013).Determination of some engineering properties of dika nut (*Irvingia gambonensis*) at Two moisture content levels as relevant to its processing. *International Journal of Eng. Research App. (IJERA), 3*(2), 182-188.

Oyerinde, A. Y. & Bello, E. I. (2016). Use of Fourier transformation in-frared (FTIR) spectroscopy for analysis of functional groups in peanut oil biodiesel and its blends. *British Journal of Applied Science and Tech*., 13(3), 1-14.

Parawira, W., Murto, M., Zvauya, R., & Matthiasson, B. (2004). Anaerobic digestion of solid potato waste alone and in combination with sugar beet leaves. *Renew. Energy, 29,* 1811-1823.

Patel, V. (1999). Cetane number of new Zealand diesel, report, office of chief gas engineer, energy inspection group. ministry of commerce Press. Wellington, New Zealand.

Petersson, A., Thompson, M. H., Hauggarard-Nielson, H., & Thomson, A. B. (2007). Potential bioethanol and biogas production using lignocellulose biomass from winter rye, oil seed rape and fata bean. *Biomass and Bionergy*, 31, 812-819.

Priya, V., Jananice, R. K & Vijayalaxmi, K. (2012). GC/MS Determination of bioactive Components *Pleurotus Ostreatus. Int Research J. Pharm 3*, 150-151.

Puhan, S., Jegan, R., Balasubbramanian, K. & Nagarajan, G. (2009) Effect of injection pressure on performance, emission and combustion characteristics of high linolenic linseed oil methyl ester in a DI diesel engine. *Renewable Energy* 34:1227–33.

Pullen, J. & Saeed, K. (2014). Factors affecting biodiesel engine performance and exhaust emissions – Part II: Experimental study, *Energy 72,* 17-34.

Qi, D. H, Geng, L. M., Chen, H., Bian, Y. Z., Liu, J., & Ren, X. C. (2009) Combustion and performance evaluation of a diesel engine fueled with biodiesel produced from soybean crude oil. *Renewable Energy* 34:2706–13.

Qiang, Z., Ryan, O. and Song-Charng, K. (2016) A comparative study of biodiesel engine performance optimization using enhanced hybrid PSO–GA and basic GA. *Applied Energy* 165, 676-684, DOI: 10.1016/j.apenergy.2015.12.044

Ra madhas, A., Jayaraj, S. & Mauraleedharara, S. E. C. (2005). Biodiesel production from high FFA rubber seed oil. *Fuel, 8*, 335-340.

Rabe, E. L. M. (2010). Jatropha oil in compression ignition engine, environment and Tanzania as supplying country. Eindhoven; Eindhoven University of Technology.

Rajendra, M., Jena, C.P. & Rahaman, H. (2009). Prediction of optimized pretreatment process parameters for biodiesel production using ANN and GA. *Fuel*, 88(5), 868 – 875.

Ramadhas, A. S., Jayara, S. and Muraleedharam, C (2005) Biodiesel production from high FFA rubber seed Fuel 84, 335-340.

Ramadhas, A. S., Jayara, S.& Muraleedharam, C (2005) Biodiesel production from high FFA rubber seed, *Fuel* 84, 335-340.

Rashid, U., Anwar, F., Ashraf, M., Saleem, M. & Yusuf, S. (2011). Application of response surface methodology for optimization tranesterification of *Moringa oleifera* oil, biodiesel production. *Energy Conversion Management, 52,* 3034-3042.

Reyero, J., Arzamendi, G., Zabala, S. & Gandia, M. L. (2015). Kinetics of NaOH-catalyzed transesterification of sun flower oil with ethanol to produce biodiesel. *Fuel processing Technology, 129*, 147-155.

Reyes, J. F. & Sepulveda, M. A. (2006). PM-10 emissions and power of diesel engine fueld with crude and refined biodiesel from salmon oil. *Fuel 85,* 1714-9.

Rizwan, A. M, Dennis, L. Y. C. & Liu, C. (2008). A review on the generation determination and mitigation of urban heat Island. *J. Environ Sci*., *20,* 120-8.

Robert, P. & Adams, D. (2007). Identification of Essential Oil components By gas Chromatography/Mass Spectrometry, 4th edition, Allured Pub Corp.

Rodrgues, J.A., Cardoso, F. P., Lachter, E. R., Estevao, L. R. M., Lima, E. & Nascimento, R.S.V. (2006). Correlating chemical structure and physical properties of vegetable oil esters. *Journal of the American Oil Chemists' Society. 83*, 353-357.

Rohman, A. (2017). Infrared spectroscopy for quantitative analysis and oil parameters of olive and virgin coconut: A review, *International journal of food properties,* 20 (7): 1447-1456.

Roman, M. B., Ekaterina I., Lomakina, R. Z. & Safieva, C. (2011). Artificial neural network (ANN) approach to biodiesel analysis: Analysis of biodiesel density, kinematic viscosity, methanol and water contents using near infrared (NIR) spectroscopy. *Fuel 90*, 2007-2015.

Rowley, A. G. (2001). Evaluating uncertainty for laboratories. A Practical Handbook.

Sahil, K., Praschant B., Akanksha M., Premjiet, S., & Davashish, R. (2011). GC-MS applications. *Int. J. pharma & Biological Archives, 2,* 1544-1560.

Sahoo, P. K., Das, L. M., Babu, M. K. G., Arora. P., Singh, V. P. & Kumar, N. R. (2009) Comparative evaluation of performance and emission characteristics of jatropha, karanja and polanga based biodiesel as fuel in a tractor engine. *Fuel* 88:1698–707.

Saifuddin, N. & Refai, H.(2014). Spectroscopy analysis of structural transesterification in biodiesel degradation. *Research Journal of Applied Sciences, Engineering and Technology, 8*(9), 1149-1159.

Sam, S. M., Akonye, L.A., Mensah, S.I., & Esenowo, G. J. (2008). Extraction and classification of lipids from seeds of *Persea Americana Miller* and *Chysophyllum albidium G. Don. Scientia Africans, 7* (2), 35-38.

Sandford, S. D., White, J. M., Shah, P. S., Wee, C., Valverde, M. A. & Meier, G. R. (2009) Feedstock and biodiesel characterization reports): Available from: http://www.biodiesel.org/resources/reports/gen/20091117.GEN-398.*pdf* (accessed 12.03.16)

Santiago-Urbina, J. A., Ventura – Canseco, L. M. C., Ayora- Talavera, T. R., Ovando – Chacon, S. L., Dendooven, L., Gutieriez-Miali, F. A. & Abud-Archila, M. (2011). Optimization of ethanol production from mango pulp using yeast strains isolated from "taberna", a Mexican fermented beverage. *Afr. J. Microbiology Res., 5*(5), 501-508.

Sarve, A., Varma, M. N. & Sonawane, S. S. (2015) Response surface optimization and artificial neural network modeling of biodiesel production from crude mahua (*Mahua indica*) oil under supercritical ethanol condition using CO_2 as co-solvent. *Royal Society of Chemists Advances*; Issue 85, article in-press.

Shahid, E. M. & Jama, J. (2011). Production of biodiesel: a technical review *Renew. Sustain. Energy Rev., 25* (9), 4732-45.

Sharma, Y. C & Singh, B. (2009). Development of biodiesel current scenarior. *Review Sustain. Energy Rev. 13*(6-7), 1646-51.

Sharmila, S. & Jeyanthi, L. R. (2012). GC-MS Analysis of esters of fatty acid present in biodiesel produced from *Cladophora vagabunda*. *Journal of Chemical and Pharmaceutical Research, 4*(11), 4883-4887.

Shut, S. H., Lee, K. L., Kamaruddin, A. H. & Tusup, S. (2010). Reactive extractions of *Jatropha curcas* seed for production of biodiesel; Process optimization study. *Environ. Sci. Technol., 44,* 4361-4367

Siddharth, J. & Sharma, M. P. (2010). Thermal stability of biodiesel and its blends: A review. *Renewable and Sustainalbe Energy Reviews 15*(1), 438-448.

Silva, G., F., Fernando, L., Camargo, F., Andrea, L. O. & Ferreira, F. , (2011). Application of response surface methodology for optimization of biodiesel production by transesterification of soybean oil with ethanol. *Fuel Processing Technology 92,* 407-413.

Singh, S. P. & Singh, D. (2010). Biodiesel production through the use of different sources and characterization of oils and their esters as the substitutes for deisel: A review. *Renew. Sustain. Energy Rev., 14*(1), 200-16.

Sivaramakrishnam, K. & Ravikumar, P. (2012). Determination of cetane number of biodiesel and its influence on physical properties. *ARFN Journal of Engineering and Applied Science*s, *7* (2), 205-211.

Smith, B. (1999). Infrared spectra interpretation. A systematic approach CRC Press. Boca Raton.

Sridhar, M. K. C, Coker, A. O., Taiwo, H. B. & Abiodun, O. (2014). Experiment on co-digestion of cow dung and water hyacinth (Eichlornia crassipes) for biogas yield. *International Journal of Science Basic and Applied Research (IJSBAR), 15*(1), 16-24.

Srincvasarao, B., Ratnan, B. W., Subbarao, S., Narasimharao, M. & Ayyanna, C. (2013). Ethanol production from cashew apple juice using statistical designs. *J. Biochem. Microb. Technol., 1,* 8-15.

Srinivas, M. R. S., Nagin, C. & Lonsane, B. K. (1994). Use of Placket-Durman design for rapid screening of several nitrogen sources, growth/product promoters, minerals and enzyme inducers

for production of alpha-galactrisidase by *Aspergillum niger* MRSS 234 in solid state fermentation system. *Bioprocess Biosyst. Eng. 10*,139-144.

Steen, E. J., Kang, Y. S., Bokinsky., G, Huzh Schirmer, A. & McClure, A.(2010). Microbial production of fatty acids derived fuels and chemicals from plant biomass. *Nature, 463*, 559-662.

Stein, S. E, & Scott, D. (1994). Optimization and testing of mass spectral library search algorithm for compound identification. *J. Am Soc. Mass Spectron, 5*, 859-866.

Stevens, C. V. & Verhen, R. (2004). Renewable bioresource: Scope and modification for non-food applications. John Willey & Sons, 208-250.

Stewart, C. N. & Joyce, B. L. (2012). Designing the perfect plant feedstock for biofuels production using the whole buffalo to diversify fuels and products. *Biotechnology advances*, *30*, 1011-1022.

Syed, A. B., Gopal, K. R. & Jebaraj, S. A. (2009). A review on biodiesel production combustion, emission and performance. *Renewable and Sustainable Energy Review, 13*, 1628-34.

Tesser, R. D., Serio, M., Giuda, M., Nastasi, M. & Santaceraria, P. (2005). Kinetics of oleic acid etherification with methanol in the presence of triglycerides. *Ind. Eng. Chem. Res.*, *44*, 7978-7982.

Thermo Fisher Scvientific, (2011). Pesticides Method Reference, 2nd edition, Austin TX,USA.

Thompson, R. C., Swan, S. H., Moore, C. J., & Vom Saal, F. S. (2009). Our plastic age. *Philos Trans R Soc B 364*,1973-6.

Thomsen, M. (2005). Complex media from processing of agricultural crops for microbial fermentation. *Applied Microbiology and Biotechnology, 68*(5), 598-606.

Tiwari, A. K., Kumar, A., & Racheman, H. (2007). Biodiesel production from jatropha oil (*Jatropha curcas*) with high FFA , an optimized process. *Biomass Bioenergy, 3*, 569-575.

Togarepi, E., Mapiye, C., Muchanyereyi, N. & Dzomba, P. (2012). Optimization of fermentation parameters for ethanol production from *Ziziziphus mauritiana* fruit pulp using

Saccharomyces cerevisiae (NA333). *International Journal of Biochemistry Research, Review 2*(2), 60-69.

Torres-jimenez, E., Jerman, M. S., Gregorc, A., Lisec, I., Dorado, M. & Kegl, B. (2011). Physical and chemical properties of ethanol-diesel fuel blends. *Fuel, 90*(2), 795-802.

Tsakins, J., Gergis, L.V., Dourtoglou, V., & Spiliotus, V. (1999). Characterization of *Moringa olifera* variety mbololo seed oil of Kenya. *J. Agric food Chem*., *47*, 4495-4499.

U.S Energy Information (2011). International Energy Outlook Available from http//www. Eia.doe.gov/oiaf/ieo/pdf, (accessed 20.02.17).

Udhayaraja, P. & Narayanan, J. S. (2012). Optimization for production of bioethanol using sorghum stovar by *Saccharomyces cerevisiae. Int. J. of Research in Pure and Applied Microbiology, 2*(4), 64-67.

Ureigho, U. N. & Ekeke, B. A. (2010). Nutrient values of *Chrysophyllum albidium linn* (African star apple) as a domestic income plantation species. *African Research Review, 4*(2), 50-56.

Uzodinma, E. O. U., Ofoefule, A. U., Eze, J. I. & Onwuka, N. D. (2007). Biogas production from blends of agro-industrial wastes trends. *Appl. Sci. Res*., *2*(6), 554-558.

Uzoh, C. F., Onukwuli, O. D., Ozofor, I. H. & Odera R. S. (2019). Encapsulation of urea with alkyd resin-starch membranes for controlled N_2 release: synthesis, characterization, morphology and optimum N_2 release. *Process safety and Environmental Protection* 121,133-142.

Varanda, M. G., Pinto, G. & Martins, F. (2011). Life cycle analysis of biodiesel production. *Fuel Processing Technology, 92* (5),1087-1094.

Veljkovic, V. B., Lakicevic, S. H., Stamenkovic, O.S., Todorovic, Z. B. And Lazic, K.L., (2006). Biodiesel production from tobacco (*Nicotiana tabacum L.*) seed oil with a high content of free fatty acids. *Fuel* 85, 2671-2675.

Venkanna, B. K., Ventaramana Reddy, C. & Wadawadagi Swati, B. (2009). Performance, emission and combustion characteristics of direct injection diesel engine running on rice bran

oil/diesel fuel blend. *International Journal of Chemical and Biological Engineering, 2*(3), 131-137.

Vujicic, D., Comic, D., Zarubica, A., Micic, R., & Boskovi, G., 2010. Kinetics of biodiesel synthesis from sunflower oil over CaO heterogeneous catalyst. *Fuel* 89, 2054– 2061.

Wahome, A., Ngunjiri, G.M.N., Shitanda, D. & Ogola, W.O. (2013). Performance Characteristics of blended rice bran biodiesel in a diesel engine. *International Journal of Engineering Science Invention, 2*(5), 35-41.

Wang, L. Jin, J. Wang, S., Wang, X. Tian, Y. & Chen, J. (2012). A novel method for identification of illegal cooking oil (1): detection of three capsaicinoids with liquid chromatography-mass spectrometry, *Chin. J. Chromatogr.* A30, pp. 1094.

Wohlgemith, R. (2009). The locks and keys to industrial biotechnology. *N. Biotechnol., 25*, 204-13.

Wu, W.N., Foglia, T.A., Marmer, W.N., & Philips, J. G. (1998). Optimizing production of ethyl esters of grease using 95% ethanol by response surface methodology. *Journal of America Oil Chemists Society, 76*, 4-10.

Xue, J., Grift, T. E. & Hansen, A. C. (2011). Effect of biodiesel on engine performances and emissions. *Renew. Sustain. energy Rev15*(2), 1098-116.

Yan, Z., & Ohlrogge, J. B. (2009). Turnover of fatty acids during natural senescence of *Arabidopsis, Brachypodium* and switchgrass and in *Arabidopsis* B-oxidation mutants. *Plant Physiol. 150*, 1981-9.

Yang, J., Golovitcher, V. L., Lurbi, P. R. & Snchez, J. J. L. (2012). Chemical kinetic study of nitrogen oxides formation trends in biodiesel combustion. *Int. J. of Chem. Eng., 2012*, 22.

Yuan, X, Liu, J., Zeng, G., Shi, J., Tong, J. & Huang, G. (2008). Optimization of conversion of waste ripe seed oil with high FFA to biodiesel using response surface methodology. *Renew. Energy, 33*, 1678-1684.

Zanchetta, P., Wheeler, P. W., Clare, J. C., Bland, M., Empringham, L. & Katsis, D. (2008). Control design of a three-phase matrix-converter-based AC-AC mobile utility power supply. *IEEE Trans. on Industrial Electronics,* 55 (1), 209-217.

Zhan, X., Wang, D., Tuinsha, M. R., Bean, S., Sieb, P. A. & Sun, X. S. (2003). Ethanol and lactic acid production as affected by sorghum genotype and location. *Ind. Crops production 18,* 245-255.

Zhan, Y. (2008). Reviving the carbohydrate economy via multi-product lignocellulose biorefiineries. *Journal of Ind. Microbiology, 35*(5), 367-375.

Zhang, J., Che, S., Yang, R. & Yan, Y. (2010). Biodiesel production from vegetable oil using heterogeneous acid and alkali Catalyst. *Fuel,* 89 (10), 2939-2944.

Zhang, L., Sheng, B., Xin, Z., Liu, Q., & Sun, S., (2010). Kinetics of transesterification of palm oil and dimethyl carbonate for biodiesel production at the catalysis of heterogeneous base catalyst. *Bioresour. Technol*. 101, 8144–8150.

Ziegenhals, K., Hubschmann, H. J., Speerk, V. & Jira, W. (2008). Fast- GC/HRMS to quantify the EU priority PAH. *J. Sep. Sci*, 31, 1779-1786.

APPENDIX 1

PICTORIAL PRESENTATION OF THE SELECTED BIOMASS

a.

b.

c.

d.

e.

f.

g.

Plate A1.1: Sweet almond fruit biomass, a. The fruit, b. Fruit cut section, c. Dried fruit pulp, d. Inner seed with coat e. The seed, f. The fruit husk, g. The ground pulp (raffinnate and 600µm particle size).

a.

b.

c.

d.

e.

f

g.

Plate A1.2: African star apple fruit biomass.

a. Fruit, b. Fruit cut section, c. ground fruit pulp, d. dried pulp, e. The seed with coat, f. The seed coat, g. The seed.

a

b

c.

d.

Plate A1.3: African pear fruit biomass sample, a. Fruit, b. Seed, c. Released seed for drying, d. Ground seed.

APPENDIX 2

ANALYTICAL PROCEDURES FOR OIL PHYSICO-CHEMICAL PROPERTIES

A2.1: Determination of Density

Materials used

- Density bottle
- Weighing balance (Ohaus, Model AR 3130. Readability: 0.001g. Range: 0-300g)
- Measuring cylinder
-

Procedure

A clean empty density bottle was weighed on an electronic balance and the weight (w_1) noted. It was then filled with the sample and weighed (w_2). All the determinations were at room temperature. The volume (V) of the density bottle was noted.

$$Density = \frac{W_2 - W_1}{V} \quad \text{(A2.1)}$$

A2.2: Determination of Flash and fire point

The flash and fire point of the fuel samples was determined as per ASTM D-93. A Pensky Martin Flash Point (closed) apparatus was used to measure the flash and fire point of the fuel samples. The sample was filled in the test cup up to the specified level and was heated and stirred at a slow and constant rate. At every 10 ^{o}C temperature rise, flame was introduced for a moment with the help of a shutter. The temperature at which a flash appeared in the form of sound and light was recorded as flash point. The fire point was recorded as the temperature at which fuel vapour catches fire and stays for minimum of five seconds. The temperature was measured with the help of a thermometer.

A2.3: Determination of Viscosity

This was done by passing the sample through one end of Oswald viscometer and allowing the sample to flow from one marked end of the bulb to the other end. The time taken for this flow to take place is noted and used in calculating the viscosity.

Viscosity (cp) $n1=\frac{n2d1t1}{d2d2}$ (A2.2)

n1= viscosity of sample

*d*1= density of sample

t1 = time of flow (sample)

n2 = viscosity of water

*d*2 = density of water

t2 = time of flow (water)

A2.4: Determination of Iodine Value (Wij's).

Materials

- Glacial acetic acid
- Potassium iodide solution (10%)
- Iodine
- Iodine Trichloride
- 0.1N sodium thiosulphate solution
- Starch indicator
- Carbon tetrachloride (chloroform)
- Wij's solution
- Glass stoppered flasks

Preparation of Wij's Solution

9g of iodine was dissolved in 300ml of Carbon tetrachloride. 8g of iodine trichloride was also dissolved in 200ml of glacial acetic acid. The two were mixed together and diluted to 1 liter with glacial acetic acid.

Procedure

The sample was melted and filtered through a filter paper. 0.5g of the sample was weighed into a clean flask. 25 ml of carbon tetrachloride and 25 ml of Wiji's solution was added to it. The glass stopper was wetted with KI solution and used to cover the flask. The flask was swirled and allowed to stand in the dark for 30 minutes. A blank test was carried out simultaneously under similar experimental conditions. After standing for 30 minutes, 15 ml of KI solution and 100 ml of water were added and the stopper rinsed. The liberated iodine was titrated with standard sodium thiosulphate solution while swirling the contents of the flask continuously until the colour of the solution changed to straw yellow. 1 ml of starch solution was added and the titration continued until the blue colour formed disappeared after shaking thoroughly.

A2.5: Determination of. Refractive Index

Materials Used

Abbe refractometer -bench type (Model: WYA-2S, Made by Searchtech Instruments)

Procedure

The power switch was pressed on and the illuminating lamp came up and the display showed 0000. A drop of the sample was introduced on the working surface of the lower refracting prism. The rotating arm and the collecting lens cone of the light gathering

illuminating units were rotated so as to make the light-intake surface of the upper light-intake prism to be illuminated evenly. The field of view was observed through the eye piece and the adjustable hand wheel was rotated so as to make the line dividing the dark and light areas fall in the cross line. The dispersion correction hand wheel was rotated so as to get a good contrast between the light and dark area and minimum dispersion. The read button was then pressed and the refractive index was displayed on the screen.

A2.6: Determination of Acid Value (MgkOH/g)

Materials

- Ethanol
- 1% phenolphthalein indicator
- 0.1N KOH

Procedure

5g of the sample was weighed into a flask. 50 ml of neutralized ethanol was poured into the flask. The contents were mixed together and boiled. It was then titrated with 0.1N KOH to a faint pink colour that persisted for at least 15 seconds.

$$A.V = \frac{56.1xNxTx100}{1000xG} \qquad \text{(A2.3)}$$

Where:

N = Normality of standard KOH used

T = Titration volume

G = weight of sample

A2.7: Determination of Saponification Value

Materials

- Alcoholic KOH (0.5N)
- Standard 0.5N HCl
- Phenolphthalein indicator (1% w/v)
- Reflux condenser with quick fit flask
- Heating mantle

Procedure

2g of the oil was weighed into the flask. 25ml of 0.5N alcoholic potassium hydroxide was added to it and boiled under reflux for one (1) hour. The excess alkali was determined by titration with 0.5N Hydrochloric acid while the solution was still hot using 0.5ml of 1.0% alcoholic solution of phenolphthalein as indicator. A blank was determined under the same condition without using the sample.

$$S.V = \frac{56.1x(B-S)xN}{W} \qquad \text{(A2.4)}$$

S = Volume in ml of standard HCl required for the sample

B = Volume in ml of standard HCl required for the blank.

N = Normality of HCl

W = Weight of oil used.

A2.8: Determination of. Cloud and pour points

The Cloud and Pour point of fuel samples were determined as per ASTM D-2500 using the Cloud and Pour point apparatus. The apparatus mainly consists of 12 cm high glass tubes of

3 cm diameter. These tubes are enclosed in an air jacket, which is filled with a freezing mixture of crushed ice and sodium chloride crystals. The glass tube containing fuel sample is taken out from the jacket at every 10°C interval as the temperature falls, and is inspected for cloud / pour point. The point at which a haze was first seen at the bottom of the sample was taken as the cloud point. The pour point was taken to be the temperature 10 °C above the temperature at which no motion of fuel was observed for five seconds on tilting the tube to a horizontalposition.

A2.9: Determination of Moisture Content

The A.O.A.C method (2000) was used. Porcelain crucibles were washed and dried in an oven at 100^{o}C for 30 minutes and allowed to cool in a desiccator. One gramme of the sample was placed into weighed crucibles and then put inside the oven set at 105^{o}C for 4 hours. The samples were removed from the oven after this period and then cooled and weighed. The drying was continued and all the samples with the crucibles weighed until a constant weight was obtained.

$$\% \text{ moisture} = \frac{A-B}{A} \times \frac{100}{1} \qquad \text{(A2.5)}$$

A = Original weight of sample

B = Weight of dried sample.

A2.10: Determination of Ash Content Determination

The residue remaining after all the moisture have been removed and the fats, proteins, carbohydrates, vitamins and organic acids burnt away by ignition at about 600^{o}C is called ash. It is usually taken as a measure of the mineral content of the sample.

Using AOAC (2000) method, 1g of the finely ground samples were weighed into porcelain crucibles which have been washed, dried in an oven at 100^{o}C, cooled in a desiccator and weighed. They were then placed inside a muffle furnace and heated at 600^{o}C for 4 hours. After this, they were removed and cooled in a desiccator and then weighed.

$$\% \text{ Ash} = \frac{A - B}{C} \times \frac{100}{1} \qquad \text{(A2.6)}$$

A = Weight of crucible + ash

B = Weight of crucible

C = Weight of original sample

APPENDIX 3

THE FT-IR SPECTRUM OF THE SEED OILS AND THEIR BIODIESELS.

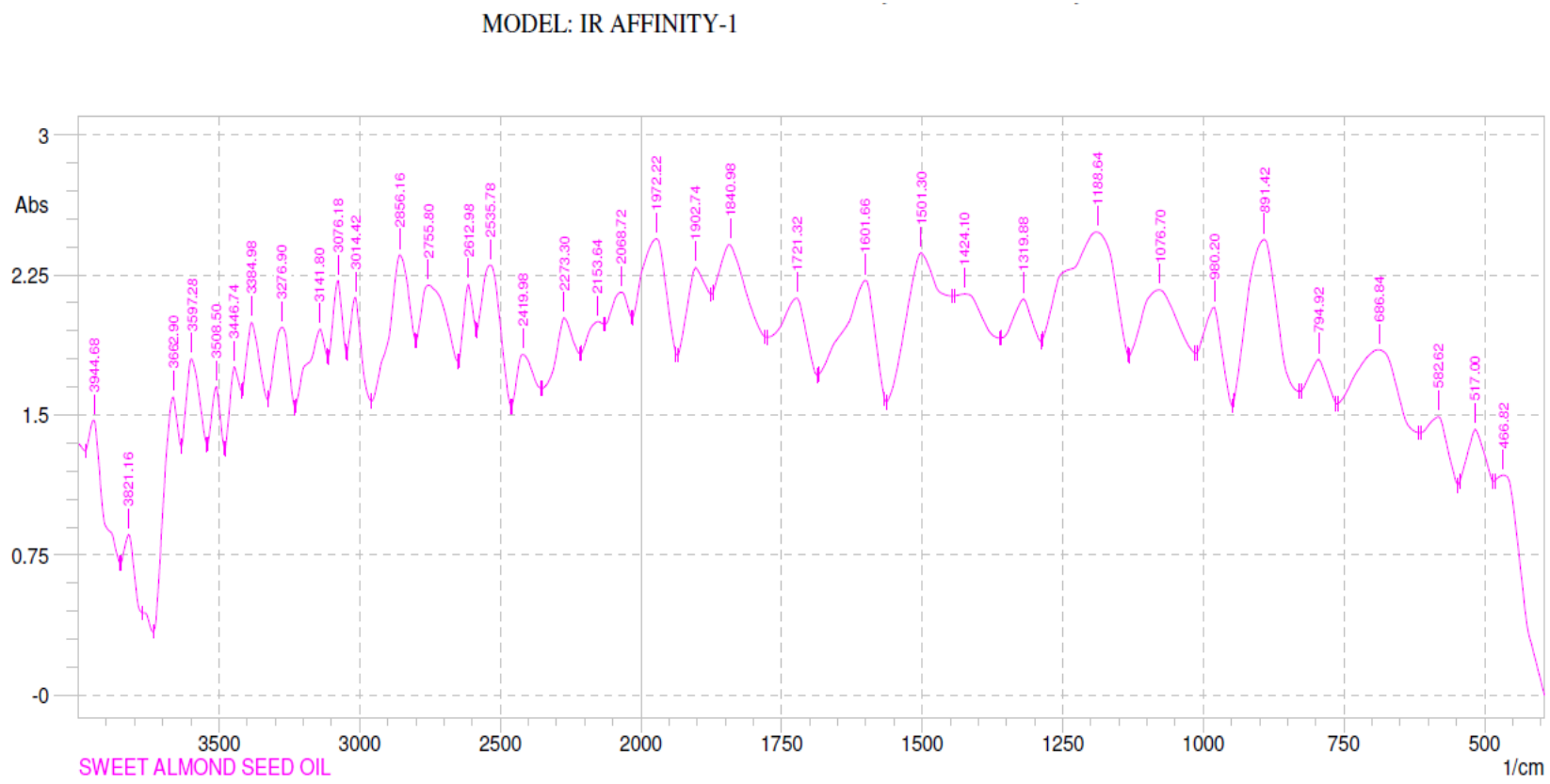

Figure A3.1: FT-IR Spectrum for SASO.

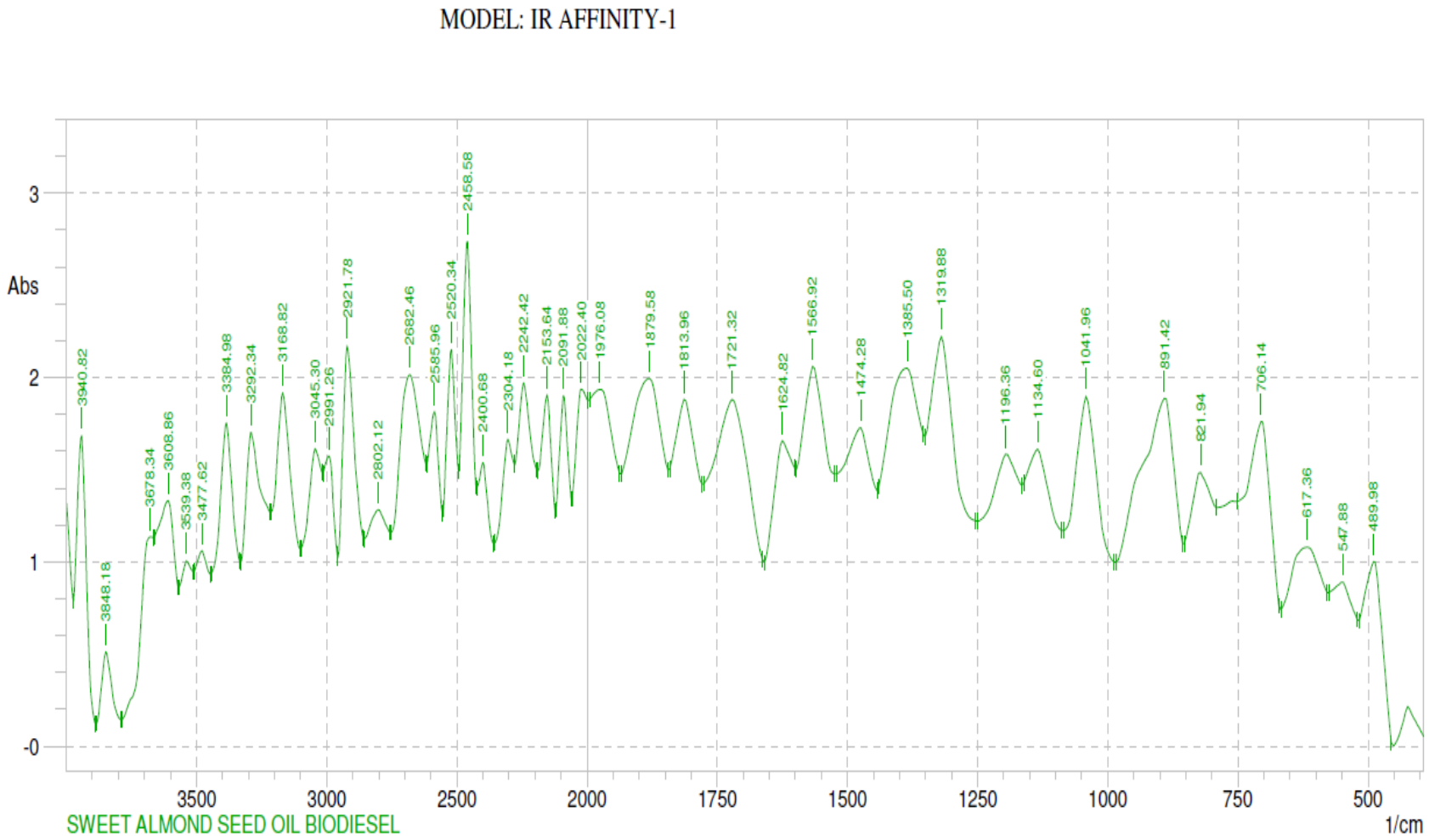

Figure A3.2: FT-IR Spectrum for SASOME.

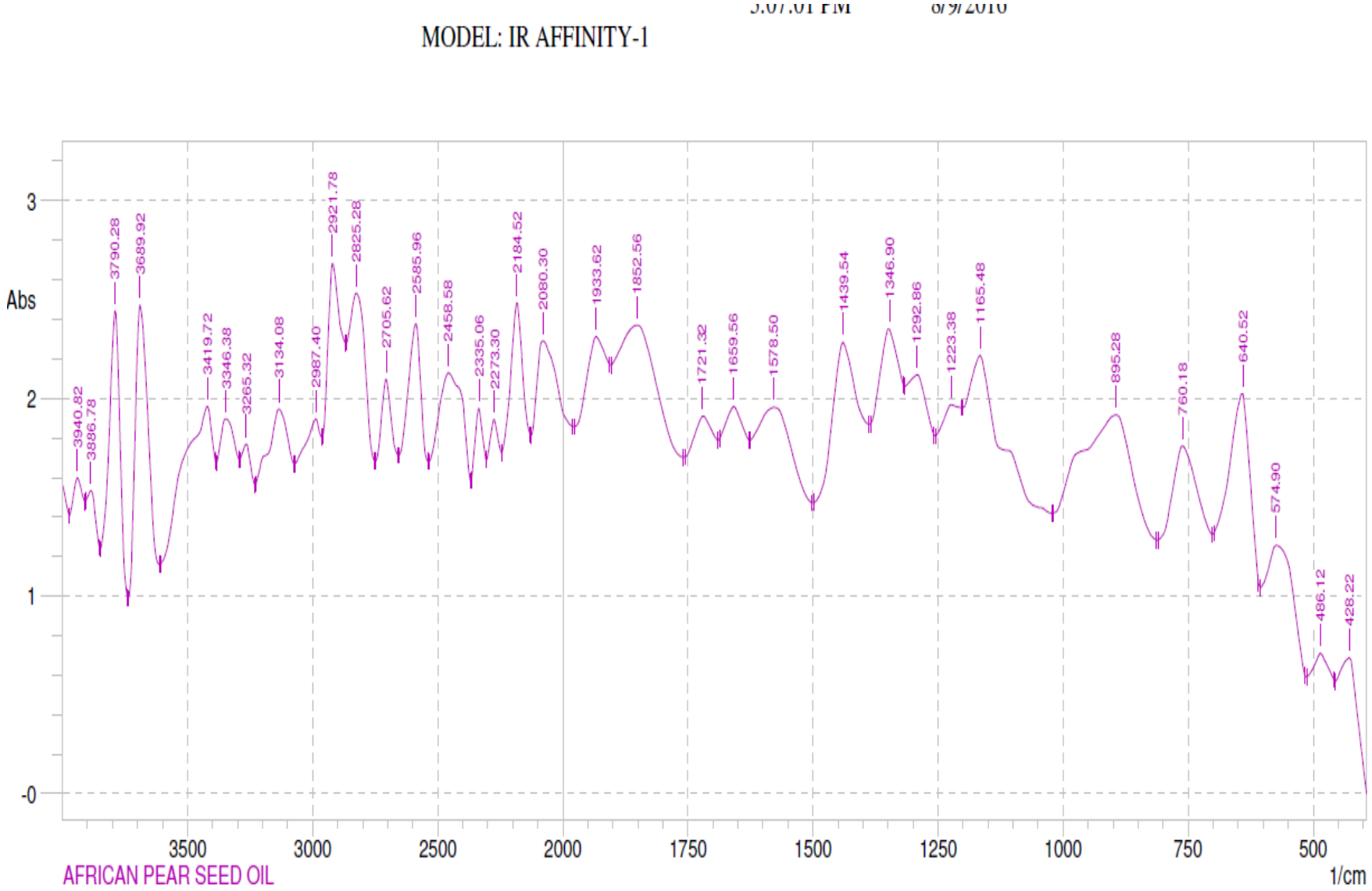

Figure A3.3: FTIR Spectrum for APSO

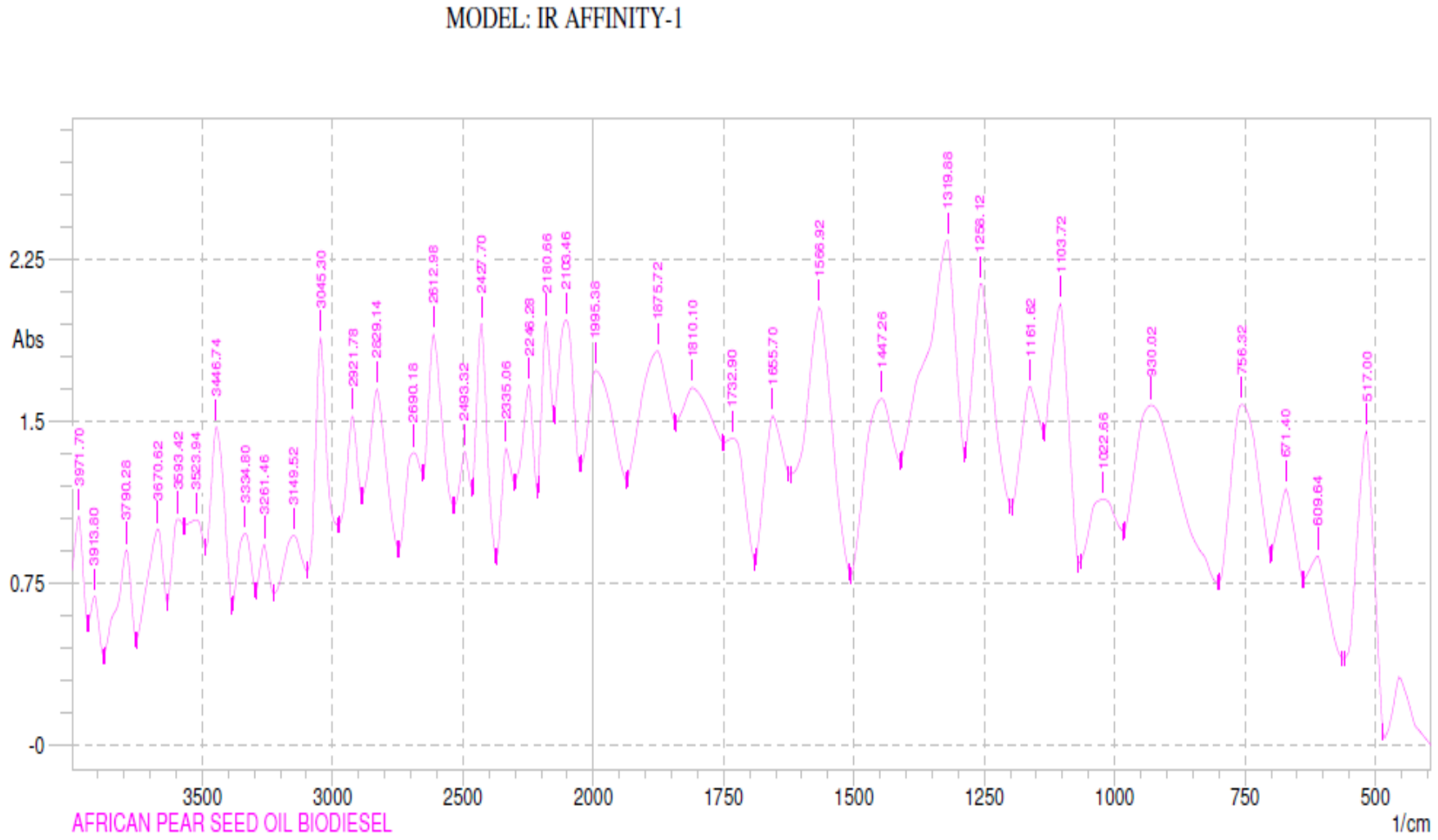

Figure A3.4: FTIR Spectrum for APSOME.

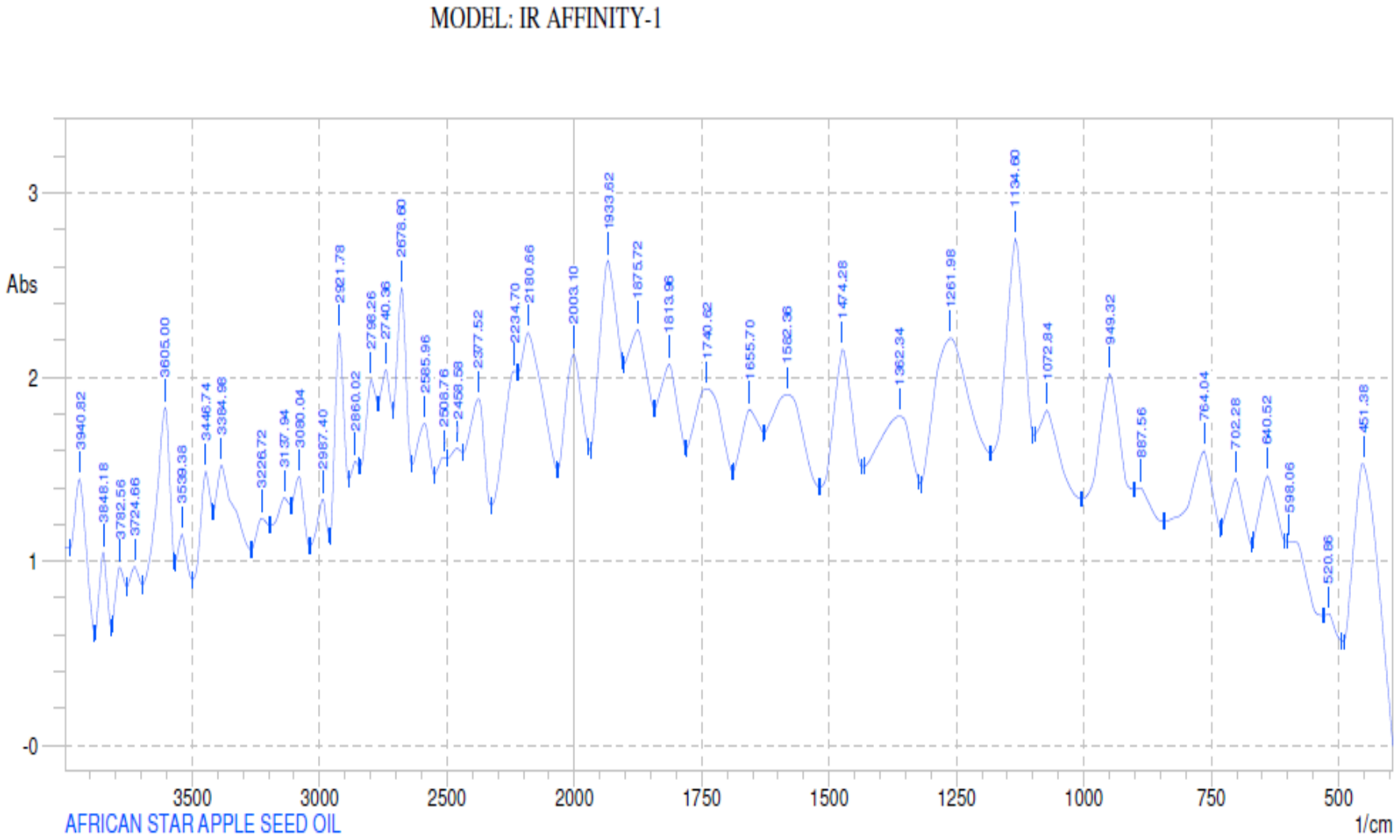

Figure A3.5: FTIR Spectrum for ASASO.

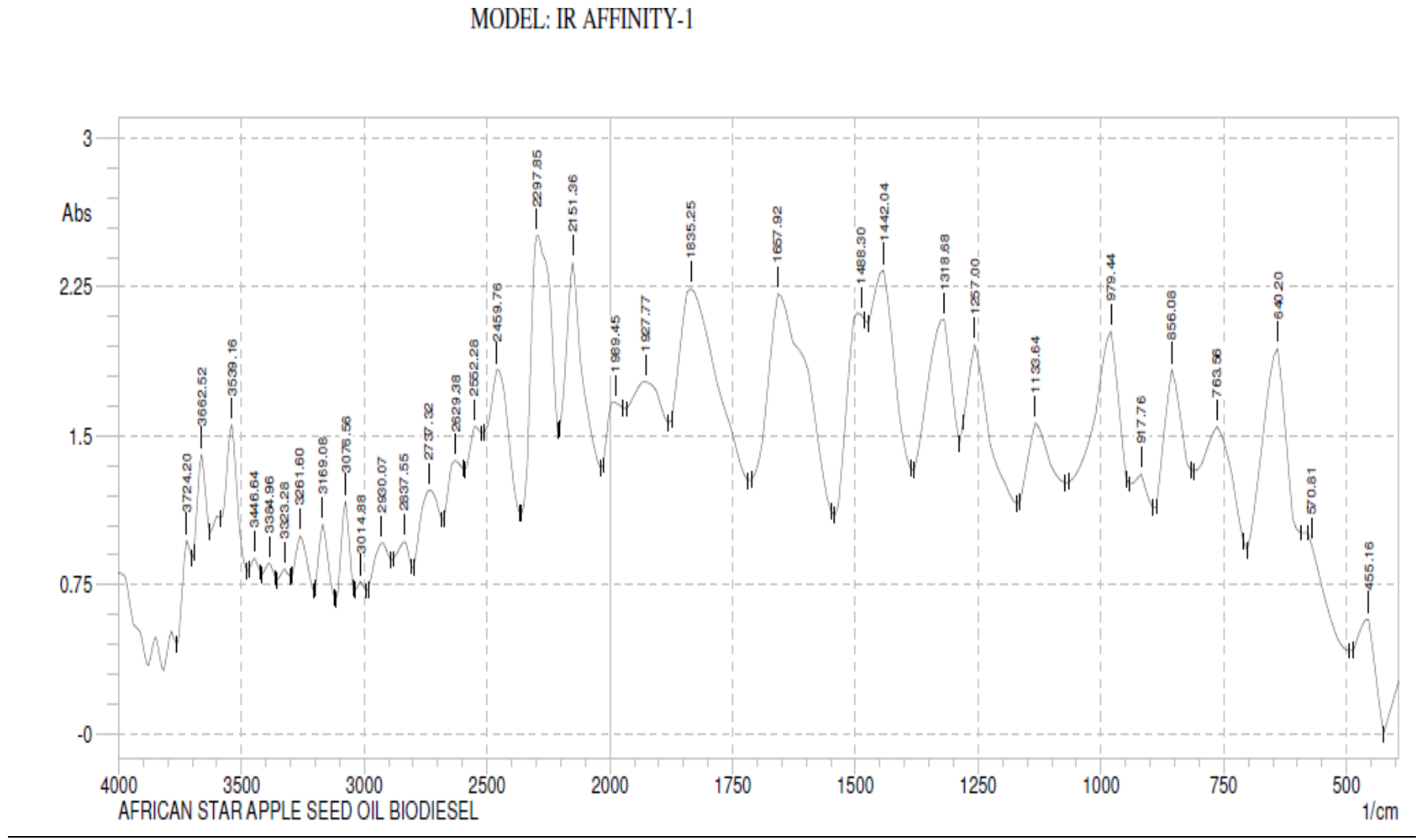

Figure A3.6: FTIR Spectrum for ASASOME.

APPENDIX 4

THE GC-MS SPECTRUM OF THE BIODIESEL

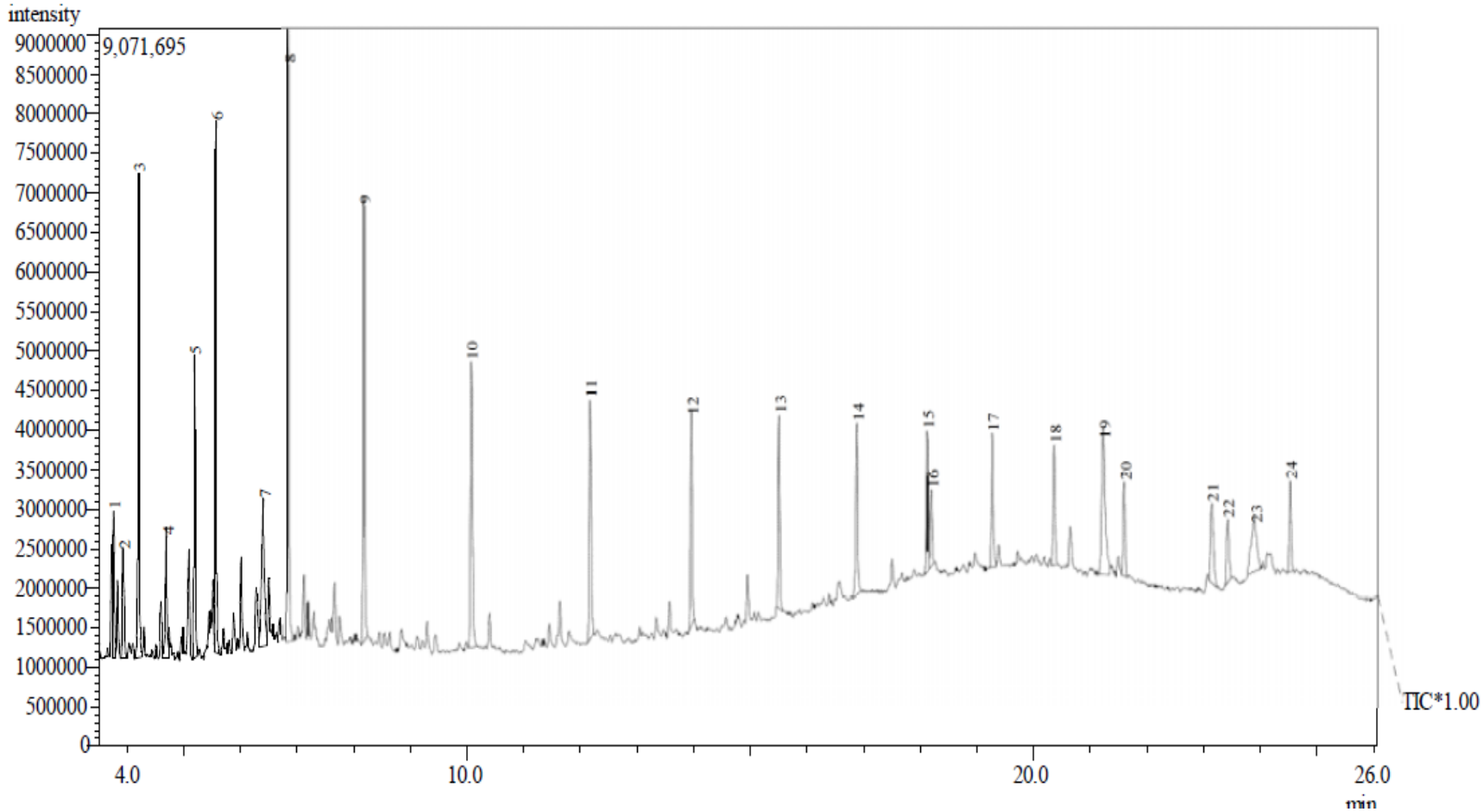

Figure A4.1: GC-MS chromatogram of SASOME.

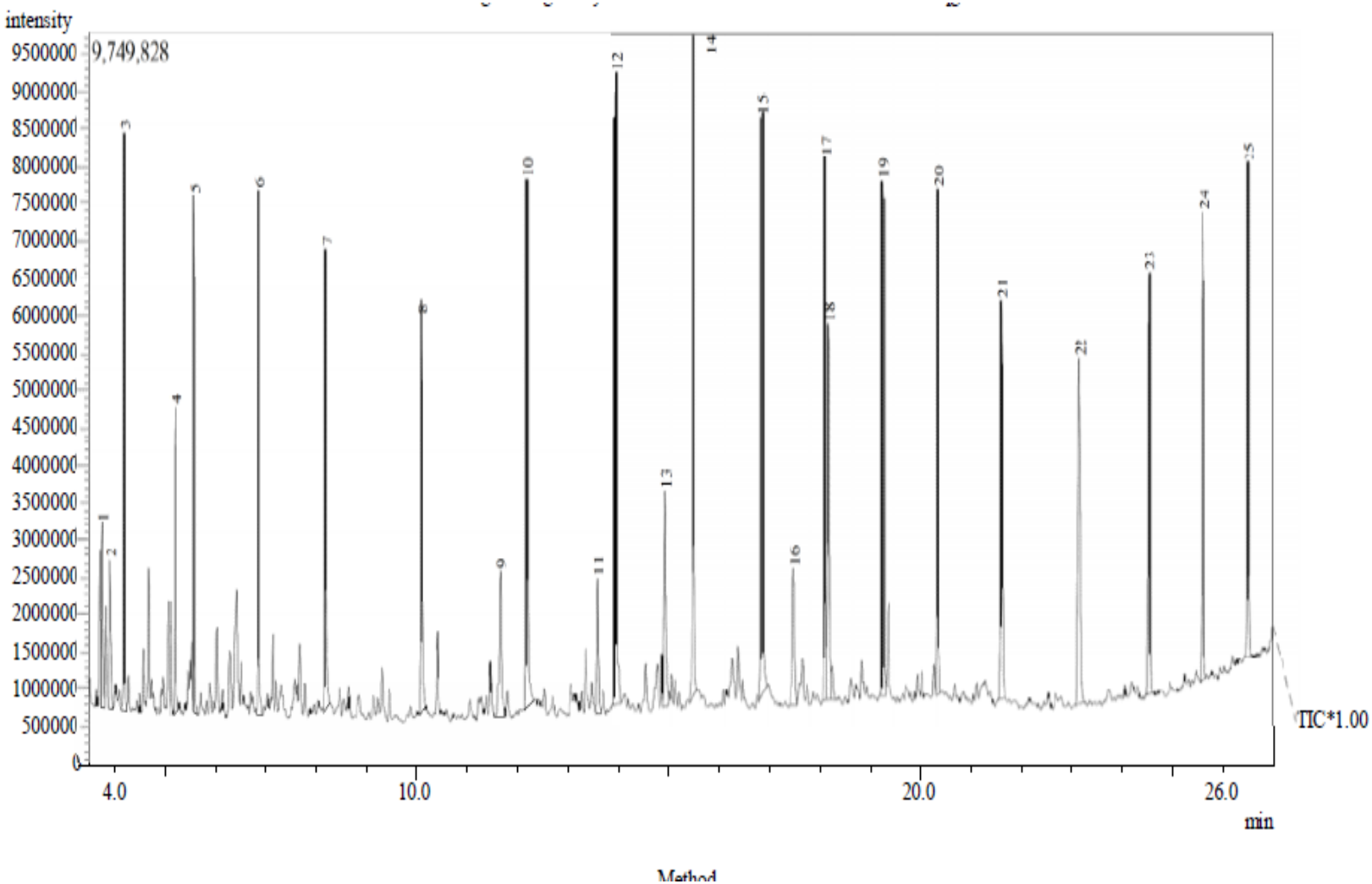

Figure A4.2: GC-MS chromatogram of APSOME.

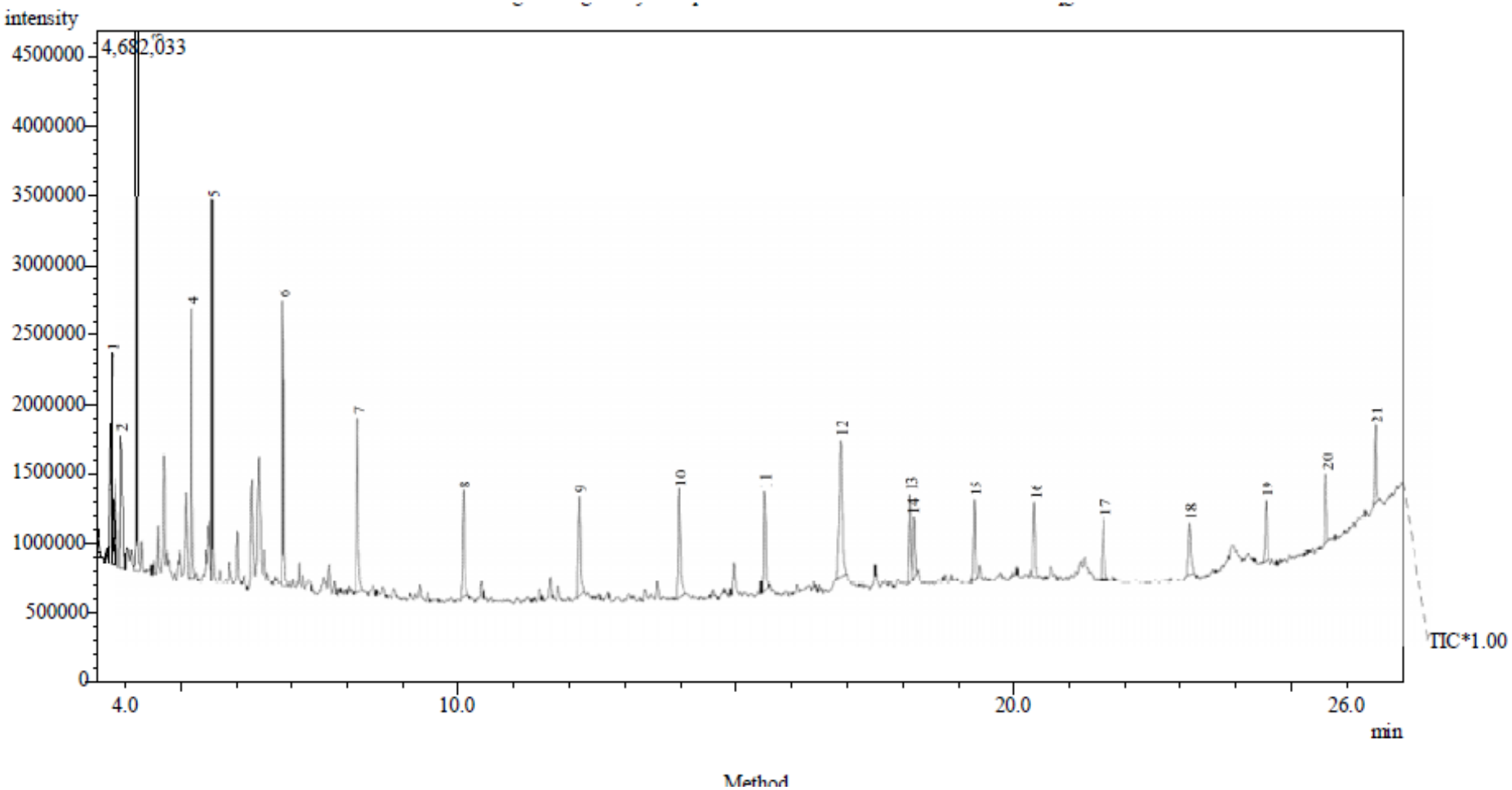

Figure A 4.3: GC-MS chromatogram of ASASOME.

APPENDIX 5

EFFECT OF OPERATING PARAMETERS ON YIELD AND VISCOSITY

Table A5.1: Biodiesel yield and viscosity obtained at different operating conditions.

Operating Parameters	Viscosity (mm^2/s)			Biodiesel yield (%)		
	ASASO FAME	SASO FAME	APSO FAME	ASASO FAME	SASO FAME	APSO FAME
Reaction time (mins)						
45	2.94	3.00	3.05	50.10	60.40	55.10
50	2.93	2.98	3.00	62.10	75.10	65.40
55	2.90	2.97	2.98	70.30	84.40	75.30
60	2.85	2.90	2.92	75.50	87.20	84.60
65	2.80	2.88	2.91	84.40	94.40	92.50
70	2.82	2.86	2.90	80.50	92.40	90.00
75	2.82	2.86	2.89	79.20	90.50	89.50
Catalyst concentration (wt%)						
0.5	3.51	4.05	4.27	70.40	75.10	65.50
1.0	3.05	3.84	3.90	72.50	85.20	75.20
1.5	2.82	3.05	3.45	82.10	91.40	86.50
2.0	2.71	2.81	3.03	86.40	93.60	86.50
2.5	2.52	2.62	2.83	84.50	90.90	86.00
3.0	2.22	2.51	2.83	80.10	86.80	82.50
Reaction temperature(^oC)						
45	3.35	3.38	3.40	55.20	68.50	60.00
50	3.38	3.40	3.45	59.60	70.70	65.10
55	3.39	3.44	3.50	65.20	80.50	75.20
60	3.40	3.46	3.52	75.30	90.60	86.70
65	3.42	3.48	3.55	80.50	95.50	94.50
70	3.43	3.50	3.57	78.80	93.00	92.10
Methanol /oil molar ratio						
3:1	3.11	3.21	3.82	57.90	65.50	60.10
4:1	3.05	3.12	3.40	70.60	78.50	73.98
5:1	2.72	2.87	3.30	75.80	85.70	80.40
6:1	2.55	2.69	2.70	81.50	89.40	84.50
7:1	2.40	2.51	2.60	84.90	91.60	87.68
8:1	2.40	2.45	2.65	85.70	92.50	88.00

APPENDIX 6

DIESEL ENGINE PERFORMANCE, COMBUSTION AND EMISSION CHARACTERISTICS DATA

Table A6.1: Raw data for petro-diesel combustion in Perkin 4:108 diesel engine

S/N	1	2	3	4	5
Oil Type	HSD	HSD	HSD	HSD	HSD
Oil Viscosity,μ (mm^2/s)	3.21	3.21	3.21	3.21	3.21
Oil Cal. Value, Q_{net} (MJ/kg)	43.5	43.5	43.5	43.5	43.5
Oil Density, ρ(kg/m^3)	830	830	830	830	830
Oil Flash Point, FP (˚C)	60	60	60	60	60
Speed, N(rpm)	1500	1500	1500	1500	1500
Torque, T(Nm)	5.0	10.0	20.0	30.0	40.0
Time, t(s)	160	136	110	94	76
Volume, v (cm^3)	50	50	50	50	50
hw (mm H_2O)	5.70	6.40	7.60	8.70	9.50
Inlet Temp (˚C)	32.0	34.0	35.0	37.0	39.0
Exit temp (˚C)	33.0	35.5	37.0	39.5	41.0
Head (cm)	12.0	15.0	15.5	15.7	15.9
Inlet Temp. (˚C)	41	51	62	74	86
Exit temp (˚C)	50	61	78	85	94
Head (cm)	16.6	14.5	13.9	11.5	10.2
Exh. Temp. (˚C)	175	205	225	240	250
CO (%)	0.072	0.050	0.055	0.059	0.25
NO_X(ppm)	210	352	550	720	760
CO_2(%)	3.50	4.0	4.7	5.5	6.9
HC (ppm)	32.50	26.51	30.50	40.50	55.1
Smoke Opacity	4.34	9.22	16.74	20.13	27.52
$V_f \times 10^{-6}(m^{3/s})$	0.3125	0.3676	0.4545	0.5319	0.6579
$M_f \times 10^{-4}$ (kg/s)	2.60	3.05	3.77	4.41	5.46
$Va(m^{3/s})$	0.0148	0.0157	0.0171	0.0183	0.0191
Ma(kg/s)	0.0163	0.0173	0.0188	0.0204	0.0211
Bp(kw)	0.785	1.570	3.141	4.712	6.283
Bmep(bar)	0.354	0.707	1.415	2.123	2.831
$Vs(m^3/s)$	0.044	0.044	0.044	0.044	0.044
Π_v (%)	33.63	35.70	38.90	41.60	43.41
Π_{BT}(%)	7.0	11.8	19.2	24.6	26.5
A_F	62.69	56.72	49.87	46.26	38.64
BSFC (kg/kwh)	1.192	0.699	0.432	0.337	0.313
BSEC (MJ/kwh)	0.052	0.030	0.019	0.015	0.014

Table A6.2: Raw data for SASOME B100 combustion in Perkin 4:108 diesel engine

5	4	3	2	1	S/N
B100	B100	B100	B100	B100	Oil Type
4.05	4.05	4.05	4.05	4.05	Oil Viscosity μ (mm^2/s)
31.18	31.18	31.18	31.18	31.18	Oil Cal. value, Qnet (MJ/kg)
849	849	849	849	849	Oil Density, ρ(kg/m^3)
136	136	136	136	136	Oil Flash Point, FP (˚C)
1500	1500	1500	1500	1500	Speed, N(rpm)
40.0	30.0	20.0	10.0	5.0	Torque, T(Nm)
87	102	151	192	201	Time, t(s)
50	50	50	50	50	Volume, v (cm^3)
9.50	8.70	7.60	6.40	5.70	hw (mm H_2O)
39.0	37.0	35.0	34.0	32.0	Inlet Temp (˚C)
42.0	39.0	37.2	36.0	33.7	Exit temp (˚C)
15.2	14.9	14.7	14.5	12.8	Head (cm)
86.0	74.0	63.0	52.0	41.0	Inlet Temp. (˚C)
94.0	85.0	78.0	61.0	50.0	Exit temp (˚C)
10.2	11.5	13.9	14.5	16.6	Head (cm)
237	220	197	180	160	Exh. Temp. (˚C)
0.26	0.057	0.049	0.050	0.06	CO (%)
830	816	600	415	270	NO_X(ppm)
7.59	6.31	4.50	4.28	3.55	CO_2(%)
30.0	26.10	15.71	12.50	11.0	HC (ppm)
					Smoke Opacity
0.575	0.490	0.331	0.291	0.249	$V_f \times 10^{-6}(m^{3/s})$
4.81	4.16	3.811	2.47	2.11	$M_f \times 10^{-4}$ (kg/s)
0.0191	0.0183	0.0171	0.0157	0.0148	$Va(m^{3/s})$
0.0211	0.0204	0.0188	0.173	0.0163	Ma(kg/s)
6.283	4.712	3.141	1.570	0.785	Bp(kw)
2.831	2.123	1.415	0.707	0.354	Bmep(bar)
0.044	0.044	0.044	0.044	0.044	$Vs(m^3/s)$
43.41	41.60	38.90	35.70	33.63	η_v (%)
41.89	36.32	35.84	20.38	11.99	η_{BT}(%)
43.87	49.04	66.88	70.04	77.25	A_F
0.28	0.32	0.32	0.57	0.96	BSFC (kg/kwh)
0.009	0.010	0.010	0.018	0.030	BSEC (MJ/kwh)

Table A6.3: Raw data for SASOME B75 combustion in Perkin 4:108 diesel Engine.

5	4	3	2	1	S/N
B75	B75	B75	B75	B75	Oil Type
4.00	4.00	4.00	4.00	4.00	Oil Viscosity μ (mm^2/s)
32.48	32.48	32.48	32.48	32.48	Oil Cal. value, Qnet (MJ/kg)
844	844	844	844	844	Oil Density, ρ(kg/m^3)
116	116	116	116	116	Oil Flash Point, FP (˚C)
1500	1500	1500	1500	1500	Speed, N(rpm)
40.0	30.0	20.0	10.0	5.0	Torque, T(Nm)
79	84	96	170	200	Time, t(s)
50	50	50	50	50	Volume, v (cm^3)
9.50	8.70	7.60	6.40	5.70	hw (mm H_2O)
40.0	37.0	35.0	34.0	32.0	Inlet Temp (˚C)
42.7	39.5	37.3	35.1	33.6	Exit temp (˚C)
15.2	14.9	14.7	14.5	12.8	Head (cm)
86.0	74	63	52.0	41.0	Inlet Temp. (˚C)
95.0	86	79	64	55.0	Exit temp (˚C)
10.5	11.5	13.9	14.5	16.6	Head (cm)
240	210	188	170	145	Exh. Temp. (˚C)
0.30	0.060	0.50	0.55	0.057	CO (%)
8.25	814	597	412	256	NO_X(ppm)
7.58	6.30	4.95	4.26	3.54	CO_2(%)
32.1	28.0	17.40	16.0	15.50	HC (ppm)
					Smoke Opacity
0.633	0.59	0.52	0.294	0.25	$V_f \times 10^{-6}(m^{3/s})$
5.34	4.97	4.39	2.489	2.11	$M_f \times 10^{-4}$ (kg/s)
0.0191	0.0183	0.0171	0.0157	0.0148	$Va(m^{3/s})$
0.0211	0.0204	0.0188	0.173	0.0163	Ma(kg/s)
6.283	4.712	3.141	1.570	0.785	Bp(kw)
2.831	2.123	1.415	0.707	0.354	Bmep(bar)
0.044	0.044	0.044	0.044	0.044	$Vs(m^3/s)$
43.41	41.60	38.90	35.70	33.63	η_v (%)
36.22	28.96	26.86	19.50	11.45	η_{BT}(%)
39.51	41.05	42.82	69.76	77.25	A_F
0.31	0.38	0.50	0.59	0.96	BSFC (kg/kwh)
0.010	0.012	0.016	0.019	0.031	BSEC (MJ/kwh)

Table A6.4: Raw data for SASOME B50 combustion in Perkin 4:108 diesel engine

5	4	3	2	1	S/N
B50	B50	B50	B50	B50	Oil Type
3.92	3.92	3.92	3.92	3.92	Oil Viscosity μ (mm^2/s)
33.88	33.88	33.88	33.88	33.88	Oil Cal. value, Qnet (MJ/kg)
840	840	840	840	840	Oil Density, ρ(kg/m^3)
107	107	107	107	107	Oil Flash Point, FP (˚C)
1500	1500	1500	1500	1500	Speed, N(rpm)
40.0	30.0	20.0	10.0	5.0	Torque, T(Nm)
91	105	129	165	199	Time, t(s)
50	50	50	50	50	Volume, v (cm^3)
9.50	8.70	7.60	6.40	5.70	hw (mm H_2O)
40.0	37.0	35.0	34.0	32.0	Inlet Temp (˚C)
42.6	39.4	37.3	35.2	33.5	Exit temp (˚C)
15.2	14.9	14.7	14.5	12.8	Head (cm)
86.0	74.0	63.0	52.0	41.0	Inlet Temp. (˚C)
92.1	84.0	79.0	61.0	52.0	Exit temp (˚C)
10.5	11.5	13.9	14.5	16.6	Head (cm)
245	215	185	165	150	Exh. Temp. (˚C)
0.38	0.059	0.049	0.050	0.056	CO (%)
820	810	595	408	254	NO_X(ppm)
7.55	6.25	4.90	4.25	3.52	CO_2(%)
33.50	27.50	15.00	13.00	12.50	HC (ppm)
26.99	24.67	19.50	15.21	8.75	Smoke Opacity
0.54	0.47	0.38	0.303	0.251	$V_f \times 10^{-6} (m^{3/s})$
4.61	4.00	3.25	2.54	2.11	$M_f \times 10^{-4}$ (kg/s)
0.0191	0.0183	0.0171	0.0157	0.0148	Va($m^{3/s}$)
0.0211	0.0204	0.0188	0.0173	0.0163	Ma(kg/s)
6.283	4.712	3.141	1.570	0.785	Bp(kw)
2.831	2.123	1.415	0.707	0.354	Bmep(bar)
0.044	0.044	0.044	0.044	0.044	Vs(m^3/s)
43.41	41.59	38.86	35.68	33.63	η_v (%)
40.22	34.76	28.53	18.24	10.98	η_{BT}(%)
45.77	51.00	57.85	68.11	77.25	A_F
0.264	0.310	0.37	0.58	0.9679	BSFC (kg/kwh)
0.009	0.010	0.013	0.020	0.0328	BSEC (MJ/kwh)

Table A6.5: Raw data for SASOME B25 combustion in Perkin 4:108 diesel engine.

5	4	3	2	1	S/N
B25	B25	B25	B25	B25	Oil Type
3.50	3.50	3.50	3.50	3.50	Oil Viscosity μ (mm^2/s)
35.2	35.2	35.2	35.2	35.28	Oil Cal. value, Qnet (MJ/kg)
835	835	835	835	835	Oil Density, ρ(kg/m^3)
98	98	98	98	98	Oil Flash Point, FP (˚C)
1500	1500	1500	1500	1500	Speed, N(rpm)
40.0	30.0	20.0	10.0	5.0	Torque, T(Nm)
80	987	105	145	172	Time, t(s)
50	50	50	50	50	Volume, v (cm^3)
9.50	8.70	7.60	6.40	5.70	hw (mm H_2O)
40.0	37.0	35.0	34.0	32.6	Inlet Temp (˚C)
42.7	39.5	37.3	35.1	33.6	Exit temp (˚C)
15.2	14.9	14.7	14.5	12.8	Head (cm)
86.0	74	63.0	52.0	41.0	Inlet Temp. (˚C)
94.0	85	78.0	61.0	50.0	Exit temp (˚C)
10.2	11.5	13.9	14.5	16.6	Head (cm)
248	220	190	175	125	Exh. Temp. (˚C)
0.45	0.078	0.049	0.050	0.055	CO (%)
858	800	589	405	250	NO_X(ppm)
7.50	6.21	4.81	4.22	3.51	CO_2(%)
35.50	31.70	17.22	16.50	15.70	HC (ppm)
25.96	21.55	19.67	10.50	6.15	Smoke Opacity
0.6250	0.5555	0.476	0.3448	0.2907	$V_f \times 10^{-6} (m^{3/s})$
5.22	4.800	3.978	2.879	2.427	$M_f \times 10^{-4}$ (kg/s)
0.0191	0.0183	0.0171	0.0157	0.0148	Va($m^{3/s}$)
0.0211	0.0204	0.0188	0.0173	0.0163	Ma(kg/s)
6.283	4.712	3.141	1.570	0.785	Bp(kw)
2.831	2.123	1.415	0.707	0.354	Bmep(bar)
0.044	0.044	0.044	0.044	0.044	Vs(m^3/s)
43.41	41.59	38.86	35.68	33.63	η_v (%)
30.00	28.00	22.39	15.45	9.17	η_{BT}(%)
40.42	42.50	47.28	60.09	67.16	A_F
0.36	0.36	0.45	0.66	1.11	BSFC (kg/kwh)
0.0127	0.016	0.016	0.023	0.039	BSEC (MJ/kwh)

Table A6.6: Raw data for APSOME B100 combustion in Perkin 4:108 Diesel Engine

5	4	3	2	1	S/N
B100	B100	B100	B100	B100	Oil Type
3.52	3.52	3.52	3.52	3.52	Oil Viscosity μ (mm^2/s)
34.42	34.42	34.42	34.42	34.42	Oil Cal. value, Qnet (MJ/kg)
852	852	852	852	852	Oil Density, ρ(kg/m^3)
125	125	125	125	125	Oil Flash Point, FP (˚C)
1500	1500	1500	1500	1500	Speed, N(rpm)
40.0	30.0	20.0	10.0	5.0	Torque, T(Nm)
105	129	140	191	216	Time, t(s)
50	50	50	50	50	Volume, v (cm^3)
9.50	8.70	7.60	6.40	5.70	hw (mm H_2O)
30.0	29.0	28.0	27.50	26.50	Oil Temp. (˚C)
101.30	101.30	101.30	101.30	101.30	Oil Pressure (N/m^2)
39.0	37.5	36.0	34.0	32.5	Inlet Temp (˚C)
41.0	39.0	37.5	36.0	34.0	Exit temp (˚C)
15.1	14.9	14.8	14.5	12.7	Head (cm)
87.0	75.0	61.5	51.0	41.0	Inlet Temp. (˚C)
94.0	85.0	77.5	62.0	51.0	Exit temp (˚C)
10.1	11.6	13.8	15.0	16.7	Head (cm)
241	225	205	186	175	Exh. Temp. (˚C)
0.28	0.062	0.054	0.06	0.07	CO (%)
840	819	604	420	280	NO_X(ppm)
7.62	6.51	4.70	4.32	4.00	CO_2(%)
32.10	28.0	17.25	13.60	12.50	HC (ppm)
29.67	24.50	17.40	11.42	7.55	Smoke Opacity
0.4762	0.3876	0.3571	0.2618	0.2315	$V_f \times 10^{-6}(m^{3/s})$
4.057	3.302	3.043	2.230	1.972	$M_f \times 10^{-4}$ (kg/s)
0.0191	0.0183	0.0171	0.0157	0.0148	Va($m^{3/s}$)
0.0211	0.0204	0.0188	0.0173	0.0163	Ma(kg/s)
6.283	4.712	3.141	1.570	0.785	Bp(kw)
2.831	2.123	1.415	0.707	0.354	Bmep(bar)
0.044	0.044	0.044	0.044	0.044	Vs(m^3/s)
43.41	41.59	38.86	35.68	33.63	η_v (%)
44.99	41.59	38.86	35.68	11.60	η_{BT}(%)
52.01	61.78	61.78	77.58	82.66	A_F
0.2324	0.2522	0.3487	0.5113	0.9043	BSFC (kg/kwh)
0.0080	0.0087	0.0120	0.01760	0.0311	BSEC (MJ/kwh)

Table A6.7: Raw data for APSOME B75 combustion in Perkin 4:108 diesel engine

5	4	3	2	1	S/N
B75	B75	B75	B75	B75	Oil Type
3.47	3.47	3.47	3.47	3.47	Oil Viscosity,μ (mm^2/s)
35.80	35.80	35.80	35.80	35.80	Oil Cal. value, Qnet (MJ/kg)
850	850	850	850	850	Oil Density, ρ(kg/m^3)
109	109	109	109	109	Oil Flash Point, FP (˚C)
1500	1500	1500	1500	1500	Speed, N(rpm)
40.0	30.0	20.0	10.0	5.0	Torque, T(Nm)
96	117	129	173	201	Time, t(s)
50	50	50	50	50	Volume, v (cm^3)
9.50	8.70	7.60	6.40	5.70	hw (mm H_2O)
29.5	28.0	27.0	25.50	25.50	Oil Temp. (˚C)
101.30	101.30	101.30	101.30	101.30	Oil Pressure (N/m^2)
41.0	37.5	35.5	34.0	32.5	Inlet Temp (˚C)
43.5	39.0	37.0	35.0	33.5	Exit temp (˚C)
15.2	14.9	14.7	14.0	12.7	Head (cm)
86.0	79.0	66.0	54.0	41.0	Inlet Temp. (˚C)
90.0	85.0	80.0	65.0	53.0	Exit temp (˚C)
11.0	12.0	13.8	14.5	16.8	Head (cm)
243	216	200	175	150	Exh. Temp. (˚C)
0.30	0.070	0.063	0.060	0.065	CO (%)
831	815	600	418	272	NO_X(ppm)
7.73	6.42	5.05	4.46	3.85	CO_2(%)
34.50	29.50	18.80	17.50	16.50	HC (ppm)
24.99	19.87	11.67	8.77	5.66	Smoke Opacity
0.5208	0.4273	0.3876	0.2890	0.2488	$V_f \times 10^{-6}(m^{3/s})$
4.427	3.632	3.294	2.457	2.114	$M_f \times 10^{-4}$ (kg/s)
0.0191	0.0183	0.0171	0.0157	0.0148	Va($m^{3/s}$)
0.0211	0.0204	0.0188	0.0173	0.0163	Ma(kg/s)
6.283	4.712	3.141	1.570	0.785	Bp(kw)
2.831	2.123	1.415	0.707	0.354	Bmep(bar)
0.044	0.044	0.044	0.044	0.044	Vs(m^3/s)
43.41	41.59	38.86	35.68	33.63	η_v (%)
39.64	36.24	26.63	17.85	1.04	η_{BT}(%)
47.66	56.16	57.07	70.41	77.11	A_F
0.25	0.28	0.38	0.56	0.97	BSFC (kg/kwh)
0.091	0.010	0.014	0.020	0.035	BSEC (MJ/kwh)

Table A6.8: Raw data for APSOME B50 combustion in Perkin 4:108 diesel engine

5	4	3	2	1	S/N
B50	B50	B50	B50	B50	Oil Type
3.40	3.40	3.40	3.40	3.40	Oil Viscosity μ (mm^2/s)
37.20	37.20	37.20	37.20	37.20	Oil Cal. value, Qnet (MJ/kg)
846	846	846	846	846	Oil Density, ρ(kg/m^3)
100	100	100	100	100	Oil Flash Point, FP (˚C)
1500	1500	1500	1500	1500	Speed, N(rpm)
40.0	30.0	20.0	10.0	5.0	Torque, T(Nm)
89	100	119	162	189	Time, t(s)
50	50	50	50	50	Volume, v (cm^3)
9.50	8.70	7.60	6.40	5.70	hw (mm H_2O)
27.5	29.0	28.0	27.0	27.5	Oil Temp. (˚C)
101.30	101.30	101.30	101.30	101.30	Oil Pressure (N/m^2)
41.5	38.5	36.0	33.50	33.0	Inlet Temp (˚C)
43.0	39.5	38.0	35.50	34.5	Exit temp (˚C)
15.4	15.0	14.8	14.0	12.5	Head (cm)
85.5	71.0	62.0	45.5	42.5	Inlet Temp. (˚C)
91.5	85.0	70.0	60.0	53.0	Exit temp (˚C)
11.0	12.5	13.5	15.0	17.0	Head (cm)
247	219	192	171	168	Exh. Temp. (˚C)
0.45	0.060	0.055	0.060	0.060	CO (%)
825	812	595	413	264	NO_X(ppm)
7.60	6.30	5.01	4.50	3.75	CO_2(%)
34.60	28.60	16.0	13.40	13.50	HC (ppm)
25.19	18.79	13.96	9.15	6.65	Smoke Opacity
0.5618	0.5000	0.4200	0.3086	0.2645	$V_f \times 10^{-6}(m^{3/s})$
4.752	4.230	3.555	2.611	2.238	$M_f \times 10^{-4}$ (kg/s)
0.0191	0.0183	0.0171	0.0157	0.0148	Va($m^{3/s}$)
0.0211	0.0204	0.0188	0.0173	0.0163	Ma(kg/s)
6.283	4.712	3.141	1.570	0.785	Bp(kw)
2.831	2.123	1.415	0.707	0.354	Bmep(bar)
0.044	0.044	0.044	0.044	0.044	Vs(m^3/s)
43.41	41.59	38.86	35.68	33.63	η_v (%)
35.54	29.94	25.82	16.16	9.43	η_{BT}(%)
44.40	48.23	52.88	66.26	72.83	A_F
0.272	0.323	0.410	0.598	1.03	BSFC (kg/kwh)
0.0101	0.020	0.015	0.022	0.037	BSEC (MJ/kwh)

Table A6.9: Raw data for APSOME B25 combustion in Perkin 4:108 diesel engine.

5	4	3	2	1	S/N
B25	B25	B25	B25	B25	Oil Type
3.30	3.30	3.30	3.30	3.30	Oil Viscosity μ (mm^2/s)
38.70	38.70	38.70	38.70	38.70	Oil Cal. value, Qnet (MJ/kg)
840	840	840	840	840	Oil Density, ρ(kg/m^3)
88	88	88	88	88	Oil Flash Point, FP (˚C)
1500	1500	1500	1500	1500	Speed, N(rpm)
40.0	30.0	20.0	10.0	5.0	Torque, T(Nm)
83	91	114	152	177	Time, t(s)
50	50	50	50	50	Volume, v (cm^3)
9.50	8.70	7.60	6.40	5.70	hw (mm H_2O)
41.0	39.0	37.0	36.0	36	Oil Temp. (˚C)
101.30	101.30	101.30	101.30	101.30	Oil Pressure (N/m^2)
40.0	38.0	36.0	34.5	32.0	Inlet Temp (˚C)
53.0	50.0	47.5	46.0	44.0	Exit temp (˚C)
15.5	15.1	14.9	14.5	12.7	Head (cm)
81.0	78.0	62.5	51.0	40	Inlet Temp. (˚C)
89.0	80.0	76.0	61.0	50	Exit temp (˚C)
10.3	11.0	13.9	14.5	17.0	Head (cm)
249	225	200	182	130	Exh. Temp. (˚C)
0.50	0.080	0.052	0.060	0.058	CO (%)
820	805	580	409	259	NO_X(ppm)
7.65	6.35	4.97	4.29	3.78	CO_2(%)
37.50	32.41	26.00	18.00	16.80	HC (ppm)
25.61	18.45	14.56	9.35	7.15	Smoke Opacity
0.6024	0.5494	0.4386	0.3289	0.2825	$V_f \times 10^{-6}(m^{3/s})$
5.06	4.615	3.684	2.763	2.373	$M_f \times 10^{-4}$ (kg/s)
0.0191	0.0183	0.0171	0.0157	0.0148	Va($m^{3/s}$)
0.0211	0.0204	0.0188	0.0173	0.0163	Ma(kg/s)
6.283	4.712	3.141	1.570	0.785	Bp(kw)
2.831	2.123	1.415	0.707	0.354	Bmep(bar)
0.044	0.044	0.044	0.044	0.044	Vs(m^3/s)
43.41	41.59	38.86	35.68	33.63	η_v (%)
32.09	26.38	22.03	14.68	68.69	η_{BT}(%)
42.20	44.20	51.03	62.61	68.69	A_F
0.29	0.35	0.42	0.54	1.09	BSFC (kg/kwh)
0.112	0.0135	0.0163	0.0210	0.042	BSEC (MJ/kwh)

Table A6.10: Variation of brake thermal efficiency with brake power of APSOME blends with diesel.

S/N	Torque(Nm)	Brake power (kW)	B100	B75	B50	B25	D
1	5.0	0.785	11.60	10.40	9.43	11.10	7.00
2	10.0	1.570	20.45	17.85	16.16	14.68	11.8
3	20.0	3.141	29.99	26.63	25.82	22.03	19.2
4	30.0	4.712	41.46	36.24	29.94	26.38	24.6
5	40.0	6.283	44.99	39.64	35.54	32.09	26.5

Table A6.11: Variation of brake thermal efficiency with brake power of SASOME blends with diesel.

S/N	Torque(Nm)	Brake power (kW)	B100	B75	B50	B25	D
1	5.0	0.785	11.99	11.45	10.98	9.17	7.0
2	10.0	1.570	20.38	19.50	18.24	15.45	11.8
3	20.0	3.141	35.68	30.86	28.53	25.39	19.2
4	30.0	4.712	40.33	28.96	34.76	29.00	24.6
5	40.0	6.283	44.00	40.22	36.22	30.00	26.5

Table A6.12: Variation of brake specific fuel consumption with brake power of APSOME blends with diesel.

S/N	Torque(Nm)	Brake power (kW)	B100	B75	B50	B25	D
1	5.0	0.785	0.9043	0.97	1.03	1.09	1.192
2	10.0	1.570	0.5113	0.56	0.598	0.64	0.699
3	20.0	3.141	0.3487	0.38	0.410	0.42	0.432
4	30.0	4.712	0.2522	0.28	0.323	0.335	0.337
5	40.0	6.283	0.2324	0.25	0.272	0.29	0.313

Table A6.13: Variation of specific fuel consumption with brake power of SASOME blends with diesel.

S/N	Torque(Nm)	Brake power (kW)	B100	B75	B50	B25	D
1	5.0	0.785	0.96	0.96	0.9679	1.11	1.192
2	10.0	1.570	0.57	0.59	0.58	0.66	0.699
3	20.0	3.141	0.32	0.50	0.37	0.45	0.432
4	30.0	4.712	0.32	0.38	0.310	0.36	0.337
5	40.0	6.283	0.28	0.31	0.264	0.36	0.313

Table A6.14: Variation of brake specific energy consumption with brake power of APSOME blends with diesel.

S/N	Torque(Nm)	Brake power (kW)	B100	B75	B50	B25	D
1	5.0	0.785	0.0311	0.035	0.037	0.042	0.052
2	10.0	1.570	0.0176	0.020	0.022	0.0260	0.030
3	20.0	3.141	0.0120	0.014	0.015	0.0163	0.019
4	30.0	4.712	0.0087	0.010	0.0120	0.0135	0.015
5	40.0	6.283	0.0080	0.009	0.0101	0.0112	0.014

Table A6.15: Variation of specific energy consumption with brake power of SASOME blends with diesel.

S/N	Torque(Nm)	Brake power (kW)	B100	B75	B50	B25	D
1	5.0	0.785	0.020	0.031	0.0328	0.039	0.052
2	10.0	1.570	0.018	0.019	0.020	0.023	0.030
3	20.0	3.141	0.014	0.016	0.017	0.018	0.019
4	30.0	4.712	0.010	0.012	0.015	0.017	0.015
5	40.0	6.283	0.009	0.010	0.011	0.013	0.014

Table A6.16: Variation of gross fuel consumption with brake power of APSOME blends with diesel.

S/N	Torque(Nm)	Brake power (kW)	B100	B75	B50	B25	D
1	5.0	0.785	1.972	2.114	2.238	2.373	2.60
2	10.0	1.570	2.230	2.457	2.61	2.763	3.05
3	20.0	3.141	3.043	3.294	3.555	3.684	4.1
4	30.0	4.712	3.502	3.632	4.230	4.41	5.01
5	40.0	6.283	4.057	4.427	4.752	5.06	5.46

Table A6.17: Variation of gross fuel consumption with brake power of SASOME blends with diesel.

S/N	Torque(Nm)	Brake power (kW)	B100	B75	B50	B25	D
1	5.0	0.785	2.11	2.21	2.31	2.427	2.60
2	10.0	1.570	2.47	2.48	2.54	2.879	3.05
3	20.0	3.141	2.811	3.39	3.502	3.696	4.13
4	30.0	4.712	3.16	3.97	4.00	4.75	5.01
5	40.0	6.283	4.81	4.99	5.05	5.17	5.36

Table A6.18: Variation of air/fuel ratio with brake power of APSOME blends with diesel.

S/N	Torque(Nm)	Brake power (kW)	B100	B75	B50	B25	D
1	5.0	0.785	82.66	77.11	72.83	68.69	62.69
2	10.0	1.570	77.58	70.41	66.26	62.61	56.72
3	20.0	3.141	61.78	57.07	52.88	51.03	49.87
4	30.0	4.712	61.78	56.16	50.23	48.20	46.26
5	40.0	6.283	52.01	47.66	44.40	42.20	38.64

Table A6.19: Variation of air/fuel ratio with brake power of SASOME blends with diesel

S/N	Torque(Nm)	Brake power (kW)	B100	B75	B50	B25	D
1	5.0	0.785	80.66	77.25	73.75	67.16	62.69
2	10.0	1.570	75.56	69.76	64.11	60.09	56.72
3	20.0	3.141	66.88	62.82	57.85	51.28	49.87
4	30.0	4.712	62.04	57.05	52.00	50.50	46.26
5	40.0	6.283	48.87	42.51	37.77	36.42	34.64

Table A6.20: Variation of brake mean effective pressure with brake power of APSOME blends with diesel.

S/N	Torque(Nm)	Brake power (kW)	B100	B75	B50	B25	D
1	5.0	0.785	0.354	0.354	0.354	0.354	0.354
2	10.0	1.570	0.707	0.707	0.707	0.707	0.707
3	20.0	3.141	1.415	1.415	1.415	1.415	1.415
4	30.0	4.712	2.123	2.123	2.123	2.123	2.123
5	40.0	6.283	2.831	2.831	2.831	2.831	2.831

Figure A6.21: Variation of brake mean effective pressure with brake power of SASOME blends with diesel.

S/N	Torque(Nm)	Brake power (kW)	B100	B75	B50	B25	D
1	5.0	0.785	0.354	0.354	0.354	0.354	0.354
2	10.0	1.570	0.707	0.707	0.707	0.707	0.707
3	20.0	3.141	1.415	1.415	1.415	1.415	1.415
4	30.0	4.712	2.123	2.123	2.123	2.123	2.123
5	40.0	6.283	2.831	2.831	2.831	2.831	2.831

Table A6.22: Variation of volumetric efficiency with brake power of APSOME blends with diesel.

S/N	Torque(Nm)	Brake power (kW)	B100	B75	B50	B25	D
1	5.0	0.785	33.63	33.63	33.63	33.63	33.63
2	10.0	1.570	35.68	35.68	35.68	35.68	35.70
3	20.0	3.141	38.86	38.86	38.86	38.86	38.90
4	30.0	4.712	41.59	41.59	41.59	41.59	41.60
5	40.0	6.283	43.41	43.41	43.41	43.41	43.41

Table A6.23: Variation of volumetric efficiency with brake power of SASOME blends with diesel.

S/N	Torque(Nm)	Brake power (kW)	B100	B75	B50	B25	D
1	5.0	0.785	33.63	33.63	33.63	33.63	33.63
2	10.0	1.570	35.68	35.68	35.68	35.68	35.70
3	20.0	3.141	38.86	38.86	38.86	38.86	38.90
4	30.0	4.712	41.59	41.59	41.59	41.59	41.60
5	40.0	6.283	43.41	43.41	43.41	43.41	43.41

Table A6.24: Variation of exhaust gas temperature with brake power of APSOME and its blends with diesel.

S/N	Torque(Nm)	Brake power (kW)	B25	B50	B75	B100	D
1	5	0.785	175	168	155	148	175
2	10	1.570	186	179	171	162	205
3	20	3.141	205	200	192	185	225
4	30	4.712	225	220	214	2055	240
5	40	6.283	247	243	240	232	250

Table A6.25: Variation of exhaust gas temperature with brake power of SASOME and its blends with diesel.

S/N	Torque(Nm)	Brake power (kW)	25	50	75	100	D
1	5	0.785	179	168	159	154	185
2	10	1.570	191	184	177	173	205
3	20	3.141	220	211	205	192	225
4	30	4.712	234	226	219	211	240
5	40	6.283	248	244	241	238	250

Table A6.26: Variation of CO emissions with brake power of APSOME and its blends with diesel.

S/N	Torque(Nm)	Brake power (kW)	100	75	50	25	D
1	5	0.785	0.07	0.065	0.060	0.058	0.072
2	10	1.570	0.06	0.06	0.060	0.06	0.050
3	20	3.141	0.062	0.07	0.060	0.080	0.059
4	30	4.712	0.054	0.053	0.050	0.052	0.055
5	40	6.283	0.280	0.320	0.450	0.500	0.250

Table A6.27: Variation of CO emissions with brake power of SASOME and its blends with diesel.

S/N	Torque(Nm)	Brake power (kW)	100	75	50	25	D
1	5	0.785	0.06	0.057	0.056	0.055	0.072
2	10	1.570	0.05	0.050	0.050	0.050	0.050
3	20	3.141	0.049	0.049	0.048	0.049	0.055
4	30	4.712	0.057	0.060	0.059	0.078	0.050
5	40	6.283	0.260	0.300	0.400	0.450	0.250

Table A6.28: Variation of CO_2 emissions with brake power of APSOME and its blends with diesel.

S/N	Torque(Nm)	Brake power (kW)	100	75	50	25	D
1	5	0.785	4.00	3.85	3.75	3.78	3.50
2	10	1.570	4.32	4.46	4.50	4.29	4.00
3	20	3.141	4.70	5.05	5.01	4.97	4.70
4	30	4.712	6.51	6.42	6.30	6.35	5.50
5	40	6.283	7.62	7.73	7.60	7.65	6.90

Table A6.29: Variation of CO_2 emissions with brake power of SASOME and its blends with diesel.

S/N	Torque(Nm)	Brake power (kW)	100	75	50	25	D
1	5	0.785	3.55	3.54	3.52	3.51	3.50
2	10	1.570	4.28	4.26	4.25	4.22	4.00
3	20	3.141	4.50	4.95	4.90	4.81	4.70
4	30	4.712	6.31	6.30	6.25	6.21	5.50
5	40	6.283	7.59	7.58	7.65	7.70	6.90

Table A6.30: Variation of NO_X emissions with brake power of APSOME and its blends with diesel.

S/N	Torque(Nm)	Brake power (kW)	100	75	50	25	D
1	5	0.785	280	272	264	259	210
2	10	1.570	604	600	595	580	550
3	20	3.141	420	418	413	409	352
4	30	4.712	819	815	812	805	720
5	40	6.283	840	831	825	820	760

Table A6.31: Variation of NO_X emissions with brake power of SASOME and its blends with diesel.

S/N	Torque(Nm)	Brake power (KW)	100	75	50	25	D
1	5	0.785	270	256	254	250	210
2	10	1.570	415	412	408	405	352
3	20	3.141	600	597	595	589	550
4	30	4.712	816	814	810	800	720
5	40	6.283	830	825	820	810	760

Table A6.32: Variation of HC emissions with brake power of APSOME and its blends with diesel.

S/N	Torque(Nm)	Brake power (kW)	100	75	50	25	D
1	5	0.785	12.5	14.50	16.50	17.80	32.50
2	10	1.570	13.60	15.50	17.40	19.00	26.81
3	20	3.141	16.00	17.25	18.80	20.00	30.50
4	30	4.712	25.60	28.00	29.50	32.41	40.50
5	40	6.283	32.10	34.50	35.60	37.50	55.10

Table A6.33: Variation of HC emissions with brake power of SASOME and its blends with diesel.

S/N	Torque(Nm)	Brake power (kW)	100	75	50	25	D
1	5	0.785	11.00	12.50	14.50	16.70	32.50
2	10	1.570	12.50	14.00	15.00	17.50	26.51
3	20	3.141	15.71	16.40	17.00	19.02	30.50
4	30	4.712	24.10	26.00	29.50	31.70	40.50
5	40	6.283	30.00	32.1	33.50	35.50	55.10

Table A6:34: Percentage change in exhaust emissions against blends of APSOME with diesel.

	CO					NO_X					CO_2					HC				
Oil Blend	5	10	20	30	40	5	10	20	30	40	5	10	20	30	40	5	10	20	30	40
B100	-2.77	20.00	-1.82	5.08	12	33.33	19.32	9.82	13.75	10.52	14.29	8.00	0.00	18.36	9.70	-61.53	-49.27	-43.44	-30.86	-41.74
B75	-9.72	20.00	-3.64	18.64	20	29.52	18.75	9.09	13.19	9.34	10.00	11.50	7.46	16.73	9.85	-49.23	-34.72	-38.36	-27.16	-37.39
B50	-16.67	20.00	-9.09	1.69	80.	25.71	17.33	8.18	12.78	8.55	7.14	12.50	6.60	14.55	10.14	-58.46	-50.02	-47.55	-29.38	-37.21
B25	-19.44	20.00	-5.45	35.59	100.	23.30	16.19	5.46	11.80	-7.89	8.00	7.25	5.74	15.45	10.87	-48.31	-32.86	-37.71	19.98	-31.94

Table A6:35: Percentage change in exhaust emissions against blends of APSOME with diesel.

	CO					NO_X					CO_2					HC				
Oil Blend	5	10	20	30	40	5	10	20	30	40	5	10	20	30	40	5	10	20	30	40
B100	-2.77	20.00	-1.82	5.08	12	33.33	19.32	9.82	13.75	10.52	14.29	8.00	0.00	18.36	9.70	-61.53	-49.27	-43.44	-30.86	-41.74
B75	-9.72	20.00	-3.64	18.64	20	29.52	18.75	9.09	13.19	9.34	10.00	11.50	7.46	16.73	9.85	-49.23	-34.72	-38.36	-27.16	-37.39
B50	-16.67	20.00	-9.09	1.69	80	25.71	17.33	8.18	12.78	8.55	7.14	12.50	6.60	14.55	10.14	-58.46	-50.02	-47.55	-29.38	-37.21
B25	-19.44	20.00	-5.45	35.59	100	23.30	16.19	5.46	11.80	-7.89	8.00	7.25	5.74	15.45	10.87	-48.31	-32.86	-37.71	19.98	-31.94

APPENDIX 7

CHEMICAL KINETICS DATA AND PLOTS

Table A7.1: Kinetics data for SASOME production at 65˚C.

S/N	Reaction Time (min)	Mg (%w/w)	$^{1}/_{Mg}$ $(\%\,^{w}/_{w})^{-1}$	Dg $(\%\,^{w}/_{w})$	$^{1}/_{Dg}$ $(\%\,^{w}/_{w})^{-1}$	Tg $(\%\,^{w}/_{w})$	$^{1}/_{Tg}$ $(\%\,^{w}/_{w})^{-1}$	FAME $(\%\,^{w}/_{w})$	GL $(\%\,^{w}/_{w})$
1	0	1.08	0.92	2.90	0.34	95.61	0.0104	0.00	0.00
2	0.3	1.18	0.84	2.90	0.34	65.71	0.0152	25.94	4.07
3	0.5	3.02	0.33	3.87	0.25	54.26	0.0184	32.75	6.05
4	1.0	5.20	0.19	4.81	0.20	37.73	0.0265	45.36	6.40
5	2.0	2.90	0.34	2.69	0.37	23.51	0.0425	63.80	7.00
6	4.0	1.99	0.50	2.48	0.40	13.39	0.0746	74.64	7.40
7	6.0	1.71	0.58	2.30	0.43	9.37	0.107	78.72	7.75
8	10.0	1.33	0.74	2.00	0.50	5.84	0.171	82.04	8.00
9	20.0	0.86	1.21	1.52	0.66	3.01	0.3316	86.49	8.08
10	40.0	0.61	1.64	1.02	0.98	1.53	0.6528	88.34	8.29
11	60.0	0.35	2.79	0.77	1.29	1.02	0.974	89.16	8.56
12	80.0	0.28	3.61	0.62	1.61	0.77	1.295	89.53	8.77
13	100.0	0.24	4.09	0.52	1.92	0.61	1.616	89.73	8.50

Table A7.2: Kinetics data for SASOME production at 60˚C.

S/N	Reaction Time (min)	Mg (%w/w)	$^{1}/_{Mg}$ $(\%\,^{w}/_{w})^{-1}$	Dg $(\%\,^{w}/_{w})$	$^{1}/_{Dg}$ $(\%\,^{w}/_{w})^{-1}$	Tg $(\%\,^{w}/_{w})$	$^{1}/_{Tg}$ $(\%\,^{w}/_{w})^{-1}$	FAME $(\%\,^{w}/_{w})$	GL $(\%\,^{w}/_{w})$
1	0	1.08	0.92	2.90	0.34	95.61	0.0104	0.00	0.00
2	0.3	2.49	0.40	3.24	0.31	74.46	0.0134	15.80	3.71
3	0.5	3.25	0.30	3.52	0.28	64.72	0.0154	22.54	5.47
4	1.0	4.65	0.21	4.02	0.24	48.78	0.0205	36.30	6.05
5	2.0	3.05	0.33	4.92	0.20	32.68	0.0306	54.34	7.00
6	4.0	0.96	1.03	2.71	0.37	19.69	0.0508	69.36	7.08
7	6.0	0.91	1.10	2.56	0.391	14.08	0.0710	74.91	7.14
8	10.0	0.82	1.21	2.35	0.42	8.98	0.1114	79.94	7.41
9	20.0	0.66	1.51	1.96	0.509	4.71	0.2124	84.63	7.84
10	40.0	0.48	2.09	1.47	0.68	2.41	0.4144	87.53	8.01
11	60.0	0.37	2.68	1.18	0.85	1.62	0.6164	88.60	8.13
12	80.0	0.31	3.26	0.98	1.016	1.22	0.8184	88.99	8.20
13	100.0	0.26	3.85	0.84	1.19	0.98	1.0204	89.21	8.41

Table A7.3: Kinetics data for SASOME production at 55˚C .

S/N	Reaction Time (min)	Mg (%w/w)	$^{1}/_{Mg}$ $(\%\,^{w}/_{w})^{-1}$	Dg $(\%\,^{w}/_{w})$	$^{1}/_{Dg}$ $(\%\,^{w}/_{w})^{-1}$	Tg $(\%\,^{w}/_{w})$	$^{1}/_{Tg}$ $(\%\,^{w}/_{w})^{-1}$	FAME $(\%\,^{w}/_{w})$	GL $(\%\,^{w}/_{w})$
1	0	1.08	0.92	2.90	0.34	95.61	0.0104	0.00	0.00
2	0.3	2.65	0.38	3.45	0.29	75.30	0.0133	14.70	3.50
3	0.5	3.54	0.28	3.70	0.27	65.79	0.0152	21.76	5.11
4	1.0	4.80	0.21	4.20	0.24	50.0	0.020	34.89	6.00
5	2.0	1.05	0.95	4.98	0.20	33.78	0.030	53.34	6.75
6	4.0	1.01	0.99	2.68	0.37	20.49	0.049	68.67	7.05
7	6.0	0.98	1.02	2.56	0.39	14.71	0.068	74.43	7.22
8	10.0	0.92	1.09	2.36	0.42	9.40	0.106	79.78	7.54
9	20.0	0.80	1.25	1.97	0.51	4.94	0.202	84.40	7.79
10	40.0	0.63	1.58	1.48	0.68	2.53	0.394	87.30	8.00
11	60.0	0.52	1.91	1.18	0.84	1.70	0.586	88.42	8.10
12	80.0	0.44	2.24	0.98	1.01	1.28	0.77	89.09	8.15
13	100.0	0.38	2.57	0.84	1.18	1.00	0.970	89.15	8.43

Table A7.4: Kinetics data for APSOME production at 65˚C.

S/N	Reaction Time (min)	Mg (%w/w)	$^{1}/_{Mg}$ $(\%\,^{w}/_{w})^{-1}$	Dg $(\%\,^{w}/_{w})$	$^{1}/_{Dg}$ $(\%\,^{w}/_{w})^{-1}$	Tg $(\%\,^{w}/_{w})$	$^{1}/_{Tg}$ $(\%\,^{w}/_{w})^{-1}$	FAME $(\%\,^{w}/_{w})$	GL $(\%\,^{w}/_{w})$
1	0	1.44	0.694	2.88	0.347	94.40	0.0106	3..45	0.0
2	0.3	1.84	0.543	3.19	0.313	70.02	0.0141	20.64	3.31
3	0.5	3.15	0.317	3.57	0.280	60.98	0.0164	28.50	3.80
4	1.0	4.06	0.240	3.98	0.251	45.04	0.0222	42.95	3.87
5	2.0	1.176	0.8502	4.10	0.244	29.58	0.0338	60.84	4.24
6	4.0	0.994	1.0064	2.11	0.474	17.54	0.0570	74.48	4.18
7	6.0	0.860	1.1626	1.86	0.537	12.26	0.0802	79.70	5.12
8	10.0	0.678	1.475	1.51	0.664	7.91	0.1264	83.94	5.96
9	20.0	0.343	2.256	1.02	0.981	4.12	0.2426	88.27	6.15
10	40.0	0.262	3.818	0.519	1.615	2.11	0.4746	90.81	6.20
11	60.0	0.156	5.380	0.444	2.249	1.41	0.7066	90.94	7.02
12	80.0	0.144	6.942	0.306	2.883	1.00	0.9386	90.95	7.50
13	100.0	0.117	8.504	0.284	3.517	0.85	1.1706	91.15	7.50

Table A7.5: Kinetics data for APSOME production at 60˚C.

S/N	Reaction Time (min)	Mg (%w/w)	$^{1}/_{Mg}$ $(\%\,^{w}/_{w})^{-1}$	Dg $(\%\,^{w}/_{w})$	$^{1}/_{Dg}$ $(\%\,^{w}/_{w})^{-1}$	Tg $(\%\,^{w}/_{w})$	$^{1}/_{Tg}$ $(\%\,^{w}/_{w})^{-1}$	FAME $(\%\,^{w}/_{w})$	GL $(\%\,^{w}/_{w})$
1	0	1.44	0.694	2.88	0.347	94.40	0.0106	3.45	0.0
2	0.3	2.07	0.483	3.23	0.310	71.63	0.0140	19.97	3.00
3	0.5	3.23	0.310	3.74	0.267	61.72	0.0162	28.00	3.28
4	1.0	4.38	0.228	4.02	0.249	45.87	0.0218	42.08	3.45
5	2.0	1.27	0.789	4.20	0.238	30.30	0.0300	60.15	4.00
6	4.0	1.13	0.883	2.47	0.405	18.05	0.0554	74.01	4.24
7	6.0	1.02	0.978	2.30	0.435	12.85	0.0778	79.38	4.35
8	10.0	0.757	1.167	2.03	0.493	8.16	0.1226	83.89	5.06
9	20.0	0.609	1.64	1.56	0.639	4.26	0.2346	87.56	6.01
10	40.0	0.387	2.586	1.01	0.931	2.18	0.4586	90.24	6.12
11	60.0	0.283	3.532	0.818	1.223	1.46	0.6826	90.52	6.92
12	80.0	0.223	4.478	0.660	1.515	1.05	0.9066	90.85	7.17
13	100.0	0.181	5.424	0.55	1.807	0.88	1.1306	90.92	7.41

Table A7.6: Kinetics data for APSOME production at 55˚C.

S/N	Reaction Time (min)	Mg (%w/w)	$^{1}/_{Mg}$ $(\%\,^{w}/_{w})^{-1}$	Dg $(\%\,^{w}/_{w})$	$^{1}/_{Dg}$ $(\%\,^{w}/_{w})^{-1}$	Tg $(\%\,^{w}/_{w})$	$^{1}/_{Tg}$ $(\%\,^{w}/_{w})^{-1}$	FAME $(\%\,^{w}/_{w})$	GL $(\%\,^{w}/_{w})$
1	0	1.44	0.694	2.88	0.347	94.40	0.0106	3.45	0.0
2	0.3	2.92	0.338	3.34	0.299	72.89	0.0137	17.76	3.02
3	0.5	3.50	0.284	3.80	0.263	63.29	0.0158	26.24	3.11
4	1.0	4.70	0.213	4.05	0.24	47.62	0.0210	40.23	3.30
5	2.0	1.345	0.743	4.59	0.218	31.85	0.0314	58.32	3.93
6	4.0	1.261	0.793	2.48	0.403	19.16	0.0522	72.91	4.19
7	6.0	1.187	0.842	2.317	0.432	13.69	0.703	78.57	4.24
8	10.0	1.063	0.941	2.049	0.488	8.72	0.1146	82.27	4.90
9	20.0	0.842	1.188	1.589	0.629	4.57	0.1286	87.04	5.96
10	40.0	0.594	1.682	1.010	0.911	2.34	0.4266	90.04	6.02
11	60.0	0.460	2.076	0.838	1.193	1.57	0.6346	90.66	6.47
12	80.0	0.374	2.670	0.678	1.475	1.18	0.8424	90.73	7.04
13	100.0	0.3160	3.064	0.569	1.757	0.95	1.0506	90.94	7.22

Table A7.7: Kinetics data for ASASOME production at 65˚C.

S/N	Reaction Time (min)	Mg (%w/w)	$^{1}/_{Mg}$ $(\%\,^{w}/_{w})^{-1}$	Dg $(\%\,^{w}/_{w})$	$^{1}/_{Dg}$ $(\%\,^{w}/_{w})^{-1}$	Tg $(\%\,^{w}/_{w})$	$^{1}/_{Tg}$ $(\%\,^{w}/_{w})^{-1}$	FAME $(\%\,^{w}/_{w})$	GL $(\%\,^{w}/_{w})$
1	0	1.17	0.855	2.34	0.427	95.04	0.0105	0.0	0.0
2	0.3	2.12	0.472	3.00	0.333	75.59	0.0132	15.24	3.05
3	0.5	2.11	0.474	3.25	0.274	66.44	0.0151	24.23	3.57
4	1.0	3.80	0.227	3.65	0.250	51.02	0.0196	37.64	3.39
5	2.0	1.067	0.9368	3.85	0.235	34.84	0.0287	60.24	4.07
6	4.0	0.9817	1.0186	1.800	0.555	21.32	0.0469	71.74	4.06
7	6.0	0.9087	1.1004	1.61	0.6196	15.36	0.0651	78.12	4.40
8	10.0	0.7911	1.264	1.34	0.748	9.85	0.1015	83.00	4.82
9	20.0	0.5977	1.673	0.94	1.069	5.19	0.1925	87.85	5.42
10	40.0	0.4014	2.491	0.58	1.711	2.67	0.3745	89.70	6.15
11	60.0	0.3022	3.309	0.42	2.353	1.80	0.5565	90.12	7.16
12	80.0	0.2423	4.127	0.23	2.995	1.35	0.7385	90.40	7.68
13	100.0	0.2022	4.945	0.27	3.637	1.0	0.9205	90.65	7.88

Table A7.8: Kinetics data for ASASOME production at 60˚C.

S/N	Reaction Time (min)	Mg (%w/w)	$^{1}/_{Mg}$ $(\%\,^{w}/_{w})^{-1}$	Dg $(\%\,^{w}/_{w})$	$^{1}/_{Dg}$ $(\%\,^{w}/_{w})^{-1}$	Tg $(\%\,^{w}/_{w})$	$^{1}/_{Tg}$ $(\%\,^{w}/_{w})^{-1}$	FAME $(\%\,^{w}/_{w})$	GL $(\%\,^{w}/_{w})$
1	0	1.17	0.854	2.34	0.427	95.04	0.0105	0.0	0.0
2	0.3	2.10	0.476	3.25	0.308	76.28	0.0131	18.37	3.00
3	0.5	2.80	0.357	3.18	0.314	67.34	0.0149	23.14	3.54
4	1.0	4.00	0.241	3.55	0.253	52.08	0.0192	36.52	3.85
5	2.0	1.08	0.928	3.90	0.238	35.84	0.0279	55.14	4.04
6	4.0	0.9976	1.002	1.82	0.549	22.08	0.0453	70.98	4.12
7	6.0	0.928	1.080	1.64	0.609	15.95	0.0627	77.11	4.37
8	10.0	0.816	1.225	1.37	0.731	10.26	0.0975	82.85	4.70
9	20.0	0.627	1.596	0.966	1.035	5.42	0.1845	87.69	5.30
10	40.0	0.428	2.338	0.609	1.643	2.79	0.3585	89.55	6.62
11	60.0	0.324	3.08	0.444	2.251	1.88	0.5325	90.03	7.32
12	80.0	0.261	3.822	0.350	2.859	1.42	0.7065	90.43	7.54
13	100.0	0.219	4.564	0.29	3.467	1.13	0.8805	90.56	7.80

Table A7.9: Kinetics data for ASASOME production at 55˚C.

S/N	Reaction Time (min)	Mg (%w/w)	$^{1}/_{Mg}$ $(\%\,^{w}/_{w})^{-1}$	Dg $(\%\,^{w}/_{w})$	$^{1}/_{Dg}$ $(\%\,^{w}/_{w})^{-1}$	Tg $(\%\,^{w}/_{w})$	$^{1}/_{Tg}$ $(\%\,^{w}/_{w})^{-1}$	FAME $(\%\,^{w}/_{w})$	GL $(\%\,^{w}/_{w})$
1	0	1.17	0.854	2.34	0.427	95.04	0.0105	0.0	0.0
2	0.3	2.34	0.427	3.45	0.290	79.18	0.0126	12.03	3.00
3	0.5	2.95	0.339	3.63	0.275	71.17	0.0141	18.88	3.37
4	1.0	4.18	0.228	4.00	0.241	56.81	0.0176	31.32	3.69
5	2.0	1.13	0.886	4.15	0.227	40.49	0.0247	50.23	4.00
6	4.0	1.09	0.918	1.91	0.523	25.71	0.0389	67.23	4.06
7	6.0	1.05	0.95	1.75	0.5704	18.83	0.0531	74.17	4.20
8	10.0	0.986	1.014	1.50	0.666	12.27	0.0815	80.62	4.62
9	20.0	0.852	1.174	1.105	0.905	6.56	0.1525	86.26	5.22
10	40.0	0.67	1.494	0.72	1.383	3.40	0.295	88.76	6.45
11	60.0	0.55	1.814	0.537	1.861	2.29	0.437	89.46	7.16
12	80.0	0.47	2.134	0.427	2.339	1.73	0.5785	89.89	7.48
13	100.0	0.41	2.454	0.35	2.817	1.39	0.7205	90.17	7.68

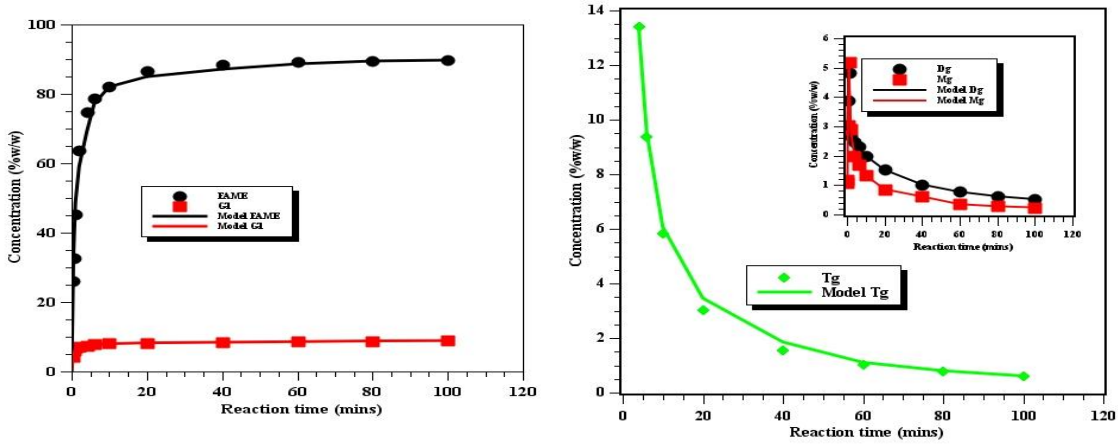

65°C

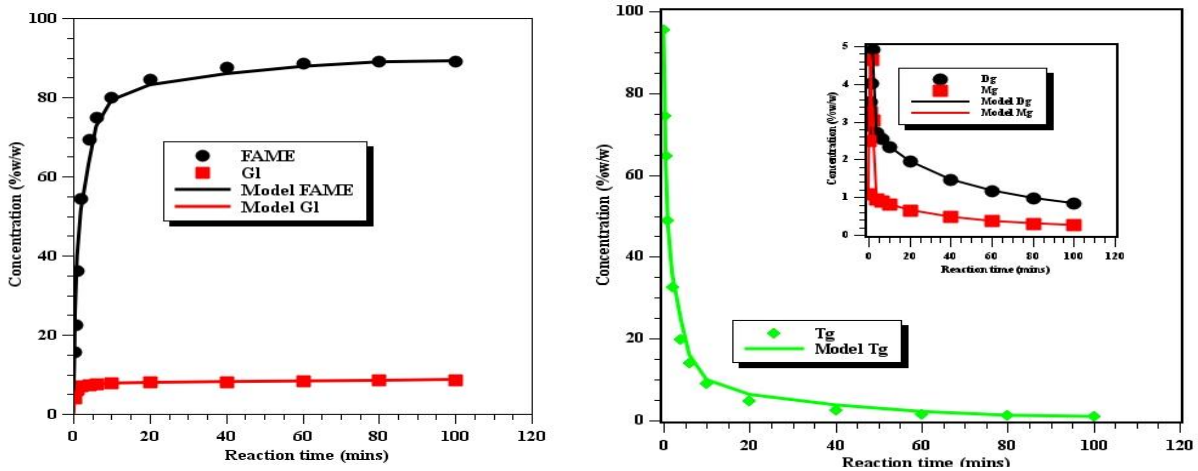

60°C

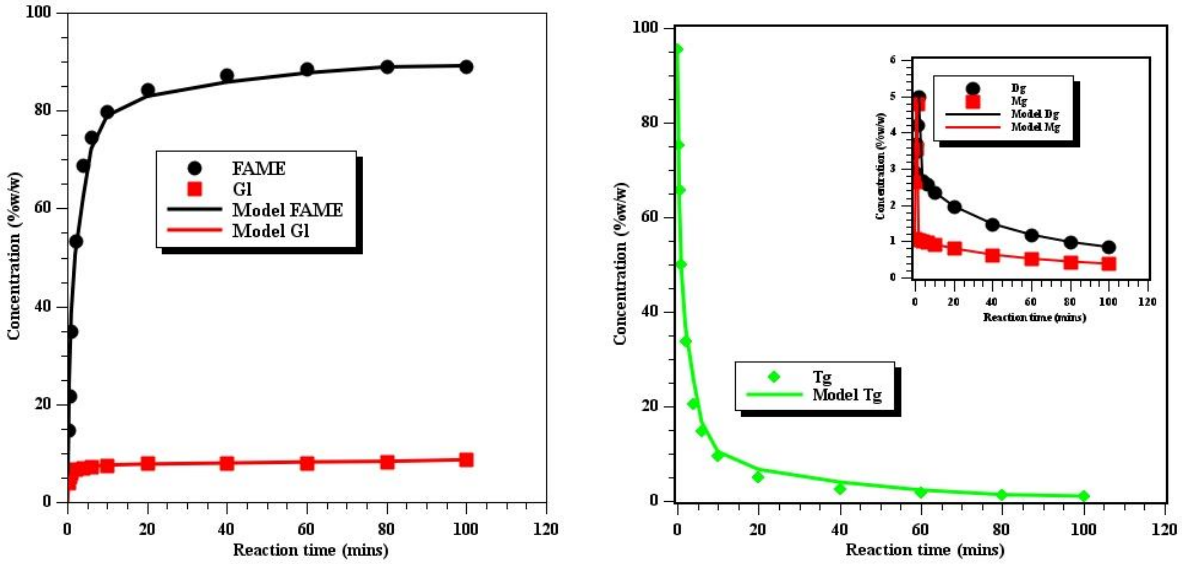

55°C

Figure A7.1: Composition of reaction products for SASOME at 65˚C, 60˚C and 55˚C

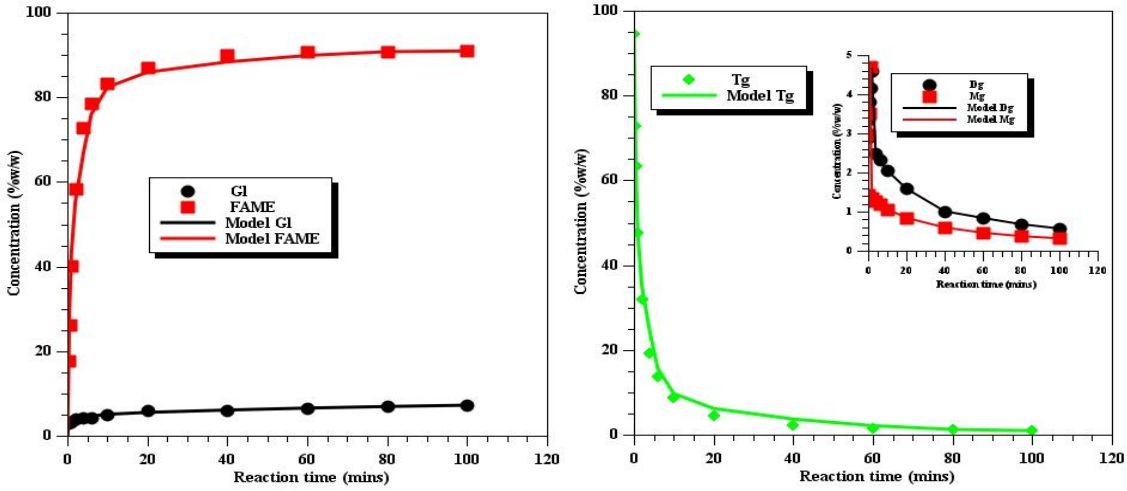

65°C

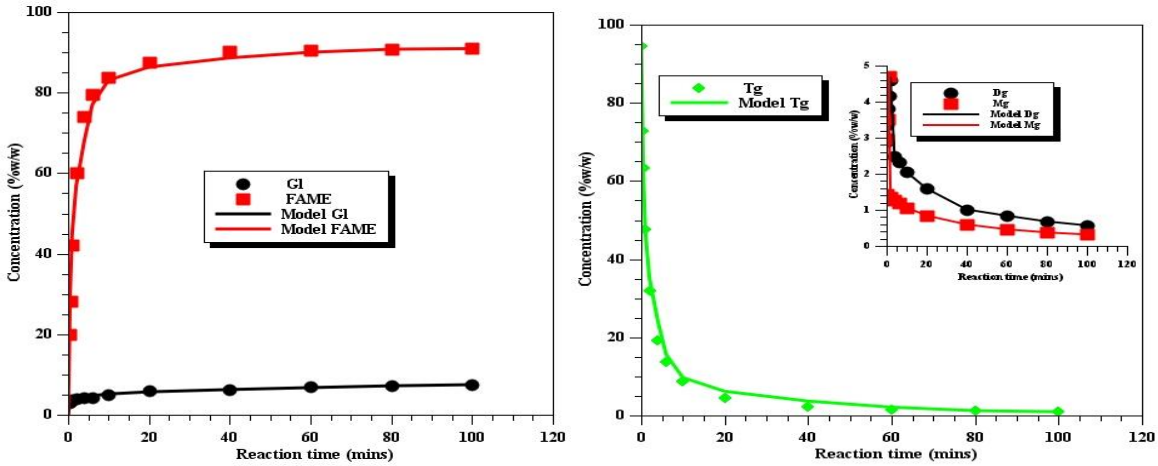

60°C

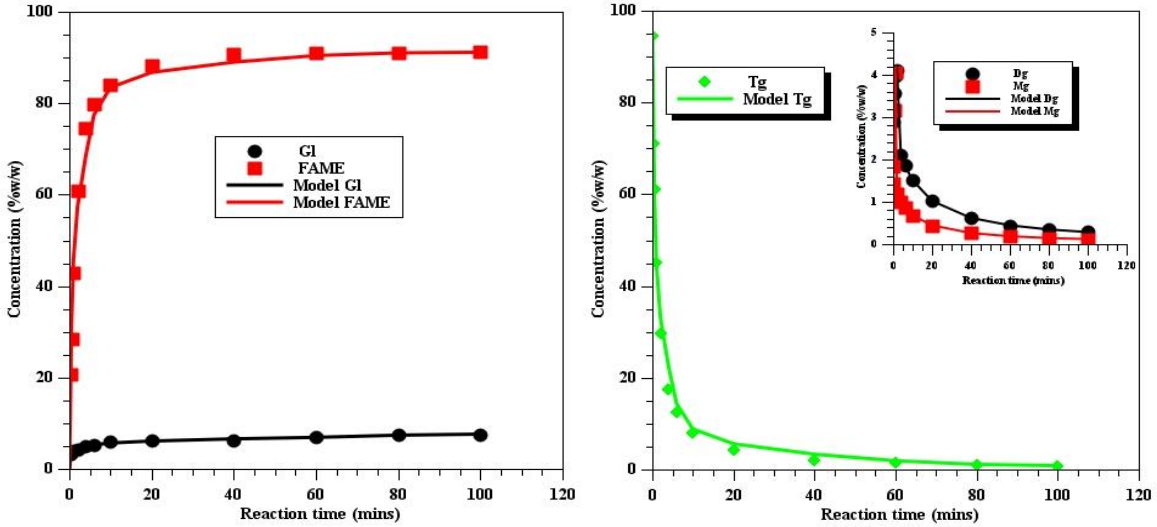

55°C

Figure A7.2: Composition of reaction products for APSOME at 65˚C, 60˚C and 55˚C.

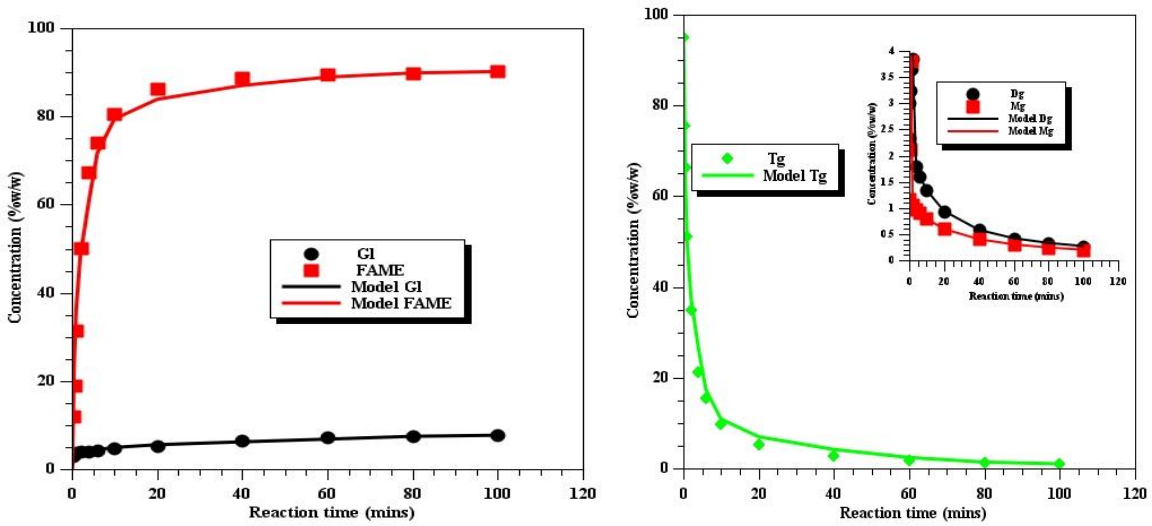

65°C

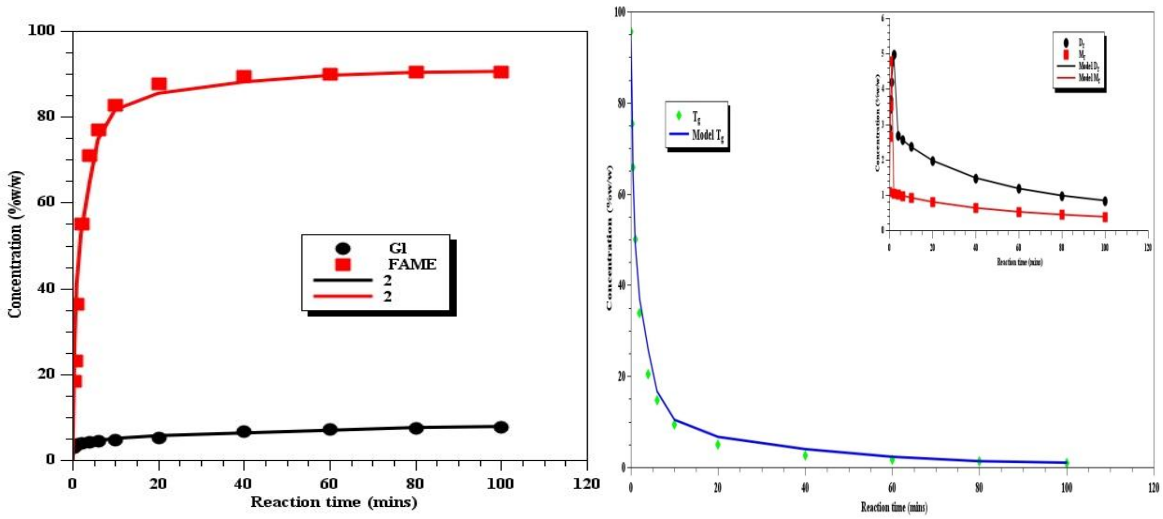

60°C

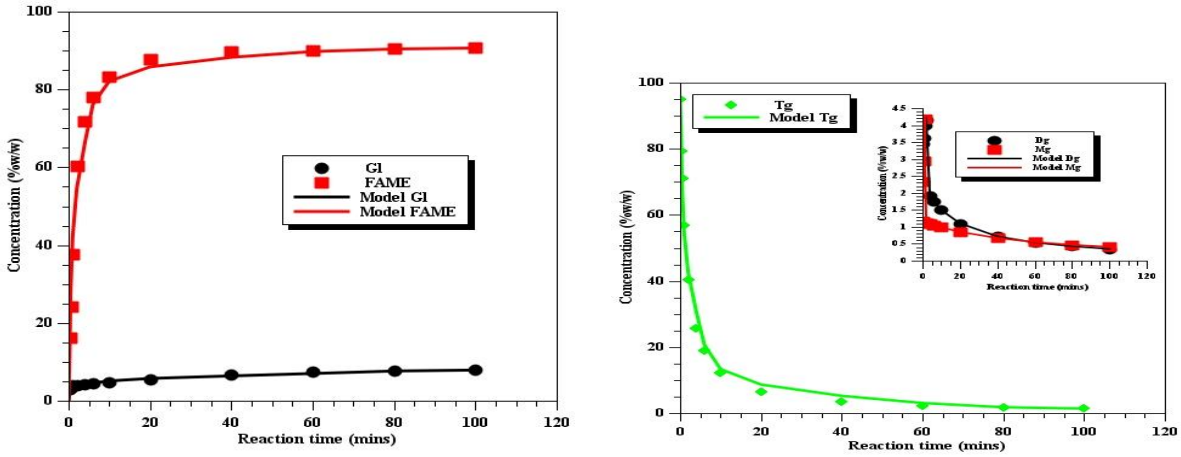

55°C

Figure A7.3: Composition of reaction products for ASASOME at 65˚C, 60˚C and 55˚C.

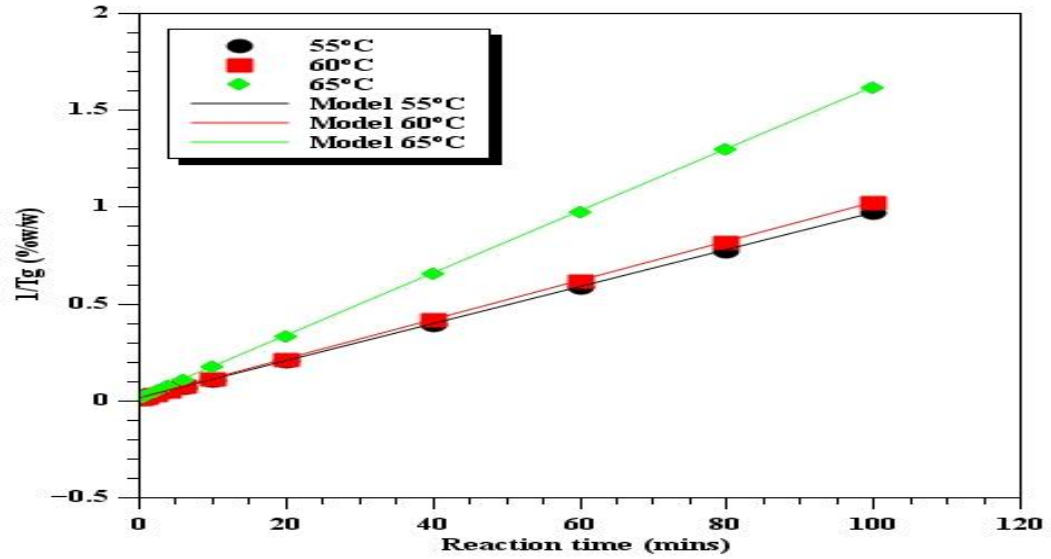

SASOME

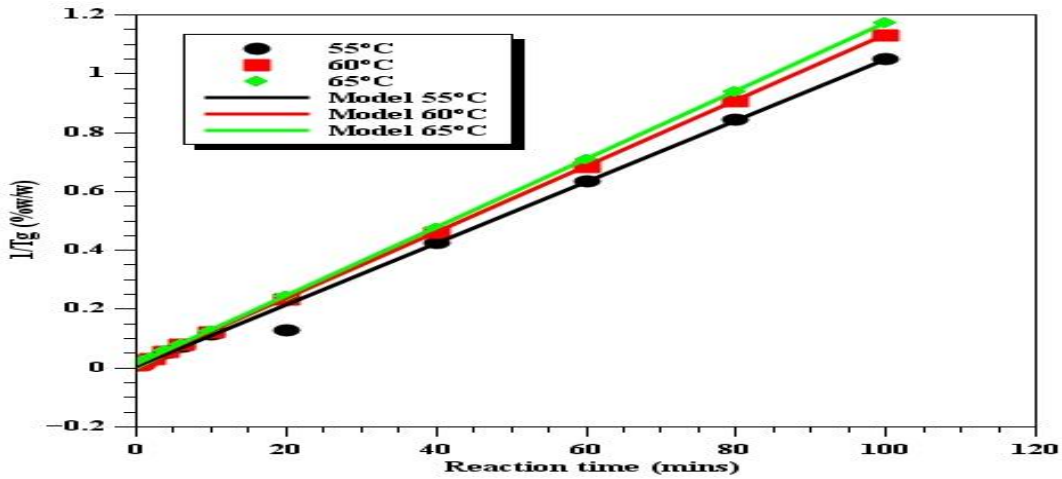

APSOME

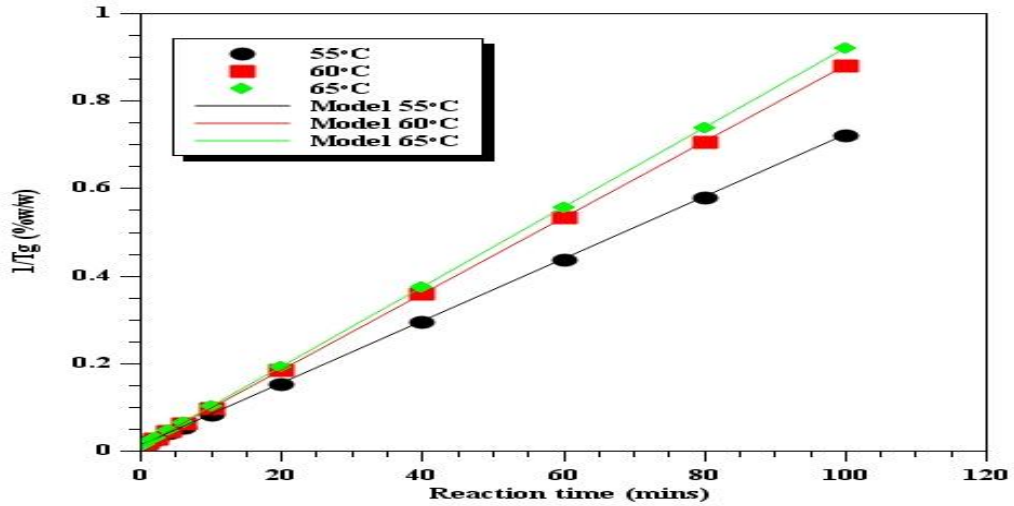

ASASOME

Figure A7.4: Second- order reaction irreversibbe model of triglycerides hydrolysis

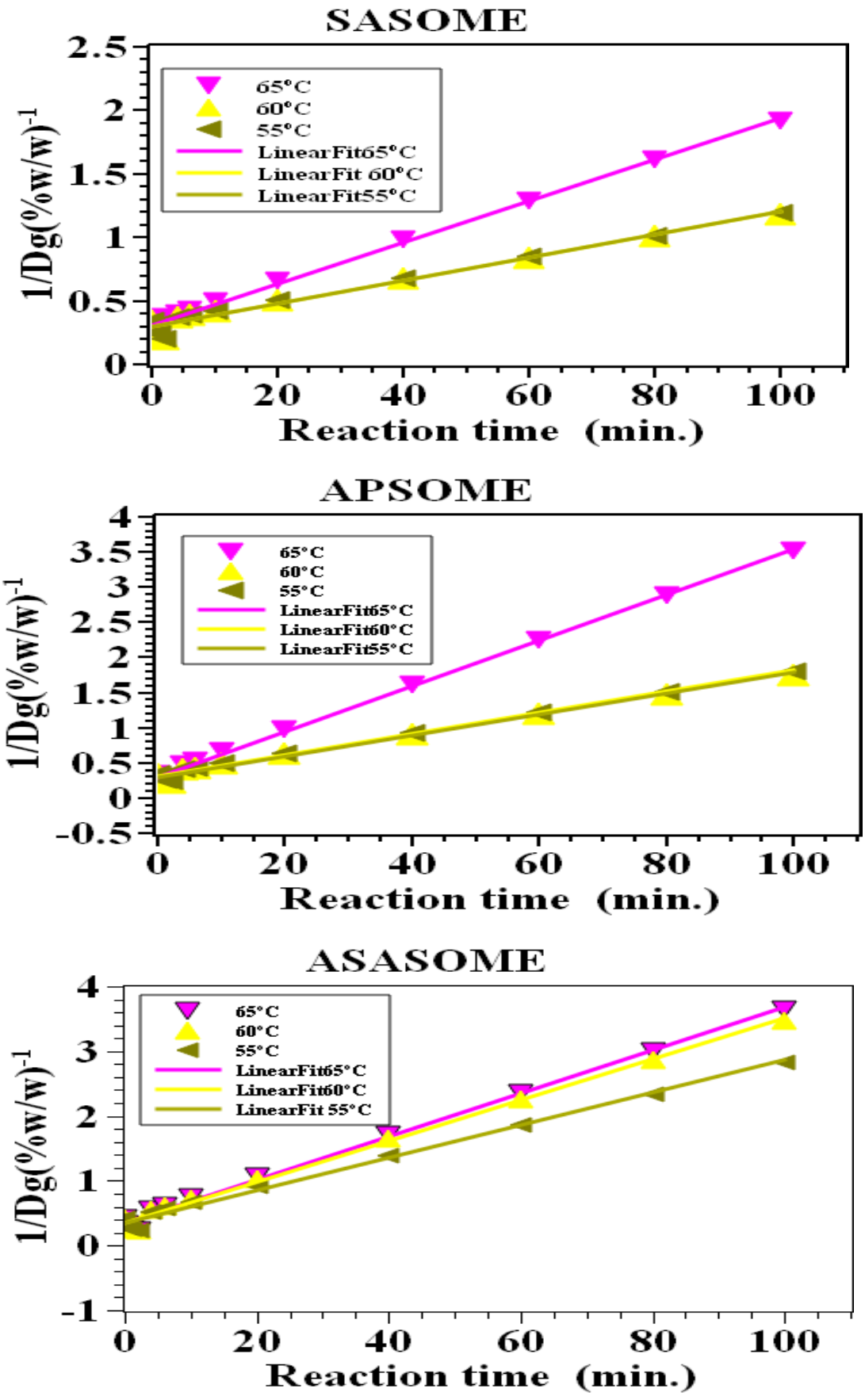

Figure A7.5: Second-order reaction irreversibbe model of diglycerides hydrolysis

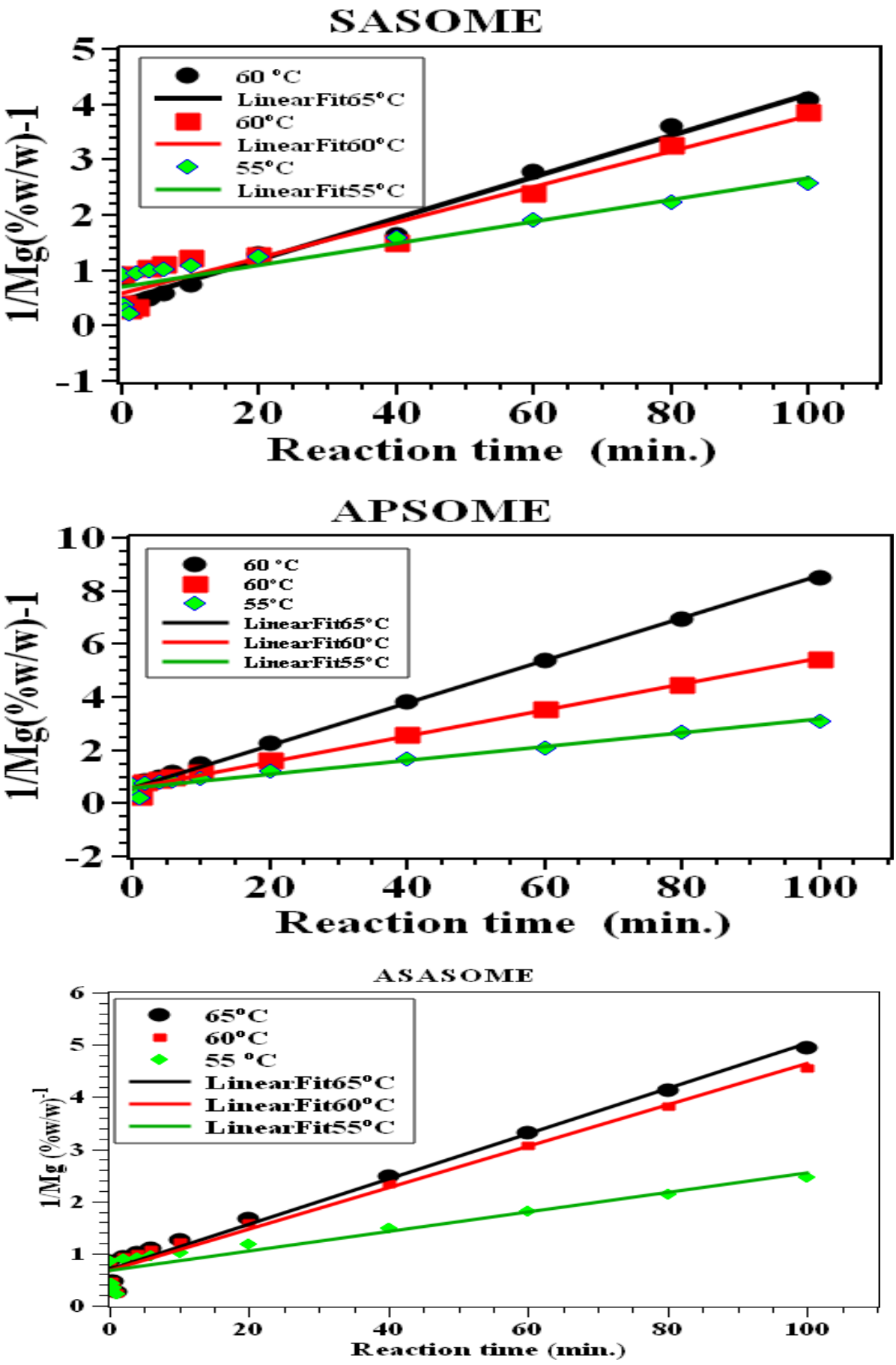

Figure A7.6: Second- order reaction irreversibbe model of monoglycerides hydrolysis

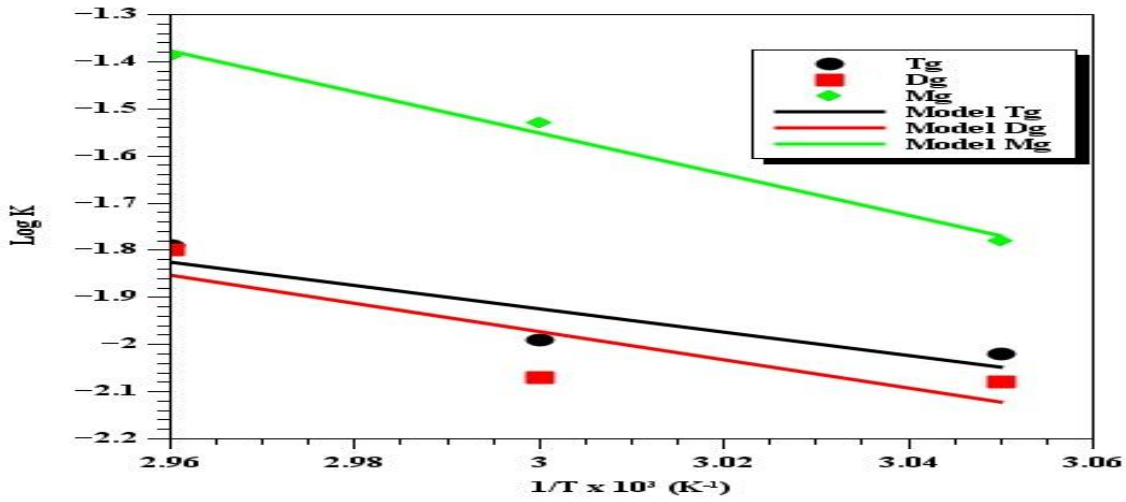

SASOME

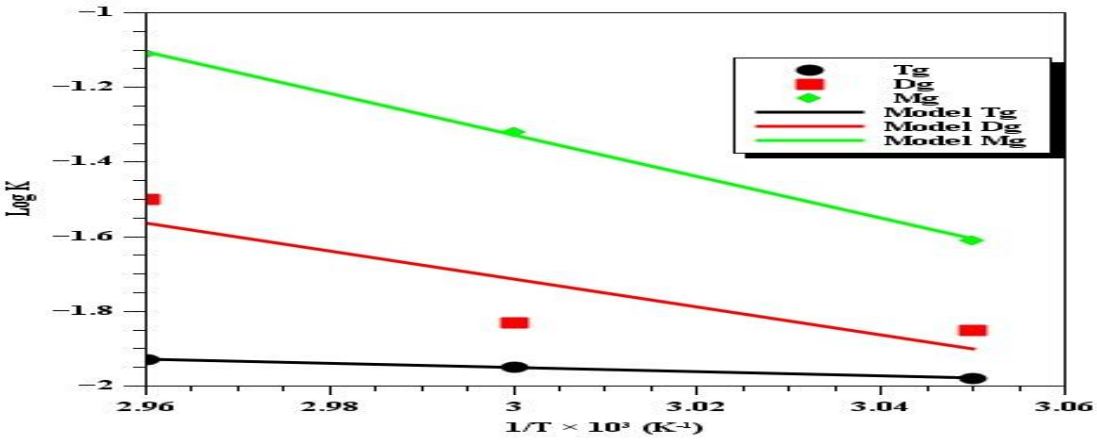

APSOME

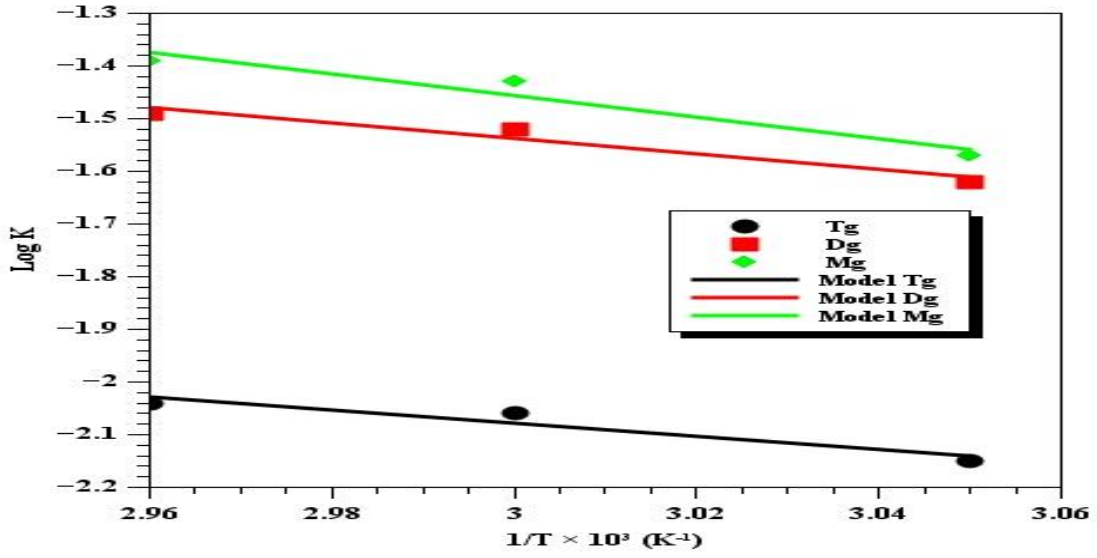

ASASOME

Figure A7.7: Arrhenius plot of irreversible model reaction rate versus temperature

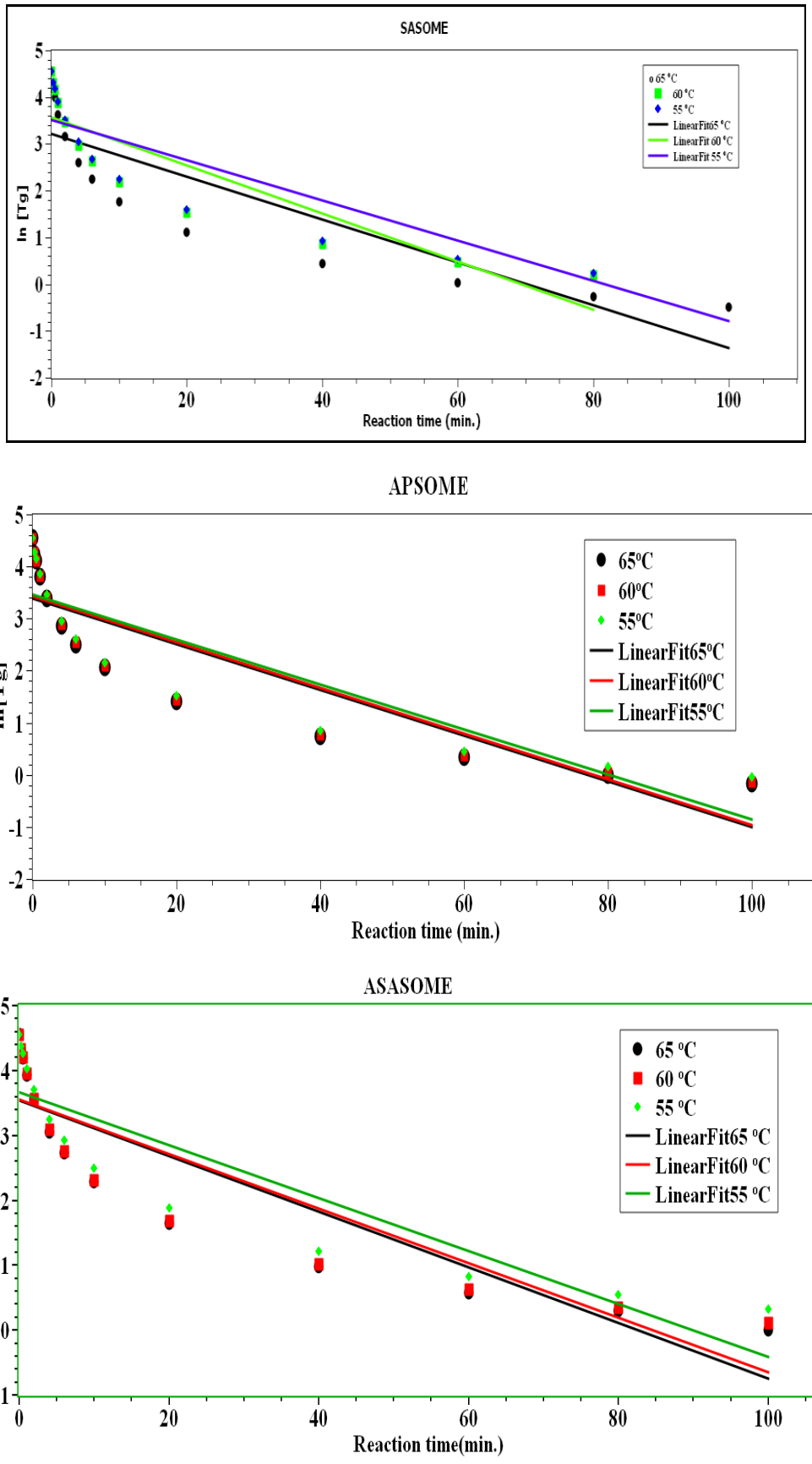

Figure A7.8: First-order plot of the triglycerides hydrolyis

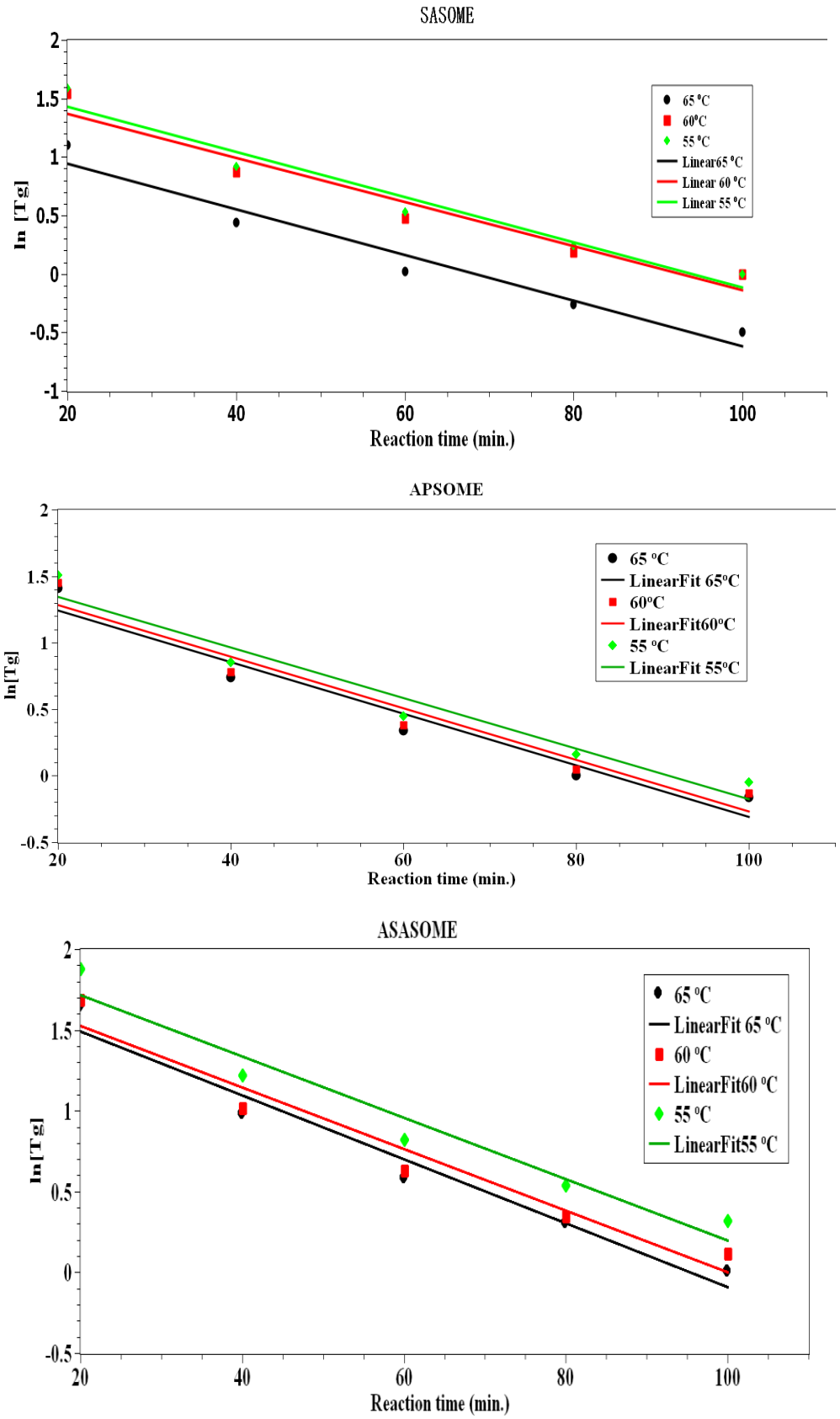

Figure A7.9: First-order plot of the latter stage (from 20 minutes) triglycerides hydrolyis

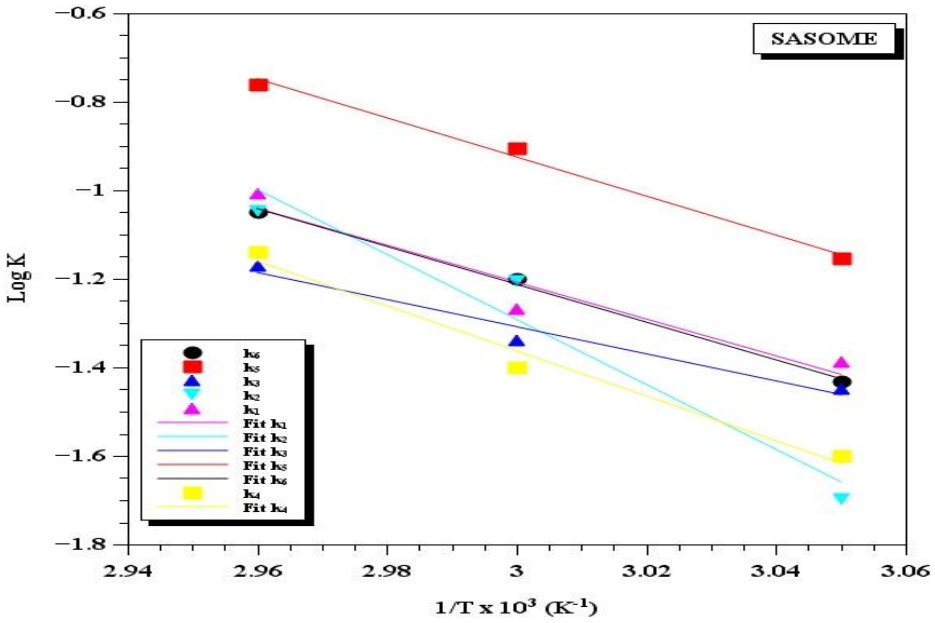

Figure A7.10: Plot of log k vs 1/T for SASOME reversible model.

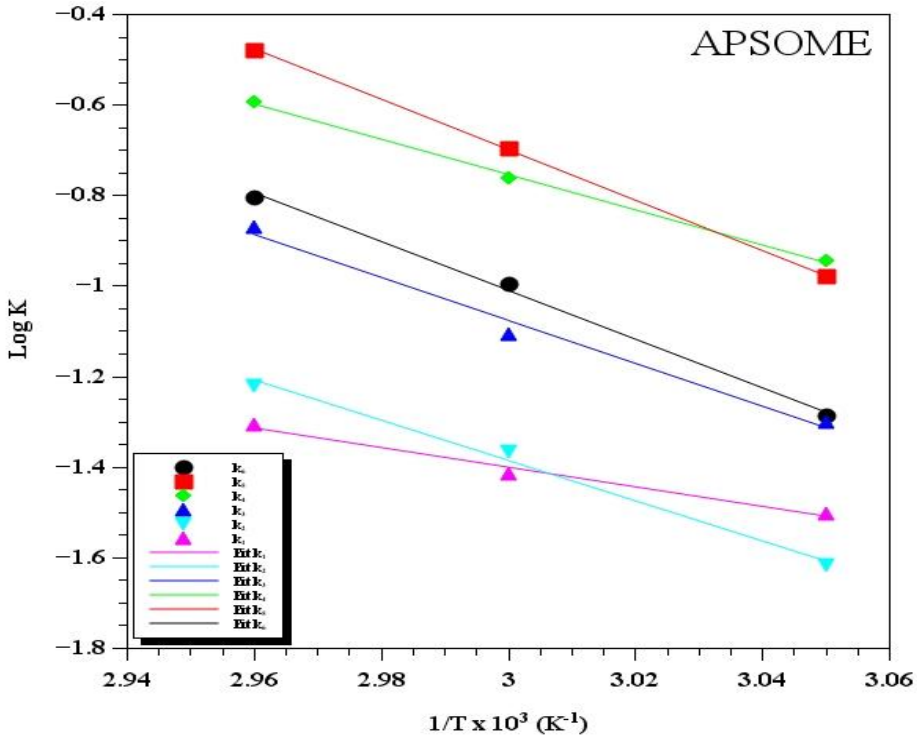

Figure A7.11: Plot of log k vs 1/T for APSOME reversible model.

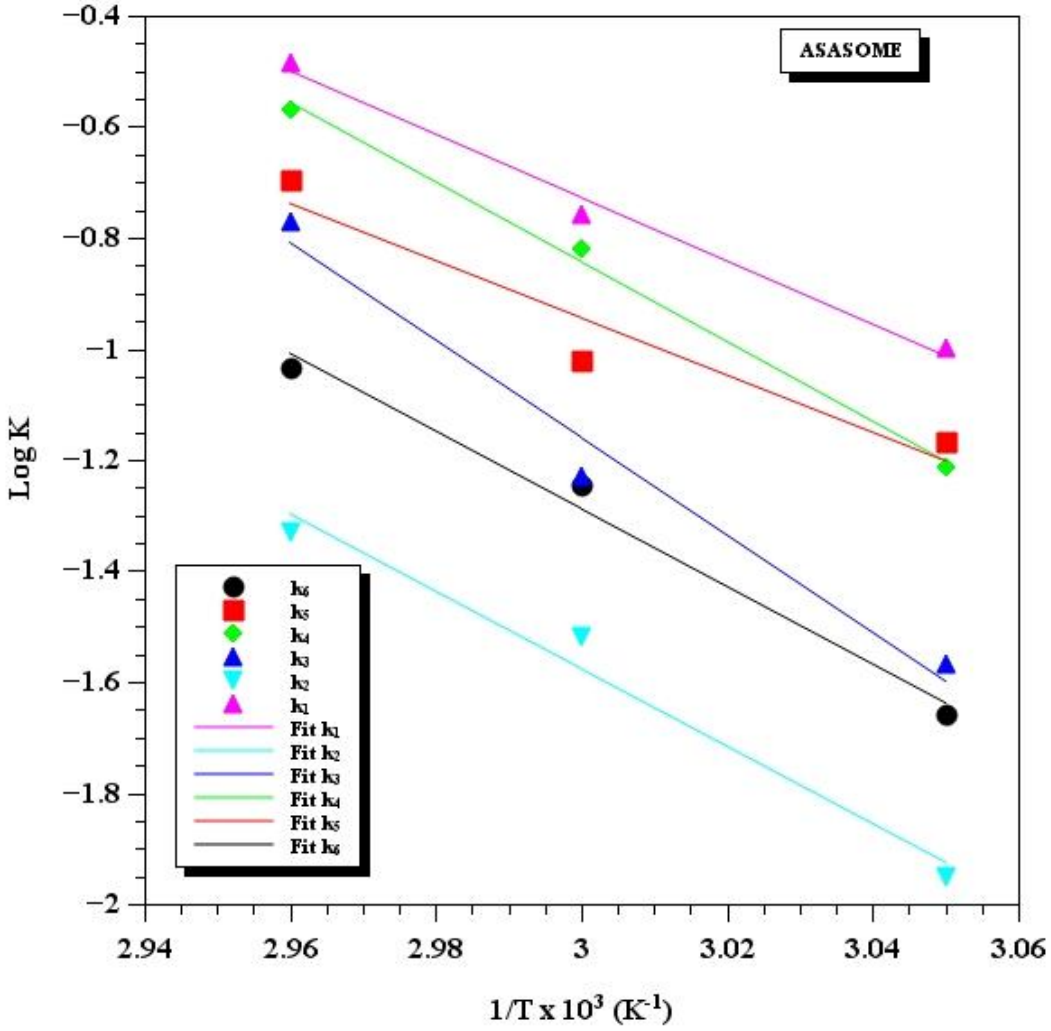

Figure A7.12: Plot of log k vs 1/T for ASASOME reversible model.

Table A7.10: Effect of mixing intensities at 60°C rate of transesterification of SASO, APSO and ASASO.

SASOME			APSOME			ASASOME		
200rpm	400rpm	800rpm	200rpm	400rpm	800rpm	200rpm	400rpm	800rpm
0.00	0.00	0.00	3.99	3.99	3.99	0.00	0.00	0.00
25.99	27.81	28.74	20.81	22.67	47.21	13.00	17.50	43.41
32.80	34.21	35.75	30.67	31.61	78.11	41.05	48.91	75.21
45.14	49.61	50.36	45.11	47.21	82.67	60.55	76.85	81.01
62.95	65.92	66.71	74.21	75.25	85.21	66.89	81.72	82.77
74.51	76.00	76.64	76.21	77.30	89.47	72.47	82.96	85.25
79.50	79.01	80.92	80.40	82.79	90.21	73.82	83.44	90.21
82.04	82.40	83.10	82.50	84.17	91.24	74.50	84.21	91.04
86.54	86.60	87.91	83.50	88.92	91.92	75.22	84.90	91.25
88.11	90.21	90.41	84.00	91.21	92.50	76.11	85.01	91.50
89.15	91.50	91.61	84.31	92.00	92.70	77.00	85.50	91.70
89.40	91.99	92.11	84.81	92.50	92.95	77.55	85.91	91.45
90.81	92.05	92.55	85.00	92.80	93.41	77.10	86.41	91.55

Appendix 8

Publications in Learned and Peer-reviewed Journals and Conference Proceedings

1. **Esonye, C**., Onukwuli, O. D. and Ofoefule, A. U. (2019). Optimization of Methyl Ester Production from *Prunus Amygdalus* Seed Oil Using Response Surface Methodology and Artificial Neural Networks. *Renewable Energy*, **130**, 62-71, http://dx.doi.org/10.1016/j.renene.2018.06.036. *Elsevier publications.*

2. **Esonye, C.,** Onukwuli, O. D. & Ofoefule, A. U. (2019) Characterization and oxidation modeling of oils from *prunus amygdalus, Dyacrodes edulis* and *Chrysophyllum albidium*. *Industrial crops and products*, **128**, 298-307.http://dx.doi.org/10.1016/j.indcrop.2018.11.029. *Elsevier publications.*

3. **Esonye, C.,** Onukwuli, O. D., Ofoefule, A. U. and Ogah, E. O. (2019) Multi-input multi-output (MIMO) ANN and Nelder-Mead's simplex based modeling of engine performance and combustion emission characteristics of biodiesel-diesel blendin CI diesel engine. *Applied Thermal Engineering*, **151**, 100-114. http://dx.doi.org/10.1016/j.applthermaleng.2019.01.101. *Elsevier publications.*

4. **Esonye, C.,** Onukwuli, O. D. and Ofoefule, A. U. (2019) Chemical Kinetics of a Two-step Transesterification of *Dyacrodes Edulis* Seed Oil Using Acid-Alkali Catalyst**.** *Chemical Engineering Research and Design*, **145,** 245-257 http://dx.doi.org/10.1016/j.cherd.2019.03.010. *Elsevier publications.*

5. Ofoefule, A. U., **Esonye, C.** Onukwuli, O. D., Nwaeze, E., Ume, C. S.(2019) Modeling and optimization of African pear seed oil esterification and transesterification using artificial neural network and response surface methodology comparative analysis. *Industrial Crops and Products*, **140,** 111707 https://doi.org/10.1016/j.indcrop.2019.111707. Elsevier publications

6. **Esonye**, C., Onukwuli, O. D. and Ofoefule, A. U. (2019). Effects of Process Variables on the Yield and Viscosity of Methyl Esters Derived from *Prunus Amygdalus, Dyacrodes Edulis* and *Chrysophyllum Albidium*, *Sigma J Eng & Nat Sci* **37** (1), 33-48.

7. **Esonye,** C., Onukwuli, O. D. and Ofoefule, A. U. (2018). The Influence of Fatty Acid Composition and Functional Groups on Fuel Related Properties of Sweet Almond (*Prunus amygdalus dulcis)* Seed Oil Methyl Esters, *Der Pharma Chemica*, **10**(7), 207-214.

8. **Esonye,** C., Onukwuli, O. D., Ofoefule, A. U. and Momoh, S. O. (2018). Modeling of Biodiesel Yield from African Pear Seed (*Dyacrodes edulis*) Oil Using Artificial Neural Networks, *Journal of the Nigerian Society of Chemical Engineers (JNSChE).* **33**(1), 26-35.

9. **Esonye**, C., Onukwuli, O. D and Ofoefule, A. U (2018). The Effects of Fatty Acid Methyl Ester-Petroldiesel Blend on the CO and NOx Emissions Toxicity in CI Diesel Engine. *Journal of Chemical and Pharmaeceutical Research*, **10**(2), 111-115.

10. **Esonye,** C., Onukwuli, O. D and Ofoefule, A. U (2017). Synthesis and Physico-Chemical studies of base Catalyzed Methanolysis of some Virgin Tropical Seed Oils, *World News of Natural Science*, **15**, 112-128.

11. Onukwuli, O. D. and **Esonye, C.** (2019). Kinetics of Consecutive Irreversible Second Order Methanolysis of *Dyacrodes Edulis* Seed Oil *Journal of Engineering and Applied Sciences, Nnamdi Azikiwe University, Awka. Accepted Manuscript.*

12. **Esonye,** C., Onukwuli, O. D. and Ofoefule, A. U. (2018). Effect of African Pear (*Dyacrodes edulis*) Seed Oil Methyl Ester – Diesel Blend on the Combustion Emission Characteristics in CI Engine, In 8th Annual & International Conference of *Renewable and Alternative Energy Society of Nigeria* (RAESON): Renewable Energy for Stable Power Supply & Environmental Sustainability at University of Portharcourt, 25th to 28th April 2018, pp53.

13. **Esonye,** C., Onukwuli, O. D. and Ofoefule, A. U. (2018). Multi-Input Multi-Output (MIMO) ANN Based Modeling of Engine Performance and Combustion Emission Characteristics of Biodiesel-Diesel Blend in CI Diesel Engine, In the Faculty of Engineering 2018 International Conference (FEIC 2018): Raw Material Processing and utilization for Sustainable Development, held on 13th and 14th August, 2018 at Nnamdi Azikiwe University, Awka, Nigeria. 368-378.